Technische Universität München

Lehrstuhl für Entwicklungsgenetik

„Generation and Analysis of Mouse Models for Alzheimer's Disease"

Anke Annette Wittmann

Vollständiger Abdruck der von der Fakultät Wissenschaftszentrum Weihenstephan für Ernährung, Landnutzung und Umwelt der Technischen Universität München zur Erlangung des akademischen Grades eines

Doktors der Naturwissenschaften

genehmigten Dissertation.

Vorsitzender: Univ.-Prof. Dr. Harald Luksch

Prüfer der Dissertation:

1. Univ.-Prof. Dr. Wolfgang Wurst
2. Univ.-Prof. Dr. Aphrodite Kapurniotu

Die Dissertation wurde am 21.03.2016 bei der Technischen Universität München eingereicht und durch die Fakultät Wissenschaftszentrum Weihenstephan für Ernährung, Landnutzung und Umwelt am 08.07.2016 angenommen.

Index of contents

Zusammenfassung

Sphingolipide (SL) wurden mit der Alzheimerschen Krankheit (AD) assoziiert, da gezeigt werden konnte, dass sie die amyloidogene Prozessierung verändern und selbst wiederum von AD-relevanten Proteinen beeinflusst werden. Ein SL dessen Rolle in der Prozessierung kontrovers diskutiert wird ist Sphingomyelin (SM). SM kann von zwei verschiedenen Enzymen, Sphingomyelin Synthase 1 (SMS1) und 2 (SMS2) produziert werden, wobei SMS1 den Hauptanteil der SM Synthese übernimmt.

Um zu untersuchen, welchen Effekt ein Verlust von SMS1 auf die Lipidzusammensetzung und die Prozessierung des Amyloid Precursor Proteins (APP) *in vivo* hat, wurden *Sms1* gene trap Mäuse analysiert und eine Doppelmutanten-Mauslinie (*Sms1* x *APPswe*) durch das kreuzen von *Sms1* gene trap Mäusen mit Tg2576 Mäusen, einem bekannten AD Maus Model, generiert und analysiert.

Es konnte gezeigt werden, dass in Hirn und in Testes gewebespezifische Splicevarianten von *Sms1* existieren. *Sms1*^{MUT} Tiere zeigten eine Verringerung der SM Level im Hirn auf 56%, daraus resultierten Defizite in der Myelinisierung des zentralen (CNS) und peripheren Nervensystems (PNS). Trotz reduzierter SMS Aktivität konnte eine Reduktion der Ceramid (Cer) Level gezeigt werden. Zusätzlich wurden kompensatorische Mechanismen im SL Stoffwechsel gefunden, welche eine Anreicherung des potentiell toxischen Cer verhindern könnten. Des Weiteren war in *Sms1*^{MUT} das Verhältnis von einfach ungesättigten Fettsäuren (MUFA)/gesättigten Fettsäuren (SFA) und von mehrfach ungesättigten Fettsäuren (PUFA)/SFA innerhalb der Diacyl-Phosphatidylcholin (PCaa) und/oder der Acyl-Ethyl-Phosphatidylcholin (PCae) reduziert. Außerdem korrelierten die Level der langkettigen (LC)-PCaa und –PCaes negativ mit der Länge der Fettsäure (FA)-kette und mit dem Satturierungsgrad. Dies weist darauf hin, dass ein Verlust von *Sms1* Elongasen und Desaturasen, besonders Δ^9-Desaturase, negativ beeinflussen könnte. In Übereinstimmung mit vorherigen Berichten konnte gezeigt werden, dass *Sms1*^{MUT} altersabhängige Splenomegalie aufweisen und dass eine mögliche Verbindungen zu reduzierter Cathepsin-D (CatD) Expression und Apoptosis Inducing Factor (AIF) vermittelter Apoptose besteht. Mit Bezug auf die Lebensweise ist bekannt, dass regelmäßige Bewegung und reduzierter chronischer Stress das AD Risiko verringern. Es konnte beobachtet werden, dass *Sms1*^{MUT} Mäuse aktiver und weniger ängstlich sind, des Weiteren wiesen sie eine veränderte Signalweiterleitung in der Hypothalamus-Hypophysen-Nebennieren (HPA)-Achse auf, die sie stressresistenter erscheinen ließ.

Es wurde weiterhin festgestellt, dass männliche *Sms1*^{MUT} Mäuse subfertil sind und eine altersabhängige Reduktion der Fruchtbarkeit zeigen. Die Ergebnisse dieses Nebenprojekts haben gezeigt dass die Keimzellen im Stadium der Pachytän-Spermatozyten und der runden Spermatiden sogenanntem „Sloughing“ unterliegen. Dies konnte auf eine Fehlfunktion der Blut-Testes-Schranke (BTB), ausgelöst durch mangelnde Kommunikation zwischen Sertoli- und Keimzellen und einer daraus resultie-

renden Veränderung des extrazellulären Milieus zurückgeführt werden, welche wiederum aus einem Mangel der für die Keimzellreifung essentiellen LC-PUFAs in den Hoden resultierten. Diese LC-PUFAs schlossen Docosahexaensäure (DHA) und Eicosapentaensäure (EPA) mit ein. Eine Zufütterung von DHA/EPA war ausreichend um den Infertilitätsphänotyp in 50% der *Sms1*^{MUT} Mäuse, die zuvor als infertil identifiziert wurden zu beheben.

Sms1^{MUT} x *APPswe*^{Tg} Mäuse wurden mit einer geringeren Mendelischen Rate als erwartet geboren und zeigten eine verfrühte Sterblichkeit mit einem Alter von acht Wochen, obwohl sowohl die *Sms1* als auch die Tg2576 Mauslinie eine normale oder leicht reduzierte Lebenserwartung aufwiesen. Außerdem gewannen *Sms1*^{MUT} x *APPswe*^{Tg} Mäuse langsamer an Gewicht und zeigten auch eine Reduktion der Gehirnmasse im Vergleich zu *Sms1*^{WT} x *APPswe*^{Tg} Mäusen. Die Reduktion im SM Level in Gehirnproben der *Sms1*^{MUT} x *APPswe*^{Tg} Mäuse war vergleichbar mit dem der *Sms1*^{MUT} x *APPswe*^{WT} und konnte mit einer Veränderten Myelinisierung assoziiert werden. Eine Anreicherung spezifischer PCaa und PCae Varianten, die als Speicher von Arachidonsäure (AA), EPA und Docosapentaensäure (DPA) dienen könnte wurde in Gehirnproben der *Sms1*^{MUT} x *APPswe*^{Tg} Mäuse gemessen. Zusammen mit erhöhten Lyso-Phosphatidylcholin (lyso-PCs) Level, könnten diese Daten auf eine gesteigerte Freisetzung dieser PUFAs hinweisen, die damit als anti-inflammatorische Faktoren dienen könnten. Unterstützend hierzu konnte eine geringfügig reduzierte Aktivität der Microglia über die Expression des CD68 Antigen und den Allocraft Inflammatory Factor 1 (Iba-1) in *Sms1*^{MUT} x *APPswe*^{WT} nachgewiesen werden. Die amyloidogene Prozessierung in *Sms1*^{MUT} x *APPswe*^{Tg} war leicht war leicht verändert und bewirkte zwar keine Reduktion der Anzahl an Aβ42 positiven Plaques und pTAU, hatte aber wohl eine geringere Anzahl an Aβ40 positiven Plaques zur Folge. Weitere Analysen haben gezeigt, dass in diesem Zusammenhang eine erhöhte Rate und Autophagieinduktion und ein schneller Autophagie-vermittelter Verdau zur Reduktion von Aβ Aggregaten beitragen könnten. Verhaltenstests zeigten höhere Aktivität, in *Sms1*^{MUT} x *APPswe*^{Tg} Tieren, verglichen mit anderen Genotypen, aber keine Auswirkungen auf die Gedächtnisleistung im frühen Alter von acht Wochen. APP wurde auch in anderen Organen sowie dem Herz und der Lunge gefunden. Hier wiesen *Sms1*^{MUT} x *APPswe*^{Tg} geringfügig höhere Mengen an Aβ auf.

Zusammenfassend zeigten diese Ergebnisse, dass der Verlust von *Sms1* möglicherweise einen protektiven Effekt auf AD relevante Aspekte wie Neuroinflammation, die Prozessierung von APP und die Bildung von Plaques im Gehirn hat, aber trotzdem zu einer frühen Sterblichkeit der *Sms1*^{MUT} x *APPswe*^{Tg} Mäuse führt. Dies könnte mit der Prozessierung von APP im Herzen und der Lunge zusammenhängen, da hier eine leicht, wenn auch nicht signifikant erhöhte Anreicherung Aβ gefunden wurde.

Summary

Sphingolipids (SL) have been connected to Alzheimer's disease (AD) as they have been shown to alter amyloidogenic processing and also to be affected by AD-related proteins. One SL with controversial reports about its influence on AD risk is sphingomyelin (SM), which can be produced by two different enzymes, sphingomyelin synthase 1 (SMS1) and 2 (SMS2), while the first takes over the major bulk of SM synthesis.

In order to investigate the effect of SMS1 disruption on lipid composition and on the processing of the amyloid precursor protein (APP) *in vivo*, a *Sms1* gene trap mouse was analyzed and a double mutant animal model (*Sms1*^{MUT} x *APPswe*^{Tg}) was generated by crossing *Sms1* gene trap mice with Tg2576 mice, representing a common AD animal model.

It could be shown that *Sms1* has tissue specific splice variants in brain and testes. *Sms1*^{MUT} animals revealed a reduction of SM in the brain to 56%, leading to myelination deficits in the central nervous system (CNS) and peripheral nervous system (PNS). Despite reduction of SMS activity, ceramide (Cer) levels were decreased and compensatory mechanisms in enzymes of the SL pathway were found to prevent toxic accumulation of Cer. Additionally, *Sms1*^{MUT} had reduced diacyl-phosphatidylcholine (PCaa) and/or acyl-ethyl-phosphatidylcholine (PCae) monounsaturated fatty acid (MUFA)/saturated fatty acid (SFA) and polyunsaturated fatty acid (PUFA)/SFA ratios and long chain (LC)-PCaa and –PCaes levels correlated negatively with fatty acid (FA) chain length and saturation state, pointing to a possible negative influence of *Sms1* disruption on elongases and Δ9-desaturase. In accordance with previous reports *Sms1*^{MUT} were found to suffer from age-dependent splenomegaly and found possible connections to reduced cathepsin-D (CatD), apoptosis inducing factor (AIF) mediated apoptosis. Concerning life-style, regular exercise and reduced chronic stress are said to reduce AD risk. *Sms1*^{MUT} animals displayed an increased amount of voluntary movement and an altered hypothalamus-pituitary-adrenal (HPA)-axis signaling, rendering them more active and stress-resistant. Furthermore, *Sms1*^{MUT} males were subfertile, showing age-dependent decline in fertility, which was investigated in a side project. Results show that sloughing of germ cells takes place between the pachytene spermatocyte and round spermatid stage due to a dysfunction of the blood-testes-barrier (BTB) caused by missing communication between Sertoli cells and germ cells and the disruption of the specific microenvironment, needed for germ cell maturation due to the lack of essential LC-PUFAs in the testes. These included docosahexaenoic acid (DHA) and eicosapentaenoic acid (EPA). DHA/EPA supplemented diet was sufficient to rescue the infertility phenotype in 50% of formerly infertile male *Sms1*^{MUT}.

Unexpectedly, *Sms1*^{MUT} x *APPswe*^{Tg} animals were born below Mendelian ratios and to suffer from pre-mature death, at an age of 8 weeks, despite a normal or slightly reduced life expectancy of both single mutant animal models. Additionally, *Sms1*^{MUT} x *APPswe*^{Tg} animals had reduced weight gain

during the first month and also reduced brain weight compared to *Sms1*^{WT} x *APPswe*^{Tg} animals. Brain SM reduction of *Sms1*^{MUT} x *APPswe*^{Tg} animals was comparable to *Sms1*^{MUT} x *APPswe*^{WT}, and could be connected to alterations in myelination. Specific PCaa and PCae species were accumulated, pointing to the possibility of a store of arachidonic acid (AA), EPA and docosapentaenoic acid (DPA). Together with enhanced lyso-phosphatidylcholines (lyso-PCs), the data propose elevated release of these PUFAs, serving as anti-inflammatory lipid mediators. Consistently, subtle reduced microglial activation, monitored by CD68 antigen and allocraft inflammatory factor 1 (Iba-1) in brain samples of *Sms1*^{MUT} x *APPswe*^{WT} could be observed. Amyloidogenic processing in these double mutants was slightly altered, without affecting Aβ42 plaque count and pTAU, but reducing Aβ40 positive plaques. Furthermore, analysis proposed alterations in the autophagic pathway, which might be contributing to degradation of Aβ. Behavioral testing revealed a higher voluntary activity of *Sms1*^{MUT} x *APPswe*^{Tg} animals, compared to other genotypes, but no effects on memory performance in early life. APP was found to be additionally expressed and cleaved in heart and lung, with slightly higher levels of Aβ generated in the *Sms1*^{MUT} x *APPswe*^{Tg}.

Thus, in summary these results showed that the mutation of *Sms1* might have a protective effect on AD related aspects such as neuro-inflammation and APP cleavage, including plaque formation in the brain, but nevertheless led to a reduced survival rate, which might be connected to APP processing in heart and lung and an enhanced accumulation of Aβ in these tissues.

1. Introduction

1.1 Alzheimer's disease

In 1907 Alois Alzheimer described the case of a 51-year-old woman, Auguste Deter, suffering from a yet unknown mental illness. In his report he mentioned several behavioral abnormalities, such as jealousy of her husband, rapid memory loss, disorientation, auditory hallucinations and persecution mania. Nevertheless, her physical condition was not altered at that time and no deficits concerning reflexes, gait or manual abilities were described. After four and a half years of progressive illness, Alzheimer's patient died (Alzheimer *et al.* 1995).

1.1.1 AD facts and numbers – prevalence, FAD and SAD classification

The prevalence of dementia in people aged over 60 lies between five and seven percent, within these Alzheimer's disease (AD) represents the most common form of dementia (50-80% of all dementia cases (Abbott 2011)), causing an economic burden estimated to be at least $100 billion/year considering US only (Fillit 2000). Nowadays AD is affecting 35.6 million people, which is about 0.5% of the world's population and is estimated to reach 81 million by 2040 (Ferri *et al.* 2005, Abbott 2011). AD has an average onset age of 65 years (Abbott 2011). Reaching that age, risk for AD doubles with each decade (Forsyth and Ritzline 1998, Jorm and Jolley 1998). The time from diagnosis to death ranges from three to four years if the person is older than 80 years. When younger persons are diagnosed ten or more years can pass until death (Alzheimer's Disease Education and Referral Center, National Institute on Aging). Due to the commonly late onset and the pathology, which reflects an enhanced progress of normal aging, AD is well known as an age-related disease. 95% of all cases start late and are classified as sporadic Alzheimer's disease (SAD) with no known genetic basis, whereas less than 5% of all cases start early with 30 to 40 years and are classified as familial Alzheimer's disease (FAD) being caused by genetic risk factors (Abbott 2011). AD furthermore has a higher prevalence in women, which at an age of 75 and older are 2.8-times more affected then men (Filley 1997).

1.1.2 AD symptoms – four stages of AD progression

Dementia types are classified according to the *Diagnostic and Statistical Manual of Mental Disorders IV (DSM-IV)*. The symptoms of AD as a progressive neurological disease are categorized into four different stages according to the Alzheimer's Disease Education and Referral Center of the National Institute on Aging (Figure 1.1).

Stage one or early AD, describes the early years (one to three) after symptomatic onset. Patients show minimal awareness of their own condition, mild anemia and personality changes. They also show decreased abilities to solve problems and to cope with difficult situations. Emotional lability, loss of abstract thinking and of short term memory, as well as speech deficits finally lead to social withdrawal of AD patients.

From year two to ten (**stage two or mild AD**) memory loss gets profound. Patients show at least two signs of cognitive impairment (Anomia – loss of name/word memory, Agnosia – loss of perception, Apraxia – loss of motor skills, or Aphasia – loss of language) and severe loss of judgment. They start to wander aimlessly, show signs of mood changes, anxiety and violent outbursts.

Stage three or moderate AD is reached approximately eight to twelve years after onset, when all cognitive functions of the patients are severely impaired. Patients give repetitive statements, have delusions and hallucinations often accompanied with suspiciousness or paranoia. They also lose their impulse control and start to undress at inappropriate time points and get aggressive towards family members or care takers. At this point physical impairment and generalized muscular rigidity, with twitches are also described. Stage three patients become incontinent, are not able to recognize family members or to perform basic activities of daily living, making personal care necessary.

In the last stage of AD (**stage four to five or severe AD**) nearly all abilities are lost. Patients start to lose weight and show difficulties in swallowing. They tend to sleep longer and to get skin infections. Speech is reduced to groaning or grunting, leaving the patient as an "isolated self" (Forsyth and Ritzline 1998).

The most frequent cause of death is aspiration pneumonia, due to impaired swallowing and breathing difficulties (Kalia 2003).

1.1.3 AD pathology

Unfortunately, the pathology of AD starts up to 50 years before the first symptoms emerge which impedes early intervention in disease progression (Ohm *et al.* 1995, Smith 2002). The observed pathology at different stages correlates with the proceeding symptoms and was characterized by Braak and Braak (1991)/Braak and Braak (1995). Two major proteinopathies are involved in AD. According to the so called "amyloid hypothesis", which was handled as the major hypothesis in AD research over several years, amyloid-β (Aβ) generation is thought to be the primary event, followed by phosphorylated microtubule associated protein tau (pTAU) accumulation, finally leading to the known AD pathology (Hardy and Higgins 1992). Although this hypothesis began to totter in the last few years (Armstrong 2014, Herrup 2015, Musiek and Holtzman 2015), the major players remained.

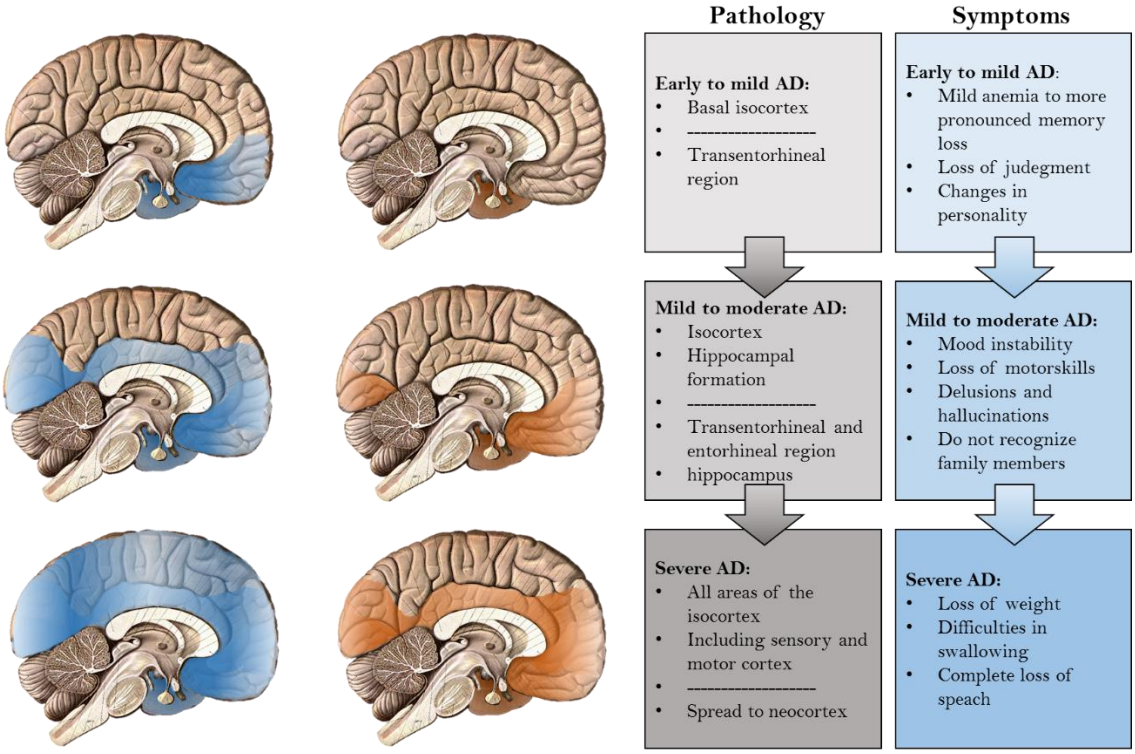

Figure 1.1: Progression of Alzheimer's disease pathology and symptoms
Illustration of pathological and symptomatic progression of Alzheimer's disease from mild and moderate up to severe stages. Spreading of plaques is depicted in blue and in the upper part of the gray panel, spreading of tangles in brown and in the lower part of the gray panels. Alzheimer's disease (AD), Classification according to (Alzheimer's Disease Education and Referral Center, National Institute on Aging) and (Braak and Braak 1991, 1995).
Schematic brain modified after: Atlas and Text-book of Human Anatomy Volume III Vascular System, Lymphatic system, Nervous system and Sense Organs.

1.1.3.1 APP and Amyloid-β

In his pathological report, Alzheimer mentioned some "minute miliary foci", forming on the cell surface and resulting from deposition of a yet unknown substance (Alzheimer, 1907). The pathology Alzheimer observed is now referred to as amyloid plaques or senile plaques (SPs; Figure 1.3).

The "special substance in the cortex", how Alzheimer called the unknown origin of the found deposits, was first identified in 1984 by Glenner and Wong (1984). It was called Aβ as it was first isolated form beta sheet fibrils of an AD brain. The origin of that 4.2kDa peptide, primarily between 40 and 42 amino acids (aa) in length, was finally tracked back by Kang *et al.* (1987) to the amyloid precursor protein (APP), a 100kDa single pass transmembrane (TM) glycoprotein (Glenner and Wong 1984, Kang *et al.* 1987). Despite extensive research it is still not yet fully clear what the major tasks of APP and its cleavage products exhibit in a healthy. Interestingly, it is assumed, that APP might function in the clearance of excess cholesterol from the brain (Puglielli *et al.* 2003b). The *APP* gene on human chromosome 21 encodes for several splice variants of APP, including APP695, the major CNS form of APP in humans (Sola *et al.* 1993, Bayer *et al.* 1999). APP is synthesized in neurons, sorted in the

Endoplasmatic reticulum (ER) and Golgi and reaches the nerve terminals by fast axonal transport (Koo *et al.* 1990). At the nerve terminals, APP can either be transferred to the plasma membrane, or be directly incorporated in endosomal compartments. It is also possible that APP is first reinternalized from the plasma membrane by clathrin-coated pits and then secondarily be directed to an endosomal compartment. However, the localization of APP plays an important role for its subsequent proteolysis as the diverse involved cleavage enzymes have preferred sites of action (Haass *et al.* 1993a, Capell *et al.* 2005, Fukumori *et al.* 2006, Haass *et al.* 2012). The cleavage process of APP leading to the generation of AD-associated amyloid plaques is discussed in section 1.1.4.

1.1.3.2 pTAU tangles

According to the amyloid hypothesis, generation and extracellular accumulation of Aβ leads to the formation of intracellular protein deposits (Hardy and Higgins 1992). These so called neurofibrillary tangles (NFTs) represent another major hallmark of AD. The protein responsible for the formation of NFTs is known as microtubule associated protein tau (MAPT or TAU) and was first discovered by Weingarten *et al.* (1975)(Figure 1.3).

Under healthy conditions TAU regulates microtubule assembly, dynamic behavior and spatial organization as well as trophic signaling enhancement and signal transduction (Weingarten *et al.* 1975, Mietelska-Porowska *et al.* 2014). It was also shown that MAPT regulates the transport of cell organelles, such as mitochondria, along the microtubules (Yu *et al.* 2005, Rodriguez-Martin *et al.* 2013, Medina and Avila 2014). Under pathological conditions however, TAU gets phosphorylated, forming pTAU and starts to accumulate inside the cell (mostly neurons) building the described tangles (Grundke-Iqbal *et al.* 1986a, Grundke-Iqbal *et al.* 1986b). It is discussed that NFT formation is a result of loss-of function, due to reduced binding abilities of the pTAU to the microtubules, but also from gain-of function, due to higher self-aggregation potential of pTAU (Johnson and Stoothoff 2004, Mietelska-Porowska *et al.* 2014). It is still not clear what is the ultimate cause for hyperphosphorylation of TAU by microtubule associated protein kinases (MAPKs), leading to destabilization of the microtubule, dysfunction of the neuron and finally cell death. However, it was shown that production of Aβ induces phosphorylation of TAU and therefore might precede and even trigger the aggregation of pTAU and neuronal death as proposed by the amyloid hypothesis (Coria *et al.* 1993, Ferrari *et al.* 2003, Hardy 2003, Johnson and Stoothoff 2004).

NFT formation spreads through the brain in a defined pattern. Braak and Braak (1995) investigated this phenomenon leading to the six Braak-stages of AD, additionally classifying progression of the disease on the pathological level with regard to SPs and NFTs (Braak and Braak 1991, 1995)(Figure 1.1).

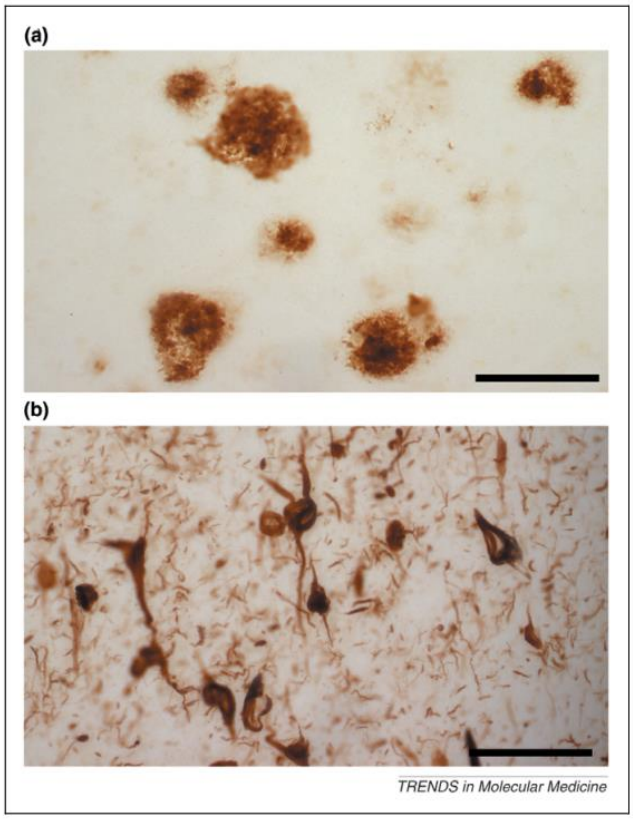

Figure 1.2: Representative pictures of amyloid plaques and neurofibrillary tangles in AD brains.
(a) Typical senile plaques derived from aggregated amyloid-beta. (b) Neurofibrillary tangles formed form phosphorylated TAU aggregates.
Picture from: Alzheimer's disease: Ab, tau and synaptic dysfunction.
Frank M. LaFerla and Salvatore Oddo, 2005

1.1.3.3 Neuronal inflammation and neuronal death

Another hallmark of AD is neuronal inflammation attended by activation of microglia. Matsuoka *et al.* (2001) observed microglia activation to go along with preceding amyloid burden in APP/PS1 mice, which was also reported in other studies (Serrano-Pozo *et al.* 2013, Marlatt *et al.* 2014). Microglia activation as a consequence of Aβ accumulation has also been connected to pTAU, therefore contributing to progression of AD pathology (Sheng *et al.* 1997, Li *et al.* 2003, Mrak 2012)(Figure 1.3).

The final and most destructive pathological features of AD is progressive loss of brain volume and expansion of the ventricles due to loss of neurons and synapses in specific brain regions. Affected neurons first start to work less, lose synaptic activity and finally die (Alzheimer's Disease Education and Referral Center, National Institute on Aging). The reduction in brain volume was also noticed in the course of the post mortem examination of Alzheimer's patient. Her brain was atrophic, with larger vascular tissue, having arteriosclerotic change (Alzheimer *et al.* 1995). Pathology starts in the medial temporal lobe (MTL), propagating to the entorhinal cortex (EHC) with its direct connection to the hippocampus, which is affected next. From here the disease spreads to the temporal cortex (Braak and Braak 1995, Scahill *et al.* 2002, Smith 2002).

1.1.3.4 Lipid accumulation

In the original case study of 1907 an additional observation was made, namely that the glia cells of the woman showed adipose saccules. However, this fact did not get much attention at first. We now know, that Alzheimer's patient suffered from progressive presenile dementia with general cortical atrophy, which is similar to Niemann Pick disease (NPD), one of several lysosomal storage diseases (LSD) (Wisniewsky et al., 1972), connecting AD to the lipid metabolism.

Today, the field of AD research is widely spread and many scientists have also shifted their research focus towards lipids. Several studies analyzing the lipid profile of AD patients showed that there are alterations in lipid content and ratios. Data linking AD to lipid metabolism is discussed in section 1.3.

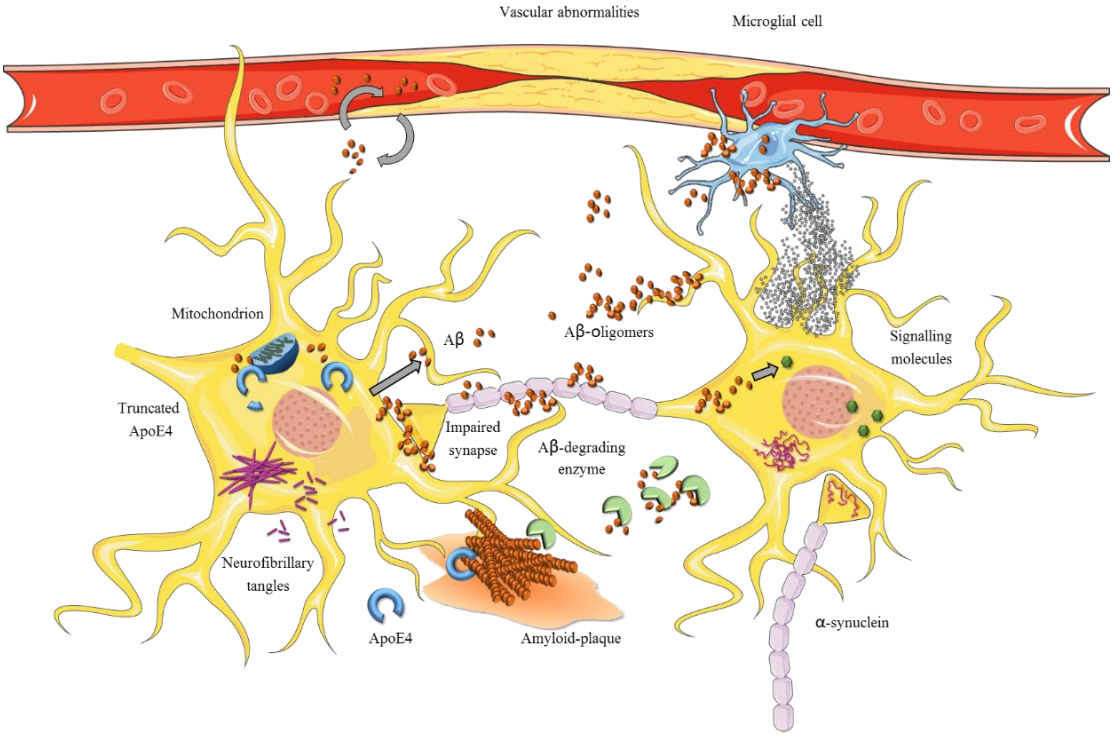

Figure 1.3: Factors involved in Alzheimer's disease pathology.
Alzheimer's disease (AD) pathology involves several different factors. Protein abnormalities include extracellular amyloid plaques, formed by aggregated amyloid-β (Aβ) and intracellular neurofibrillary tangles formed by phosphorylated microtubule associated protein tau (pTAU). Mutations in Aβ-degrading enzymes lead to further formation of plaques. These protein aggregates are thought to lead to impaired synaptic function. Additionally genetic risk factors, such as ApoE4 and vascular abnormalities are known to contribute to AD risk. Furthermore, mitochondrial defects and inflammatory factors are discussed to be involved in AD pathology.
Illustration created with the use of: http://www.servier.com/Powerpoint-image-bank

1.1.4 APP processing – amyloidogenic and non-amyloidogenic pathway

There are two major ways how APP is processed involving three different cleavage enzymes and two subsequent steps of ectodomain shedding and intramembrane proteolysis, summarized as regulated intramembrane proteolysis (Lichtenthaler *et al.* 2011). In the non-amyloidogenic pathway APP is

cleaved first by alpha-secretase (α-secretase, ADAM10) and subsequently by γ-secretase, without the formation of Aβ monomers. The amyloidogenic pathway however, requires cleavage by β-site APP cleavage enzyme 1 (β-secretase, BACE1) and γ-secretase, leading to the production of the neurotoxic Aβ monomers, which accumulate, form oligomers, fibrils and finally SPs. Both pathways therefore comprise one first (N-terminal) extra- and one second (C-terminal) intramembranous enzymatic cleavage step of APP (Haass *et al.* 2012)(Figure 1.4).

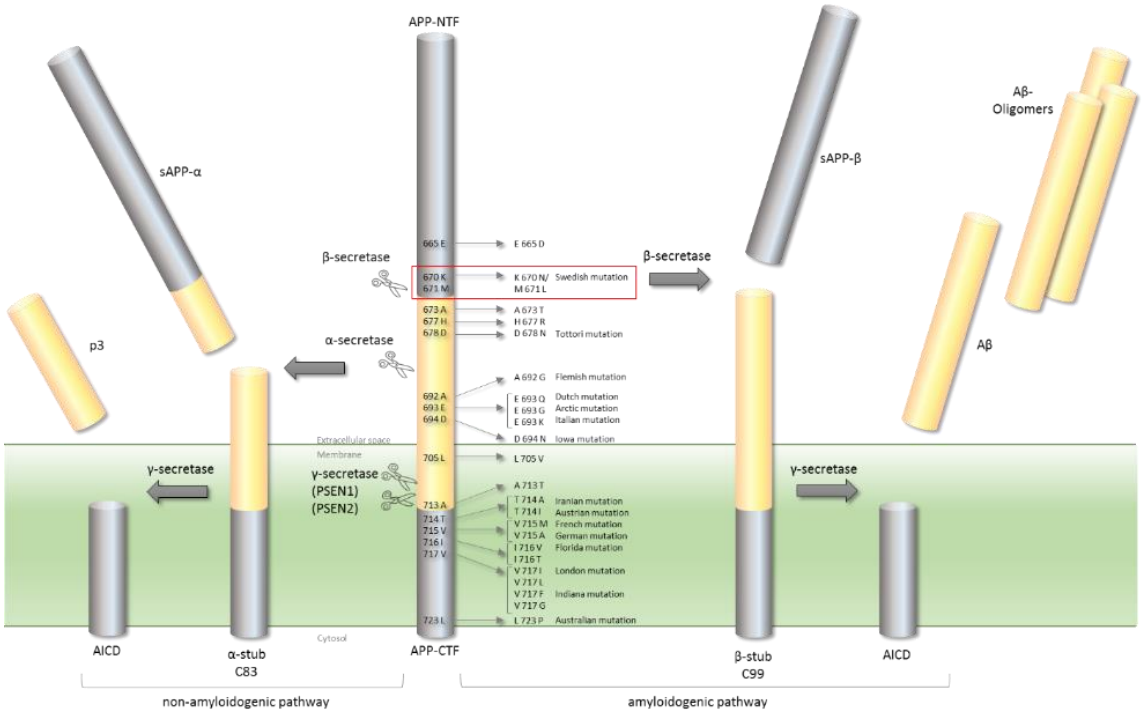

Figure 1.4: Processing of the amyloid precursor protein by the non-amyloidogenic and amyloidogenic pathway.
The amyloid precursor protein (APP), a type-I transmembrane protein, is processed by two different major pathways. Processing by the non-amyloidogenic pathway involves cleavage by α-secretase, producing a membrane-residing 83aa α-stub and soluble APP-α (sAPP-α). Subsequent cleavage by γ-secretase results in an APP intracellular domain (AICD) and a smaller extracellular fragment (p3). The amyloidogenic pathway starts by β-secretase cleavage, leading to a membrane-residing 99aa β-stub, and soluble APP-β (sAPP-β). Subsequently the β-stub is cleaved by γ-secretase, producing AICD and amyloid-β (Aβ). Aβ forms dimers, oligomers and finally fibrils, leading to the generation of amyloid plaques.
Important APP mutations and cleavage sites of the major processing enzymes are indicated. The Swedish mutation (*APPswe*) is highlighted by a red box.
N-terminal fragment (NTF), C-terminal fragment (CTF).
Illustration modified after: Van Dam and De Deyn (2006)

1.1.4.1 ADAM 10

Although several disintegrin and metalloproteases (ADAM9, ADAM10 and ADAM17) have been proposed to poses α-secretory activity, ADAM10 seems to be the principle α-secretase involved in cleavage of APP in neurons (Asai *et al.* 2003, Kuhn *et al.* 2010). α-secretory APP processing occurs mostly on the cell surface of the plasma membrane and represents the first enzymatic step in the non-amyloidogenic pathway (Parvathy *et al.* 1999). This cleavage step takes place within the Aβ peptide domain (Esch *et al.* 1990, Sisodia *et al.* 1990). This first step creates two peptides, the soluble

amyloid precursor peptide-α (sAPP-α) and the C-terminal 83aa long α-stub (α-stub, C83) integrated in the membrane. This α-stub is further processed by γ-secretase. However, as the cleavage site of ADAM10 is inside the Aβ sequence, the subsequent action of γ-secretase does not lead to the release of Aβ monomers from an ADAM10 cut α-stub. Instead a smaller N-terminal peptide (p3) and the APP intracellular domain (AICD) are released (Haass *et al.* 1993b, Lichtenthaler and Haass 2004) (Figure 1.4).

1.1.4.2 BACE1

BACE1, described first by Hussain *et al.* (1999), is accepted to be the only enzyme with β-secretase activity (Cai *et al.* 2001, Roberds *et al.* 2001). Under native conditions BACE1 is active as a homodimer (Westmeyer *et al.* 2004) with an acidic pH optimum, rendering compartments of the secretory pathway such as endosomes, but also the trans-Golgi-network (TGN) the preferred environment for APP processing via BACE1 (Kinoshita *et al.* 2003, Rajendran *et al.* 2006, Cole and Vassar 2007). On the N-terminal site of APP, BACE1 truncates the precursor protein after the Asp^{+1} residue, producing the transmembranous 99aa long C-terminal beta-stub (β-stub, C99) and the soluble amyloid precursor peptide-beta (sAPP-β) (Roher *et al.* 1993, Cole and Vassar 2007). As it was already stated for α-secretase, the C-terminal fragment (CTF) is substrate for further degradation via γ-secretase, which leads to the release of Aβ monomers (Figure 1.4).

1.1.4.3 γ-secretase

γ-secretase is not a simple enzyme, but rather an aspartyl protease complex with four major components assembled in the ER and transported to the plasma membrane (Capell *et al.* 2005). Nicastrin (NCT) is thought to interact with the amino-terminal stubs of previously cleaved transmembrane proteins, anterior pharynx defective 1 (APH-1) is needed for the formation of a pre-complex, which binds the catalytic components presenilin 1 and 2 (PS1 and PS2), which are cleaved by presenilin enhancer 2 (PEN-2) entering the complex last. The cleaved forms of PS1 and PS2 are crucial for the γ-secretase activity (Edbauer *et al.* 2003, Takasugi *et al.* 2003, Bergmans and De Strooper 2010, De Strooper *et al.* 2012). APP proteolytic cleavage by γ-secretase is performed intramembranous by its presenilin component (Haass and Steiner 2002) and generally takes place after aa 40 or 42 (Figure 1.4). It is important to mention, that γ-secretase is found on the plasma membrane, where it completes APP processing by α-secretase, but also in endosomal compartments, where it metabolizes the BACE1 truncated form of APP (β-stub) (Fukumori *et al.* 2006). In case of prior processing by BACE1, γ-secretase cleavage mainly leads to the production of amyloid-β 40 (Aβ-40) and amyloid-β 42 (Aβ-42). In general, Aβ-40 comprises about 90% of the generated Aβ, in AD the ratio is shifted towards Aβ-42, which possesses higher self-affinity and agglomeration potential. Therefore in AD Aβ-42 rich plaques are created faster than in normal aging (Jarrett *et al.* 1993).

1.1.5 AD genetics – Risk factors for FAD

It might be obvious, that the major genetic risk factors known to cause FAD are alterations in the genes encoding for proteins or enzymes involved in APP (and TAU) processing. There are for example 32 *APP* (compare to Figure 1.4), 179 *PSEN1* (locus of PS1) and 14 *PSEN2* (locus of PS2) mutations known, which act autosomal dominant and result in early-onset, fully penetrant AD (O'Brien and Wong 2011). Additionally to these autosomal dominant mutations, there are certain susceptibility genes, which may add quantitatively to an individual's risk. The most important ones nowadays are *APOE*, *BIN1*, *CLU*, *ABCA7*, *CR1*, *PICALM*, *MS4A6A*, *CD33*, *MS4A4E* and *CD2A*. Interestingly, several of the AD associated genes are involved in lipid metabolism and transport (for a recent review see: Alagiakrishnan *et al.* (2012)).

Of these, *Apolipoprotein E* (*ApoE*) represents the most important susceptibility gene. The gene encoding for ApoE has three different alleles, namely two, three and four (Mahley 1988, Weisgraber 1994) The epsilon 2 and epsilon 3 allele are thought to be protective concerning the risk for AD, the epsilon 4 allele is disease promoting (DeMattos *et al.* 2001, DeMattos 2004, Bosco *et al.* 2005, Morris *et al.* 2010). There is also a dosage effect, which can be recognized between hetero- and homozygous carriers of the epsilon 4 allele, which means a 3-fold or 4-13 times higher risk to develop AD and a 90% to almost 100% chance to develop AD at an age above 80 years, respectively (Corder *et al.* 1993, Strittmatter *et al.* 1993, Greenberg *et al.* 1995, Raber *et al.* 2004). ApoE occurs in high density lipoprotein (HDL) particles and is responsible for the transfer of cholesterol from the astroglial to the neuronal compartment, which might be altered in connection with ApoE4 allele frequency and AD pathology (Mahley 1988, DeMattos *et al.* 2001, Anstey *et al.* 2008, Bandaru *et al.* 2009) Furthermore, ApoE interacts directly with Aβ, thus reduces its amount in the circulation, preventing its accumulation and promoting its clearance by the microglial lysosomal pathway. This effect seems to be reduced in ApoE4 carriers, as it is thought to depend on ApoE lipidation status (DeMattos 2004, Jiang *et al.* 2008, Jones *et al.* 2010).

1.2 Sphingolipid metabolism

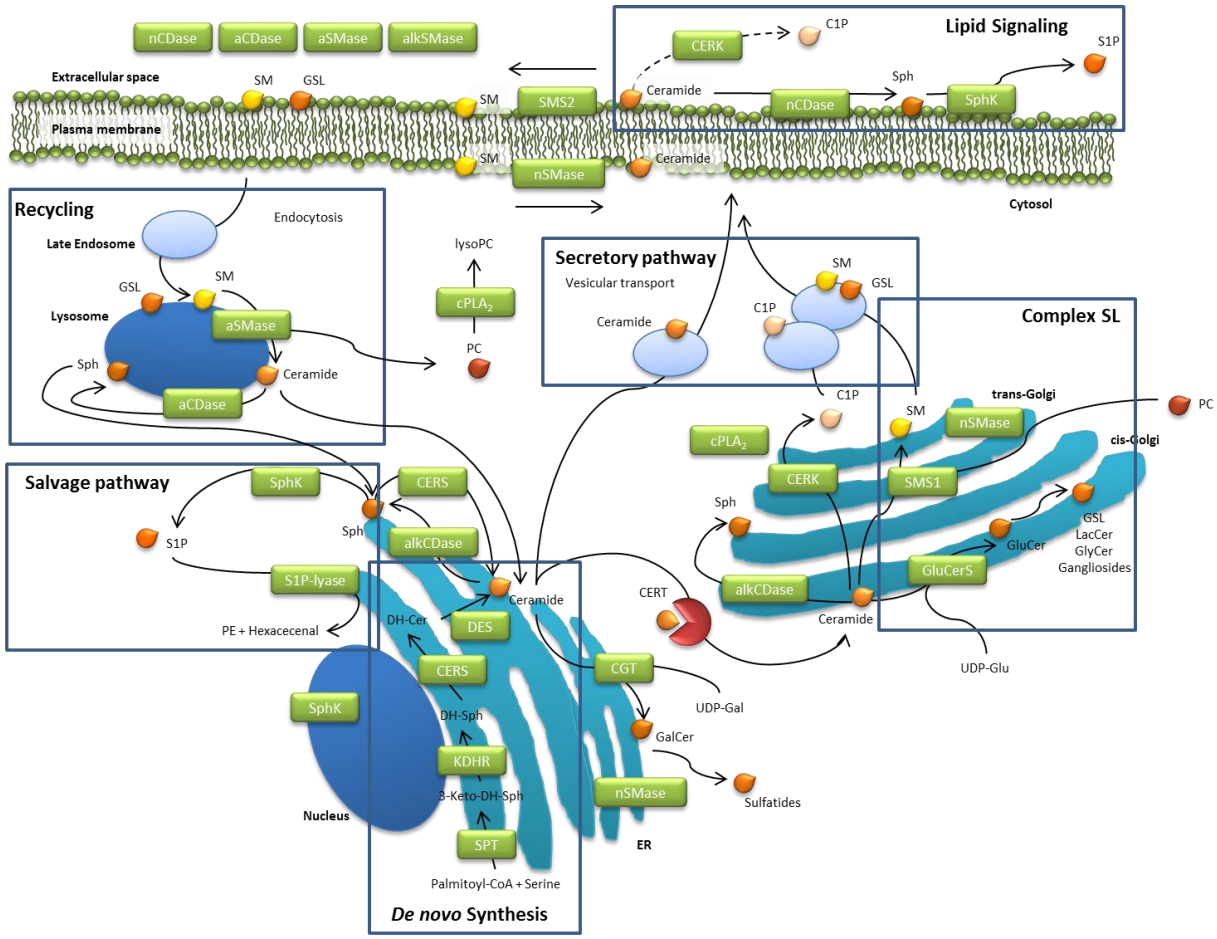

Figure 1.5: Cellular location of enzymes of the anabolic and catabolic sphingolipid pathway.
De novo synthesis of ceramide form palmitoyl-CoA and serine takes place in the ER and involves several enzymatic steps. SPT represents the first and rate limiting enzyme for ceramide *de novo* synthesis. CERT is responsible for the transport of ceramide to the Golgi apparatus, where more complex SL, such as SM or GSL are generated. These are delivered to the plasma membrane by vesicular transport and are incorporated in the lipid bilayer. In the plasma membrane lipids serve as structural components and are involved in lipid signaling. Recycling of SL occurs by the lysosomal pathway, and enzymatic degradation. Lipids are further degraded by the salvage pathway, delivering essential components back to the ER, where they can be used for synthesis of new lipid species.
Endoplasmatic reticulum (ER), ceramide transfer protein (CERT), serine palmitoyl transferase (SPT), 3-keto-dihydro-sphingosine reductase (KDHR), ceramide synthase (CERS), desaturase (DES), ceramide galactosyltransferase (CGT), acidic sphingomyelinase (aSMase), alkaline sphingomyelinase (alkSMase), neutral sphingomyelinase (nSMase), acidic ceramidase (aCDase), alkaline ceramidase (alkCDase), neutral ceramidase (nCDase), glucosylceramide-synthase (GluCerS), sphingomyelin synthase (SMS), ceramide kinase (CERK), cytosolic phospholipase A2 (cPLA2), sphingosine kinase (SphK), sphingosine-1-phosphatlyase (S1P-lyase).

1.2.1 Anabolic pathway

1.2.1.1 De novo Synthesis of Ceramide

De novo synthesis of ceramide (Cer) starts in the ER. Here, as the first and rate limiting step, serine-palmitoyl transferase (SPT) catalyzes the condensation of serine and palmitoyl-CoA for the production of 3-keto-dihydro-sphingosine, which is rapidly reduced via 3-keto-dihydro-sphingosine reductase to dihydro-sphingosine (Mandon *et al.* 1992, Beeler *et al.* 1998, Hanada 2003, Kihara and Igarashi 2004) (Figure 1.5). The next step is carried out by six different ceramide synthases (CerS1-6). Each of them has distinct preferences for different FA acyl-CoA, which they use, together with

dihydro-sphingosine to synthesize different dihydro-Cer species (Venkataraman *et al.* 2002, Riebeling *et al.* 2003, Mizutani *et al.* 2005, 2006, Laviad *et al.* 2008, Mizutani *et al.* 2008). These CerS do not only differ in affinity to their substrates, but also in tissue specific expression pattern, which makes it likely, that the precise dihydro-Cer set created per tissue takes over distinct tasks (Laviad *et al.* 2008, Mullen *et al.* 2012). As dihydro-Cer is desaturated by dihydro-Cer desaturase to Cer, this variety of dihydro-Cer species is also reflected in the Cer profile (Geeraert *et al.* 1997) (Figure 1.5).

1.2.1.2 Transport of Ceramide for further processing

As all these basic steps take place in the ER, Cer needs to be transported to the site of further processing. Delivery of Cer to the Golgi apparatus, is either conducted by the cytosolic ceramide transfer protein (CERT) (Hanada *et al.* 2007), or by vesicular transport (Giussani *et al.* 2008). CERT shuttles between ER and Golgi to supply the enzymes of the more complex sphingolipid (SL) pathway with their substrates (Figure 1.5). Interestingly, CERT possesses a serine repeat-motive, which gets phosphorylated to down regulate transport activity. This phosphorylation state is controlled by the amount of sphingomyelin (SM) and cholesterol (Chol), depletion of which is leading to dephosphorylation and activation of CERT to ensure the supply for their own synthesis (Kumagai *et al.* 2007). CERT was found to have a certain substrate specificity and a bias for Cer species, with a higher affinity to those, carrying acyl chains less than 22 carbons in length (Kumagai *et al.* 2005).

1.2.1.3 Complex Sphingolipids, Ceramide-1-Phosphate and their synthesizing enzymes

Cer represents the basic structure for the more complex SL, such as the following hexosylceramides.

When Cer reaches the cis-Golgi there are several processing pathways (Figure 1.5). One possibility is the turnover into glucosylceramide by glucosylceramide-synthase with the use of UDP-glucose (Jeckel *et al.* 1990, Futerman and Pagano 1991, Jeckel *et al.* 1992). Glucosylceramide is a very essential SL, as it serves as a precursor for most glycosphingolipids (GSL). Total loss of glucosylceramide-synthase results in embryonic lethality starting at E7.5 with complete resorption of embryonic tissue at E9.5 (Yamashita *et al.* 1999), while neuronal loss leads to severe postnatal defects including cerebellar dysfunction, reduced axon branching of Purkinje cells and myelination deficiency resulting in premature death at postnatal days 22-24 (Jennemann *et al.* 2005, Yamashita *et al.* 2005).

Cer-galactosyltransferase (Stahl *et al.* 1994) resides in the ER and can utilize *de novo*-synthesized Cer directly, together with UDP-galactose to generate galactosylceramide on the ER lumen. Cer-galactosyltransferase has a very distinct tissue expression pattern and affects oligodendrocyte function, myelination, nerve conduction and motor abilities, but also fertility, growth and survival rates, as it was shown in Cer-galactosyltransferase knockout mice (Coetzee *et al.* 1996, Fujimoto *et al.* 2000, Zoller *et al.* 2005). However, galactosylceramide is also the precursor of sulfatides, which are generated through the action of galactosylceramide-sulfotransferase (Figure 1.5). Sulfatides are also important for brain function, as major myelination defects were reported in galactosylceramide-

sulfotransferase deficient mice, which are thought to result from reduced myelin maintenance (Marcus *et al.* 2006).

Another essential SL is SM. SM is the most abundant complex SL and accumulates in the outer leaflet of the plasma membrane (Andrieu-Abadie and Levade 2002, Tafesse *et al.* 2007). Like glucosylceramide it is synthesized mostly in the Golgi apparatus. Additionally SM can be produced at the plasma membrane. At both sites, sphingomyelin synthases (SMSs) are responsible for the catalytic step, generating SM and diacylglycerol (DAG) from phosphatidylcholine (PC) or phosphatidylethanolamine (PE) and Cer (Huitema *et al.* 2004). For further information see 1.4. While Cer derives from the ER as described above, *de novo* synthesis of PC and PE takes place by the so called Kennedy pathway. This pathway is split in two branches. The first starts from choline, involves the formation of phosphocholine, the turnover in CDP-choline with the use of CTP and finally the production of PC by DAG : CDP-choline cholinephosphotransferase utilizing DAG or alkyl-acylglycerol as lipid anchor. The second branch includes similar steps starting from ethanolamine (Gibellini and Smith 2010).

If Cer is not transformed into complex SL, it can also be phosphorylated by ceramide kinase (CERK) in the trans-Golgi to form ceramide-1-phosphate (C-1-P; Figure 1.5 (Sugiura *et al.* 2002, Boath *et al.* 2008)). Knockout experiments on *Cerk*$^{-/-}$ and *CerkL*$^{-/-}$ mice suggest CERK to be the only enzyme for C-1-P synthesis in the rodent brain and retina (Mitsutake *et al.* 2007, Graf *et al.* 2008).

1.2.2 Catabolic pathways

1.2.2.1 Sphingomyelinases

Cer is not only produced through the anabolic pathway by metabolizing serine and palmitoyl-CoA, but also by the degradation process of SM into PC and Cer. SM breakdown can be catalyzed by several enzymes of the sphingomyelinase (SMase) family, which are classified into three different subgroups, according to their optimum pH

Neutral SMase (nSMase) is encoded by *SMPD2, SMPD3 and SMPD4* (Clarke *et al.* 2006). Whether the *SMPD2* encoded enzyme nSMase1 really functions as a SMase is questioned (Sawai *et al.* 1999, Zumbansen and Stoffel 2002). The best characterized nSMase is nSMase2 (encoded by *SMPD3*), which is a membrane anchored protein (Tani and Hannun 2007a). In small amounts it is found at the Golgi apparatus, while most of it localizes to the plasma membrane (Figure 1.5), where it resides in the inner leaflet (Marchesini *et al.* 2004, Tani and Hannun 2007a, b). nSMase3, encoded by the *SMPD4* gene, is a TM protein predominantly found in skeletal and cardiac muscle where it localizes to the ER (and Golgi apparatus) (Krut *et al.* 2006, Corcoran *et al.* 2008). Here again, it is still under investigation how an ER localized SMase can affect SM levels, which are highest in Golgi and the plasma membrane.

Acid SMase (aSMase) is encoded by the *SMPD1* gene. Illnesses connected to aSMase dysfunction (or *SMPD1* disruption) include Niemann Pick Disease A and B (NPD-A, NPD-B). NPD-A includes pro-

gressive neurodegenerative disease accompanied by psychomotor retardation, hepatosplenomegaly, lung disease, red spots in the retina and premature death. NPD-B is less severe, but nevertheless provokes hepatosplenomegaly and lung disease (Horinouchi *et al.* 1995, Marathe *et al.* 2000, Schuchman 2007). aSMase, as the name reveals, has an acidic pH optimum and is mainly located in lysosomal compartments, responsible for the metabolism of endosomal SM (Reviewed by: Jenkins *et al.* 2009). Despite the lysosomal SM depots, aSMase is also able to degrade plasma SM, after it was secreted to extracellular space, where it is referred to as secretory SMase (sSMase; Figure 1.5) (Schissel *et al.* 1996, Jenkins *et al.* 2009).

Alkaline SMase (alkSMase) is a member of the ecto-nucleotide phosphodiesterase family. It preferentially cleaves phosphocholine but not choline for lyso-phosphatidylcholine species (Duan *et al.* 2003a). The ectoenzyme has an optimal pH at 8.5 and is responsible for the digestion of dietary SM in the liver and the intestines (Duan *et al.* 2003a, Duan *et al.* 2003b).

1.2.2.2 Ceramidases

With the breakdown of complex SL into Cer, a central crossing point in SL metabolism is reached. Cer can serve as backbone for anabolic reactions, but it can also be further degraded. One of these catabolic pathways is the turnover of Cer into sphingosine and S-1-P. The first of these two reactions is carried out by a family of ceramidases, which deacetylate Cer to form sphingosine. Similar to SMases, the ceramidases are classified according to their optimal pH.

Neutral Ceramidase (nCDase, encoded by *ASAH2* gene) has its pH optimum between 7 and 9. nCDase with its ubiquitously expression is mainly responsible for the digestion of dietary Cer and therefore mostly expressed in intestinal tissues but is also highly expressed in heart, skeletal muscles, kidney and liver (El Bawab *et al.* 2000, Tani *et al.* 2000, Kono *et al.* 2006). nCDase is produced as a TM protein and resides at the plasma membrane and in intracellular compartments such as the mitochondrion but is also peripherally associated with the outer leaflet of the plasma membrane (El Bawab *et al.* 2000, Tani *et al.* 2003, Kono *et al.* 2006)(Figure 1.5).

Depending on the pH acid Ceramidase (aCDase, encoded by *ASAH1* gene) is capable of hydrolysis (pH 4.5) and Cer synthesis (pH 5.5). Low pH is achieved, when the ceramidase reaches the lysosomal compartment. (Koch *et al.* 1996, Okino *et al.* 2003). Similar to nCDase, a small portion of aCDase is secreted to extracellular space (Bernardo *et al.* 1995) (Figure 1.5). Deficiencies in *ASAH1* are correlated to Faber disease, resulting from Cer accumulations. Patients suffering from this LSD show symptoms like arthritis, swollen lymph nodes, psychomotor difficulties and vocal cord pathology. *Asah*$^{-/-}$ mice, are not viable, while *Asah*$^{+/-}$ show signs of LSD (Li *et al.* 2002).

The third group of ceramidases are the alkaline Ceramidases (ACERs), which are made up of three different members, residing in the ER-Golgi network with an optimal pH between 8.0 and 9.5 (Mao *et al.* 2001, Mao *et al.* 2003, Xu *et al.* 2006). ACER1, encoded by *ASAH3* is expressed in the ER. Im-

portantly, ACER1 is the Ceramidase mainly expressed in epidermis. It is supposed that the high substrate specificity of ACER1 towards C24:0 and C24:1 Cer and its exclusion of dihydro-Cer and phytoceramides explains the enrichment of these Cer species in the skin (Mao *et al.* 2003, Sun *et al.* 2008). *ASAH3L* encodes for ACER2. This Ceramidase localizes to the Golgi apparatus and is less substrate specific then ACER1, as it also metabolizes C16, C18 and C20 Cer, as well as LC dihydro-Cer and unsaturated phytoceramides (Mao and Obeid 2008, Gault *et al.* 2010). ACER3 (encoded by *PHCA* gene) is expressed rather ubiquitously with high levels in placenta and localizes to both, ER and Golgi apparatus (Mao *et al.* 2001, Mao and Obeid 2008). It is the Ceramidase responsible for the turnover of phytoceramide, dihydro-Cer and Cer carrying an unsaturated fatty acid (FA) residue with 20 or less carbons (Mao *et al.* 2001, Gault *et al.* 2010).

1.3 AD and lipids

1.3.1 How do lipids influence AD associated proteins?

1.3.1.1 Lipid rafts

But why might lipids be important for the development and progression of AD?

One important aspect of the amyloid-pathway, as mentioned before, is the fact, that the processing of APP takes place at cellular membranes (Parvathy *et al.* 1999, Haass and Steiner 2002, Westmeyer *et al.* 2004, Lichtenthaler *et al.* 2011). All involved proteins are membrane-associated proteins and are therefore tightly affected by membrane conditions, such as fluidity, which is regulated by so called "lipid rafts". Lipid rafts are small domains of about 10-200nm (Pike 2006).They are heterogeneous, highly dynamic and represent a more viscous liquid-ordered condition of the plasma membrane, which can form greater platforms by influencing and being influenced by protein-protein and protein-lipid interaction (Lingwood and Simons 2010). The major lipids found in raft-like structures are cholesterol (Chol) and SL (Simons and Ikonen 1997, Simons and Vaz 2004, Pike 2006). The sterol ring of Chol favors the interaction with more rigid saturated than with more bulky unsaturated SL, contributing to the less fluid, viscous character of lipid rafts (Lingwood and Simons 2010).

It is important to notice, that the different secretases have preferred lipid environments, regulating the accessibility of APP to its cleavage enzymes. APP itself is thought to have two pools in- and outside raft-like structures (Parkin *et al.* 1999, Ehehalt *et al.* 2003). ADAM10 however, is found primarily in non-raft areas (Harris *et al.* 2009), while the γ-secretase complex (Hur *et al.* 2008) and BACE1 in their activated forms reside in raft-like structures (Ehehalt *et al.* 2003, Kalvodova *et al.* 2005), making lipid rafts the subcellular site of amyloidogenic processing of APP and Aβ generation (Rushworth and Hooper 2010, Williamson and Sutherland 2011, Hicks *et al.* 2012)(Figure 1.6). Changing the lipid composition of the plasma membrane would therefore lead to an attraction or repulsion of amyloidogenic or non-amyloidogenic enzymes and APP. This was shown e.g. by Simons *et al.* (1998) and Marquer *et al.* (2011), with the depletion of Chol from hippocampal neurons, or by

FILM-FRET technique, which showed that Chol levels positively influence APP relocalization to raft domains, thereby influencing Aβ generation or by Kojro *et al.* (2001), who reported a stimulatory effect of reduced Chol on ADAM10 activity, without affecting expression rates, thereby promoting the non-amyloidogenic pathway.

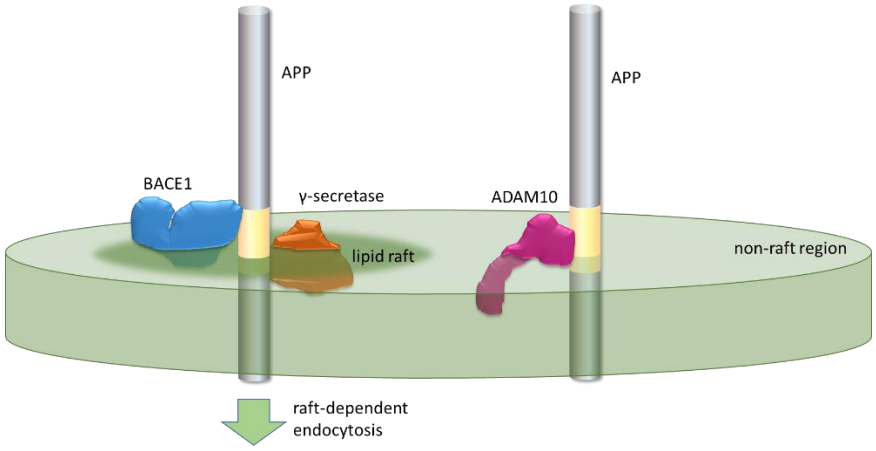

Figure 1.6: Localization of amyloid precursor protein and its processing enzymes within the membrane.
It is discussed that APP exists in two different pools inside and outside of lipid rafts. BACE1 and γ-secretase in their active forms are thought to reside inside lipid-rafts. Raft-dependent endocytosis promotes amyloid generation. ADAM10 on the other hand is found mainly outside of lipid-rafts, enhancing the non-amyloidogenic processing in the lipid unordered phase.
Amyloid precursor protein (APP), beta site APP cleavage enzyme 1 (BACE1), disintegrin and metalloproteinase domain-containing protein 10 (ADAM10).

In normal aging, the amount of Chol and SM in the cellular membrane increases, however AD patients and AD animal models (APP/PS1) show accelerated aging of rafts-like domains, which was partially attributed to faster and earlier increase in typical raft-associated lipids such as SM. Furthermore, the saturation state of FAs is shifted from omega-6 (n-6) and omega-3 (n-3) long chain polyunsaturated fatty acids (LC-PUFAs) towards saturated fatty acids (SFA), contributing to larger viscous raft-like areas. These alterations might lead to enhanced amyloidogenic processing and plaque formation (Diaz *et al.* 2012, Fabelo *et al.* 2012, Diaz *et al.* 2014, Fabelo *et al.* 2014).

On the other hand, it is also known that APP derivates influence the composition of lipid membranes. Aβ enhances phase separation of lipids via the interaction between Aβ and ganglioside GM1 (GM1) as well as triggering the uptake of raft components in the cell during the aggregation process of Aβ (Sasahara *et al.* 2013), or by regulating synthesis of important raft lipids such as SM and Chol (Grimm *et al.* 2005). AICD e.g. was found to be regulating the activity of SPT via expression regulation of its SPTLC2 subunit. In FAD and SAD cases, the generation of the SPTLC2 subunit was increased, due to the lack of a functional AICD (Grimm *et al.* 2011b). As outlined before, SPT represents the rate limiting step in sphingolipid *de novo* synthesis. Therefore, this enzyme is especially involved in the generation and metabolism of ceramide, sphingosine, sphingomyelin and glycosphingolipids (Hannun *et al.* 2001).

1.3.1.2 Endocytosis and Autophagy

Lipid rafts also represent the major sites of endocytosis (Sharma *et al.* 2002). Not only does Aβ-42 activate the endocytotic process, a proposed mechanism of clearance of fibrils (Nuutinen *et al.* 2007), but an enhanced endocytotic process also triggers the formation of Aβ, leading to a vicious circle (Ehehalt *et al.* 2003, Rajendran *et al.* 2006, Grimm *et al.* 2012, Tam *et al.* 2014). Lee *et al.* (2014) recently showed that aSMase reduction in APP/PS1/ASM$^{+/-}$ animals ameliorated autophagic defects - linked to higher aSMase activity, detected in plasma and fibroblasts of AD patients - reduced Aβ levels and improved memory performance. A higher autophagic rate might therefore account for a lysosome/autophagosome-mediated degradation of the neurotoxic peptide by the major acidic aspartyl protease CatD (McDermott and Gibson 1996)

1.3.1.3 Direct interaction

Direct interaction between lipids and proteins is another way how lipids influence the amyloid pathway.

As stated before Kojro *et al.* (2001) reported a stimulatory effect of Chol reduction on ADAM10 activity, but also BACE1's proteolytic activity can be stimulated by neutral glycosphingolipids (cerebrosides), anionic glycerosphingolipids (potentially due to PE) and sterols (Chol) (Kalvodova *et al.* 2005). Additionally BACE1 is stabilized in a ceramide rich environment, which promotes the processing of APP to Aβ, without affecting γ-secretase activity (Puglielli *et al.* 2003a).

γ-secretase activity also depends on its lipid environment, such as on Chol, which has a stimulating effect (Wahrle *et al.* 2002). Even more, it could be shown that proteoliposomes containing SL led to enhanced γ-secretase activity, while the addition of phosphatidylinositol reduced the enzyme activity compared to PC-only proteoliposomes. The major effect again, could be seen with the addition of Chol, which increased activity and cleavage of APP and Notch-like substrates in a bell-shaped dose dependent manner (Osenkowski *et al.* 2008).

1.3.2 Observed lipid alterations in AD patients

In AD patients several lipids have been found to be altered in comparison to normal controls. These include amongst others SM, Chol, ceramides, PL and plasmalogens but also sulfatide, sphingosine, galactoceramides, sphingosine-1-phosphate and gangliosides (Grimm *et al.* 2012). A more detailed view on SM and several lipids closely connected to SM synthesis is given below.

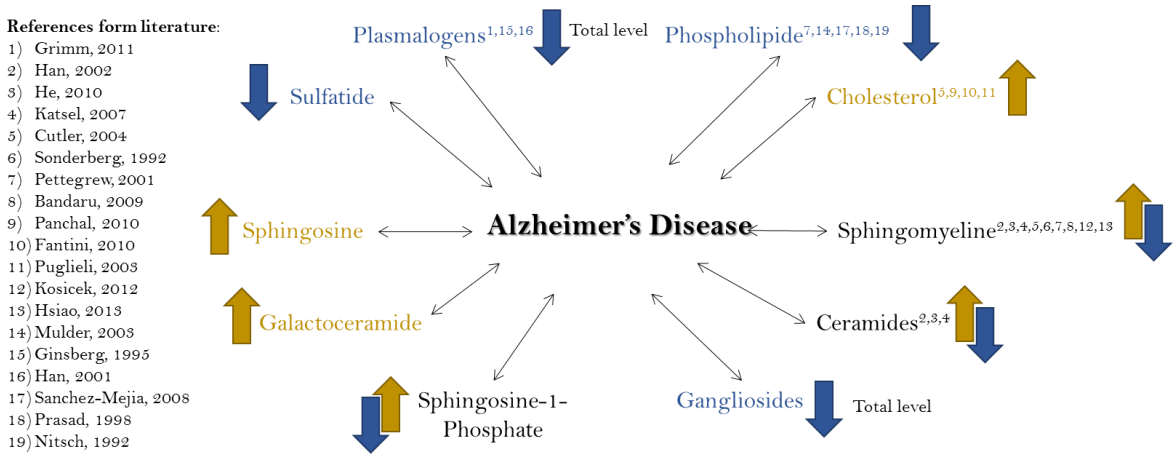

Figure 1.7: Overview on important lipid alterations observed in AD patients
Higher levels are indicated in orange and reduced levels are indicated in blue. Modified after (Grimm *et al.* 2012).

1.3.2.1 Ceramide

Most studies reported elevated ceramide levels in gray and white matter of AD patients or AD mouse models (Han *et al.* 2002, Cutler *et al.* 2004, Katsel *et al.* 2007, Bandaru *et al.* 2009, He *et al.* 2010, Mielke *et al.* 2010). He *et al.* (2010) showed that aSMase, one of the enzymes responsible for the breakdown of SM to ceramide was more active in AD frontotemporal gray matter compared to controls. The higher activity was leading to higher ceramide levels, while the amount of SM was reduced. Furthermore, activity of this enzyme was positively associated with pTAU and Aβ in this region (He *et al.* 2010). It was also stated, that there is a more pronounced ceramide elevation in early, very mild stages of AD, while levels seem to drop in more severe stages (Han *et al.* 2002) Additionally, specific species such as the C24:0 ceramides and especially galactosylceramides were highly increased, while C24:0 SM levels were lower in AD compared to normal controls (Cutler *et al.* 2004). Consistently, LC-ceramide controlling enzymes were upregulated (Katsel *et al.* 2007), pointing out, that certain lipid species might play a more significant role than others. MCI patients, possess lower overall levels of saturated ceramides compared to normal controls and AD patients, but also higher levels of very long-chain (VLC) plasma ceramides (C22:0 and C24:0). These were found to be predictive of cognitive decline and loss of hippocampal volume in progression of the disease (Mielke *et al.* 2010). Ceramide is able to move freely across the plasma membrane (Mitsutake and Igarashi 2007), therefore disturbances in ceramide homeostasis might lead to disruption of plasma membrane dynamics. The accumulation of ceramide might thus affect cellular transmembrane signal transduction (Stancevic and Kolesnick 2010), being one possible cause for the observed neuronal death in AD brains. Underlining that role, ceramide is known to cause neuronal cell death in culture and to be upregulated during neuronal apoptosis (Toman *et al.* 2002).

Correlations between Ceramide and Aβ or pTAU levels, were also shown by direct investigation. The addition of Aβ25-35 to cultured oligodendrocytes e.g. led to activation of nSMase and as consequence to accumulation of intracellular Ceramide, inducing death of oligodendrocytes (Lee *et al.* 2004). As a mechanism it was often proposed, that Aβ provokes oxidative stress, which leads to activation of SMase (Lee *et al.* 2004, for a summary see: Butterfield *et al.* 2007), but it could also be shown that Aβ directly acts on nSMase, resulting in higher enzymatic activity (Grimm *et al.* 2005). A similar effect could be observed in neurons, where oligomeric Aβ1-40 and Aβ1-42 led to increased nSMase and additionally aSMase activation, higher Ceramide levels and neuronal cell death (Malaplate-Armand *et al.* 2006, He *et al.* 2010). However, by inhibitor experiments Cutler *et al.* (2004) revealed Aβ-mediated accumulation of ceramide in cultured neurons to result rather from increased SPT activity, than due to stimulation of its degrading enzymes.

1.3.2.2 Sphingomyelin

Only one enzymatic step separates ceramide from SM. However, despite the consistent findings on ceramide, the alterations in SM levels detected in AD post-mortem brain tissue are not so straight forward (Soderberg *et al.* 1992, Pettegrew *et al.* 2001, Cutler *et al.* 2004, Bandaru *et al.* 2009, He *et al.* 2010).

It could be observed that higher SM levels correlated positively with the number of Aβ SPs, but not with NFTs (Pettegrew *et al.* 2001). Another study reported elevated gene expression levels of the major SM synthesizing enzyme, SMS1 in the hippocampus of AD brains. In addition inhibition of SMS1 activity resulted in dose and time dependent reduction in Aβ levels, without affecting APP expression or cell viability (Hsiao *et al.* 2013). Elevated SM levels were not only observed in brain tissue of AD patients, but also in cerebro-spinal fluid (CSF) of prodromal AD cases, although this elevation could not be seen between patient groups with mild and moderate AD compared to normal controls (Kosicek *et al.* 2012). Although, the gene expression for enzymes controlling SM and GSL turnover into ceramide was not found to be altered with age, *TMEM23* (*SMS1*) was slightly upregulated in correlation with Braak stages (Katsel *et al.* 2007). Bandaru *et al.* (2009) reported a region-specific increase of SM levels in AD patients identified as ApoE4 carriers.

In accordance with He *et al.* (2010) a study of Han *et al.* (2002), reports that SM levels could be neither correlated with the state of the disease, during AD progression, nor with AD patients at all, compared to normal controls.

An early study on lipid composition in AD brain regions stated reduced levels of SM in white matter and therefore also in regions with high myelin content such as hippocampus, pons and medulla oblongata (Soderberg *et al.* 1992).

1.3.2.3 Phospholipids – Phosphatidylcholine, phosphatidylethanolamine and plasmalogens

In parallel with elevated SM, reductions in PE and phosphatidylinositol were reported from AD brains (Pettegrew *et al.* 2001). Prasad *et al.* (1998) specifically reported decreased levels of AA-containing PL in AD, which was later on connected to an upregulation of cPLA2 (Sanchez-Mejia *et al.* 2008). In another study a decrease in PC, as well as in PE was described. Not only the PLs, but also their precursors, choline and ethanolamine were decreased, while PL deacylation was increased, as measured via the deacetlyation product glycerophosphocholine. These results point to an increased degradation of membrane PLs (Nitsch *et al.* 1992). Contradictory to the results described above, no difference in PC, linoleic acid or AA containing species was reported by Mulder *et al.* (2003). However, it was found that there is a lower lyso-PC/PC ratio in CSF of patients with AD. The researchers state that these findings reflect alterations in the processing of choline-containing phospholipids (PL) in AD brains (Mulder *et al.* 2003).

Whole plasmalogen content was found to be reduced in white matter of patients with mild AD. In gray matter, the decrease correlated with the disease progression, but did not affect cerebellar brain regions (Han *et al.* 2001). Ethanolamine plasmalogens being selectively reduced in areas of AD pathology, but not altered in non-affected brain structures was seen before (Ginsberg *et al.* 1995). This was more recently connected to a reduction in alkyl-dihydroxyacetonephosphate-synthase, which represents the rate-limiting step in the synthesis of plasmalogens, and enhanced ROS mediated oxidation of plasmalogens (Grimm *et al.* 2011c).

1.3.2.4 Cholesterol

Chol is one of the most important lipids concerning AD. As already mentioned earlier it plays a crucial role in lipid raft formation, maintenance and regulation, therefore modifying APP processing by its cleavage enzymes (compare 1.3.1.1). Additionally it acts directly as a regulating factor on APP processing enzymes.

Elevated Chol is also thought to be an early marker for AD (Pappolla *et al.* 2003). Free Chol levels in AD brains correlated positively with state of disease and are also elevated as a response to Aβ incubation of neurons *in vitro* (Cutler *et al.* 2004). The Chol levels are specifically increased around senile plaques (Panchal *et al.* 2010). (For more detailed information on the impact of Chol on AD progression see: Fantini and Yahi (2010) and Puglielli *et al.* (2003b)).

1.3.3 Effects of life-style on AD

Besides age and the described genetic risks, there is also evidence, that certain life-styles increase the risk of developing AD. Life-style factors influencing cognitive performance and mortality of AD patients include diet and stress, but also physical exercise (Williams 2015).

1.3.3.1 Diet and AD

There is a growing line of evidence, that diet and AD are strongly correlated. In this context antioxidant nutrients, such as Vitamin-E, fish, containing high amounts of monounsaturated fatty acids (MUFAs) and PUFAs, moderate alcohol consumption and B-vitamins are mentioned to have protective effects on the risk to develop age-related cognitive decline and AD, while nutrition promoting high blood Chol levels is thought to elevate AD risk (Solfrizzi *et al.* 2008, Morris 2009).

Saturated and unsaturated fats

In course of the Chicago Health and Aging Project (CHAP) it was reported that the intake of SFAs doubled the risk of developing AD, the consumption of trans-unsaturated fats was associated with a two to three times higher risk for AD, while participants of the study who consumed most n-6 PUFAs reduced their risk to develop AD by 70% (Morris *et al.* 2003a). With additional adjustment for the intake of FA linked to MUFA consumption the study revealed that increased intake of MUFAs also reduced AD risk by 80% (Morris *et al.* 2003a).

Other studies on the topic of fat consumption and AD risk were performed by Luchsinger *et al.* (2002) in New York and Kalmijn *et al.* (1997) in Rotterdam. Both studies could confirm the link between higher AD risk and total fat and saturated fat intake in a four and a two year trial, respectively. However, the study performed by Luchsinger et al. (2002) could not confirm the correlation between PUFA consumption and AD risk. Furthermore, it remains to mention that a follow up of the Rotterdam study after six years did not reveal any correlation of the mentioned dietary fats with AD (Kalmijn *et al.* 1997, Engelhart *et al.* 2002, Luchsinger *et al.* 2002).

These studies show, that due to study design a straight forward connection of the profitable effects of unsaturated FAs on cognitive performance is difficult to make, while evidence on the negative effects of saturated fats accumulates.

Omega-3 FAs

Within the unsaturated FAs, however, there are several candidates which are promising to have a positive influence on memory performance or risk for dementia. n-3 FAs as a type of PUFAs are important for brain development, especially docosahexaenoic acid (DHA) as the major n-3 FA in the brain was subject to several studies, linking it to prenatal brain development and maintenance of brain function (Salem *et al.* 1996, Lauritzen *et al.* 2001). There is also evidence, that n-3 enriched diet promotes learning and memory in rodents (Yamamoto *et al.* 1987, Jensen *et al.* 1996, Lim and Suzuki 2000). Additionally, aging implicates a reduction in n-3 FAs, which is associated with a reduction of neuronal membrane excitability, lower capacity of transmission in rodents and oxidative damage (Delion *et al.* 1996, McGahon *et al.* 1999).

Epidemiological studies suggest a protective effect of fish consumption, which supplies the body with the mentioned essential n-3 FAs (Kalmijn *et al.* 1997, Barberger-Gateau *et al.* 2002, Yamada *et al.* 2002, Kalmijn *et al.* 2004). These positive effects could also be seen in ApoE4 carriers, which implies the importance of nutrition even on a background with a genetic risk to develop AD (Barberger-Gateau *et al.* 2007).

For example the above mentioned CHAP and the Rotterdam study could show, that the consumption of at least one fish meal per week lowered the risk of AD by 60% or 70%, respectively, while the CHAP furthermore found the strongest correlation within the n-3 FAs for DHA intake. However, like already mentioned the six-year follow up of the Rotterdam study could not confirm the findings observed after two years (Kalmijn *et al.* 1997, Engelhart *et al.* 2002, Morris *et al.* 2003b, Morris *et al.* 2005).

The importance of DHA levels was also underlined by the Framingham Study, which observed dementia-free participants with an age of about 76 years over a period of 9 years. The results show that high levels of PC-DHA lowered the risk for developing dementia by 47% (Schaefer *et al.* 2006).

The Etude du Vieillisement Arteriel Study and the Three-City cohort study also confirmed to protective effect of n-3 FA on the development of dementia. They furthermore noticed, that a consumption of n-6 FAs lacking the balance with n-3 FAs has a negative effect, increasing the risk for dementia (for more detailed information see: Heude *et al.* (2003) and Barberger-Gateau *et al.* (2007)).

In a pilot study on middle-aged patients, performed in Portland, additionally to n-3 FA, alpha-lipoic acid was found to have beneficial effects on cognitive and functional decline, which were most effective if both substances were combined (Shinto *et al.* 2014).

Cholesterol

Whether Chol intake is associated with a higher risk to develop dementia is still under discussion. Contradictory results e.g. come from the Rotterdam study and its follow up study. While Kalmijn et al. 1997) found a positive correlation between AD risk and Chol intake this could not be confirmed later on (Kalmijn *et al.* 1997, Engelhart *et al.* 2002). A study on middle-aged subjects performed by the same research group as the original Rotterdam study could verify the findings of a positive correlation between dietary Chol consumption and a reduction of cognitive functions (Kalmijn *et al.* 2004), while another study evaluating food intake of people aged 65 and older did not find such a connection (Morris *et al.* 2003a). Evidence for a connection of high Chol intake and the development of AD-like pathology was found in an animal study on Chol fed rabbits, which showed intracellular amyloid beta accumulation, which was not found in rabbits fed with a control diet (Sparks *et al.* 1994). More recently Chol-fed rats showed similar results, with a degeneration of pyramidal cells of the CA1 region, thickening of blood vessels, astrogliosis and AD-like pathology (Abo El-Khair *et al.* 2014). Heverin *et al.* (2015) dedicated the effects of Chol on memory performance and development of patho-

logical hallmarks to 27-hydrocholesterol, which is able to pass the blood-brain-barrier (BBB) and was found to be a mediator of the observed effects.

1.3.3.2 Stress and AD

Additionally to diet, chronic stress is one important life-style factor, which is set into focus of the field of neurological research. Chronic restraint stress was found to have a negative effect on learning and memory performance in mice. The declining performance in the Morris water maze in this study was thought to be connected to enhanced ER stress in the frontal cortex and the hippocampus (Huang *et al.* 2015). Machado et al. (2014) summarized recently the effects of chronic stress on the different mechanism thought to be involved in AD and additionally referred to some of the epidemiologic studies performed on this topic (Machado *et al.* 2014). Importantly it was also found that chronic stress affects the lipid homeostasis of the brain. Mice treated with the chronic unpredictable stress paradigm showed profound alterations in the PL and SL metabolism, with an increase in ceramide and a decrease in SM and dihydro-SM, furthermore a decrease in PE and acyl-ethyl-PC (PCae) and an increase in lyso-PE were found. Lyso-PC was elevated in prefrontal cortex (PFC) and associated with blood corticosterone (CORT) levels (Oliveira *et al.* 2015).

1.3.3.3 Physical exercise and AD

In a society where desk work consumes a substantial amount of most people's daily time physical exercise, as a preventing measure against the development of several diseases, became an important topic of discussion. A cohort study using wrist actigraphy on cognitively normal elderly persons revealed that over 3.5 years a higher level of physical activity was associated with a lower risk for MCI and AD (Schlosser Covell *et al.* 2015). Additionally AD mortality in correlation with the level of exercise was investigated in participants of the National Runners' and Walkers' Health Studies. Results show that compared to participants, which run less than 1.07km/day an increase in activity correlated negatively with AD mortality, resulting in an up to 40.1% decreased risk for those who run more than 3.6km/day (Williams 2015). The evidence for a positive effect of physical activity on dementia is also underlined by animal studies. After 10 weeks of voluntary wheel running double transgenic *APPswe*/PS1ΔE9 mice showed not only a better performance in the Morris water maze, but also a decrease in Aβ, pTAU, astrogliosis and increased cellular proliferation in the hippocampus (Tapia-Rojas *et al.* 2015).

All in all, these results point out that a healthy life-style, including a diet with PUFAs (n-3 FAs), and low Chol, reduced chronic stress and increased exercise contributes to a reduced risk for the development of AD and AD mortality.

1.4 The sphingomyelin synthase family

SM species represent the most abundant complex SL in mammalian cells (Gault *et al.* 2010). SMSs belong to a family of phosphatidylcholine:ceramide cholinephosphotransferases and comprises three different enzymes including SMS1, SMS2 and sphingomyelin synthase related protein (SMSr) (Huitema *et al.* 2004, Tafesse *et al.* 2006). The SMS family members have six transmembrane domains (TMD), with their catalytic site oriented towards the Golgi lumen or the extracellular space (Tafesse *et al.* 2006, Villani *et al.* 2008). While SMS1 and SMS2 convert PC and ceramide to SM and DAG by transferring the phosphorylcholine moiety from PC to the primary hydroxyl of ceramide, SMSr has no SM synthase activity (Villani *et al.* 2008, Vacaru *et al.* 2009)

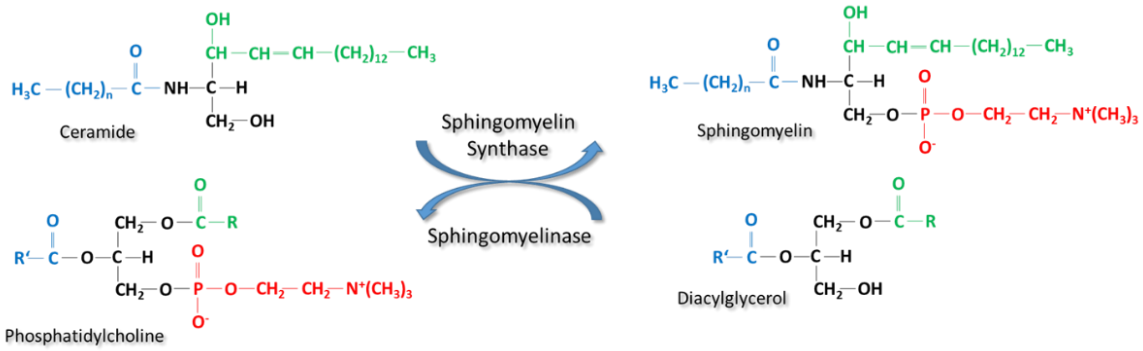

Figure 1.8: Sphingomyelin synthesis by sphingomyelin synthase.
Sphingomyelin (SM) is generated by enzymatic action of sphingomyelin synthases (SMS). The phosphatidyl head group of diacyl-phosphatidylcholine, acyl-ethyl-phosphatidylcholine (PC) or phosphatidylethanolamine (PE) species is transferred to the primary hydroxyl of ceramide due to ceramide cholinephosphotransferase activity of SMS. The enzymatic reaction leads to the production of SM, but also of diacylglycerol (DAG) known to act as a lipid signaling molecule. Two fatty acid resides on the choline-P donor are required to be recognized as a substrate. Sphingomyelinases are responsible for SM degradation. R=mostly poly-unsaturated FAs, R´= mostly saturated FAs.

1.4.1 Sphingomyelin synthase 1 and 2

SMS1 is located at the trans-Golgi apparatus and in small amounts at the plasma membrane, with the catalytic site facing either towards the Golgi lumen or the cell surface, while SMS2 is mainly located in the plasma membrane and just in small amounts present in the Golgi apparatus (Jeckel *et al.* 1990, Huitema *et al.* 2004, Yamaoka *et al.* 2004, Tafesse *et al.* 2007, Yeang *et al.* 2008). A study by Yeang *et al.* (2011) defined the domains in both SMSs , responsible for the subcellular targeting of SMS1 and SMS2. They found a Golgi retention or retrieval sequence between aa residues 332 and 410 of SMS1 and a complete loss of plasma membrane targeting of SMS2, when its most C-terminal 67aa were removed. Both enzymes are ubiquitously expressed (Huitema *et al.* 2004). Tafesse *et al.* (2007) also investigated SMS1 and SMS2 and found that SMS1 is responsible for the synthesis of the major bulk of SM (60-80%), while SMS2 is responsible for the generation of the remaining 40-20%. Both enzymes showed common substrate specificity towards ceramide, which delivers the backbone for SM production, PC serves as donor for the phosphatidyl head group. Besides PCaa, also PCae or PE could serve as head group donor (Ullman and Radin 1974, Voelker and Kennedy 1982, Tafesse *et*

al. 2006)(Figure 1.8). Depending on the quantity of the metabolites, SMS2 can also catalyze the *vice versa* reaction of SM synthesis and be responsible for its break down. This topic is more controversially discussed for SMS1, which is also proposed to use lyso-PC as a poor substrate for enzymatic turn over (Marggraf and Kanfer 1984, van Helvoort *et al.* 1994, Huitema *et al.* 2004, Ternes *et al.* 2009).

A tight regulation of SMSs represents an important mechanism. On the one hand important to balance amounts of SM and PC, in order to maintain the composition of the cell membrane, on the other hand SMSs also balance the production of the lipid mediator ceramide and DAG, which possess pro- or anti-apoptotic activity, respectively. (Hannun 1994, Geilen *et al.* 1997, Hannun *et al.* 2001, Claus *et al.* 2009). Therefore, SMS function and level of activity might be crucial for cell proliferation and viability (Tafesse *et al.* 2006, Tafesse *et al.* 2007, Van der Luit *et al.* 2007, Ding *et al.* 2008, Separovic *et al.* 2008, Shakor *et al.* 2011, Taniguchi and Okazaki 2014).

1.4.1.1 The human SMS1 gene

Human *SMS1* was formerly described as *medulla oblongata derived protein* (*MOB)* or *transmembrane protein 23* (*TMEM23)* and it was stated, that *MOB* is expressed in small amounts in almost every tissue, but that highest expression levels were found in the brain (Vladychenskaya *et al.* 2002, Huitema *et al.* 2004, Vladychenskaya *et al.* 2004). Rozhkova *et al.* (2011) characterized the *SMS1* gene, located on human chromosome 10, further and found several tissue specific splice variants, resulting from at least 5 different promoters, alternative splicing of the 24 exons, alternative polyadenylation and alternative termination of transcription. The different transcripts give rise to either the full length, 6-pass TMD protein or a truncated two-pass TMD protein (Rozhkova *et al.* 2011).

1.4.1.2 The mouse SMS1 gene

A 2364bp mouse cDNA was cloned and investigated on several levels. It was coding a 413-aa residue protein with 97% identity to the human SMS1. The mouse *Sms1* gene is localized on the reverse strand of chromosome 19, has a length of 266,987bp and at least 14 to 16 exons. Similar to the human form of *SMS1*, mouse *Sms1* undergoes alternative splicing (ensembl.org)(Yang *et al.* 2005). There are 14 splice variants known today out of which six are protein coding. Three of these encode the full length 419aa protein and one is known to encode a shorter 34aa single pass transmembrane protein. The two other splice variants (217aa and 222aa) are removed by nonsense mediated decay (ensembl.org). These results however, are not in total accordance to an earlier description of gene transcription and translation by Yang *et al.* (2005), who proposed two shorter two-pass TM proteins of SMS1 additionally to the full length protein (Figure 1.9).

1.4.1.3 SMS1 protein structure

SMS1 has a sterile alpha motif (SAM) domain, six TMDs and a phosphatidic acid phosphatase type 2/haloperoxidase (PAP2) domain. The six TMDs are α-helices connected by hydrophilic regions that from extra-membranous loops (Huitema *et al.* 2004)(Figure 1.9). SAM domains have a conserved

structure. They spread over 70 residues and exhibit a five helix bundle structure with two orthogonally packed alpha-hairpins. Functionally, SAM domains are involved in protein-protein interaction for homo- and heterodimer formation (Kim and Bowie 2003) as well as in DNA and RNA binding (Aviv *et al.* 2003). The PAP2 domain represents the catalytic site of the enzyme, facing the Golgi lumen or the cell surface. In general, it is responsible for the binding of phosphatidate and its dephosphorylation to obtain DAG and inorganic phosphate (Huitema *et al.* 2004, Carman and Han). The core structure of the PAP2 domain is also a five helical bundle. Out of these five helices, the third is responsible for the cofactor binding (Ishikawa *et al.* 2000).

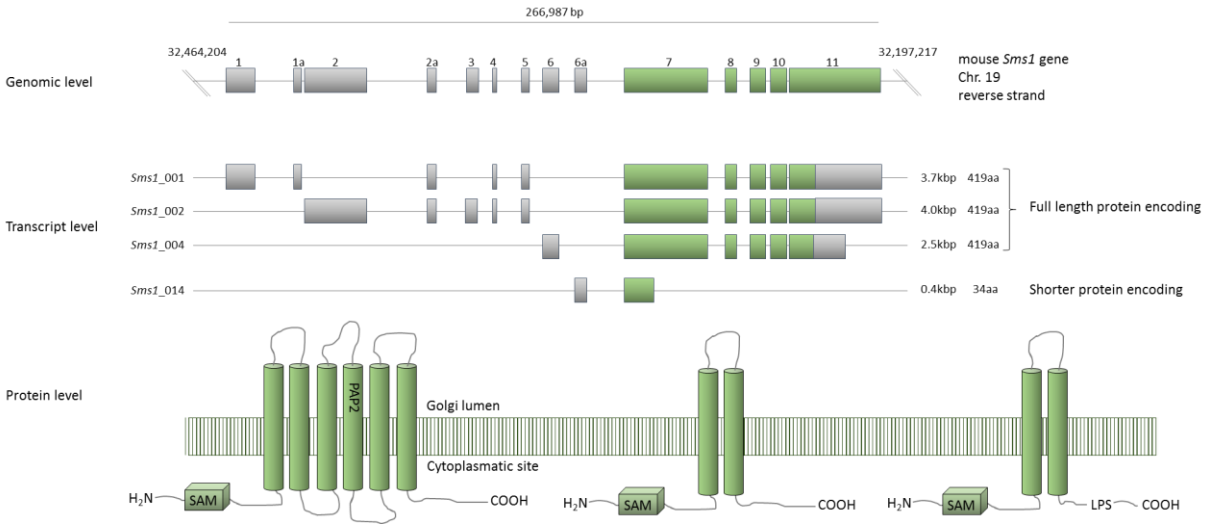

Figure 1.9: Sphingomyelin synthase 1 on genomic, transcriptional and protein level.

The mouse *Sms1* is located on the reverse strand of chromosome 19, is 266,987bp in lengths and 14 exons. Exon 1-6a are non-coding (gray boxes), while exon 7 contents the start codon and is the first of 5 coding exons (green boxes). On the transcript level there are 15 splice variants, of those 6 are protein-coding, two of them are degraded by NMD, three encode for the full length protein with 419aa. Additionally two shorter proteins are produced, differing only by three aas. The full length protein with enzymatic activity consists of six TMDs, while the other two protein variants have two TMDs. They differ from another by a tripeptide, which is found just in one variant mainly expressed in testes and heart. All protein variants contain a SAM domain, encoded by exon 7. Just the full length protein contains a PAP2 domain with the catalytic site, facing towards the Golgi lumen or the extracellular space.
Sterile alpha motif (SAM), phosphatidic acid phosphatase type 2 (PAP2) transmembrane domain (TMD).
Modified according to (Yang *et al.* 2005).

1.4.2 Sphingomyelin synthase related protein

SMSr resides in the ER (Vacaru *et al.* 2009) and, in human, has less than 22% sequence identity to SMS1 and SMS2 showing a distant relationship (Huitema *et al.* 2004). Instead of SM, SMSr synthesizes small amounts of the SMS analogue ceramide phosphoethanolamine (Vacaru *et al.* 2009). Nevertheless, blocking of SMSr leads to a substantial rise in ER ceramide and connected with it to a structural collapse of the early secretory pathway (Vacaru *et al.* 2009). SMSr expression on the other hand, is known to suppress ceramide-mediated cell death and to serve as suppressor or ceramide-induced mitochondrial apoptosis (Tafesse *et al.* 2014).

1.5 The Tg2576 or APP Swedish mouse - a common AD model

1.5.1 Genetic characteristics

The mouse model for AD we took advantage of, was the so called Tg2576 (MGI: 2385631) a common mouse model for AD. These mice bear a random insertion of the human *APP695* cDNA with the Swedish double mutation K670N/M671L (*APPswe*), which was found to be correlated with increased AD risk (Mullan *et al.* 1992). The transgene is expressed under the control of a hamster prion protein gene promoter (Hsiao *et al.* 1996). The cosmide vector was introduced into a C57Bl/6J x SJL host and the hybrid mice were backcrossed for two generations to C57Bl/6J. Investigations showed that h*APPswe* is found in brain, lung, heart, spleen, muscle and bone tissue of Tg2576 animals (Kawarabayashi *et al.* 2001). The mutation is positioned at the BACE1 cleavage site, which renders the h*APPswe* more prone to amyloidogenic cleavage, as the affinity of BACE1 to its substrate is increased (Tomasselli *et al.* 2003, Barman *et al.* 2011)(Figure 1.4).

1.5.2 Neuropathological characteristics

The neuropathological observations in Tg2576 mice include a 5.6-fold higher expression of the transgenic hAPP compared to endogenous APP, 5-fold higher Aβ1-40 and 14-fold higher Aβ1-42. (Hsiao *et al.* 1996).

This AD model develops AD pathology rather late. With 6-7 months SDS-insoluble forms of Aβ1-40 and Aβ1-42 appear. Between 6 and 10 months only few Aβ cores can be detected. In aged animals (12-23 months) neuritic plaques with amyloid cores, as well as diffuse plaques and overall higher Aβ levels increase to resemble levels found in AD patients (Kawarabayashi *et al.* 2001). The higher production of Aβ also leads to numerous Congo red positive cortical and limbic plaques. In the plaque area dystrophic neurites (Irizarry *et al.* 1997) and pTAU could be observed (Tomidokoro *et al.* 2001). Additionally, amyloid angiopathy and indications for increased oxidative stress were reported. However, even aged Tg2576 do not show neuronal loss or reduction in synaptic density in hippocampus or cortex, as it is seen in AD patients (Irizarry *et al.* 1997, Takeuchi *et al.* 2000), but signs of focal neuronal inflammation by activation of microglia and astrocytes (Frautschy *et al.* 1998, Gelissen *et al.* 1998, Benzing *et al.* 1999, Mehlhorn *et al.* 2000).

1.5.3 Behavior and life expectancy

Impairment of Y-maze spontaneous alterations at the age of 3-10 month was seen by Hsiao *et al.* (1996), together with a progressive impairment in the Morris water maze at 9-10 months. However, data on Morris water maze performance are not explicit, as studies report controversial results (Holcomb *et al.* 1998, Holcomb *et al.* 1999, King and Arendash 2002). A more recent study on behavioral performance of Tg2576, using a set of behavioral tasks, did not show widespread cognitive deficits even with 19 months of age (King and Arendash 2002). Memory deficits restricted to transgenic animals were revealed via Y-maze task only (King and Arendash 2002).

Tg2576 animals are known to have a reduced life span. Through the first 19 months of age they show a survival rate 63% with the most prominent loss of mutants during the first 6-12 months (King and Arendash 2002).

1.5.4 Lipid alterations

Lipidomic analysis in *APPswe* only mice revealed further alterations, such as minor reduction in total PCaa levels, while PCae and lyso-PCs are slightly elevated. Lyso-PCs with PUFAs however, are reduced in this AD mouse model (Grimm *et al.* 2011a). Mice with the *APPswe* and London mutation (APP^{SL}) show ceramide accumulation in the cerebral cortex (Grimm *et al.* 2005). Additionally, mice carrying human APP^{V71F} and *APPswe* possess decreased sulfatide levels in their brains (Cheng *et al.* 2010).

1.6 Sphingomyelin Synthase 1 knock out mice

Yano *et al.* (2011) created $Sms1^{-/-}$ mice, in which exon 2, yielding the ATG translation initiation codon, the SAM domain and two transmembrane regions was replaced by a neo cassette. The received chimeras were mated to C57Bl/6J. In this original description it is stated, that these animals showed moderate neonatal lethality, however, a later study by Lu *et al.* (2012) described these animals to appear normal. The original description additionally mentioned a reduction in body weight and loss of fat tissue mass. Deficiency in insulin secretion could also be shown. The animals suffered from oxidative stress, as mitochondria showed hyperpolarized membrane potential and high levels of reactive oxygen species, mediated by pancreatic ß-cell dysfunction.

Dong *et al.* (2012) investigated the mice created by Yano *et al.* (2011) further. Their analysis was focused on the immune system. They could show, that $CD4^+$ cells of their $Sms1^{-/-}$ animals had reduced levels of membrane SM. This led to cellular proliferation defects and production of interleukin (IL)-2 and interferon-γ (IFN-γ) by co-crosslinking of CD3 and CD4. Additionally $CD4^+$ cells had defects in tyrosine phosphorylation and its association with ZAP-70. Furthermore, clustering and co-localization of T-cell receptor with lipid rafts was altered. In the mice, they could show decreased serum levels of IL-6 and IFN-γ by ConA injection. Besides these major findings, slight splenomegaly and male infertility was reported.

SMS1 also seemed to have influence in hearing, as measurement of the auditory brainstem response revealed, that $Sms1^{-/-}$ animals suffer from hearing impairment in a low frequency range (4-16kHz) (Lu *et al.* 2012)

Li *et al.* (2012) generated $Sms1^{-/-}$ animals by partial deletion of exon1 (also claiming to hit the initiation codon there) and proved their gene knockout by southern blot. Their comparative investigation of $Sms1^{-/-}$ and $Sms2^{-/-}$ animals revealed a tissue specific responsibility of SM synthase activity, with SMS1 being more important in brain, spleen, lung and macrophages, while SMS2 is the major SMS

enzyme in small intestine, kidneys and liver. Furthermore bone marrow transplantation from *Sms1*$^{-/-}$ seemed to have a positive effect on arteriosclerotic lesions in *Ldlr*$^{-/-}$ animals.

In 2013, the researchers of the Yano lab found a reduction of white adipose tissue with increasing age of the animals. The plasma triglyceride concentrations in *Sms1*$^{-/-}$ mice were upregulated, lipoprotein lipase activity and FA uptake into white adipose tissue was reduced. In accordance with the detection of white adipose tissue protein modifications through oxidative stress, they found an upregulation of genes related to mitochondrial stress and apoptosis, a reduction of ATP content in white adipose tissue and reduced levels of mitochondrial respiratory chain complexes (Yano *et al.* 2013).

1.7 Aim of the study

The observation that the SL metabolism is highly altered in AD-patients and AD mouse models led us to the analysis of the impact of *Sms1*, as a crucial player in the SL pathway, on AD relevant parameters. To do so we used *Sms1* gene trap mice, which were analyzed according to their general phenotype and behavior but also specifically for alterations in myelination and stress resistance. Furthermore, we addressed the before mentioned topic of splenomegaly and male infertility in *Sms1*$^{-/-}$ in the *Sms1* gene trap animals.

To obtain AD-relevant read out we crossed *Sms1* gene trap animals to Tg2576, as a standard mouse model for AD. These double mutants were also analyzed according to their general phenotype and behavior. We specifically addressed the question of alterations in APP processing and plaque formation and a possible effect on memory performance of these animals. Furthermore a possible effect on systemic and neuronal inflammation was assessed.

Thus this study should provide a first overview on the sites and pathways of interaction between SMS1 and h*APPswe* and the results show, that the double mutant animals model could serve as a promising tool to investigate the intersection of SL metabolism and AD.

2. Material and Methods

2.1 Material

2.1.1 Animals

2.1.1.1 *Sms1* mouse line

The mutant *Sms1* allele (MGI: *Sms1*$^{Gt(E201D11)Wrst}$, subsequently referred to as *Sms1*^{GT}) was generated by gene trap technology as described previously (Schnutgen *et al.* 2005). Heterozygous animals, obtained from chimera mating were interbred to obtain homozygous mutants. Males were backcrossed six times to female C57Bl/6J mice (Charles River Laboratories). Animals of the *Sms1* line carrying no *Sms1*^{GT} allele are labeled as *Sms1*^{WT}, animals heterozygous for the *Sms1*^{GT} allele are labeled as *Sms1*^{HET} and those carrying two *Sms1*^{GT} alleles are labeled as *Sms1*^{MUT}. If just the mouse line is meant without distinguishing of genotypes it is labeled as *Sms1* mouse line.

2.1.1.2 Tg2576 mouse line

Tg2576 were purchased from Taconic. These mice carry the hAPP695 with the Swedish mutation. In the following mice carrying the heterozygous hAPP695$^{K670N/M671L}$ are referred to as *APPswe*^{Tg}, while mice without the hAPP695$^{K670N/M671L}$ are referred to as *APPswe*^{WT}. ^{Tg}2576 homozygous for the human transgene are not viable.

2.1.1.3 *Sms1* x *APPswe* mouse line

The *Sms1* x *APPswe* mouse line was generated by mating of *Sms1*^{MUT} with *APPswe*^{Tg}. Subsequently *Sms1*^{HET} x *APPswe*^{Tg} and *Sms1*^{HET} x *APPswe*^{WT} double mutants were mated to obtain animals for the *Sms1* x *APPswe* mouse line. If just the mouse line is meant without distinguishing the genotypes it is labeled as *Sms1* x *APPswe* mouse line. Furthermore, if all genotypes for the gene locus of *Sms1* are meant, but there was a difference observed depending on the *APPswe* genotype, animals were labeled as *Sms1* x *APPswe*^{WT} and *Sms1* x *APPswe*^{Tg}. Respectively, the same was done if all genotypes of *APPswe* were meant, but it was distinguished between the genotypes of *Sms1*. Consequential the nomenclature of *Sms1*^{WT} x *APPswe*, *Sms1*^{HET} x *APPswe* and *Sms1*^{MUT} x *APPswe* was used.

2.1.2 Antibodies

Table 2.1: Primary and secondary antibodies used for Western Blot and Immunostaining
Immunogen, respective dilutions, IDs and companies are listed.

Primary antibodies				
Immunogen	**Dilution WB**	**Dilution IHC**	**ID**	**Company**
Sphingomyelin Synthesis				
Anti-SMS1 (N-13), rabbit polyclonal	1:1000 (49kDa)	1:100	AP05279PU-N	Acris
Anti-SMS1 (E-5), mouse monoclonal	1:1000 (49kDa)		sc-166436	Santa Cruz
Anti-SMS1, rabbit polyclonal	1:1000 (49kDa)		ab135365	abcam
Anti-SMS2 (N-13), goat polyclonal	1:1000 (43kDa)	1:50 - 1:500	sc-34048	Santa Cruz
Junction Proteins				
Anti-Occludin, rabbit polyclonal	1:500 (63kDa, 59 kDa)	1:100	ab31721	abcam
Anti-β-Catenin, rabbit monoclonal	1:8000 (92kDa, 86kDa)	1:500 (1:500)	ab32572	abcam
Anti-Connexin 43 / GJA1, rabbit polyclonal	1:8000 (43kDa)	1:1000	ab11370	abcam
Histone Marker				
Anti-phospho-histone H2A.X, mouse monoclonal		1:250	05-636	Millipore
Anti-Histone 3 tri methyl K9, rabbit polyclonal		1:750	ab8580	abcam
Anti-Histone 3 tri methyl K4, rabbit polyclonal		1:150	ab8898	abcam
HPA-axis components				
Anti-Glucocorticoid receptor alpha (GRα), rabbit polyclonal	4µg/ml (90kDa, 86kDa)		ab3580	abcam
Anti-Multi drug resistance protein 1 (MDR1), rabbit polyclonal	1:3000 (141kDa)	1:250	ab170904	abcam
anti-MFSD2A, rabbit polyclonal	1:1000 (60kDa)		ab105399	abcam
Anti-ACTH, rabbit polyclonal		1:100	ab74976	abcam
Inflammatory response				
Anti-CD3, rabbit polyclonal	1:200 (23kDa)	1:100	ab16669	abcam
Anti-IgG2b, rabbit monoclonal	1:5000 (50kDa, 30kDa)	1:500	ab190482	abcam
Anti-TGF beta, rabbit polyclonal	1:750 (13kDa)	1:300	ab66043	abcam
Anti-CD68, rabbit polyclonal	1:50 (37kDa)	1:100	ab125047	abcam
Anti-Iba-1, goat polyclonal	1µg/ml (17kDa)	1:1000	ab5076	abcam
Anti-BDNF, rabbit polyclonal	1:1000 (28kDa)		ab46176	abcam
Housekeeper				
Anti-beta Actin, mouse	1:5000		GTX26276	GeneTex
Anti-Gapdh, mouse monoclonal	1:5000		GTX627408	GeneTex
Anti-HPRT, rabbit polyclonal	1:2000		FL-218	Santa Cruz

Anti-beta tubulin III, rabbit		1:500	ab18207	abcam
APP processing				
10A8, rat	1:40 (80kDa)		NRG13 10A8	Kremmer
192wt, rabbit	1:900 (100kDa)			ELAN
192swe, rabbit	1:2000 (100kDa)			ELAN
22C11, mouse monoclonal	1:5000 (100kDa)		MAB348	Chemicon/Millipore
2C2, mouse	1:1000 (120kDa)		2C2	Kremmer
2D8, rat	1:1000 (4kDa)		2D8	Kremmer
5313, rabbit polyclonal	1:4000 (100kDa)		5313	Kremmer
AD10, rabbit polyclonal	1:4000 (60/85kDa)		AB19026	Calbio-chem/Chemicon
B1 (cs), rabbit monoclonal	1:1000 (70kDa)		5606	Cell signaling
APP-CTF, rabbit monoclonal	1:3000 (100kDa)		A8717	Sigma
M3.2, mouse	1:2000 (4-7kDa)		SIG-39155-200	Signet
Aβ-rod, rabbit	1:2000 (4-7kDa)		SIG-39151	Signet
A8718 = APP-CTF				Willem
6E10, mouse monoclonal	1:2000 (100kDa)	1:500	SIG-39300	Signet
Anti-beta-Amyloid (1-40), mouse monoclonal	1:100 - 1:1000 (4kDa)	1:150	SIG-39140	Signet
Anti-beta-Amyloid (1-42), mouse monoclonal	1:100 - 1:1000 (4kDa)	1:500	SIG-39142	Signet
Anti-Tau, mouse monoclonal	1 :1000		ANB0042	Invitrogen
Anti-pTAU, goat polyclonal	1:500		sc-16896	Santa Cruz
Myelin Marker				
Anti-Myelin Basic Protein (MBP), rabbit polyclonal	1µg/ml (18kDa, 45kDa)	1:150	ab40390	abcam
Anti-Myelin Oligodendrocyte Glycoprotein (MOG, C-term), goat polyclonal	0.2µg/ml (28kDa)	1:100	AP08806PU-N	Acris
Autophagy marker				
anti-LAMP1 (1D4B), rat monoclonal	1:500 (110 - 140kDa)		ab25245	abcam
anti-EEA1 (N-19), goat polyclonal	1:800 (162kDa)	1:50	sc-6415	Santa Cruz
anti-EEA1, rabbit polyclonal	1µg/ml (180kDa)		ab2900	abcam
anti-LAMP1 (1D4B), rat monoclonal	1:500 (120kDa)	1:50	sc-19992	Santa Cruz
Anti-p62 (C-terminal), guinea pig	1:2000 (62kDa)		5318	Cell signaling
Anti-AIF (D29D2), rabbit	1:1000 (47kDa)		ab6313	abcam
Anti-LC3, rabbit polyclonal	1:500 (LC3I 18kDa, LC3II 16kDa)		sc-28266	Santa Cruz

Secondary antibodies				
Immunogen	**Dilution WB**	**Dilution IHC**	**ID**	**Company**
Fluorescent				
anti-mouse Alexa594 (red)		1:500	A-21203	Life technologies
anti-rabbit Alexa594 (red)		1:500	A-21207	Life technologies
anti-goat Alexa594 (red)		1:500	A-11050	Life technologies
anti-rabbit Alexa 488 (green)		1:500	A-21206	Life technologies
HRP-conjugated				
goat anti-mouse	1:10000			Dianova
goat anti-rabbit	1:10000			Dianova
rabbit anti-goat	1:10000			Dianova
Anti-Rabbit IgG (H+L)	1:10000		W4011	Promega
Anti-Mouse IgG (H+L)	1:10000		W4021	Promega
goat anti-rat IgG	1:4000		sc-2006	Santa Cruz
donkey anti-goat IgG	1:4000		sc-2020	Santa Cruz
Biotin-conjugated				
rabbit anti-goat		1:300	305-065-006	Dianova
goat anti-rabbit		1:300	111-065-003	Dianova

2.1.3 Buffers, Gels and Media

1X PBS	
NaCl	8.0g
KCl	0.2g
Na_2HPO_4	1.42g
KH_2PO_4	0.27g
dH_2O	add to 1L

10x TAE	
Tris	48.4g
Glacial acetic acid	11.4ml
EDTA disodium salt	3.7g
dH_2O	add to 1L

10X TRIS-HCL	
Tris	60.57g
dH_2O	add to 1L
	Adjust to pH 7.4 – pH7.6

10X TBS	
Tris-HCl (1M) pH 7.6	200ml
NaCl (5M)	300ml
dH_2O	500ml

LYSIS BUFFER – FOR DNA ISOLATION	
KCl (1M)	1ml
Tris (1M)	2ml
Non.N40 (10%)	9ml
Tween (10%)	9ml
dH_2O	add to 100ml
+ 10µl Proteinase K (20mg/µl) per 500µl buffer	

LACZ-WASH-BUFFER	
MgCl2 (1M)	240µl
Sodium-deoxycholat (5%)	240µl
NP-40 (10%)	240µl
PBS	add to 120ml

LACZ-STAINING-SOLUTION	
$K_3Fe(CN)_6$ (0.5M)	600µl
$K_4Fe(CN)_6$ (0.5M)	600µl
X-gal (20mg/µl)	3µl
LacZ-wash-buffer	add to 60ml

10X FA-GEL BUFFER – STOCK SOLUTION FOR NORTHERN BLOT GELELECTROPHORESIS	
MOPS (1M)	200ml
Sodium acetate (1M)	50ml
EDTA (500mM)	20ml
dH_2O	add to 1L
	adjust to pH 7.0

1X FA-GEL RUNNING BUFFER - FOR NORTHERN BLOT GELELECTROPHORESIS	
10x FA-gel buffer	100ml
Formaldehyde (12.3M; 37%)	20ml
dH_2O	add to 1L

1.2% FA-GEL - FOR NORTHERN BLOT GELELECTROPHORESIS	
Agarose	1.8g
10x FA-gel buffer	15ml
dH_2O	add to 150ml

10X SSC	
NaCl	1.5M
Sodium citrate	250mM
in dH_2O	

CHURCH BUFFER	
Na_2HPO_4	1M
NAH_2PO_4	1M
BSA	1%
SDS	7%
EDTA	1mM
ssDNA	0.1mg/ml
in dH_2O	
	Adjust to pH7.4

PFA 20% - STOCK SOLUTION FOR PERFUSION	
paraformaldehyde	200g
1xPBS	add to 1L
	adjust to pH 7.4

PFA 4% - WORKING SOLUTION FOR PERFUSION	
PFA (20%)	200ml
1xPBS	add to 1L

1X RIPA – FOR STANDARD PROTEIN ISOLATION	
Tris-HCl pH7.5	50mM
NaCl	150mM
Triton X-100	1%
DOC	0.50%
SDS	0.10%
EDTA pH8.0	2mM
in dH_2O	

5X RIPA – STOCK SOLUTION USED FOR APP PROFILE WESTERN BLOT	
Tris-HCl pH7.4	100mM
NaCl	750mM
NP40	5%
Triton X-100	0.20%
Sodiumdesoxycholat	2.50%
in dH_2O	

1X RIPA- WORKING SOLUTION FOR APP PROFILE WESTERN BLOT	
RIPA (5x)	2ml (1X)
EDTA (0.5M)	50µl
Protease Inhibitor Mix (500x)	20µl
dH_2O	add to 10ml

DEA – WORKING SOLUTION FOR APP PROFILE WESTERN BLOT	
DEA	0.20%
NaCl	50mM
	adjust to pH10
Proteinase Inhibitor Mix (500x)	

DEA-T – NEUTRALIZED DEA	
DEA working solution	
Tris-HCl pH6.8	0.5M

COLLECTION GEL	
Acrylamide	1.0ml
Tris-HCl pH6.8	2.5ml
TEMED	30µl
APS	30µl
in H_20	

SEPARATION GEL	
Acrylamide	3.2ml
Tris-HCl pH8.8	4ml
TEMED	30µl
APS	30µl
in H_20	

RUNNING-BUFFER – FOR APP PROFILE WESTERN BLOT	
Tris-Glycine Buffer (10x)	200ml (1X)
SDS	0.01%
H_2O	add to 2L

RUNNING-BUFFER – FOR STANDARD WESTERN BLOT	
Running-Buffer (20x) NuPAGE® Running buffer (MES) MOPS buffer	50ml (1X)
dH_2O	add to 1L

10X TRIS-GLYCINE BUFFER – FOR APP PROFILE WESTERN BLOT	
Tris	151g (250mM)
Glycine	720g (800mM)
dH_2O	add to 5L

TRANSFER-BUFFER – FOR APP PROFILE WESTERN BLOT	
Tris-Glycine Buffer (10x)	200ml (1X)
H_2O	add to 2L

TRANSFER-BUFFER – FOR STANDARD WESTERN BLOT	
Transfer-Buffer (20x)	12.5ml (1X)
Methanol	25ml (10%)
dH_2O	add to 250ml

STRIPPING BUFFER – FOR WESTERN BLOT	
Tris	0.76g
SDS	2.0g
β-Mercaptoethanol	700µl
dH_2O	add to 100ml
	adjust to pH 6.8

TBS-T (0.05% - 0.1%) – USED FOR WESTERN BLOT	
10 x TBS	100ml
Tween®-20	0.5 - 1ml
dH_2O	add to 1L

SKIM MILK (5%) – FOR WESTERN BLOT	
Skim Milk powder	5g
TBS-T (0.05% Tween)	add to 100ml

MEFS MEDIUM	

FCS (PAN)	10%
L-Glutamin	1%
Pen/Strep	0-2%
in 1x DMEM	

2.1.4 Chemicals and basic substances

CHEMICALS	ABBREV.	COMPANY
3, 3'-diaminobenzidine	DAB	DCS LabLine
4', 6-diamidino-2-phenylindole	DAPI	Carl Roth
β-mercaptoethanol		Sigma
Agarose		Biozym
Ampicillin		Sigma
Ampuwa		Fresenius
Bis-Tris		Sigma
Chloroform		Sigma
Citric acid		Sigma
Formic acid	FA	Sigma
Dimethyl sulfoxide	DMSO	Sigma
Desoxy-Nucleotid triphosphates	dNTPs	Fermentas
Ethanol	EtOH	Merck
Ethidiumbromide	EtBr	Fluka
Ethylene diamine tetraacetic acid	EDTA	Sigma
Ethylene glycol tetraacetic acid	EGTA	Sigma
Ethylene glycol		Roth
Eosin		Roth
Fetal calf serum	FCS	PAN, Hybond
Formaldehyde		Sigma
Glutaraldehyde		Sigma
Glycerol		Sigma
Goat serum		Sigma
Haematoxylin (Mayer's)		Sigma
Hydrochloric acid	HCl	Sigma
Isopropyl-β-D-thiogalactopyranosid	IPTG	Fermentas
Isopropanol		Merck
Indocyanine Green	ICG	Provided by Dr. Steven Ford
Isoflourane		Baxter
liquid nitrogen	Liquid N_2	Linde gas
Lithium carbonate		Roth
L-Glutamine 200nM (100x)		Gibco
Magnesium chloride	MgCl	Merck
Methanol	MeOH	Merck
MOPS	MOPS	Sigma
N-laurylcarcosine Sodium Salt Solution		Sigma
Ninident P40	NP-40	Fulka
Paraffin		Sigma
Paraformaldehyde		Sigma
Formalin		Roth
Phosphatase Inhibitor (tablet)		Roche
Potassium chloride	KCl	Roth
Protease Inhibitor (tablet)		Roche
Proteinase K		Roche
Rapamycin		Sigma
RNA loading dye		Thermo scientific

Dnase		Sigma
Rnase inhibitor		Roche
Rnase Zap®		Sigma
Skim milk powder		BD Bioscience
SOC. Medium		Invitrogen
Sodium acetate		Merck
Sodium Cacodylate Buffer (0.1M) with 2.5% glutaraldehyde (pH7.4)		Science Services
Sodium choride	NaCl	Merck
Sodium citrate		Sigma
Sodium dodecyl sulfate	SDS	Sigma
Sodium hydrogen carbonate		Sigma
Streptavidin-peroxidase solution		KPL
Toluidine blue		Sigma
TriReagent		Sigma
Trizol		Invitrogen
Tris		Sigma
Triton X-100		BioRad
Trypsin/EDTA 0.05% (1x)		Gibco
Tween-20		Sigma
X-Gal		Fermentas
Xylol		Carl Roth

2.1.5 Consumables and other material

CONSUMABLES AND OTHER MATERIAL	COMPANY
5x Sample Loading buffer	Invitrogen
20 x NuPAGE® Running buffer	Invitrogen
20x NuPAGE® Transfer buffer	Invitrogen
20x XT MOPS running buffer	BioRad
10x Tris/Glycine buffer	BioRad
Antibody dilution buffer	DCS LabLine
Aquapolymount	Polysciences
Blades, Microtome, S35	Feather
Blades, Cryostate, C35	Feather
Coverslips	Roth
Cryotubes	Nunc
Electrophoresis chambers	Peqlab
Eppendorf tubes 1.5ml	Eppendorf
Eppendorf tubes 2.0ml	Eppendorf
Falcon tube 15ml	Roth
Falcon tube 50ml	Roth
Flat bottom 96-Well plates	Nunc
Filter paper	Whatman 3mm
Gloves	Meditrade, Kimtech Science
Gel blotting systems	BioRad
Dulbecco's Modified Eagle's Medium 1x	Gibco
Dulbecco's Modified Eagle's Medium 1x plus Ca^{2+}/Mg^{2+}	Gibco
Dulbecco's Phosphate Buffered Saline 1x	Gibco
Full-Range Rainbow molecular weight marker	Amersham
GeneRuler 100pb and 1kb	Fermentas
Glass pipettes	Hirschmann
Glassware	Schott
Glas pipetts	Biozym

Glas slides	Roth
Neubauer counting chamber	Brand
NuPAGE® LDS Sample Buffer (4x)	Invitrogen
O.C.T. freezing medium	Polysciences
Pertex mounting medium	Polysciences
PCR stripes	Eppendorf
PCR lids	Eppendorf
PCR plates	
PCR cover foil	Eppendorf
Petri dishes	Nunc
Pipetts and pipette tips	Gilson
Poter and pistl	Roth
Platic pipetts	Greiner
PVDF membrane	Millipore
Tender cooker	Nordic Ware
Raser blades	Wilkinson
Tris-Glycin Gel 4-12%, 10%	Invitrogen, BioRad
Wipes	Klimtech Science

2.1.6 Enzymes and Vectors

ENZYMES AND VECTORS	COMPANY
Proteinase K	Roche
EcoRI	Roche
DNaseI	Roche
pCRII-TOPO / TOPO TA cloning vector	Invitrogen

2.1.7 Fatty acid diet

The omega-3 fatty acid composition (Omega-3 90 EE) used for supplementary diet experiments was kindly provided by KD-Pharma Bexback GmbH.

2.1.8 Kits

KITS	COMPANY
5 PRIME MasterMis (PCR)	5 PRIME
ECL Detection KIT	Amersham
iScriptTM Select cDNA Synthesis Kit	BioRad
M.O.M.™ Kit	Vector Laboratories
PAS staining kit	Sigma
Pierce® BCA Protein Assay Kit	Thermo Scientific
Qiagen Plasmid Maxi Kit	Qiagen
Qiagen Plasmid MiniPrep Kit	Qiagen
QIAquick Gel Extraction Kit	Qiagen
Rneasy® Mini Kit	Qiagen
Rnase-free Dnase Set	Qiagen
SuperScript® VILO cDNA Synthesis Kit	Life Technologies
TaqMan® Universal Master Mix	Applied Biosystems
TOPO TA Cloning® Kit (Dual promoter)	Invitrogen
TUNEL kit	Millipore

2.1.9 Machinery

INSTRUMENT	TYPE	COMPANY
Autoclave	667-1ST	Aigner
Balances	LC6201S	Satorius
	LC220-S	Satorius
Centrifuges	Evolution RC	Sorvall
	5417R	Eppendorf
	5424	Eppendorf
	Varifuge 3.0R	Heraeus
Cryostate	HM 560M	Microm
Developing machine	Curix 60	Agfa
Digital camera	AxioCam MRc	Zeiss
Electric Homogenizer	Ultra-Turrax T25 basic	IKA
Freezer (-20°C)		Liebherr
Freezer (-80°C)	HFU 686 Basic	Heraeus
Fridges (4°C)		Liebherr
Gel documentation system	E.A.S.Y.	Herolab
Heating plate	BV SW 85	Adamas Instrument
Ice machine	AF 30	Scotsman
Incubators for bacteria	Innova 4230	New Brunswick Scientific
Incubators for MEFs		Heraeus
Light source for microscopy	KL 1500	Leica
Magnetic heater, stirrer	MR3001	Heidolph
Microscope for fluorescent imaging	Axiovert 200M	Zeiss
Microtom	SM2000R	Leica
Microwave oven		Sharp
Oven (37°C)		Memmert
Oven (67°C)		Memmert
PCR machines	MasterCycler Gradient	Roche
Perfusion pump	401U/D1	Watson-Marlow Bredel
pH meter	pH Level 1	InoLab
Photopeter	Biophotometer 6131	Eppendorf
Pipette filler, electric	Easypet	Eppendorf
Plate reader	Power wave	BioTek
Power supplies	E443	Consort
Real-time PCR system	7900HT	Applied Biosystems
Roll incubator	SRT6D	Stuart
Shaker	Polymax1040	Heidolph
Sonifier	Cell disrupter B15	Branson
Thermomixer	Comfort	Eppendorf
Vacuum pump	VP 86	VWR
UV-lamp	N-36	Benda
UV/VIS-spectral photometer	NanoDrop® ND-1000	Peqlab
Vortexer	Vortex genie 2	Secientific industries
Water baths	U3	Julabo
	AQUAline AL 12	LAUDA
Water conditioning system	MilliQ biocel	Millipore

2.1.10 Primer sets for genotyping, splice variant detection and probe generation

Primer sets were ordered from Metabion, dissolved in dH_2O and vortexed vigorously to generate a 100pM stock solution, which was stored at 4°C or at -20°C for long term storage (Table 2.2). Primers were used in the listed assays in a working concentration of 10pM.

Table 2.2: Primer sequences used for detection of splice variants, genotyping and for generation of Northern blot probes. Primer probe sets for TaqMan assays are also listed.
Sequences are listed in 5'-3' direction. Assay IDs correspond to order ID listed by lifetechnologies.com.

Primers for genotyping	
variant	**primer sequence**
*Sms1*_fw	GCCGGAAATTAAAAAGAACAATGA
*Sms1*_rv	GCAATGCAGGGTGCTTCTTCC
Spli_rv2	GCCAAACCTACAGGTGGGGTCTTT
APP1501	AAGGGGCCAAAGCCTGGAGGGTGGAACA
APP1501X	GTGGATAACCCCTCCCCCAGCCTAGACCA
APP1502	GTTGAGCCTGATGCCCGCCCTGC

Primers for detection of *Sms1* splice variants	
variant	**primer sequence**
Sms1-001_fw	GCAGCCCGAGGTTCCAAGTC
Sms1-001_rv	CGCTCCGGTTCTGGCATGGG
Sms1-002_fw	GAAGTGTTGTCACAAGAGGTGG
Sms1-004_fw	CTGGCCACTCCCAACCGCTG
Sms1-014_fw	CTGGCGCTGCCTGTGAAACC
Sms1-014_rv	CAGCAGCCAGTCTGCCACCTTC
Info	*Sms1*-001_rv also used for *Sms1*-002 and -004

Primers for generation of Northern probes	
variant	**primer sequence**
*Sms1*_e7fw	GCGAACGAATGTTTGGACACCG
*Sms1*_e7rv	GCAGCCACTGAAATAGCCAGAGT
Gapdh_fw	TCTCCGCCCCTTCTGCCGATG
Gapdh_rv	CAGCCCCGGCATCGAAGGTG

2.1.11 Primer probe sets for TaqMan assays

Table 2.3: Primar probe sets used for TaqMan assays

Bestellnr.	Mm00522643_m1		
Gen	Sgms1	Ref-Seq	Protein
Spans exons	7-8	NM_001168525.1	NP_001161997.1
Bestellnr.	Mm00512327_m1		
Gen	Sgms2	Ref-Seq	Protein
Spans exons	5-6	NM_028943.5	NP_083219.2
Bestellnr.	Mm00460332_m1		
Gen	Acer1	Ref-Seq	Protein
Spans exons	5-6	NM_139306.2	NP_647467.1
Bestellnr.	Mm01264988_m1		
Gen	Acer2	Ref-Seq	Protein
Spans exons	5-6	NM_139306.2	NP_647467.1
Bestellnr.	Mm00502940_m1		
Gen	Acer3	Ref-Seq	Protein
Spans exons	1-2	NM_025408.2	NP_079684.2
Bestellnr.	Mm00480021_m1		
Gen	Asah1	Ref-Seq	Protein
Spans exons	4-5	NM_019734.2	NP_062708.1
Bestellnr.	Mm00479659_m1		
Gen	Asah2	Ref-Seq	Protein
Spans exons	7-8	NM_018830.1	NP_061300.1
Bestellnr.	Mm01258345_g1		
Gen	Lass2	Ref-Seq	Protein
Spans exons	8-9	NM_029789.1	NP_084065.1
Bestellnr.	Mm03990709_m1		
Gen	Lass3	Ref-Seq	Protein
Spans exons	1-2	NM_001164201.1	NP_001157673.1
Bestellnr.	Mm00482658_m1		
Gen	Lass4	Ref-Seq	Protein
Spans exons	9-10	NM_026058.4	NP_080334.3
Bestellnr.	Mm00510998_m1		
Gen	Lass5	Ref-Seq	Protein
Spans exons	9-10	NM_028015.2	NP_082291.1
Bestellnr.	Mm00556165_m1		
Gen	Lass6	Ref-Seq	Protein
Spans exons	5-6	NM_172856.3	NP_766444.1
Bestellnr.	Mm00488319_g1		
Gen	Smpd1	Ref-Seq	Protein
Spans exons	3-4	NM_011421.2	NP_035551.1
Bestellnr.	Mm01188195_g1		
Gen	Smpd2	Ref-Seq	Protein
Spans exons	5-6	NM_009213.2	NP_033239.1
Bestellnr.	Mm00491359_m1		
Gen	Smpd3	Ref-Seq	Protein
Spans exons	3-4	NM_021491.3	NP_067466.1

Bestellnr.	Mm00547173_m1		
Gen	Smpd4	Ref-Seq	Protein
Spans exons	8-9	NM_001164609.1	NP_001158081.1
Bestellnr.	Mm00435874_m1		
Gen	Pomc	Ref-Seq	Protein
Spans exons	2-3	NM_008895.3	NP_032921.1
Bestellnr.	Mm01192208_m1		
Gen	Mfsd2a	Ref-Seq	Protein
Spans exons	13-14	NM_029662.2	NP_083938.2
Bestellnr.	Mm00432670_m1		
Gen	Crhr1	Ref-Seq	Protein
Spans exons	3-4	NM_007762.4	NP_031788.1
Bestellnr.	Mm00438303_m1		
Gen	Crhr2	Ref-Seq	Protein
Spans exons	1-2	NM_009953.3	NP_034083.2
Bestellnr.	Mm00434865_s1		
Gen	Mc2r	Ref-Seq	Protein
Spans exons	4-4	NM_001271716.1	NP_001258645.1
Bestellnr.	Mm00433832_m1		
Gen	Nr3c1	Ref-Seq	Protein
Spans exons	1-2	NM_008173.3	NP_032199.3
Bestellnr.	Mm01241596_m1		
Gen	Nr3c2	Ref-Seq	Protein
Spans exons	7-8	NM_001083906.1	NP_001077375.1

2.1.12 Software

SOFTWARE	COMPANY
Axio Vision	Zeis
Excel 2010	Microsoft
SDS2.4	Applied Biosystems
ImageJ2x	Rawak Software
KC4	BioTek
GraphPad Prism	GraphPad Software, Inc.

2.2 Methods

This section describes the methods used in the thesis. For detailed information about buffer ingredients and composition please see the corresponding section in the material or the supplementary part.

2.2.1 Animal housing

All animal experiments were carried out in accordance with the European Communities Council Directive (86/609/EEC). Littermates of the *Sms1* or *Sms1* x *APPswe* mouse line were used in this study. Animals were group housed in standard cages, with a maximal occupancy of five. Housing conditions included 22 ± 1°C, 55 ± 5% humidity a 12-hour light-dark cycle and *ad libitum* access to food and water.

2.2.2 Accession of birth rates

Birth rates of different sexes and genotypes were assessed according to the number of animals counted and genotyped at the age of weaning (3 weeks). The total number of *Sms1*^{WT} x *APPswe*^{WT} animals counted was set to be 100% of the expected Mendelian ratio. Other genotypes are shown as % of expected Mendelian ratio.

2.2.3 Accession of body weight gain

Animals of the *Sms1* x *APPswe* mouse line were weighted on a weekly basis, starting with weaning at the age of 3 weeks. Data were grouped according to age and are presented as mean per genotype ± SEM.

2.2.4 Accession of death rates

Survival of obtained offspring was monitored and listed for the first 25 weeks of live. The precise date or the week within an animal was found dead was noted. Each death event was listed according to genotype and age. The total number of offspring per genotype was set to 100%, each event of death within this genotype was represented by an according percent loss of total percent surviving. Data are presented as percent surviving.

2.2.5 PUFA diet experiments

2.2.5.1 Fertility experiment

We tested eight and 20 week old male *Sms1* mice for fertility. Therefore, *Sms1*^{WT} and *Sms1*^{HET} males, serving as control, and *Sms1*^{MUT} males were each provided with an eleven week old C57Bl/6J female. After three weeks these females were separated from the males and kept for additional three weeks. The litters obtained in this period were recorded. Subsequently to separation of the first batch of females, the *Sms1* males were provided with a second female each. In parallel, a mix of omega-3 fatty acid ethylesters (Omega-3 90 EE) including 38% DHA and 46% EPA (KD Pharma, Bexbach) was manually fed to the male *Sms1* mutants in an oral dose of 9mg-total omega-3 fatty acids con-

tent/day/animal for 13 weeks. After the feeding experiment, the animals were sacrificed, perfused and testes were prepared for H&E staining.

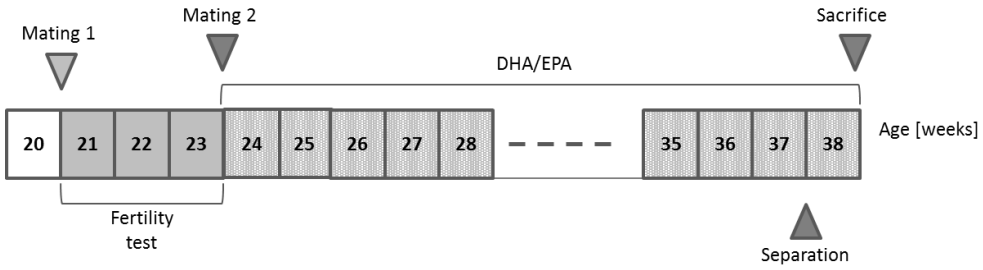

Figure 2.1: Feeding scheme for fertility experiment
Schematic time course of the infertility test mating scheme, with subsequent DHA/EPA supplementation. *Sms1*^{WT} (n=2), *Sms1*^{HET} (n=4) and *Sms1*^{MUT} (n=6) were mated at the age of 20 weeks to an 11 week old C57Bl/6J female (mating 1) for a test of fertility. After three weeks these mating were terminated and the female was replaced by a new 11 week old C57Bl/6J female (mating 2). These mating were maintained for 13 weeks, before they were terminated (separation). With the start of mating 2 all males were provided with a DHA/EPA diet supplementation (9mg total omega-3 content/animal/day, oral dose) for the duration of 14 weeks. At the age of 38 weeks males were sacrificed and testes were analyzed.

2.2.5.2 Weight gain experiment

Sms1^{HET} x *APPswe*^{Tg} and *Sms1*^{HET} x *APPswe* ^{WT} animals were mated to obtain offspring as littermates of the relevant genotypes (*Sms1*^{WT} x *APPswe*^{Tg}, *Sms1*^{HET} x *APPswe*^{Tg}, *Sms1*^{MUT} x *APPswe*^{Tg}). With the start of mating, females were manually fed with a supplementary diet of omega-3 fatty acid ethylesters (Omega-3 90 EE) including 38% DHA and 46% EPA (9mg-total omega-3 FA content/day/animal KD Pharma, Bexbach) to ensure a supply of essential PUFAs for the offspring during embryonal development. With weaning, pups themselves were fed with DHA/EPA diet (3mg-total omega-3FA content/day/animal until 4 weeks of age; 9mg-total omega-3FA content/day/animal from 4 weeks of age onwards). Weight gain and death rates were monitored as described above. Weight data is presented as percent difference in weight gain between DHA/EPA fed and non-fed animals of the respective genotype ± SEM.

2.2.6 Behavioral Tests

Behavioral testing was either performed in the GMC or was done by Dr. Annemarie Zimprich and Dr. Lillian Garret in accordance with the GMC protocols (see below). The cohort for GMC analysis consisted of 10 mice per sex and genotype and was transferred to the GMC two weeks prior to start of the testing battery (Gailus-Durner *et al.* 2005) for habituation.

A brief summary of the behavioral test procedures, which are discussed in more detail in this thesis is given below, for a more detailed information and a collection of GMC protocols, please see: http://www.eumorphia.org/EMPReSS.

All test apparati were cleaned between the assessment of behavioral performances of different mice.

2.2.6.1 Open Field

The open field (OF) test apparatus consists of a square-shaped testing arena (ActiMot), surrounded by transparent walls (45.5 x 45.5 x 39.5cm) and a light intensity of 150 – 200lux in the periphery or the center, respectively. It has a defined periphery, which is set as a corridor of 8cm along the walls and a resulting center zone. The OF is frequently used to assess general behavior such as locomotion distance and speed, but also for anxiety-related parameters For testing, animals are placed in the middle of the arena and are monitored and videotaped for 20'. Data acquisition included 1) the latency for the first re-entry in the center zone, 2) number of center zone entries, 3) their speed, 4) distance and 5) time in the different compartments as well as 6) number of rearings were assessed.

2.2.6.2 Y-Maze

For acquisition of spatial memory performance based on the retrograde working memory, mice were tested on the Y-Maze. The Y-Maze apparatus consists of three arms, which are organized in 120° angles. At the beginning of the test, animals were placed at the end of one arm and were allowed to explore the Y-Maze for 5'. Data acquisition included 1) time to first arm entry, 2) total number of entries, 3) completed triads, 4) arm alterations and entrance sequences.

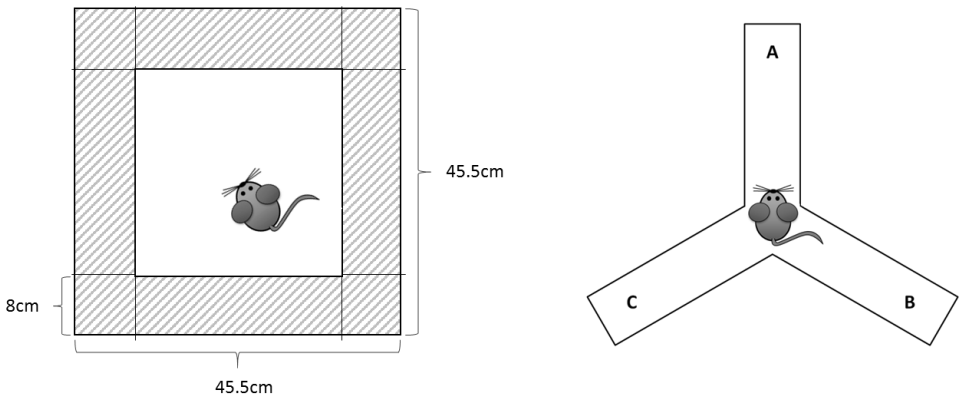

Figure 2.2: Open field and Y-Maze arena
Schematic drawing of the Open Field and the Y-Maze arena, which were used for assessment of standard behavioral data, anxiety-related behavior and memory performance.

2.2.6.3 Grip strength

Grip strength was assessed with a horizontal metal grid attached to a force sensor. The mouse is allowed to grip the grid and is then pulled by its tail. The strength applied until the mouse loses hold of the grid is measured in three subsequent trials performed within one minute. Mean values are used to represent the grip strength. This test is performed with the mouse either grasping the grid with two or with four paws.

2.2.6.4 Rotarod test

For assessment of motor coordination the rotarod test was applied. The rotarod (Bioseb, Chaville, France), consisting of a rotating spindle with five individual lanes, one for each mouse, is driven by a computer controlled rotating rod allowing the device to accelerate in a predefined way. The speed was set to accelerate from 4–40 rpm for 300" with 15' between each trial. Three trials were performed with each animals and the mean performance was presented.

2.2.6.5 Stress reactivity test (SRT)

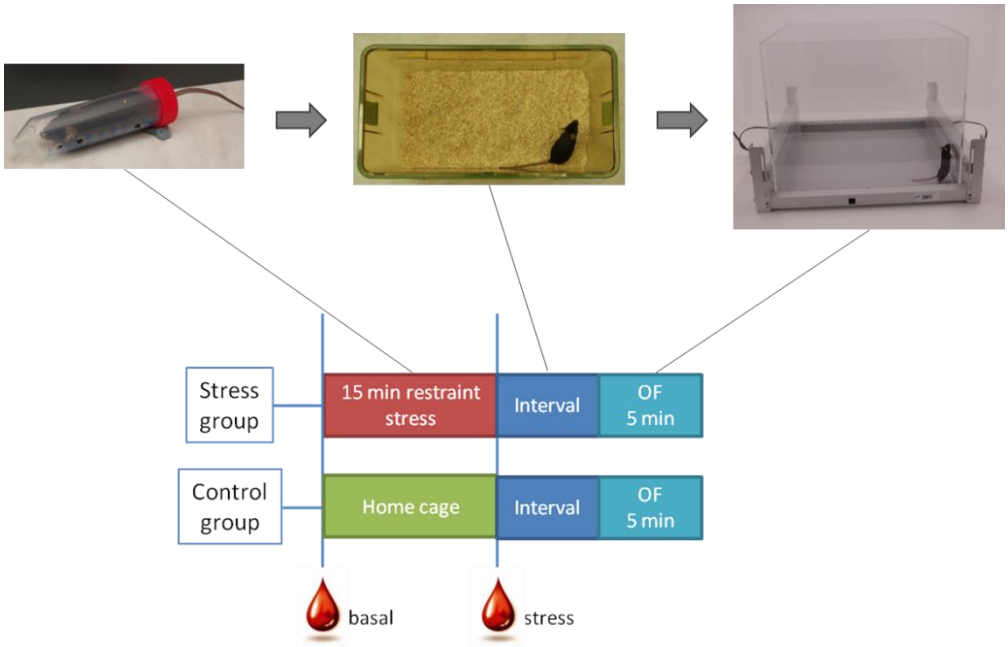

Figure 2.3: Schematic illustration of the stress reactivity test (SRT) setup
Animals were grouped into a stress and a control group. A blood sample was taken from each animals to assess basal CORT levels. Animals of the stress group were exposed to a restraint stress, by placing them into a 50ml falcon tube for a defined period, while animals of the control group remained in their home cages. After this period a second blood sample was taken from each animal to assess stress CORT levels. All animals were placed back into their home cages for an interval needed to stop the wound from bleeding. Animals were subsequently tested in a OF arena and their behavior during the first 5min of testing was analyzed. Pictures were taken by Dr. Annemarie Zimprich.

SRT tests were performed by Dr. Annemarie Zimprich according to the scheme shown below (Figure 2.3). Female and male animals of the *Sms1* mouse line were grouped into a stress and a control group. From each animal a blood sample was taken from the tail vein to assess basal CORT levels. Animals of the stress group were exposed to a restraint stress of either 15' or 2h., by placing them into a 50ml falcon tube. Animals of the control group remained in their home cages. After this period a second blood sample was taken from each animal to assess CORT levels after stress. All animals were placed back into their home cages for an interval of either 5' or 20'. Subsequently, animals were tested in a OF arena as described above (section 2.2.6.1) and their behavior during the first 5min of testing was analyzed.

2.2.7 Animal blood and organ preparation

2.2.7.1 Blood taking

Blood taking for the analysis of steroids in the GMC was done retro-bulbar from isoflourane narcotized mice. Plasma was obtained by centrifugation and was stored at -20°C until further analysis. For a more detailed information and a collection of GMC protocols, please see: http://www.eumorphia.org/EMPReSS.

2.2.7.2 Pathological analysis

Pathological analysis was performed in the Institute of Pathology. Therefore *Sms1* x *APPswe* animals, which were found dead (*post-mortem* interval < 3h) were collected and, together with age-matched controls, macroscopically and histologically analyzed by Dr. Frauke Neff.

2.2.7.3 Perfusion

2.2.7.3.1 Organ preparation and perfusion with PBS

Mice were sacrificed by carbon dioxide inhalation and transcardially perfused with 50-70ml ice-cold PBS prior to brain and organ preparations. Organs were put to 2ml Eppendorf tubes. The brain was separated into its two hemispheres, while the left half or the right half were used for protein preparations or immunological investigations, respectively, before freezing in dry ice cooled isopentane and storage at -80°C.

2.2.7.3.2 Organ preparation and perfusion with PFA

Mice were sacrificed by carbon dioxide inhalation and transcardially perfused with 50-70ml ice-cold PBS followed by 50ml 4% PFA. Organs were dissected, placed into 15ml falcon tubes and postfixed in 4% PFA at 4°C overnight. Subsequently organs were dehydrated and paraffin embedded.

2.2.7.4 Tissue embedding

Table 2.4: Times used for tissue dehydration and embedding into paraffin blocks
Embedding procedures for different tissues are listed. Xylol:Paraffin was mixed in a 1:1 ratio. Incubation times were as indicated. Overnight (O/N).

	Brain	Heart	Lung	Spleen	Adrenals	Piuitary
4%PFA	O/N	O/N	O/N	O/N	2h	2h
70%EtOH	4h or O/N	4h or O/N	4h or O/N	4h or O/N	1h	1h
95%EtOH	2h	2h	2h	2h	30'	30'
100%EtOH	2h	2h	2h	2h	30'	30'
Xylol	2h	2h	2h	2h	1h	1h
Xylol:Paraffin	1h	1h	1h	1h	skip	skip
Paraffin	O/N	O/N	O/N	O/N	O/N	O/N

After PFA fixation overnight. Organs were dehydrated by increasing EtOH row (70-100%), cleared with Xylol and embedded into paraffin. For detailed information on incubation times see

Table 2.4. Incubation with 4% PFA was done at 4°C, Xylol:Paraffin and Paraffin only incubations were performed at 67°C. All other steps were carried out at RT. Paraffin blocks were slowly cooled down and stored at 4°C until further processing

2.2.7.5 Cutting of tissues

2.2.7.5.1 Microtome cutting

Paraffin embedded tissues were cut with the microtome. 4°C pre-cooled paraffin blocks were fixed to the microtome, allowing them to be cooled during the whole cutting process. Tissues were cut into 6 to 8µm thick sections in a series of 4 or 8 slides, depending on the tissue. Sections were put into a 37-40°C warm water bath, allowing them to unfold for 2-5'. Subsequently, the sections were mounted onto glass slides using a soft brush. Slides were dried at 40°C on a heating plate for 20-30' and then dried over night at 67°C in an oven.

2.2.7.5.2 Cryostate cutting

Heart tissue, frozen and stored in O.C.T (Tissue Tek) were cut with the cryostate into 6µm thick sections. The frozen cubes were mounted onto the cryostate section plates and fixed by rapid freezing (-55°C). Temperatures for the specimen was put to -22°C and for the blade to -17°C. Sections were immediately mounted onto glass slides and dried on a heating plate set to 30°C. Sections were subsequently stored at -80°C until further processing.

2.2.7.6 Organ withdrawal for RNA and Protein Isolation

Mice were sacrificed by cervical dislocation. Organs were dissected, cleared from blood in ice-cold 0.9% NaCl, taped dry, put a 1.5ml cryotube, placed on dry ice or shock frozen in liquid nitrogen and subsequently stored at -80°C or in the gas phase of liquid nitrogen until further investigations.

2.2.7.7 Dissection of HPA-axis related brain parts and organs for RNA isolation

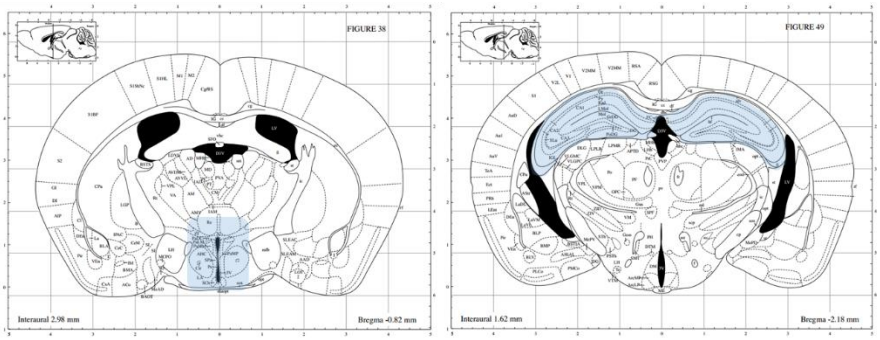

Figure 2.4: Brain areas dissected for HPA-axis relevant analysis of expression levels.
The first panel highlights the area dissected for the analysis of the hypothalamic areas including the paraventricular nucleus. The second panel shows the hippocampus, which was dissected completely.

For investigation of HPA-axis relevant brain areas, the animals were killed by cervical dislocation, brains were quickly removed and brain regions were isolated on ice. The hippocampus was dissected by separation and careful loosening of the cortical tissue around the hippocampus (Figure 2.4). Sub-

sequently, the highlighted area (Figure 2.4) of the hypothalamic area was taken. Furthermore, the pituitary and the adrenal glands were removed. Tissues were snap frozen in a 1.5ml cryotube in liquid nitrogen and stored at -80°C until further processing.

2.2.7.8 Organ withdrawal for Lipid profiling and enzyme activity measurements

Animals were sacrificed by cervical dislocation in order to prevent any inconvenience in the enzyme activities caused by carbon dioxide. After cervical dislocation, the animals were weighted. The brain was removed and directly placed into 4°C pre-cooled 0.9 % NaCl. The brain was tapped dry on a tissue towel, weighted, put in a 1.5ml cryotube and was shock frozen in liquid nitrogen. The heart, lung, liver, spleen and (for male animals) the testis were dissected and treated the same way as the brain. All organs were stored in the gas phase of liquid nitrogen until shipping on dry ice and further processing.

2.2.8 Accession of organ weight

The weights of the organs, obtained by the method described above, were analyzed as absolute data and as relative data compared to the body weight of the respective animal. Data are presented as mean per genotype ± SEM.

2.2.9 Histological analysis and organ pathology

Histological analysis and organ pathology was performed within the GMC as described (Gailus-Durner *et al.* 2009). A total of 46 mice of the *Sms1* mouse line at different ages were analyzed for morphological changes.

Animals were sacrificed with CO_2. Body weight, body length and weight of internal organs such as heart, spleen and liver were determined. Tail tips were cut and stored at -70°C for genetic reconfirmation. Organs were fixed in 4% formalin and embedded in paraffin as described above (see section 2.2.7.4), 4µm sections were cut with the microtome (see section 2.2.7.5.1) and stained with hematoxylin and eosin (H&E; see section 2.2.12.2) for histological examination. Periodic acid shiff (PAS; see section 2.2.12.3) staining was applied for visualization of glycolipids. Images of tissue sections were acquired with an automated slidescanner (NanoZoomer-NDP-Hamamatsu, Germany). All slides were independently reviewed and interpreted by 2 pathologists, experienced in mouse pathology.

2.2.10 Nucleic acid based methods

2.2.10.1 DNA based methods

2.2.10.1.1 DNA Isolation

Genomic DNA was isolated from tail tips (0.5mm) by incubation with 500µl of Lysis-Buffer and 20µg of Proteinase-K per tail tip at 60°C for at least 3h. For Proteinase-K inactivation samples were heated to 95°C for 10' prior to centrifugation and separation of the supernatant. Isolated DNA was stored at 4°C until further processing.

2.2.10.1.2 Genotyping – PCRs

Genotyping was performed by triplet-PCR amplification according to the pipette scheme listed below (Table 2.5). The *Sms1* genotype was identified using the primers listed in Table 2.2. A band of 577bp represents the mutant fragment and 999bp represents the wild-type fragment. The genotype of the h*APPswe* allele was identified using the primers listed in Table 2.2. A band of 470bp represents the mutant fragment and 750bp represents the wild-type fragment. PCR cycling settings for the reactions were set according to Table 2.5. All PCR fragments were sequence-verified initially.

Table 2.5: Pipetting scheme for standard-PCR and cycle settings for *Sms1* and h*APPswe* genotyping PCR reactions

Standard-PCR	
5' PCR reaction Mix	10µl
Primer, each	1µl
DNA template	1µl
H_2O	add 20µl

Cycle settings - *Sms1* genotyping		
95°C	3.0'	
94°C	0.5'	35x
60°C	1.0'	
72°C	0.5'	
72°C	7.0'	

Cycle settings - *hAPPswe* genotyping		
95°C	3.0'	
94°C	0.5'	35x
56°C	1.0'	
72°C	1.0'	
72°C	7.0'	

2.2.10.1.3 Gel-electrophoresis

For standard DNA based gel-electrophoresis, a 2.5% agarose gel (based on 1xTAE-buffer) was prepared After heating in the microwave (900W for 5-8'), the gel was allowed to cool down and $2x10^{-5}$ Vol% of EtBr were added. The gel was purred into an electrophoresis jar and allowed to cure, before 1xTAE-buffer was added as a conductor. Subsequently 4x DNA loading dye was added to the DNA sample and DNA was applied to the gel. Gel-electrophoresis was performed at 90-130V for 1h depending on the size of the jar. Gel images were taken under UV light.

2.2.10.1.4 Sequencing

Sequencing of DNA samples was done in the GATC. DNA and primer samples were prepared as follows. PCR amplified or gel-isolated DNA was diluted to 40ng/µl of DNA per 30µl of Volume. Primer for the sequencing reaction were diluted to 10pmol/µl and 20µl were provided.

2.2.10.2 RNA based methods

For all RNA work RNase free material was used. Pipettes and machinery was prepared to be RNase free using RNaseZap®.

2.2.10.2.1 RNA Isolation

1ml Trizol was added per sample. Samples were homogenized and incubated for 5' at RT prior to centrifugation at 15000g for 10' at 4°C. After taking off of the supernatant, 200µl of Chloroform were added and samples were mixed and incubated for 8' at RT. Subsequently samples were centrifuged at 15000g for 15' at 4°C. The supernatant was mixed with 530µl of Isopropanol and again incubated at -20°C, overnight. Remaining RNA-isolation steps were carried out using the RNeasy Kit (Qiagen) according to the manufacturer's instructions, including DNase treatment.

Briefly, 700µl of the lysate were applied to a RNeasy column and centrifuged. 350µl of RW1 Buffer were applied to the column, which was again centrifuged, for washing. DNase treatment took place by mixing 70µl of RDD Buffer and 10µl DNaseI, which was again applied to the column and incubated at RT for 15'. After repeated washing using RW1 buffer and twice 500µl of RPE buffer, RNA was eluted from the column by applying twice 30µl RNase free H_2O and centrifugation. If tissue samples were smaller than 30µg, RNA isolation was directly done with RNeasy Kit (Qiagen) starting with tissue homogenization in RLT buffer (RLT buffer, 1% beta-Mercaptoethanol) and subsequent loading of the sample to a RNeasy column. All following steps were performed as described above.

All centrifugation steps were set to 8000g, RT, 15sec, if not mentioned otherwise. RNA yield was measured at the NanoDrop with an OD_{260}. An optimal purity, assessed by the OD_{260}/OD_{280} ratio of 1.8 to 2.1 was aimed for. RNA was stored at -80°C until further processing.

2.2.10.2.2 RNA – cDNA conversion / RT-PCR

Reverse transcription polymerase chain reaction (RT-PCR) of isolated RNA was performed via the iScript™ Select cDNA Synthesis Kit (BioRad) for detection of splice variants via semi-quantitative RT-PCR. 4µl of 5x iScript-Selection-Reaction-Mix, 1µl of Reverse Transcriptase and 1µl of RNA (1.0µg) were added to 14µl of RNase free H_2O. RT-PCR reaction settings were 5', 25°C – 30', 42°C – 5', 85°C for activation, elongation and inactivation and were carried out on heat block. cDNA was stored at -20°C until further processing.

Reverse transcription of RNA for TaqMan Assays was performed via the Vilo-Kit (Invitrogen) according to the manufacturer's instructions. Briefly, 4µl of 5x Vilo Reaktion Mix and 2µl of 10x Superscript Enzyme Mix was added to 14µl of RNA (total 2.0µg per reaction). RT-PCR reaction settings were 10', 25°C – 60', 42°C – 5', 85°C. cDNA was stored at -20°C until further processing.

2.2.10.2.3 Detection of splice variants

The four protein coding transcripts of *Sms1* were analyzed by semi-quantitative cDNA-based PCR using specific primer combinations (Table 2.2). The PCR setup was done according to the standard PCR pipetting scheme (Table 2.5). PCR cycling settings were 95°C, 5' – (94°C, 1' – 56°C, 1' – 72°C, 1') x 35 – 72°C, 7' for all reactions.

2.2.10.2.4 Generation of Northern blot probes

PCR amplification of probe sequences

For Northern Blot probes 801bp of *Sms1* exon 7 were PCR-amplified using the primers *Sms1*_e7fw (5' – GCGAACGAATGTTTGGACACCG – 3') and *Sms1*_e7rv (5' – GCAGCCACTGAAATAGCCAGAGT – 3'; compare Table 2.2) and a genomic DNA template. The PCR setup was done according to the standard PCR pipetting scheme (Table 2.5). PCR cycling settings were 95°C, 5' – (94°C, 1' – 56°C, 1' – 72°C, 1') x 35 – 72°C, 7'.

A *Gapdh* probe was PCR-amplified using the primer pair of *Gapdh*_fw (5' – TCTCCGCCCCTTCTGCCGATG – 3') and *Gapdh*_rv (5' – CAGCCCCGGCATCGAAGGTG – 3'; compare Table 2.2). The PCR setup was done according to the standard PCR pipetting sheme (Table 2.5). PCR cycling settings were 95°C, 5' – (94°C, 1' – 56°C, 1' – 72°C, 1') x 35 – 72°C, 7'.

A *lacZ* probe was provided, to control for expression of the gene trap cassette and to validate genotypes.

Gel-electrophoresis and gel-extraction

For selection and isolation of specifically amplified DNA sequences, gel-electrophoresis was performed as described before.

The amplified sequences were visualized after gel-electrophoresis using UV light. The respective bands were cut out of the agarose gel with a scalpel and collected separately in a 2ml Eppendorf tube. Isolation of specifically amplified DNA sequences was performed with the Gel Extraction Kit (Qiagen) according to the manufacturer's instructions. Briefly, 450µl of BQ buffer were added to the isolated agarose cube and dissolved at 50°C for 10'. 150µl of Isopropanol were added and the solution and mixed. Subsequently, the solution was loaded on a provided column and was centrifuged, before 500µl of BQ buffer were added to the column. After another round of centrifugation 750µl of PE buffer were added to the column and were incubated for 3' at RT. After incubation the column was centrifuged twice. For elution of the DNA, 50µl of H_2O were added to the column and it was again centrifuged. After isolation DNA yield and quality was controlled by optical density (OD) OD_{260} and OD_{260}/OD_{280} ratio.

All centrifugation steps were carried out for 1' at 13krpm and the flow-through was discarded. Except for the elution step, when flow-through, containing DNA was collected.

Transformation of chemically competent E.coli DH5α bacteria

LB^{+Amp} agar plates were prepared. Therefore 400ml of LB-Agar were boiled in the microwave (2' at 670W, short cool down, 7' at 270W). Agar was allowed to cool down to 50°C and 1ml of Ampicillin (50mg/µl) was added and agar was distributed to 6cm petri dishes. After cool down, petri dishes were sealed with parafilm and stored at 4°C.

Prior to plating of cells, petri dishes were prepared for blue/white-selection. Therefore 50µl of X-Gal and 50µl of IPTG were added to the petri dishes and were incubated at 37°C for 1h.

For amplification of the isolated sequence, TOPO-vector cloning was performed. "TOP10"-cells (chemically competent E.coli DH5α bacteria) were allowed to taw on ice. 4µl of TOPO-vector mix (see Table 2.6) were added to 100µl of bacteria, mixed cautiously and placed on ice for 30'. A heat shock was performed for 45" at 42°C for permeabilization of the plasma membrane. Subsequently, the reaction was stopped and bacteria were placed on ice for 1-2'. Bacteria were allowed to divide by

adding 50µl SOC Medium and by incubating for 1h at 37°C on a shaker, prior to plating on the prepared LB^{+Amp} agar plates. To obtain colonies for selection, plates were incubated at 37°C overnight.

Table 2.6: TOPO-vector mix composition.

TOPO-vector mix	
DNA product	1µl
Vector	1µl
Salt	1µl
H_2O	3µl

Amplification and isolation of plasmid DNA

For control and selection of correctly transformed plasmids, a positive (white) colony was picked from the agar plate and put into 3ml LB^{+Amp} medium at 37°C overnight. 2ml of the culture were transferred to a 2ml Eppendorf tube, while the remaining culture was kept at 4°C.

For isolation of the plasmid using the Plasmid MiniPrep Kit (Qiagen) the 2ml of culture were centrifuged at 13krpm, 10'. The supernatant was discarded and the pellet was used for plasmid isolation according to the manufacturer's instructions. Briefly, the pellet was resuspended in 250µl of P1 buffer by pipetting, 250µl of P2 buffer were added and the solution was mixed by inverting of the tube. After incubation for 5' at RT, 350µl of N3 buffer were added and the tube again inverted. After centrifugation for 10' at 13krpm, the supernatant was added to 600µl of Isopropanol and again centrifuged for 15' at 13krpm. For washing 1ml of 70% EtOH was added to the pellet. Subsequently to centrifugation for 10' at 13krpm, EtOH was discarded and the pellet was dried at RT in the inverted tube. The pellet was dissolved in 30µl H_2O or EB.

For further amplification and a higher yield of sequence verified plasmids, the remaining culture stored at 4°C was used for amplification of the plasmid and put to 250ml of LB^{+Amp} medium at 37°C overnight. Plasmid isolation from a high volume of culture was performed with the Plasmid Maxi-Prep Kit (Qiagen). The culture was transferred to centrifugation beakers, balanced and centrifuged in a 4°C pre-cooled GSA Rotor (5000rpm, 15'). The supernatant was discarded and the pellet either stored at -20°C or directly processed further. Therefore 10ml of P1 buffer was added and the pellet was resuspended. 10ml of P2 buffer were added, the solution was mixed and incubated for 5' at RT. 10ml of P3 buffer were added and the solution was incubated for 30' on ice. Subsequently the solution was transferred to a 50ml falcon tube and centrifuged for 20', 5krpm at 4°C. Filter columns were prepared and equilibrated with 10ml of QBT buffer per column. Filter hoppers and filter were put on top and the supernatant was added to the filter. After the supernatant passed the filter column, the column was washed twice with QB buffer. The plasmids were eluted from the column by adding 15ml QF buffer and were captured in a prepared 50ml falcon tube, containing 10.5ml Isopropanol. The solution was mixed thoroughly and centrifuged for 1h at 5000rpm and 4°C, the supernatant was discarded and the pellet was washed with 5ml 70%EtOH. After an additional round of centrifugation

(1h, 5000rpm, 4°C), EtOH was removed and the pellet was dried at RT. Finally the pellet was dissolved in 100µl H_2O or EB.

Concentration of isolated plasmid DNA was measured at 260nm and was checked for purity, by aiming for an optimal OD_{260}/OD_{280} ratio of 1.8. DNA was stored at 4°C until further processing.

Restriction digestion of plasmid DNA

For digestion of isolated plasmid DNA, a digestion mix was set up using EcoRI as restriction enzymes and Buffer H according to the manufacturer's instruction. The enzymatic digestion was performed at 37°C overnight.

Table 2.7: Digestion mix composition.

Digestion mix	
DNA plasmid	3µl
Buffer H	2µl
EcoRI	1µl
H_2O	14µl

2.2.10.2.5 Northern blot

20µg per RNA sample were mixed with 15µl of RNA loading dye and heated to 50°C for 30' before the samples were applied to a 1.2% formaldehyde- agarose (FA)-gel. Gel electrophoresis took place in FA-running buffer at 100V for 3h, with a change of buffer after half of the running time. RNA integrity was checked by visualization of the 18S and 28S band under UV light. The gel was washed in dH_2O and two changes of 10x SSC for 15' each. The RNA was blotted overnight on an Amersham HybondTM-N+ membrane using 10x SSC, subsequently UV-crosslinked and pre-hybridized in Church Buffer at 65°C for 1h, to prevent unspecific binding.

Probes were P^{32}-labeled using the Rediprime II random labeling System (Amersham). Therefore, 25ng of probe DNA was denatured by heating to 100°C for 5' in TE-buffer. Subsequently cooled on ice for 5' and added to the labeling system following the manufacturer's instructions. Labeled probes were diluted in Church Buffer to 1,500 counts/µl (*Sms1* probe) and 1,000 counts/µl (Gapdh probe). After blocking, the membrane was incubated with labeled cDNA-hybridization-probes at 65°C, overnight. Redundant radioactivity was removed by washing with 2x SSC (RT, 2x 10'), 2x SSC-1% SDS (RT, 10'), 1x SSC-1% SDS (65°C, 10'). Kodak X-ray films were applied overnight.

Band intensities were measured with ImageJ2x. Statistical analysis was performed using the two-tailed Student's T-test. Statistical significance was considered at * $p \leq 0.05$, ** $p \leq 0.01$ and *** $p \leq 0.001$

2.2.10.2.6 TaqMan assay

Generated cDNA (minimum n=3 per genotype, reverse transcribed from standardized RNA quantities) was analyzed in triplicates using specific primer and probe sets for each gene of interest (Table

2.3). Samples were analyzed via SDS 2.4, adjusted to β-*actin* expression and statistically validated by the $2^{-\Delta\Delta CT}$ method (Livak and Schmittgen 2001). Statistical analysis was performed using the two-tailed Student's T-test. Statistical significance was considered at * $p \leq 0.05$, **$p \leq 0.01$ and *** $p \leq 0.001$.

Table 2.8: TaqMan reaction mix and cycle settings for the TaqMan assay

TaqMan-reaction mix	
cDNA (30ng)	9µl
2x TaqMan® Universal Master Mix	9µl
20x TaqMan® Assay	1µl

Cycle settings – TaqMan assay		
95°C	10.0'	
95°C	15.0''	40x
60°C	1.0'	

2.2.10.2.7 Microarray and evaluation

Due to the expected and observed phenotype brain and testes samples were analyzed. Muscle tissue served as a control. Organs were collected from mice at the age of 17 weeks as described above. Microarrays were performed as part of the GMC pipelines. Briefly, total RNA was isolated (*Sms1* wild-type, n=6; and *Sms1* mutant, n=6) according to manufacturer's protocol using RNeasy Mini kits (Qiagen). RNA integrity was controlled on an FA-gel and concentration was calculated from $OD_{260/280}$ measurement. 500ng of high quality total RNA was amplified using the Illumina TotalPrep RNA Amplification kit (Ambion). The amplified cRNA was hybridised to MouseRef-8 v2 Expression BeadChips (Illumina, San Diego, CA, USA) and after 16h incubation, staining and scanning were done according to the Illumina expression protocol. For normalization of the data, we used the GenomeStudioV2011.1 software processing using the quantile normalization and background subtraction. The identification of significant gene regulation was performed by Dr. Dietrich Trümbach using SAM (Significant Analysis of Microarrays) included in the TM4 software package as described (Tusher *et al.* 2001). The selection of the top differentially expressed genes with reproducible up- or down-regulation includes about 5% false positives (false discovery range (FDR), estimated by calculation of 1000 permutations) in combination with fold change > 1.4. Array data are available in the GEO database (http://www.ncbi.nlm.nih.gov/geo/?roo=md) under GSE39585.

In addition to the univariate SAM method described above, Dr. Dietrich Trümbach performed Support Vector Machine with Recursive Feature Elimination (SVM-RFE) according to Augustin *et al.* (2011) and Zhou and Tuck (2007) on normalized microarray data of $Sms1^{MUT}$ and $Sms1^{WT}$ mice. The combination of univariate and multivariate analyses in this case SAM and SVM-RFE, respectively, allowed the comparison of the most discriminatory genes from both methods and to select overlapping genes (Soon *et al.* 2009). For SVM prediction the function svm from the e1071 package in R (http://www.r-project.org/) was used with default settings except the parameters type = 'C-classification', kernel = 'linear' and cost = 0.01. SVM-RFE algorithm grouped the samples of the microarray dataset ($Sms1^{WT}$, n=6; and $Sms1^{MUT}$, n=6) into stratified 5-folds and all combinations of 4-folds were used for mSVM-RFE. This grouping into folds was done ten times and SVM-RFE al-

gorithm was applied 50 times on different subsets of the original dataset. Finally, 50 different probe-set selections, each consisting of the best 500 probe-sets for classification according to the cost function of the SVM classifier, were obtained. The frequency of each probeset occurring in all the probeset selections was computed to identify the most important probesets.

Differentially expressed genes occurring in at least 5 probeset selections were functionally investigated for enrichment in Gene Ontology (GO) categories cellular component and biological process by the program Pathway Studio 9.0 (Elsevier). For calculation of p-values a Fisher's exact test was performed. Afterwards a FDR correction (Benjamini and Hochberg 1995) was applied by the R function p.adjust (with the parameter method="fdr").

2.2.11 Protein based methods

2.2.11.1 Protein Isolation standard procedure

Organ samples were manually homogenized using a glass pistil and ice cold RIPA-buffer with added Complete Protease Inhibitor Cocktail and Complete Phosphatease Inhibitor Cocktail (1 tablet each per 10ml of buffer, Roche). Depending on the amount of tissue 500µl to 1ml RIPA-buffer were used. Samples were incubated for 30' on ice, sonicated with 3 pulses and RIPA-buffer soluble and insoluble protein fractions were separated by centrifugation (15000g, 20', 4°C). The supernatant was separated from the pellet and both were stored at -80°C.

2.2.11.2 Protein Isolation for APP profiling

For immunoblotting of APP and cleavage products, brain, heart and lung protein was isolated subsequently with DEA-buffer and RIPA-buffer resulting in two fractions of soluble and membrane bound proteins. Protein isolation was performed in the lab of Dr. Michael Willem (LMU) with kind assistance.

1ml DEA-buffer was used per hemisphere of mouse brain for the homogenization. Homogenization was performed with potter and pistil (10 strokes per brain). The homogenized samples were transferred to a pre-cooled 1.5ml Eppendorf tube. Potter and pistil were cleaned with cold H2O each time before a new set of genotypes was handled. Samples were kept on ice during the homogenization procedure. DEA-buffer was used to dissolve and enrich extracellular APP cleavage products such as Aβ, sAPPβ or sAPPα. DEA-buffer dissolved samples were centrifuged (5000g, 10min, 4°C). 500µl of the supernatant, containing DEA-buffer soluble protein, was transferred to a new 1.5ml Ultracentrifuge Eppendorf tube, the remaining supernatant was discarded and the pellet was saved for RIPA-buffer protein isolation. The 500µl DEA-buffer soluble protein were again centrifuged (130000g, 60min, 4°C). 450µl of the supernatant were transferred to a new 1.5ml Eppendorf tube and 10% 0.5M Tris pH6.8 were added for neutralization. Neutralized DEA-buffer soluble protein was kept at –80°C until further processing.

The pellet obtained by ultracentrifugation of DEA-buffer soluble protein was also kept for the isolation of RIPA-buffer soluble protein.

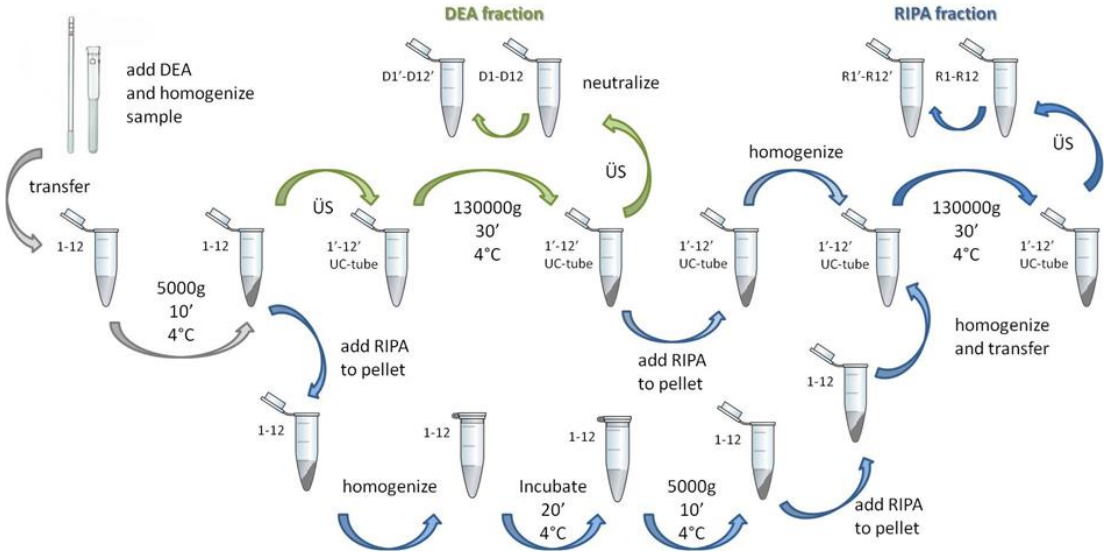

Figure 2.5: Illustration of DEA and RIPA based isolation procedure of APP and protein derivates for the analysis of APP processing
The steps highlighted in green were used to obtain the DEA-soluble protein fraction, while the steps highlighted in blue were used to obtain the RIPA-soluble protein fraction.

RIPA-buffer was used to disrupt the cells and obtain all cytoplasmic and membranous components such as full length APP, C99, C83 and AICD. 1ml of RIPA-buffer was added to the pellet, gained by the first centrifugation step and 100µl RIPA-buffer were added to the pellet obtained by the second ultracentrifugation step. Both pellets were resuspended with blue or yellow pipette tips, respectively. The first resuspended pellet was put on the shaker for 30min at 4°C for RIPA-buffer incubation and was subsequently centrifuged at 5000g for 10min at 4°C. Afterwards, 900µl of the supernatant was transferred to an ultracentrifuge Eppendorf tube. During that time, the second resuspended pellet was kept on ice and was now combined with the first sample in the ultracentrifugation Eppendorf tube. 500µl of combined pre-RIPA lysate was put for centrifugation (130000g, 60min, 4°C). The supernatant, containing RIPA-buffer soluble protein was taken off and stored at -80°C until further processing.

The pellets, remaining after isolation of RIPA-buffer soluble protein contained unsoluble and plaque associated APP derivates, which were kept at -80°C for further investigation.

40µl of neutralized DEA-buffer soluble protein and 40µl of RIPA-buffer soluble protein were used for BCA measurement as described below.

2.2.11.3 Protein quantification / BCA assay

Protein concentration was assessed by the bicinchoninic acid (BCA) Protein Assay Reagent (Thermo scientific) according to the manufacturer's instructions. Briefly, 25µl of BSA standards, ranging from

25µg/µl to 2mg/µl, and sample dilutions (1:10 up to 1:100, depending on the tissue) were applied to a 96 well flat bottom plate and incubated for 30' at 37°C with 200µl of BCA working reagent (CuSO4/bicinchoninic acid (1:50)) per well. Samples were analyzed in triplicates with three different dilutions, depending on tissue volume. Absorbance at 562nm was measured and samples concentrations were calculated in Excel depending on the standard curve results.

2.2.11.4 Westernblot standard procedure

RIPA-soluble protein samples were slowly thawed on ice and diluted in dH_2O to the desired concentration. 15µl (containing 10µg to 40µg) of diluted protein per sample were mixed with 5µl NuPAGE® LDS Sample Buffer (4x) and 0.2µl β-Mercaptoethanol for denaturation of the protein. To ensure denaturation, samples were additionally heated to 95°C for 3min, cooled down to RT and shortly vortexed, to abolish any concentration gradient.

For SDS-PAGE using the invitrogen blotting system 20µl of heated protein samples and 10µl of SeeBlue® Plus2 Pre-Stained Standard were applied to a NuPAGE® Novex Bis-Tris 4-12% (or 10%) Gel. Gelelectorphoresis was performed in 1 x NuPAGE® MES SDS Running Buffer for 1h at 200V. Proteins were transferred to PVDF membranes using Transfer Buffer (1 x NuPAGE® Transfer Buffer, 5% MeOH) for 1.5h at 30V.

For SDS-PAGE using the BioRad blotting system the same amount of protein samples and 10µl of Full Range Rainbow marker or AppliChem VI protein marker were applied to a 4-12% (or 10%) Bis-Tris Gel. Gelelectorphoresis was performed in 1 x MOPS Running Buffer for 1h at 200V. For protein transfer, two Whatmann paper were used below the gel and above the membrane, to ensure a tight packing for blotting. For the transfer PVDF membranes and Transfer Buffer (1 x_Tris-Glycin Buffer, 20% MeOH) were used. Blotting took place over night (~18h) at 20V and 4°C.

For both systems the following steps were the same. Unspecific binding of the primary antibody was prevented by blocking the membrane with 5% skim milk (in TBS-T (0.01% Tween 20)) for 1h at RT either in a 50ml falcon tube, or in an open box. Subsequently, the membrane was incubated with the primary antibody in a falcon tube (50ml) at the given dilution (see Table 2.1) at 4°C ON. After incubation with the first antibody the membrane was washed three times for 10' with TBS-T (0.01% Tween 20). The secondary antibody, was applied to the membrane (for dilutions see Table 2.1) for 1h at RT.

After three rounds of washing (TBS-T (0.01% Tween 20), 10') the membrane was developed using the ECL system. Briefly, the membrane was put between two layers of transparent film and covered with ECL (1:1 mixture, 1ml per 55cm^2). The membrane was incubated with ECL for 1min in the dark and subsequently chemoluminescent films were used for signal dectection. Exposure times were 3min, 1min and 30sec and were adjusted according to the detected signal. Films were developed with a developing machine.

Quantification of the protein signal intensities, was performed using ImageJ2x.

2.2.11.5 Westernblot APP profile

Western blots for the analysis of APP and its derivates were carried out at the LMU with friendly support of Dr. Michael Willem, similar to the above described standard procedure, with some alterations.

20µg of DEA or RIPA-soluble protein per sample was incubated together with with 5µl NuPAGE® LDS Sample Buffer (4x; Invitrogen) and 0.2µl β-Mercaptoethanol at 95°C for 3', to obtain denatured protein. Protein samples and 10µl of SeeBlue® Plus2 Pre-Stained Standard (Invitrogen) were applied in different lanes either to a Novex® 10-20% Tricine Protein Gel or to self-purred acrylamide-Gels (protein-gel combination see Table 2.9).

Gel electrophoresis was performed using Tris-Glycine running buffer for 1h at 100-120V, RT. Proteins were transferred to PVDF or Nitrocellulose membranes for 1.5h at 0.4A per gel, RT. The nitrocellulose membranes were heated in PBS for 2x2.5' at 900W using a microwave and were allowed to cool down between heating steps. Unspecific binding of antibodies was blocked by incubation of membranes with I-Block for 1h, RT. Membranes were subsequently incubated with primary antibodies, diluted in I-Block, at 4°C, overnight (for antibody specifications see Table 2.1). After washing with 0.05% PBS-T, the secondary antibody was applied to the membrane in a 1:10000 dilution for 1h, RT. After 3 x 10' in 0.05% PBS-T, the blot was developed using Hyperfilm ECL and the ECL detection reagents (Amersham).

Table 2.9: Gel antibody combinations used for analysis of the APP profile
Either 8% polyacrylamide gels (8%) or Bis-Tris gels (π) were used for size dependent separation of proteins. Antibody/gel combinations are listed and fragment detection info is shown.

DEA-buffer soluble protein

%-age of Gel	Antibody	Info
8%	22C11	sAPPα/β
8%	Aß-rod	Endogenous sAPPα, Aβ
8%	2D8	sAPPα, Aβ
8%	192wt	Endogenous APP full length
8%	192swe	Transgene APP full length
8%	10A8	sAPPα/β
π	2D8	sAPPα, Aβ
π	M3.2	Aβ

RIPA-buffer soluble protein

%-age of Gel	Antibody	Info
8%	22C11	APP full length
8%	AD10	ADAM10
8%	B1	BACE1
8%	5313	Transgene APP full length
π	APP-CTF	CTF
π	2C2	APP full length
π	A8718	CTF

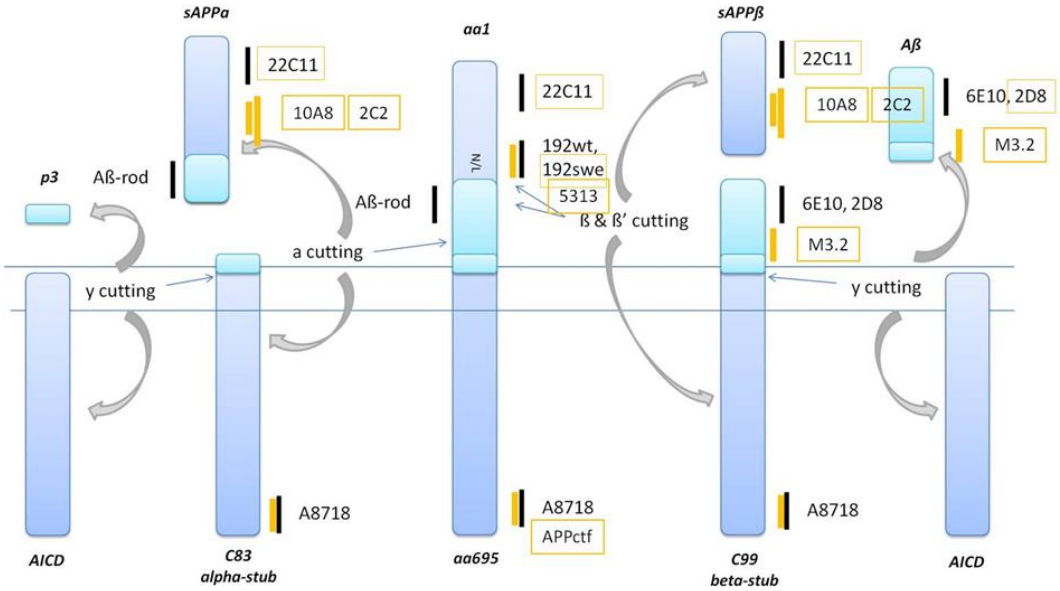

Figure 2.6: Illustraions of the antibody binding sites for the detection of APP expression and processing using western blot analysis
The dark blue column represents the APP and the light blue column the Aβ. α-, β- and γ-cutting sites are indicated.The black and yellow lines indicate the approximate binding sites of the used antibodies, allowing the recapitulation of cleavage and processing events of APP and APP derivates.

All incubation steps were performed in trays on a shaker. Quantification of the protein signal, was performed using ImageJ2x. Statistical analysis was performed using the one-way ANOVA with *post hoc* Tukey test. Statistical significance was considered at * $p \leq 0.05$, ** $p \leq 0.01$ and *** $p \leq 0.001$.

2.2.12 Staining procedures

Table 2.10: Immunohistochemistry protocol
Standard IHC steps are listed in white and gray, yellow boxes outline special treatment for the detection of APP and APP derivates, green boxes outline the treatment in cases when a secondary antibody of mouse orignin was used. Steps1-6 represent standard rehydration procedure and steps 25-29 standard dehydration procedure.

Solution	Percentage	Duration	Temperature
Xylol		30'	RT
EtOH	100%	Rinse thoroughly	RT
EtOH	96%	Rinse thoroughly	RT
EtOH	85%	Rinse thoroughly	RT
EtOH	70%	Rinse thoroughly	RT
VE H_2O		Rinse thoroughly	RT
Citrate Buffer pH6		30'	900W pressure cooker
TBS-T	0.05%	Rinse thoroughly	RT
Formic acid	70%	20'	RT
TBS-T	0.05%	Rinse thoroughly	RT
H_2O_2 + MeOH	3%	5'	RT
VE H_2O	0.05%	Rinse thoroughly	RT
Goat serum	3%	30'	RT
1ary AB		over night	4°C
TBS-T	0.05%	Rinse thoroughly	RT
2ary AB		30'	RT
TBS-T	0.05%	Rinse thoroughly	RT
Streptavidin peroxidase		30'	RT
TBS-T	0.05%	Rinse thoroughly	RT
Avidin-Block		15'	RT
TBS-T	0.05%	Rinse thoroughly	RT
Biotin-Block		15'	RT
TBS-T	0.05%	Rinse thoroughly	RT
DAB substrate		dependant on staining	RT
H2O		Rinse thoroughly	RT
VE H_2O		Rinse thoroughly	RT
EtOH	70%	Rinse thoroughly	RT
EtOH	85%	Rinse thoroughly	RT
EtOH	96%	Rinse thoroughly	RT
EtOH	100%	Rinse thoroughly	RT
Xylol		30'	RT

Formic acid treatment: used for APP, Aβ-40 and Aβ-41 antigen retrieval
Avidin/Biotin-Block: used if 2ary anit-mouse antibodies were applied

If not mentioned otherwise, paraffin embedded tissue sections were deparaffinized and hydrated as outlined in Table 2.10 steps 1-6 and subsequently to the staining procedure dehydrated and cleared

according to the final 6 steps of Table 2.10. Steps where the sections should be rinsed thoroughly could be replaced by incubation for 2-5' at RT.

2.2.12.1 Immunohistochemistry protocols

2.2.12.1.1 IHC / DAB staining

Standard immunohistochemical staining was performed according to Table 2.10. Briefly, slides were deparaffinized in Xylol and rehydrated in a decreasing EtOH row, sections were rinsed in VE H_2O to get rid of remaining EtOH and heat mediated antigen retrieval was performed in 1x sodium citrate buffer (pH6) at 900W for 30' in a pressure cooker. Slides were brought to RT in TBS-T (0.05% Tween-20). Peroxidase inactivation was performed with 3% H_2O_2 for 5'. Remaining MeOH was rinsed off in VE H2O. Unspecific antibody binding was blocked by incubation of slides in 3% goat serum for 30'. Slides were washed in TBS-T. Primary antibodies were diluted in antibody-dilution buffer (DCS) according to Table 2.1 and 200µl of the dilution were applied per slide. Sections were incubated with the primary antibody over night at 4°C. Slides were washed with TBS-T and secondary antibodies were applied in the listed dilutions (see Table 2.1) for 30'. Sections were washed in TBS-T and incubated with streptavidin-peroxidase for 30'. After washing in TBS-T, DAB working solution (1ml buffer, 40µl 3,3'-diaminobenzidine (DAB)) was added to the sections for 5'-10' dependent on strength of the staining. The reaction was stopped in tap H2O and slides were rinsed in VE H_2O prior to Haematoxylin counterstaining for 1.5' and blueing in running tap H_2O for 10'. Slides were rinsed in VE H_2O, dehydrated, cleared and covered with Pertex and a coverslip. Sections were dried over night at RT.

2.2.12.1.2 IHC / DAB staining anti-mouse

In case a secondary anti-mouse antibody was used IHC staning was performed with the usage of the M.O.M.™ Kit to prevent high background of anti-mouse secondary antibodies on mouse tisse.

Staining was done as recommended by the manufacturer. Therefore Mouse IgG Blocking reagent was used instead of normal goat serum. Additionally to blocking subsequent Avidin- and Biotin-Blocking was performed for 15' at RT. Antibodies were diluted in M.O.M.™ Kit protein concentrate and the M.O.M.™ Kit provided secondary antibody was used.

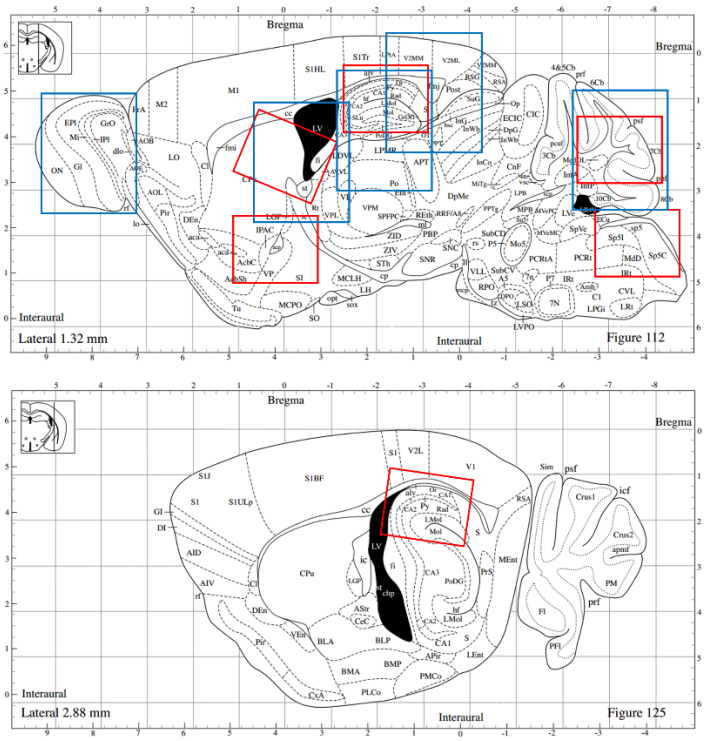

Figure 2.7: Imaging areas for visualization of lipidation and MBP expression
MBP expression, shown in Figure 3.11 D was visualized in areas highlighted by red boxes, and lipidation patern monitored by Klüver Barrera staining in Figure 3.11 A was visualized in areas highlighted in blue boxes.

2.2.12.1.3 APP, Aß40 and Aß42 immunostaining and plaque counting

Immunohistochemical staining was carried out on 8µm sections of paraffin-embedded tissues. Paraffin sections were rehydrated and subjected to heat-mediated antigen retrieval using 1x Citrate-Buffer pH6. For staining of APP, Aß40 or Aß42 antigen retrieval was additionally mediated by incubation with formic acid (70%, 20', RT; compare to Table 2.10). Endogenous peroxidase was inhibited with 3% H_2O_2 for 5', RT. The slides were incubated with blocking-solution (TBS-T (0.1%), 3% goat serum) for 30', RT. If secondary anit-mouse antibodies were used Avidin- and Biotin-blocking was performed for 15', RT, each. Primary antibodies or an antibody-complex were applied (for dilutions see Table 2.1; incubation was done over night, 4°C). Incubation with the secondary antibodies (for dilutions see Table 2.1; 30', RT) was followed by 30' incubation with Streptavidin Peroxidase and application of 3,3'-diaminobenzidine (DAB) as substrate. Haematoxylin was used for counterstaining. Between each step, despite after blocking, slides were washed in TBS-T (0.1%).

Plaques were counted on coronal brain sections between -1.06mm and -2.54mm from Bregma. An average of nine sections was counted per animal (*Sms1*^{WT} x *APPswe*^{Tg} n=3; *Sms1*^{MUT} x *APPswe*^{Tg} n=5) Data is shown as mean number of plaques per section ± SEM. Statistical analysis was done using the two-tailed Student's T-test. Statistical significance was considered at * $p \leq 0.05$, ** $p \leq 0.01$ and *** $p \leq 0.001$.

2.2.12.1.4 IHC / Fluorescent staining

Fluorescent staining was performed similar to DAB standard stainings, but without peroxidase inactivation (compare to Table 2.10). After incubation of the slides with the primary antibody over night, the sections were washed with TBS-T and subsequently incubated for 1h with the fluorescent labeled secondary antibody diluted in blocking solution (for dilutions used see Table 2.1). After incubation the antibody was washed off with TBS-T and sections were counter stained with DAPI. DAPI stainin solution was cleared from the slides with PBS and sections were covered with Aqua Polymount and coverslips, dried over night in a dark chamber and subsequently analyzed.

2.2.12.2 Haematoxylin & Eosin staining

H&E staining was carried out at RT. Slides were deparaffinized and rehydrated according to the standard procedure listed above (Table 2.10). Afterwards, slides were stained with Haematoxylin for 1.5', blued with running tap water for 10'. Slides were couterstained with 0.25% Eosin for 12', cleared in tap water and dehydrated according to the standard procedure listed above. Sections were covered with Pertex, covered with a coverglas and dried over night at RT.

2.2.12.3 Peridoic acid – Schiff's reagent staining

Periodic acid – Schiff's reagent (PAS) staining was carried out at RT using the Periodic Acid-Schiff (PAS) Kit (Sigma) according to the manufacturer's instructions. After deparaffinizing and rehydrating of the tissue sections (Table 2.10), slides were incubated with periodic acid solution for 5' and again cleared under running VE H_2O, before they were transferred to Schiff's reagent for 15'. Schiff's reagent was cleared from the slides in running tap H_2O for 5'. Heamatoxylin was used as a counterstain. Slides were incubated for 1', before blueing in tap H_2O. Sections were dehydrated and cleared as described for the standard procedure. Slides were covered with Pertex and a coverglas and dried over night at RT.

2.2.12.4 Klüver-Barrera staining

After deparaffination of the slides in Xylol for 30', slides were brought to 95% EtOH and stained in Luxol fast Blue (LFB) over night at 58°C. Slides were rinsed in 95% EtOH to remove excess stain and differentiated in lithium carbonate (0.1%) and 70% EtOH for 8s each. Differentiation was stopped in tap H_2O before counterstaining with cresyl-violet (0.1%) for 10' at RT and differentiation in 95% EtOH and 95% EtOH with 0.01% acidic acid for 15s each. Slides were covered with Pertex and coverslips and dried over night at RT.

2.2.12.5 TUNEL staining and counting of TUNEL positive cells

TUNEL staining was performed with the ApopTag® Peroxidase *In Situ* Apoptosis Detection Kit (Millipore, California) according to the manufacturer's instructions. Briefly, formalin fixed, paraffin embedded testes sections were deparaffinized and rehydrated according to the listed standard procedure (Table 2.10). Slides were put to PBS for 5' at RT, subsequently treated with Proteinase K

(20µg/ml) for 15' at RT and afterward washed in two changes of dH_2O to remove remaining Proteinase K. Following the pretreatment, endogenous peroxidase was quenched by incubating the sections with 3% H_2O_2 in PBS for 5' at RT. Remaining H_2O_2 was removed by washing in two changes of PBS. Equilibration buffer was applied (80µl/slide) for 1' at RT. Remaining liquid was taped off and working strength TdT enzyme (100µl/section) was applied. Sections were incubated for 1h at 37°C. After prolongation of single- and double-strand breaks the reaction was stopped by incubation with working strength stop/wash buffer for 10', RT. Subsequently slides were washed in three changes of PBS, before the anti-digoxigenin conjugate was applied (80µl/slide) for 30' at RT. Slides were washed again in four changes of PBS, remaining liquid was removed and the peroxidase substrate (80µl/slide, DCS, two component kit) was added to the sections for 10' RT. Sections were counterstained with Haematoxylin for 1.5', RT, blued, dehydrated and covered and analyzed by light microscopy.

TUNEL-positive cells in testes seminiferous tubules were counted in subsequent TUNEL stained sections, with an average of 435 tubules per animal counted. Data was listed as average number of TUNEL-positive cells per tubule ± SEM.

2.2.12.6 B-glactosidase staining

For lacZ staining embryos (E12.5) and adult brains were dissected as described (see section 2.2.16.1 and 2.2.7.3). Subsequently the tissue was post-fixed in 4% PFA over night at 4°C. Tissue was washed in LacZ-wash-buffer for 10' at RT in a 50ml falcon tube on a rotor. After washing the tissue was stained over night at 30°C using LacZ-staining-solution. LacZ staining was performed by Irina Rodionova.

2.2.13 Transmission electron microscopy

Animals (*Sms1*^{MUT} n=2, *Sms1*^{WT} n=2, age: 12 weeks) were transcardially perfused with 50ml ice cold PBS, prior to perfusion with 70ml of transmission electron microscopy (TEM) fixing solution. Brains or testes and epididymides were removed. Regions of interest were isolated and cut into 1mm3 cubes, which were post fixed in 2.5% glutaraldehyde containing 0.1M sodium cacodylate buffer (pH 7.4) at 4°C over night. Tissues were given to Dr. Michaela Aichler for further processing and subsequent imaging by TEM. Briefly, tissues were postfixed in 2% aqueous osmium tetraoxide (Dalton, 1955), dehydrated in gradual ethanol (30–100%) and propylene oxide, embedded in Epon and cured for 24 hours at 60°C. Cubes were cut into semi-thin sections and stained with toluidine blue. Ultrathin sections of 50 nm were collected onto 200 mesh copper grids, stained with uranyl acetate and lead citrate before examination by transmission electron microscopy (transmission electron microscope Zeiss Libra 120 Plus; Carl Zeis NTS GmbH; Oberkochen, Germany). Pictures were acquired using a Slow Scan CCD-camera and iTEM software (Olympus Soft Imaging Solution; Münster, Germany).

2.2.14 Multispectral optoacoustic tomography

Multispectral optoacoustic tomography (MSOT) was performed by Dr. Steven Ford and the experiment was approved by the TVA 55.2-1-54-2531-189-12. Therefore, animals were transferred to the Institute of Biological and Medical Imaging (IBMI), pla-ced under isoflurane anesthesia and imaged using a MSOT system described previously (Razansky *et al.* 2011). In brief, mice were shaved using depilation cream on the head and around the testes region for imaging. Animals were placed in a prone position in the MSOT imaging system. Ultrasound coupling gel and water were used to provide acoustically-matched coupling between the tissue and acoustic detector array. The animals were positioned in the detector array to provide tomographic slices in the region of interest (ROI; brain, testes). The tissue was illuminated over a range of wavelengths (700, 730, 760, 800, and 860 nm) and the resulting optoacoustic responses were used to reconstruct cross-sectional images through the testes using a back-projection algorithm (Kruger *et al.* 1995). During imaging, 2mg/kg bodyweight Indocyanine Green (ICG) was injected via the tail vein of each animal and serial multispectral images were acquired following injection. Finally, multispectral unmixing was done using linear regression (Laufer *et al.* 2007, Razansky *et al.* 2007) to derive the ICG absorbance signal. ROI analysis of the unmixed signal provided the quantitative time course of ICG distribution and clearance within the brain or testes with a time resolution of ~ 5 seconds. Quantification of the ICG absorbance signal was determined by taking the mean pixel intensity value of the ICG signal within specified regions of the brain or the inner region of the testes.

2.2.15 Lipid profiling and enzyme activity assay

Organ preparation for the generation of a lipid profile was performed as described above. Upon freezing in liquid nitrogen, samples were stored in the gas phase of liquid nitrogen and were shipped on dry ice to Homburg, University of Saarland. Here Prof. Dr. Tobias Hartmann and Dr. Marcus Grimm performed the further analysis, including lipid measurements and enzyme activity measurements in their lab. A brief summary of the applied methods is given below.

2.2.15.1 Protein Isolation and quantification

2.2.15.1.1 Testes preparation

Organs were dissected and homogenized in H_2O on ice using a PotterS (Braun, Melsungen, Germany) at 1500 revolutions per minute and 50 strokes. Homogenates were adjusted to Protein amount of 10mg/ml with H_2O, snapfrozen in liquid nitrogen and stored at -80°C for further experiments.

2.2.15.1.2 Protein amount determination

Protein determination was performed according to Smith *et al.* (1985). Briefly, we used a standard curve of bovine serum albumin with a concentration range of 0.1-1.2 µg/µl. 20µl of the standard solutions was pipetted onto a 96-well plate (Nunc, Langenselbold, Germany) and further 1-2µl of each sample was pipetted in triplicates onto the 96-well plate. 200µl reagent buffer, consisting of

$CuSO_4$/bicinchoninic acid (1:39; v/v) was added to each well using a multichannel pipette (Eppendorf, Germany). The plate was incubated for 15' at 37°C followed by incubation at RT for 15' while shaking (IKA, Staufen, Germany) at 300 revolutions per minute. Absorbance was measured using a MultiscanEX (Thermo Fisher Scientific, Schwerte, Germany) at a wavelength of 550nm.

2.2.15.2 Mass spectrometry

All measurements were performed using a 4000 quadrupole linear-ion trap (QTrap) mass spectrometer equipped with a Turbo Spray ion source (AB SCIEX, Darmstadt, Germany): The QTrap was connected to a Agilent Cap HPLC comprising of 1200 Capillary Pump, 1200 Micro Wellplate Sampler and 1200 Thermostat Module (Agilent, Böblingen, Germany). Data analysis was carried out using Analyst 1.5 software (AB SCIEX, Darmstadt, Germany). For determination of phosphatidylcholine, phospatidylcholine-plasmalogen, lyso-phosphatidylcholine, phospatidylethanolamine, sphingomyelin and ceramide levels 20µl sample was injected into sample loop with the following running solvent gradient (0.0 – 2.4min, 30µl; 2.4 – 3.0min, 200µl; 3.0min, 30µl). Mass spectrometry settings and composition of running solvents used is specified below.

2.2.15.2.1 Measurement of diacylphosphatidylcholine (PCaa), phospatidylcholine-plasmalogen (PCae), lyso-phosphatidylcholine (lysoPC) and sphingomyelin (SM) levels

Measurement was performed according to Grimm *et al.* (2011a). Briefly, 10µl of homogenates was applied onto a solvinert 96well plate with a 0.45µm sterile filter at the bottom (Millipore, Schwalbach, Germany). Samples were further incubated in a 5% phenylisothiocyanate solution diluted in C_2H_5OH/H_2O/pyridine (1:1:1; v/v/v) for 20'. Samples were extracted using 5mM ammonium acetate buffer (300µl) in methanol using a multichannel pipette (Eppendorf, Germany) into a 1ml 96well deep well plate (Nunc, Langenselbold, Germany) and further diluted with 600µl of 5mM ammonium acetate dissolved in CH_3OH/H_2O, which also served as the only running solvent.

2.2.15.2.2 Measurement of ceramide levels

Ceramide measurement was performed according to Gu *et al.* (1997). In brief, 50µl of each samples was mixed with 500µl CH_3OH/H_2O/12M HCl (95/5/0,5; v/v/v) and sonicated for 1' at 4°C. Mixture was shaken for 10' at RT at maximum speed (Multireax, Heidolph Instruments, Schwabach, Germany). After adding 300µl H_2O and 500µl $CHCl_3$ samples were shaken for another 10' at RT. Samples were centrifuges at 5000rpm for 10' and the lower phase was transferred to a new tube. 700µl $CHCl_3$ was added to the remaining two phases and mixture was shaken for 10' at RT at maximum speed. After another centrifugation step as described above, the two lipid containing phases were combined and dried in a vacuum concentrator. Finally, lipids were dissolved in 300µl $CHCl_3/CH_3OH$ (95/5; v/v) and transferred into a 96-deep well plate (Nunc, Langenselbold, Germany). Prior to injection the samples were diluted with 600µl 5mM ammonium acetate dissolved in

CH_3OH and shaken at 300rpm (IKA, Staufen, Germany) for 10'. The running solvent for ceramide analyses was composed of CH_3OH/ H_2O (97/3; v/v).

2.2.15.3 Enzyme activity assay

To assess enzyme activity solubilized membrane preparations were put on a black 96-well plate. The measurement was done in triplicates. For BACE1 activity the samples were diluted 1:1 with 1xPBS (pH 4.5). With the addition of the substrate, turnover was surveilled continuously in a fluorometer with precise emission- and extinction wavelengths and defined cycles (Table 2.11).

Table 2.11: Wavelength, cycle number and intervals for enzyme activity measurements.

Secretase	Extinction wavelength	Emission wavelength	Cycle number and intervall
BACE1	345 ± 5nm	500 ± 2.5nm	180, 60sec
γ-secretase	355 ± 10nm	440 ± 10nm	50, 180sec

To control for specificity of the turnover of each secretase, activity was also measured in the presence of specific inhibitors (for BACE1: 2µM β-secretase inhibitor II (Calbiochem), for γ-secretase: 50µM γ-secretase inhibitor X (Calbiochem)).

2.2.16 Cell culture experiments

2.2.16.1 Generation of mouse embryonic fibroblasts

Mouse embryonic fibroblasts (MEFs) were generated from E13.5 embryos. Therefore *Sms1* x *APPswe* mating were set up with *Sms1*^{HET} x *APPswe*^{Tg} males and *Sms1*^{HET} x *APPswe*^{WT} females. Females were controlled for plugs on the morning after the mating was set up and uteri were dissected 13 days afterwards. Embryos were removed from the uterus and washed in PBS before the heads were cut off and stored at 4°C for genotyping (see section 2.2.10.1 and 2.2.10.1.2). Heart, inner organs and blood vessels of the embryonic bodies were removed. The remaining epithelium was again washed in PBS, transferred to a new petri dish (6cm diameter) and cut into small pieces using scissors. 2ml Trypsin (0.05%) was added per petri dish and tissue was incubated for 5' at 37°C, 7% CO_2. Lysed tissue was additionally homogenized using a 1ml pipet tip and again incubated for 5' at 37°C, 7% CO_2, before it was transferred to a 15ml falcon tube and centrifuged for 4' 2500rpm. The supernatant was discarded and the cell pellet was dissolved in DMEM (10% FCS, 1% glutamine, 1% Pen/Strep). Cells were grown at 37°C, 7% CO_2.

2.2.16.2 Rapamycin treatment

For Rapamycin treatment MEFs (passage 2 or passage 4) were plated on 6-well or 12-well plates and grown in DMEM (10%FCS, 1%glutamin, 1%Pen/Strep) to be 90% confluent. Rapamycin (2.74nM) was diluted in DMEM (10%FCS, 1%glutamin) to obtain a working concentration of 10nM or 100nM Rapamycin. Additionally 42µl of DMSO, corresponding to the maximum value of DMSO diluted Rapamycin was diluted in DMEM (10%FCS, 1%glutamin). Medium was removed, cells were

washed with PBS and subsequently treated with either 200µl 10nM Rapamycin, 100nM Rapamycin, or DMSO only, as a control. MEFs were incubated for 4h or 8h at 37°C, 7% CO_2, to obtain concentration and time dependent results.

2.2.16.3 Protein Isolation from MEFs

After the incubation Rapamycin or DMSO solutions were removed and MEFs were covered with 200µl ice-cold RIPA buffer, put on ice and incubated for 20', while shaking. Subsequently, MEFs were transferred to 1.5ml Eppendorf tubes, vortexed and centrifuged (25', 4°C, 25krpm). The supernatant was removed and stored at -80°C until further processing.

2.2.17 Statistical evaluation

The exact number of animals used per experiment is either listed in the method section or with the respective table or figure illustrating the results of the experiment. Statistical analysis for the comparison of two groups was done by two-tailed Student's t-test. If three or more groups were compared one-way ANOVA was performed. *Post hoc* analysis, for correction of multiple testing after performance of ANOVA, was done either by application of Sidak or Tukey test, depending if a heteroscedastic or homoscedastic distribution could be assumed.

For statistical evaluation of the lipid profile all experiments were performed using at least five different animals per genotype and were analyzed in triplicates. Statistical analysis of the data of the *Sms1* mouse line was determined by two-tailed Student's t-test, while the data of the *Sms1* x *APPswe* mouse line was analyzed by one-way ANOVA with *post hoc* Tukey's test.

CORT data, obtained by SRT was analyzed separately for a treatment and genotype effect by two-way ANOVA. *Post hoc* analysis was done by Sidak for the treatment effect and with Tukey's test for the genotype effect, respectively. Behavioral data from the SRT was analyzed by two-way ANOVA with *post hoc* Sidak test per analyzed parameter.

Data on fertility in the *Sms1* mouse line after DHA/EPA feeding was analyzed by two-way ANOVA with *post hoc* analysis by Tukey's test. Data on weight gain in *Sms1* x *APPswe* animals was analyzed by two-tailed Student's t-test as only fed and non-fed groups per genotype were compared.

Behavioral data of the *Sms1* x *APPswe* mouse line was analyzed separately per parameter by one-way ANOVA and *post hoc* Tukey's test.

TaqMan assays were analyzed via SDS 2.4, adjusted to β-*actin* expression and statistically validated by the $2^{-\Delta\Delta CT}$ method (Livak and Schmittgen 2001). Statistical analysis for significance was performed using the two-tailed Student's t-test.

Statistical significance was set at $^{\#}$ $p < 0.1$, * $p \leq 0.05$, **$p \leq 0.01$ and *** $p \leq 0.001$ and $^{n.s.}$ $p > 0.1$ as not significant.

3. Results

3.1 *Sms1* gene trap model

3.1.1 Validation of insert localization

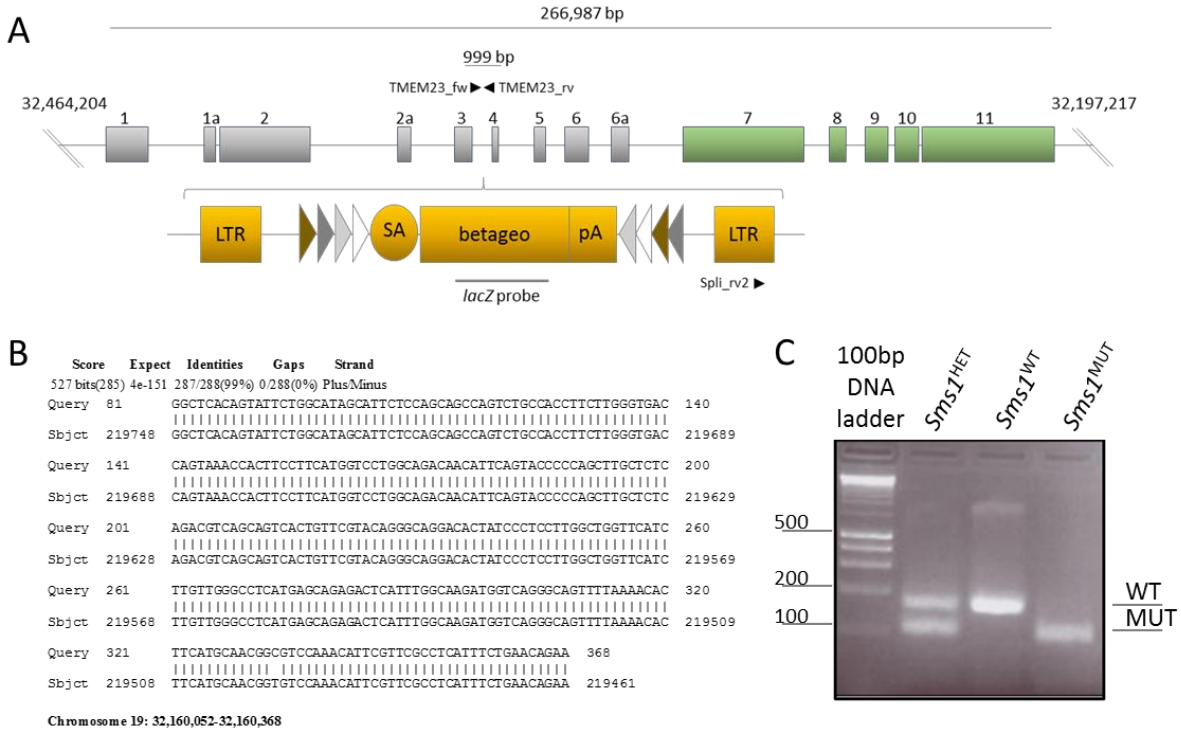

Figure 3.1: The gene trap β-galactosidase cassette construct is located in intron five of the *Sms1* gene. (A) Schematic drawing of the mouse *Sms1* gene on chromosome 19. *Sms1* has 267 kbp and 14 exons. It is located on the reverse strand. Exons are shown as boxes, non-coding exons are marked in gray, coding exons are marked in green. The gene trap β-galactosidase (betageo) cassette is integrated in intron five and is composed of a splice adapter (SA), the beta-galactosidase cDNA sequence (betageo) and a polyA (pA) signal. The cassette is flanked by two long terminal repeats (LTRs), frt (olive green), flip (dark grey), loxP (light grey), and lox511 (white) sites. (B) Sequence alignment mapping the gene trap insertion to intron five of the *Sms1* gene. (C) DNA-gel-electrophoresis, showing genotyping results after PCR with specific primer sets (shown in (A)) for $Sms1^{WT}$, $Sms1^{HET}$ and $Sms1^{MUT}$ animals.

The *Sms1* gene trap model was created by random insertion of a gene trap cassette (Figure 3.1 A) into the mouse genome (Schnutgen *et al.* 2005). The gene trap clone (MGI: $Sms1^{Gt(E201D11)Wrst}$; Figure 3.1 A), which was the origin of the *Sms1* mouse line, listed the insertion in exon three. Genotyping primers were provided (Table 2.2). In order to validate the localization of the gene trap cassette the genotyping PCR products were sequenced and the cassette was found to positioned in intron number five (Figure 3.1 A, B).

Genotyping of the mice was performed by triplet-PCR on genomic tail tip DNA. PCR results as depicted in Figure 3.1 C show the homozygous wild-type band (999bp; $Sms1^{WT}$), the homozygous mutant band (577bp; $Sms1^{MUT}$) and the heterozygous bands for animals bearing one wild-type and one mutant allele of the *Sms1* gene (999bp plus 577bp; $Sms1^{HET}$).

3.1.2 The *Sms1* gene trap mouse model showed remaining expression of *Sms1* and brain specific splice variants

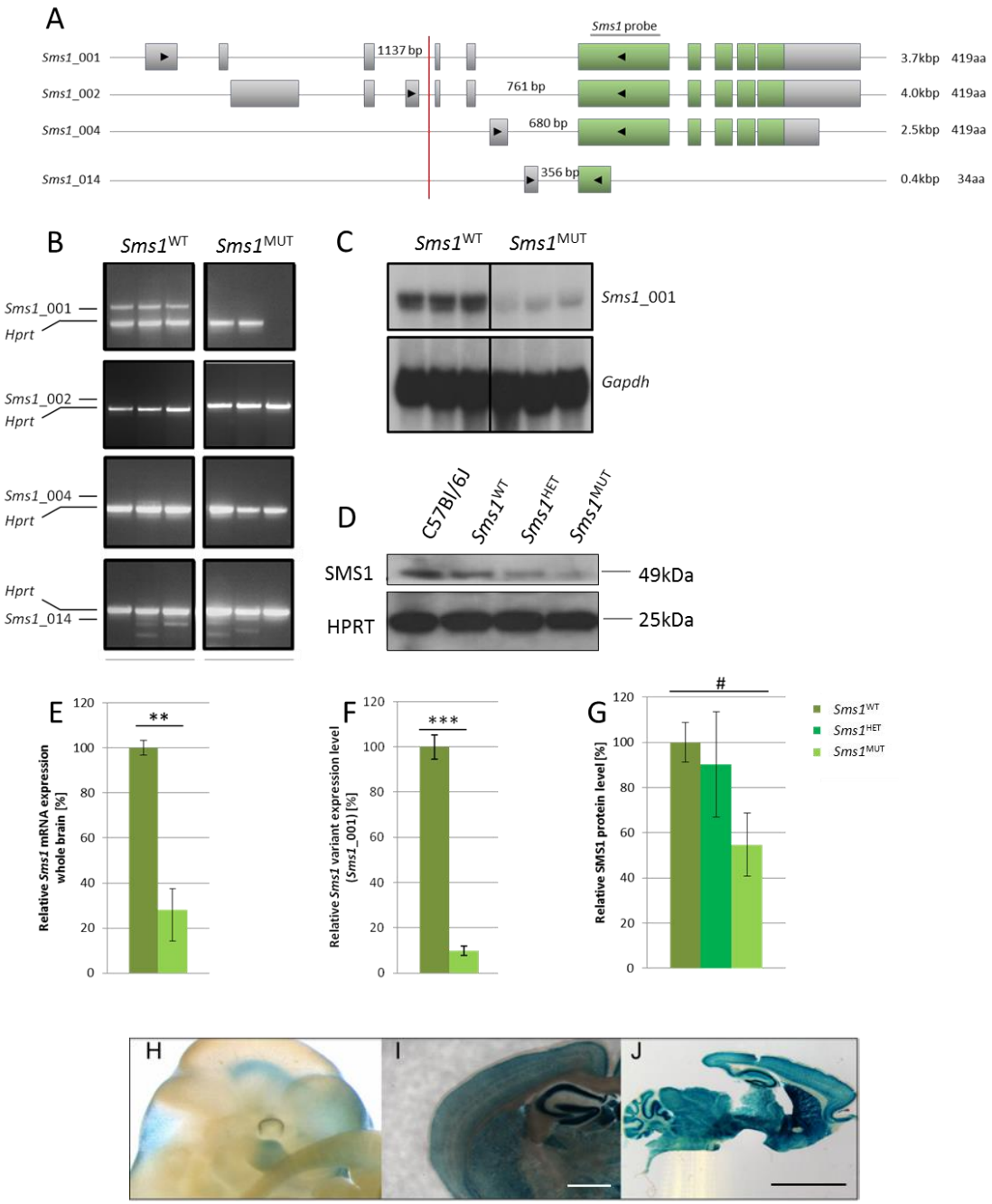

Figure 3.2: *Sms1* showed remaining RNA and protein expression. The *Sms1_001* splice variant was the only *Sms1* variant expressed in brain tissue and was reduced in *Sms1*^{MUT} animals.

(A) Schematic drawing of the four protein coding splice variants of *Sms1*. Exons are depicted as green boxes and introns as connecting lines. Primer pair localizations (black arrowheads) and *Sms1* probe localization on the first coding exon (gray line) are shown. The gene trap cassette insertion is marked by a red line. (B) RT-PCR results of the analysis of *Sms1* splice variants expressed in *Sms1*^{WT} and *Sms1*^{MUT} brain tissue, with specific primer pairs for the four protein coding transcripts. (C) Northern blot on *Sms1*^{WT} and *Sms1*^{MUT} whole brain RNA with specific probes for *Sms1* and *Gapdh*. (D) Representative Western blot results for remaining SMS1 protein expression of C57bl/6J, *Sms1*^{WT}, *Sms1*^{HET} and *Sms1*^{MUT} brain samples. (E) *Sms1* mRNA expression analyzed by TaqMan assay with a specific primer probe set on whole brain samples from *Sms1*^{WT} (n=3) and *Sms1*^{MUT} (n=4) animals, relative to *Sms1*^{WT} levels, which were set to 100%. (F) Quantification of Northern blot results for *Sms1_001* splice variant

levels in brain tissue from *Sms1*^{MUT} (n=3) animals, compared to levels of *Sms1*^{WT} (n=3) animals, which were set to 100%. (G) Quantification of SMS1 protein levels (n=3 per genotype), relative to *Sms1*^{WT} levels, which were set to 100%. (H-J) β-galactosidase staining of *Sms1* in (H) embryonic (E12.5) and (I, J) adult brain of *Sms1*^{MUT} animals (photo: Dr. Thomas Floss). Scale bar (I) 1mm and (J) 5mm. Data was analyzed by two-tailed Student's T-test (E, F) and one-way ANOVA with *post hoc* Tukey's test (G). Data is shown as mean ± SEM. p≤0.1$^{\#}$, p≤0.05*, p≤0.01**, p≤0.001***.

The intronic insertion was located upstream of the first coding exon of *Sms1*. Therefore the open reading frame, starting with exon 7 (Figure 3.1 A, green bars) was not directly affected by the gene trap cassette insertion. To validate the disruption of the gene and to quantify *Sms1* expression, qPCR, taking advantage of specific TaqMan primer probe sets (Table 2.3), was performed. Results from mRNA isolated from whole brains of *Sms1*^{WT} and *Sms1*^{MUT} male animals, showed a significant reduction in *Sms1* expression to 28.1 ± 9.2% of the wild-type level (100 ± 3.2%; p=0.003; Figure 3.2 E).

Sms1 is widely expressed and found in diverse organs and tissues (Yang *et al.* 2005). The aim was to clarify which of these variants is the most abundant in brain and if the remaining expression was due to "leakiness" of the gene trap construct, or if an additional promoter located downstream of the insertion site could be the reason for the remaining 28% of *Sms1* mRNA we measured. Therefore a RT-PCR on brain mRNA (converted into cDNA) was performed. Figure 3.2 A shows the diverse protein coding splice variants, which were investigated, including the primer localizations for the different mRNA variants and size of the RT-PCR products. In *Sms1*^{WT} brain samples only the *Sms1*_001 transcript was found to be expressed, while *Sms1*_002, _004 and the shorter _014 product could not be detected (Figure 3.2 B). In *Sms1*^{MUT} samples the *Sms1*_001 product was not detected, showing a disruption of *Sms1* gene expression, due to the gene trap cassette insertion in intron 5 (Figure 3.2 B). As RT-PCR is not suitable for quantitative analysis of RNA expression a Northern blot on *Sms1*^{WT} and *Sms1*^{MUT} whole brain RNA samples was performed additionally. By Northern blot just the *Sms1*_001 transcript and none of the other protein coding mRNA variants was detected, validating the results obtained by RT-PCR (Figure 3.2 B, C). It could clearly be seen, that in *Sms1*^{MUT} samples the *Sms1*_001 variant was expressed at a lower level compared to *Sms1*^{WT} samples. Quantification revealed a 90.2 ± 2.0% reduction of the *Sms1*_001 transcript relative to the wild-type expression levels (Figure 3.2 F).

Discrepancy between remaining mRNA expression of 28% in TaqMan assay and 9.8% in Northern blot, is due to hybridization site of the TaqMan primer probe set (spanning exon 7 to 8; Table 2.3). Due to this localization the TaqMan assay also detects other splice variants additionally to *Sms1*_001. Due to their smaller size, these were not be detected by Northern blot. The smaller variants are supposed to be subject of nonsense-mediated decay (NMD) and are not translated into protein.

SMS1 protein levels were reduced to 54.7 ± 14.1% in *Sms1*^{MUT} compared to *Sms1*^{WT} levels (p=0.0800). *Sms1*^{HET} animals did not differ significantly from *Sms1*^{WT} animals concerning SMS1 levels (Figure 3.2 D, G).

B-galactosidase staining of embryonic and adult brains of *Sms1*^{MUT} animals showed a strong expression throughout the brain tissue, starting already at embryonic stages (E12.5; Figure 3.2 H-J).

In summary, *Sms1* was expressed ubiquitously in the brain of embryonic and adult mice. *Sms1* disruption by insertion of the gene trap cassette led to a reduction in *Sms1* mRNA and protein levels of the brain, but did not cause a complete knock-out.

3.1.3 *Sms1*^{MUT} animals appear normal in most instances

Sms1^{MUT} animals appeared normal in size, and development and without crucial behavioral alterations, despite a subtle reduced anxiety-like behavior, when observed in their home cage. Furthermore a slight reduction in body weight was observed in *Sms1*^{MUT} and *Sms1*^{HET} animals in comparison to *Sms1*^{WT} animals. These reductions were not fully persistent at different ages of the animals and were dependent on sex. However, mean body weights never exceeded *Sms1*^{WT} levels (Figure 3.3)

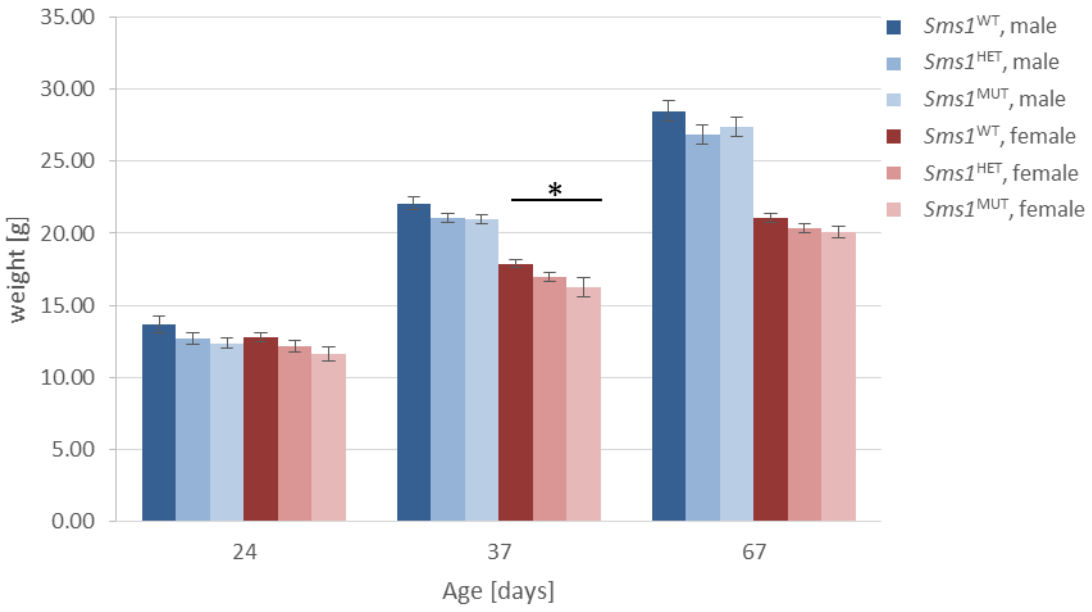

Figure 3.3: *Sms1*^{HET} and *Sms1*^{MUT} tended to have a reduced body weight, depending on age.
Body weight was measured in *Sms1*^{WT}, *Sms1*^{HET} and *Sms1*^{MUT} animals of both sexes at different time points. Body weight [g] at the corresponding age [days] is shown. Males: *Sms1*^{WT} (n=18), *Sms1*^{HET} (n=33), *Sms1*^{MUT} (n=14); females: *Sms1*^{WT} (n=22), *Sms1*^{HET} (n=23), *Sms1*^{MUT} (n=13). Data was analyzed by one-way ANOVA with *post hoc* Tukey's test. Data is shown as mean ± SEM. p≤0.1#, p≤0.05*, p≤0.01**, p≤0.001***.

3.1.4 *Sms1*^{MUT} animals show slight alterations in heart an spleen

At the age of 16 weeks organ weights were measured in the GMC. *Sms1*^{MUT} males had a reduced median liver weight in relationship to body weight, in comparison to male *Sms1*^{WT} controls (*Sms1*^{WT}: 49.98 mg/g (IQR: 2.17), *Sms1*^{MUT}: 47.24 mg/g (IQR: 5.09), p=0.026; supplementary Table 10.1). In female *Sms1*^{MUT} liver weights relative to body weight were higher in comparison to *Sms1*^{WT} controls (*Sms1*^{WT}: 49.44 mg/g (IQR: 2.65), *Sms1*^{MUT}: 51.63 mg/g (IQR: 0.85); supplementary Table 10.1). Heart weights relative to body weight were increased in *Sms1*^{MUT} of both sexes (*Sms1*^{WT} males: 5.16 mg/g (IQR: 0.10), *Sms1*^{MUT} males: 5.34 mg/g (IQR: 0.04); *Sms1*^{WT} females: 5.08 mg/g (IQR: 0.40), *Sms1*^{MUT} females: 5.54 mg/g (IQR: 0.32); p=0.029; supplementary Table 10.1). Additionally in males the diastolic posterior wall width of the heart was reduced to 0.69mm (IQR: 0.05) in comparison to *Sms1*^{WT} males with a median thickness of 0.78mm (IQR: 0.05: supplementary Table 10.2).

Median spleen weights relative to body weight were also increased in male and female *Sms1*^{MUT} at an age of 16 weeks, in comparison to *Sms1*^{WT} controls, but reached a trend in males only (*Sms1*^{WT} males: 3.38 mg/g (IQR:0.20), *Sms1*^{MUT} males: 3.77 mg/g (IQR: 1.04), p=0.699; *Sms1*^{WT} females: 2.54 mg/g (IQR: 0.65), *Sms1*^{MUT} females: 3.29 mg/g (IQR: 1.1), p=0.093; supplementary Table 10.1).

3.1.5 Lipid profile

3.1.5.1 Sphingomyelin species

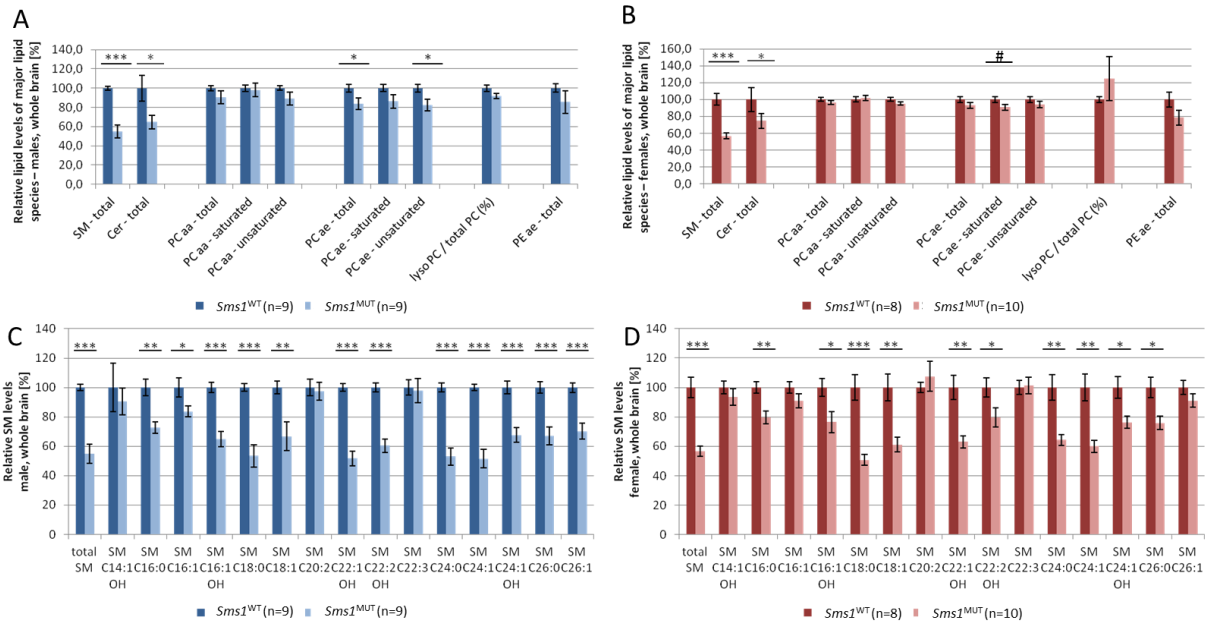

Figure 3.4: Lipid levels of the most important sphingolipids, metabolites and sphingomyelin measured in brain samples from male and female *Sms1*^{MUT} in comparison to *Sms1*^{WT} animals.
(A) Relative lipid levels of male *Sms1*^{WT} (n=9) and *Sms1*^{MUT} (n=9) brain samples. (B) Relative lipid levels of female *Sms1*^{WT} (n=8) and *Sms1*^{MUT} (n=10) brain samples. (C) Relative SM levels of male *Sms1*^{WT} (n=9) and *Sms1*^{MUT} (n=9) brain samples. (D) Relative SM levels of female *Sms1*^{WT} (n=8) and *Sms1*^{MUT} (n=10) brain samples. Sphingomyelin (SM), ceramide (Cer), diacyl-phosphatidylcholin (PCaa), phosphatidylcholine plasmalogene (PCae), phosphatidylcholin (PC), phosphatidylethanolamine (PE). Data was analyzed by two-tailed Student's T-test. Data is shown as mean ± SEM. $p<0.01^{\#}$ $p\leq0.05$*, $p\leq0.01$**, $p\leq0.001$***.

To analyze the functional consequences of the *Sms1* disruption, several lipid species of the SL pathway were quantified with the help of Prof. Dr. Tobias Hartmann and Dr. Marcus Grimm. It should be analyzed which amount of SM is still produced, which levels of the direct substrates of SMS1 can be found and if the production of closely related SL species is affected.

SM itself was significantly reduced to 54.9 ± 6.6% ($p<0.0001$) in male and to 56.7 ± 3.4% ($p=0.0002$) in female brain tissue. Concerning total SM levels, it seemed that male animals were slightly more affected than females (Figure 3.4 A, B). The remaining SM detected might either arise from SMS2 activity, which is not disrupted in our model, or from leaky SMS1 expression, which was shown to be at 55% (Figure 3.2 D, G).

The analysis of the different SM species showed, that most of them were affected by the *Sms1* disruption. Exceptions were SM C14:1 OH, SM C20:2 and SM C22:3, which were neither reduced in males, nor in females (Figure 3.4 C, D). However, analysis of the sex difference showed that these three SM

species were the only ones regulated between males and females with lower levels in males compared to their female counterparts (supplementary Table 10.9).

SM species with the most prominent reduction in *Sms1*^{MUT} compared to *Sms1*^{WT} animals included SM C18:0 (53.5 ± 7.6%, p<0.0001; 50.7 ± 3.7%, p=0.0004), SM C18:1 (66.7 ± 9.8%, p=0.0068; 61.1 ± 5.1%, p=0.0030), SM C24:0 (53.0 ± 5.8%, p<0.0001; 64.4 ± 3.8%, p=0.0041) and SM C24:1 (51.6 ± 6.4%, p<0.0001; 60.0 ± 4.1%, p=0.0024) which were amongst the five most reduced SM species in males and females, respectively. In male mutants additionally SM C22:1 OH (51.7 ± 5.1%, p<0.0001) was found to be the second most regulated species right after SM C24:1. Concerning the saturation state of SM species, the saturated SM species tended to be more strongly reduced than their unsaturated versions. This effect got lost with increasing FA chain length, especially in male *Sms1*^{MUT} compared to male *Sms1*^{WT} animals. The LC SM species were stronger reduced in *Sms1*^{MUT} males, compared to female *Sms1*^{MUT} animals (Figure 3.4 C, D).

Overall, the insertion of the *Sms1* gene trap cassette and the resulting reduction in SMS1 protein led to reduced levels of SM of 56%, with a strong reduction in C18:0, C18:1, C24:0 and C24:1.

3.1.5.2 Ceramide

With the reduction in SM levels, it would be expected to see an increase in total Ceramide levels, as the missing turnover of this substrate should result in its accumulation. However, Ceramide levels were not increased in *Sms1*^{MUT} compared to *Sms1*^{WT} animals, but rather showed decreased levels. The reduction of Ceramide was between 64.7 ± 6.8% (p=0.0124) and 74.6 ± 8.8% (p=0.0416) in males and females, respectively. Here again, the effect of *Sms1* disruption was more pronounced in males, than in females (Figure 3.4 A, B).

3.1.5.3 Phosphatidylcholines and Plasmalogens

Besides Ceramide, PC is the second substrate for the synthesis of SM (Huitema *et al.* 2004, Tafesse *et al.* 2006), therefore the content of PCaa and PCae species in brain tissue of *Sms1*^{WT} and *Sms1*^{MUT} animals was analyzed. The total amount of PCaa was not changed in either sex. Analysis of PCaa saturation levels between *Sms1*^{MUT} and *Sms1*^{WT} samples, however, showed a slight but not significant reduction in unsaturated species, which was again more pronounced in males, than in females (Figure 3.4 A, B).

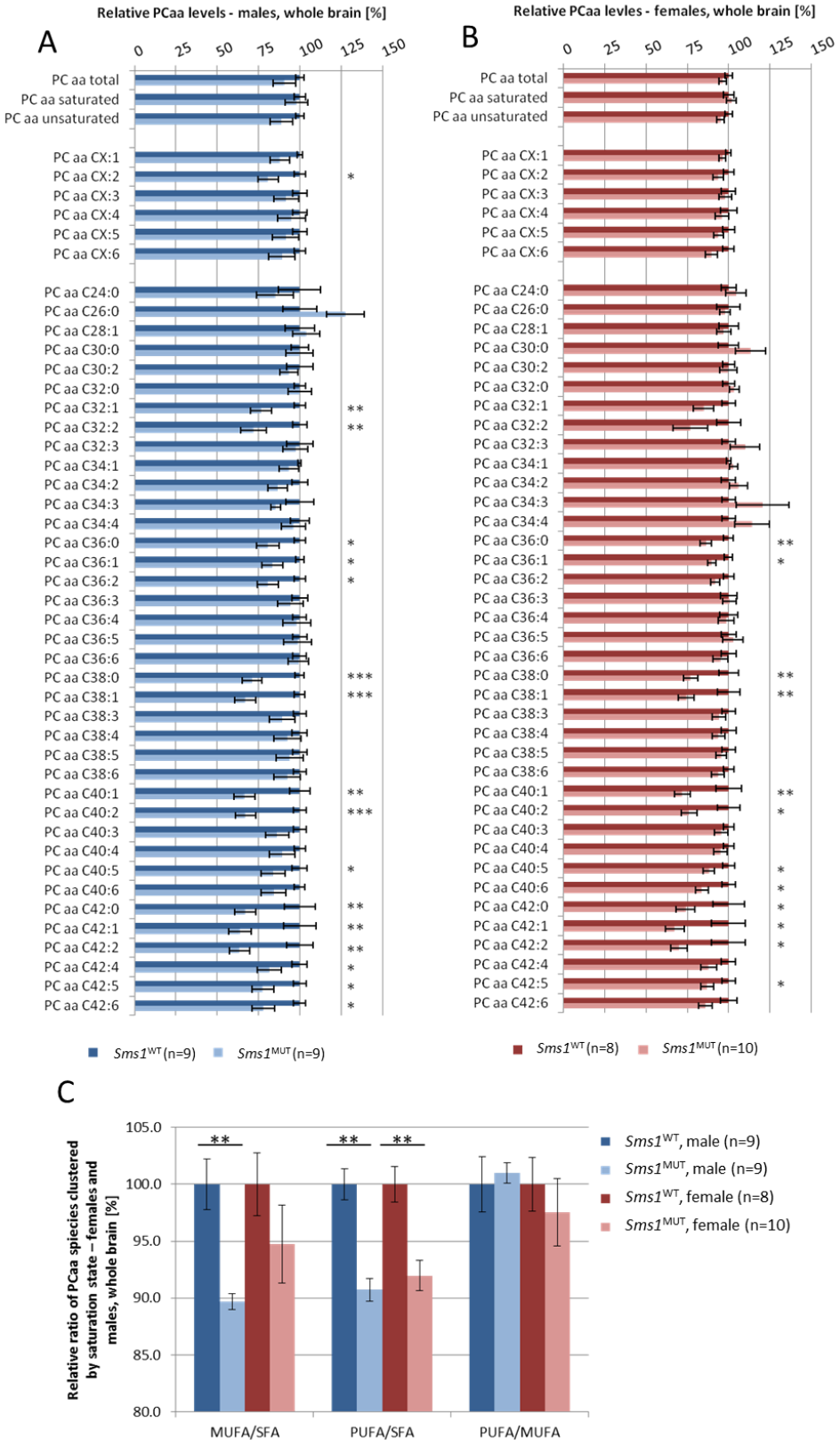

Figure 3.5: Levels of diacyl-phosphatidylcholine species, measured in brain samples from male and female *Sms1*^{MUT} in comparison to *Sms1*^{WT} animals.

(A) Relative PCaa levels of male *Sms1*^{WT} (n=9) and *Sms1*^{MUT} (n=9) brain samples. (B) Relative PCaa levels of female *Sms1*^{WT} (n=8) and *Sms1*^{MUT} (n=10) brain samples. (C) Relative ratio of PCaa species of male and female brain samples clustered by saturation state.
Diacyl-phosphatidylcholin (PCaa), mono-unsaturated fatty acid (MUFA), poly-unsaturated fatty acid (PUFA), saturated fatty acid (SFA). Data was analyzed by two-tailed Student's T-test. Data is shown as mean ± SEM. p≤0.05*, p≤0.01**, p≤0.001***.

PCae levels in female *Sms1*^{MUT} mice were not significantly changed. Nevertheless, there was a tendency (p=0.0752) to reduced saturated PCae levels (90.7 ± 3.3%; Figure 3.4 B). In contrast, unsaturated PCae in male *Sms1*^{MUT} animals were significantly reduced by 17.5 ±5.9% (p=0.0267) compared to *Sms1*^{WT} levels, leading to an overall reduction in PCae content to 83.8 ± 6.3% in male *Sms1*^{MUT} brain samples (Figure 3.4 A).

Although there were no or just marginal changes in total PC content between *Sms1*^{WT} and *Sms1*^{MUT} animals, the single PCaa and PCae species revealed some alterations.

In both sexes there were no alterations in PCaa C24:0 to PCaa C32:0 levels, but with increasing FA chain length the PCaa profile of the *Sms1*^{MUT} started to differ more from that of the *Sms1*^{WT} animals. In males PCaa C32:1 and PCaa C32:2 were reduced to 76.5 ± 6.5% (p=0.0057) and 72.0 ± 7.8% (p=0.0065), respectively. A similar alteration could be seen for the C36 containing PCaa species (PCaa C36:1 with 83.4 ± 6.6%, p=0.0306; PCaa C36:2 with 80.6 ± 6.5%, p=0.0175). Here the fully saturated PCaa C36:0 content was also reduced in *Sms1*^{MUT} compared to wild-type animals (80.6 ± 6.7% (p=0.0196). PCaa C38 showed a reduction in saturated and monounsaturated (PCaa C38:0, 71.2 ± 6.0, p=0.0005; PCaa C38:1, 67.1 ± 6.4, p=0.0003), but like observed in PCaa C32 and C36, no alterations in highly unsaturated FA carrying species. PCaa C40 species also followed this pattern. PCaa C40:1 and PCaa C40:2 were reduced to 66.6 ± 6.3% (p=0.0015) and 67.1 ± 6.2% (p=0.0004), respectively, while PCaa C40:3 to PCaa C40:6 did not differ significantly between *Sms1*^{MUT} and *Sms1*^{WT} male brain samples. This pattern changed with PCaa species of a total carbon chain length of 42. Here an overall reduction in PCaa C42 species was found. Nevertheless, the reduction was more pronounced in saturated to di-unsaturated PCaa C42 (PCaa C42:0, 66.9 ± 6.3%, p=0.0095; PCaa C42:1, 63.6 ± 6.8%, p=0.0077; PCaa C42:2, 63.4 ± 6.2%, p=0.0021) than in PCaa C42:4 (81.6 ±7.2%, p=0.0465) to PCaa C42:6 (77.8 ± 6.8%, p=0.0109; Figure 3.5 A).

As seen before, female changes were more subtle than those observed in males. Female *Sms1*^{MUT} did not show any alterations in PCaa levels, with a total carbon chain length shorter than 36. Similar to male mutants, they showed reduced levels of PCaa C36:0 (86.2 ± 3.4%, p=0.0076), PCaa C36:1 (89.6 ± 2.6%, p=0.0107), PCaa C38:0 (77.0 ± 4.4%, p=0.0086) and PCaa C38:1 (74.3 ± 4.7%, p=0.0078). No alterations in PCaa C38:2 levels in female *Sms1*^{MUT} compared to *Sms1*^{WT} animals were found. However, PCaa C40:1 and PCaa C40:2 were reduced to 72.0 ± 5.0% (p=0.0093) and 76.0 ± 4.9% (p=0.0122), respectively which revealed a similar, but again less pronounced down-regulation in

female *Sms1*^{MUT} animals, with respect to their male counterparts. Also in females, the long-chain PCaa C42 species showed the strongest alterations ranging from 67.4 ± 5.7% (p=0.0176) of PCaa C42:1 to 87.0 ± 3.9% (p=0.0390) of PCaa C42:5. In contrast to male brain samples, no significant alterations in PCaa C42:4 and PCaa C42:6 levels were found. The only PCaa species, which were significantly reduced in females only were PCaa C40:5 and PCaa C40:6. These sphingolipids were reduced by 12.0 ± 3.4% (p=0.0253) and 16.2 ± 3.8% (p=0.0110), respectively (Figure 3.5 B).

Analysis of PCaa subtypes revealed a more pronounced down-regulation of saturated and mono- or di-unsaturated than of poly-unsaturated species. To investigate this topic further, the ratios between saturation types were calculated.

Ratios revealed a reduction in mono-unsaturated fatty acids (MUFAs) and poly-unsaturated fatty acids (PUFAs) in comparison to saturated fatty acids (SFAs). Characterization of these ratios in the different sexes, showed that males exhibit again the stronger phenotype compared to females. In more detail, MUFA/SFA ratio in *Sms1*^{MUT} females was reduced by 5.2 ± 3.4% (p=0.2491) without reaching a significant difference to *Sms1*^{WT} levels. In *Sms1*^{MUT} males the MUFA/SFA ratio was significantly reduced with a value of 94.8 ± 0.7% (p=0.0012). In both sexes the ratio between PUFAs and SFAs was reduced in *Sms1*^{MUT} animals. Female *Sms1*^{MUT} reached only 92.0 ± 1.3% (p=0.0014) and male *Sms1*^{MUT} 90.7 ± 1.0% (p=0.0077) of the respective *Sms1*^{WT} values. The PUFA/MUFA ratio was not changed in *Sms1*^{MUT} compared to *Sms1*^{WT} animals (Figure 3.5 C).

A second class of PCs is made up by plasmalogens (PCae), which differ from diacyl-phosphatidylcholines by the addition of their FA chain at sn-1 position via a vinyl-ether-bond instead of an ester bond.

The levels of several PCae species in *Sms1*^{MUT} male brain samples were reduced. Among these were PCae C34:2, with a value of 78.0 ± 5.2% (p=0.0041) followed by PCae C36:1 to PCae C36:3 (78.5 ± 5.0%, p=0.0059; 74.3 ± 4.3%, p=0.0015; 79.0 ± 5.0%, p=0.0092). PCae C38, PCae C40 and PCae C42 showed a reduction in their mono- and di-unsaturated species (PCae C38:1, 67.2 ± 4.8%, p=0.0001; PCae C30:2, 67.1 ± 4.6%, p=0.0001; PCae C40:1, 74.9 ± 6.0%, p=0.0023; PCae C40:2, 69.1 ± 5.8%, p=0.0003; PCae C42:1, 75.8 ± 6.5%, p=0.0120; PCae C42:2, 79.2 ± 6.7%, p=0.0270). Of these the PCae C38 species showed the strongest decrease in *Sms1*^{MUT} compared to *Sms1*^{WT} mice. The long chain PCae C42 species were additionally reduced in their fully saturated state (PCae C42:0, 71.7 ± 7.3%, p=0.0025). The levels of all PCae C44 species from *Sms1*^{MUT} animals were significantly lower than those of *Sms1*^{WT} male mice (PCae C44:3, 81.3 ± 7.6%, p=0.0417; PCae C44:4, 79.5 ± 7.4%, p=0.0415; PCae C44:5, 76.7 ± 8.5%, p=0.0234; PCae C44:6, 77.8 ± 6.1%, p=0.0251; Figure 3.6 A).

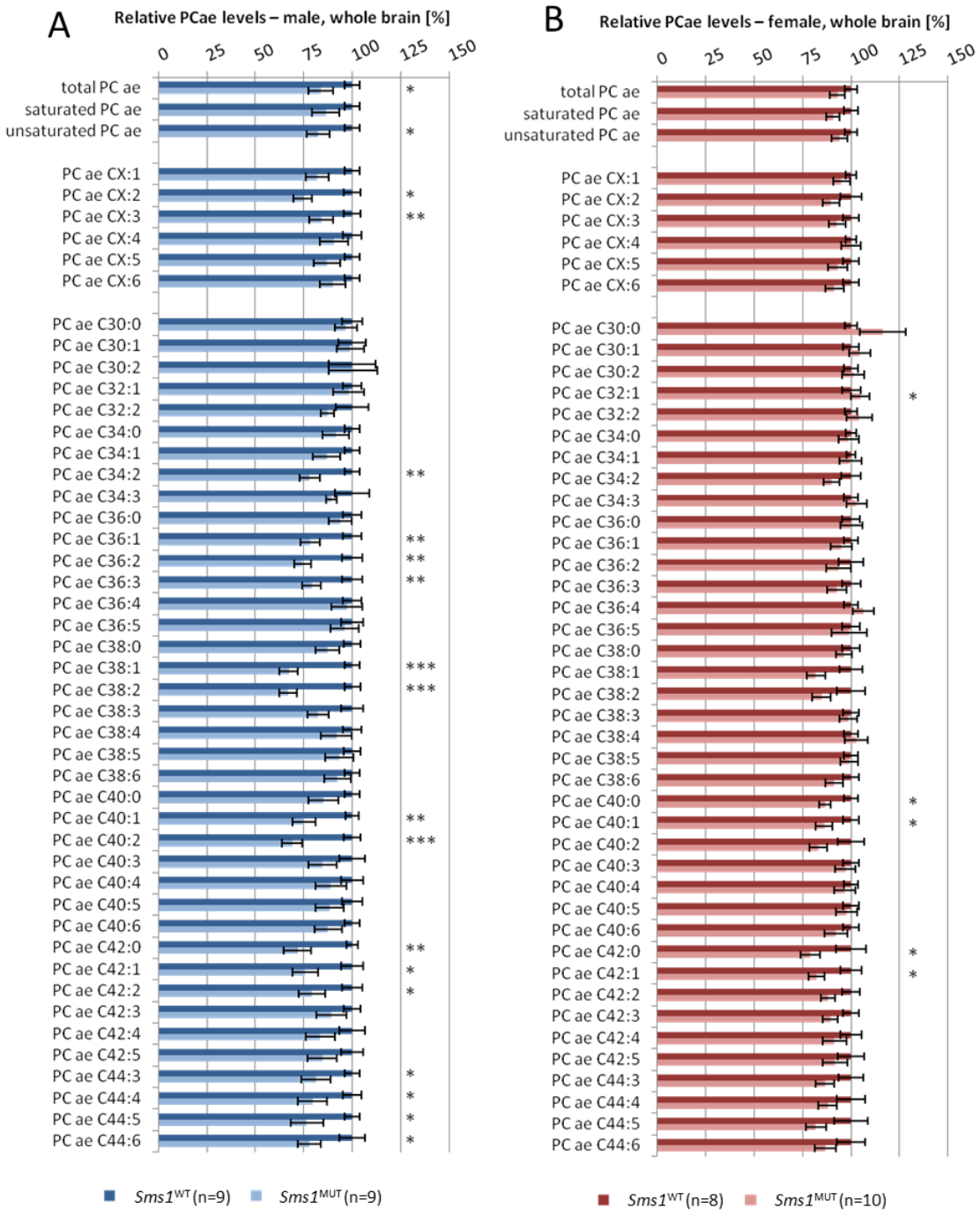

Figure 3.6: Levels of acyl-alkyl-phosphatidylcholine (plasmalogene) species, measured in brain samples from male and female *Sms1*^{MUT} in comparison to *Sms1*^{WT} animals.

(A) Relative PCae levels of male *Sms1*^{WT} (n=9) and *Sms1*^{MUT} (n=9) brain samples. (B) Relative PCae levels of female *Sms1*^{WT} (n=8) and *Sms1*^{MUT} (n=10) brain samples.

Phosphatidylcholin plasmalogene (PCae). Data was analyzed by two-tailed Student's T-test. Data is shown as mean ± SEM. p≤0.05*, p≤0.01**, p≤0.001***.

In female *Sms1*^{MUT} only five PCaa species were significantly altered in comparison to *Sms1*^{WT} mice. All of these were either SFA or MUFA carrying PCae species, with rather long chain lengths. PCae C38:1 was reduced to 81.9 ± 4.7% (p=0.0325), PCae C40:0 to 86.7 ± 3.0% (p=0.0149) and PCae C40:1 to 86.2 ± 4.2% (p=0.0299). PCae C42:0 showed the strongest reduction to 79.9 ± 4.9% (p=0.0407) and PCae C42:1 was reduced to 82.3 ± 4.2% (p=0.0202). In contrast to male *Sms1*^{MUT} neither PCae species with chain lengths shorter than 38 or longer than 42, nor PCae species with more than one unsaturated residue were affected (Figure 3.6 B).

Furthermore, the ratio of PCae MUFAs or PUFAs to SFAs were analyzed, respectively. There were no significant changes detected. Also the ratio between PUFAs and MUFAs did not show any alterations between *Sms1*^{MUT} and *Sms1*^{WT} animals of either sex (supplementary Table 10.12 and Table 10.13).

Detailed analysis of the PCaa data sets revealed a wave like pattern, regarding FA chain length and saturation state of PCaa species. It could be seen that the level of PCaas negatively correlated with FA chain length and with saturation state of the distinct species (Figure 3.7 A).

Like PCaa levels, PCae levels also correlated negatively with chain length. However, the decrease in PCae levels was less pronounced than it was in PCaa. The wave like pattern was not so clear in PCae, but still the highly unsaturated FA containing PCae species were less reduced than those with mono- or di-unsaturated FA residues. As already stated before, these findings were stronger in male animals, than in females (Figure 3.7 B).

In summary, Cer, PCaa and PCae levels were rather reduced in *Sms1*^{MUT} animals, despite showing the expected elevation. Importantly, for PCaa and PCae species, the reduction was positively correlated with FA chain length and saturation state, resulting in a wave-like pattern of LC-PCaas and LC-PCaes, when mapped against *Sms1*^{WT} levels. This alterations could be a result of changes in elongase and desaturase activities.

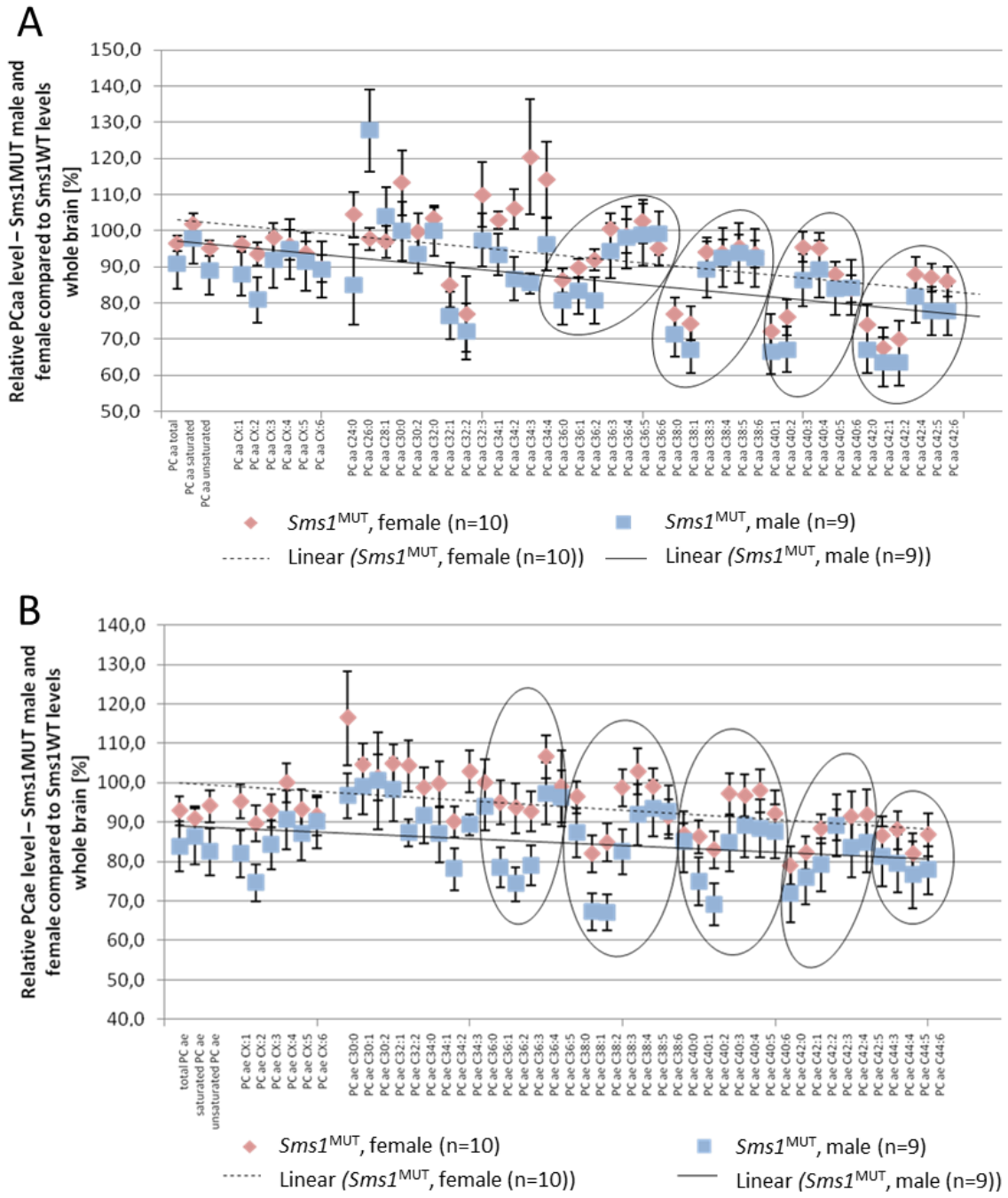

Figure 3.7: Long-chain FA containing diacyl-phosphatidylcholines and phosphatidylcholine plasmalogene species showed a wave like pattern depending on chain length and saturation state in male and female *Sms1*^{MUT} in comparison to *Sms1*^{WT} animals.

(A) Relative PCaa levels of *Sms1*^{MUT} male and female brain samples in comparison to *Sms1*^{WT} levels, which were set to 100% (B) Relative PCae levels of *Sms1*^{MUT} male and female brain samples in comparison to *Sms1*^{WT} levels, which were set to 100%. Lipid species with the same total FA chain length are clustered in gray rings.

Diacyl-phosphatidylcholine (PCaa), phosphatidylcholin plasmalogene (PCae). Male *Sms1*^{WT} (n=9) and *Sms1*^{MUT} (n=9), female *Sms1*^{WT} (n=8) and *Sms1*^{MUT} (n=10). Data was analyzed by two-tailed Student's T-test. Data is shown as mean ± SEM. p≤0.05*, p≤0.01**, p≤0.001***.

3.1.5.4 Lyso-Phosphatidylcholine species

To analyze if PC levels are reduced due to higher degradation lyso-PC levels were measured. The only species which was significantly elevated in male *Sms1*^{MUT} was lyso-PC 17:0 (125.6 ± 7.5%, p=0.0167). Lyso-PC 6:0 also showed higher values (116.0 ± 4.6%), but only a statistical tendency to be elevated (p=0.0637). The levels of all other significantly altered lyso-PC levels were lower in *Sms1*^{MUT} compared to *Sms1*^{WT} animals. These include lyso-PC 20:4, which showed the strongest reduction to 72.6 ± 6.7% (p=0.0291), followed by lyso-PC 18:0 and lyso-PC 18:1 with a reduction to 75.0 ± 5.6% (p=0.0111) and 76.6 ± 5.8% (p=0.0132), respectively. Additionally lower levels of lyso-PC 16:0 (82.1 ± 6.8%, p=0.0411) and lyso-PC 20:3 (86.2 ± 6.3%, p=0.0394) were detected (Figure 3.8 A).

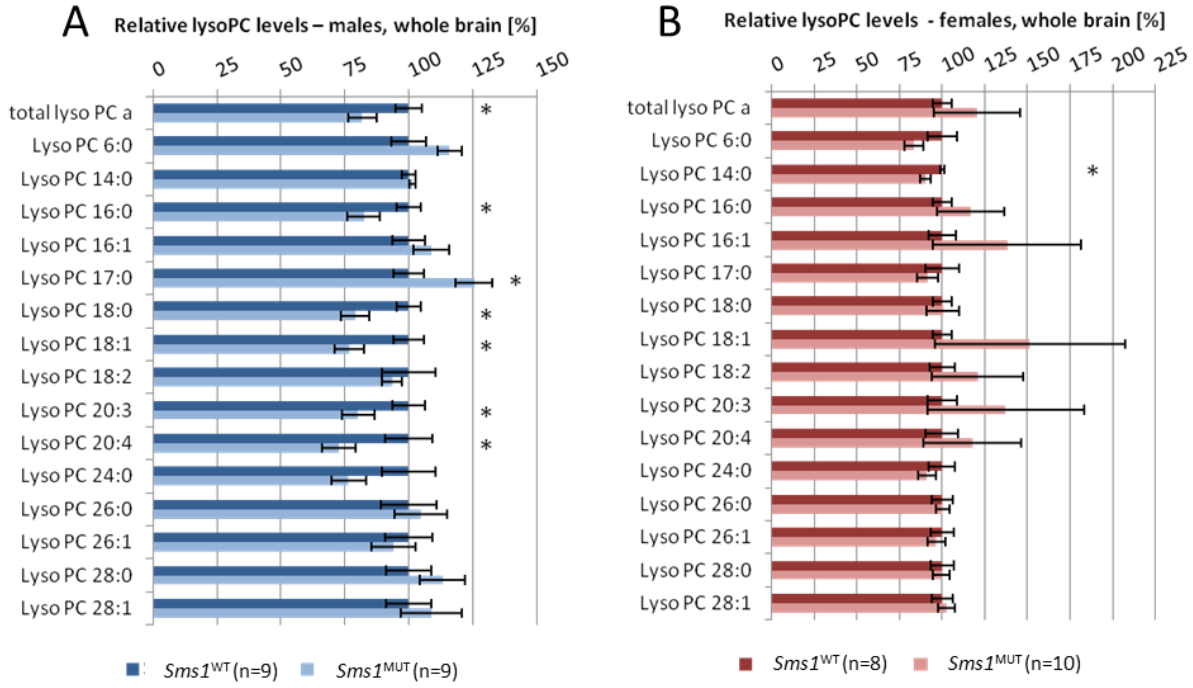

Figure 3.8: Levels of lyso-phosphatidylcholine species, measured in brain samples from male and female *Sms1*^{MUT} in comparison to *Sms1*^{WT} animals.

(A) Relative lyso-PC levels of male *Sms1*^{WT} (n=9) and *Sms1*^{MUT} (n=9) brain samples. (B) Relative lyso-PC levels of female *Sms1*^{WT} (n=8) and *Sms1*^{MUT} (n=10) brain samples.

Lyso-phosphatidylcholin (lyso-PC). Data was analyzed by two-tailed Student's T-test. Data is shown as mean ± SEM. p≤0.05*, p≤0.01**, p≤0.001***.

The only lyso-PC, which had significantly different levels between *Sms1*^{MUT} and *Sms1*^{WT} was lyso-PC 14:0. Its levels were down to 90.1 ± 3.3% (p=0.0105). Female brain samples, other than those of males, had high SEM values, which could mask possible elevations of certain lyso-PC species (Figure 3.8 B).

All in all, the reduced levels of lyso-PC point to altered processing of PC species and could reveal a reduction in PLA_2 activity and reduced free FA release.

3.1.5.5 Cholesterol and Phosphatidylethanolamine

Phosphatidylethanolamine (PEae) is closely related to PCae, bearing an ethanolamine instead of a choline head group. Significant changes in PEae levels were only found in male brain samples. PEae C38:6 was reduced to 75.5 ± 9.3% (p=0.0327), while there was a trend to lower levels of PEae C36:2 and PEae C40:6 (76.3 ± 11.7%, p=0.0776; 76.5 ± 10.6%, p=0.0661). Results on female PEae levels did not differ significantly between *Sms1*^{MUT} and *Sms1*^{WT} levels (Figure 3.9 A).

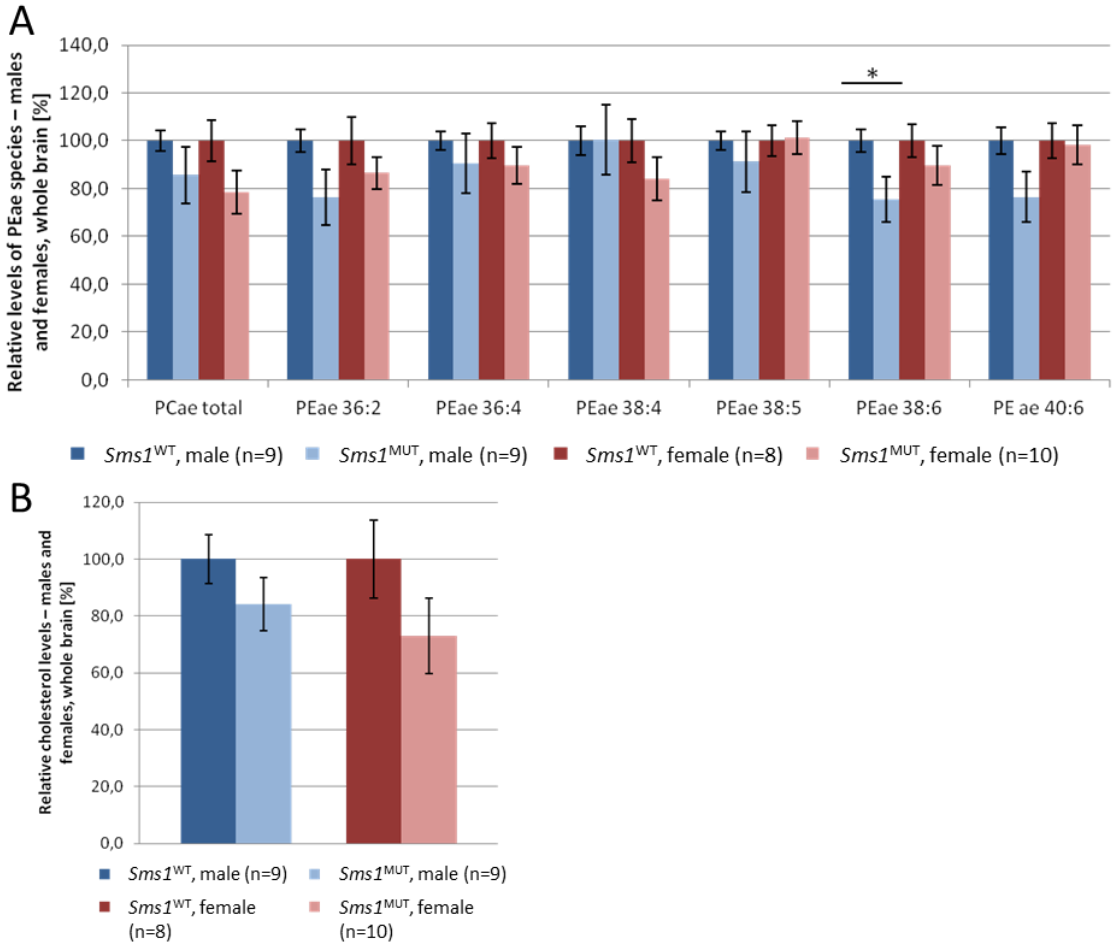

Figure 3.9: Levels of phosphatidylethanolamine species and cholesterol, measured in brain samples from male and female *Sms1*^{MUT} in comparison to *Sms1*^{WT} animals.
(A) Relative PE levels of male and female brain samples. (B) Relative cholesterol levels in male and female brain samples. *Sms1*^{WT} data from male and female animals is shown in dark blue or dark red, *Sms1*^{MUT} data from male and female animals is shown in light blue or light red, respectively. Male *Sms1*^{WT} (n=9), *Sms1*^{MUT} (n=9) and female *Sms1*^{WT} (n=8), *Sms1*^{MUT} (n=10). Phosphatidylethanolamine (PEae). Data was analyzed by two-tailed Student's T-test. Data is shown as mean ± SEM. p≤0.05*, p≤0.01**, p≤0.001***.

Another SL, highly enriched in lipid rafts, besides SM is cholesterol. Therefore, it should be clarified if a down-regulation in SM synthesis would also affect this major sterol. Cholesterol levels in *Sms1*^{MUT} brain samples in comparison to *Sms1*^{WT} samples were measured and found to be slightly reduced in the *Sms1*^{MUT} samples (males: 84.18 ± 9.32%, p=0.2283; females: 72.98 ± 13.33%, p=0.1754, in comparison to the respective *Sms1*^{WT} samples, which were set to 100%). Here, for the first time female levels were more affected than those of males. However, results on cholesterol levels did not reach significance. (Figure 3.9 B).

3.1.6 Enzymes of the Sphingolipid pathway

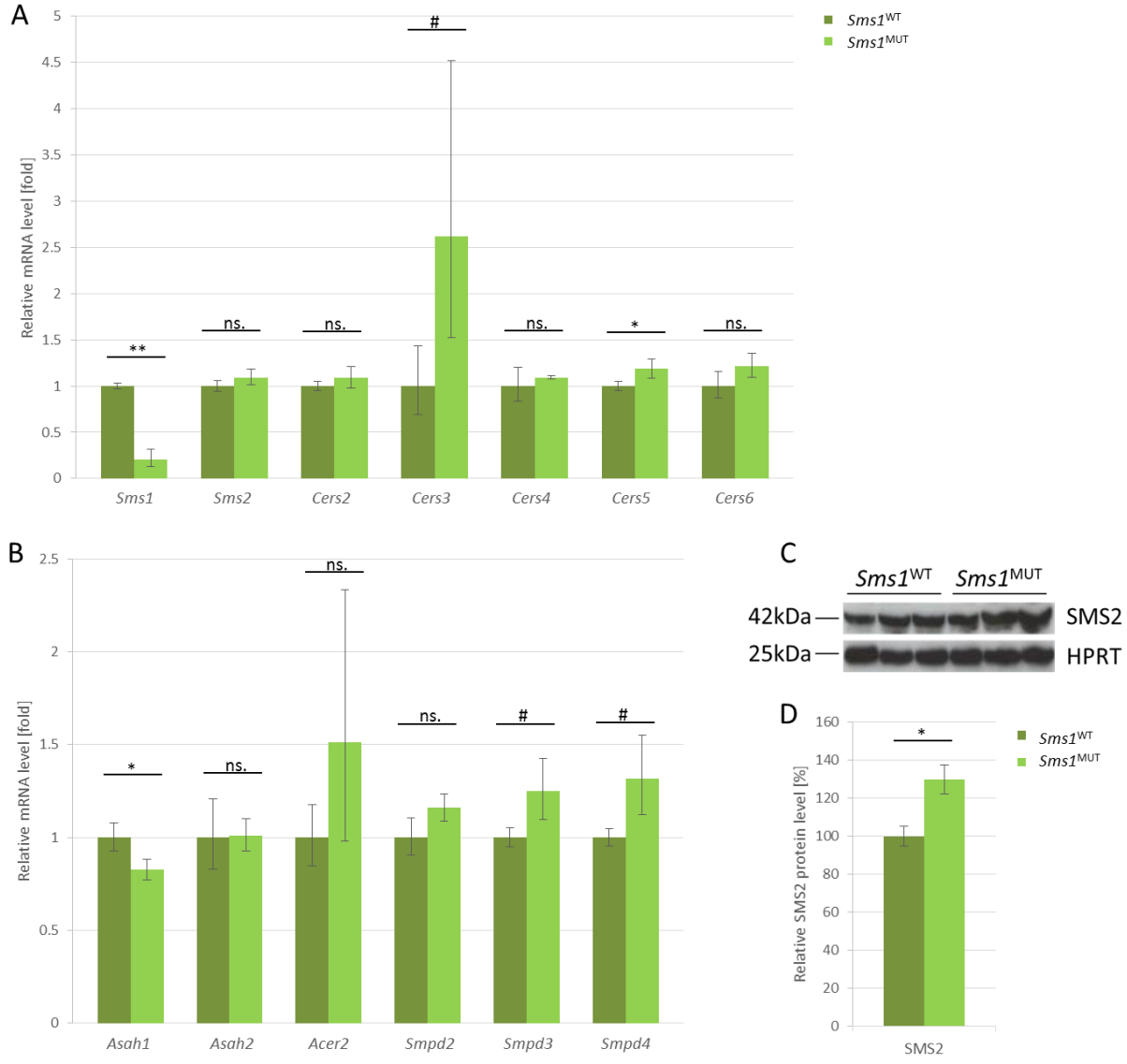

Figure 3.10: mRNA expression levels of enzymes involved in the SL pathway, measured in brain samples male *Sms1*^{MUT} in comparison to *Sms1*^{WT} animals.

(A) Relative mRNA expression levels of *Sms1*, *Sms2*, *Cers2-6*, detected by TaqMan assays. (B) Relative mRNA expression levels of *Asah1-2*, *Acer2*, *Smpd2-4*, detected by TaqMan assays. (C) Immunoblot against SMS2 from whole brain protein lysates of adult *Sms1*^{WT} and *Sms1*^{MUT} brain. (D) Quantification of immunoblot against SMS2. TaqMan assay: *Sms1*^{WT} n=3, *Sms1*^{MUT} n=5; immunoblot *Sms1*^{WT} n=3, *Sms1*^{MUT} n=3. *Sms1*^{WT} data is shown in dark

green, *Sms1*^{MUT} data is shown in light green. TaqMan assay data was analyzed by the $2^{-\Delta\Delta CT}$ method (Livak and Schmittgen, 2001). Statistical analysis was done by two-tailed Student's T-test (A, B, C). Data is presented as mean ± SEM. $p<0.1^{\#}$, $p\leq0.05$*, $p\leq0.01$**, $p\leq0.001$***.

The down regulation of SM levels was regarded as proof of principle for the disruption of the *Sms1* gene expression by the gene trap cassette insertion. However, it should further be clarified if a disruption of SMS1 function might trigger an up-regulation of *Sms2* expression in order to compensate for the loss in total SM synthesis activity. Therefore a quantification of *Sms2* mRNA by TaqMan assay and SMS2 protein levels by Western blot was performed. While mRNA analysis did not show a significant up-regulation of *Sms2* expression, the protein levels of SMS2 were slightly increased in *Sms1*^{MUT} (129.8 ± 7.5%, p=0.0372) compared to *Sms1*^{WT} controls (Figure 3.10 A, C, D). Nevertheless, as it could be seen from the lipid profile of *Sms1*^{MUT} mice, the slight up-regulation of SMS2 levels were not sufficient to fully restore SM levels in *Sms1*^{MUT} brain tissue (Figure 3.4 A-D).

The lipid analysis of the *Sms1*^{MUT} and *Sms1*^{WT} animals revealed some unexpected results. For example, ceramide did not increase in *Sms1*^{MUT} animals, as it would have been expected due to the disruption of SMS1 function. Additionally, the PC species were down regulated according to their chain lengths and saturation state. Therefore, the expression of enzymes in the SL pathway were controlled for alterations, as these might compensate high and toxic ceramide levels, for example. To see if the enzymes are differently regulated an expression microarray analysis on whole brain samples of 5 months old male *Sms1*^{WT} and *Sms1*^{MUT} animals was performed in the GMC. Supplementary Table 10.22 lists the results according to the detected frequency. Subsequently, the expression microarray results by GO terms for biological process (supplementary Table 10.23) and cellular compartment (supplementary Table 10.24) were analyzed. Genes listed in the high ranked GO categories involved in the SL pathway, lipid metabolism, or regulatory processes crucial for the SL homeostasis are summarized in Table 3.1 and described below.

Table 3.1: Highest ranked GO categories for biological processes
GO category analysis based on expression microarray results of whole brain samples of 5 months old male *Sms1*^{WT} (n=3) and *Sms1*^{MUT} (n=4) mice. False discovery range (FDR). Data was analyzed by **Dr. Dietrich Trümbach**.

Name	Total Entities	Overlap	Percent Overlap	Overlapping Entities	p-value	FDR
cellular lipid metabolic process	141	3	2	PRKAA2,GPAM,TECR	0,0521873	0,158527693
ceramide biosynthetic process	19	2	10	SMPD2,LASS4	0,00562757	0,100422529
fatty acid biosynthetic process	89	3	3	PRKAA2,TPI1,TECR	0,0161705	0,131775508
lipid biosynthetic process	128	4	3	PRKAA2,TPI1,TECR,LASS4	0,00728675	0,112792818
lipid catabolic process	116	2	1	CLPS,PLA1A	0,151754	0,247809279
lipid metabolic process	372	6	1	GDPD1,PDE3A,CLPS,PLA1A,ACER1,TECR	0,0242895	0,138530469
regulation of lipid metabolic process	30	2	6	PRKAA2,ACER1	0,0137163	0,127153901
sphingolipid metabolic process	57	2	3	ACER1,LASS4	0,0453534	0,158527693
steroid biosynthetic process	85	2	2	PRKAA2,TECR	0,0912108	0,192501197

3.1.6.1 Alterations in expression levels of catabolic enzymes

One regulated gene was *Smpd2* (sphingomyelin phosphodiesterase 2; *nSMase*, neutral membrane sphingomyelinase 2). The expression of *Smpd2*, listed in ceramide biosynthetic process, in *Sms1*^{MUT} animals, compared to *Sms1*^{WT} mice was lowered to 81% (Table 3.1; supplementary Table 10.22). nSMase2 is responsible for the breakdown of SM into Ceramide and PC and is mainly located at the inner leaflet of the plasma membrane (Tomiuk *et al.* 1998). A down regulation would therefore reduce SM degradation. However, other studies claim, that nSMase2 has rather lysophosphatidase than sphingomyelinase function. They propose, that its major enzymatic reaction is the hydrolysis of 1-acyl-2-lyso-sn-glycero-3-phosphocholine (lyso-PC) and 1-O-alkyl-2-lyso-sn-glycero-3-phosphocholine (lyso-platelet-activating factor, lyso-PAF) into glycerophosphocholine and a carboxylate. PAF is considered to be the physiological substrate (Sawai *et al.* 1999). Considering this substrate specificity a down regulation in *Smpd2* could alter lyso-PC and lyso-PAF processing.

One other regulated gene, encoding for an enzyme with catabolic function is *Pla1a* (phospholipase A1 member A; listed in the category: lipid catabolic process; Table 3.1). Its expression level in *Sms1*^{MUT} animals was 20% lower compared to that of *Sms1*^{WT} animals (supplementary Table 10.22). PLA1A has restricted enzymatic activity against phosphatidylserine and lyso-PS, hydrolyzing their ester bonds at the sn-1 position, thereby producing 2-acyl lyso-phospholipids. PC, PE, phosphatidic acid (PA) or phosphatidylinositol (PI) are not considered as substrates (Sato *et al.* 1997, Nagai *et al.* 1999).

Asah3/Acer1 (alkaline Ceramidase 1) encodes for another hydrolyzing enzyme, degrading ceramides to sphingosine and was listed in three different GO categories (Table 3.1). However, its expression in brain is rather low and it is mainly found in epidermis, which underlines its substrate affinity to-

wards very long chain ceramides (Houben *et al.* 2006). The up regulation in *Asah3* expression to 124%, which was detected in *Sms1*^{MUT} mice compared to *Sms1*^{WT} animals, would lead to an enhanced degradation of VLC-ceramide, preventing its toxic accumulation (supplementary Table 10.22). Nevertheless, as stated above *Asah3* plays a minor role in the brain.

Gdpd1 (glycerophosphodiester phosphodiesterase domain containing 1) encodes for a catabolic enzyme. It is located in the cytoplasm, near the perinuclear region and belongs to a protein family hydrolyzing deacylated glycerophospholipids to glycerol phosphate and alcohol (Chang *et al.* 2008). In the microarray analysis *Gdpd1* showed an elevated expression level of 110% in *Sms1*^{MUT} compared to *Sms1*^{WT} samples (supplementary Table 10.22).

Clps (pancreatic colipase preproprotein), which was also listed in the GO category lipid catabolic process (Table 3.1), is a cofactor of the pancreatic lipase, which allows the anchoring of lipase to the surface of micelles and additionally stabilizes the active confirmation of the lipase (Sugar *et al.* 2003). Without CLPS, the lipase would be washed and loose its efficiency. CLPS was believed to play a role only in pancreatic acinar cells, but preprocolipase expression was also found in the rat brain (York *et al.* 2006). The expression differences detected in brain (*Sms1*^{MUT}: 80%, compared to *Sms1*^{WT} levels, supplementary Table 10.22) could therefore lead to altered lipase efficiency.

3.1.6.2 Alterations in expression levels of anabolic enzymes

As it was mentioned before, the tight regulation of ceramide levels is crucial for cell function and viability. Therefore, not just the degradation of ceramide by ceramidases, but also the synthesis of ceramide represents an important point of metabolic regulation. *Lass4/Cers4* (ceramide synthase 4) was 18% down-regulated in *Sms1*^{MUT} in comparison to *Sms1*^{WT} animals, which would result in a reduced synthesis of ceramide (supplementary Table 10.22). Lass4 was listed in three different GO categories linked to lipid metabolism (Table 3.1).

Another regulated gene, involved in the generation of lipids, is *Prkaa2* (protein kinase, AMP-activated, alpha 2 catalytic subunit), which encodes for the catalytic subunit of the AMP-activated protein kinase (AMPK), functioning as an energy sensor in response to cellular metabolic stress. If AMPK is activated it leads to acetyl-CoA carboxylase (ACC) and beta-hydroxy beta-methylglutaryl-CoA reductase (HMGCR) inhibition by phosphorylation of these enzymes (Hardie 1992, Aguan *et al.* 1994)-read again. Both of these enzymes are key enzymes for lipid synthesis pathways. We found Prkaa2 listed in 5 GO categories (Table 3.1). *Prkaa2* expression was reduced to 84% in *Sms1*^{MUT} in comparison to *Sms1*^{WT} animals, which would point to an up regulation in energy consuming processes such as the two mentioned steps in lipid synthesis (supplementary Table 10.22).

Gpsn2/Tecr (trans-2, 3-enoyl-CoA reductase) was listed in four GO categories (Table 3.1) and was found to be 16% higher expressed in *Sms1*^{MUT} than in *Sms1*^{WT} animals (supplementary Table 10.22).

GPSN2 represents a multi-pass membrane protein, which is located in the ER and belongs to the steroid 5-alpha reductase family. The protein catalyzes the reduction of 6:1 to 16:1, with highest activity with 10:1 CoA (Das, Uhler et al. 2000). In another study GPSN2 was found to be responsible for the last of 4 sequential reactions in the elongation of microsomal long and very long chain FA. This step is the reduction of trans-2, 3-enoyl-CoA to saturated acyl-CoA (Das *et al.* 2000, Moon and Horton 2003). Therefore the slightly elevated levels of Gpsn2 expression might lead to higher levels of SFA.

An enzyme, which is located farther down the lipid synthesis pathway is the mitochondrial glycerol-3-phosphate acyl transferase, encoded by *Gpam*. GPAM has a substrate preference for SFA containing acyl-ACP. The acyl-group of these acyl-ACPs is transferred to the sn-1 position of glycerol-3-phosphate in an esterification reaction (Yet *et al.* 1993, Igal *et al.* 2001). This step is essential for the generation of glycerolipids (Lehner and Kuksis 1996). *Gpam* expression was reduced to 75% in *Sms1*^{MUT} brain samples compared to controls (supplementary Table 10.22) and it was listed in the GO category cellular lipid metabolic process (Table 3.1).

Tpi1 (triosephosphat isomerase 1) encodes for an enzyme responsible for the isomerization of glyceraldehyde-3-phosphate and dihydroxy-acetone phosphate in course of glycolysis and gluconeogenesis (Brown *et al.* 1985, Gruning *et al.* 2014). It was listed in the GO categories fatty acid biosynthetic process and lipid biosynthetic process and down regulated to 90% of the *Sms1*^{WT} expression levels (Table 3.1; supplementary Table 10.22).

Pde3a (cyclic GMP-inhibited phosphodiesterase A) encodes for one of eleven subtypes of phosphodiesterases. It is involved in many different cellular processes and is responsible for the degradation of cAMP and cGMP, therefore contributing to the amplitude and duration of these intracellular messengers (Degerman *et al.* 1994, Kuthe *et al.* 1999, Feijge *et al.* 2004, Zhang and Colman 2007).

These expression differences are based on microarray data and should therefore be validated. Nevertheless, these candidate genes provide interesting evidence for further analysis and investigations.

To validate the expression levels of enzymes of the SL pathway, which are closely connected to SM synthesis, the RNA samples from *Sms1*^{WT} and *Sms1*^{MUT} animals were analyzed by gene-specific TaqMan assays.

Sms1 expression in *Sms1*^{MUT} was verified in these samples to be significantly down-regulated to 20 ± 7-11% (p=0.0017) of *Sms1*^{WT} levels, while no altered expression of *Sms2* on the mRNA level was found (Figure 3.10 A). However, a 29.77 ± 7.53% (p=0.0372) up regulation of SMS2 protein levels were detected (Figure 3.10 C, D), which points to posttranslational regulation of the isoenzyme.

The SMases analyzed per TaqMan assay were all altered in the same direction, namely to higher expression levels in *Sms1*^{MUT} compared to *Sms1*^{WT} mice (Figure 3.10 B). *Smpd2* and *Smpd3* were 16

± 8-7% and 25 ± 18-15% upregulated, respectively, reaching a trend to elevated mRNA levels (p=0.0953 and p=0.0504). *Smpd4* showed 32 ± 23-20% higher mRNA levels, which differ significantly from *Sms1*^{WT} values (p=0.0462, Figure 3.10 B). *Smpd3* and *4* were not found to be regulated with the microarray approach, while *Smpd2* was found to be down-regulated to 81% in *Sms1*^{MUT} samples (supplementary Table 10.22).

Quantification of the relative expression values of *Sms1*^{WT} and *Sms1*^{MUT} *CerS2-6* was performed. Although, the microarray data suggested a down-regulation of *CerS4/Lass4*, this could not be verified by TaqMan expression analysis supplementary Table 10.22; Figure 3.10 A). Here *CerS* mRNA expression did not differ between *Sms1*^{WT} and *Sms1*^{MUT} brain samples. In contrast, *CerS3* and *CerS5*, which did not show any expression differences in the microarray were upregulated in *Sms1*^{MUT} animals in comparison to *Sms1*^{WT} mice. The *CerS3* mRNA level with a value of 262 ± 189-110% did not reach significance but a trend (p=0.0628), due to the high standard deviation. *CerS5* levels, however were significantly upregulated to 119 ± 11-10% (p=0.0414; Figure 3.10 A).

The microarray data showed an up-regulation of *Asah3/Acer1* expression in *Sms1*^{MUT} animals. However, this alteration of mRNA levels could not be validated by TaqMan assay, as expression levels were under detection limits. *Acer2* and *Acer3* were found to be equally expressed with both methods (supplementary Table 10.22; Figure 3.10 B). For *Acer2* high standard deviations were found in the *Sms1*^{MUT} samples. In contrast to the alkaline ceramidases (*Acer1-3*), which were not altered or rather upregulated, the acid and neutral ceramidases showed a tendency to be down-regulated. *Asah1* was significantly lower expressed in *Sms1*^{MUT} samples (83 ± 6-5%, p=0.0313), compared to *Sms1*^{WT} levels, while *Asah2* down-regulation did not reach significance (Figure 3.10 B).

Validation of the microarray data by TaqMan assay showed, that microarray data should be handled with care. Nevertheless, in summary, the results point out that the SL metabolism especially concerning enzymes regulating Cer levels is sensitive to changes in the system. Importantly, compensation of the SMS1 reduction by an upregulation of SMS2 levels was detected, which would explain remaining SM levels in brain of 56% despite the disruption of the major SM synthesis enzyme.

3.1.7 Myelination deficits in the brain and the spinal cord of *Sms1*^{MUT}

As reported before, the lipid profile of the *Sms1*^{MUT} animals was profoundly changed, with a high reduction in SM levels. SM is, as its name indicates, one of the major components of the myelin sheaths, built up by the plasma membrane of oligodendrocytes in the brain (Kilkus *et al.* 2008). Therefore it should be clarified if this reduction in brain SM levels might result in any myelination deficits, hampering isolation integrity and brain function.

Klüver Barrera Staining, a basic staining method to highlight lipids on tissue sections revealed a possible reduction in lipidation in the hippocampus and cortex of *Sms1*^{MUT} animals, whereas the lipid

composition in the cerebellum, striatum and the olfactory bulbs seemed to be unchanged (Figure 3.11 A).

To clarify if these staining differences reliably report differences in myelination myelin basic protein (MBP) was analyzed, as it represents one of the highest expressed proteins in myelin sheaths (Boggs 2006, Jahn *et al.* 2009). Sagittal sections of *Sms1*^{WT} and *Sms1*^{MUT} animals were immunohistochemically stained and analyzed. MBP was found to be expressed differently mostly in hippocampal regions (Figure 3.11 D, upper right and middle left panel) and the nucleus accumbens (Figure 3.11 D, middle right panel), while the expression pattern in the cerebellum, striatum and brain stem seemed to be mostly unaffected (Figure 3.11 D, upper left, lower left and lower right panel).

Western Blot quantification of another abundant myelin protein (myelin oligodendrocyte glycoprotein, MOG) underlined the findings from MBP staining. MOG was significantly reduced to 70.6 ± 5.5% (p=0.0497) in *Sms1*^{MUT} in comparison to *Sms1*^{WT} animals (Figure 3.11 B, C). These findings indicate a disturbance in myelination in *Sms1*^{MUT} animals.

Myelination in the spinal cord was also investigated. In the 3xTg animals a clear reduction in myelin integrity could be seen, as myelin sheaths seemed to be less tightly wrapped around the axons (Figure 3.11 E). Also the space between the axons in the bundle seemed to be enlarged in the 3xTg animal model. The *Sms1*^{MUT} in comparison to *Sms1*^{WT} also showed looser packing of axons inside the bundle and one could observe a less dense closure of myelin sheaths around the axons, although these results were less striking as in the 3xTg animal model (Oddo *et al.* 2003) used as positive control (Figure 3.11 E).

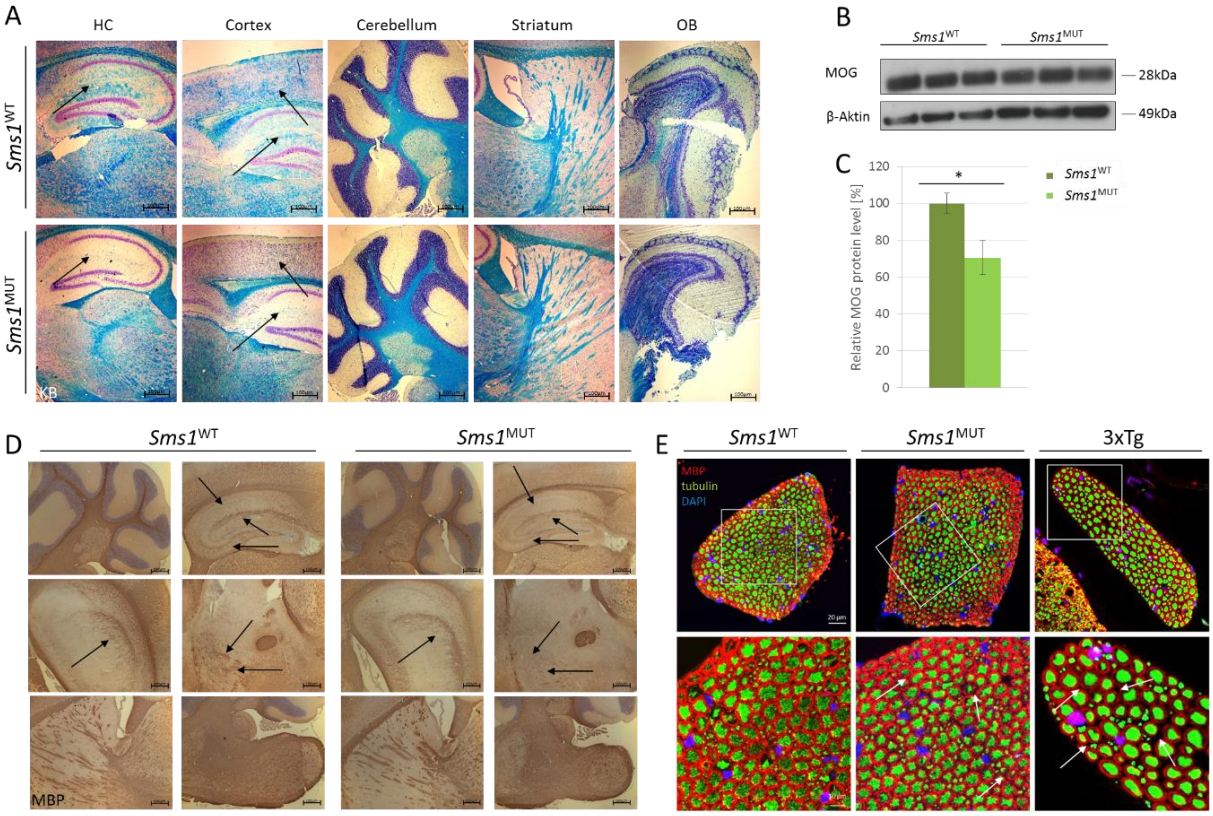

Figure 3.11: *Sms1*^{MUT} revealed hints to myelination deficit in brain and spinal cord.
(A) Klüver Barrera staining of sagittal brain sections from *Sms1*^{WT} and *Sms1*^{MUT} animals. Arrow indicate areas of reduced staining in HC and Cortex regions. Scale bar: 500µm (B) Immunoblot against myelin oligodendrocyte glycoprotein (MOG) and (C) quantification relative to *Sms1*^{WT} levels, which were set to 100% (WB and quantification by Peter Braun). (D) Immunostaining against myelin basic protein (MBP) on sagittal brain sections from *Sms1*^{WT} and *Sms1*^{MUT} animals. Scale bar: 500µm (E) Fluorescent immunostaining of MBP and tubulin on sections of lumbar exon bundles from *Sms1*^{WT}, *Sms1*^{MUT} and 3x^{Tg} animals (picture by Peter Braun). Scale bar: 20µm. Data was analyzed by two-tailed Student's T-test. Data is presented as mean ± SEM. p≤0.05*, p≤0.01**, p≤0.001***.

3.1.8 Strength, coordination and nociception changes in *Sms1*^{MUT}

The observed alterations in myelination in the brain might affect brain function and behavioral performance. Furthermore, the loose-fitting myelin sheaths around axons and the larger gaps between the single axon fibers in lumbar axon bundles could have an effect on muscle function and signaling speed in the PNS. To elucidate these questions data obtained by the GMC, concerning grip strength and coordinator performance was checked.

Sms1^{MUT} had significantly reduced forepaw grip strength (p<0.001). *Sms1*^{WT} and *Sms1*^{MUT} differed by 6.55g. Separation of sexes revealed, that these differences are mostly due to alterations in female mice. Grip strength with all four paws was not changed between genotypes (supplementary Figure 10.1, supplementary Table 10.3 and Table 10.4). These observations point to a reduced muscle strength in the forepaws, while the two hind paws seem to be largely unaffected.

To test for coordination performance, a rotarod test was performed and the latency until the animals fall off the rotating and accelerating rod was measured. *Sms1*^{MUT} mice performed slightly worse than their *Sms1*^{MUT} controls. *Sms1*^{MUT} had an overall reduction of 22.6 ± 14.2s in mean latencies over all three test cycles until the animals fall off from the rotarod. However, these results did not reach significance (p=0.1200; see supplementary Figure 10.2 and Table 10.5).

Additionally to muscle innervation and coordination, the integrity of axons is also important for the conductance of sensory stimuli. The hotplate test for nociception was performed and showed a reduction in the second response time (p=0.022). While *Sms1*^{WT} females and males started licking their feet after 14.5 ± 3.9s or 19.0 ± 7.0s, respectively, *Sms1*^{MUT} mice showed a second response to the stimulus after 17.5 ± 4.7s and 23.5 ± 3.6s. The sex difference in this second response time also reached significance (p=0.002). Neither males nor females had genotype specific differences in first response time (shaking; see supplementary Figure 10.3 and Table 10.6).

3.1.9 Blood-Brain-Barrier alterations

As it was shown, the dysregulation in lipid composition of the plasma membrane and cellular compartments might lead to the misrepresentation of several important myelin-related proteins. It could be shown that myelin components are reduced in *Sms1*^{MUT}. Therefore it should be analyzed what influence the shift in lipids might have on other proteins of the cellular plasma membrane. Especially junction proteins, crucial components of the blood-brain-barrier (BBB) came in the focus, as the BBB is one of the most important defense mechanisms of the brain and is often discussed in AD research.

Protein levels of distinct junction proteins, namely β-Catenin (β-Cat), Connexin 43 (CX43) and Occludin (Occl), which contribute to adherents, gap and tight junctions, respectively were analyzed. *Sms1*^{MUT} brain samples had 19.2 ± 1.0% higher levels of β-Catenin and 19.3 ± 3.7% higher levels of CX43 than *Sms1*^{WT} brain samples. Both values were significantly different to those of wild-type controls (β-Cat: p=0.0496; CX43: p=0.0409; Figure 3.12 A, B, D, E). Occludin levels also followed the same pattern and were slightly elevated, but without reaching significant difference (Occl-115kDa: 118.4 ± 1.8%, p=0.1420; Occl-59kDa: 136.5 ± 12.5%, p=0.1032; Figure 3.12 C, F).

These findings indicate, that the myelination and additionally the BBB might be affected by lipid alterations observed in the *Sms1*^{MUT} brain. Up regulation of junction proteins could indicate a compensatory mechanism to strengthen a weakened BBB. After all, the question remained, whether the observed changes would lead to leakiness or reduced integrity of the BBB. To answer this question, Dr. Steven Ford conducted MSOT measurements, using Iodocyanin green (ICG), an under normal conditions BBB impermeable dye, to analyze BBB functionality.

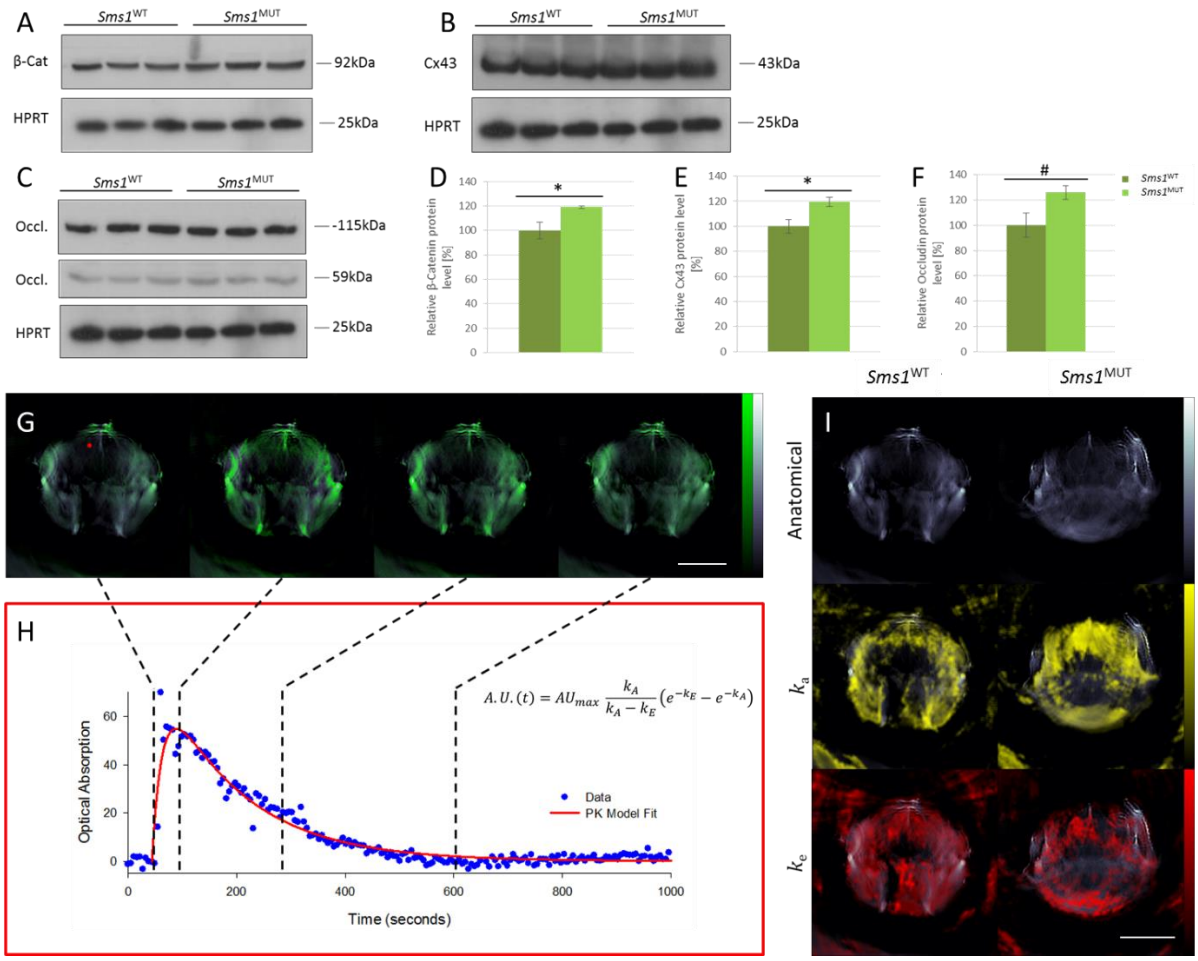

Figure 3.12: The blood-brain barrier of *Sms1*^{MUT} seemed to be comprised in its functionality.
(A-C) Immunoblot and (D-F) quantification against (A, D) β-Catenin, (B, E) Connexin 43 and (C, F) Occludin. Data was analyzed by two-tailed Student's T-test. Data is presented as mean ± SEM. p≤0.05*, p≤0.01**, p≤0.001***. (G, H) Time series of Iodocyanin (ICG, green) distribution before and after injection of ICG, where the corresponding time points for image capture are indicated by the dashed lines. Scale bar: 4mm. (H) Representative ICG distribution profile for a given pixel in the brain (indicated by a red dot in panel G), and the fitted one-compartment pharmacokinetic model described by the equation in (H). (I) Upper panel shows anatomical images of the *Sms1*^{WT} and *Sms1*^{MUT} brain sections, determined by an average of all frames at 900 nm wavelength. (I) Middle and lower panel images show the rate constant parameters for the absorption and elimination of ICG, respectively. The color bars for each image are set constant for comparison between *Sms1*^{WT} (n=5) and *Sms1*^{MUT} (n=3) images. Scale bar: 4mm. Data was obtained and analyzed by Dr. Steven Ford. Max values on the color bars correspond to: k_A = 0.01 s-1; k_E = 0.55 s-1.

The aim of this analysis was to investigate BBB permeability in the sense of influx (k_A) and efflux (k_E) parameters of ICG in *Sms1*^{WT} and *Sms1*^{MUT} animals over time (Figure 3.12 G, H). Preliminary data might indicate a possible higher influx and reduced efflux in *Sms1*^{MUT}, as it is shown in Figure 3.12 I. This would indicate a higher permeability of the BBB in these animals. However, due to resolution problems of the method and a missing positive control, these measurement should be handled with caution.

Additional measurements are recommended with a higher number of animals and imaging of comparable brain sections per genotype. Furthermore, different BBB passing and non-passing dyes could help to identify regions of BBB leakiness and permeability characteristics such as size tolerance or clearance rates.

3.1.10 HPA axis alterations

3.1.10.1 Basic results related to stress-coping and anxiety-like behavior

The primary behavioral screen of the *Sms1* mouse line, performed within the GMC standard panel, gave results about several changes connected to overall activity and alertness, anxiety-like and stress-coping behavior. Data obtained by OF testing for 20min showed that *Sms1*^{MUT} animals covered a longer distance in all four time intervals, while the highest difference could be seen in the first five minutes. Here the mean distance covered by *Sms1*^{MUT} was 36% longer than by *Sms1*^{WT} (Figure 3.13 A). Additionally the whole average speed of *Sms1*^{MUT} animals was faster than that of *Sms1*^{WT} animals. *Sms1*^{MUT} reached a value of 20.75 ± 0.95cm/s, which was 3.77cm/s faster than the average speed of *Sms1*^{WT} animals (Figure 3.13 D). Both results were pointing to hyperactivity of *Sms1*^{MUT} animals.

As a parameter of anxiety-like behavior the latency to the first entry to the center zone of the OF arena was assessed additionally to the number of transits. Furthermore, the distance travelled and time spent in the central area were measured. *Sms1*^{WT} animals entered the center zone after an average of 7.74 ± 1.21s, while it took *Sms1*^{MUT} animals 13.75 ± 2.65s (Figure 3.13 E). Although, *Sms1*^{MUT} entered the center zone later than *Sms1*^{WT} controls, the number of transits to this area was larger in *Sms1*^{MUT} (*Sms1*^{WT}: 215.35 ± 17.39, *Sms1*^{MUT}: 308.30 ± 22.02; $p<0.01$, Figure 3.13 F). These results might appear contradictory, as a longer latency is thought to reflect more anxiety-like and a higher number of transits a less anxiety-like behavior.

Sms1^{WT} animals covered between 28.5 ± 1.45% and 31.79 ± 1.55% of the whole distance travelled in the center zone, while this percentage in *Sms1*^{MUT} animals was between 33.56 ± 2.00% and 39.26 ± 1.74% (Figure 3.13 B). Calculated over all four time intervals, *Sms1*^{MUT} animals travelled a 6.13 ± 1.35% longer distance in the center zone compared to *Sms1*^{WT} animals. In addition to a longer distance covered in the center zone, *Sms1*^{MUT} also spent more time in this inner circle of the testing arena. Separating data from male and female animals revealed a more pronounced genotype effect in female mice. In all four intervals of the testing time, *Sms1*^{MUT} females spent a higher percentage in the center zone, compared to their *Sms1*^{WT} controls (Figure 3.13 C). Over the whole 20min of testing *Sms1*^{MUT} female mice reached 31.61 ± 1.60%, while *Sms1*^{WT} female mice only reached 20.11 ± 2.03% of the whole testing time spent in the center zone. Male *Sms1*^{MUT} mice in comparison spent 24.75 ± 2.27% and male *Sms1*^{WT} mice 22.43 ± 1.62% of the whole testing time in the center zone (compare Figure 3.13 C). The overall distance and time spent in the center zone underlined a less anxiety-like

behavior of *Sms1*^{MUT} animals, which could be already seen in the number of transits. The separation of male and female data also points to a more pronounced reduction in anxiety in female animals.

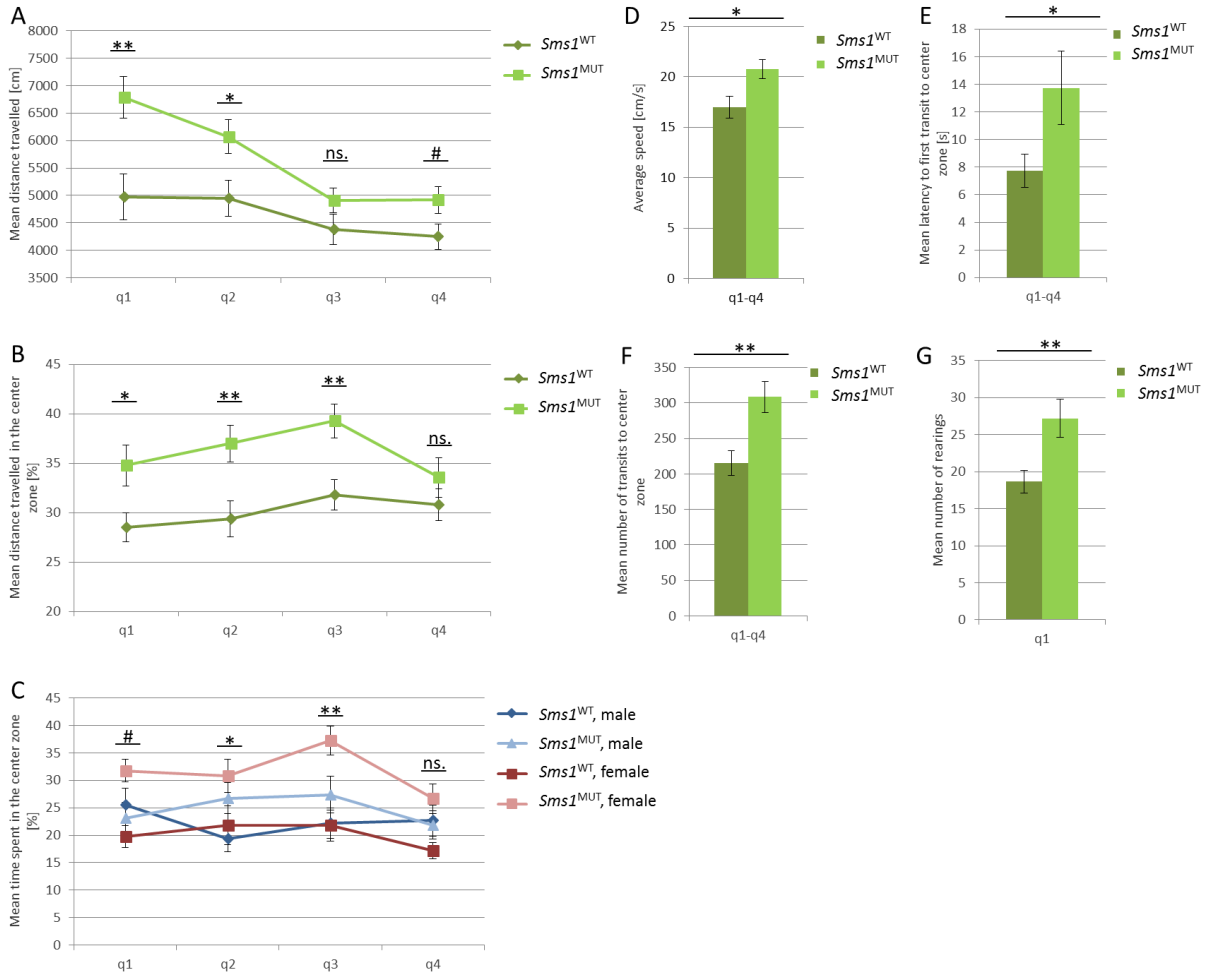

Figure 3.13: *Sms1*^{MUT} showed alterations in anxiety-related behavior.
(A-G) Open field (OF) results from *Sms1*^{MUT} compared to *Sms1*^{WT} animals, (A-C) separated by quartiles of the testing period or (D-F) over the whole testing period. (A) Mean distance traveled in OF. (B) Mean distance travelled in the center zone. (C) Mean time spent in the center zone. (D) Average speed in OF test. (E) Mean latency to first transit to center zone. (F) Mean number of transits to the center zone. (G) Mean number of rearings in the first quartile of the testing period. *Sms1*^{WT} data is shown in dark blue and dark red for males and females, respectively, or in dark green for combined data of both sexes. *Sms1*^{MUT} data is shown in light blue and light red for males and females, respectively, or in light green for combined data of both sexes. Data was analyzed by a linear model (A-C) and by two-tailed Student's T-test (D-G). Data is presented as mean ± SEM. $p<0.01^{\#}$, $p\leq0.05^{*}$, $p\leq0.01^{**}$, $p\leq0.001^{***}$.
Testing and partial data analysis was performed by Dr.Anne-Marie Zimprich.

Rearing behavior was assessed as a parameter of exploration. However, the number of rearings only differed significantly in the first five minutes of OF testing time. Here *Sms1*^{MUT} showed a higher number of rearings with an average of 27.2 ± 2.56 compared to *Sms1*^{WT} mice with an average of

18.65 ± 1.53 ($p<0.01$; Figure 3.13 G). After the first five minutes, the number of rearings in *Sms1*^{MUT} dropped and even sank below the *Sms1*^{WT} mean value, but without reaching significance.

An elevated number of rearings in the first testing quarter could be interpreted as higher initial alertness. The reduction over time might reflect a habituation effect of the *Sms1*^{MUT} animals, which is not seen in *Sms1*^{WT} animals, as their number of rearings stays more or less constant over time.

3.1.10.2 Stress reactivity tests

3.1.10.2.1 Stress reactivity test with 15 min restraint stress

All of these behavioral areas involve signaling via the HPA axis. Therefore we started to investigate this topic in more detail, by the setup of a SRT and quantification of the major players of the HPA axis.

To get more detailed information about the stress reaction in *Sms1*^{WT} and *Sms1*^{MUT} animals we performed an SRT with 15min restraint stress followed by a 20min interval and a subsequent 10min OF test.

Similar to the GMC data, *Sms1*^{MUT} females and *Sms1*^{WT} females of the control group differed concerning the distance covered in the whole arena after the full 10min testing time. *Sms1*^{MUT} females covered 6237.67cm more than *Sms1*^{WT} females of the control group. However, *Sms1* males of the control group did not differ significantly in the covered distance (data not shown). Overall locomotion speed was not altered between any of the male groups, however female *Sms1*^{MUT} ran faster than their *Sms1*^{WT} controls of either group (*Sms1*^{WT} control: 20.80cm/s (IQR: 10.15), *Sms1*^{MUT} control: 31.10cm/s (IQR: 11.10), $p=0.0007$; *Sms1*^{WT} stress: 25.70cm/s (IQR: 5.10), *Sms1*^{MUT} stress: 30.10cm/s (IQR: 3.6), $p>0.9999$; Figure 3.14 G). This effect was blunted after exposure to stress. However, neither *Sms1*^{WT}, nor *Sms1*^{MUT} showed a significant effect of stress on locomotion speed, when comparing the treatment effect within the genotypes (Figure 3.14 G).

For anxiety-like linked parameters, namely the distance travelled and time spent in the center zone, as well as the number of transits to the center zone similar results to the primary screen were found. The male control groups did not reach significantly different levels in the distance travelled in the center zone. After 15min restraint stress, however *Sms1*^{MUT} males covered a longer distance in the center area compared to their wild-type controls (*Sms1*^{WT} stress: 24.8% (IQR: 6.8), *Sms1*^{MUT} stress: 39% (IQR: 7.0), $p=0.0542$; Figure 3.14 D). Both of the female groups differed between *Sms1*^{MUT} and *Sms1*^{WT} animals, with the *Sms1*^{MUT} animals showing a longer distance travelled in the center zone (*Sms1*^{WT} control: 25.8% (IQR: 3.95), *Sms1*^{MUT} control: 35.1% (IQR: 1.4), $p=0.0332$; *Sms1*^{WT} stress: 24.2% (IQR: 5.7), *Sms1*^{MUT} stress: 39.9% (IQR: 15.6), $p=0.0056$; Figure 3.14 D). Regarding the time spent in the center zone, similar results were found. In the male stress group *Sms1*^{WT} mice spent 19.20% (IQR: 8.05) and *Sms1*^{MUT} mice 34.1% (IQR: 6.7) of the test time in the center zone ($p=0.0468$,

Figure 3.14 E). Female animals differed between genotypes in both groups (*Sms1*^{WT} control: 18.8% (IQR: 4.73), *Sms1*^{MUT} control: 31.1% (IQR 6.6), p=0.0072; *Sms1*^{WT} stress: 19.3% (IQR: 6.5), *Sms1*^{MUT} stress: 33.4% (IQR: 17.5), p=0.0025; Figure 3.14 E). No effect concerning distance travelled or time spent in center zone could be seen either in male or female animals due to the exposure to restraint stress (Figure 3.14 D, E). Only female animals of the control group differed between genotypes in the number of transits to the center zone. *Sms1*^{MUT} animals crossed the line to the central area more often than their *Sms1*^{WT} controls (*Sms1*^{WT} control: 126.5 (IQR: 50.0), *Sms1*^{MUT} control: 232 (IQR: 88), p=0.0003; Figure 3.14 F). *Sms1* male animals did not show any difference in transits to the center zone and none of the groups showed a restraint stress related effect (Figure 3.14 F).

Two different blood samples were taken during the SRT, one at the beginning of the test to assess the basal CORT level of both groups of the *Sms1* mice (control, basal and stress, basal) and a second directly after the 15min resting period in the home cage (control, 15min), or 15min restraint stress (stress, 15min), respectively. *Sms1*^{WT} and *Sms1*^{MUT} animals had comparable basal CORT levels in the control and also in the stress group. *Sms1*^{WT} and *Sms1*^{MUT} animals of the stress group show elevated CORT levels in their second blood sample (15min), taken .after the 15min restraint stress period (*Sms1*^{WT} stress basal: 81.18nmol/L (IQR: 94.04), *Sms1*^{WT} stress 15min: 392.54nmol/L (IQR: 310.46), p<0.0001; *Sms1*^{MUT} stress basal: 139.63nmol/L (IQR: 183.19), *Sms1*^{MUT} stress 15min: 468.31nmol/L (IQR: 222.97), p<0.0001; Figure 3.14 A). Elevation of CORT due to an activation of the HPA axis points to a normal reaction of both genotypes to the stimulus (15min restraint stress). Basal samples of *Sms1*^{WT} and *Sms1*^{MUT} of the control group did not differ either. In contrary, the blood samples taken from the control groups 15min after the initial blood sample differed. Although these animals were not exposed to restraint stress, *Sms1*^{WT} animals show higher CORT levels in their second blood sample (*Sms1*^{WT} control basal: 62.74nmol/L (IQR: 147.82), *Sms1*^{WT} control 15min: 344.57nmol/L (IQR: 260.13), p=0.0001; Figure 3.14 A). *Sms1*^{MUT} animals did not have significantly elevated CORT levels in their second blood sample (*Sms1*^{MUT} control basal: 61.84nmol/L (IQR: 100.891), *Sms1*^{MUT} control 15min: 188.33nmol/L (IQR: 102.46), p=0.5036). *Sms1*^{WT} and *Sms1*^{MUT} CORT levels differed by 156.24 nmol/L (p=0.0297; Figure 3.14 A).

Detailed analysis of SRT data revealed that basal CORT levels, which seemed not to differ between *Sms1*^{WT} and *Sms1*^{MUT} need to be regarded separately concerning sex of the animals. However, basal CORT levels in male *Sms1*^{MUT} and *Sms1*^{WT} controls did not differ (*Sms1*^{WT} control basal: 121.59nmol/L (IQR: 261.77), *Sms1*^{MUT} control basal: 36.22nmol/L (IQR: 23.69), p= 0.7277; *Sms1*^{WT} stress basal: 67.61nmol/L (IQR: 143.99), *Sms1*^{MUT} stress basal: 48.42nmol/L (IQR: 47.05), p>0.9999; Figure 3.14 B). The same could be seen for basal CORT levels in females. Levels in *Sms1*^{MUT} were not significantly elevated in comparison to *Sms1*^{WT} females (*Sms1*^{WT} control basal: 62.74nmol/L (IQR: 96.35), *Sms1*^{MUT} control basal: 145.76nmol/L (IQR: 39.69), p=0.9174; *Sms1*^{WT} stress basal:

106.07nmol/L (IQR: 53.83), *Sms1*^{MUT} stress basal: 220.08nmol/L (IQR: 33.91), p=0.6711; Figure 3.14 B).

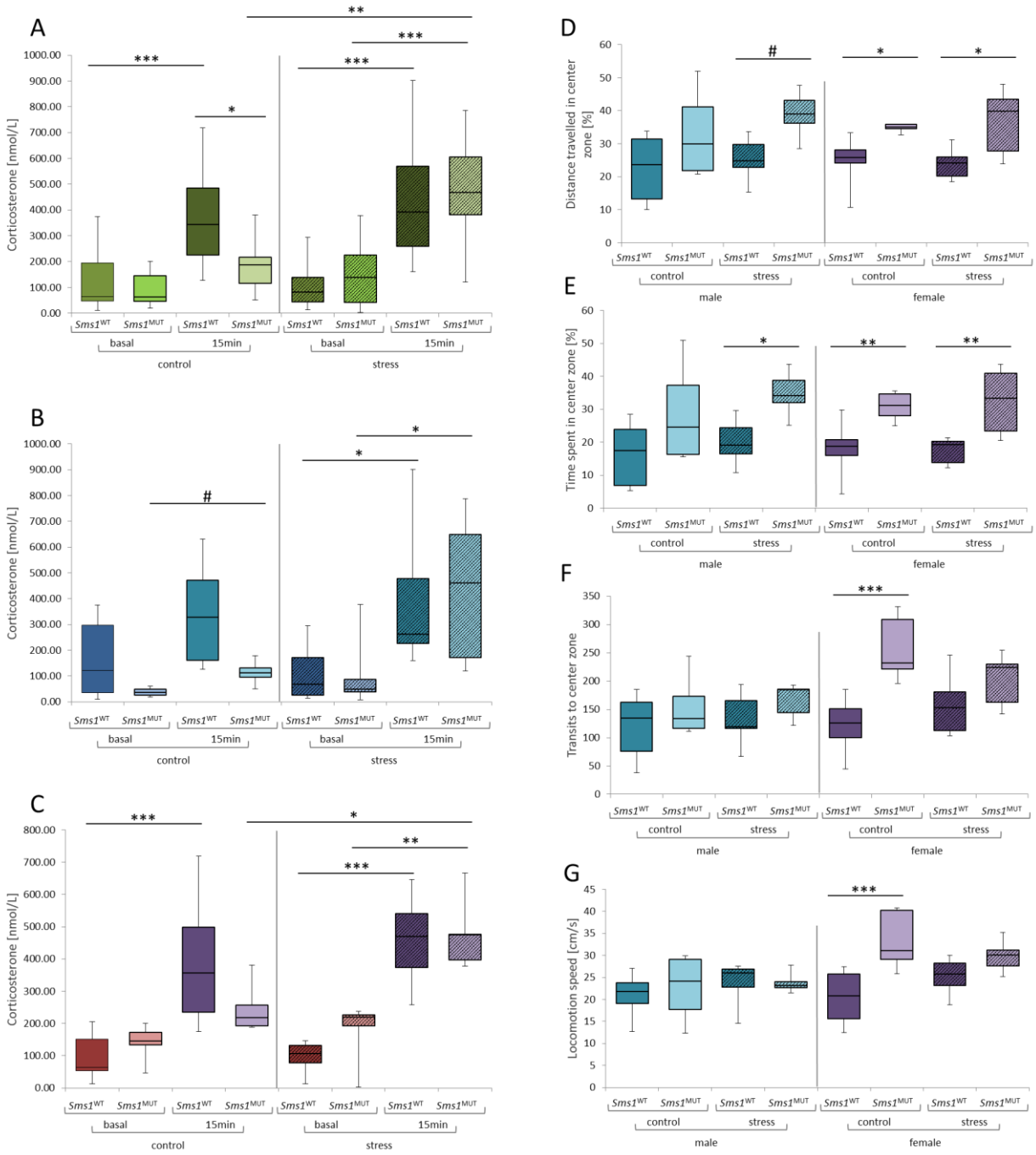

Figure 3.14: 15min stress-reactivity test (SRT) reveals alterations in stress coping behavior and corticosterone alterations in *Sms1*^{MUT} animals.

(A-C) Corticosterone levels of tail vein blood taken at time point 0 (basal) of the SRT and 15min after SRT start (15min). *Sms1*^{WT} and *Sms1*^{MUT} animals were grouped into control (control) and stress (stress) groups, indicating if they received 15min restrained stress or not. (D-G) Parameter assessed by open field test after 15min SRT in control and stress groups. *Sms1*^{WT} data is shown in dark blue and dark red for males and females, respectively, or in dark green for combined data of both sexes. *Sms1*^{MUT} data is shown in light blue and light red for males and females, respectively, or in light green for combined data of both sexes. Data obtained from stress groups is

highlighted by dashed boxes. Male *Sms1*^{WT} control n=6, stress n=9; *Sms1*^{MUT} control n=4, stress n=5; Female *Sms1*^{WT} control n=8, stress n=7; *Sms1*^{MUT} control n=5, stress n=5. Data was analyzed separately for genotype and treatment effects. Comparison was done by two-way ANOVA with *post hoc* Sidak for treatment and Tukey's test for genotype effects, respectively. Behavioral data was analyzed by two-way ANOVA and *post hoc* Sidak test. Data is presented as median ± quartiles. $p<0.01^{\#}$, $p\leq0.05^{*}$, $p\leq0.01^{**}$, $p\leq0.001^{***}$.
Testing and partial data analysis was performed by Dr. Anne-Marie Zimprich.

3.1.10.2.2 Stress reactivity test with 2h restraint stress

To elucidate if CORT levels in *Sms1*^{MUT} did not rise at all, or were dropping faster, the restraint stress period was extended to 2h. Afterwards animals were allowed a 20min resting interval and another OF test was performed.

OF retesting of male animals of the control group after 2h in their home cage did not reveal any statistically significant genotype specific differences. However, *Sms1*^{MUT} males showed a slightly elevated distance travelled in the whole area and in the center zone over the whole 10min of OF testing period in comparison to *Sms1*^{WT} controls (Figure 3.15 E, D). Also the locomotion speed was slightly increased and they crossed the border to the center zone more often (Figure 3.15 G, C). Concerning the time spent in this inner area, results reached a statistical trend in male animals of the stress group, tested after the reception of 2h restraint stress. *Sms1*^{MUT} spent a higher percentage of the whole testing time in the center zone, compared to their *Sms1*^{WT} controls (*Sms1*^{WT} stress 2h: 21.60% (IQR: 16.95), *Sms1*^{MUT} stress 2h: 37.80% (IQR: 8.70), p=0.0907; Figure 3.15 E, F). *Sms1*^{MUT} males did not differ significantly in their behavioral performance with or without the reception of restraint stress (Figure 3.15 C-H). *Sms1*^{WT} males, however, showed an increase in their distance travelled in the whole area, their locomotion speed and the number of rearings, when they were exposed to a 2h period of restraint stress (Distance: *Sms1*^{WT} control 2h: 6902.60cm (IQR: 3260.70), *Sms1*^{WT} stress 2h: 11283.50cm (IQR: 2333.80), p=0.0251; Speed: *Sms1*^{WT} control 2h: 11.70cm/s (IQR: 5.50), *Sms1*^{WT} stress 2h: 19.90cm/s (IQR: 4.15), p=0.0214; Rearings: *Sms1*^{WT} control 2h: 26.50 (IQR: 4.75), *Sms1*^{WT} stress 2h: 40.00 (IQR: 17.50), p=0.0905; Figure 3.15 D, G, H).

In *Sms1* females of the control group, the differences which were indicated in the male animals of the control group became significant (or at least reached a tendency to be different) in some criteria tested. These included the whole distance travelled, locomotion speed and rearings (Distance: *Sms1*^{WT} control 2h: 6108.25cm (IQR: 3309.08), *Sms1*^{MUT} control 2h: 11689.90cm (IQR: 3964.10), p=0.0261; Speed: *Sms1*^{WT} control 2h: 10.45 cm/s (IQR: 5.63), *Sms1*^{MUT} control 2h: 22.40cm/s (IQR: 6.10), p=0.0094; Rearings: *Sms1*^{WT} control 2h: 20.50 (IQR: 7.00), *Sms1*^{MUT} control 2h: 58.00 (IQR: 14.00), p=0.0014). In all of these criteria, *Sms1*^{MUT} control females had higher values compared to *Sms1*^{WT} control females (Figure 3.15 D, G, H). With the perception of 2h restraint stress, *Sms1*^{WT} females showed higher values in these criteria, reaching the levels seen in *Sms1*^{MUT} females of the control group, while *Sms1*^{MUT} animals did not increase their values with perception of the stressor. I found

no significant difference between the behavioral performance of *Sms1*^{MUT} control females and *Sms1*^{MUT} stress females (Figure 3.15 C-H). Therefore, with 2h restraint stress, the mentioned differences between *Sms1*^{WT} control 2h and *Sms1*^{MUT} control 2h were leveled out equalizing their OF behavior (Figure 3.15 C-H). However, in *Sms1*^{WT} females, perception of restraint stress elevated most parameters measured. Most of them were activity related, such as the whole distance travelled, number of transits to the center, the locomotion speed and the number of rearings (Distance: *Sms1*^{WT} control 2h: 6108.25cm (IQR: 3309.08), *Sms1*^{WT} stress 2h: 14383.70cm (IQR: 5736.50), p=0.0032; Transits: *Sms1*^{WT} control 2h: 57.50 (IQR: 55.25), *Sms1*^{WT} stress 2h: 188.00 (IQR: 124.00), p=0.0262; Speed: *Sms1*^{WT} control 2h: 10.45cm/s (IQR: 5.63), *Sms1*^{WT} stress 2h: 25.50cm/s (IQR: 10.25), p=0.0023; Rearings: *Sms1*^{WT} control 2h: 20.50 (IQR: 7.00), *Sms1*^{WT} stress 2h: 49.00 (IQR: 16.00), p=0.0058; Figure 3.15 D, C, G, H). There was no elevation in the distance travelled in the center zone nor in the time spent in the center zone, which would indicate a reduced anxiety-like behavior (Figure 3.15 E, F).

In the 15min SRT it was noticed, that male and female data needed to be regarded separately. Also the behavioral data of the 2h SRT points out, that stress-related behavior should be analyzed in separate sets concerning sex. Therefore, the CORT data of the 2h SRT was split into male and female data sets.

Male *Sms1*^{WT} and *Sms1*^{MUT} basal CORT levels did not differ between genotypes or groups (*Sms1*^{WT} control basal: 54.12nmol/L (IQR: 23.88), *Sms1*^{MUT} control basal: 39.98nmol/L (IQR: 55.65), p=0.8876; *Sms1*^{WT} stress basal: 66.53nmol/L (IQR: 42.00), *Sms1*^{MUT} stress basal: 46.47nmol/L (IQR: 45.39), p=0.9669; Figure 3.15 A). After 2h in their home cage neither the *Sms1*^{WT}, nor the *Sms1*^{MUT} control group showed any alterations compared to their basal CORT data (*Sms1*^{WT} control basal: 54.12nmol/L (IQR:23.88), *Sms1*^{WT} control 2h: 69.20nmol/L (IQR: 25.08), p=0.9397; *Sms1*^{MUT} control basal: 39.98nmol/L (IQR: 55.65), *Sms1*^{MUT} control 2h: 81.90nmol/L (IQR: 5.41), p=0.9240; Figure 3.15 A). The elevation of CORT levels with the experience of 2h restraint stress was significant in both, *Sms1*^{WT} and *Sms1*^{MUT} males of the stress group (*Sms1*^{WT} stress basal: 66.53nmol/L (IQR: 42.00), *Sms1*^{WT} stress 2h: 280.70nmol/L (IQR: 153.34), p<0.0001; *Sms1*^{MUT} stress basal: 46.47nmol/L (IQR: 45.39), *Sms1*^{MUT} stress 2h: 238.12nmol/L (IQR: 28.86), p=0.0006; Figure 3.15 A). These CORT levels, reached after 2h of restraint stress, are also significantly higher than those measured in the control groups after 2h (*Sms1*^{WT} control 2h: 69.20nmol/L (IQR: 25.08), *Sms1*^{WT} stress 2h: 280.70nmol/L (IQR: 153.34), 2h, p=0.0006; *Sms1*^{MUT} control 2h: 81.90nmol/L (IQR: 5.41), *Sms1*^{MUT} stress 2h: 238.12nmol/L (IQR: 28.86), p=0.0164 Figure 3.15 A).

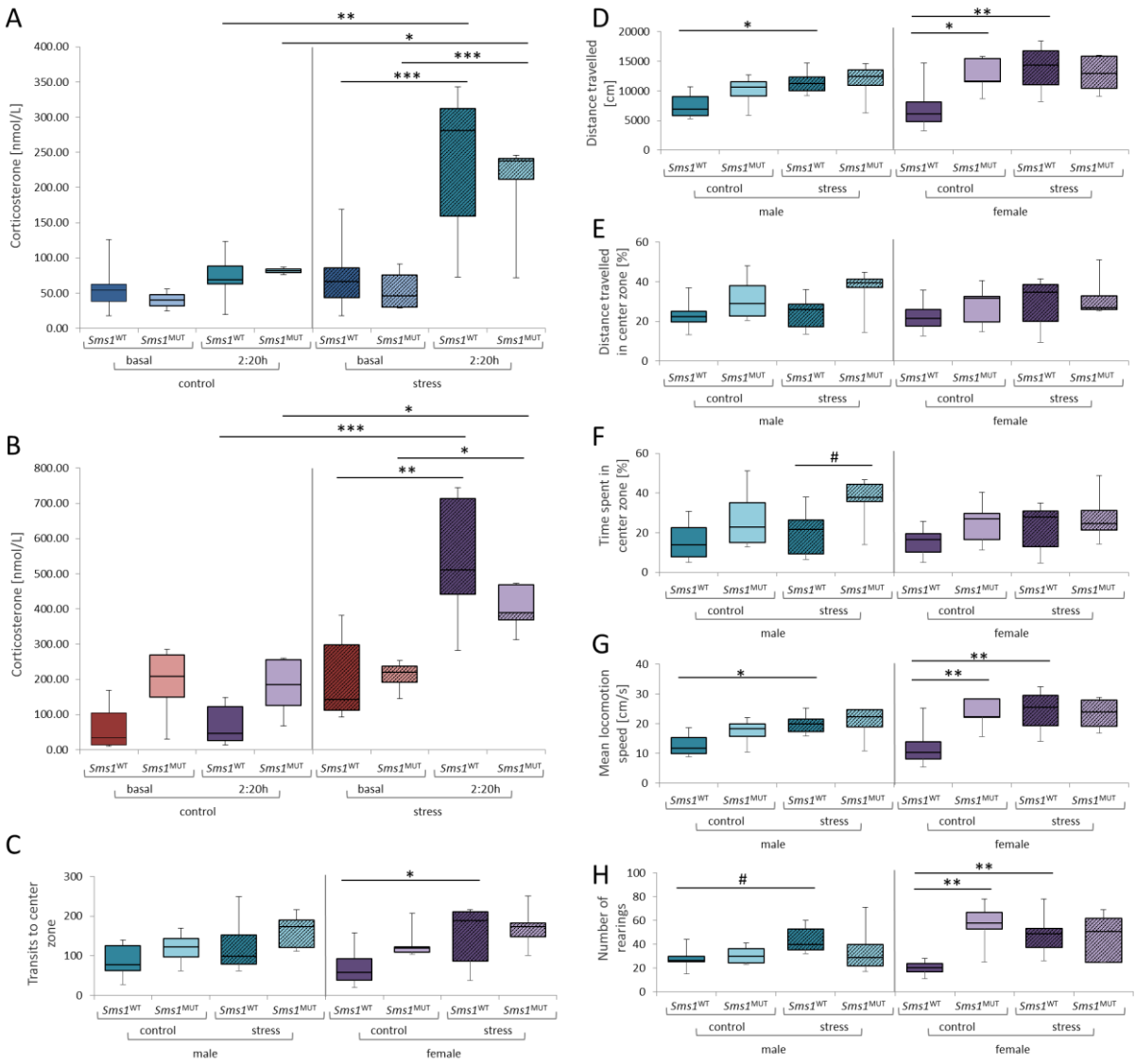

Figure 3.15: 2h stress-reactivity test (SRT) reveals alterations in stress coping behavior and corticosterone alterations in *Sms1*^{MUT} animals.

(A, B) Corticosterone levels of tail vein blood taken at time point 0 (basal) of the SRT and 2:20h after SRT start (2:20h). *Sms1*^{WT} and *Sms1*^{MUT} animals were grouped into control (control) and stress (stress) groups, indicating if they received 15min restrained stress or not. (C-H) Parameter assessed by open field test after 2:20h SRT in control and stress groups. *Sms1*^{WT} data is shown in dark blue and dark red for males and females, respectively. *Sms1*^{MUT} data is shown in light blue and light red for males and females, respectively. Data obtained from stress groups is highlighted by dashed boxes. Male *Sms1*^{WT} control n=6, stress n=7; *Sms1*^{MUT} control n=3, stress n=5; Female *Sms1*^{WT} control n=8, stress n=6; *Sms1*^{MUT} control n=4, stress n=4. Data was analyzed separately for genotype and treatment effects. Comparison was done by two-way ANOVA with *post hoc* Sidak for treatment and Tukey's test for genotype effects, respectively. Behavioral data was analyzed by two-way ANOVA and *post hoc* Sidak test. Data is presented as median ± quartiles. $p<0.01^{\#}$, $p\leq0.05^{*}$, $p\leq0.01^{**}$, $p\leq0.001^{***}$.
Testing and partial data analysis was performed by Dr. Anne-Marie Zimprich.

In females, the basal CORT levels of the control group differed slightly between genotypes, without reaching significance (*Sms1*^{WT} control basal: 33.63nmol/L (IQR: 91.71), *Sms1*^{MUT} control basal:

208.90nmol/L (IQR: 119.78), p= 0.2843). The same was seen after 2h (*Sms1*^{WT} control 2h: 47.05nmol/L (IQR: 95.10), *Sms1*^{MUT} control 2h: 185.45nmol/L (IQR: 128.98), p=0.4567; Figure 3.15 B). The exposure to 2h restraint stress led to higher CORT levels in *Sms1*^{WT} and *Sms1*^{MUT} females, while no genotype-dependent difference was observed after perception of restraint stress (*Sms1*^{WT} stress 2h: 511.24nmol/L (IQR: 273.30), *Sms1*^{MUT} stress 2h: 389.29nmol/L (IQR: 100.12), p=0.5626; Figure 3.15 B). CORT values differences between *Sms1*^{WT} control 2h (47.05nmol/L (IQR: 95.10)) and *Sms1*^{WT} stress 2h (511.24nmol/L (IQR: 273.30)) were highly significant (p<0.0001) with the higher value found in the stress group after the exposure to 2h restraint stress. CORT values of *Sms1*^{MUT} control 2h (185.45nmol/L (IQR: 128.98)) and *Sms1*^{MUT} stress 2h (389.29nmol/L (IQR: 100.12) were also significantly different (p=0.0376). Here as expected, the higher values were again measured after perception of stress (Figure 3.15 B).

Overall, females show higher CORT levels than their male counterparts. The difference noticed between *Sms1*^{WT} and *Sms1*^{MUT} females of the control group is not reflected in males.

Comparison of both SRTs

Comparing data sets from both SRTs (15min and 2h restraint stress), showed that males of the control groups had a similar CORT pattern. Although, CORT levels were higher in the 15min SRT than in the 2h SRT. *Sms1*^{MUT} animals always had lower CORT values compared to their *Sms1*^{WT} controls, although these differences were not significant. In both SRTs the control groups had slightly elevated CORT values, when the second blood sample was taken after 15min and 2h time spent in their home cages. After 15min, these differences still reached a trend in *Sms1*^{MUT} males, but not after 2h interval between the first and the second blood taking event (Figure 3.14 B, Figure 3.15 A).

In females, the overall CORT values were comparable in height between the 15min and the 2h SRT. The hint to elevated CORT levels under basal conditions in *Sms1*^{MUT} compared to *Sms1*^{WT}, which could be assumed in the 15min SRT already, seemed to persist in the 2h SRT. One major difference could be seen in the *Sms1*^{WT} control group, where in the 15min SRT animals showed higher CORT values after 15min but not after 2h in their home cage. The same tendency could be seen in *Sms1*^{MUT}, but to a lesser extent. Concerning the CORT values after 15min or 2h perception of restraint stress, both *Sms1*^{WT} and *Sms1*^{MUT} showed an elevation in CORT with comparable levels. However, the *Sms1*^{MUT} levels seemed to be a bit lower after 2h of restraint stress than those of *Sms1*^{WT} females (Figure 3.14 C, Figure 3.15 B).

After 2h, neither *Sms1*^{WT} nor *Sms1*^{MUT} controls differed in their basal CORT levels, indicating that the CORT elevation seen in *Sms1*^{WT} animals 15min after basal blood collection had already returned to basal levels after 2h. With regard to the stress groups, male and female *Sms1*^{MUT} data indicated

lower levels of CORT compared to *Sms1*^{WT} animals, after the perception of 2h restraint stress. This might indicate, that CORT levels were indeed faster down regulated in *Sms1*^{MUT} animals.

On the behavioral level 15min restraint stress did not affected behavior of *Sms1*^{WT} or *Sms1*^{MUT} animals of either sex (Figure 3.14 C-G). After 2h of restraint stress, behavioral differences became obvious. Male and female *Sms1*^{WT} animals showed elevation in the whole distance travelled, locomotion speed, and number of rearings. Females also differed in the number of transits to the center zone. Importantly, these differences were just seen in *Sms1*^{WT} animals, while no effect was noticed in *Sms1*^{MUT} animals (Figure 3.15 C-H). In summary these results showed that *Sms1*^{MUT} animals are more stress-resistant, not showing altered behavior after perception of a stressor, such as restraint stress.

3.1.10.3 Analysis of the major HPA axis components

The alterations in stress-coping behavior and CORT values found in *Sms1*^{MUT} pointed to changes in HPA axis signaling. Therefore the expression levels of the major players in HPA axis signaling were analyzed in organs involved in stress-axis signaling, namely the brain, pituitary gland and adrenals.

3.1.10.3.1 Pituitary and Adrenal morphology

Structural analysis of the pituitary did not show any major alterations between *Sms1*^{WT} and *Sms1*^{MUT} animals. Anterior, intermediate and posterior lobe were of comparable thickness and cellular structure (Figure 3.16 H). Also the adrenal structure was similar, although one *Sms1*^{MUT} analyzed showed an enlargement of the X-zone of the adrenal cortex (Figure 3.16 H, J, K). However, the other *Sms1*^{MUT} adrenals analyzed did not show any alterations in comparison to *Sms1*^{WT} adrenals.

3.1.10.3.2 Expression level of genes involved in HPA axis signaling

If we assume an accelerated down regulation of CORT levels after a stress reaction, there are several regulatory levels in the HPA axis described above, where the stress reaction could be altered. Therefore the major players in the HPA axis-regulated stress response were quantified by qPCR (TaqMan Assay) and Western Blot.

No alteration was found in Nr3c1 (GR) or Nr3c2 (MR) mRNA levels in whole brain samples, or in hypothalamic brain samples (Figure 3.16 A, C). But in the hippocampus Nr3c2 levels were 1.59 fold higher in *Sms1*^{MUT} in comparison to *Sms1*^{WT} animals ($p=0.0477$; Figure 3.16 C). Under basal conditions *Sms1*^{MUT} animals had 1.63 fold higher Pomc mRNA levels in their pituitary gland ($p=0.0175$; Figure 3.16 D). However, ACTH staining in the pituitary gland revealed, that although Pomc as a precursor showed elevated mRNA levels in *Sms1*^{MUT}, ACTH itself seemed to be reduced in *Sms1*^{MUT} compared to *Sms1*^{WT} (Figure 3.16 I). Furthermore, *Sms1*^{MUT} had a reduction in adrenal Mc2r mRNA levels (0.43 fold, $p=0.0619$; Figure 3.16 B). With a reduction of ACTH and a reduction in its receptor (Mc2r) it might be that the stress reaction in *Sms1*^{MUT} is slower compared to *Sms1*^{WT} standards.

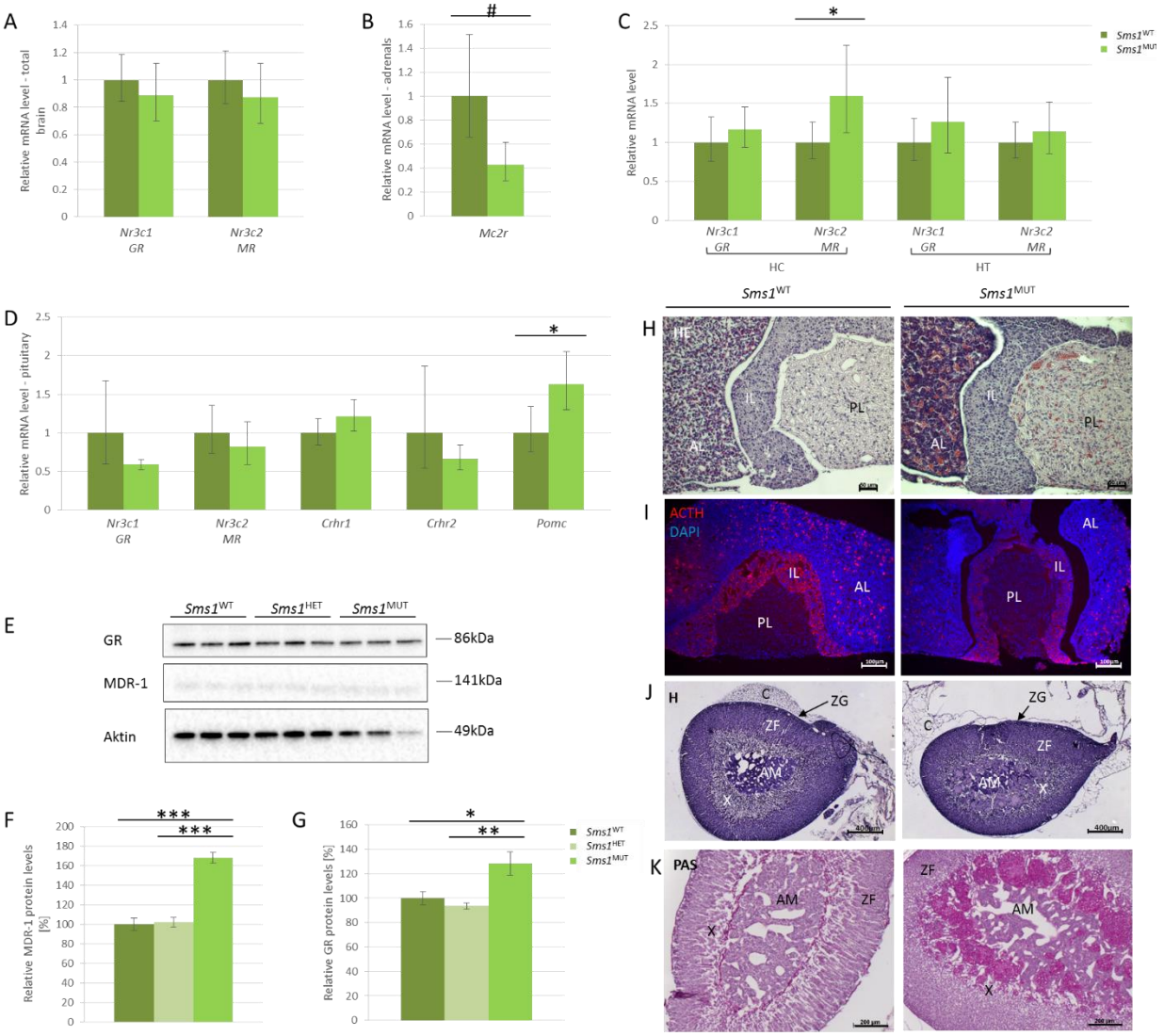

Figure 3.16: *Sms1*^{MUT} showed alterations in some of the major HPA axis components.

(A-D) Relative expression level of major HPA axis components, measured by TaqMan assays using RNA samples of (A) whole brain, (B) adrenals, (C) hippocampus (HC) and hypothalamus (HT) and (D) pituitary of *Sms1*^{WT} and *Sms1*^{MUT} female animals. (E) Representative Immunoblot and (F, G) quantification of multi-drug resistant protein 1 (MDR-1) and glucocorticoid receptor (GR), performed on whole brain protein samples. (H) H&E staining of pituitary sections of *Sms1*^{WT} and *Sms1*^{MUT} animals. Scale bar: 50µm. (I) Fluorescent immunostaining of pituitary sections of *Sms1*^{WT} and *Sms1*^{MUT} using a commercial antibody against ACTH (red) and DAPI (blue). Scale bar: 100µm. (J) Haemalaun and (K) Periodic acid-Shiff (PAS) staining of *Sms1*^{WT} and *Sms1*^{MUT} adrenal sections. Scale bar: 400µm and 200µm.

Anterior lobe (AL), intermediate lobe (IL), posterior lobe (PL), capsule (C), zona glomerulosa (ZG), zona fasciculate (ZF), X-zone(X), adrenal medulla (AM) qPCR data: *Sms1*^{WT} n=3-4, *Sms1*^{MUT} n=4-6; data is presented as mean ± SD. Immunoblot data: *Sms1*^{WT} n=6, *Sms1*^{HET} n=6, *Sms1*^{MUT} n=4. TaqMan assay data was analyzed by the $2^{-\Delta\Delta CT}$ method (Livak and Schmittgen, 2001). Statistical analysis was done by two-tailed Student's T-test (A-D) or one-way ANOVA with *post hoc* Tukey's test (F, G). Data is presented as mean ± SEM; $p<0.01^{\#}$, $p\leq0.05^{*}$, $p\leq0.01^{**}$, $p\leq0.001^{***}$.

Regarding protein expression only whole brain GR levels could be detected, which were elevated to 184.6 ± 13.2% in *Sms1*^{MUT} animals, compared to *Sms1*^{WT} controls (p=0.0158; Figure 3.16 G). Unfortunately it was not possible to detect MR protein levels, due to low expression levels and bad antibody performance.

An additional player in the HPA axis is the multidrug resistance protein 1(MDR-1). It is responsible for the efflux of CORT from the brain to the periphery. MDR-1 therefore regulates CORT levels in the brain, binding to receptors and negative feedback regulation. In whole brain samples, MDR-1 was elevated to 148.3 ± 25.4% (p<0.0001) in *Sms1*^{MUT} animals in comparison to *Sms1*^{WT} levels (Figure 3.16 F).

The same tendencies for MDR-1 and GR were also found in *Sms1*^{MUT} x *APPswe*^{Tg} in comparison to *Sms1*^{WT} x *APPswe*^{Tg} mice (see supplementary data: Figure 10.12). Underlining the relevance of *Sms1* expression on MDR-1 and GR protein levels also on an *APPswe* transgenic background.

3.1.11 Aged *Sms1*^{MUT} animals show splenomegaly

For *Sms1* knock-out animals it is known that they suffer from mild splenomegaly (Dong *et al.* 2012) and *Sms1* and *Sms2* knock-out animals show several other alterations concerning their immune system (Qin *et al.* 2010, Dong *et al.* 2012, Hayashi *et al.* 2014). Therefore spleen histology, cytokine and immunoglobulin levels of *Sms1* animals were investigated.

Three out of four *Sms1*^{MUT} females, aged between 1.7 and 2.3 years, had major splenomegaly. Figure 3.17 shows the most prominent enlargement found in *Sms1*^{MUT} animals.

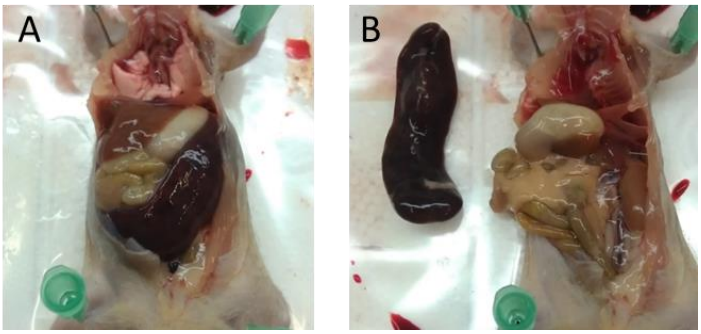

Figure 3.17: Major splenomegaly was found in aged female *Sms1*^{MUT} animals.
(A, B) Pronounced splenomegaly was seen in 3 out of 4 female *Sms1*^{MUT} animals with 1.7 and 2.3 years of age.

To analyze the spleen phenotype of these female mice in more detail PAS staining was performed to monitor overall spleen histology. Furthermore a first check of T-cell and B-cell distribution pattern and quantification by IHC and Western blots, respectively was done.

PAS staining of cross sections of aged *Sms1*^{WT} and *Sms1*^{MUT} spleens showed a loss of spleen structure, with blurred borders between white (WP) and red pulp (RP) and a disruption of the mantel zone (MZ; Figure 3.17 A). PAS staining revealed the presence of golden brownish pigments, representative for either hemosiderin or ceroid or lipofuscin, both found in the cytoplasm of macrophages. While hemosiderin reflects the removal of effete red blood cells ceroid or lipofuscin appears with the oxidation and polymerization of FAs. However, there were no obvious alterations in the extent of hemosiderin or ceroid or lipofuscin staining between *Sms1*^{WT} and *Sms1*^{MUT} spleens (Figure 3.17 A).

As former data showed hints to a possible alteration of specific T- and B-cell count (compare supplementary Table 10.7) Western blots and immunostaining against CD3, which if found in most T-cell types was performed. A high variance of CD3-positive cells in *Sms1*^{WT} and also in *Sms1*^{MUT} could be seen, with no significant alteration between the genotypes (Figure 3.17 B, D, E). *Sms1*^{MUT} 2 and 4, which had most enlarged spleens, did not show any CD3-positive signal in Western blots (Figure 3.17 D). Additionally IgG2b, one of the four different IgGs in mice, and TGF-β, which triggers the class switch from IgG3 to IgG2b were analyzed. IgG2b was not altered in *Sms1*^{MUT} compared to *Sms1*^{WT} (*Sms1*^{WT} 100.00 ± 23.48%, *Sms1*^{MUT} 60.95 ± 15.95%, p=0.2379). The same could be seen for TGF-β (*Sms1*^{WT} 100.00 ± 25.81%, *Sms1*^{MUT} 37.31 ± 18.31%, p=0.1180; Figure 3.17 D, E).

A dysfunctional lysosomal pathway or altered cell degradation might contribute to the spleen enlargement. To prove this hypothesis, markers for endocytosis or autophagy (early endosome antigen1, EEA1; ubiquitin binding protein p62, p62; catepsin-D, CatD, microtubule-associated protein 1 light chain 3 beta, LC3) and apoptosis (apoptosis inducing factor; AIF) were analyzed.

While a high variances of p62 levels and LC3II/LC3I ratios were found in *Sms1*^{MUT} samples, the early endosomal marker EEA1 showed elevated levels in *Sms1*^{MUT} spleen samples (*Sms1*^{WT} 100.00 ± 5.54%, *Sms1*^{MUT} 154.92 ± 10.35%, p=0.0474; Figure 3.17 F, G) and CatD levels showed a trend to be reduced to 40.10 ± 15.71% in *Sms1*^{MUT}s compared to *Sms1*^{WT} levels (100.00 ± 19.28%, p=0.0665). Additionally, AIF levels were lower in *Sms1*^{MUT} compared to *Sms1*^{WT} spleen samples (*Sms1*^{WT} 100.00 ± 4.56%, *Sms1*^{MUT} 60.57 ± 3.75%, p=0.0024; Figure 3.17 F, G).

To check if the increase in spleen volume is correlated to reduced apoptosis of spleen-residual cells, TUNEL staining was performed. Events of cell death could be identified clearly and in high number in *Sms1*^{WT} spleens, while in *Sms1*^{MUT} only the not enlarged spleen showed cell death events in similar intensity to those of *Sms1*^{WT} animals (Figure 3.17 H).

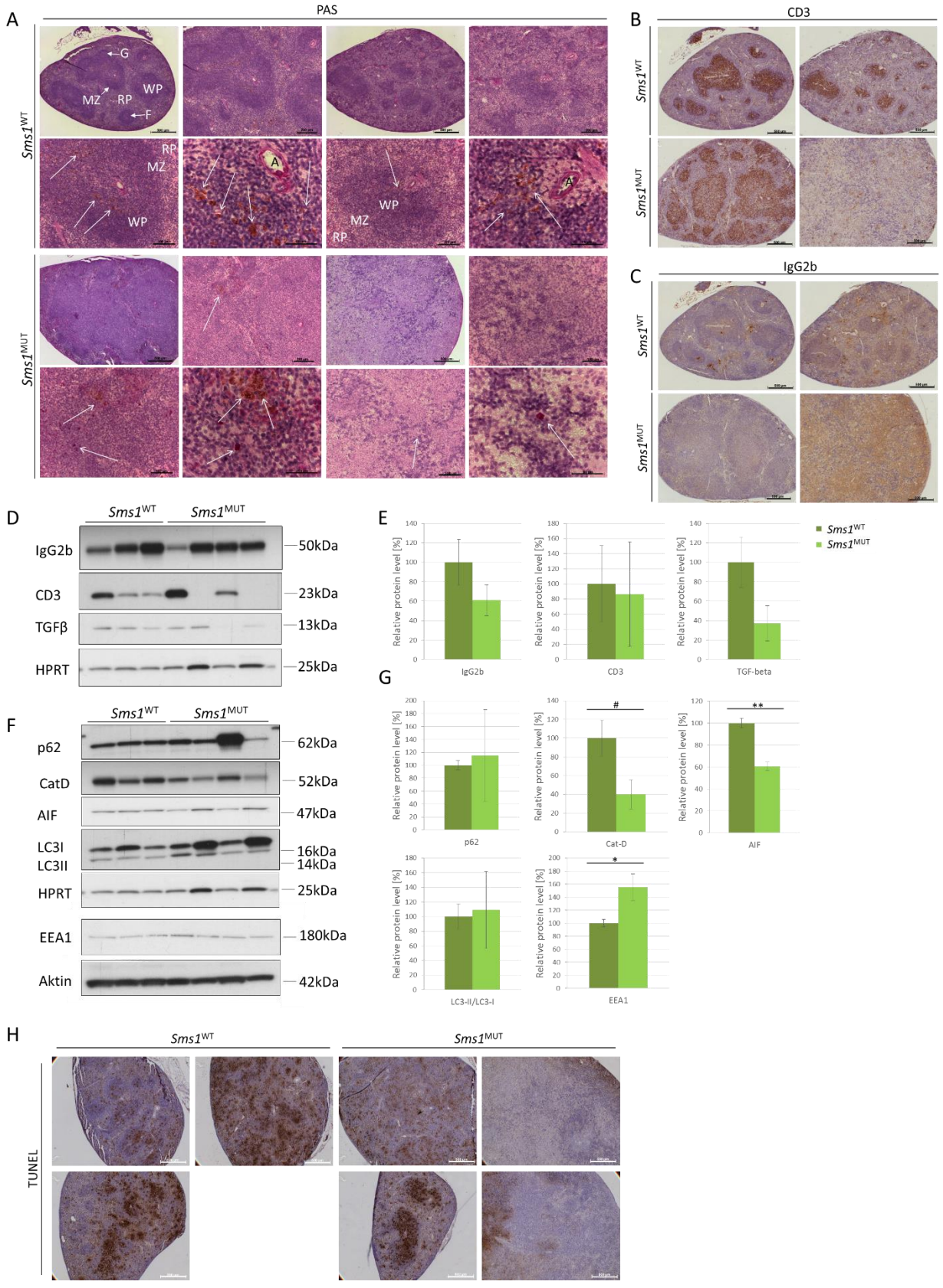

Figure 3.18: *Sms1*^{MUT} showed age-dependent splenomegaly, disruption of spleen structure with possible alterations in lysosomal and apoptotic pathways.

(A-C) Staining of spleen sections form aged (1.7 – 2.3 years) female *Sms1*^{WT} and *Sms1*^{MUT} mice. (A) Periodic acid

shiff (PAS) staining. Different structural and functional zones of the spleen are labeled. Hemosiderin or ceroid or lipofuscin positive pigments are marked (white arrows). Schale bars: 500µm, 200µm, 200m and 50µm with increasing magnification. (B, C) Immunostaining against (B) CD3 and (C) IgG2b. Scale bars: 500µm. (D-G) Immunoblots and quantification of (D, E) proteins of the immune system and (F, G) markers for endocytosis, autophagy or apoptosis. (H) TUNEL staining for *Sms1*^{WT} and *Sms1*^{MUT} spleens. Scale bars: 500µm.
Artery (A), follicle (F), granular zone (G), marginal zone (MZ), red pulp (RP), white pulp (WP). *Sms1*^{WT} n=3, *Sms1*^{MUT} n=4. Statistical analysis was done by two-tailed Student's T-test. Data is presented as mean ± SEM; $^{\#}p<0.01$ *p≤0.05, **p≤0.01, ***p≤0.001.

3.1.12 *Sms1*^{MUT} showed altered testes histology and partially comprised fertility

As a side project *Sms1*^{MUT} were analyzed with respect to testes functionality and fertility as it was known that *Sms1*$^{-/-}$ animals suffer from male infertility (Dong *et al.* 2012). However, to my knowledge no further research was performed on that topic. Therefore, testes and epididymides samples and sections of *Sms1*^{WT} and *Sms1*^{MUT} were analyzed regarding several points of interest.

3.1.12.1 Testes specific transcripts and protein levels of *Sms1* were strongly reduced in *Sms1*^{MUT} animals

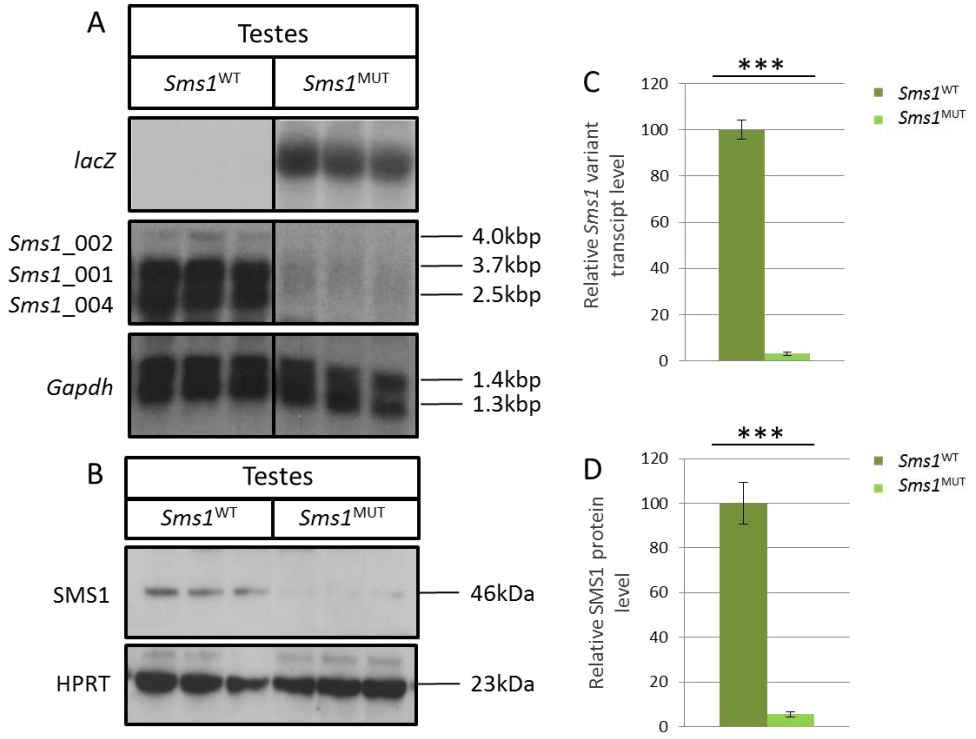

Figure 3.19: The gene trap cassette insertion disrupted expression of testes specific transcripts and reduced SMS1 protein levels.

(A) Northern blot of testes RNA. Specific probes against exon7 of *Sms1* (compare Figure 3.2) and against Gapdh were used for identification and quantification of testes specific *Sms1* transcripts. A lacZ probe, hybridizing to the gene trap cassette (compare Figure 3.1), was used for additional genotype confirmation. (B) Immunoblot analysis of testes tissue from *Sms1*WT and *Sms1*MUT animals. A commercial antibody against SMS1 was used. HPRT served as a loading control. (C) Quantification of the *Sms1*_001 and *Sms1*_004 splice variants in testes of *Sms1*^{MUT} in comparison to *Sms1*^{WT} animals. (D) Quantification of testes SMS1 protein levels of *Sms1*^{MUT} in comparison to *Sms1*^{WT} animals. *Sms1*^{WT} n=3, *Sms1*^{MUT} n=3. Statistical analysis was done by two-tailed Student's T-test. Data is shown as mean ± SEM; *p≤0.05, **p≤0.01, ***p≤0.001.

As stated before, *Sms1* has several tissue specific transcripts. In order to determine and quantify, which *Sms1* transcripts are present in testes and which variants are disrupted by the intronic gene trap insertion Northern blots were performed. Therefore, testes RNA was used and a probe covering 801bp of the first coding exon 7, which was created for the analysis of brain transcripts already

(compare: 2.2.10.2.5; Figure 3.2 C). The alternative transcripts *Sms1*-004 (2.5kb) and *Sms1*-001 (3.7kb) were the major transcripts detected in testes, showing a strong mean reduction to 3.1 ± 0.7% (p=0.0001) in the *Sms1*^{MUT} as compared to *Sms1*^{WT} levels (Figure 3.19 A, C). The transcript *Sms1*-002 (4.0kb), initiating upstream of the insertion site, was expressed only in marginal amounts in *Sms1*^{WT} only and was not detected in *Sms1*^{MUT} testes. The short *Sms1*-014 transcript was not detected in neither genotype (Figure 3.19 A, C). A probe against β-galactosidase mRNA was used to validate the expression of the inserted gene trap cassette in *Sms1*^{MUT} (Figure 3.19 A). SMS1 protein levels, analyzed by immunoblotting with a commercial antibody (Santa Cruz), was reduced to 5.5 ± 1.2% (p=0.0005) in *Sms1*^{MUT} animals, as compared to protein levels in the *Sms1*^{WT} (Figure 3.19 B, D).

3.1.12.2 Testes of *Sms1*^{MUT} showed specific reduction in lipid levels, which differed from changes observed in brain tissue

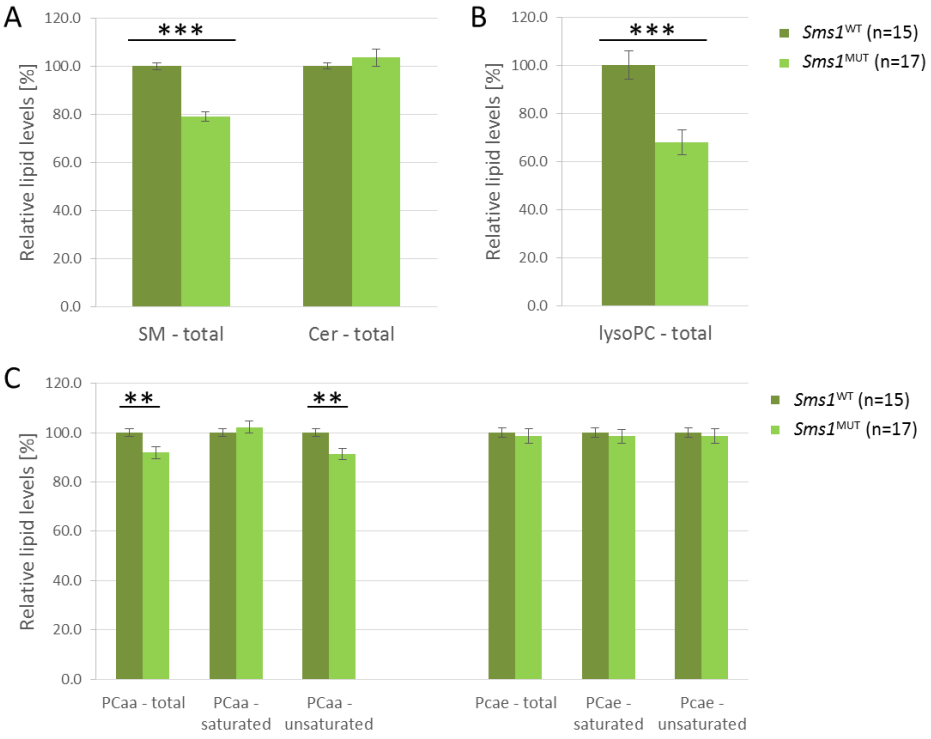

Figure 3.20: Lipid profile of *Sms1*^{MUT} testes, as compared to *Sms1*^{WT} controls.
(A-C) Relative lipid levels of (A) total sphingomyelin (SM) and ceramide (Cer), per 100µg or 500µg protein (B) total lyso-phosphatidylcholin (lyso-PC) per 100µg protein and (C) total diacyl-phosphatidylcholin (PCaa) and phosphatidylcholine-plasmalogene (PCae) levels per 100µg protein. PCaa and PCae levels are also shown separated by fatty acid saturation state.
All graphs show lipid levels of *Sms1*^{MUT} in comparison to *Sms1*^{WT} testes, which were set to 100%. *Sms1*^{WT} n=15, *Sms1*^{MUT} n=17. Statistical analysis was done by two-tailed Student's T-test. Data is presented as mean ± SEM; *p≤0.05, **p≤0.01, ***p≤0.001.

To determine SMS1 enzyme activity in testes, lipid profiles from testes of *Sms1*^{WT} and *Sms1*^{MUT} littermates were established. Comparable to brain, substrates of SMS1, Cer and PC as well as SM, lyso-

PC, PCaa and PCae of different chain length and saturation states were analyzed. Compared to *Sms1*^{WT} levels, SMs were reduced to 78.9 ± 2.0% ($p<0.0001$) in *Sms1*^{MUT} (Figure 3.20 A; supplementary Table 10.16). Cer levels were almost unaffected in testes samples (Figure 3.20 A).

Analysis of PCaa revealed a reduction to 91.9 ± 2.4% ($p=0.0089$) in *Sms1*^{MUT}, which mainly resulted from a reduction of unsaturated PCaa (91.3 ± 2.4%; $p=0.0056$). The amount of saturated PCaa was comparable to *Sms1*^{WT} levels (Figure 3.20 C). Neither PCae levels of saturated, nor of unsaturated species were altered in *Sms1*^{MUT} testes samples, compared to *Sms1*^{WT} levels. (Figure 3.20 C).

A more detailed dispatch of the most abundant PCaa and PCae species revealed a significant reduction in MUFA- and PUFA-containing species in *Sms1*^{MUT} compared to *Sms1*^{WT} (Table 3.2 A). Most striking results among the FAs with a highly significant reduction were found for the PCaa species C38:5 and C38:6, indicative of a loss of Arachidonic acid (AA; C20:4), DHA (C22:6) or EPA (C20:5, compare to Table 3.2 A). In the PCae profile C38:6 was also one of the lipids showing strong reduction, pointing to a possible reduction of DHA and EPA incorporation (compare to Table 3.2 B). Interestingly, the total level of lyso-PCs was significantly reduced to 73.4 ± 0.2% ($p=0.001$) in testes of *Sms1*^{MUT} in comparison to the level in *Sms1*^{WT} samples (Figure 3.20 B). This reduction was found to be present in all of the major lyso-PC species with high significance (compare to Table 3.2 C).

Table 3.2: Lipid profile of *Sms1*^{MUT} testes PCaa, PCae and lyso-PC species, compared to *Sms1*^{WT} levels. Lipid levels with the highest intensities are shown for diacyl-phosphatidylcholines (PCaa, A) acyl-alkyl-phosphatidylcholines (PCaes, B) and lyso-phosphatidylcholines (lyso-PCs, C). Additionally, predicted major fatty acids are listed. *Sms1*^{WT} n=15, *Sms1*^{MUT} n=17. Statistical analysis was done by two-tailed Student's T-test. Data is presented as mean percentage ± SEM, with *Sms1*^{WT} levels set to 100%, *p≤0.05, **p≤0.01, ***p≤0.001.

A

PC aa species	Sms1WT (n=15)			Sms1MUT (n=17)			significance		
	Intensity	%	SEM %	Intensity	%	SEM %	ttest	significance	
PC aa total	10,445,747	100.0	1.6	9,602,725	91.9	2.4	0.0089	**	
PC aa saturated	560,581	100.0	1.5	573,085	102.2	2.5	0.4548		
PC aa unsaturated	9,885,166	100.0	1.6	9,029,640	91.3	2.4	0.0056	**	
PC aa CX:1	2,430,350	100.0	1.5	2,400,435	98.8	2.2	0.6527		
PC aa CX:2	724,364	100.0	2.1	637,658	88.0	2.7	0.0016	**	
PC aa CX:3	829,606	100.0	1.8	729,132	87.9	2.6	0.0008	***	
PC aa CX:4	2,744,306	100.0	1.7	2,572,597	93.7	2.3	0.0353	*	
PC aa CX:5	2,326,950	100.0	1.7	1,977,048	85.0	2.4	0.0000	***	
PC aa CX:6	829,590	100.0	2.3	712,770	85.9	3.2	0.0015	**	predicted major FA
PC aa C38:5	1,950,614	100.0	1.6	1,641,727	84.2	2.4	0.0000	***	20:5 20:4 22:5 18:0 18:1 16:0
PC aa C34:1	1,798,063	100.0	1.3	1,786,400	99.4	2.1	0.7968		
PC aa C36:4	1,618,575	100.0	1.4	1,506,247	93.1	2.4	0.0210	*	
PC aa C38:4	981,771	100.0	2.3	928,077	94.5	2.3	0.1033		
PC aa C38:6	585,682	100.0	2.2	486,001	83.0	3.6	0.0006	***	22:6 22:5 20:5 20:4 18:1 18:2 16:0 16:1
PC aa C36:3	561,250	100.0	1.8	470,413	83.8	3.0	0.0001	***	18:1 18:2
PC aa C36:1	456,553	100.0	2.9	458,581	100.4	3.4	0.9221		
PC aa C32:0	380,136	100.0	1.4	407,912	107.3	2.7	0.0259	*	
PC aa C34:2	357,430	100.0	2.5	284,356	79.6	3.0	0.0000	***	18:2 16:1 14:0

B

PC ae species	Sms1WT (n=15)			Sms1MUT (n=17)			significance		
	Intensity	%	SEM %	Intensity	%	SEM %	ttest	significance	
total PC ae	2,308,270	100	2.01591613	2,276,965	99	2.95707438	0.70788908		
saturated PC ae	135,666	100	1.8	133,692	99	2.8	0.6667		
unsaturated PC ae	2,172,604	100	2.0	2,143,273	99	3.0	0.7113		
PC ae CX:1	445,538	100	2.3	526,086	118	4.3	0.0012	**	
PC ae CX:2	152,595	100	2.3	152,839	100	2.9	0.9659		
PC ae CX:3	108,640	100	2.2	110,663	102	2.9	0.6097		
PC ae CX:4	390,514	100	2.3	393,153	101	3.3	0.8680		
PC ae CX:5	595,251	100	2.2	554,955	93	3.0	0.0751		
PC ae CX:6	480,066	100	2.2	405,577	84	3.2	0.0005	***	predicted major FA
PC ae C38:5	440,375	100	2.2	408,858	93	3.1	0.0682		
PC ae C38:6	435,848	100	2.2	361,284	83	3.3	0.0002	***	22:6 20:5 20:4 18:1 18:2 16:0
PC ae C34:1	283,881	100	2.9	373,995	132	5.6	0.0001	***	18:0 18:1 16:0 16:1
PC ae C36:4	207,666	100	2.5	204,587	99	3.6	0.7362		
PC ae C38:4	121,855	100	2.2	123,640	101	3.1	0.7023		
PC ae C40:5	92,162	100	2.5	92,797	101	3.3	0.8679		
PC ae C32:1	77,986	100	1.7	66,307	85	2.6	0.0001	***	
PC ae C34:2	73,002	100	3.2	67,181	92	4.0	0.1318		
PC ae C40:0	55,709	100	2.6	54,825	98	3.2	0.7015		
PC ae C36:5	51,057	100	2.2	42,016	82	2.5	0.0000	***	

C

lyso PC a species	Sms1WT (n=15)			Sms1MUT (n=17)			significance	
	Intensity	%	SEM %	Intensity	%	SEM %	ttest	significance
total lyso PC a	434258.4	100.0	5.9	294251.0	67.8	5.2	0.0003	***
Lyso PC 16:0	160184.4	100.0	6.2	102757.1	64.1	6.0	0.0002	***
Lyso PC 20:4	91537.0	100.0	7.6	58978.2	64.4	6.1	0.0010	***
Lyso PC 18:1	71646.4	100.0	6.9	50157.9	70.0	5.9	0.0025	**
Lyso PC 18:0	58547.4	100.0	4.7	43893.5	75.0	4.6	0.0007	***
Lyso PC 20:3	17463.1	100.0	7.7	10297.6	59.0	6.1	0.0003	***
Lyso PC 18:2	15400.3	100.0	7.9	8920.0	57.9	5.1	0.0001	***
Lyso PC 14:0	3701.9	100.0	1.7	3340.3	90.2	1.3	0.0001	***
Lyso PC 16:1	3526.8	100.0	6.3	2312.6	65.6	5.2	0.0002	***
Lyso PC 26:0	3344.8	100.0	10.3	4216.3	126.1	19.2	0.2444	

3.1.12.3 *Sms1*^{MUT} testes showed strongly changed histology and enhanced apoptosis

Testes of *Sms1*^{MUT} were smaller in size and showed strikingly different histology compared to normal *Sms1*^{WT} testes (Figure 3.21 A - J). In *Sms1*^{MUT} epididymides, mostly round spermatids, lacking acrosome structures and tails, were accumulated, while mature spermatozoa were rarely seen (Figure 3.21 C, D). Additionally, in *Sms1*^{MUT} seminiferous tubules of different stages, large vacuoles were frequently encountered (Figure 3.21 F, J; Figure 3.22 B). In testes, comparison of *Sms1*^{WT} and *Sms1*^{MUT}s revealed that round and elongated spermatids were strongly reduced in number and that only a few spermatozoa were observed in *Sms1*^{MUT} (Figure 3.21 E, F, I, J).

Testosterone levels were not significantly decreased in male mutants (*Sms1*^{WT}: 1.21 + 1.45, - 1.15nmol/L; *Sms1*^{MUT}: 0.92 + 1.17, - 0.74nmol/L; p=0.203; Supplementary Figure 10.10). Meaning a lack of testosterone, causing spermatogenesis deficits could be excluded.

Expression and localization of SMS1 (Figure 3.21 E-F) and SMS2 (Figure 3.21 I, J) were determined by immunohistochemistry on testes sections. Both SMSs were prominently visible in the acrosome of developing *Sms1*^{WT} spermatids and spermatozoa, a structure that was rarely visible in *Sms1*^{MUT} (Figure 3.21. F, J). SMS1 was diffusely seen at sites of intercellular contacts such as the blood-testis-barrier (BTB; Figure 3.21 E) made up by Sertoli cells and the blood-epididymis-barrier (BEB; Figure 3.21 G), where it was strongly expressed in the Principal cells. SMS1 expression overall was strongly reduced in *Sms1*^{MUT} testes and epididymides, but not totally absent (Figure 3.21 F, H). SMS2 was absent from the BTB in *Sms1*^{WT} testes, but expressed in elongating spermatids. In *Sms1*^{MUT} testes, SMS2 expression was reduced to a small dot found in spermatids (Figure 3.21 I, J).

To answer the question if the observed vacuoles result from enhanced apoptosis in *Sms1*^{MUT} testes, TUNEL staining was performed. Testes of *Sms1*^{MUT} had clusters of apoptotic germ cells in the basal compartment of the seminiferous tubules (Figure 3.21 K, L). Additionally, apoptotic material accumulated in the lumen of the tubules (Figure 3.21 L). Counting of cell death events (TUNEL positive cells per tubule) resulted in a 1.9-fold higher rate in *Sms1*^{MUT} testes, compared to *Sms1*^{WT} testes (Figure 3.21 M).

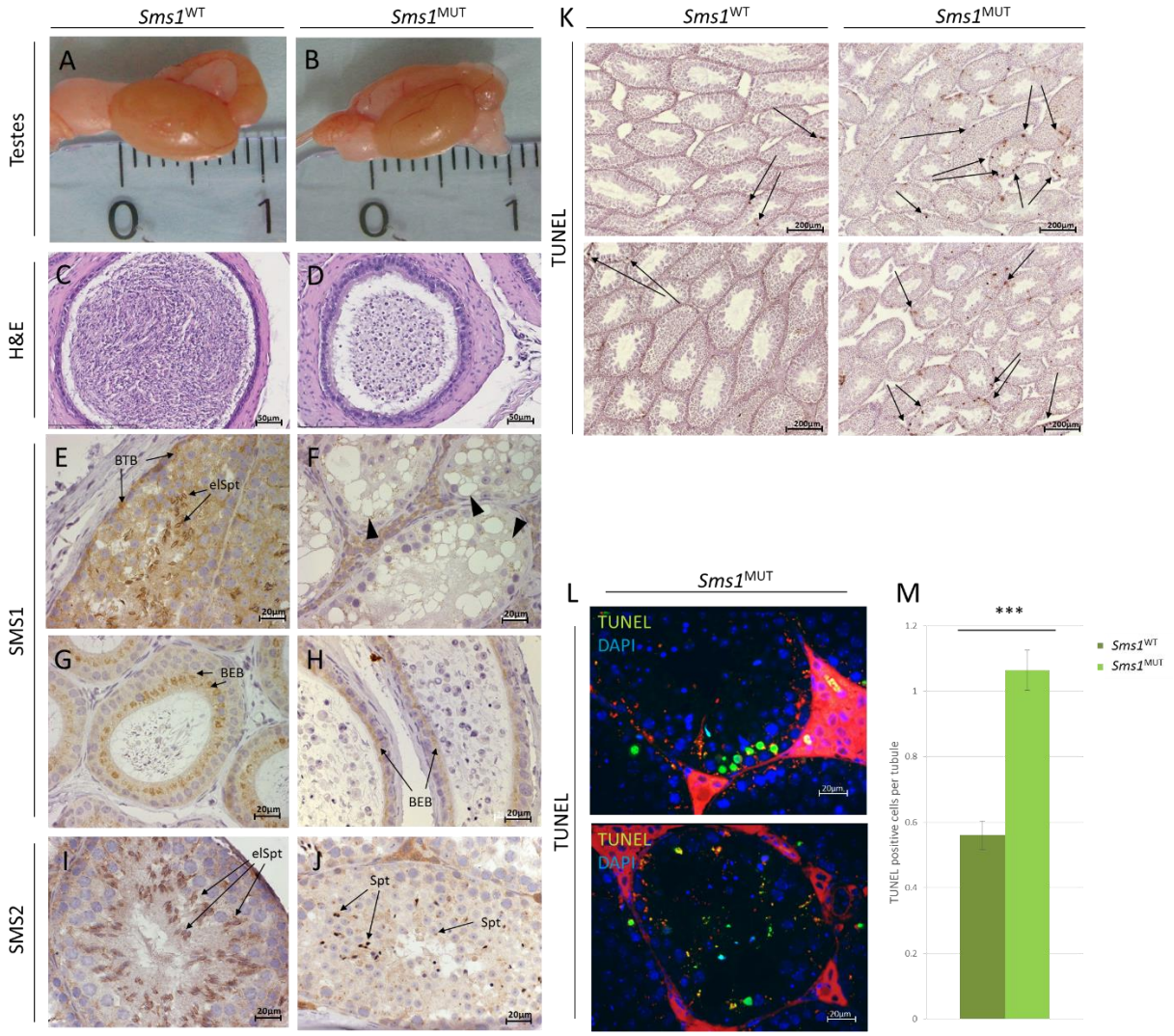

Figure 3.21: *Sms1*^{MUT} males had smaller testes with strikingly different histology compared to *Sms1*^{WT} males.

(A-B) Representative images of 10 weeks old (A) *Sms1*^{WT} and (B) *Sms1*^{MUT} testes. (C-D) Haemalaun and Eosin staining of 16 weeks old (C) *Sms1*^{WT} and (D) *Sms1*^{MUT} epididymides. Scale bar: 50µm. (E-J) Immunostaining against (E-H) SMS1 and (I-J) SMS2 in (E, I) *Sms1*^{WT} and (F, J) *Sms1*^{MUT} testes and (G) *Sms1*^{WT} and (H) *Sms1*^{MUT} epididymides. Sites of SMS1 and SMS2 localization (black arrows) and frequently observed vacuoles (black arrow heads) are indicated. Scale bar: 20µm. (K) TUNEL staining of *Sms1*^{WT} and *Sms1*^{MUT} testes are shown. Arrows point to TUNEL positive cells. Scale bar: 200µm. (L) Fluorescent TUNEL staining of *Sms1*^{MUT} testes, showing representative cell death events at the basal lamina (upper image) and apoptotic material in the tubule lumen (fluorescent image; image by Harry Schertan). Scale bar: 20µm. (M) Counting of TUNEL positive cells per tubule in *Sms1*^{WT} and *Sms1*^{MUT} seminiferous tubules. TUNEL counting: *Sms1*^{WT} n=3, *Sms1*^{MUT} n=4. Statistical analysis was done by two-tailed Student's T-test. Data is presented as mean number of TUNEL positive cells/tubule ± SEM, with an average of 435 tubules counted per animal; *p≤0.05, **p≤0.01, ***p≤0.001.

3.1.12.4 Sloughing of immature germ cell takes place between pachytene and round spermatid stage

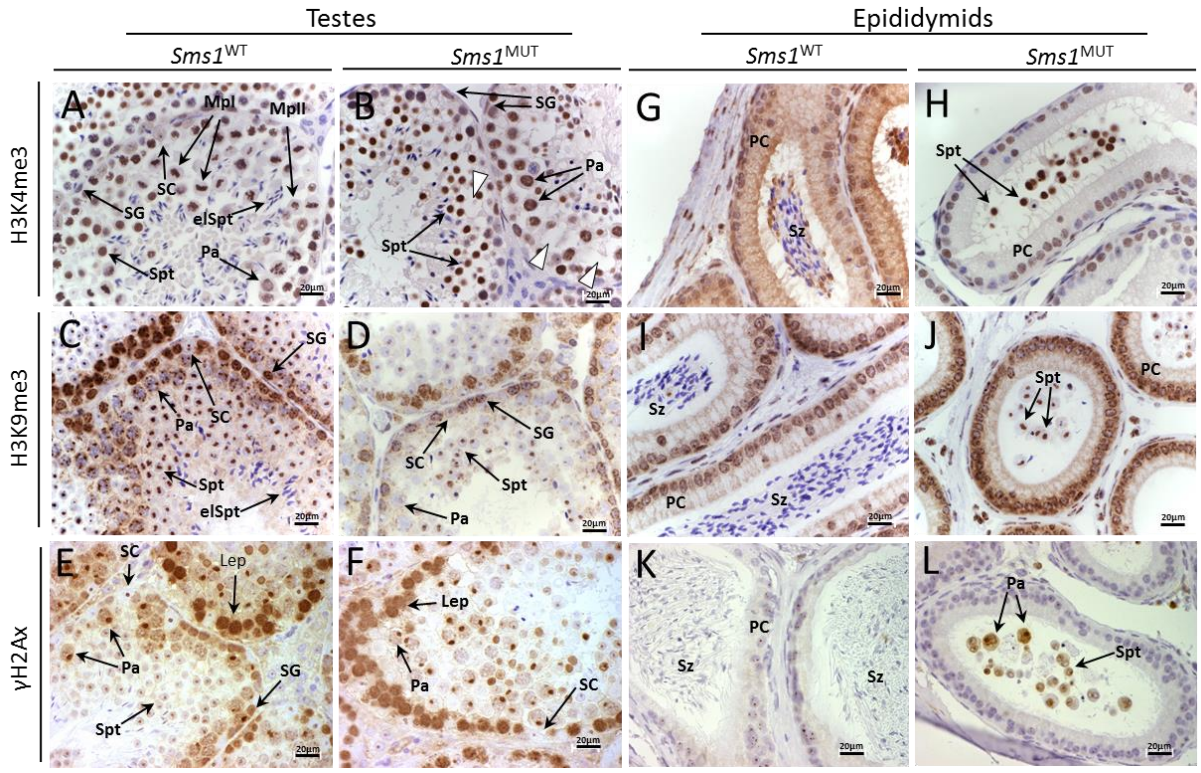

Figure 3.22: Specification of spermatogenesis stages with specific histone markers via immunohistochemistry (IHC) on testes sections of *Sms1*^{MUT} compared to *Sms1*^{WT} animals. Presence of histone modifications in epididymis illustrated sloughing of pachytene spermatocytes to round spermatid stages.
(A-L) IHC using the indicated specific antibodies for histone variants on sections of *Sms1*^{WT} and *Sms1*^{MUT} (A-F) seminiferous tubules or (G-L) epididymides. Stages of spermatogenesis are labeled. Vacuoles, frequently encountered in *Sms1*^{MUT} testes are marked (white arrow heads). Scale bar: 20µm.
Tri-methylated lysine 4 of histone 3 (H3K4me3); tri-methylated lysine 9 of histone 3 (H3K9me3); elongating spermatids (elSpt) leptotene spermatocytes (Lep), mitosis phase I (MpI), mitosis phase II (MpII), pachytene spermatocytes (Pa), Principal cells (PC); Sertoli cell (SC), spermatogonia (SG), spermatids (Spt), spermatozoa (Sz).

From these findings, I hypothesized sloughing of spermatid stages into *Sms1*^{MUT} testes lumen and their accumulation in the epididymides. In order to determine, the exact stage of spermatogenesis at which germ cells of *Sms1*^{MUT} lose contact to Sertoli cells, the expression of specific histone modifications, taking place during the course of spermatogenesis, were analyzed. Histone modifications during meiosis include tri-methylation of histone H3 at lysine residue 4 (H3K4me3) prior to meiotic foci formation, a modification that is associated with active chromatin (Khalil *et al.* 2004, Khalil and Driscoll 2006, Godmann *et al.* 2007). The expression pattern of H3K4me3 was determined and found the histone modification was found to be expressed weakly in *Sms1*^{WT} Sertoli cells and in the spermatogonia nuclei. H3K4me3 was also detectable in pachytene spermatocytes and covered the entire nucleus of spermatids, but was again absent from mature spermatozoa (Figure 3.22 A, B). In epididymides H3K4me3 was mainly found in Principal cells (Figure 3.22 G). Expression of H3K4me3 in

Sms1^{MUT} testes showed equal results as in *Sms1*^{WT} animals (Figure 3.22 A, B, G, H). H3K4me3 expression marks the entire nucleus of spermatids, which were found in the lumen of *Sms1*^{MUT} epididymides. Elongated spermatids found in the *Sms1*^{WT} lumen of the epididymides were not H3K4me3 positive (Figure 3.22 H).

Histone H3 lysine 9 becomes first tri-methylated (H3K9me3) in spermatogonia, a modification that is associated with inactive chromatin. While H3K9me3 is not found in the XY-body of pachytene spermatocytes, it is detectable in the heterochromatin clusters of spermatogonia up to the round spermatid stages (Mermoud *et al.* 2002, Peters *et al.* 2002). This modification was seen in *Sms1*^{WT} as well as in *Sms1*^{MUT} testes (Figure 3.22 C, D). Expression pattern of H3K9me3 in *Sms1*^{WT} and *Sms1*^{MUT} testes was strongest in spermatogonia and pachytene spermatocytes and was maintained until spermatid stage (Figure 3.22 C, D). In epididymides H3K9me3 was mainly found in Principal cells. (Figure 3.22 I, J). In the *Sms1*^{MUT} epididymides lumen spermatids contained the typical heterochromatin cluster stained by H3K9me3, indicating sloughing of histone-retaining spermatocytes cells up to late spermatid stages (Figure 3.22 J).

Histone H2Ax becomes phosphorylated at serine residue 139 (γH2AX) (Kubler *et al.* 2011) formation during S-phase and meiotic prophase (Rogakou *et al.* 1998, Mahadevaiah *et al.* 2001). γH2Ax formation occurs during S-phase in B-type spermatogonia and remains detectable until the pachytene-stage, where it localizes to the XY-body (Hamer *et al.* 2003). γH2Ax formation initiates during leptotene – zygotene where it is necessary for homologous recombination-mediated DNA repair (Mahadevaiah *et al.* 2001, Govin *et al.* 2004). However, this histone modification is only faintly detectable in spermatid heterochromatin (Peters *et al.* 2002, Khalil *et al.* 2004, Khalil and Driscoll 2006). In both, *Sms1*^{WT} and *Sms1*^{MUT} γH2Ax staining of B-type spermatogonia and of the XY-body in pachytene spermatocytes could be detected. Staining was maintained until spermatid stage (Figure 3.22 E, F). γH2Ax -positive cells were not observed in the epididymal lumen of *Sms1*^{WT} mice (Figure 3.22 K), while γH2Ax-positive spermatocytes and haploid spermatids were present in mutant epididymides (Figure 3.22 L), indicating that sloughing involved pachytene to late spermatid stages and thus a compromised function of the seminiferous epithelium.

3.1.12.5 *Sms1*^{MUT} testes showed alterations in junction protein expression and localization and in blood-testes-barrier functionality

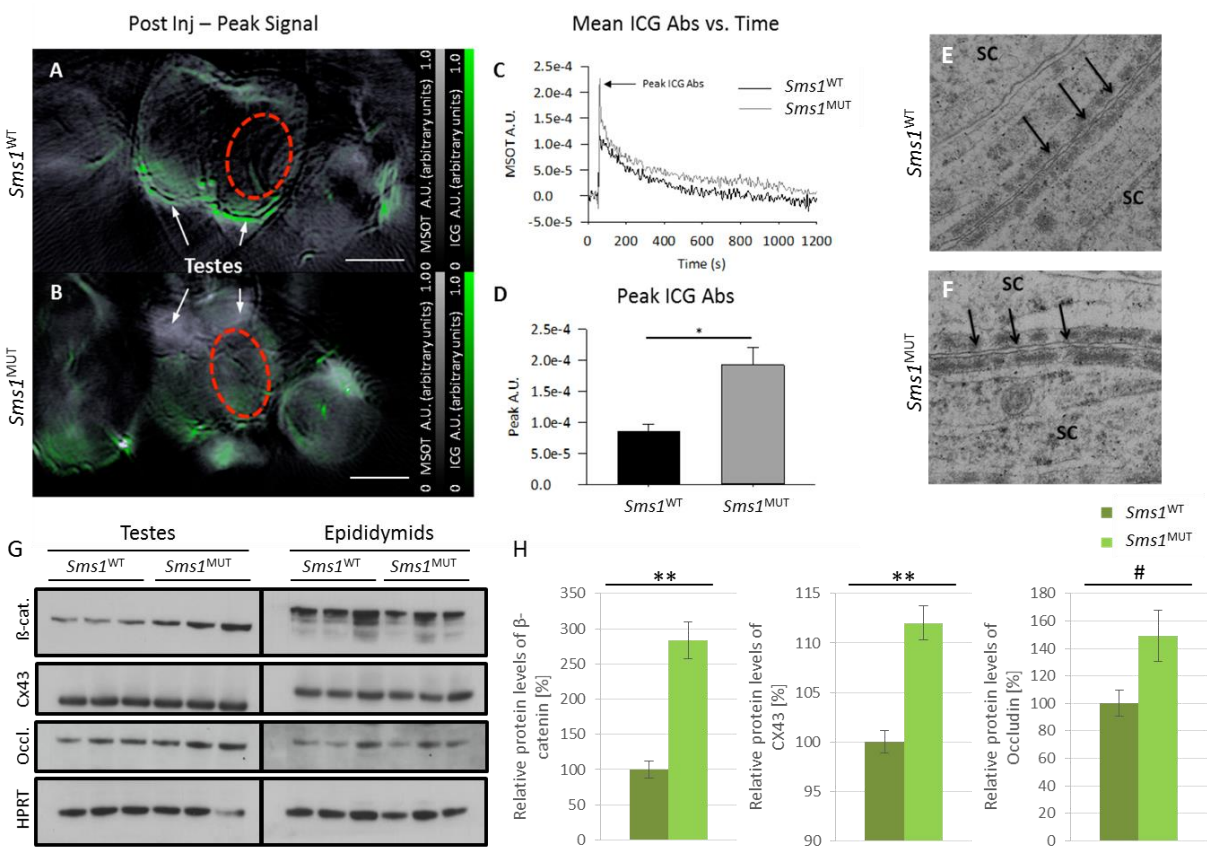

Figure 3.23: The blood-testes-barrier of *Sms1*^{MUT} appeared to be established but impaired.
(A, B) Unmixed Iodocyanin green (ICG) signal (green) overlayed on anatomical images (reconstructed image at 860nm) of (A) *Sms1*^{WT} and (B) *Sms1*^{MUT} testes, immediately following ICG injection. Color maps are shown for the overall absorbance signal in the anatomical images and (grey) and multispectrally-unmixed ICG signal (green). Mean pixel intensity was determined in the area of the testes, as indicated by red ellipsoids, and plotted vs. time. Scale bar: 3mm (C) Representative ICG-absorbance vs. time curves for *Sms1*^{WT} (black trace) and *Sms1*^{MUT} (grey trace) animals. (D) Peak values of the ICG absorbance vs. time curves. MSOT A.U. values are normalized by subtracting the overall signal by the baseline signal measured prior to ICG injection (Image by Dr. Steven Ford). (E, F) Transmission electron microscopy (TEM) of Sertoli cell (SC) boundaries in the testes of (E) *Sms1*^{WT} and (F) *Sms1*^{MUT} mice. Tight-junctions (black arrows), necessary for the formation and integrity of the BTB between SC could be shown. Magnification: x 50000. (G) Immunoblot of junction markers. B-catenin (β-cat) was used as adherence junction marker, connexin 43 (Cx43) as gap junction marker and occluding (Occl) as tight junction marker. (H) Quantification of immunoblot results on testes samples.
MSOT data: *Sms1*^{WT}, nobs=3 from 3 animals; *Sms1*^{MUT}, n_{obs}=6 from 3 animals; Immunoblot data: *Sms1*^{WT} n=3, *Sms1*^{MUT} n=3. Statistical analysis was done by two-tailed Student's T-test. Data is presented as mean ± SEM; *p≤0.05, **p≤0.01, ***p≤0.001. Absorption units (A.U).

It was hypothesized that the specific reduction of PUFAs (AA, EPA, DPA and DHA) in *Sms1*^{MUT} testes may cause sloughing of pachytene spermatocytes and spermatids due to a disturbance of the integrity of the BTB, as proposed by Stoffel et al., (2008) (Stoffel *et al.* 2008). In order to test the hypothesis of a compromised BTB, testes of *Sms1*^{MUT} animals were analyzed on different levels.

By TEM it could be shown that tight junctions between Sertoli cells were established equally in *Sms1*^{WT} and *Sms1*^{MUT} testes (Figure 3.23 E, F).

However, when the protein levels of representative junction markers were quantified in testicular and epididymal samples by immunoblotting, β-catenin (β-cat, 283.3 ± 26.0%, p=0.0054) and connexin 43 (Cx43, 112.0 ± 1.7%, p=0.0084) as subunits of adherents- or gap-junctions, respectively, were significantly elevated in *Sms1*^{MUT} testes (Figure 3.23 G, H), while their protein levels in the epididymides were unchanged (supplementary Figure 10.11). Occludin levels in the *Sms1*^{MUT} showed a tendency to be elevated in testes (Occl, 149.1 ± 18.7%, p=0.0776) but were also not altered in the epididymides compared to *Sms1*^{WT} levels (Figure 3.23 G, H and supplementary Figure 10.11).

I wondered if the elevated expression levels of junctional proteins might correlate with hampered protein trafficking to their site of destination. A misregulation of protein trafficking to the cellular surface or an altered distribution between basal and apical compartment might lead to profound defects in germ cell maturation due to guidance and communication deficits between Sertoli cells and maturating germ cells. Therefore I checked for localization of the respective markers in testes and epididymides tissue. Immunostaining, using β-catenin and anti-Connexin 43 antibodies showed their location in *Sms1*^{WT} and *Sms1*^{MUT} near the BTB and in the adluminal compartment of the testes, respectively (Figure 3.23 A, B, G, H). No alteration between *Sms1*^{WT} and *Sms1*^{MUT} could be detected. For β-catenin, however, a dislocation in the caput of the epididymides in *Sms1*^{MUT} was found. While in *Sms1*^{WT} testes β-catenin localized mostly to the adluminal compartment it was found to be more abundantly distributed in *Sms1*^{MUT} (Figure 3.23 C, D). In the epididymal cauda no alteration of β-catenin location between both genotypes was detected (Figure 3.23 E, F). Connexin 43 was equally expressed in the epididymides of *Sms1*^{WT} and *Sms1*^{MUT} (Figure 3.23 I-L). The tight-junction marker occludin was less prominent near the BTB in *Sms1*^{MUT} (Figure 3.23 M, N) and was found to be more prominent in the adluminal part of the tubules in the epididymal cauda compared to *Sms1*^{WT} (Figure 3.23 Q, R).

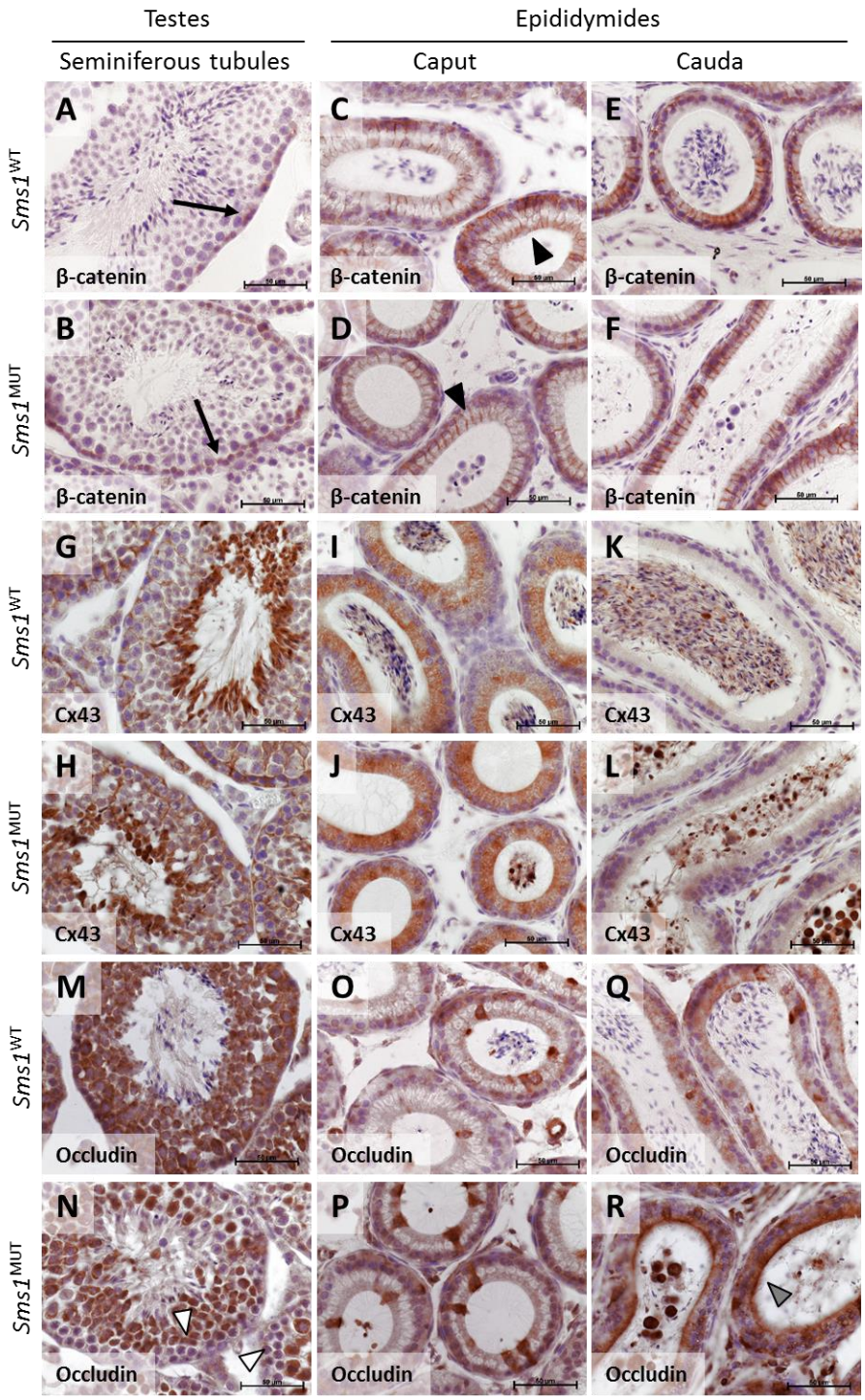

Figure 3.24: Sertoli/Sertoli and Sertoli/germ cell junction marker showed partial dislocation in *Sms1*^{MUT} testes or epididymides.

(A-R) Immunostaining against junction proteins on sections of *Sms1*^{WT} and *Sms1*^{MUT} testes and epididymides. Representative pictures of (A-F) β-catenin staining as adherence junction marker, (G-L) Connexin 43 (Cx43) staining as gap junction marker and (M-R) Occludin staining as tight junction marker are shown. Scale bar: 50µm. Localization of β-catenin near the BTB (black arrows) in *Sms1*^{WT} and *Sms1*^{MUT} testes and its delocalization towards the basal compartment in the epididymal caput (black arrow heads) in *Sms1*^{MUT} is indicated. In *Sms1*^{MUT} the retraction of Occludin from the BTB (white arrow heads) and its accumulation in the adluminal compartment of the epididymal cauda (gray arrow head) is shown. Blood-testes-barrier (BTB).

The up regulation of junction proteins and their partial delocalization in the testes and/or epididymal tissue could lead to a comprised function of the BTB. In order to elucidate this hypothesis *in vivo*, Multi-Spectral Optoacoustic Tomography (MSOT) imaging of Iodocyanin Green (ICG) distribution in the testes was performed. Following ICG injection, *Sms1*^{WT} testes show little ICG peak signal within testes, while, a qualitatively higher signal was detected in *Sms1*^{MUT} testes (Figure 3.23 A, B). Representative time courses of ICG distribution in the *Sms1*^{WT} and *Sms1*^{MUT} mice are shown in Figure 3.23 C, indicating higher peak ICG levels and slower clearance of ICG in the *Sms1*^{MUT} animals when compared to the *Sms1*^{WT} values ($8.43e^{-5} \pm 1.25e^{-5}$, p=0.040, Figure 3.23 D).

The elevated levels of junction markers might indicate a compensatory mechanism between Sertoli cells and germ cells in order to maintain functional cross-talk and adhesion. It may also indicate reduced trafficking of these junctional proteins to the cellular membrane, as it was shown for both SMSs to have an impact on TGN-mediated trafficking and secretion (Subathra *et al.* 2011). Nevertheless, the higher ICG signal in the *Sms1*^{MUT} animals indicates increased permeability of the BTB, since a loss of integrity results in ICG leaking from vessels to testicular tissue.

3.1.12.6 *Sms1*^{MUT} showed partial reduction in fertility, which could be ameliorated by DHA/EPA diet

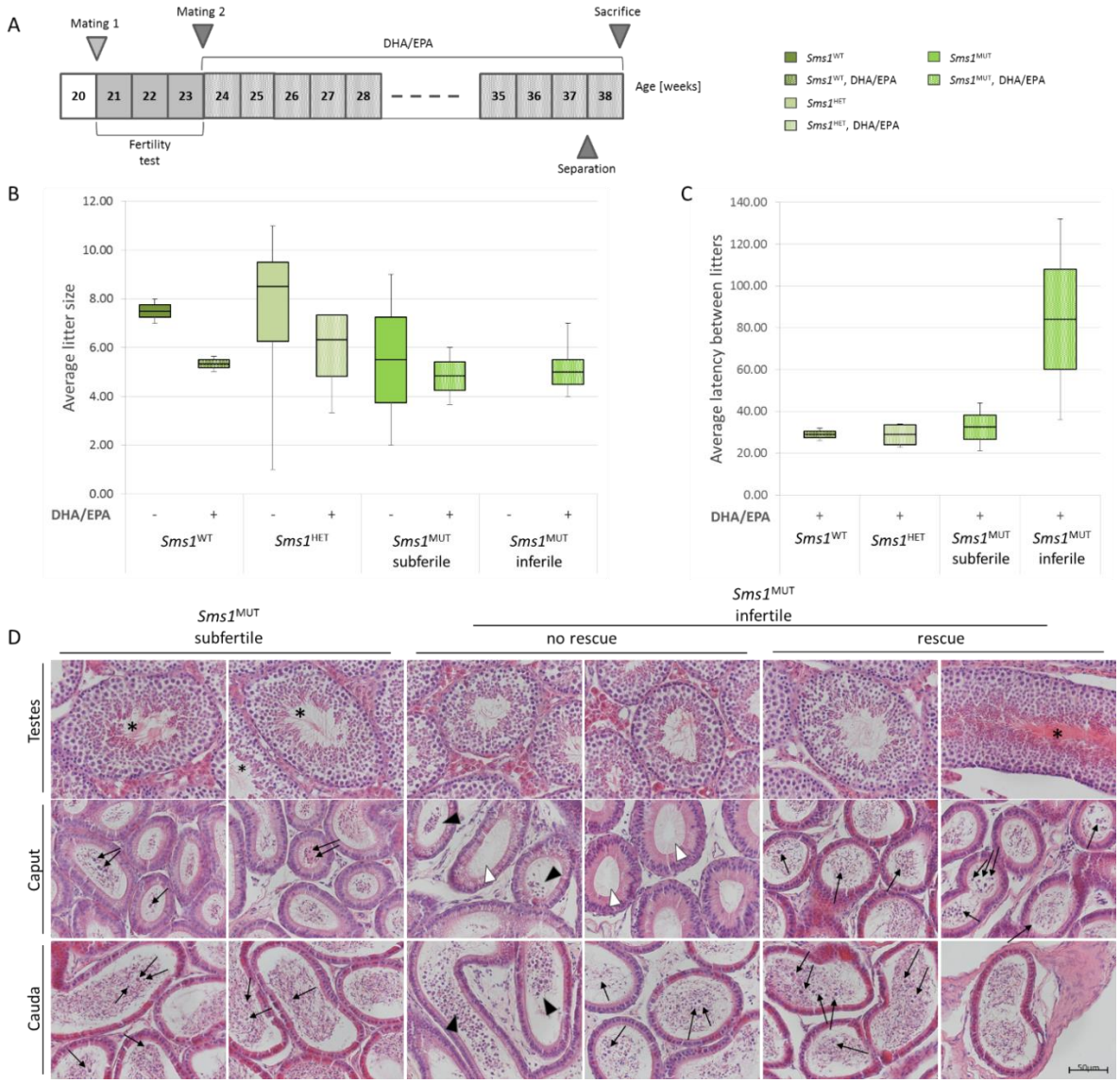

Figure 3.25: DHA/EPA enriched diet led to partial rescue of the sloughing phenotype in infertile *Sms1*^{MUT}. (A) Schematic time course of the infertility test mating scheme, with subsequent DHA/EPA supplementation. *Sms1*^{WT}, *Sms1*^{HET} and *Sms1*^{MUT} were mated at the age of 20 weeks to an 11 week old C57Bl/6J female (mating 1) for a test of fertility. After three weeks these mating were terminated and the female was replaced by a new 11 week old C57Bl/6J female (mating 2). These mating were maintained for 13 weeks, before they were terminated (separation). With the start of mating 2 all males were provided with a DHA/EPA diet supplementation (9mg total omega-3 content/animal/day, oral dose) for the duration of 14 weeks. At the age of 38 weeks males were sacrificed and testes were analyzed. (B) Mean number of offspring produced by *Sms1*^{WT}, *Sms1*^{HET}, *Sms1*^{MUT} fertile and *Sms1*^{MUT} infertile without (green boxes) and with DHA/EPA diet supplementation (dotted green boxes). (C) Mean latency between litters with DHA/EPA diet supplementation. (D) Representative images of H&E stained testes of fertile *Sms1*^{MUT}, infertile not rescued *Sms1*^{MUT} and infertile rescued *Sms1*^{MUT} are shown after receiving DHA/EPA diet. Arrows point to remaining Pa and Spt in seminiferous tubules. Accumulation of immature germ cells (dark arrow heads) and empty tubes (white arrow heads) are shown. Scale bar: 50µm, for all pictures. Pachytene spermatocytes (Pa), spermatids (Spt). *Sms1*^{WT} n=2, *Sms1*^{HET} n=4 and *Sms1*^{MUT} n=6. Statisical analysis was done by two-way ANOVA with *post hoc* Tukey's test. Data is shown as median ± quartiles.

When *Sms1*^{MUT} males were initially mated at the age of 8 weeks I found that 33% were not able to produce offspring. At the age of 20 weeks the fully prominent testis dysmorphology in six out of six mutant males as described above was present in *Sms1*^{MUT} (Figure 3.21 C, D). Therefore, I wondered about the fertility state of males of the *Sms1* mouse line at that age. In total twelve male animals including all genotypes were analyzed (*Sms1*^{WT} n=2, *Sms1*^{HET} n=4, *Sms1*^{MUT} n=6). First the fertility status was determined in a mating set up with C57Bl/6J females (age: eleven weeks) for a three week period. Infertility of *Sms1*^{MUT} was assumed in this experiment when a male failed to produce offspring during the mating time of 3 weeks (Figure 3.25 A). All *Sms1*^{WT} and *Sms1*^{HET} males tested produced offspring. However, just two out of the six *Sms1*^{MUT} were fertile (33%), while four failed to produce offspring (66%). These results point to an early age related decrease of total fertility in *Sms1*^{MUT} males compared to *Sms1*^{HET} and *Sms1*^{WT} controls. The litter size was also analyzed. Fertile *Sms1*^{MUT} males produced 5.50 (IQR: 3.5) pups per litter, while *Sms1*^{HET} and *Sms1*^{WT} males produced 8.5 (IQR: 3.25) and 7.50 (IQR: 0.5) pups per litter, respectively (Figure 3.25 B). Therefore, at the age of 20 weeks, fertile *Sms1*^{MUT} males could be considered as subfertile compared to controls.

The observed reduction in DHA (Table 3.2 A, B) and its profound role in spermatogenesis clearly indicated that a loss of this FA might be responsible for the observed male sub-/infertility phenotype (Figure 3.25 B).Therefore, I decided to treat *Sms1* males with a supplement of 38% DHA and 46% EPA (kindly provided by KD-Pharma GmbH, Bexbach) in order to see if the sub-/infertility phenotype could be reversed.

The supplementary diet experiment was set up as a follow up to the fertility analysis. After the three weeks period, in which the fertility status was determined, *Sms1* males of all genotypes were re-mated to an eleven week old C57Bl/6J female and were manually fed with an oral dose (9mg/day/animal) of the omega-3 FA containing oil on a daily basis for the duration of 13 weeks (Figure 3.25 A). During that testing period, *Sms1*^{WT} and subfertile *Sms1*^{MUT} males produced an average of 2.50 ± 0.71 litters, each. *Sms1*^{HET} males produced 3.00 ± 0.00 litters in average. Of the confirmed infertile *Sms1*^{MUT} 50% produced offspring with feeding, while the other 50% failed to generate offspring. The *Sms1*^{MUT} with rescued fertility had produced one litter each during the testing period of 13 weeks. The mean latency between litters was also determined. The results for *Sms1*^{WT} (29.00 (IQR: 3.0) days) and *Sms1*^{HET} males (29.00 (IQR: 9.5) days) were similar (Figure 3.25 C,). Subfertile *Sms1*^{MUT} and infertile *Sms1*^{MUT} males needed more time for reproduction (subfertile *Sms1*^{MUT}: 32.50 (IQR: 11.5) days, infertile *Sms1*^{MUT}: 84.00 (IQR: 48.0) days; Figure 3.25 C). It must be noted, that infertile *Sms1*^{MUT} just obtained one litter each during the testing period, therefore the average latency between litters could not be determined, but it rather reflected the latency to the first litter. I noted, that for *Sms1*^{WT} and *Sms1*^{HET} males the number of offspring was reduced with the feeding of the DHA/EPA diet to an average of 6.33 (IQR: 2.5) pups per litter for *Sms1*^{WT} and to 5.33 (IQR: 0.33) pups per litter for *Sms1*^{HET} males (Figure 3.25 B). This was most likely due to the stress associated

with the daily feeding procedure. Previously subfertile *Sms1*^{MUT} males also produced less offspring after feeding (4.84 (IQR: 1.17) pups per litter).The 50% previously infertile males, which started to reproduce obtained an average of 2.00 (IQR: 4.5) pups per litter (Figure 3.25 B).

All offspring was heterozygous, confirming homozygosity of the males, which was also confirmed by re-genotyping via triplex-PCR (data not shown).

Mating were terminated and males sacrificed after one additional week of DHA/EPA enriched diet. As it is shown in Figure 3.25 D, progression of spermatogenesis reflects the number of offspring obtained. Only few rounded spermatids were visible in fertile *Sms1*^{MUT} mutant epididymides after feeding, while the majority of cells had matured into spermatozoa (Figure 3.25 D). In the *Sms1*^{MUT} males, which remained infertile after DHA/EPA diet we found empty epididymal caput tubules and also a large amount of round spermatids in the lumen of the epididymal cauda tubules. In the rescued formerly infertile *Sms1*^{MUT} animals spermatogenesis was found to progress normally in some seminiferous tubules, with a large number of major sperm produced. However round spermatids remained present in the epididymides (Figure 3.25 D). The histological results therefore reflect the findings on the level of reproduction.

3.2 *Sms1* x *APPswe* mouse model

3.2.1 General characterization of the *Sms1* x *APPswe* mouse model

3.2.1.1 Birth rates

The genotype distribution of the born pups was analyzed. As homozygous *APPswe*^{Tg} are not viable the expected distribution of the remaining six genotypes was calculated and the expected percentages were compared to the actual numbers (Table 3.3).

Table 3.3: Birth ratios of the different genotypes of *Sms1* x *APPswe* mice.
Percent of genotypes born, in respect to genotypes expected by birth rates in Mendelian ratios. Homozygous *APPswe*^{Tg} animals were not viable. Therefore *APPswe*^{Tg} refers to heterozygous *APPswe*^{Tg} animals. The *Sms1* genotype is labeled *Sms1*^{WT} for wild-type, *Sms1*^{HET} for heterozygous and *Sms1*^{MUT} for homozygous gene trap cassette insertion carriers.

% of expected genotype distribution	*APPswe*^{WT}			*APPswe*^{Tg}			Total
	Sms1^{WT}	*Sms1*^{HET}	*Sms1*^{MUT}	*Sms1*^{WT}	*Sms1*^{HET}	*Sms1*^{MUT}	
male	80.12	77.26	89.48	30.69	34.21	33.30	49.08
female	120.18	86.62	88.96	35.64	35.38	39.54	56.19
male and female	100.15	81.94	89.22	33.17	34.79	36.42	52.63

If one assumes that *Sms1*^{WT} x *APPswe*^{WT} animals were born in a normal rate, it was found that only 52.63% of all expected pups are born. The distribution between male and female pups was in an almost normal range with 49.08% of all expected male pups and 56.19% of all expected female pups born, which represented a slight deviation of the 1:1 ratio between males and females (Table 3.3).

With regard to the *Sms1*^{WT} x *APPswe*^{WT} animals 20.18% more females than expected were counted, while only 80.12% of the expected males were born. This higher representation of females was seen in all genotypes except of *Sms1*^{MUT} x *APPswe*^{WT}, where 89.48% of expected male and 88.96% of expected female pups were born (Table 3.3).

All three possible genotypes with the *APPswe*^{WT} background were reduced to 90.44%, while these genotypes with an *APPswe*^{Tg} background were reduced to 34.79%. Therefore about two third of all animals bearing the *APPswe*^{Tg} background seemed not to be born (Table 3.3).

In summary, a slight reduction in male pubs born and a loss of about 2/3 of h*APPswe* transgene bearing pubs, prior to birth, was noticed.

3.2.1.2 Survival rates

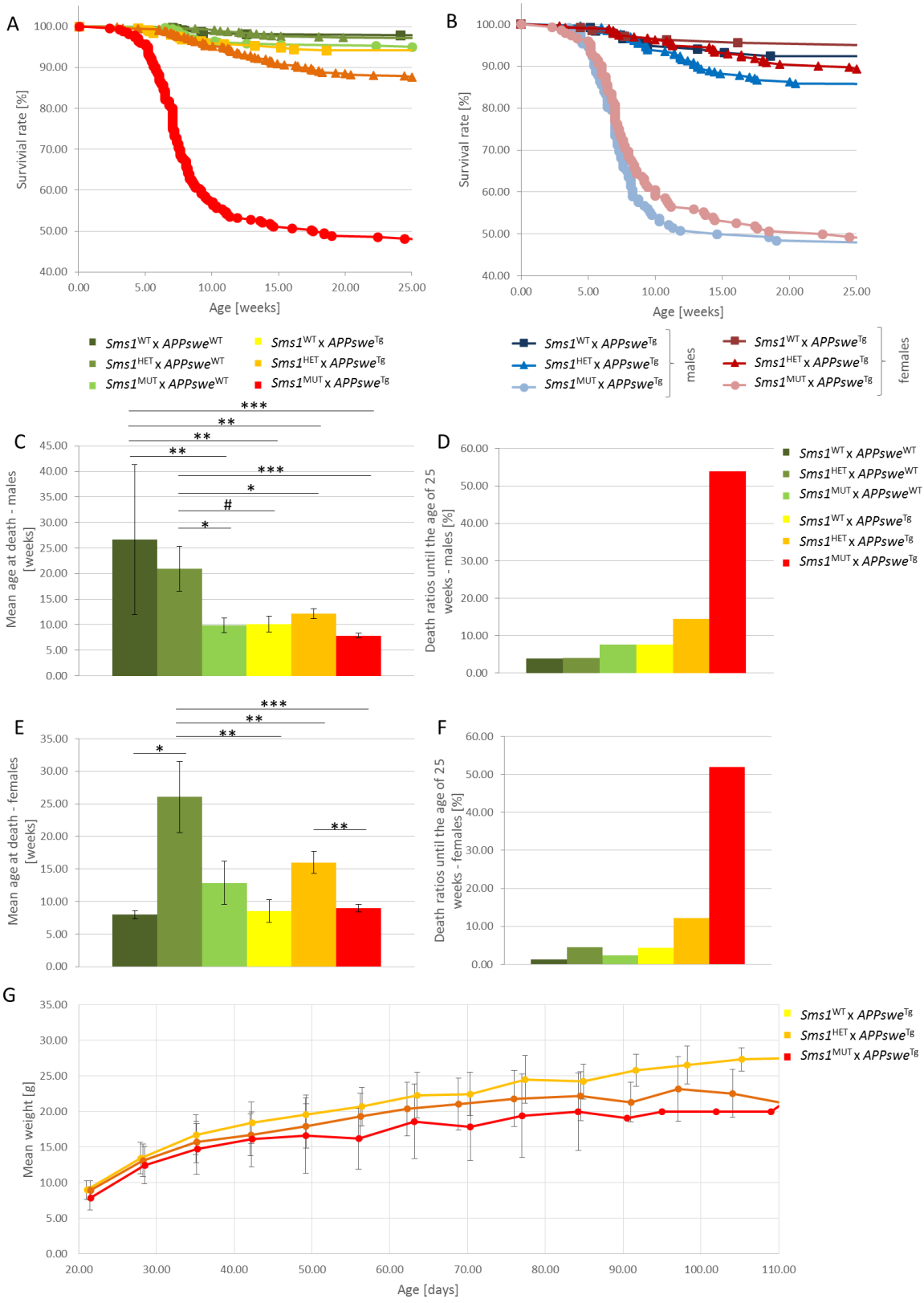

Figure 3.26: *Sms1*^{MUT} x *APPswe*^{Tg} animals showed reduced survival rates and reduced weight gain compared to *Sms1*^{WT} x *APPswe*^{Tg} animals.

(A, B) Survival rates of *Sms1* x *APPswe* animals, grouped by (A) genotype and (B) genotype and sex. (C, E) Mean

age at death of (C) male and (E) female animals. (D, F) Death ratios calculated over the first 25 weeks of (D) male and (F) female animals. (G) Weight gain during the first 110 days. Survival data: males: *Sms1*^{WT} x *APPswe*^{WT} n=154, *Sms1*^{HET} x *APPswe*^{WT} n=297 , *Sms1*^{MUT} x *APPswe*^{WT} n=172, *Sms1*^{WT} x *APPswe*^{Tg} n=118, *Sms1*^{HET} x *APPswe*^{Tg} n=263, *Sms1*^{MUT} x *APPswe*^{Tg} n=128; females: *Sms1*^{WT} x *APPswe*^{WT} n=231, *Sms1*^{HET} x *APPswe*^{WT} n=333 , *Sms1*^{MUT} x *APPswe*^{WT} n=171, *Sms1*^{WT} x *APPswe*^{Tg} n=137, *Sms1*^{HET} x *APPswe*^{Tg} n=272, *Sms1*^{MUT} x *APPswe*^{Tg} n=152; data is presented as percent of total pups born per genotype, or as mean ± SEM; weight data: *Sms1*^{WT}x *APPswe*^{Tg} n=14-3, *Sms1*^{HET} x *APPswe*^{Tg} n=31-5, *Sms1*^{MUT} x *APPswe*^{Tg} n=24-2. Statistical analysis was done by one-way ANOVA with *post hoc* Tukey's test. Data is presented as mean ± SEM $p<0.01^{\#}$, $p\leq0.05^{*}$, $p\leq0.01^{**}$, $p\leq0.001^{***}$.

In course of the breeding I noticed, that *Sms1*^{MUT} x *APPswe*^{Tg} animals died within their first few weeks. Therefore the survival rates of the six different genotypes were analyzed during the first 25 weeks after birth.

Sms1^{MUT} x *APPswe*^{Tg} animals showed a massive decline in animal numbers during the first 25 weeks, with a 50% death rate within the first 17.43 weeks (Figure 3.26 A). The mean age at death of male pups was 7.83 weeks, while female pups lived shortly longer with a mean age of 8.99 weeks (Figure 3.26 C, E). In the 25 weeks period 53.91% of male *Sms1*^{MUT} x *APPswe*^{Tg} and 51.97% of the female mice died (Figure 3.26 B, D and F). The remaining survivors died successively within the next 2 year period.

Although death rates were less dramatic compared to *Sms1*^{MUT} x *APPswe*^{Tg} also the *Sms1*^{HET} x *APPswe*^{Tg} and *Sms1*^{WT} x *APPswe*^{Tg} showed a reduction in their life span. In *Sms1*^{HET} x *APPswe*^{Tg} death rates ranged from 12.13% in females to 14.45% in males (Figure 3.26 B, D, F). The mean age at death lied between 12.15 weeks and 15.99 weeks in males and females, respectively (Figure 3.26 C, E). 7.63% of all male and 4.38% of all female *Sms1*^{WT} x *APPswe*^{Tg} animals died within the first 25 weeks, while male animals reached a mean age of 10.13 weeks and females of 8.5 weeks. This showed, that although *Sms1*^{HET} x *APPswe*^{Tg} have a higher death rate compared to *Sms1*^{WT} x *APPswe*^{Tg}, the average age at death is higher in both sexes (Figure 3.26 C-F).

Death rates in the remaining three genotypes analyzed (*Sms1*^{WT} x *APPswe*^{WT}, *Sms1*^{HET} x *APPswe*^{WT} and *Sms1*^{HOM} x *APPswe*^{WT}) ranged from 1.30% in female *Sms1*^{WT} x *APPswe*^{WT} to 7.62% in male *Sms1*^{WT} x *APPswe*^{Tg} animals. The 3.90% of *Sms1*^{WT} x *APPswe*^{WT} males found dead had a mean age of 26.67 weeks, the 4.04% of *Sms1*^{HET} x *APPswe*^{WT} of 20.98 weeks and the *Sms1*^{MUT} x *APPswe*^{WT} of 9.87 weeks, which showed a clear genotype related life expectancy on the *APPswe*^{WT} genetic background. In females, this correlation is not so clear, as the 1.30% of *Sms1*^{WT} x *APPswe*^{WT} animals, which were found dead had a mean age of 7.95 weeks. However, this percentage of animals found dead can be regarded to be in a normal range. *Sms1*^{HET} x *APPswe*^{WT} and *Sms1*^{MUT} x *APPswe*^{WT} females showed a 4.50% and 2.34% death rate and a mean age of 26.07 and 12.86 weeks at death, respectively (Figure 3.26 A-F).

These show a genotype related effect on life expectancy, dependent on the *Sms1* genotype, but also on the *APPswe* background, with animals having a homozygous insertion of the gene trap cassette in *Sms1* additionally to carrying the *hAPPswe* transgene having the least life expectancy. Additionally males were more prone to premature death than females.

3.2.1.3 Body and organ weight

Shortly before death some of the *Sms1*^{MUT} x *APPswe*^{Tg} animals looked skinny, while others did not show any signs of approaching death. The weight of *Sms1*^{WT} x *APPswe*^{Tg}, *Sms1*^{HET} x *APPswe*^{Tg} and *Sms1*^{MUT} x *APPswe*^{Tg} was measured on a weekly basis and genotype specific weight differences were found. These differences were increasing with age (Figure 3.26 G, Figure 3.26 A, C and supplementary Figure 10.4 and Table 10.8).

The weight of *Sms1*^{HET} x *APPswe*^{Tg} animals was reduced 0.24% at the mean age of 21.33 days in comparison to *Sms1*^{WT} x *APPswe*^{Tg}. This difference had increased with advancing age up to 23.37% at the mean age of 110.71 days. These observed weight differenced were even more pronounced in *Sms1*^{MUT} x *APPswe*^{Tg} animals. The smallest weight reduction of 7.37% in comparison to *Sms1*^{WT} x *APPswe*^{Tg} animals was recorded at the mean age of 28.22 days. The highest difference was again reached at a mean age of 110.71 days, when both genotypes differ by 27.40% (Figure 3.26 G and supplementary Table 10.8). Male and female data did not differ in weight incline and increasing weight differences (see supplementary Figure 10.4, Table 10.8).

As mentioned before, *Sms1*^{MUT} x *APPswe*^{Tg} animals dyed with an age between 7.83 and 8.99 days. Therefore I decided to dissect *Sms1*^{WT} x *APPswe*^{WT}, as a control, *Sms1*^{MUT} x *APPswe*^{WT} and *Sms1*^{WT} x *APPswe*^{Tg} as components and *Sms1*^{MUT} x *APPswe*^{Tg} as the double mutant at the age of 8 weeks in order to analyze the different organs for alterations, which might be responsible for the premature death.

The body weight of these animals dissected at the age of 8 weeks revealed a decline in weight depending on the genotype. Male *Sms1*^{MUT} x *APPswe*^{WT} (26.31 ± 0.81g) showed already slightly, but not significantly reduced body weight compared to *Sms1*^{WT} x *APPswe*^{WT} (27.52 ± 1.12g). *Sms1*^{WT} x *APPswe*^{Tg} and *Sms1*^{MUT} x *APPswe*^{Tg} males showed further and significantly reduced body weight of 23.60 ± 0.82g (p=0.0288) and 20.04 ± 1.14g (p=0.0001), respectively (Figure 3.27 A).

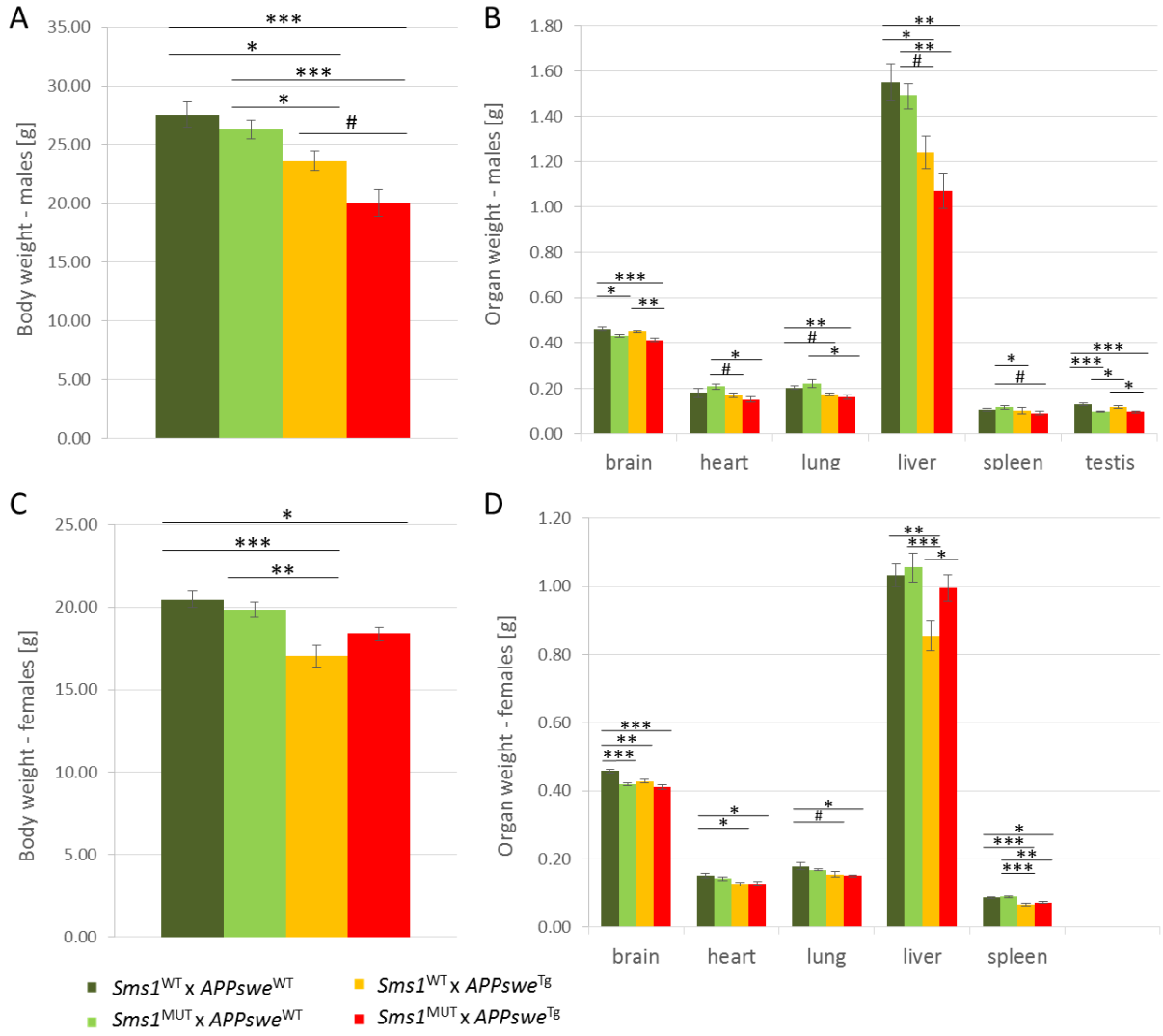

Figure 3.27: *Sms1* x *APPswe* animals showed alterations in body and organ weights depending on genotype.

(A, C) Absolute body weight of (A) male and (C) female animals at the age of 8 weeks. (B, D) Absolute organ weights of (B) male and (D) female animals at the age of 8 weeks. Males: *Sms1*^{WT} x *APPswe*^{WT} (n=8), *Sms1*^{MUT} x *APPswe*^{WT} (n=12), *Sms1*^{WT} x *APPswe*^{Tg} (n=16), *Sms1*^{MUT} x *APPswe*^{Tg} (n=10); females: *Sms1*^{WT} x *APPswe*^{WT} (n=12), *Sms1*^{MUT} x *APPswe*^{WT} (n=21), *Sms1*^{WT} x *APPswe*^{Tg} (n=11), *Sms1*^{MUT} x *APPswe*^{Tg} (n=12). Statistical analysis was done by one-way ANOVA with *post hoc* Tukey's test. Data is presented as mean ± SEM; $p<0.01^{\#}$, $p\leq0.05^{*}$, $p\leq0.01^{**}$, $p\leq0.001^{***}$.

In order to analyze organ weights the measured weights relative to the body weight was calculated (supplementary Figure 10.6). In male animals there was no significant difference in lung or liver weights. Brain weight in *Sms1*^{WT} x *APPswe*^{WT} control males was 1.70 ± 0.06% of the body weight. The brain weight of *Sms1*^{MUT} x *APPswe*^{WT} (1.65 ± 0.05%) did not differ from that of controls, while *Sms1*^{WT} x *APPswe*^{Tg} and *Sms1*^{MUT} x *APPswe*^{Tg} had a higher relative brain weight of 1.94 ± 0.06% (p=0.0980) and 2.11 ± 0.11% (p=0.0061), respectively. It is important to notice that the absolute

brain weight showed a *Sms1* genotype dependent reduction in both *Sms1*^{MUT} x *APPswe*^{WT} (0.43 ± 0.01g, p=0.0267) and *Sms1*^{MUT} x *APPswe*^{Tg} (0.41 ±0.01g, p=0.0007) in comparison to *Sms1*^{WT} x *APPswe*^{WT} controls (0.46 ± 0.01g; Figure 3.27 B). In Addition, the absolute brain weight of *Sms1*^{MUT} x *APPswe*^{Tg} males was again significantly lower than that of *Sms1*^{WT} x *APPswe*^{Tg} component males (0.45 ± 0.01g, p=0.0029; Figure 3.27 B). However, as stated before, this reduction in brain weight did not persist the body weight loss correction.

The relative heart, lung and liver weights of males did not differ compared to controls (supplementary Figure 10.6 A).

In the spleen *Sms1*^{MUT} x *APPswe*^{WT} (0.44 ± 0.03%, p=0.0005); and *Sms1*^{MUT} x *APPswe*^{Tg} males (0.45 ± 0.02%, p=0.0004) showed higher relative weights compared to *Sms1*^{MUT} x *APPswe*^{Tg} males (0.33 ± 0.03%; supplementary Figure 10.6 A).

Highly significant differences in relative organ weight was also noticed in testes. Testes weight in relation to body weight in *Sms1*^{WT} x *APPswe*^{WT} reaches 0.47 ± 0.02%. *Sms1*^{MUT} x *APPswe*^{WT} only reach a value of 0.38 ± 0.01% (p=0.0042). *Sms1*^{WT} x *APPswe*^{Tg} males, with 0.50 ± 0.02%, and *Sms1*^{MUT} x *APPswe*^{Tg} males with 0.49 ±0.02% did not show alterations (p=0.6272, p=0.8859). However, in comparison to *Sms1*^{MUT} x *APPswe*^{WT}, both *Sms1* x *APPswe*^{Tg} genotypes had highly significantly elevated testes weights (p<0.0001, p=0.0002; supplementary Figure 10.6 A).

Females of the *Sms1* x *APPswe* line showed the same genotype specific pattern of body mass decline as it was recorded in male mice.

Sms1^{WT} x *APPswe*^{WT} control females had a mean body mass of 20.46 ± 0.49g, which is about 7g less than their male counterparts. This reflects the normal sex difference in mice. Significantly lower body weight, in comparison to controls, was reached in *Sms1*^{WT} x *APPswe*^{Tg} and *Sms1*^{MUT} x *APPswe*^{Tg} females, which had a mean weight of 17.02 ± 0.67g (p<0.0001) and 18.40 ±0.39g (p=0.0266), respectively (Figure 3.27 C). In contrast to males, female *Sms1* x *APPswe*^{Tg} mice did not show a further reduction dependent on the *Sms1* genotype (Figure 3.27 C).

In female mice, relative heart weights were not correlated to the genotype (supplementary Figure 10.6 B), while liver weights of *Sms1*^{MUT} x *APPswe*^{Tg} females showed a trend to be higher than those of *Sms1*^{WT} x *APPswe*^{WT} controls (p=0.0925) and of *Sms1*^{WT} x *APPswe*^{Tg} (p=0.0530).

Regarding brain weight, *Sms1*^{WT} x *APPswe*^{Tg} females, with a mean relative brain weight of 2.54 ± 0.08% had a significantly higher weight than controls (*Sms1*^{WT} x *APPswe*^{WT}: 2.25 ± 0.05%, p=0.0010). With the additional mutation in *Sms1* both, *Sms1*^{MUT} x *APPswe*^{WT} and *Sms1*^{MUT} x *APPswe*^{Tg}, lost relative brain mass. *Sms1*^{MUT} x *APPswe*^{WT} had mean relative brain weight of 2.13 ± 0.04% and *Sms1*^{MUT} x *APPswe*^{Tg} of 2.25 ± 0.04%, representing a 0.12% and 0.29% reduction of rela-

tive brain weight in comparison to *Sms1*^{WT} x APPswe^{WT} controls (p=0.1944) or *Sms1*^{WT} x *APPswe*^{Tg} compounds (p=0.0013), respectively (supplementary Figure 10.6 B).

In the lungs I found the same pattern as seen in the brain, although the weight differences were less pronounced. The relative lung weight of *Sms1*^{MUT} x *APPswe*^{WT} (0.85 ± 0.02%) was slightly but not significantly lower than in *Sms1*^{WT} x *APPswe*^{WT} controls (0.87 ±0.06%), while the relative lung weight of *Sms1*^{MUT} x *APPswe*^{Tg} (0.82 ± 0.02%) was again lower than in *Sms1*^{WT} x *APPswe*^{Tg} (0.91 ± 0.04%, p=0.0478; supplementary Figure 10.6 B). These results, as mentioned for the brain, reflected a *Sms1* genotype dependent reduction of relative lung mass in female mice amplified on an *APPswe*^{Tg} background.

The absolute spleen weights of *Sms1*^{MUT} x *APPswe*^{WT} (0.089 ± 0.003g) and *Sms1*^{MUT} x *APPswe*^{Tg} (0.072 ± 0.003g) showed marginal elevation in comparison to *Sms1*^{WT} x *APPswe*^{WT} controls (0.086 ± 0.003g) and *Sms1*^{WT} x *APPswe*^{Tg} components (0.066 ± 0.004g), respectively (Figure 3.27 D). However, with correction for body mass loss, the elevation on the *APPswe*^{Tg} background got lost (*Sms1*^{WT} x *APPswe*^{Tg}: 0.39 ± 0.02%, *Sms1*^{MUT}x *APPswe*^{Tg}: 0.39 ± 0.02%), while it persisted on *APPswe*^{WT} background (*Sms1*^{WT} x *APPswe*^{WT}: 0.42 ±0.01%, *Sms1*^{MUT} x *APPswe*^{WT}: 0.45 ± 0.01%; supplementary Figure 10.6 B).

In summary the genotype-dependent weight reduction noticed before could be validated. As discussed before, the differences were more pronounced in male animals. Importantly, in both male and female animals, brain weight was reduced in genotypes homozygously carrying the *Sms1* gene trap cassette. This could demonstrate a modification of brain structure due to disrupted SM synthesis.

3.2.2 Lipid profile

Regarding the life expectancy and body weight gain, crucial differences between *Sms1*^{MUT} x *APPswe*^{WT} and *Sms1*^{MUT} x *APPswe*^{Tg} were found, which led me to the question, if the additional expression of the *APPswe* transgene also has further influence on the already altered lipid metabolism of the *Sms1* mouse line. Therefore a profile of the most important lipids concerning SM synthesis in brains was generated of *Sms1*^{WT} x *APPswe*^{WT} control, *Sms1*^{MUT} x *APPswe*^{WT} and *Sms1*^{WT} x *APPswe*^{Tg} component and *Sms1*^{MUT} x *APPswe*^{Tg} double mutant mice with the help of Dr. Marcus Grimm and Prof. Tobias Hartmann.

3.2.2.1 Sphingomyelin

In both, male and female Sms1MUT x APPsweWT animals sphingomyelin (SM) levels were down regulated to 57.61 ± 4.49% (p<0.0001) and 56.02 ± 4.47% (p<0.0001) of the respective Sms1WT x APPsweWT control (Figure 3.28 A, B). Sms1WT x APPsweTg animals showed similar levels to controls (Sms1WT x APPsweTg male: 111.85 ± 3.53%, Sms1WT x APPsweTg female: 96.75 ± 2.66%). Therefore there was also no further significant reduction or elevation of SM levels in the

Sms1MUT x APPsweTg double mutant animals in comparison to Sms1MUT x APPsweWT compound mice. Sms1MUT x APPsweTg male and female had SM levels between 55.18 ± 1.15% ($p<0.0001$) and 49.35 ± 4.40% ($p<0.0001$) of controls, respectively (Figure 3.28 A, B).

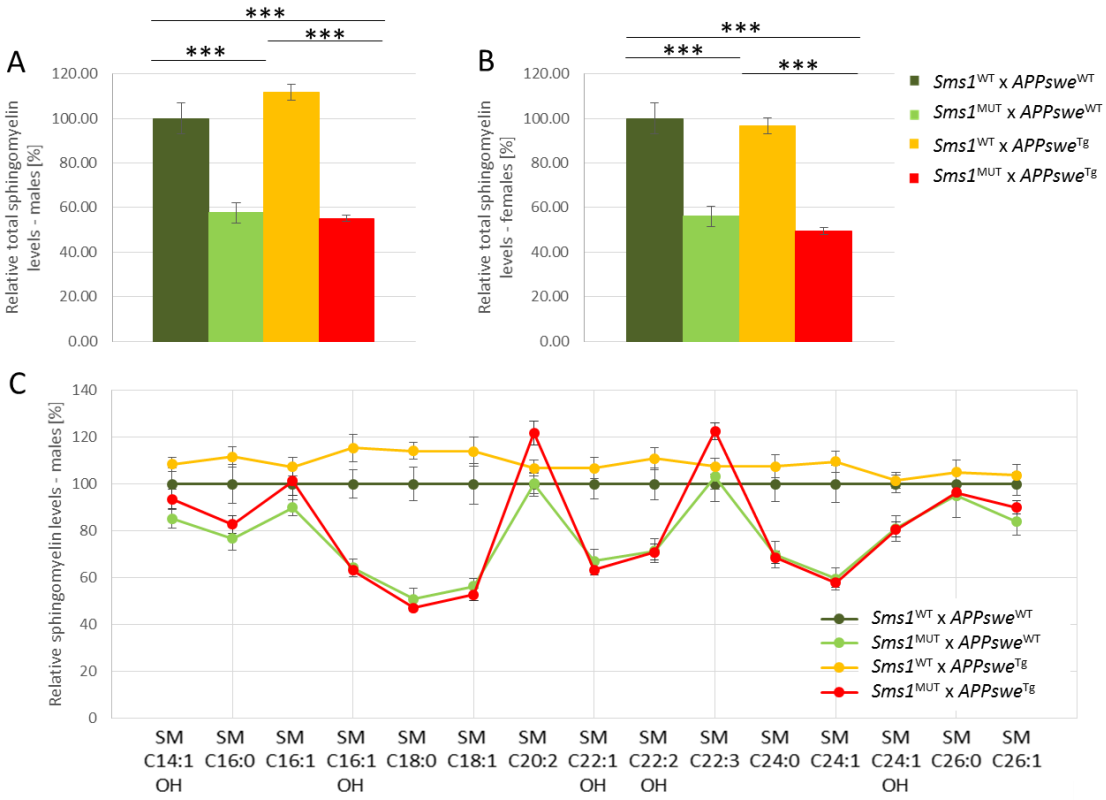

Figure 3.28: Brain sphingomyelin was reduced to a similar extend in *Sms1*^{MUT} x *APPswe*^{WT} and *Sms1*^{MUT} x *APPswe*^{Tg} at the age of 8 weeks.

(A, B) Relative sphingomyelin (SM) levels of (A) male and (B) female brain tissue. (C) Relative levels of the distinct SM species in brain tissue. Combined data from both sexes. Males: *Sms1*^{WT} x *APPswe*^{WT} n=5, *Sms1*^{MUT} x *APPswe*^{WT} n=6, *Sms1*^{WT} x *APPswe*^{Tg} n=11, *Sms1*^{MUT} x *APPswe*^{Tg} n=6; females: *Sms1*^{WT} x *APPswe*^{WT} n=6, *Sms1*^{MUT} x *APPswe*^{WT} n=11, *Sms1*^{WT} x *APPswe*^{Tg} n=13, *Sms1*^{MUT} x *APPswe*^{Tg} n=5. Statistical analysis was done by one-way ANOVA with *post hoc* Tukey's test. Data is presented as mean ± SEM; $p<0.01^{\#}$, $p\leq0.05$*, $p\leq0.01$**, $p\leq0.001$***.

Comparing the different SM species between males and females revealed that females did not have generally more or less SM, but differ dependent on the SM species. *Sms1*^{WT} x *APPswe*^{WT} females had higher levels of the abundant C16:1 OH, C18:0 and C18:1 species. The same could be seen in Smd1^{MUT} x *APPswe*^{WT} females, although C16:1 OH and C18:0 levels dropped due to the disruption of *Sms1*. *Sms1*^{WT} x *APPswe*^{Tg} females had overall lower SM levels compared to their male counterparts. The SM levels of the *Sms1*^{MUT} x *APPswe*^{Tg} double mutant females followed those of the *Sms1*^{MUT} x *APPswe*^{WT} component females, however, due to their *APPswe*^{Tg} background, levels were even lower in comparison to their male counter parts. With increasing FA chain length (> SM C22:1 OH), female mice of all genotypes had lower SM levels, compared to males (supplementary Figure 10.7).

In male animals the levels of the different SM species of the *Sms1*^{WT} x *APPswe*^{Tg} compound mice were generally elevated in comparison to *Sms1*^{WT} x *APPswe*^{WT} controls (Figure 3.28 C), while female *Sms1*^{WT} x *APPswe*^{Tg} mice did not differ much from *Sms1*^{WT} x *APPswe*^{WT} levels (supplementary Table 10.17).

Male and female mice carrying the *Sms1* gene trap cassette showed the expected reduction in most of the SM species. The highest reduction was seen in the most abundant SM species C18:0 (*Sms1*^{MUT} x *APPswe*^{WT} male: 50.86 ± 4.70%, p<0.0001; female: 47.31 ± 4.26%, p<0.0001; *Sms1*^{MUT} x *APPswe*^{Tg} male: 41.57 ±4.79%, p<0.0001, female: 41.57 ± 4.79%, p<0.0001), C18:1 (*Sms1*^{MUT} x *APPswe*^{WT} male: 56.17 ± 3.30%, p=0.0009; female: 54.84 ± 5.19%, p<0.0001; *Sms1*^{MUT} x *APPswe*^{Tg} male: 48.39 ± 8.04%, p=0.0004, female: 48.39 ± 8.04, p<0.0001) and C24:1 (*Sms1*^{MUT} x *APPswe*^{WT} male: 59.41 ± 4.59%, p=0.0003; female: 62.54 ± 5.66%, p=0.0004; *Sms1*^{MUT} x *APPswe*^{Tg} male: 55.36 ± 4.95%, p=0.0002; female: 55.36 ± 4.95%, p=0.0004; Figure 3.28 C, supplementary Table 10.17).

Exceptions from down regulation were C16:1, C20:2, C22:3 and C26:0 (Figure 3.28 C). C20:2 was even higher in *Sms1*^{MUT} x *APPswe*^{Tg} mice (male: 121.77 ± 4.06%, p=0.0223; female: 117.49 ± 5.54%, p=0.0594) in comparison to *Sms1*^{WT} x *APPswe*^{WT} controls. The same was seen for C22:3 (*Sms1*^{MUT} x *APPswe*^{Tg} male: 112.51 ± 2.78%, p=0.0283; female: 124.45 ± 6.81%, p=0.0100; (Figure 3.28 C, supplementary Table 10.17).

Overall, the disruption of *Sms1* led to a reduction of SM levels of more than 40% without striking differences between sexes. The reduction affected all commonly found SM species except of SM C20:2 and SM C22:3.

3.2.2.2 Diacyl-phosphatidylcholine species

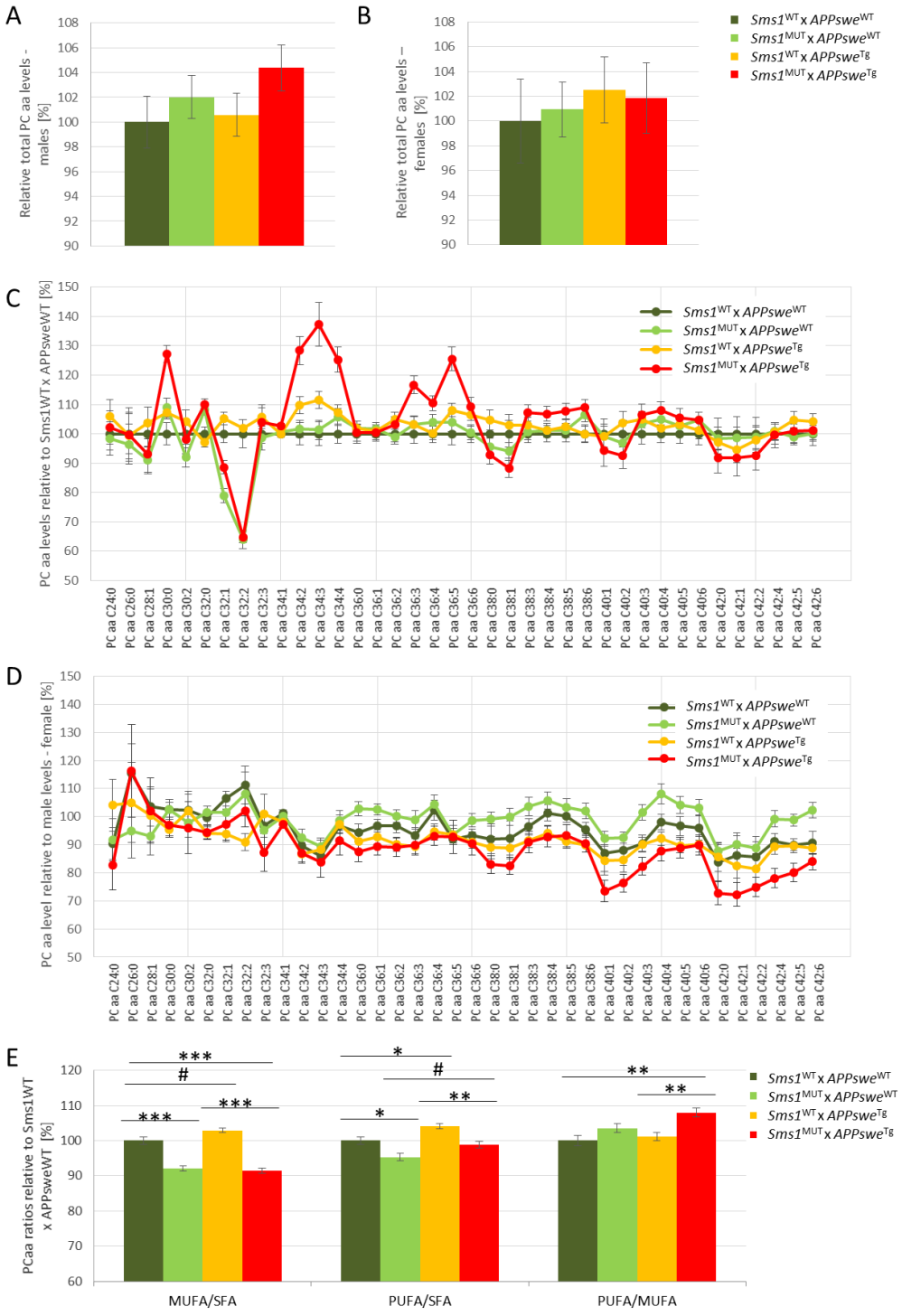

Figure 3.29: Brain diacyl-phosphatidylcholin showed alterations between genotypes amongst others, concerning saturation state.

(A, B) Relative diacyl-phosphatidylcholin (PCaa) levels of (A) male and (B) female brain tissue. (C) Relative levels of the distinct PCaa species in brain tissue. Combined data from both sexes. (D) Comparison of female lipid levels relative to male levels, which were set to 100%. (E) Relative PCaa ratios of mono-unsaturated (MUFA), poly-unsaturated (PUFA) and saturated fatty acids (SFA). Males: *Sms1*^{WT} x *APPswe*^{WT} n=5, *Sms1*^{MUT} x *APPswe*^{WT} n=6, *Sms1*^{WT} x *APPswe*^{Tg} n=11, *Sms1*^{MUT} x *APPswe*^{Tg} n=6; females: *Sms1*^{WT} x *APPswe*^{WT} n=6, *Sms1*^{MUT} x *APPswe*^{WT} n=11, *Sms1*^{WT} x *APPswe*^{Tg} n=13, *Sms1*^{MUT} x *APPswe*^{Tg} n=5. Age 8 weeks. Statistical analysis was done

by one-way ANOVA with *post hoc* Tukey's test. Data is presented as mean ± SEM; p<0.01#, p≤0.05*, p≤0.01**, p≤0.001***.

PCaa as one of the precursor molecules of SM was not significantly elevated in *Sms1*^{MUT} x *APPswe*^{Tg} (104.37 ± 1.85%, p=0.4034) animals compared to *Sms1*^{WT} x *APPswe*^{WT} controls, which were set to 100% (Figure 3.29 A, B).

Comparison of the distinct PCaa species per genotype showed a massive regulation of certain distinct PCaas, mainly in the *Sms1*^{MUT} x *APPswe*^{Tg} double mutant mice. PCaa C30:0, C34:2, C34:3, C34:4, C36:3, C36:4 and C36:5 were elevated most, while C32:2 was significantly lower. In the LC-FA range of PCaa I did not see peaks of that extend as in short-chain FA containing PCaa, however, the levels still follow a wave like pattern (Figure 3.29 C). PCaa levels of *Sms1*^{MUT} x *APPswe*^{Tg} animals seemed to be amplified in comparison to the levels found in *Sms1*^{WT} x *APPswe*^{Tg} compound mice. In more detail, the peak in C34:2 to C34:4 could be detected in *Sms1*^{WT} x *APPswe*^{Tg} mice, with the highest level in C34:3. C34:3 in those animals was 11.5 ± 2.98% (p=0.2214) higher than in *Sms1*^{WT} x *APPswe*^{WT} mice, in *Sms1*^{MUT} x *APPswe*^{Tg} mice, however, the levels of this lipid species reached 137.33 ±7.50% (p<0.0001) of controls (Figure 3.29 C). The same could be noticed for the C36:3 to C36:5 peak. Here *Sms1*^{WT} x *APPswe*^{Tg} animals reached a level of 108.06 ± 2.25% (p=0.2869) for C36:5 while in *Sms1*^{MUT} x *APPswe*^{Tg} this level was amplified to 125.54 ± 4.04% (p<0.0001) of *Sms1*^{WT} x *APPswe*^{WT} controls (Figure 3.29 C). With regard to the LC-FA containing PCaas (starting with C36), *Sms1*^{MUT} x *APPswe*^{Tg} double mutant animals had low levels in the SFA-, MUFA- and di-unsaturated FA- (DUFA-) containing LC-PCaas, while levels of LC-PCaa species with three or more unsaturated residues were elevated (Figure 3.29 C). This was also reflected in the MUFA/SFA and PUFA/SFA ratio of male and female animals, where these ratios dropped in both, *Sms1*^{MUT} x *APPswe*^{WT} and *Sms1*^{MUT} x *APPswe*^{Tg}, to a similar extend (MUFA/SFA: *Sms1*^{MUT} x *APPswe*^{WT} male: -7.24%, female: -8.42%; *Sms1*^{MUT} x *APPswe*^{Tg} male: -8.22%, female: -8.46%; PUFA/SFA: *Sms1*^{MUT} x *APPswe*^{WT} male: -5.87%, female: -3.80%; *Sms1*^{MUT} x *APPswe*^{Tg} male: -0.46%, female: -2.32%; Figure 3.29). Results on the PUFA/MUFA ratio differed between males and females. Female animals with the *Sms1*^{MUT} x *APPswe*^{WT} and the *Sms1*^{MUT} x *APPswe*^{Tg} genotype had a 5.04% and 6.71% higher PUFA/MUFA ratio, respectively, in comparison to *Sms1*^{WT} x *APPswe*^{WT} and *Sms1*^{WT} x *APPswe*^{Tg} animals (Figure 3.29 E). In males, I did not find an elevation of the PUFA/MUFA ratio in *Sms1*^{MUT} x *APPswe*^{WT} animals, but again *Sms1*^{MUT} x *APPswe*^{Tg} animals had an 8.44% higher ratio in comparison to *Sms1*^{WT} x *APPswe*^{WT} controls (Figure 3.29 E). It is worth to mention, that except of the female PUFA/MUFA ratio, *Sms1*^{WT} x *APPswe*^{Tg} animals showed slightly higher ratios compared to *Sms1*^{WT} x *APPswe*^{WT} controls (Figure 3.29 E).

The differences between male and female PCaa data can be found in Figure 3.29 D. *Sms1*^{WT} x *APPswe*^{WT} females had a distinct pattern of PCaa species level in comparison to males. However, this

pattern got less pronounced with the mutation of *Sms1*, while it got more pronounced with the expression of the *APPswe* transgene. In detail, female animals of all genotypes, in comparison to male animals, had a reduced levels of LC-PCaas with SFA-, MUFA- of DUFA-residues, while their reduction in PUFA-LC-PCaas was less pronounced, or in case of *Sms1*^{MUT} x *APPswe*^{WT} females rose above male levels. These results became clearer with increasing FA-chain length (Figure 3.29 D).

In summary, PCaa levels were upregulated in male *Sms1* gene trap carrying genotypes, but not in females. PCaa analysis showed that some distinct species are highly upregulated and that LC-PCaas followed a wave like pattern, reflected in the PUFA/SFA and MUFA/SFA ratios, which were reduced in *Sms1* gene trap carrying genotypes.

3.2.2.3 Acyl-alkyl-phosphatidylcholine (plasmalogene) species

Total levels of plasmalogens (PCaes), which differ from PCaas by an ether bond at the sn-1 position, were not crucially changed in male or female animals of either genotype (Figure 3.30 A).

Overall, female mice had lower levels of PCaes than males (Figure 3.30 C). Comparison of male and female data sets revealed a similar pattern to PCaas, with *Sms1*^{MUT} x *APPswe*^{WT} females having less reduced level of LC-PCaes and *Sms1*^{MUT} x *APPswe*^{Tg} females having the strongest reduction compared to their male counterparts (Figure 3.30 C, supplementary Table 10.19 A, B).

PCae C36:4 and C36:5 were elevated in *Sms1*^{MUT} x *APPswe*^{Tg} male and female mice, similar to the above described PCaa pattern (PCae C36:4 in *Sms1*^{MUT} x *APPswe*^{Tg} males: 115.61 ± 0.84%, p=0.1485, females: 118.34 ± 4.49%, p=0.1086; PCae C36:5 in *Sms1*^{MUT} x *APPswe*^{Tg} males: 113.11 ± 4.08%, p=0.3898, females: 107.86 ± 3.60%, p=0.7832). The same could be seen for C38:5 (PCae C38:5 in *Sms1*^{MUT} x *APPswe*^{Tg} males: 111.32 ± 1.15%, p=0.3218, females: 109.64 ± 4.28%, p=0.4535; supplementary Table 10.19 A, B). However, in PCaes, just C36:4 reached significantly different levels compared to *Sms1*^{WT} x *APPswe*^{WT} animals. The mostly reduced PCaes in *Sms1*^{MUT} x *APPswe*^{Tg} mice was C38:1. In males these reduced levels were almost the same between *Sms1*^{MUT} x *APPswe*^{WT} (86.85 ± 6.48%, p=0.8870) and *Sms1*^{MUT} x *APPswe*^{Tg} animals (87.59 ± 3.34%, p=0.3943), while in *Sms1*^{MUT} x *APPswe*^{Tg} females (80.88 ± 5.05%, p=0.0610), the levels dropped far below that of *Sms1*^{MUT} x *APPswe*^{WT} females (95.22 ± 2.85%, p=0.8621) in comparison to *Sms1*^{WT} x *APPswe*^{WT} levels of the respective sex (supplementary Table 10.19 A, B). C38:2 and C40:2 represented the second most reduced PCae species in both, male and female *Sms1*^{MUT} x *APPswe*^{Tg} animals (supplementary Table 10.19 A, B). Of these only female PCae C40:2 with 84.10 ± 3.99% of *Sms1*^{WT} x *APPswe*^{WT} levels was significantly lower (p=0.0450). Results summarized for both sexes are shown in Figure 3.30 B.

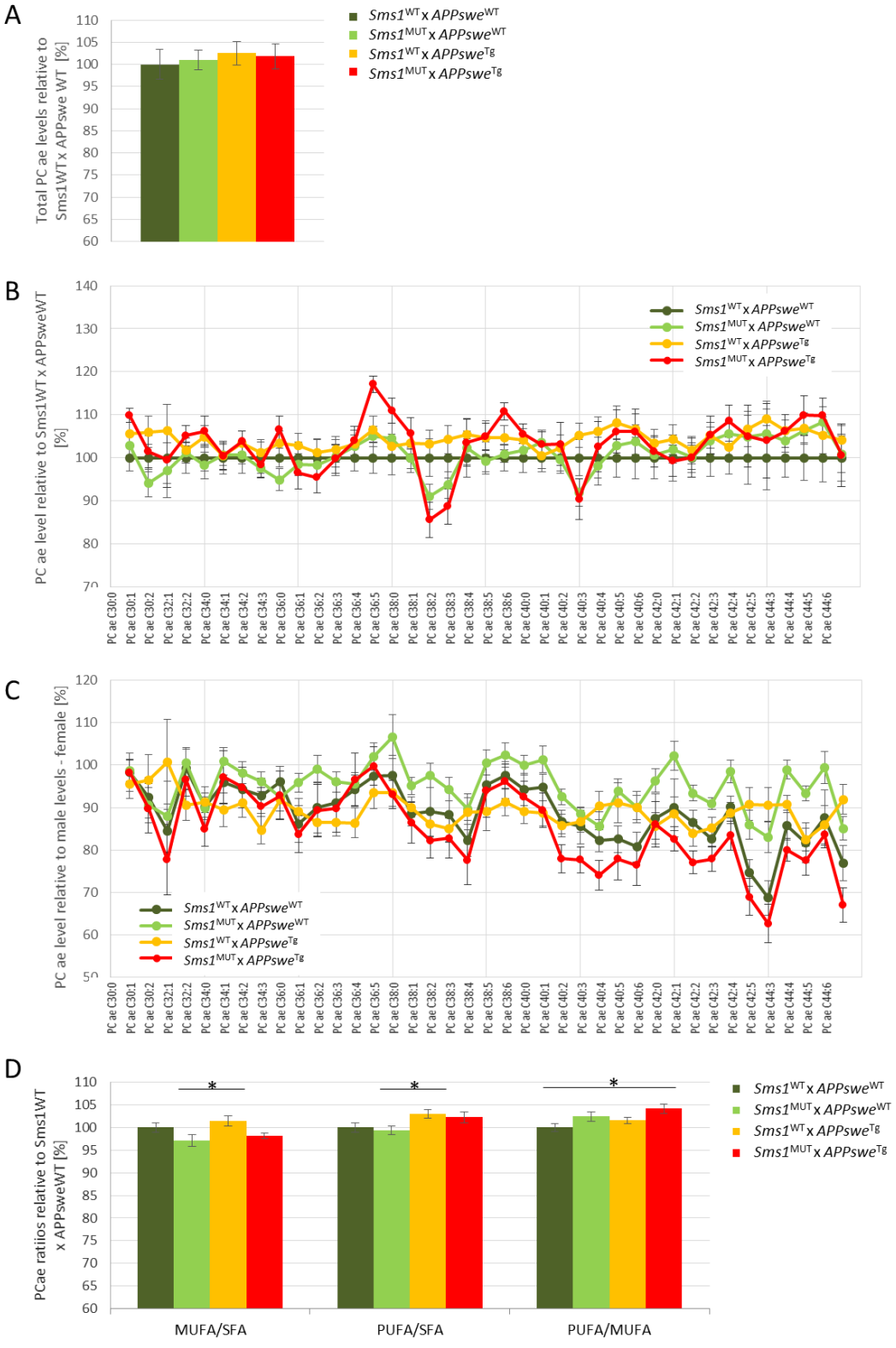

Figure 3.30: Distinct brain acyl-alkyl-phosphatidylcholines showed alterations between genotypes amongst others, concerning saturation state.

(A) Relative acyl-alkyl-phosphatidylcholin (PCae) levels of brain tissue. (B) Relative levels of the distinct PCae species in brain tissue. (C) Comparison of female lipid levels relative to male levels, which were set to 100%. (D)

Relative PCae ratios of mono-unsaturated (MUFA), poly-unsaturated (PUFA) and saturated fatty acids (SFA). Combined data form both sexes. Males: *Sms1*^{WT} x *APPswe*^{WT} n=5, *Sms1*^{MUT} x *APPswe*^{WT} n=6, *Sms1*^{WT} x *APPswe*^{Tg} n=11, *Sms1*^{MUT} x *APPswe*^{Tg} n=6; females: *Sms1*^{WT} x *APPswe*^{WT} n=6, *Sms1*^{MUT} x *APPswe*^{WT} n=11, *Sms1*^{WT} x *APPswe*^{Tg} n=13, *Sms1*^{MUT} x *APPswe*^{Tg} n=5. Age 8 weeks. Statistical analysis was done by one-way ANOVA with *post hoc* Tukey's test. Data is presented as mean ± SEM; $p<0.01^{\#}$, $p\leq0.05^{*}$, $p\leq0.01^{**}$, $p\leq0.001^{***}$.

LC-PCaes were regulated differently in male and female mutants. While male *Sms1*^{MUT} x *APPswe*^{WT} LC-PCaes levels dropped below the *Sms1*^{WT} x *APPswe*^{WT} levels, the female *Sms1*^{MUT} x *APPswe*^{WT} levels of these lipid species were higher than those of their *Sms1*^{WT} x *APPswe*^{WT} controls (supplementary Table 10.19 A, B). For the double mutant SMS1^{MUT} x *APPswe*^{Tg} animals, the opposite regulation was detected (supplementary Table 10.19 A, B).

In contrast to PCaas, in the PCaes no clear correlation between lipid level and saturation sate could be detected (Figure 3.29 E, Figure 3.30 D). Only a minor but not significant reduction of MUFA/SFA levels was found in both *Sms1* defective genotypes (Figure 3.30 D). The PUFA/SFA ratios were unchanged in males and slightly elevated in female *Sms1*^{WT} x *APPswe*^{Tg} animals. PUFA/MUFA ratios pointed to a possible elevation of PUFAs against MUFAs with the disruption of *Sms1* (Figure 3.30 D).

The results in PCae species resembled those found in PCaa, with several species being elevated and a kind of wave-like pattern in the LC-PCaes. The MUFA/SFA ratio resembled the pattern seen in the *Sms1* mouse line, however, it was less prominent. The PUFA/SFA ratios did not show any alteration depending on the *Sms1* genotype.

3.2.2.4 Lyso-PC species

PC species get degraded by phospholipases, which cut of the mainly unsaturated FAs at the sn-2 position, to generate so called lyso-PCs. The analysis of PCaa and PCae showed a selective loss or elevation of several species. Therefore it should be clarified if the lyso-PC composition could give any hint on how the PCaa and PCaes get metabolized.

Total levels of lyso-PCs were similar in *Sms1*^{MUT} x *APPswe*^{WT} (10.508 ± 4.38%, p=0.5104) and in *Sms1*^{MUT} x *APPswe*^{Tg} (15.18 ± 6.16%, p=0.2728) animals (Figure 3.31 A). Neither male, nor female levels differed significantly between genotypes (supplementary Table 10.20 A, B). With regard to sex, the different lyso-PC species were again differently regulated between males and females (Figure 3.31 D).

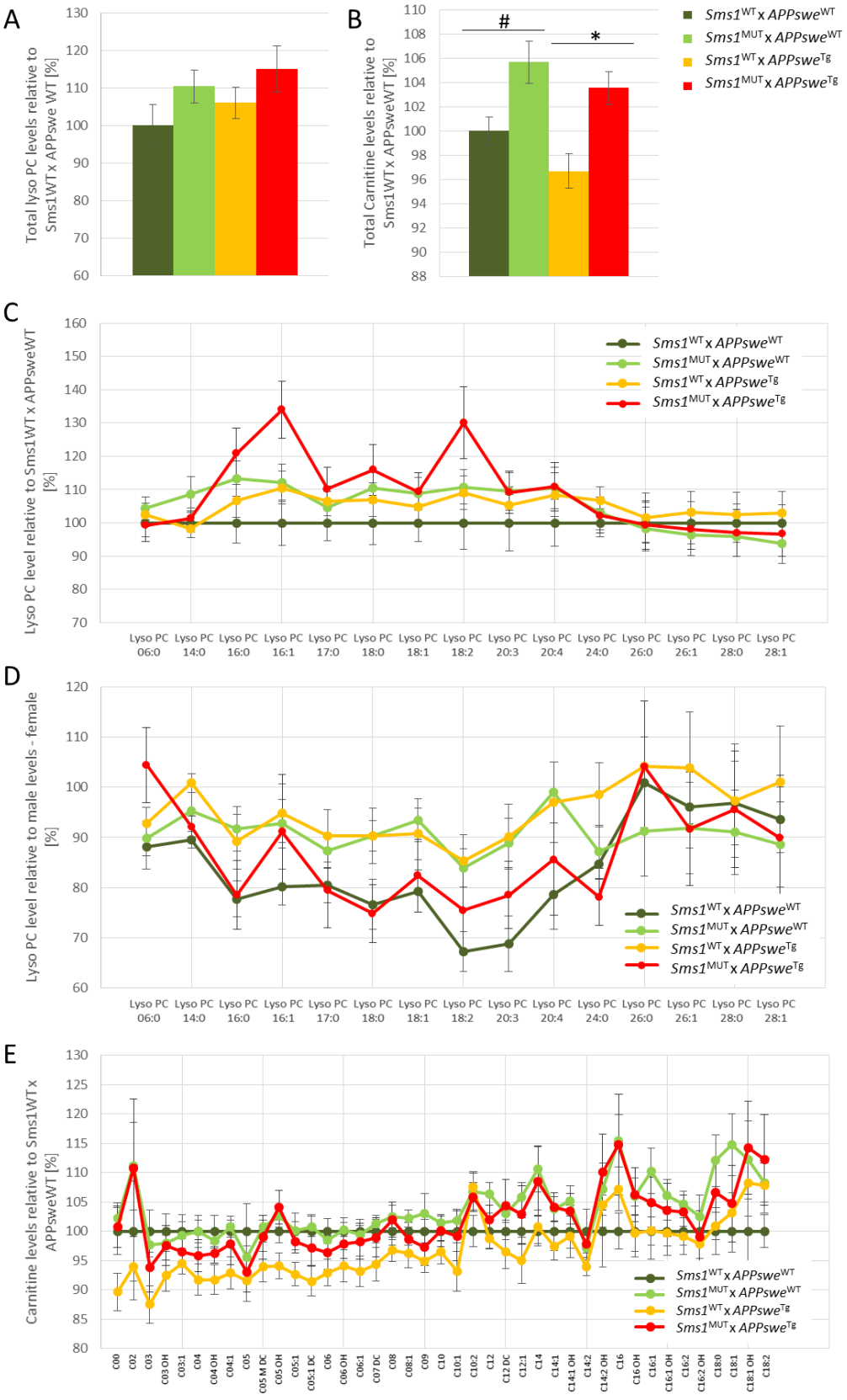

Figure 3.31: Lyso-phosphatidylcholine and carnitine levels are partially elevated in *Sms1*^{MUT} x *APPswe*^{WT} and in *Sms1*^{MUT} x *APPswe*^{Tg} animals.

(A) Relative lyso-phosphatidylcholine (lyso-PC) levels of brain tissue. (B) Relative carnitine levels of brain tis-

sue. (C) Relative levels of lyso-PC species. Combined data form both sexes. (D) Comparison of female lyso-PC levels relative to male levels, which were set to 100%. (E) Relative levels of carnitine species. Combined data form both sexes. Males: *Sms1*^{WT} x *APPswe*^{WT} n=5, *Sms1*^{MUT} x *APPswe*^{WT} n=6, *Sms1*^{WT} x *APPswe*^{Tg} n=11, *Sms1*^{MUT} x *APPswe*^{Tg} n=6; females: *Sms1*^{WT} x *APPswe*^{WT} n=6, *Sms1*^{MUT} x *APPswe*^{WT} n=11, *Sms1*^{WT} x *APPswe*^{Tg} n=13, *Sms1*^{MUT} x *APPswe*^{Tg} n=5. Age 8 weeks. Statistical analysis was done by one-way ANOVA with *post hoc* Tukey's test. Data is presented as mean ± SEM; p<0.01#, p≤0.05*, p≤0.01**, p≤0.001***.

The lyso-PC species differed between genotypes in C16:0 and C24:0, where both compound animals (*Sms1*^{MUT} x *APPswe*^{WT} and *Sms1*^{WT} x *APPswe*^{Tg}) and the double mutant animals (*Sms1*^{MUT} x *APPswe*^{Tg}) had elevated levels in comparison to *Sms1*^{WT} x *APPswe*^{WT} controls (Figure 3.31 C).

With higher FA chain length the lyso-PC levels of all genotypes analyzed were comparable to those of *Sms1*^{WT} x *APPswe*^{WT} controls (Figure 3.31 C). Peak values of lyso-PC levels were reached in *Sms1*^{MUT} x *APPswe*^{Tg} animals for the lyso-PCs C16:0 (120.87 ± 7.53%, p=0.1585), C16:1 (133.99 ± 8.67%, p=0.0094) and C18:2 (130.01 ± 10.82%, p=0.0496; Figure 3.31 C).

Due to the sex differences in total lyso-PC levels, I also analyzed lyso-PC species for both sexes separately. In both sexes, the levels of lyso-PCs in *Sms1*^{WT} x *APPswe*^{Tg} compound animals was lower than in *Sms1*^{MUT} x *APPswe*^{WT} compound animlas (supplementary Table 10.20 A, B). When these levels were compared to *Sms1*^{WT} x *APPswe*^{WT} control levels of the respective sex, however, female levles of both compound lines were well above those of controls (lyso-PC C16:0 to C20:4; supplementary Table 10.20 B), while male compound levles were more similar to those of controls (supplementary Table 10.20 A). The levles of lyso-PC species in double mutant *Sms1*^{MUT} x *APPswe*^{Tg} males and females had a similar pattern in both sexes (supplementary Table 10.20 A, B). Nevertheless, in females the peaks at lyso-PC C16:1 (141.59 ± 12.39%, p=0.0474) and 18:2 (134.94 ± 10.33%, p=0.0915) were more pronounced in comparison to male peaks (lyso-PC C16:1: 124.48 ± 7.03%, p=0.3433; C18:2: 120.15 ± 10.28%, p=0.4850), related to the respective *Sms1*^{WT} x *APPswe*^{WT} control levles (supplementary Table 10.20 B).

When female lyso-PC levels per genotype were mapped against male lyso-PC levels, it could be seen that both *Sms1*^{WT} x *APPswe*^{WT} controls differed most, with the female level well below that of males (Figure 3.31 D). The same could be seen for *Sms1*^{MUT} x *APPswe*^{Tg} animals, while the levels of compound mice (*Sms1*^{MUT} x *APPswe*^{WT} and *Sms1*^{WT} x *APPswe*^{Tg}) were more close to those of male animals (Figure 3.31 D).

3.2.2.5 Carnitines

In comparison to *Sms1*^{WT} x *APPswe*^{WT} controls, *Sms1*^{MUT} x *APPswe*^{WT} (105.66 ± 1.75%, p=0.0972) had the tendency to elevated Carnitine levels. The same was seen for *Sms1*^{MUT} x *APPswe*^{Tg} mice (103.54 ± 1.46%, p=0.0185) in comparison to *Sms1*^{WT} x *APPswe*^{Tg} animals. Here a significant difference was reached (Figure 3.31 B). With regard to the different carnitine species *Sms1*^{MUT} x

APPswe^{WT} and *Sms1*^{MUT} x *APPswe*^{Tg} animals showed elevated levels of species carrying FA chains with more than ten carbon residues (Figure 3.31 E). Total intensities of carnitines were rather low, therefore these results should be handled carefully.

3.2.3 DHA/EPA diet reduced hampered weight gain, but did not affect death rates

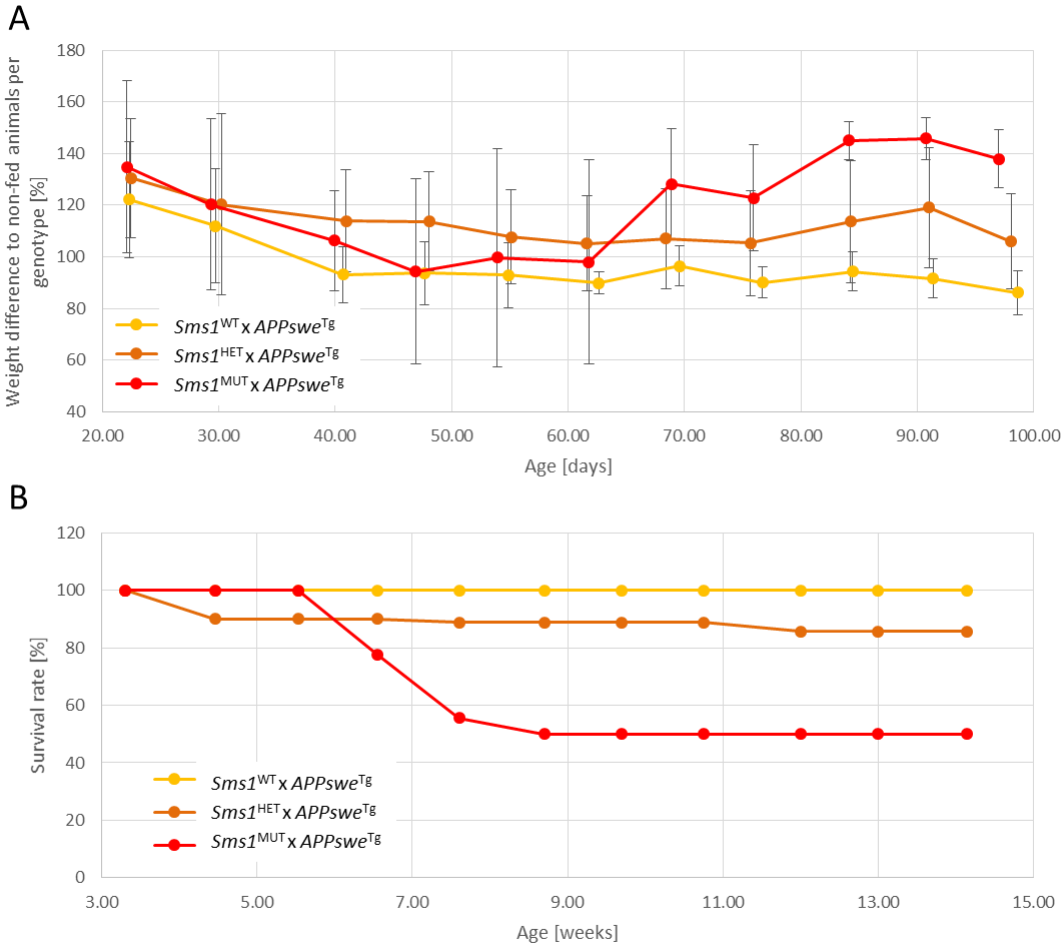

Figure 3.32: DHA/EPA supplemented diet rescued hampered weight gain, but did not improve survival of *Sms1*^{MUT} x *APPswe*^{Tg} animals.

(A) Weight increase of DHA/EPA fed *Sms1* x *APPswe*^{Tg} animals sorted by genotype in comparison to non-fed animals of the same genotype which were set to 100%. (B) Survival rates of DHA/EPA fed *Sms1* x *APPswe*^{Tg} animals. Combined data form both sexes. *Sms1*^{WT} x *APPswe*^{Tg} n=6, *Sms1*^{HET} x *APPswe*^{Tg} n=10, *Sms1*^{MUT} x *APPswe*^{Tg} n=9. Statistical analysis was done by one-way ANOVA with *post hoc* Tukey's test. Data is presented as mean ± SD; $p<0.01^{\#}$, $p\leq0.05$*, $p\leq0.01$**, $p\leq0.001$***.

As mentioned before, a reduction in MUFAs and PUFAs compared to SFAs was found in mice with the *Sms1*^{MUT} genotype. It is well known, that unsaturated FA are crucial for development and health (Kihara 2012). Therefore I wondered if a supplemental diet with omega-3 and omega-6 FA could help to improve the body weight gain and life expectancy of the affected genotypes of the *Sms1* x

APPswe mouse line. Due to the fact, that MUFAs and PUFAs play already a role in early development and represent an important parameter of mother milk, which is influenced by fatty acid uptake by nutrition (Antonakou *et al.* 2013, Nishimura *et al.* 2014), I started the feeding experiment already with the breeding pair females. They obtained omega-3 FAs (9mg total omega-3 FAs/animal/day) in addition to normal diet from the first day of the mating until weaning of the pubs. With weaning the pups themselves were fed the FA diet at a concentration of 4.5mg total omega-3 FAs/animal/day, which was doubled when they reached the age of 4 weeks.

3.2.3.1 Weight gain

Body weight gain of the fed animals improved compared to their non-fed controls of the corresponding genotype. All three genotypes had slightly increased body weight at weaning, which declined to the level of non-fed controls at the age of 40 to 60 days. From that age onwards, the increase in body weight improved and at the age of 90 days *Sms1*^{WT} x *APPswe*^{Tg} animals reached 91.51 ± 7.56% (p=0.0697), *Sms1*^{HET} x *APPswe*^{Tg} animals 119.01 ± 23.33% (p=0.0301) and *Sms1*^{MUT} x *APPswe*^{Tg} 145.93 ± 8.17% (p=0.0155) of the body weight of respective non-fed controls. It is important to notice that animals of the *Sms1*^{MUT} x *APPswe*^{Tg} genotype, which had the most restricted weight gain, in the non-fed cohort, showed the best improvement in weight gain, compared to the other genotypes *Sms1*^{HET} x *APPswe*^{Tg} and *Sms1*^{WT} x *APPswe*^{Tg} (Figure 3.32 A).

3.2.3.2 Life expectancy

Live expectancy in *APPswe* transgenic animals did not change due to the supplementary feeding of omega-3. At the age of 13 weeks survival rates of *Sms1*^{WT} x *APPswe*^{Tg} animals were 100%, while survival rates in *Sms1*^{HET} x *APPswe*^{Tg} animals were down to 85.71% and in *Sms1*^{MUT} x *APPswe*^{Tg} to 50% (Figure 3.32 B).

Taken together DHA/EPA supplement could rescue the genotype-related hampered weight gain observed in animals of the *Sms1* x *APPswe* mouse line, with best results for *Sms1*^{MUT} x *APPswe*^{Tg} animals. Nevertheless, survival could not be increased with supplement diet.

3.2.4 APP processing

3.2.4.1 APP cleavage products

APP and its cleavage enzymes, BACE1, ADAM10 and γ-secretase, are all transmembrane proteins. The lipid profile of *Sms1*^{MUT}x *APPswe*^{Tg} animals was profoundly changed and this change in lipid composition is likely to affect plasma membrane functionality, such as formation of lipid rafts and vacuoles, lipid-protein interactions and lipid signaling. All of these events are likely to influence APP cleavage. To analyze if the lipid composition changes due to *Sms1* disruption led to a shift in APP cleavage products, I set up an APP profile from brain samples of 8 week old male animals of the *Sms1* x *APPswe* mouse line (Figure 3.33). In addition BACE1 and γ-secretase activity in brain samples of 8

week old male and female animals of this line was measured (Figure 3.34) to asses direct or indirect effects of lipid alterations on their enzymatic activity.

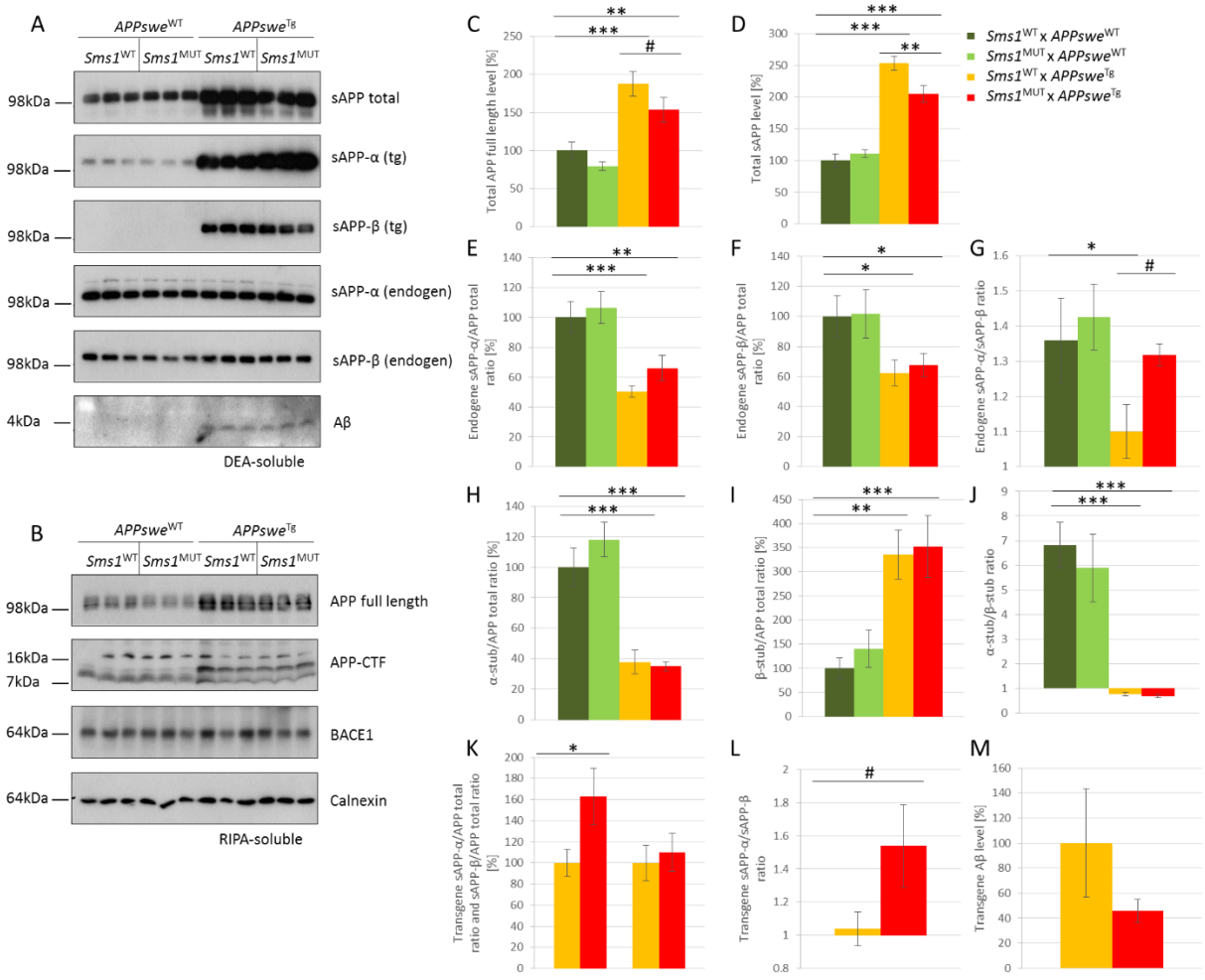

Figure 3.33: Amyloid beta precursor protein (APP) cleavage profile revealed a shift towards non-amyloidogenic processing in *Sms1*^{MUT} x *APPswe*^{Tg} animals.

(A) Immunoblot of DEA-soluble APP cleavage products. (B) Immunoblot of RIPA-soluble APP cleavage products and BACE1. (C-L) Quantification of immunoblot results for (D) total full lengths APP. (D) total soluble APP, (E-G) endogenous sAPP-α, sAPP-β including their ratio, (H-J) α-stub, β-stub including their ratio and (K, L) transgene sAPP-α, sAPP-β including their ratio. Immunoblots were performed on male whole brain samples, n=3 per genotype, age 8 weeks. Statistical analysis was done by one-way ANOVA with *post hoc* Tukey's test. Data is presented as mean ± SEM; $p<0.01^{\#}$, $p\leq0.05^{*}$, $p\leq0.01^{**}$, $p\leq0.001^{***}$.

In the RIPA fraction isolated from total brain samples, the membrane bound products for the APP profile can be found, such as total APP full length, C-terminal fragments (APP-CTF) and BACE1. Total APP full length levels were expectedly higher in *APPswe* transgenic animals (*Sms1*^{WT} x *APPswe*^{Tg} and *Sms1*^{MUT} x *APPswe*^{Tg}, mean APP full length: 190.03 ± 26.09%), which express endogenous *App* and human *APPswe* in comparison to *APPswe* non transgenic animals (*Sms1*^{WT} x

APPswe^{WT} and *Sms1*^{MUT} x *APPswe*^{WT}, mean APP full length: 100.00 ± 15.13%, p<0.0001), which just express endogenous *App* (Figure 3.33 B, C).

Additionally, *Sms1*^{MUT} x *APPswe*^{WT} animals had slightly reduced APP full length levels, which were down to 79.61 ± 5.76% (p=0.0502) of *Sms1*^{WT} x *APPswe*^{WT} control levels. A similar tendency, without significance could be found in *Sms1*^{MUT} x *APPswe*^{Tg} double mutant mice in comparison to *Sms1*^{WT} x *APPswe*^{Tg} compound mice. Here the total APP full length level 82.00 ± 8.61% of *Sms1*^{WT} x *APPswe*^{WT} level (p=0.2878; Figure 3.33 B, C).

After the first cleavage by either BACE1 or ADAM10, soluble APP-beta (sAPP-β) or soluble APP-alpha (sAPP-α), respectively, can be found to be released from the cellular membrane. These APP products could be detected in the DEA fraction. Additionally, the APP C-terminal fragment (APP-CTF; C99, 16kDa or C83, 7kDa respectively) remains membrane bound and could be found in the RIPA fraction of brain protein. The total level of sAPP (sAPP total) was not changed between *Sms1*^{WT} x *APPswe*^{WT} and *Sms1*^{MUT} x *APPswe*^{WT} (Figure 3.33 A, D).

In *APPswe* transgenic animals, first of all higher levels of sAPP total were found (mean sAPP total: 217.66 ± 27.17%) in comparison to *APPswe* non transgenic animals (mean sAPP total: 100.00 ± 9.20%, p<0.0001), due to the additional expression of human *APPswe* and its processing (Figure 3.33 A, D). Furthermore, a correlation between the reduced levels of APP full length and sAPP total could be detected in *Sms1*^{MUT} x *APPswe*^{Tg} animals. sAPP total was also reduced to 80.89 ± 5.13% (p=0.0020) in *Sms1*^{MUT} x *APPswe*^{Tg} animals compared to *Sms1*^{WT} x *APPswe*^{Tg} compound mice, which reflected the reduced APP full length expression in these animals.

After the cleavage by ADAM10 or BACE1 alpha-stubs (α-stubs) or beta-stubs (β-stubs) remain in the cellular membrane, while soluble APP-alpha (sAPP-α) or soluble APP-beta (sAPP-β) are released, respectively.

α-stub/APP total ratio was found to be higher in *APPswe* non-transgenic compared to *APPswe* transgenic animals. *Sms1*^{MUT} x *APPswe*^{WT} had an 18.04 ± 11.41% higher, but not significantly different (p=0.1666), ratio than *Sms1*^{WT} x *APPswe*^{WT} controls. *Sms1*^{WT} x *APPswe*^{Tg} and *Sms1*^{MUT} x *APPswe*^{Tg} animals, however had lower ratios of 37.79 ± 7.80% (p=0.0002) and 34.99 ± 3.16% (p=0.0001), respectively compared to *Sms1*^{WT} x *APPswe*^{WT} controls (100.00 ± 12.42%; Figure 3.33 B, H). These results indicated, that a higher amount of the total APP full length in *APPswe* non-transgenic animals, was processed to α-stubs in comparison to *APPswe* transgenic animals, where a lower percentage of the produced APP full length was cleaved in the α-secretory pathway.

With regard to the β-stub/APP total ratio, contrary results were found. *Sms1* x *APPswe*^{Tg} animals had higher ratios (*Sms1*^{WT} x *APPswe*^{Tg}: 335.29 ± 50.70%, p=0.0012; *Sms1*^{MUT} x *APPswe*^{Tg}: 351.79 ±

64.20%, p=0.0007) than *Sms1* x *APPswe*^{WT} animals (*Sms1*^{MUT} x *APPswe*^{WT}: 140.47 ± 38.75%, p=0.7187) compared to *Sms1*^{WT} x *APPswe*^{WT} control animals (100.00 ± 21.66%; Figure 3.33 B, I). These higher β-stub/APP total ratios showed a preference in *APPswe* transgenic animals for the β-secretory pathway. That shift towards BACE1 cleavage was expected, as the *APPswe* mutation leads to a higher affinity of BACE1 towards APP as its substrate and therefore promotes the generation of β-stubs over the generation of α-stubs.

The preference towards BACE1-mediated cleavage in *Sms1* x *APPswe*^{Tg} animals could also be seen in the α-stub/β-stub ratio itself. While *Sms1* x *APPswe*^{WT} animals had ratios between 5.88 ± 1.37 (*Sms1*^{MUT} x *APPswe*^{WT}) and 6.82 ± 0.92 (*Sms1*^{WT} x *APPswe*^{WT}), representing a higher amount of α-stubs over β-stubs (p<0.0001). *Sms1* x *APPswe*^{Tg} animals had ratios between 0.76 ± 0.7 (*Sms1*^{WT} x *APPswe*^{Tg}) and 0.68 ± 0.07 (*Sms1*^{MUT} x *APPswe*^{Tg}), pointing to higher amounts of β-stubs over α-stubs (Figure 3.33 B, J).

No differences were found within *Sms1* x *APPswe*^{WT} or *Sms1* x *APPswe*^{Tg} animals, correlating with the *Sms1* genotype.

sAPP-α and sAPP-β were measured with specific antibodies, making it possible to distinguish between endogenous and transgenic cleavage products.

Endogenous sAPP-α/total APP ratio was lower in *Sms1* x *APPswe*^{Tg} animals (*Sms1*^{WT} x *APPswe*^{Tg}: 50.38 ± 3.89%, p=0.0006; *Sms1*^{MUT} x *APPswe*^{Tg}: 66.11 ± 8.60 %, p=0.0068) than in *Sms1* x *APPswe*^{WT} animals (*Sms1*^{MUT} x *APPswe*^{WT}: 106.61 ± 10.73%, p=0.7987) compared to *Sms1*^{WT} x *APPswe*^{WT} controls (100.00 ± 10.48%; Figure 3.33 A, E). The lower levels in sAPP- α/total APP ratio in the *Sms1* x *APPswe*^{Tg} animals compared to *Sms1* x *APPswe*^{WT} animals reflect the concurrence between endogenous APP and transgenic *APPswe*. From the total amount of APP full length, present in these animals, a lower percentage of endogenous APP was processed via the α-secretory pathway, as transgenic *APPswe* competes as a substrate for ADAM10.

Endogenous sAPP-β/total APP ratio showed a similar pattern as sAPP-α/total APP ratio, with *Sms1* x *APPswe*^{Tg} animals having a lower ratio (*Sms1*^{WT} x *APPswe*^{Tg}: 62.25 ± 8.76%, p=0.0210; *Sms1*^{MUT} x *APPswe*^{Tg}: 67.76 ± 7.79%, p=0.0454) than *Sms1* x *APPswe*^{WT} animals (*Sms1*^{MUT} x *APPswe*^{WT}: 101.72 ± 15.98%, p=0.9980) in comparison to *Sms1*^{WT} x *APPswe*^{WT} controls (100.00 ± 13.80%; Figure 3.33 A, F). I did not find any *Sms1* correlated alterations between genotypes. Similar to the sAPP- α/total APP ratio these results showed the competition between endogenous APP and transgenic *APPswe*, which resulted in a lower percentage of endogenous APP to be cleaved by BACE1.

In all four genotypes, the ratio between endogenous sAPP-α and sAPP-β indicated a higher amount of sAPP-α produced. Nevertheless a lower sAPP-α/sAPP-β ratio was found in *Sms1*^{WT} x *APPswe*^{Tg} animals (1.10 ± 0.08) compared to *Sms1*^{WT} x *APPswe*^{WT} controls (1.36 ± 0.12, p=0.0273). This reduction could not be found in *Sms1*^{MUT} x *APPswe*^{Tg} animals (1.32 ± 0.03, p=0.9335; Figure 3.33 A, G). These results could point out, that in *Sms1*^{WT} x *APPswe*^{Tg} compound mice had a slightly shifted processing of endogenous APP towards the β-secretory pathway, which was revoked with the additional mutation in *Sms1*. However, this possible observation needs to be clarified further.

Transgenic sAPP-α and sAPP-β were also measured in *Sms1* x *APPswe*^{Tg} animals. In comparison to total APP levels there was a 62.82 ± 26.76% higher ratio of sAPP-α/APP total in *Sms1*^{MUT} x *APPswe*^{Tg} double mutant animals compared to *Sms1*^{WT} x *APPswe*^{Tg} compound mice (100.00 ± 12.69%, p=0.0379; Figure 3.33 A, K), while there was no difference in sAPP-β/APP total between both genotypes (Figure 3.33 A, K). Direct comparison of both soluble products in the sAPP-α/sAPP-β ratio also showed an elevation of sAPP-α levels in the *Sms1*^{MUT} x *APPswe*^{Tg} mice (1.53 ± 0.25), compared to *Sms1*^{WT} x *APPswe*^{Tg} animals (1.04 ± 0.10, p=0.0583; Figure 3.33 A, L).

At the age of 8 weeks no endogenous Aβ could be detected in either *Sms1*^{WT} x *APPswe*^{WT} or *Sms1*^{MUT} x *APPswe*^{WT} animals (Figure 3.33 A). In brain samples of *Sms1*^{WT} x *APPswe*^{Tg} and *Sms1*^{MUT} x *APPswe*^{Tg} animals of the same age small amounts of Aβ were found, with *Sms1*^{MUT} x *APPswe*^{Tg} animals having less Aβ then *Sms1*^{WT} x *APPswe*^{Tg}. This reduction was not significant (Figure 3.33 A).

3.2.4.2 Activity of APP processing enzymes

Due to the hints obtained from the APP profile, that *APPswe* processing in *Sms1*^{MUT} x *APPswe*^{Tg} animals compared to *Sms1*^{WT} x *APPswe*^{Tg} animals was shifted to the α-secretory pathway leading to higher amounts of sAPP-α, compared to sAPP-β, it should be analyzed whether this shift was linked to alterations in secretase activity. Therefore, activities of BACE1 and γ-secretase was measured in male and female brain samples, collected at the age of 8 weeks.

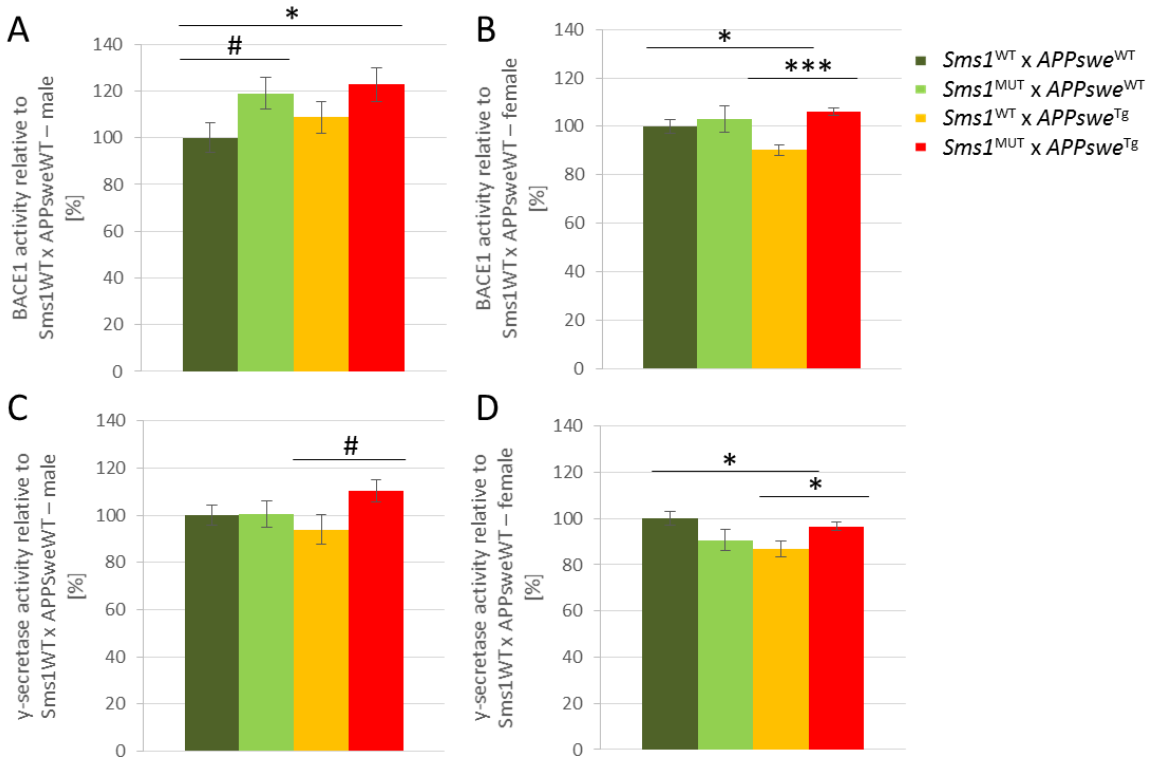

Figure 3.34: Secretase activity was altered in *Sms1* x *APPswe* animals.
(A, B) Beta site APP cleavage enzyme 1 (BACE1) activity in (A) male and (B) female brain samples. (C, D) γ-secretase activity in (C) male and (D) female brain samples. Males: *Sms1*^{WT} x *APPswe*^{WT} n=5, *Sms1*^{MUT} x *APPswe*^{WT} n=6, *Sms1*^{WT} x *APPswe*^{Tg} n=11, *Sms1*^{MUT} x *APPswe*^{Tg} n=6; females: *Sms1*^{WT} x *APPswe*^{WT} n=6, *Sms1*^{MUT} x *APPswe*^{WT} n=11, *Sms1*^{WT} x *APPswe*^{Tg} n=13, *Sms1*^{MUT} x *APPswe*^{Tg} n=5. Age 8 weeks. Statistical analysis was done by one-way ANOVA with *post hoc* Tukey's test. Data is presented as mean ± SEM; p<0.01#, p≤0.05*, p≤0.01**, p≤0.001***.

3.2.4.2.1 BACE1 activity

Compared to *Sms1*^{WT} x *APPswe*^{WT} controls, BACE1 activity in male brain samples was elevated to a similar extend, when *Sms1* was disrupted, independent on the *APPswe* background. Additionally, the expression of the *APPswe* transgene led to a slightly higher, but not significantly increased BACE1 activity compared to *Sms1* x *APPswe*^{WT} animals (*Sms1*^{WT} x *APPswe*^{WT}: 100.00 ± 6.45%; *Sms1*^{MUT} x *APPswe*^{WT}: 118.96 ± 6.70%, p=0.0759; *Sms1*^{WT} x *APPswe*^{Tg}: 108.68 ± 6.94%, p=0.3866; *Sms1*^{MUT} x *APPswe*^{Tg}: 122.83 ± 7.23%, p=0.0463; Figure 3.34 A). In female samples the elevation of BACE1 activity with the mutation in *Sms1*^{MUT} x *APPswe*^{Tg} was also found compared to *Sms1*^{WT} x *APPswe*^{Tg}, however, BACE1 activity was reduced in *Sms1*^{WT} x *APPswe*^{Tg} compound mice in comparison to *Sms1*^{WT} x *APPswe*^{WT} control animals (*Sms1*^{WT} x *APPswe*^{WT}: 100.00 ± 2.96%; *Sms1*^{MUT} x *APPswe*^{WT}: 102.94 ± 5.46%, p=0.6497; *Sms1*^{WT} x *APPswe*^{Tg}: 90.23 ± 2.12%, p=0.0278; *Sms1*^{MUT} x *APPswe*^{Tg}: 105.91 ± 1.44, p=0.1105; Figure 3.34 B). Although these results were not persistent within sex, they give a hint that BACE1 activity might be negatively influenced by *Sms1* expression.

3.2.4.2.2 Γ-secretase complex activit

Γ-secretase represents the second step in the amyloidogenic pathway of APP processing, but is also responsible for the second cleavage in the non-amyloidogenic pathway. No significant alterations of γ-secretase activity in male or female animals on a *Sms1* x *APPswe*^{WT} background were found (male: *Sms1*^{WT} x *APPswe*^{WT}: 100.00 ± 4.22%; *Sms1*^{MUT} x *APPswe*^{WT}: 100.52 ± 5.45%, p=0.9419; female: *Sms1*^{WT} x *APPswe*^{WT}: 100.00 ± 3.02%; *Sms1*^{MUT} x *APPswe*^{WT}: 90.58 ± 4.53%, p=0.1217; Figure 3.34 C, D). On an *Sms1* x *APPswe*^{Tg} background, however, both, male and female data revealed an up regulation of γ-secretase activity with the disruption of *Sms1* in comparison to *Sms1*^{WT} x *APPswe*^{Tg} compound mice (male: *Sms1*^{WT} x *APPswe*^{Tg}: 100.00 ± 6.25%; *Sms1*^{MUT} x *APPswe*^{Tg}: 117.61 ± 4.63%, p=0.0660; female: *Sms1*^{WT} x *APPswe*^{Tg}: 100.00 ± 3.47%; *Sms1*^{MUT} x *APPswe*^{Tg}: 111.36 ± 1.86%, p=0.0366; Figure 3.34 C, D). Without the additional mutation in *Sms1*, there was a down regulation of γ-secretase activity in *Sms1*^{WT} x *APPswe*^{Tg} animals in comparison to *Sms1*^{WT} x *APPswe*^{WT} controls, which reached significance in female animals only (male: *Sms1*^{WT} x *APPswe*^{WT}: 100.00 ± 4.22%; *Sms1*^{WT} x *APPswe*^{Tg}: 93.93 ± 6.25%, p=0.4433; female: *Sms1*^{WT} x *APPswe*^{WT}: 100.00 ± 3.02%; *Sms1*^{WT} x *APPswe*^{Tg}: 86.68 ± 3.47%, p=0.0199; Figure 3.34 C, D). For *Sms1* x *APPswe*^{Tg} animals, these results indicated, that *Sms1* expression might also facilitate γ-secretase activity.

3.2.5 pTAU/TAU ratio

Additionally to the human *APPswe* transgene endogenous TAU and pTAU levels in the brains of *Sms1* x *APPswe* mice were analyzed to check if the changes in the APP processing pathway affect the phsophorylation of TAU.

With an age of 8 weeks, pTAU/TAU ratios were not significantly different between the genotypes of the *Sms1* x *APPswe* mouse line.

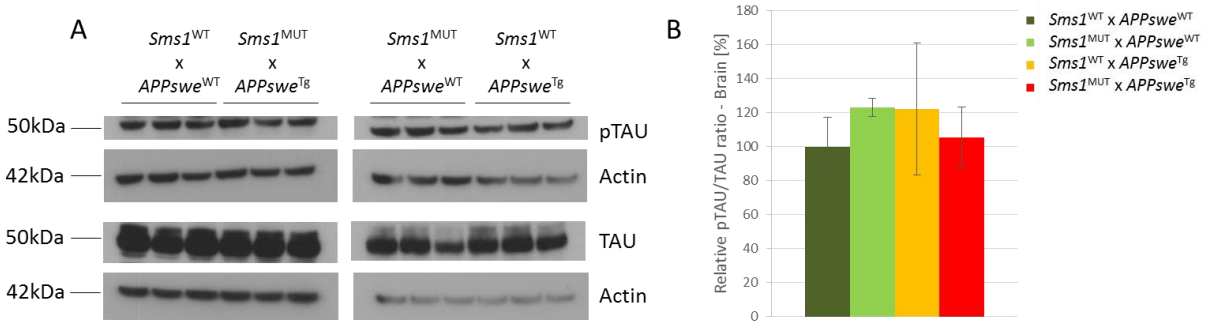

Figure 3.35: TAU and pTAU levels in the brains of *Sms1* x *APPswe* mice.
(A) Immunoblot against TAU and pTAU in brain samples of 8 week old Sms1 x APPswe animals. (B) Relative quantification of pTAU/TAU ratios with Sms1WT x APPsweWT set to 100%. Sms1WT x APPsweWT n=3, Sms1MUT x APPsweWT n=3, Sms1WT x APPsweTg n=3, Sms1MUT x APPsweTg n=3. Statistical analysis was done by one-way ANOVA with post hoc Tukey's test. Data is presented as mean ± SEM; p<0.01#, p≤0.05*, p≤0.01**, p≤0.001***.

3.2.6 Brain histology of *Sms1* x *APPswe* mice

As Aβ generation could be detected in *Sms1*^{MUT}x *APPswe*^{Tg} and *Sms1*^{WT} x *APPswe*^{Tg} mice, immunohistochemical staining was performed to check for possible formation of plaques. I decided to directly stain and distinguish Aβ-40 and Aβ-42 positive plaques to analyze possible aggregation differences in the *Sms1* x *APPswe*^{Tg} animals. Aβ-40 positive plaques were found in *Sms1*^{WT} x *APPswe*^{Tg} and in *Sms1*^{MUT} x *APPswe*^{Tg} animals. Representative pictures of Aβ-40 plaques found in cortical and thalamic regions are shown in Figure 3.36 A, B. However, when Aβ-40 positive plaques were counted *Sms1*^{MUT} x *APPswe*^{Tg} animals with a mean number of 1.28 ± 0.17 plaques per section had less plaques compared to *Sms1*^{WT} x *APPswe*^{Tg} animals with a mean number of 2.44 ± 0.53 plaques per section (p=0.0449; Figure 3.36 E). These results were most significant in the hypothalamic region (Figure 3.36 F). Aβ-42 positive plaques were also rarely found, but mostly in *Sms1*^{WT} x *APPswe*^{Tg} animals (Figure 3.36 C, D). Quantification of Aβ-42 positive plaques did not reveal any significant alteration between genotypes (Figure 3.36 G). Importantly, the observed Aβ-40 and Aβ-42 positive plaques had a rather diffuse structure, missing an aggregation core (Figure 3.36 C, D). Regarding the overall low number of plaques counted per section the Aβ pathology should be regarded as minor.

To check for antibody performance and plaque authenticity Thioflavin-S staining was performed. Detected plaques were Thioflavin-S positive (compare supplementary Figure 10.5), underlining the results mentioned above.

In summary the reduction in Aβ-40 positive plaques could contribute to the finding on a possible shift towards the α-secretory pathway in *Sms1*^{MUT} x *APPswe*^{Tg} animals in comparison to *Sms1*^{WT} x *APPswe*^{Tg} animals.

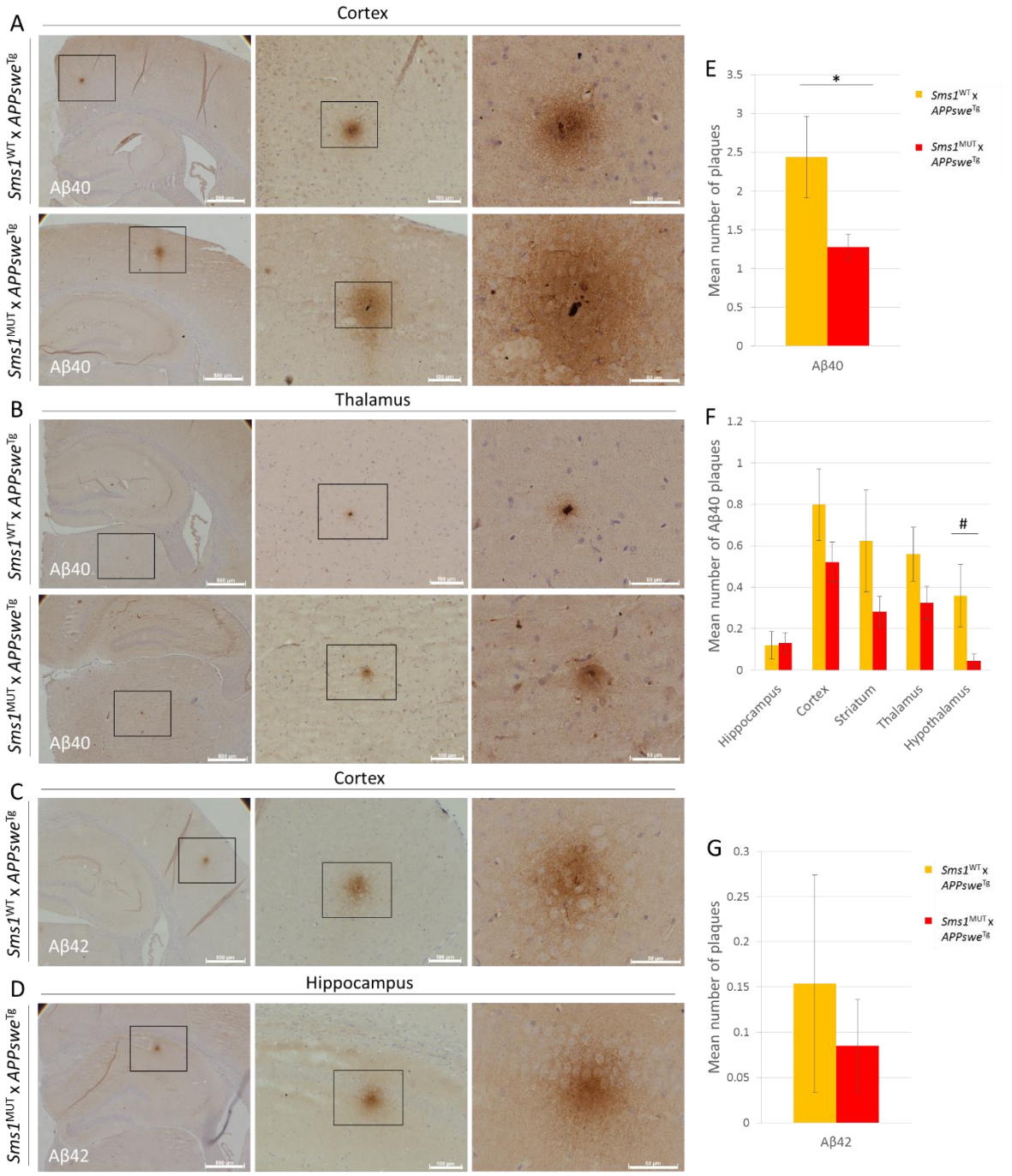

Figure 3.36: Aβ-40 and Aβ-42 positive plaques were found in *Sms1* x *APPswe*^{Tg} animals, with a reduction of Aβ-40 positive plaques in *Sms1*^{MUT} x *APPswe*^{Tg} mice.

(A, B) Representative immunostaining of Aβ-40 positive plaques in the (A) cortex and (B) thalamus of *Sms1*^{WT} x *APPswe*^{Tg} and *Sms1*^{MUT} x *APPswe*^{Tg} animals. (C, D) Representative immunostaining of Aβ-42 positive plaques in the (C) cortex and (D) hippocampus of *Sms1*^{WT} x *APPswe*^{Tg} animals. Scale bars for A-D: 500µm, 100µm and 50µm with increasing magnification. (E) Mean number of Aβ-40 positive plaques per section. (F) Mean number of Aβ-40 positive plaques per section shown by brain region. (G) Mean number of Aβ-42 positive plaques per section. *Sms1*^{WT} x *APPswe*^{Tg} n=3, *Sms1*^{MUT} x *APPswe*^{Tg} n=5, with 7-10 brain sections counted per animal. Age 8 weeks. Statistical analysis was done by two-tailed Student's t-test. Data is presented as mean ± SEM; $p<0.01^{\#}$, $p\leq0.05^{*}$, $p\leq0.01^{**}$, $p\leq0.001^{***}$.

3.2.7 Studies on general behavior and memory performance

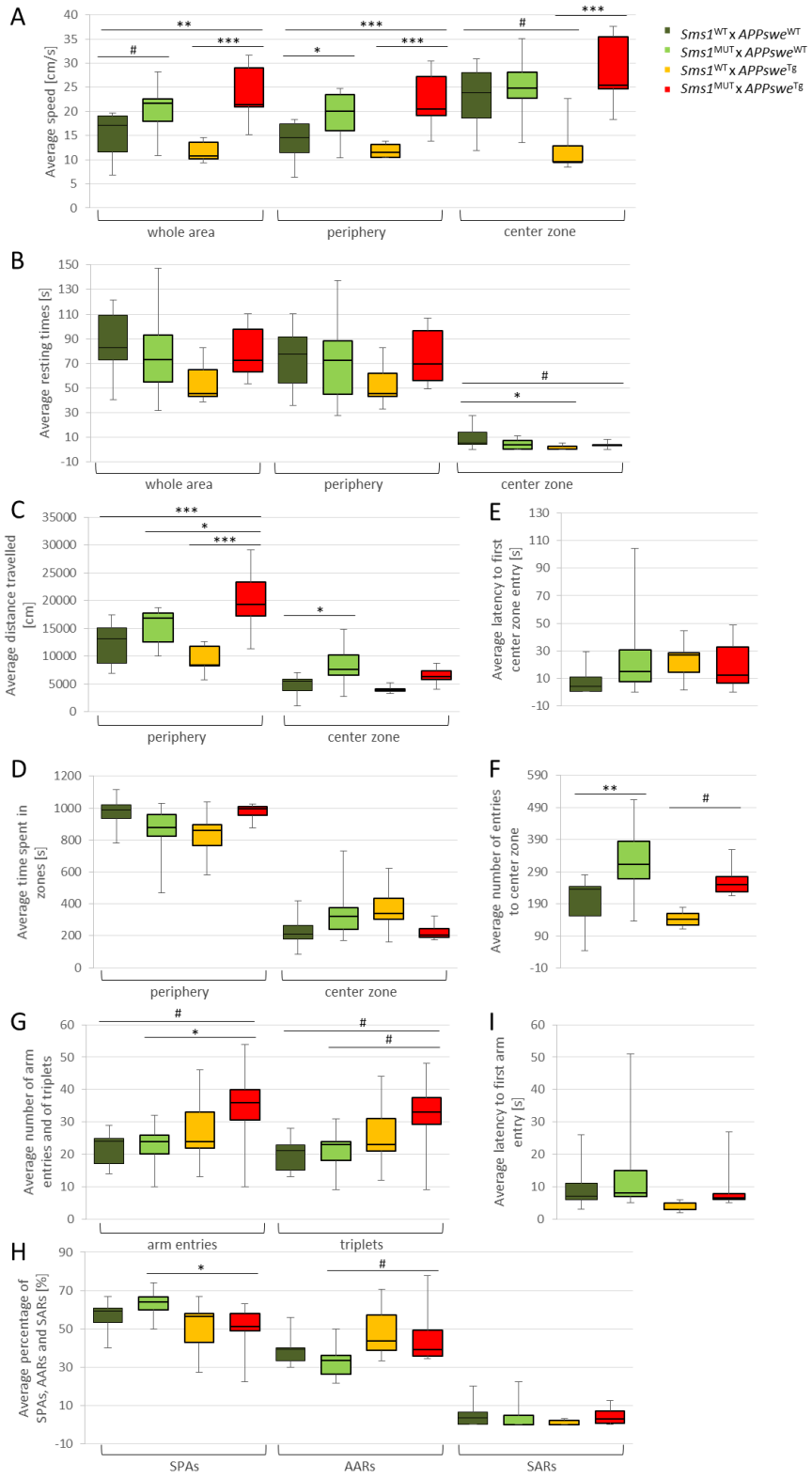

Figure 3.37: Behavioral studies did not reveal any alterations in memory performance in *Sms1* x *APPswe*^{Tg} animals at the age of 8 weeks.

(A-F) Open field (OF) results. (A) Average speed in whole area, periphery and center zone. (B) Average resting time in periphery and center zone. (C) Average distance travelled in periphery and center zone. (D) Average time

spent in periphery and center zone. (E) Average latency to enter center zone. (F) Average number of transits to the center zone. (G-I) Y-Maze results. (G) Average number of arm entries and performed triplets. (H) Average percentage of spontaneous alterations (SPAs), alternate arm returns (AARs) and same arm returns (SARs). (I) Average latency to first arm entry. *Sms1*^{WT} x *APPswe*^{WT} n=9, *Sms1*^{MUT} x *APPswe*^{WT} n=13, *Sms1*^{WT} x *APPswe*^{Tg} n=5, *Sms1*^{MUT} x *APPswe*^{Tg} n=8. Age 8 weeks. Data represents results of the whole testing period for each test. Statistical analysis was done by one-way ANOVA with post hoc Tukey's test. Data is presented as median ± quartiles; $p<0.01^{\#}$, $p\leq0.05^{*}$, $p\leq0.01^{**}$, $p\leq0.001^{***}$.

The detection of plaques at the age of eight weeks, although without a major Aβ pathology, provoked the question if one would be able to detect behavioral deficits in animals of the *Sms1* x *APPswe* mouse line, at this early age. The question was, if these animals show signs of general behavioral alterations and especially of memory performance. As there was the need to perform these tests with young animals at the age of eight weeks they should be regarded as preliminary results. Open field (OF) results showed a higher average speed in *Sms1*^{MUT} x *APPswe*^{WT} (21.7cm/s (IQR: 4.6), p=0.0507) and in *Sms1*^{MUT} x *APPswe*^{Tg} (21.4cm/s (IQR: 8.0), p=0.0002) animals compared to *Sms1*^{WT} x *APPswe*^{WT} (17.1cm/s (IQR: 7.5)) and *Sms1*^{WT} x *APPswe*^{Tg} (10.7cm/s (IQR: 3.4)) animals, respectively, pointing to an alteration of behavior based on the *Sms1* mutation. The average speed of each genotype except of *Sms1*^{WT} x *APPswe*^{Tg} animals did again differ between periphery and center zone of the OF, with a higher speed seen in the center zone (Figure 3.37 A). *Sms1*^{WT} x *APPswe*^{Tg} animals did not just show the lowest average speed but also had shortest resting times while the OF test performance (45.8s (IQR: 21.5)). These reached significance when comparing the center zone data (Figure 3.37 B). The relation between genotypes found for the average speed were also reflected in the average distance travelled during OF (*Sms1*^{WT} x *APPswe*^{Tg} < *Sms1*^{WT} x *APPswe*^{WT} < *Sms1*^{MUT} x *APPswe*^{WT} < *Sms1*^{MUT} x *APPswe*^{Tg}). For all genotypes the distance travelled in the periphery was longer than that travelled in the center zone (Figure 3.37 C). The same relation between periphery and center zone could be seen for the time spent in the respective area. However, here *Sms1*^{MUT} x *APPswe*^{WT} (322.8s (IQR: 134.8)) and *Sms1*^{WT} x *APPswe*^{Tg} (338.5s (IQR: 133.9)) animals spent longer time in the center zone compared to *Sms1*^{WT} x *APPswe*^{WT} (212.6s (IQR: 85.2)) and *Sms1*^{MUT} x *APPswe*^{Tg} animals (203.8s (IQR: 56.2)), although, these data did not reach significance (Figure 3.37 D). The average latency to enter the center zone for the first time during the OF test did not differ between genotypes (Figure 3.37 E), while the average number of entries to the center zone was higher in *Sms1*^{MUT} x *APPswe*^{WT} (312 (IQR: 116), p=0.0057) and in *Sms1*^{MUT} x *APPswe*^{Tg} (249 (IQR: 48)) animals compared to *Sms1*^{WT} x *APPswe*^{WT} (236 (IQR: 91), p=0.0544) and *Sms1*^{WT} x *APPswe*^{Tg} animals (142 (IQR: 36)), respectively (Figure 3.37 F).

In order to measure memory performance, a Y-Maze test was conducted. The average number of arm entries and performed triplets showed similar to the OF test, that *Sms1*^{MUT} x *APPswe*^{Tg} animals had a higher activity and travelled more compared to *Sms1*^{WT} x *APPswe*^{WT} animals (Figure 3.37 G). However, in comparison to the OF test in the Y-Maze I did not find the correlation between higher

activity (average speed and distance travelled or number of arm entries and performed triplets) and the mutation in *Sms1*, as *Sms1*^{MUT} x *APPswe*^{WT} animals had similar numbers of arm entries and triplets like *Sms1*^{WT} x *APPswe*^{WT} animals (Figure 3.37 A, C, G). Concerning the latency until the first arm entry the Y-Maze test verified the results obtained by the OF, with no difference between genotypes detected (Figure 3.37 E, I).

Concerning memory performance parameters of the Y-maze no striking differences were found between the genotypes. The number of same arm return (SAR), was similarly small in all tested genotypes with average numbers between 1.0 and 2.8 (1.1 to 4.5%; Figure 3.37 H). Interestingly, spontaneous alteration performance (SAP), measuring the tendency to enter another arm than the most recently visited, was worse in *Sms1*^{MUT} x *APPswe*^{Tg} (51.04% (IQR: 9.31) compared to *Sms1*^{MUT} x *APPswe*^{WT} animals (64.00% (IQR: 6.67), p=0.0481), while alternate arm returns (AAR) were observed more often (*Sms1*^{MUT} x *APPswe*^{WT}: 36.00% (IQR: 9.91), *Sms1*^{MUT} x *APPswe*^{Tg}: 49.21% (IQR: 13.48), p=0.0872; Figure 3.37 H). This points to an effect of *hAPPswe* expression on memory performance, although no effect was observed between *Sms1*^{WT} x *APPswe*^{Tg} and *Sms1*^{WT} x *APPswe*^{WT} animals.

In total, the higher activity described in *Sms1*^{MUT} animals was also seen in *Sms1*^{MUT} x *APPswe*^{WT} and *Sms1*^{MUT} x *APPswe*^{Tg} animals. Anxiety-like behavior seemed to be reduced in *Sms1*^{MUT} x *APPswe*^{WT} compared to *Sms1*^{WT} x *APPswe*^{WT} animals, but gave controversial results on *Sms1*^{MUT} x *APPswe*^{Tg} animals, as they showed a reduced time spent in the center zone, but elevated number of center zone entrances and a longer distance travelled in the center zone. With regard to memory, no major effect of *Sms1* disruption, which could be connected to Aβ or plaque load observed in the brains of *Sms1*^{WT} x *APPswe*^{Tg} and *Sms1*^{MUT} x *APPswe*^{Tg} animals, could be detected.

3.2.8 APP Expression pattern of APPswe in different organs

There were no major alterations in brains of *Sms1* x *APPswe* animals detected, which could explain the early death phenotype. Therefore *Sms1* x *APPswe* animals, which were found dead (*post-mortem* interval < 3h) together with age-matched controls were transferred to the Institute of Pathology for pathological investigation by Dr. Frauke Neff. Macroscopic and histological analysis revealed slight alterations in heart, lung and liver. Those included dilation of one or both ventricles of the heart, hyperemia of the lung and microgranuloma and/or glycogen storage of different severity in the liver. However, none of these findings was restricted to *Sms1*^{MUT} x *APPswe*^{Tg} or could give an obvious hint to the cause of death (see supplementary data Table 10.21).

In an earlier description of the *APPswe*/Tg2576 mouse model (Kawarabayashi *et al.* 2001) it is mentioned, that the h*APPswe* is not just expressed in the brain of these animals, but is also found in heart, lung and spleen. Therefore I checked for h*APPswe* expression in different organs of the *Sms1* x *APPswe* mouse model.

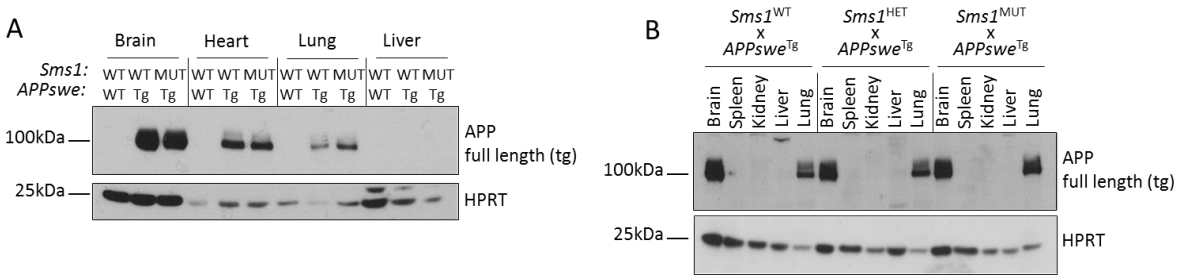

Figure 3.38: Tissue specific expression of h*APPswe* in the *Sms1* x *APPswe* mouse line.
(A, B) Immunoblot against h*APPswe* using the commercial 6E10 antibody and protein samples of different organs from 8 week old animals of the *Sms1* x *APPswe* mouse line.

The h*APPswe* was found to be expressed in brain, heart and lung, as it was expected from literature ((Kawarabayashi *et al.* 2001); Figure 3.38 A, B). Expression was high in heart samples, followed by brain and less pronounced in lung samples. However, it is necessary to mention, that HPRT expression is not equal between the tested tissues, and that comparison of protein amount therefore is not straight forward. Different to literature, the expression of h*APPswe* could not confirmed in spleen samples of the *Sms1* x *APPswe* mouse model. There was also no expression in liver and kidney (Figure 3.38 A, B).

As the differences found in brain samples were not crucial, it should be investigated, wheather *APPswe* processing in one of the other organs was profoundly changed. Preliminary analysis of the APP profile in lung and heart in comparison to brain revealed different levels of full length APP to be expressed in the analyzed organs (heart>brain>lung), without differences between *Sms1*^{WT} x *APPswe*^{Tg} and *Sms1*^{MUT} x *APPswe*^{Tg} animals (Figure 3.39 A, B). Immunoblot analysis did not reveal any statistical significant differences in expression of BACE1 or ADAM10, APP full length, APP-CTF or Aβ between genotypes (Figure 3.39 A-F). Nevertheless, 5- to 15-fold higher Aβ levels were found in lung and heart compared to the traces detected in the brain samples (heart>lung>brain). Additionally, slightly enhanced, but not statistically different, levels of Aβ were found in *Sms1*^{MUT} x *APPswe*^{Tg} in comparison to *Sms1*^{WT} x *APPswe*^{Tg} animals in both organs (Figure 3.39 A, D). Expression of the cleavage enzymes differed between the tissues with BACE1 having similar levels in lung and heart, while its expression in brain was 5-fold higher. ADAM10 expression wax 2.5-fold higher in heart and 4.8-fold to 5.8-fold higher in lung in comparison to brain samples (Figure 3.39 A, E, F). The α-stub/β-stub ratio was 2- to 3-fold higher in the heart and more than 10-fold higher in the lung compared to the brain (Figure 3.39 A, C). These results correlated with the expression of the APP cleavage enzymes of the non-amyloidogenic and amyloidogenic pathway (Figure 3.39 A, C, E, F).

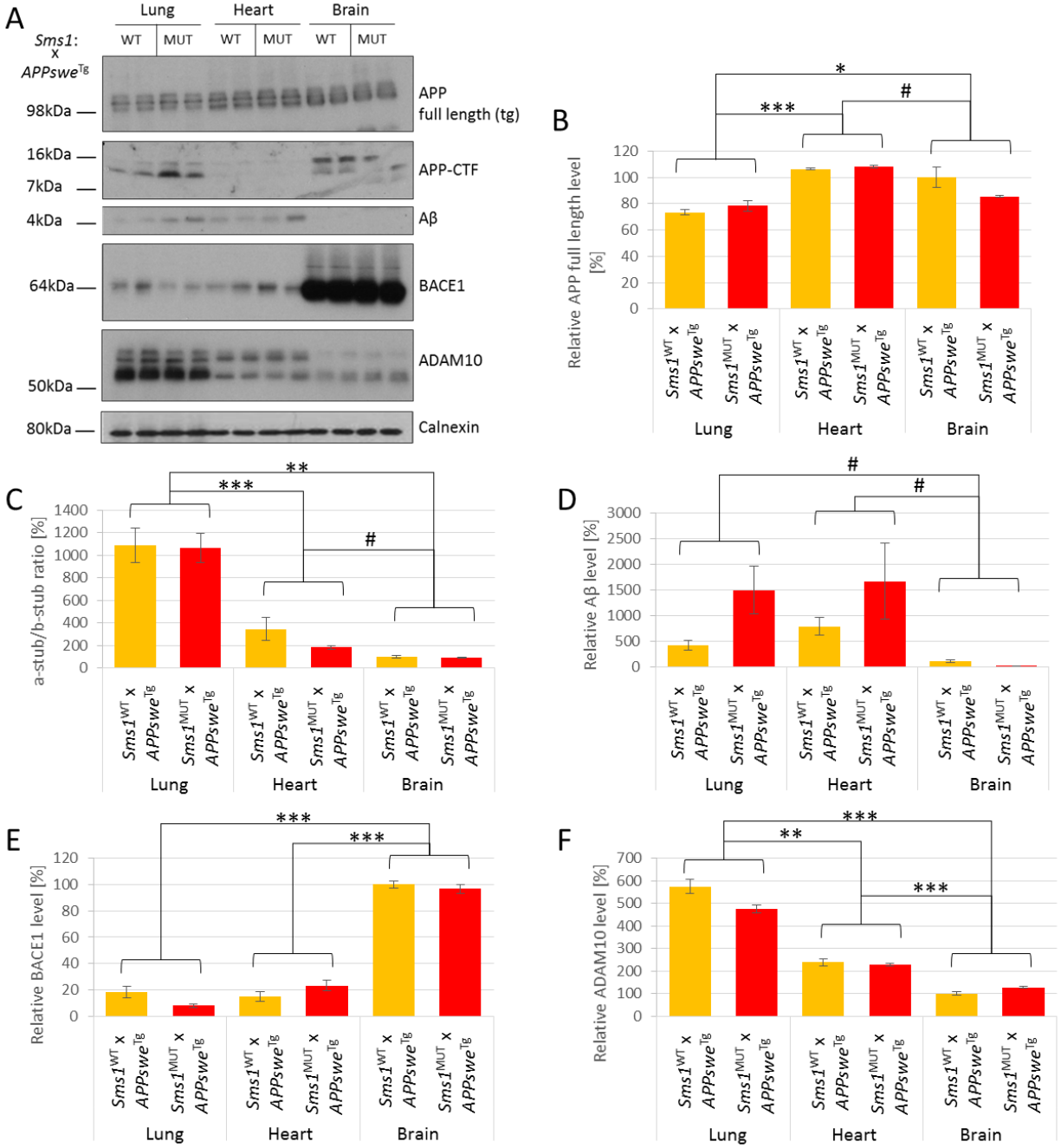

Figure 3.39: APP profile of lung and heart in comparison to brain samples

(A) Immunoblot of APP full length, major cleavage products and cleavage enzymes of lung, heart and brain protein samples. (B-F) Quantification of APP full length (B), α-stub/β-stub ratio (C), Aβ (D), BACE1 (E) and ADAM10 (F) of lung, heart and brain samples. Calnexin was used as house keeping protein.

Immunoblots were performed on male whole brain samples, n=2 per genotype, age 8 weeks. Statistical analysis was done by two-tailed Student's t-test. Data is presented as mean ± SEM; $p<0.01^{\#}$, $p\leq0.05^{*}$, $p\leq0.01^{**}$, $p\leq0.001^{***}$.

In summary the analysis of h*APPswe* expression and cleavage in organs other than the brain, revealed that expression of the transgene was found in heart and lung and could potentially lead to accumulation of Aβ in these tissues. Additionally a high rate of AICD production in these organs could alter intracellular signaling and affect transcription as AICD is known to act as a regulator on transcriptional level e.g. on enzymes of the SL pathway (Slomnicki and Lesniak 2008, Grimm *et al.* 2011b).

3.2.9 Myelination was altered between *Sms1*^{WT} x *APPswe*^{Tg} and *Sms1*^{MUT} x *APPswe*^{Tg} animals depending on the brain region

The *Sms1* mouse model showed alterations in myelination pattern in the CNS and PNS due to the deficit in SMS1. The expression of h*APPswe* as a transmembrane protein could additionally alter the formation of myelin sheaths. Therefore, the myelination state of *Sms1*^{WT} x *APPswe*^{Tg} and *Sms1*^{MUT} x *APPswe*^{Tg} animals was investigated. As brain regions for the analysis the cortex and hippocampus, representing regions of AD pathology, were chosen. In both genotypes myelin sheaths appeared normal in shape (Figure 3.40 A-P). The mean axon diameter in cortex of *Sms1*^{MUT} x *APPswe*^{Tg} animals was 0.16 ± 0.07µm smaller in comparison to *Sms1*^{WT} x *APPswe*^{Tg} animals (2.66 ±0.06µm, p=0.0955; Figure 3.40 Q). In hand with a reduced axon diameter, the thickness of myelin sheath was decreased from 0.37 ± 0.01µm in *Sms1*^{WT} x *APPswe*^{Tg} to 0.30 ± 0.01µm in *Sms1*^{MUT} x *APPswe*^{Tg} animals (p<0.0001; Figure 3.40 R). Axon diameter in the hippocampus remained unaffected and was accompanied by an increase in myelin thickness (Figure 3.40 S, T). In average hippocampal myelin sheaths of the *Sms1*^{MUT} x *APPswe*^{Tg} animals were 0.03 ± 0.01µm thicker than those of *Sms1*^{WT} x *APPswe*^{Tg} animals (Figure 3.40 T).

Taken together the disruption of *Sms1* affected myelination not only in adult *Sms1*^{MUT} animals, but also in young *Sms1*^{MUT} x *APPswe*^{Tg} animals. As seen before axon diameter and packing of myelin sheaths was altered. However in the brain of *Sms1*^{MUT} x *APPswe*^{Tg} animals the loss of SMS1 lead to brain region specific decrease (as seen in the cortex) or increase (as seen in the hippocampus) of myelin thickness. Thus, region specific brain capacity could be altered, leading to changes in action potential transmission and signaling.

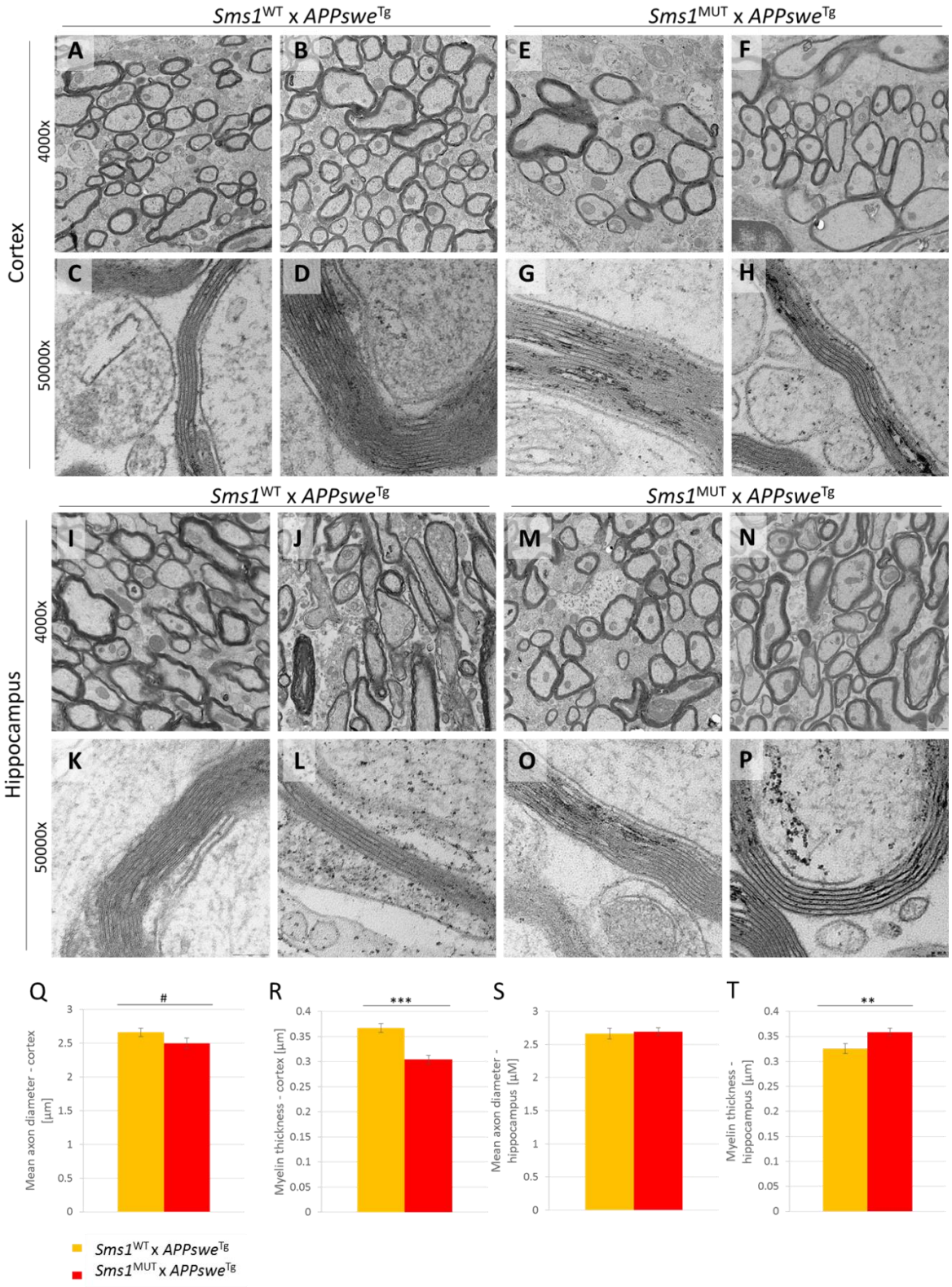

Figure 3.40: Axon diameter and myelin sheaths thickness in the cortex were reduced in *Sms1*^{MUT} x *APPswe*^{Tg} animals, while in the hippocampus myelin thickness was increased

(A-P) TEM images from (A-H) the cortex and (I-P) the hippocampus of *Sms1*^{WT} x *APPswe*^{Tg} and *Sms1*^{MUT} x *APPswe*^{Tg} animals. Magnification as indicated. (Q, S) Mean axon diameter in the (Q) cortical and (S) hippocampal region of *Sms1*^{WT} x *APPswe*^{Tg} (n=2) and *Sms1*^{MUT} x *APPswe*^{Tg} (n=2) animals, with an average of 170 axons measured per animal. (R, T) Mean myelin thickness in the (R) cortical and (T) hippocampal region of *Sms1*^{WT} x

APPswe^{Tg} (n=2) and *Sms1*^{MUT} x *APPswe*^{Tg} (n=2) animals, with an average of 240 axons measured per animal. Magnification x4000 and x 50000. Statistical analysis was done by two-tailed Student's t-test. Data is presented as mean ± SEM, $p<0.01^{\#}$, $p\leq0.05$*, $p\leq0.01$**, $p\leq0.001$***.

3.2.10 Inflammatory hints

AD is known to be related in brain inflammation, including microglia activation and release of inflammatory factors.

High levels of IgG were detected in heart samples of *Sms1*^{MUT} x *APPswe*^{Tg} animals by unspecific binding in immunoblots directed against APP derivates (supplementary Figure 10.8 A). To validate these findings and get a first overview on immunological reactions additional immunoblots on heart samples from animals of the *Sms1* x *APPswe* mouse line were performed in order to specifically detect IgG2b (IgGs are sequestered to the blood by activated B-lymphocytes) and CD3 (a common marker expressed on most T-cells) levels. IgG2b levels were highly variant amongst the analyzed genotypes. Nevertheless, IgG2b levels suggested an influence of the *Sms1* genotype on their levels (*Sms1*^{MUT} x *APPswe*^{WT} (276.86 ± 51.56%) and in *Sms1*^{MUT} x *APPswe*^{Tg} animals (488.55 ± 31.60%) in comparison to *Sms1*^{WT} x *APPswe*^{WT} (100.00 ± 95.94%) and *Sms1*^{WT} x *APPswe*^{Tg} (184.87 ± 66.29%), compare: supplementary Figure 10.8 B, E). CD3, as a common T-cell marker, was just found in mutant genotypes, but not in *Sms1*^{WT} x *APPswe*^{WT} animals. No significant differences in protein level were detected (supplementary Figure 10.8 B, D, E).

In *Sms1*^{MUT} animals a possible alteration of BBB functionality was proposed. Therefore, it should be elucidated if the high levels of IgG found in heart samples would also be reflected in the brain due to a defect in the BBB. If so, this could lead to neuro-inflammatory processes in animals of the *Sms1* x *APPswe* mouse model. To address this question, immunoblotting and quantification of several inflammatory markers in whole brain protein lysates was performed.

The high levels of IgG2b found in heart samples were reflected in the brain. Despite a higher representation of IgG2b in the heart of *Sms1*^{MUT} x *APPswe*^{WT} animals compared to *Sms1*^{WT} x *APPswe*^{Tg}, the relationship in brain was vice versa. *Sms1*^{MUT} x *APPswe*^{WT} reached 158.76 ± 53.31% and *Sms1*^{WT} x *APPswe*^{Tg} 180.99 ± 28.33% of *Sms1*^{WT} x *APPswe*^{WT} levels. However, similar to the heart, *Sms1*^{MUT} x *APPswe*^{Tg} (748.47 ± 289.21%, p=0.0692) showed the highest IgG2b levels in the brain in comparison to *Sms1*^{WT} x *APPswe*^{WT} (Figure 3.41 A, F).

IgGs represent the most important class of Igs of the specific immune system. During the process of an immune response, different IgGs are generated and a so called class switch takes place. The switch from IgG3 to IgG2b is triggered by TGF-β, therefore the level of this mediator was measured in the heart and the brain to elucidate if enhanced levels of IgG2b occur due to an enhanced class switch mediated by TGF-β. TGF-β levels in the heart had a high intra-genotype variability,

but did not reveal any significant difference between the genotypes (supplementary Figure 10.8 B, F). In the brain TGF-β levels were slightly lower in those animals carrying the *Sms1* gene trap cassette, but there were no significant differences detected (Figure 3.41 A, E).

I wondered if the IgG2b levels detected in brain reflect the levels found in heart due to blood remaining in both tissues, upon preparation and protein lysate generation, or if IgG2b was able to enter the brain tissue due to a misfunctional BBB. MFSD2A represents a rather recently discovered FA-transporter expressed in the BBB, regulating the passage of LC-lyso-PCs into the brain, being connected to transcytosis of Igs across epithelial barriers, and being crucial for embryonic development and adult maintenance of the BBB (Ben-Zvi *et al.* 2014, Nguyen *et al.* 2014, Guemez-Gamboa *et al.* 2015). A high abundance of IgG2b could correlate with a higher transcytosis or a partially permeable BBB, which could both be credited to alterations in MFSD2A expression. There were no alterations in MFSD2A levels in the heart (supplementary Figure 10.8 B, C), which was analyzed as a control tissue, but indeed I found reduced levels of MFSD2A in *Sms1*^{MUT} x *APPswe*^{WT} (79.94 ± 1.91%, p=0.0400) and in *Sms1*^{MUT} x *APPswe*^{Tg} animals (86.73 ± 2.89%, p=0.0197) compared to *Sms1*^{WT} x *APPswe*^{WT}, correlating with the observed higher rates of IgG2b (Figure 3.41 A, G).

To check if reduced expression of MFSD2A would allow the passage of IgG2b through the BBB epithelium, immunostaining against IgG2b was performed on brain sections of *Sms1*^{WT} x *APPswe*^{Tg} and *Sms1*^{MUT} x *APPswe*^{Tg} animals. Results showed clearly more IgG2b positive staining in the brain vessels of *Sms1*^{MUT} x *APPswe*^{Tg} animals, but no infiltration into brain tissue itself (Figure 3.41 B).

In summary IgG2b levels in the brain correlated just in part with the levels of the heart. Nevertheless, in both tissues IgG2b levels were highest in the *Sms1*^{MUT} x *APPswe*^{Tg} animals. I was not able to identify alterations in TGF-β mediated class switch from IgG3 to IgG2b as a reason for IgG2b accumulation. Furthermore, despite a reduction in MFSD2A levels, IgG2b was restricted to brain vessels, but did not infiltrate the brain tissue of *Sms1*^{MUT} x *APPswe*^{Tg} animals.

Inflammation is reflected in the brain by specific activation of microglia. Although, these differences did not reach significant levels, CD68 and Iba-1 expression, as two different markers for microglia activation showed, that with the expression of the h*APPswe* transgene the potential for neuroinflammation might be increased, while a disruption of *Sms1* could lead to a reduced activation of microglia. Thus, *Sms1*^{MUT} x *APPswe*^{WT} (88.80 ± 5.03%) and *Sms1*^{MUT} x *APPswe*^{Tg} animals (95.11 ± 9.05%) had reduced levels of CD68 in comparison to *Sms1*^{WT} x *APPswe*^{WT} (100.00 ± 8.74%) or *Sms1*^{WT} x *APPswe*^{Tg} animals (121.16 ± 4.72%), respectively (Figure 3.41 A, H). Quantification of Iba-1 gave similar results (*Sms1*^{WT} x *APPswe*^{WT}: 100.00 ± 5.18%, *Sms1*^{MUT} x *APPswe*^{WT}: 85.10 ± 5.25%, *Sms1*^{WT} x *APPswe*^{Tg}: 115.08 ± 6.15%, *Sms1*^{MUT} x *APPswe*^{Tg}: 101.93 ± 7.60; Figure 3.41 A, I).

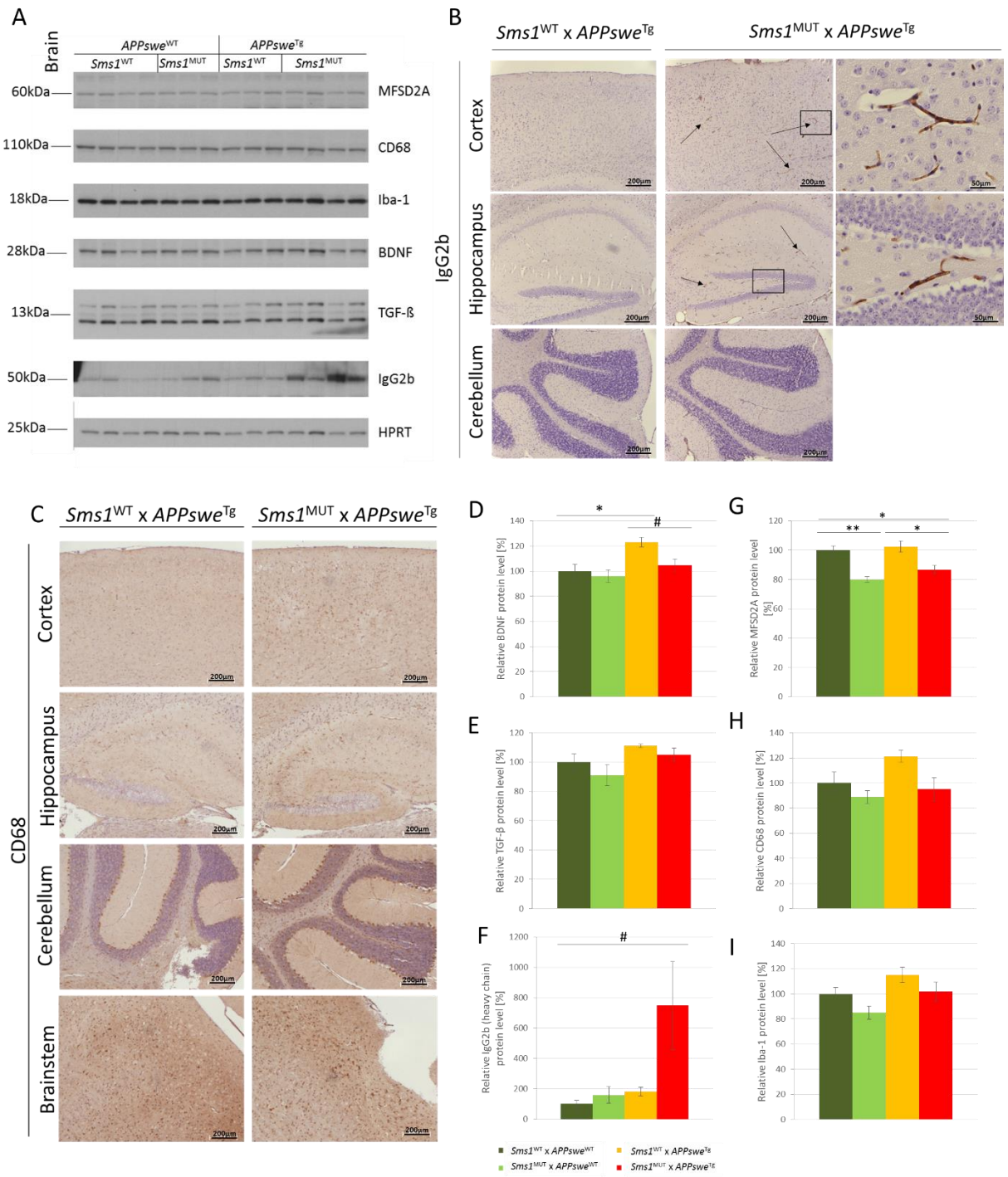

Figure 3.41: Inflammatory markers of the brain in *Sms1* x *APPswe* mouse model.
(A) Immunoblot of brain samples from 8 week old animals of the *Sms1* x *APPswe* mouse line using antibodies against immunological markers. (B) Representative immunostaining against IgG2b on brain sections of *Sms1*^{WT} x *APPswe*^{Tg} and *Sms1*^{MUT} x *APPswe*^{Tg} animals. Areas of IgG2b positive staining are indicated (black arrows) and magnified. Scale bars: 200µm and 50µm with increasing magnification. (C) Representative immunostaining against CD68 on brain sections of *Sms1*^{WT} x *APPswe*^{Tg} and *Sms1*^{MUT} x *APPswe*^{Tg} animals. Scale bar: 200µm. (D-I) Quantification of immunoblot results relative to *Sms1*^{WT} x *APPswe*^{WT} levels, which were set to 100%. *Sms1*^{WT} x *APPswe*^{WT}: n=4, *Sms1*^{MUT} x *APPswe*^{WT}: n=3, *Sms1*^{WT} x *APPswe*^{Tg}: n=3, *Sms1*^{MUT} x *APPswe*^{Tg}: n=5. Statisical analysis was done by one-way ANOVA with *post hoc* Tukey's test. Data is presented as mean ± SEM, $p<0.01$#, $p\leq0.05$*, $p\leq0.01$**, $p\leq0.001$***.

The reductions in CD68 and even more in Iba-1 were just marginal. Nevertheless, CD68 differences reached a statistical trend, when just two genotypes were copared directly. Therefore immunostaining against CD68 was performed. Expression was found in the cortex, the hippocampus, as well as in Bergmann glia next to cerebellar Purkinje cells, without any major differences between *Sms1*^{WT} x *APPswe*^{Tg} and *Sms1*^{MUT} x *APPswe*^{Tg} brain sections (Figure 3.41 C).

Persistent inflammation is known to upregulate BDNF expression in the brain and to be connected to AD pathology (Laske *et al.* 2006, Faria *et al.* 2014). Therefore I checked for BDNF protein levels and found them to negatively correlate with levels of CD68 and Iba-1, with highest levels detected in *Sms1*^{WT} x *APPswe*^{Tg} animals (123.16 ±3.81%, p=0.0322) compared to *Sms1*^{WT} x *APPswe*^{WT} levels and a decrease of 18.42 ±4.81% in *Sms1*^{MUT} x *APPswe*^{Tg} in comparison to *Sms1*^{WT} x *APPswe*^{Tg} animals (p=0.0947; Figure 3.41 A, D).

That a loss of glia cells might be responsible for the lower levels of markers could be excluded by the absence of TUNEL-positive cells in brain sections of *Sms1* x *APPswe* animals (data not shown).

Taken together microglial activation marker analysis could point to a hampered activation of microglia in genotypes of the *Sms1* x *APPswe* mouse line carrying the *Sms1* gene trap cassette. Additionally a reduction in BDNF levels in *Sms1*^{MUT} x *APPswe*^{Tg} in comparison to *Sms1*^{WT} x *APPswe*^{Tg} animals underlines a possible effect of *Sms1* disruption on brain inflammation.

3.2.11 Autophagy alterations in brain and MEFs of *Sms1* x *APPswe* nimals

Changes in the lipid metabolism of the cell profoundly affect the composition of the cell membrane, but also of intracellular membranes and therefore might alter vesicle formation. Formation of vesicles is an important step in several crucial cellular processes, such as vesicular transport, endo- and exocytosis and autophagy, which are also tightly connected to AD-relevant protein processing.

In brain lysates of untreated animals of the *Sms1* x *APPswe* mouse line EEA1, a marker for early endosomes, did not show any alteration between genotypes. Especially in *Sms1*^{MUT} x *APPswe*^{Tg} animals a high variability was detected (Figure 3.42 A, B).

LC3II/LC3I ratio and expression levels of p62 represent two different indicators for the autophagic flux. LC3I is processed to LC3II with the formation of autophagosomes and incorporated into the vesicular membrane. Autophagosomes enclose particles which are primed for degradation. P62 binds ubiquitinated/phosphorylated proteins, designated for enzymatic degradation and is taken up into lysosomes. Fusion of autophagosomes with lysosomes leads to the formation of autolysosmes, the final cellular compartment for enzymatic degradation of redundant protein. It seemed that induction of autophagic degradation was higher in *Sms1*^{MUT} x *APPswe*^{Tg} animals, as the LC3II/LC3I ratio was 58.47 ± 50.84% higher compared to *Sms1*^{WT} x *APPswe*^{WT} (100.00 ± 30.15%, p=0.0197). In addition the disruption of *Sms1* led to lower levels of p62 (*Sms1*^{MUT} x *APPswe*^{WT}: 69.91 ± 9.48%; *Sms1*^{MUT} x

APPswe^{Tg}: 61.03 ± 10.94%) in comparison to *Sms1*^{WT} x *APPswe*^{WT} (100.00 ± 16.87%, p=0.0291) and to *Sms1*^{WT} x *APPswe*^{Tg} (83.21 ± 7.05%, p=0.0919) animals, respectively (Figure 3.42 A, D, C).

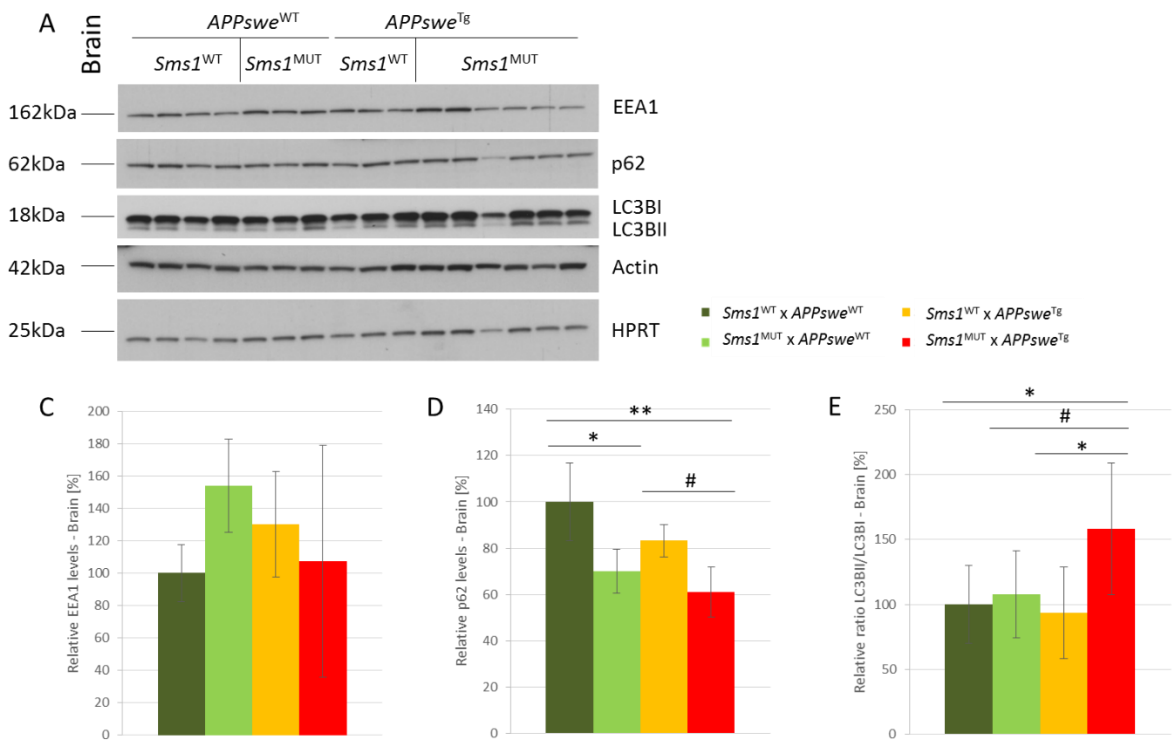

Figure 3.42: Alterations in protein expression linked to autophagy induction and lysosomal degradation were detected in the brain of *Sms1* x *APPswe* mouse line.
(A) Immunoblot against markers for early endosomes (EEA1), autophagosomes (LC3II/LC3I) and lysosomes (p62) on whole brain protein lysates of 8 week old animals the *Sms1* x *APPswe* mouse line. (B-D) Quantification of the immunoblot results relative to *Sms1*^{WT} x *APPswe*^{WT} levels, which were set to 100%. *Sms1*^{WT} x *APPswe*^{WT}: n=4, *Sms1*^{MUT} x *APPswe*^{WT}: n=3, *Sms1*^{WT} x *APPswe*^{Tg}: n=3, *Sms1*^{MUT} x *APPswe*^{Tg}: n=6. Statisical analysis was done by one-way ANOVA with *post hoc* Tukey's test. Data is presented as mean ± SEM, p<0.01#, p≤0.05*, p≤0.01**, p≤0.001***.

A higher induction of autophagy in *Sms1*^{MUT} x *APPswe*^{Tg} animals, together with a better rate of lysosomal clearance could contribute to an enhanced degradation of redundant intracellular proteins and derivates.

To check for autophagy induction and autophagic flux, MEFs were generated from a *Sms1* x *APPswe* breeding. The obtained primary cell lines originating from E13.5 siblings were treated with either DMSO as a control or 10µM or 100µM Rapamycin to induce mTOR mediated autophagy. Expression levels of autophagic markers were checked by immunoblot 4h or 8h after induction.

After 4h, results showed a lower production rate of LC3I in *Sms1*^{MUT} x *APPswe*^{WT} and *Sms1*^{MUT} x *APPswe*^{Tg} MEFs, while the turnover of LC3I into LC3II seemed to be similar between the genotypes

(supplementary Figure 10.9). This difference in LC3I generation led to a higher LC3II/LC3I ratio in *Sms1*^{MUT} x *APPswe*^{Tg} with 10µM and 100µM Rapamycin treatment compared to the other genotypes. In *Sms1*^{MUT} x *APPswe*^{WT} this effect was less pronounced, but similar (Figure 3.43 A, D). 8h after induction LC3I production was nearly stopped except in *Sms1*^{MUT} x *APPswe*^{WT} animals, here also still LC3II levels were increasing (Figure 3.43 A, D). 10µM Rapamycin treatment led to an elevation of p62 levels 4h after induction, while 100µM Rapamycin led to a drastic decrease in p62 levels, strongest in *Sms1*^{MUT} x *APPswe*^{Tg} MEFs, although these findings were similar in MEFs of all analyzed genotypes (Figure 3.43 A, C). After 8h, the elevation due to 10µM Rapamycin was only seen in *Sms1*^{MUT} x *APPswe*^{WT} animals, but a reduction of p62 levels with 100µM Rapamycin treatment was still observed (Figure 3.43 A, C).

These results of *Sms1*^{MUT} x *APPswe*^{Tg} MEFs were similar to the results obtained from *Sms1*^{MUT} x *APPswe*^{Tg} brain lysates, with high LC3II/LC3I ratios and a strong reduction in p62 levels. In summary this could point to a strong induction of autophagy and a rapid degradation process, just as seen for the brain samples. Additionally *Sms1*^{MUT} x *APPswe*^{WT} MEFs seemed to react slower to the autophagy-inducing trigger as other genotypes.

EEA1 and LAMP1 represent markers for early and late endosomes, respectively and should not be directly influenced by induction of mTOR-mediated autophagy. Nevertheless 4h after treatment, *Sms1*^{WT} x *APPswe*^{WT} and *Sms1*^{WT} x *APPswe*^{Tg} MEFs reacted to 10µM and 100µM Rapamycin treatment with an up regulation of EEA1 and LAMP1 levels. For LAMP1 this up regulation was more dosage-dependent in comparison to EEA1 results (Figure 3.43 A, B, E). 8h after induction elevated EEA1 persisted in *Sms1*^{WT} x *APPswe*^{Tg} MEFs, but were down in *Sms1*^{WT} x *APPswe*^{WT} MEFs. Additionally *Sms1*^{MUT} x *APPswe*^{WT} MEFs showed a highly variable up regulation of EEA1. Different to EEA1, LAMP1 levels in *Sms1*^{WT} x *APPswe*^{WT} MEFs treated with Rapamycin for 8h remained upregulated, but were unaltered or down regulated in *Sms1*^{WT} x *APPswe*^{Tg} MEFs. Levels of LAMP1 were also increased in *Sms1*^{MUT} x *APPswe*^{Tg} MEFs. Again *Sms1*^{MUT} x *APPswe*^{WT} MEFs reacted with a massive and highly variant increase in LAMP1 levels. (Figure 3.43 A, B, E).

The time shifted reaction of *Sms1*^{MUT} x *APPswe*^{WT} animals could be seen for p62, EEA1 and LAMP1, which might point to an altered capability of vesicle formation in MEFs of that genotype. A strong reaction in EEA1 and LAMP1 production after Rapamycin treatment was already 4h after induction was only seen in *Sms1*^{WT} x *APPswe*^{WT} MEFs, which might point to a connection between autophagy and endocytosis. As LAMP1 levels were still higher than EEA1 the turnover of newly formed early endosomes to late endosomes might be already proceeded 4h after Rapamycin treatment.

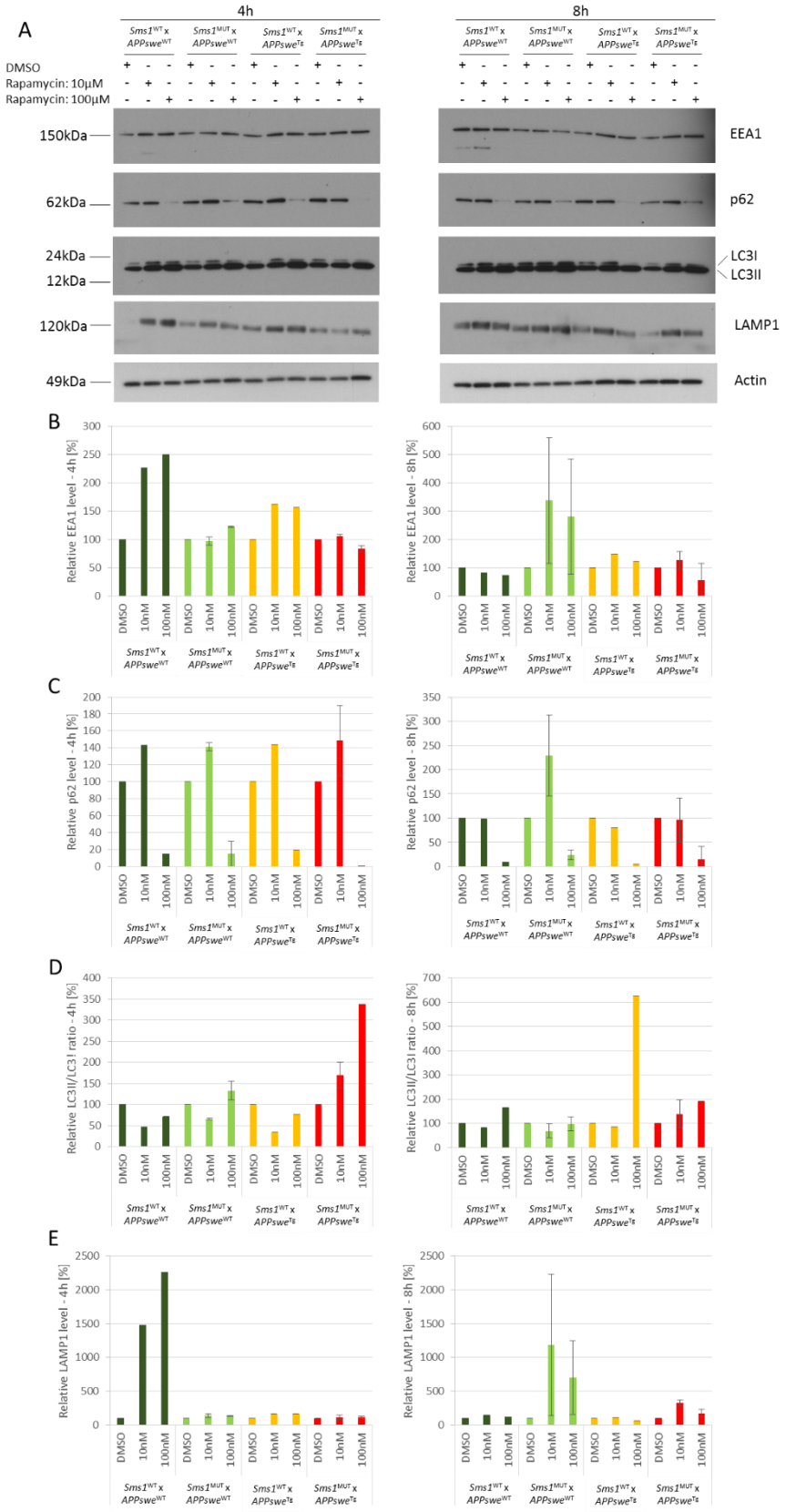

Figure 3.43: Preliminary data on time and dosage-dependent autophagy induction in MEFs obtained from breedings of the *Sms1* x *APPswe* mouse line

Sms1^{WT} x *APPswe*^{WT} (n=1), *Sms1*^{MUT} x *APPswe*^{WT} (n=2), *Sms1*^{WT} x *APPswe*^{Tg} (n=1) and *Sms1*^{MUT} x *APPswe*^{Tg} (n=4) MEFs obtained from E13.5 littermate embryos were treated with DMSO, 10µM or 100µM Rapamycin for

4h or 8h, respectively. (A) Immunoblot against autophagy makers in protein lysates of treated MEFs with 4h or 8h incubation times. (B-E) Quantification of immunoblots with 4h or 8h incubation times relative to DMSO control, which was set to 100%. Data was not statistically analyzed as n-numbers were too small. Data is presented as mean ± SEM.

4. Discussion

4.1 *Sms1* has tissue specific transcripts in mice

Human and mouse *SMS1* is known to be expressed in a large variety of tissues and to have different tissue-specific splice variants (Huitema *et al.* 2004, Yang *et al.* 2005, Rozhkova *et al.* 2011). Therefore the expression of mouse *Sms1* splice-variants in brain and testes samples were analyzed. In brain the full length protein coding transcript *Sms1*_001 was found to be the only splice variant expressed. These results differ from previous findings, which describe two different full length protein coding *Sms1* variants and one shorter variant to be expressed in brain (Yang *et al.* 2005). Reports on human *Sms1* mRNA state that the major bulk of mRNA found in brain encodes for the full length protein, which is in line with the data on the *Sms1* mouse line (Dergunova *et al.* 2013). Furthermore, it was shown recently that circular RNAs (circRNAs) of *Sms1* exists in the brain of humans and mice. These special variants are thought to be part of the system regulating *Sms1* gene functionality (Filippenkov *et al.* 2015).

In testes three variants could be detected. *Sms1*_001 and *Sms1*_004 were found to be prominently expressed with comparable levels. The *Sms1*_002 variant could be detected in traces only. All of these splice-variants are protein coding and are known to get translated into the six-pass TMD protein with enzymatic activity. In former studies, the two described shorter *Sms1* variants were shown to be most prominent in testes, while just one of two full length protein encoding transcripts was detected (Yang *et al.* 2005). It might be that the different methods (Northern blot and RT-PCR) account for the discrepancies in detection. The amplification step in RT-PCR could lead to alterations in transcription efficiency depending on the sequence. Nevertheless, the long transcripts all encode for the six-pass TMD protein found in both analyzed tissues, while the shorter variants encode for proteins with yet unknown function and misses the catalytic site for SM synthesis.

4.2 The intronic gene trap cassette insertion leads to a tissue-specific reduction in SMS1

The *Sms1* mouse model is based on a gene trap clone with a random insertion of a *β-galactosidase* cDNA carrying cassette (Schnutgen *et al.* 2005). The gene trap cassette could be localized in intron five after exon three of the *Sms1* gene. The intronic insertion did not completely abolish gene expression, although the main *Sms1* promoter is located upstream of the insertion site (Yang *et al.* 2005, Rozhkova *et al.* 2011 , Rozhkova *et al.* 2015). Exon skipping or leakiness of the cassette's polyA could be a cause of remaining *Sms1* mRNA and protein expression. Furthermore, for human *SMS1* it was suggested that there are additional tissue-specific promoters located downstream of the gene trap cassette insertion site, which may explain remaining expression and differences in expression levels between tissues (Rozhkova *et al.* 2011, Rozhkova *et al.* 2015). In both tissues, brain and testes, mRNA

levels in the *Sms1*^{MUT} animals were significantly reduced compared to *Sms1*^{WT} levels. However, remaining full length SMS1 protein levels were still at 55% in brain, whereas in testes SMS1 protein levels were down to 5.5%. These differences point out that the *Sms1_001* transcript found in brain is more stable and efficiently translated. It was indicated by Rozhkova *et al.* (2011) and other studies (Sudarkina *et al.* 2015), that regulation of human *SMS1* expression occurs mainly at the post-transcriptional, but also on the transcriptional and the translational level, which was verified by Filippenkov *et al.* (2015) through the investigation of circRNAs of human *SMS1* and mouse *Sms1*. In this context it was recently shown that in human tissue the expression of *SMS1* variants might also depend on polyadenylation of intronic regions, leading to the formation of truncated transcripts, which account for shorter proteins prone to NMD and represent one mechanism of regulation of SMS1 levels (Dergunova *et al.* 2013). In accordance with previous findings shorter protein variants of SMS1 could not be detected by immunoblotting (Sudarkina *et al.* 2015).

4.3 The tissue-specific SMS1 reduction is not fully compensated by SMS2

As mentioned before, SMS1 is located in the trans-Golgi apparatus and is therefore responsible for the synthesis of the major bulk of SM (Huitema *et al.* 2004, Yamaoka *et al.* 2004, Tafesse *et al.* 2007), but it is not the only SM synthesizing enzyme. SMS2 as its isoenzyme is mainly located in the outer plasma membrane, where it is responsible for the synthesis of 70% of the local SM (Tafesse *et al.* 2007). It is still discussed if, due to activity similarities, its main function is similar to that of SMSr at the ER, meaning to participate in monitoring and regulating Cer levels at the membrane to avoid apoptosis induction (Vacaru *et al.* 2009, van Meer and Hoetzl 2010, Tafesse *et al.* 2014). Furthermore, SMS2 is found in a smaller portion in the Golgi apparatus and therefore can contribute to SM *de novo* synthesis from ER derived Cer and PC (Huitema *et al.* 2004, Tafesse *et al.* 2007). No enhanced mRNA levels of *Sms2* in brain or testes could be detected, but a slight elevation of SMS2 protein levels in brain, pointing to post-translational regulation or higher stability, as it was also seen for brain SMS1 (Rozhkova *et al.* 2011). That disruption of *Sms1* does not affect *Sms2* mRNA levels was also found in liver and macrophages of *Sms1* knock-out animals (Li *et al.* 2012). Whether higher protein levels correlate with higher activity of SMS2 was not measured in the *Sms1* mouse line. However, SM levels in the brain of *Sms1*^{MUT} mice were significantly reduced to 55-57% of *Sms1*^{WT} levels, with a similar reduction found on *APPswe*^{WT} and *APPswe*^{Tg} background, while in the testes still 79% of *Sms1*^{WT} SM levels were produced. Pointing out, that SMS2 was not capable to fully compensate the loss of SMS1 in neither tissue. An incomplete redundancy between SMS1 and SMS2 was also stated previously (Tafesse *et al.* 2007). Tafesse *et al.* (2007) claimed that in human HeLa cells SMS1 is responsible for 60-80% of the SMS activity in the cell, while SMS2 takes over the remaining 20-40%. The remaining protein levels and the up-regulation of SMS2 levels found in *Sms1*^{MUT} mice could contribute to the less severe reduction of SM in these animals. Additionally, the differences need to be treat-

ed carefully as different cell system or tissue were used for data generation. Furthermore, SM can also be produced in three steps from Cer by generation of sphingosine and sphingosylphosphocholine as intermediate products, bypassing SMS1 (Sribney 1966, Fujino *et al.* 1968). This was also noticed by Tafesse *et al.* (2007), who report only a minor reduction of SM levels of about 20%, after treatment of HeLa cells with siRNA against both, SMS1 and SMS2.

In brain, *Sms1*^{MUT} showed 67% of *Sms1*^{WT} SMS1 protein levels remaining but a mean reduction of 56% in SM levels, while in testes just 6% of *Sms1*^{WT} SMS1 protein levels were observed, while SM levels were still at 79%. These differences might either depend on a tissue-specific enzymatic activity of SMS1, or one can state that in the testes, compared to the brain, SMS1 plays a reduced role in SM production. Another option would be, that SMS2 is able to compensate better for the loss of SMS1 in testes, compared to the brain.

4.4 *Sms1* disruption affects birth rates and survival depending on expression of *hAPPswe*^{Tg}

There were no alterations in birth rates between the different genotypes of the *Sms1* mouse line. Furthermore, mice of all genotypes had a normal life expectancy. This is controversial to reports from *Sms1* knock-out animals, which are known to be born at a lower Mendelian ratio and show moderate neonatal lethality (Yano *et al.* 2011, Dong *et al.* 2012). As described above, depending on the tissue, *Sms1*^{MUT} animals still have 6 to 67% of *Sms1*^{WT} SMS1 protein levels, and 56 to 79% remaining SM, which accounts for the missing effects on birth rates and life span in comparison to complete *Sms1* knock-out animals.

Homozygous Tg2576 mice are not viable, thus Tg2576 are grouped in transgene positive and transgene negative animals for investigations (Hsiao *et al.* 1996, King and Arendash 2002). Animals of the *Sms1* x *APPswe* mouse line carrying a *hAPPswe* transgene (*APPswe*^{Tg}) were born with approximately 2/3 reduced Mendelian frequency, with no additional effect of the *Sms1* mutation on birth rates.

Tg2576 animals are known to have a reduced life span with 63% survival rates through 19 months of age and a most prominent loss of transgene positive animals during the first 6-12 months (King and Arendash 2002). With the mating of Tg2576 mice to *Sms1* animals this phenotype was amplified. Thus, *Sms1*^{HET} x *APPswe*^{Tg} and *Sms1*^{MUT} x *APPswe*^{Tg} animals showed higher death rates compared to the other genotypes. Highest rates were found in *Sms1*^{MUT} x *APPswe*^{Tg} animals with just 52-54% survival in the first 25 weeks and a mean age at death of 8-9 weeks, depending on sex. Male animals were affected stronger than female animals. These results suggest a synergism between *Sms1* and the *hAPPswe* transgene or its derivates. In accordance with these results, APP/PS1/aSMase$^{-/-}$ animals show early death and other deficits (Lee *et al.* 2014), linking amyloidogenic processing to SM homeostasis with effects on the life span. Additionally, the higher survival rates of females, point to a sex-

dependent mechanism which might be based on the altered lipid and energy metabolism between males and females (Blaak 2001).

4.5 *Sms1* disruption leads to reduced body weight or weight gain

Sms1 knock-out animals show reduced growths and body weight (Yano *et al.* 2011, Dong *et al.* 2012). Assessment of weight in *Sms1*^{WT}, *Sms1*^{HET} and *Sms1*^{MUT}animals of both sexes could not fully confirm these findings. *Sms1*^{HET} and *Sms1*^{MUT} had just slightly reduced body weight compared to *Sms1*^{WT} animals of the same sex, at an age between 24 and 67days. Furthermore, the observed weight differences were not persistent or amplified with age. Nevertheless, the mean weight of *Sms1*^{HET} or *Sms1*^{MUT} animals never exceeded the mean weight of *Sms1*^{WT} animals.

Studies about weight in Tg2576 are partially controversial. Some report no weight differences in comparison to wild-type animals at all (d'Uscio *et al.* 2012), others state minor, not progressing weight reduction (Luo *et al.* 2012), or they show a slight but significant reduction in body weight gain positively correlated to age (Ishii *et al.* 2014). Animals observed in these studies were all between two and 20 months old. *Sms1*^{HET} x *APPswe*^{Tg} and *Sms1*^{MUT} x *APPswe*^{Tg} animals showed reduced weight gain between four to 16 weeks of age. *Sms1*^{MUT} x *APPswe*^{Tg} animals were affected most and differences got more pronounced with proceeding age. Although, these data did not reach significance there is a clear tendency to a genotype- and age-dependent eased body weight gain. The reported and/or observed reduction in weight of Tg2576 and *Sms1*^{MUT} was less pronounced than that observed in *Sms1*^{MUT} x *APPswe*^{Tg} animals compared to *Sms1*^{WT} or *Sms1*^{WT} x *APPswe*^{Tg} controls, respectively. Confirming the proposed synergetic effect between the amyloidogenic pathway and the SM metabolism and the need for a control of SM levels.

4.6 Disruption of *Sms1* triggers further changes in SL-metabolism, which are magnified on a *hAPPswe*^{Tg} background

4.6.1 Maintenance of Cer homeostasis as an important aspect in the brain of *Sms1*^{MUT}

Besides the reduction in SM several other changes in SL content were found in the *Sms1*^{MUT} brain and testes. Cer represents a substrate for SMSs (Huitema *et al.* 2004) and it was thought to accumulate upon SMS1 disruption. However, total Cer levels were 25-35% reduced in brains of female and male *Sms1*^{MUT}, respectively, but were not affected in the testes samples. Thus, a stronger reduction in SM levels went hand in hand with a stronger reduction of Cer.

Cer is known to function as lipid signaling molecule, amongst others leading to cell cycle arrest and promoting apoptosis (Spiegel and Merrill 1996, Toman *et al.* 2002, Tafesse *et al.* 2014), but also SM itself is associated with cell death and apoptosis (Taniguchi and Okazaki 2014). It is therefore likely, that transient shifts in the SM/Cer ratio are immediately processed, to prevent any cytotoxic accumulation. Thus, the elevated level of SMS2, measured in the brain, might contribute to the rapid turn

over of Cer as soon as it reaches the PM. It might also be that SMSr as specified Cer sensor (Tafesse *et al.* 2014) maintains the amount of this lipid mediator at a tolerated level by direct intervention at the ER. Expression levels of additional enzymes involved in the SL pathway and in Cer regulation were analyzed in the brain by microarray and TaqMan assays in order to check for specific compensatory mechanisms contributing to Cer homeostasis. The lower expression of *Smpd2*, and *CerS4*, both Cer producing enzymes (Clarke *et al.* 2006, Mullen *et al.* 2012), and the upregulation of *Asah3* expression, degrading Cer to sphingosine (Mao *et al.* 2003, Sun *et al.* 2008), in microarray analysis made them promising candidates for the maintenance of Cer homeostasis upon *Sms1* disruption. However, these data sets could not be validated by TaqMan assays. Data from brain samples were quite controversial and did not deliver persistent results, which would allow a clear statement on regulatory enzymatic actions.

Nevertheless, microarray analysis of brain samples gave several promising hints for new candidate genes, which could be affected by a disruption of *Sms1*. These genes could contribute to alterations in the SL pathway. They include *Pla1a*, which cleaves exclusively PS and lyso-PS at their sn-1 position (Sato *et al.* 1997), thereby potentially altering their content in the plasma membrane and the availability and release of SFA from these substrates. Importantly, a PS-mediated uptake of Aβ into microglia for degradation was described by Yuyama *et al.* (2012), linking *Pla1a* to AD. PS is amongst others implicated in apoptosis and blood coagulation, thus lower *Pla1a* expression could contribute to an upregulation of these mechanisms (Turner *et al.* 1970, Rimon *et al.* 1997, Sato *et al.* 1997, Uchida *et al.* 1998, Nagai *et al.* 1999, Lentz 2003). Second, *Prkaa2*, with reduced expression in *Sms1*^{MUT}, represents a subunit of AMPK. AMPK is said to act as an energy sensor for metabolic stress and upon activation inhibits HMGCR and ACC by phosphorylation. HMGCR is responsible for the formation of mevalonate, by reduction of two hydroxyl methylglutaryl-CoA with NADPH as a cofactor. Mevalonate represents the major precursor for the subsequent synthesis of Chol and other sterols. ACC with ATP and Biotin as cofactors represents the rate limiting step for the synthesis of FAs. It catalyzes the formation of malonyl-CoA, the basis for the FA elongation cycle (Hardie 1992, Aguan *et al.* 1994). Importantly *Prkaa2* mRNA reduction was also found in 6 month old APPswe/PS1dE9 mice, suggesting a change in energy metabolism prior to the development of major AD pathology (Pedros *et al.* 2014). Another gene involved in FA elongation is *Tecr*, the third candidate gene with higher expression in *Sms1*^{MUT}. It is responsible for the last of four steps in the formation of LC- and VLC-FAs (Das *et al.* 2000, Moon and Horton 2003). Targeting *Sms1* might therefore also influence elongation of FAs.

However, enzyme levels do not necessarily reflect enzymatic activity. Therefore, one would need to measure substrate turnover rates of all these enzymes to clearly state how the disruption of SMS1 triggers compensatory mechanisms of the SL pathway. The quantification of enzyme activities would not be possible without isolation and purification of the enzyme in question. Here another problem

arises, as enzymatic activity is at least in part dependent on the surrounding membrane composition. This was shown e.g. by Silva *et al.* (2009) analyzing SMase activities in dependence of lipid rafts and especially of Chol. Both are important parameters in the *Sms1* mouse line and would be altered by the isolation process.

4.6.2 The disruption of *Sms1* affects PC species, with specific saturation and elongation states in *Sms1*^{MUT} animals

Besides Cer, PC represents a substrate for SMS1 (Huitema *et al.* 2004). PC is regarded as a crucial lipid for the maintenance of membrane integrity, as it accounts for approximately 40% of all PL in most cellular membranes (Klein 2000). Total PCaa levels were found to be slightly elevated in *Sms1*^{MUT} x *APPswe*^{Tg} animals compared to controls without *Sms1* disruption, showing a parallel to APP/PS1/aSMase$^{-/-}$ animals, in which the disbalance of SM homeostasis evoked PC elevation as well (Lee *et al.* 2014). In *Sms1*^{MUT} female and/or male brain samples, reduced MUFA/SFA and PUFA/SFA ratios of PCaa species compared to *Sms1*^{WT} were found, while there was no additional reduction in the PUFA/MUFA ratio. These ratios were not affected in PCae species. In the *Sms1* x *APPswe* mouse line, the PCaa results were similar to those found in the *Sms1* mouse line and the disruption of *Sms1* led to a lower MUFA and PUFA content, with a more pronounced reduction in MUFAs. Furthermore, MUFA/SFA ratios of PCaes were significantly reduced, leading to elevated PUFA/MUFA ratios for both PCs measured. Thus, *Sms1*^{MUT} x *APPswe*^{WT} and *Sms1*^{MUT} x *APPswe*^{Tg} animals were especially deprived of MUFA-PCaa and -PCae content (MUFA<PUFA<SFA).

Taken together, these data sets could potentially point to altered regulation of desaturases in animals with a *Sms1* disruption. Δ9-desaturase is responsible for the generation of MUFAs (C16:1 and C18:1) from palmitic acid (C16:0) or stearic acid (C18:0), respectively (Kihara 2012). The lack of MUFAs, could therefore result from reduced expression or lower activity of Δ9-desaturase. Δ12-desaturase is needed for the transformation of oleic acid (C18:1) to linoleic acid (C18:2) the shortest FA of the n-6 PUFAs. Δ15-desaturase is responsible for the generation of α-linoleic acid (C18:3), representing the first n-3 PUFA. For further desaturation steps of n-6 or n-3 PUFA Δ6- and Δ5-desaturase are needed (Kihara 2012). As MUFAs are significantly more reduced than PUFAs, the results would be in agreement with an interpretation that the lack in PUFAs might rather result from reduced substrate availability, than from altered Δ12- or Δ15-desaturase activity and that the metabolism of generated MUFAs to PUFAs could lead to a deprivation of Δ9-desaturase-generated FAs.

Additionally to specific saturation states, also PC elongation states were selectively altered in *Sms1*^{MUT} animals. The PCaa levels and PCae levels correlated negatively with the FA chain length. This shows, that additionally to desaturases also elongases are potentially affected by the disruption of *Sms1*. These effects were background- or age-specific as they could not be reproduced in the *Sms1* x *APPswe* mouse line. Nevertheless, together with the proposed candidate genes *Prkaa2* and *Tecr*

these findings provide additional evidence that SMS1 could be involved in regulation of FA elongation steps especially for LC and VLC-FAs.

Lipids with their special head groups and specific FA composition do not only contribute to the membrane properties of the PM and cellular organelles such as thickness, fluidity or curvature, but also influence TM proteins (Gil *et al.* 1998, van Meer *et al.* 2008, Holthuis and Menon 2014). The loss of LC-FA containing PCs would lead to reduced thickness and fluidity of membranes, altering protein trafficking and embedding of transmembrane proteins. An overall shift in saturation states towards SFA containing PCs would result in a more rigid membrane constitution and reduced trafficking, which might be able to balance the loss of SM with its rigidity promoting characteristics. The reduction in LC-PCaas on the other hand was positively correlated with saturation state, which would render thicker membranes less stable as their fluidity increases (Li *et al.* 2000, Rawicz *et al.* 2000, Zhai *et al.* 2014).

4.6.3 *Sms1*^{MUT} x *APPswe*^{Tg} accumulate PCaa and PCae species which could influence inflammation and acetylcholine availability

PCaas and PCaes differ from another at their sn-1 position. While in PCaas FAs are bound by an ester bond, PCaes form an enol-ether bond. Despite this difference, both PCs carry mostly a C16:0 or C16:1 or a C18:1 FA residue at their sn-1 position (Vance 1989).

Total PCaa levels were not changed significantly. Nevertheless, two specific peaks were observed in the PCaa profile. PCaa C34:2, C34:3 and C34:4 built up the first peak in *Sms1*^{MUT} x *APPswe*^{Tg}, this reflects an accumulation of C16:0/C16:1 or C18:1 combinations with other unsaturated C16/C18 FAs. These components represent the major building and energy FAs (Vance 1989). The second peak was found in the PCaas C36:3, C36:4 and C36:5. This elevation points e.g to EPA (C20:5, n-3 FA) combined with C16:0 (reflected in C36:5) and AA (C20:4, n-6 FA) combined with C16:0 or 16:1 (reflected in C36:4 or C36:5). An elevation of potentially AA containing PCae species (C36:4, C36:5, C38:5 combined with C16:0, C16:1 or C18:1, respectively) was also found. PCae C36:4 and C38:5 additionally could be composed of C16:0 in combination with EPA or DPA (C22:5, n-6 FA), respectively. High levels of AA, EPA and DPA bound in PCaa and PCae species, could serve as a reserve pool in lipid signaling and inflammatory response (reviewed by: Yacoubian and Serhan (2007), Serhan *et al.* (2008)).

PCs are not only used as a substrate for the synthesis of complex SL, but can also be cleaved at the sn-2 position, releasing lyso-PCs and a free FA as a byproduct. This cleavage is mediated by $cPLA_2$ (Farooqui and Horrocks 2006). As the sn-2 position is mostly occupied by unsaturated FAs the increased abundance of several lyso-PC species as it was indicated for *Sms1*^{MUT} x *APPswe*^{Tg} in comparison to *Sms1*^{WT} x *APPswe*^{WT} animals could be linked to the release of free unsaturated FAs. $cPLA_2$ is e.g. activated by C1P involving the action of CPTP an C1P transfer protein (Pettus *et al.* 2004,

Simanshu *et al.* 2013). The generation of C1P might be one way, how Cer levels are kept on a non-cytotoxic level. Therefore, it might be interesting to measure and compare C1P levels in the different genotypes of the *Sms1* x *APPswe* mouse model. $cPLA_2$-mediated release of bound AA, represents the rate limiting step for the production of lipoxins and free EPA is processed further to resolvins of the E series (RvE; (Serhan *et al.* 2008)), connecting these lipids to anti-inflammatory processes. Interestingly, it was also shown, that four month of AA and DHA (as a downstream product of EPA) supplemented diet positively influence memory performance in 13 month old Tg2576 animals and that additional 6 month of supplemented diet also decreased the burden of SP in these animals (Hosono *et al.*, Hosono *et al.*). Therefore, these alterations in PUFA-containing PCs was of special interest within the *Sms1* x *APPswe* mouse line, as they represent one possible link to AD parameters.

However, the question remains, if elevated levels of AA, EPA and DPA containing PCs account for a greater availability of these PUFAs or if the cleavage by cPLA2 is hampered and these PCs accumulate without providing PUFAs to the organism.

Furthermore, PCaa plays also a crucial role as choline storage for the production of acetyl-choline (ACh). ACh, one of the most important neurotransmitters in the brain, is reduced in AD patients and was shown to contribute to memory performance in rats (Whitehouse *et al.* 1981, Whitehouse *et al.* 1982, Nyakas *et al.* 2011, Schliebs and Arendt 2011). The administration of PCaa elevated ACh release and led to improvement in memory performance in AD mice (Chung *et al.* 1995). An elevation in total PCaa levels as it was seen in *Sms1*^{MUT} x *APPswe*^{WT} and in *Sms1*^{MUT} x *APPswe*^{Tg} males could lead to enhanced availability of choline for synthesis of ACh, thus mimicking in part the effect of AChE inhibitors, which are often used in AD therapy and are still studied to prevent or resolve AD pathology (Duan *et al.* 2015, Lee *et al.* 2015, Ye *et al.* 2015).

These important aspects give rise to the question, whether the observed lipid alterations affect two major pathways related to AD, namely neuronal inflammation and ACh metabolism. ACh metabolism was not further investigated in these animals, but they might represent a model to study the impact of lipid alterations on the cholinergic system.

Interestingly, the most prominently altered PCaes in *Sms1*^{MUT} x *APPswe*^{Tg} reflect well the alterations found in mean human AD brain samples (Grimm *et al.* 2011a). In both cases PCae C36:4, C36:5 and C38:5 were strongly upregulated, while PCae C38:1, 38:2 and 40:2 were the lipid species with most reduced levels. Therefore the *Sms1*^{MUT} x *APPswe*^{Tg} animals can be considered as a good model to study AD-relevant changes in PCaes.

4.7 EPA/DHA supplemented diet improves weight gain, without influencing life span of *Sms1*^{MUT} x *APPswe*^{Tg} animals

As free FAs themselves were not measured, it could not be finally clarified if SFA-, MUFA- and PUFA-PCs, as well as the reserve pools of potentially AA-, EPA- and DPA-containing PCaas and PCaes were metabolized and free FAs were released, or if the higher levels of these PCaa and PCae species represent a lack in processing of these special FAs due to a reduced cPLA$_2$-mediated release from the reserve pool. To check if the important PUFAs were lacking and if a supply of these essential FAs would improve weight gain and survival rates of *Sms1* x *APPswe* animals, these mice were fed an n-3 FA diet containing EPA and DHA. DHA is also known to positively influence PLA$_2$ activity (Rao *et al.* 2007a). Already during matings females were fed with the supplementary diet, ensuring a sufficient supply of FA during embryogenesis and after birth by maternal milk (Antonakou *et al.* 2013, Nishimura *et al.* 2014). Subsequently the offspring was supplied with the supplementary diet. *APPswe*^{Tg} animals, regardless of their *Sms1* genotype, were already born with slightly elevated body weight, compared to animals from litters, where the mother did not receive n-3 supplemented food. This higher weight was maintained until weaning, when it started to drop continuously until it reached the level of non-fed controls at the age of 40 to 60 days. However, with proceeding age, the n-3 fed animals gained body weight faster than their controls, with the *Sms1*^{MUT} x *APPswe*^{Tg} animals having the highest difference compared to non-fed animals of the same genotype. This indicates, that the supplementation with n-3 FAs is crucial for development and body weight gain in *Sms1* x *APPswe*^{Tg} animals and is influenced by both, the *Sms1* genotype and the *APPswe*^{Tg} background. In humans a similar beneficial role of n-3 LC-PUFAs is discussed, however, also controversial data is reported (for a review see: Imhoff-Kunsch *et al.* (2012)). The results indicate, that the observed loss in MUFA and PUFA containing lipids contribute for the observed weight phenotype and that EPA/DHA supplemented diet enabled the fed animals to overcome the reduction in weight gain caused by *Sms1* disruption, either through direct availability of EPA and DHA or by promoting cPLA$_2$-mediated FA release.

Although, body weight gain was improved by supplementary feeding of n-3 FAs, the survival of *Sms1*^{HET} x *APPswe*^{Tg} and *Sms1*^{MUT} x *APPswe*^{Tg} animals was not affected in the first 15 weeks. As a higher survival rate with age could not be expected, the feeding experiment was aborted after 15 weeks. Thus, the early death phenotype caused by the proposed synergistic effect between *Sms1* and h*APPswe* could not be rescued by EPA/DHA supplementary diet, but might rather be caused by other effects of *Sms1* disruption.

4.8 Changes in lipid composition lead to altered myelination patterns in CNS and PNS

Besides the total body weight, also brain weight was affected by *Sms1* disruption. As the brain, different to other organs, is not directly connected to size and body weight (Herschel 1972), absolute

brain weight was analyzed the in *Sms1* x *APPswe* mice without correction for the body weight loss. In both *Sms1*^{MUT} genotypes a reduction in brain weight of about 6.7 to 10.6% in comparison to *Sms1*^{WT} x *APPswe*^{WT} brain weight was found, or a reduction of 3.7 to 8.1% in comparison to *Sms1*^{WT} x *APPswe*^{Tg} animals. This reduction in weight correlates with the measured reduction of total SM in the brain of both *Sms1*^{MUT} genotypes to 53-57% of *Sms1*^{WT} x *APPswe*^{WT} levels, as SM makes up 10% of brain lipids (lipidlibrary.aocs.org).

Myelin is unique amongst the plasma membranes, as its dry weight is made up by an unusually high amount of 70-75% of lipids and SM as a crucial component of myelin sheaths is highly abundant in the brain. Furthermore, myelin is specifically enriched in plasmalogens, which make up 12-15% of myelin lipids, in Chol and in VLC-SFAs (C22:0 – C24:0) (Norton and Poduslo 1973, Morell and Jurevics 1996, Imgrund *et al.* 2009). SMSs represent important enzymes in oligodendrocytes, which are responsible for the formation of myelin sheaths. The ratio of SM/Cer in oligodendrocytes is 9:1, while in neurons a ratio of 1.5/1 was reported (Kilkus *et al.* 2008). Consistently, *in vitro* experiments revealed low SMS and high SMase activity in neurons, while in three days old oligodendrocytes activities are *vice versa* (Kilkus *et al.* 2008). It should be clarified to which extent the observed reduction in SM to half of *Sms1*^{WT} levels and the reduction of MUFAs and PUFAs containing PCaas and PCaes affect the myelination pattern in *Sms1*^{MUT} and *Sms1*^{MUT} x *APPswe*^{Tg} animals.

Using Klüver Barrera staining for brains of *Sms1*^{MUT} animals a changed lipidation pattern with a reduction in the cortex and the hippocampus but equal staining intensity in the cerebellum, striatum and the OB was discovered. These findings were validated by reduced abundancy of MOG and MBP in protein lysates or immunostainings, respectively. MBP, as a major protein in myelin sheaths, makes up 8% of all myelin proteins and is thought to mediate the adhesion between the surfaces of the myelin layers (Boggs 2006, Jahn *et al.* 2009). Reduced MBP levels were detected in the hippocampus and the nucleus accumbens while the cerebellum, striatum and brain stem seemed unaffected by the reduction. The nucleus accumbens was discussed to contribute to memory formation (Goldenberg *et al.* 1999) but is mostly known to regulate the reward system and was found to be reduced in volume in late onset AD (Fjell and Walhovd 2010, Pievani *et al.* 2013) Thus, the myelination pattern was altered in brain areas affected in AD, while areas, which are less affected by AD had normal levels of lipidation and of MBP expression.

Reduction in axon diameter and a reduced myelin thickness was also observed by TEM in the cortex of 8 week old *Sms1*^{MUT} x *APPswe*^{Tg} in comparison to *Sms1*^{WT} x *APPswe*^{Tg} animals. However, in the hippocampus, axon diameter was not altered and myelin sheaths were even slightly thicker. This might be connected to higher physical activity levels in *Sms1*^{MUT} x *APPswe*^{Tg} mice, which is discussed below, as running exercise was shown to specifically enhance myelination in the hippocampal dentate gyrus in 6-month-old APP/PS1 transgenic mice (Chao *et al.* 2015). It might also be that the loss of SM and the accompanied changes in SL homeostasis might have a progressing age-related

demyelination effect as it was suggested to happen in AD (Svennerholm and Gottfries 1994, Bartzokis 2004, Carmeli *et al.* 2013).

An imbalance in the unique lipid composition of myelin could affect its structure and properties, as it is known form LSDs. Studies on Krabbe or NPA and diverse animal studies were addressing this topic (Chrast *et al.* 2011). E.g. aSMase knock-out mice, a model for NPC, accumulated SM, GM2 and GM3, leading to reduced expression of myelin-associated proteins in the cerebellum and cortical regions (Buccinna *et al.* 2009). In this study the defects were linked to reduced oligodendrocyte metabolism, which might be reflected in the reduced levels of MOG found in *Sms1*^{MUT} animals, as MOG is said to be expressed in oligodentrocytes with remyelination potential (Crang *et al.* 2004). That SM elevation as well as reduction could influence proteins linked to myelination highlights the need for a tight control of SM levels in the brain.

Furthermore, a recent study combining ultra-high-resolution imaging mass spectrometry and *in situ* hybridization revealed that especially SM d18:1/24:1 is found in white matter, due to the specific expression of *CerS2* in these regions, which selectively provides SMS with its substrate (Sugimoto *et al.* 2015). SM 24:1 levels were reduced in all *Sms1*^{MUT} genotypes of both mouse lines investigated in this study and expression levels of *CerS2* in the brain were upregulated in *Sms1*^{MUT}. This could be interpreted as a compensatory mechanism, trying to overcome the myelination deficits, ensuring delivery of VLC-SFAs. In line with its expression in highly myelinated regions, CerS2 deficient mice, lacking VLC-SFAs have been shown to have myelination deficits and suffer from gradual demyelination predominantly in the PNS (Imgrund *et al.* 2009). In *Sms1*^{MUT} animals reduced axon diameters were found in the lumbar exon bundles of the PNS and axonal MBP-positive myelin showed a less dense packing. Therefore, it would also be interesting to analyze the SM levels and *CerS* expression and activity directly in the PNS.

The results suggest, that the disruption of *Sms1* leads to deficits in myelin generation or maintenance. In both mouse models there were no severe effects of these alterations on daily life performance, however, *Sms1*^{MUT} showed reduced fore paw grip strengths, slightly worse motor coordination and partial reduced nociception. These alterations might be connected to myelination deficits in the CNS and PNS. The relevance of this data needs to be investigated in more detail. Myelin sheaths should be isolated and analyzed concerning their lipid and protein composition. Furthermore, thickness and isolation parameters of the myelin sheaths should be measured. Thus, electrophysiological measurements are suggested to analyze signal conductance in the CNS and PNS.

4.9 Is the disruption of *Sms1* protective concerning AD pathology of the brain?

4.9.1 The APP level seems to be influenced by *Sms1*

Numerous studies have focused on the correlation between membrane lipids and the generation of amyloid in AD patients and in mouse models for AD (for a recent summary on human studies see: Reitz (2013)). From the latter its known that lipids can influence APP trafficking, cleavage or degradation by direct interaction with relevant proteins or by alteration of lipid raft-mediated processing steps (Ehehalt *et al.* 2003, Cordy *et al.* 2006, Kim *et al.* 2006, Fabelo *et al.* 2012, Hicks *et al.* 2012, Bhattacharyya *et al.* 2013, Walter and van Echten-Deckert 2013, Fabelo *et al.* 2014). Furthermore, it was shown, that Aβ itself could influence phase separation of lipids, through its interaction with the ganglioside GM1, triggering the uptake of those lipid components into Aβ aggregates, leading to reduced membrane fluidity (Sasahara *et al.* 2013) or by influencing Chol and SM metabolism by alteration of HMGR or nSMase activity (Grimm *et al.* 2005). In this way lipids and APP or its cleavage products, alter each other, with the ability to crucially change cellular function. To study the effects of *Sms1* disruption-mediated brain lipid composition changes on the processing of endogenous APP and transgenic hAPPswe, the levels of these precursors and their cleavage products, as well as the enzymes of the amyloidogenic pathway were analyzed.

As expected in *Sms1* x *APPswe*^{Tg} animals a higher amount of full length APP was detected, due to the additional expression of the human transgene. That the elevation is mostly due to higher expression rates, was shown earlier, as hAPPswe and endogenous APP have approximately the same processing rate, although hAPPswe has a tendency to be more stable as 50% of initially generated hAPPswe but just 30% of endogenous APP persisted in brain after 23h (Morales-Corraliza *et al.* 2009). The current data revealed a 2-fold elevation in full length APP on the protein level in 8 week old *Sms1*^{WT} x *APPswe*^{Tg} in comparison to full length APP levels in *Sms1*^{WT} x *APPswe*^{WT}. This elevation was less than the origninally described 5.6-5.8% in ten to 61 week old Tg2576 animals (Hsiao *et al.* 1996). It might be that the age difference accounts for the inconsistency of APP levels, but it is more likely that the different background due the crossing of the *Sms1* to the Tg2576 mouse line altered protein expression levels, or that ongoing breeding of Tg2576 animals in different facilities led to strain specific alterations compared to the original description by Hsiao *et al.* (1996).

Sms1 seems to positively influence APP levels, as the levels of the full length protein were 18-21% reduced in *Sms1*^{MUT} x *APPswe*^{WT} and in *Sms1*^{MUT} x *APPswe*^{Tg} animals in comparison to their controls not bearing the *Sms1* mutation. As TGN-mediated protein trafficking depends on SMS activity (Subathra *et al.* 2011), an altered delivery of APP to the cell surface and back could possibly affect APP processing and total levels (Choy *et al.* 2012). *In vitro* experiments on Chinese hamster ovary (CHO) cells stably expressing *hAPP695*, however, could not show an altered expression of APP upon SMS1 inhibitor-mediated reduction of SM synthesis (Hsiao *et al.* 2013). It might be that the dif-

ferent cell type and/or the different promoters controlling *hAPP695* expression in both cases account for the discrepancy (Hsiao *et al.* 1996, Hsiao *et al.* 2013).

sAPP total was found in similar amounts in *Sms1*^{WT} x *APPswe*^{WT} and *Sms1*^{MUT} x *APPswe*^{WT} animals, therefore the reduction mediated by *Sms1* disruption was not reflected in this processed product. In *Sms1*^{WT} x *APPswe*^{Tg} and *Sms1*^{MUT} x *APPswe*^{Tg} animals, the genotype-specific 20% reduction in APP total level was still mirrored in the levels of total sAPP. Further comparison revealed 25-33% higher levels of sAPP in comparison to the respective APP full length levels. This could be interpreted to be in compliance with a reduced clearance rate and therefore a higher half-life of transgene derived soluble hAPP (Morales-Corraliza *et al.* 2009).

In summary there are indications that *Sms1* influences full length hAPPswe and, to a lesser extent, endogenous full length APP levels in a positive manner, which might be connected to TGN alterations. sAPP was processed in a similar rate but seemed to be more stable on in *Sms1* x *APPswe*^{Tg} animals.

4.9.2 *hAPPswe* expression shifts APP processing of towards the β-secretory pathway

In general, APP can be processed either via the α-secretory (non-amyloidogenic) or the β-secretory (amyloidogenic) pathway (compare 1.1.4). In *Sms1* x *APPswe*^{WT} animals the endogenous APP was preferentially processed via the α-secretory pathway. Thus reflecting physiological conditions and generating an α-stub/β-stub ratio of 6-7:1. The AD-associated double mutation (K670N/M671L) in the h*APPswe* leads to a higher affinity of BACE1 towards this substrate, resulting in a 50-60-fold increased efficiency of β-site cleavage of h*APPswe* compared to wild-type APP (Tomasselli *et al.* 2003, Barman *et al.* 2011). Consistent with this data, the β-secretory pathway was clearly preferred in *APPswe* transgenic mice, leading to an α-stub/β-stub ratio of 0.7-0.8:1.

sAPP-α/sAPP-β ratios were compared with specific antibodies allowing to distinguish endogenous and transgenic APP. Interestingly, for endogenous APP the same shift towards β-cleavage, with a 20% reduction in endogenous sAPP-α/sAPP-β ratios in *Sms1*^{WT} x *APPswe*^{Tg} compared to *Sms1*^{WT} x *APPswe*^{WT} animals was found. Pointing out, that expression of the transgene also impacts processing of the endogenous BACE1 substrate.

4.9.3 Is there an impact of *Sms1* disruption on APP processing?

The endogenous sAPP-α/sAPP-β ratio in *Sms1*^{MUT} x *APPswe*^{Tg} was comparable to *Sms1*^{WT} x *APPswe*^{WT} animals, despite a lower ratio found in *Sms1*^{WT} x *APPswe*^{Tg}. Thus, the reduction in the sAPP-α/sAPP-β ratio, evoked by the expression of the transgene, was revoked with the additional disruption of *Sms1* expression. The same increase in the ratio of about 20% was seen for the transgenic sAPP-α/sAPP-β ratio comparing *Sms1*^{WT} x *APPswe*^{Tg} and *Sms1*^{MUT} x *APPswe*^{Tg} animals.

These results could be interpreted as a *Sms1* disruption-dependent shift of APP processing towards the α-secretory pathway, while β-secretory cleavage was not affected.

Overall, Aβ was not detectable in *Sms1* x *APPswe*^{WT} animals and just small amounts were found in both *Sms1* x *APPswe*^{Tg} genotypes. Between the latter, no significant differences were found. It might nevertheless be that differences in Aβ levels became visible or more pronounced, if *Sms1* x *APPswe* animals of a higher age would have been analyzed.

That a reduction in SL levels could influence APP processing in direction of the α-secretory pathway without alteration of β-cleavage products was shown by Sawamura *et al.* (2004), who found that inhibition of SPT in CHO-cells resulted in an elevation of sAPP-α and α-stubs. A tight connection between SPT and APP was also found by Grimm *et al.* (2011b), who proposed, that AICD downregulates the expression of the catalytic subunit of SPT. A reduction in SL or SM in particular could thus be protective, preventing further processing of APP via the β-secretory pathway. In agreement with this hypothesis SPT and SMS1 were found upregulated in a subgroup of sporadic AD patients or AD patients without significant neuropathology, respectively (Geekiyanage and Chan 2011, Hsiao *et al.* 2013). The data from AD patients revealed, that *SMS1* expression is elevated in the hippocampus, while it is unchanged in the cerebellum. These findings could be connected to a dose-dependent reduction in Aβ levels upon inhibition of SMS1 in CHO cells (Hsiao *et al.* 2013). In PC-12 cells it could be shown that SM promotes the accumulation of Aβ bound to gangliosides, especially GM1 (Yuyama and Yanagisawa 2010). These studies provide additional cues for a possible positive effect of *Sms1* disruption on Aβ generation. It might be that lipid alterations precede plaque pathology and that regulations in enzyme expression levels promote or delay disease progression.

The data obtained from the APP profile and the activity measurements of enzymes of the amyloidogenic-pathway seemed controversial, because *Sms1*^{MUT} x *APPswe*^{Tg} showed an up regulation of amyloidogenic enzymes (BACE1 and y-secretase). ADAM10 and BACE1 protein levels were not altered, but its enzymatic activity of ADAM10 was not measured. Thus, it remains to be clarified if the up regulation of BACE1 and γ-secretase activity is counter balanced by an increased activity of α-secretase, which could explain the higher abundance of sAPP-α in *Sms1*^{MUT} x *APPswe*^{Tg}.

Another possible explanation would be, that despite a higher activity of BACE1, APP access to this enzyme is limited in *Sms1*^{MUT} x *APPswe*^{Tg} animals, due to their altered membrane composition. If one considers an influence of lipid rafts on the APP cleavage, APP could be drifting out of lipid rafts, with the reduction in SM and Chol and the accompanying loss of rigidity. If APP is found more in the non-raft regions of the membrane, it might be more frequently exposed to ADAM10-mediated cleavage and be processed by the non-amyloidogenic pathway (Ehehalt *et al.* 2003), despite higher enzymatic activity of BACE1. Increased Chol levels in NPC-cells contributed to higher colocalization

rates of APP and BACE1 in endosomes, increasing BACE1-mediated processing of APP (Malnar *et al.* 2012), while HEK-cells depleted of Chol demonstrated increased APP processing via the α-secretory pathway due to a 6-fold higher activity of ADAM10, while its expression was not changed (Kojro *et al.* 2001). These interesting results suggest further investigation of APP processing in the *Sms1* x *APPswe* mouse.

4.9.4 *Sms1* x *APPswe*^{Tg} animals develop diffuse plaques early in life and a reduced number of Aß-40 positive plaques with the disruption of *Sms1*

At 8 weeks of age no plaques were expected in Tg2576, which are known to develop plaques with 6 month of age (Kawarabayashi *et al.* 2001). Nevertheless, Aβ could be detected by immunoblotting and both Aβ-40 and Aβ-42 positive plaques were present in brain sections of *Sms1* x *APPswe*^{Tg} animals. Detected plaques had a diffuse structure, often missing an aggregation core. These kind of plaques are also detected in human AD brains (Alafuzoff *et al.* 2008) and represent an early stage of plaque development (Griffin *et al.* 1995). Interestingly, plaques did not mainly appear in cortical or hippocampal regions, where they would have been expected due to the expression pattern of h*APPswe* under the hamster prion promoter (Irizarry *et al.* 1997).

Aβ-42 positive plaques formed very rarely and were not changed in number between genotypes. It was shown, that soluble Aβ-42 activates nSMase leading to reduction in SM (Grimm *et al.* 2005). As no significant alteration in the number of Aβ-42 plaques was found an additive effect of this APP cleavage product on SM levels was not expected. Aβ-40 positive plaques were reduced in *Sms1*^{MUT} x *APPswe*^{Tg}. If this reduction can be connected to the elevated sAPP-α/sAPP-β ratio in *Sms1*^{MUT} x *APPswe*^{Tg} mice is not clear.

It would be worth to have a deeper look on plaque analysis including Chol alterations in the *Sms1* x *APPswe* mouse model, as this sterol plays an important role in membrane structuring, regulation of AD-enzyme activities, substrate mobilization and processing (Simons *et al.* 1998, Kojro *et al.* 2001, Grimm *et al.* 2005, Grimm *et al.* 2008, Fantini and Yahi 2010, Kosicek *et al.* 2010, Liu *et al.* 2010, Malnar *et al.* 2012). Chol is known to accumulate around senile plaques (Panchal *et al.* 2010) and to be connected to Aβ generation. Elevated Aβ40 results in reduced HMGR activity, thereby reducing the synthesis of Chol, but in turn the inhibition of HMGR also leads to reduced Chol and hence reduced Aβ formation (Fassbender *et al.* 2001, Grimm *et al.* 2005). Reduced Chol could shift lipid-raft mediated APP cleavage in a protective manner, evoking redistribution of proteins, altering endocytosis and elevating ADAM10 levels (Simons *et al.* 1998, Kojro *et al.* 2001, Harris *et al.* 2009, Marquer *et al.* 2011). Thus, there might be a possible additive effect of shifted Chol levels and changed SM levels, which could be investigated in aged *Sms1*^{HET} x *APPswe*^{Tg} animals.

4.9.5 Memory performance is not altered between the different genotypes of the *Sms1* x *APPswe* mouse line

It was of interest, if the detected alterations in APP processing and plaque formation would be reflected on a behavioral level. Therefore, a Y-maze test was set up in order to check for memory performance of animals of the *Sms1* x *APPswe* mouse line. Tg2576 are known to show altered performance in the Y-maze test, although they do not show widespread cognitive deficits (King and Arendash 2002). However, due to the early death phenotype behavioral testing had to start at a rather early age of 7.5 weeks, rendering results rather indicative then clear-cut.

No major alterations in spatial memory performance were found in animals of the *Sms1* x *APPswe* mouse line. The number of SARs, was not altered between the genotypes. SAP was worse in *Sms1*^{MUT} x *APPswe*^{Tg} compared to *Sms1*^{MUT} x *APPswe*^{WT}, but not in *Sms1*^{WT} x *APPswe*^{Tg} compared to *Sms1*^{WT} x *APPswe*^{WT}. Tg2576 show reduced SAP at 9-10 months of age (Hsiao *et al.* 1996). At an age of 9-10 month, equal memory deficits were seen in the Morris Water Maze. Here Tg2576 were also tested at 3-6 months of age, with no deficits compared to wild-type animals (Hsiao *et al.* 1996). These results show the age-dependent decline in memory performance in Tg2576 mice and explain, why there was no strinking and persistant alteration detected in *Sms1* x *APPswe* animals at an early age of 7.5 weeks.

Nevertheless, it would be of interest to see if the disruption of *Sms1* and the changed lipid composition in brain has an effect on memory performance and amyloid generation in later periods of life. Therefore studies should be continued with *Sms1*^{HET} x *APPswe*^{Tg} animals, which have a higher life expectancy. Spatial and social memory as well as brain structure and pathology should be assessed in those animals. Furthermore, conditional *Sms1* knock-out animals might provide a promising tool to study the impact of a disrupted SL-homeostasis on AD relevant parameters and behavior.

4.10 Do *Sms1*^{MUT} and *Sms1*^{MUT} x *APPswe* animals show indications related to a "healthier life style" in humans with respect to AD risk?

4.10.1 *Sms1*^{MUT} and *Sms1*^{MUT} x *APPswe*^{Tg} animals show a higher physical activity rate

With respect to AD, frequent exercise is discussed to be preventive against development of dementia (Loprinzi 2015, Tapia-Rojas *et al.* 2015, Williams 2015). *Sms1*^{MUT} and *Sms1*^{MUT} x *APPswe*^{Tg} animals showed a higher level of locomotor activity and higher speed in the OF in comparison to *Sms1*^{WT} or *Sms1*^{WT} x *APPswe*^{WT}, respectively. The Y-maze test underlined the previously seen changes in behavior, such as enhanced locomotion and reduced anxiety-like behavior detected by the OF test. Correlations between these two behavioral tasks especially in young animals were also seen by (Arendash and King 2002), who analyzed correlation parameters of different behavioral tests in

Tg2576 animals at different ages. To my knowledge, there are no studies, reporting about locomotor activity in *Sms1* knock-out animals so far.

The higher levels of activity might have attenuating effects on the development of an AD-like phenotype in animals of the *Sms1* x *APPswe* mouse line. Thus, the level of exercise potentially could correlate negatively with amyloidogenic processing of APP and Aβ40 plaque counts. Additionally, as discussed above voluntary running could contribute to the observed thicker myelin sheaths in the hippocampus of *Sms1*^{MUT} x *APPswe*^{Tg} *animals.*

4.10.2 *Sms1*^{MUT} show altered stress-coping behavior

Standard behavioral testing showed additionally to higher locomotor activity higher exploratory activity in *Sms1*^{MUT} animals, measured by the number of rearings. *Sms1*^{MUT} animals were calmer and less anxious compared to *Sms1*^{WT}, when handled in their home cages. This was reflected in a longer distance travelled in the center zone of the OF and a smaller latency to the first entry in the center zone, indicative of reduced anxiety-related behavior. Thus, *Sms1*^{MUT} appear less anxious and more tolerant to stress compared to their *Sms1*^{WT} controls, which might be beneficial with respect to AD, as chronically high stress levels are thought to enhance the risk of disease development (Machado *et al.* 2014, Huang *et al.* 2015).

The HPA axis is the main endocrine system regulating a stress reaction (Smith and Vale 2006, Papadimitriou and Priftis 2009). Briefly, on perception of a stressor corticotrophin-releasing-hormone (CRH) and Vasopressin, generated by neuroendocrine neurons of the hypothalamic paraventricular nucleus (PVN), are secreted by the neurosecretory nerve terminals of the median eminence and released via the portal blood vessels to the pituitary gland. Here they bind to specific receptors (corticotrophin-releasing-hormone receptor (CRHR1; (Vita *et al.* 1993)) and vasopressin receptor 1b (V1B; (Hernando *et al.* 2001)) and trigger the release of adrenocorticotrophin releasing hormone (ACTH) from the anterior lobe (Vale *et al.* 1981, Rivier and Vale 1983). ACTH is one of several peptide hormones generated form the prohormone pro-opiomelanocortin (POMC) by subsequent cleavage (Lacaze-Masmonteil *et al.* 1987, Raffin-Sanson *et al.* 2003). ACTH is distributed by the blood stream and functions as an endocrine hormone. It binds to the adrenocorticotrophic receptor (MCR, encoded by the *Mc2r* gene) located in the adrenocortical zona fasciculata (Mountjoy *et al.* 1992, Schioth *et al.* 1996), leading to steroidogenesis and CORT release from the adrenals into the blood circulation (Walker *et al.* 2015). Here CORT is bound by albumin and the corticosteroid binding globulin (CBG) and is transported to target organs and tissues, to elicit specific stress reactions on a metabolic or cardiovascular level (Slaunwhite and Sandberg 1959, Pardridge and Mietus 1979). CORT is also transported back to the brain, where (if it is not bound to CBG) it is able to pass the BBB (Pardridge and Mietus 1979) and to act as an agonist for two different kinds of steroid receptors, which trigger the negative feedback response, namely mineralocorticoid receptors (MR, encoded by *Nc3r2*) and glucocorticoid receptors (GR, encoded by *Nc2r1*) (Arriza *et al.* 1988). GRs are

abundant in brain with highest levels in the hippocampus, septum, cortical and thalamic regions, while MRs are mainly found in the hippocampus and the lateral septum (Reul and de Kloet 1985, 1986). Both receptor types regulate CORT-mediated negative feedback on the HPA-axis. MRs, with a five to ten times higher affinity to CORT are thought to mediate the circadian feedback regulation, while GRs get occupied if CORT levels rise in the brain and therefore take over the negative feedback regulation in a stress reaction (Reul and de Kloet 1985, 1986).

The SRT tests underlined the observation of an altered stress-coping behavior in *Sms1*^{MUT} animals. Interestingly, a high elevation in CORT levels was found in the *Sms1*^{WT} control animals 15min after the initial blood taking, but without receiving restraint stress, while CORT was just slightly higher in *Sms1*^{MUT} animals. This could be interpreted in three different ways; 1) *Sms1*^{MUT} animals are restricted in the synthesis or release of CORT upon perception of a stressor; 2) *Sms1*^{MUT} perceive the first blood taking as a less stressful event compared to *Sms1*^{WT} animals, underlining a reduced anxiety-related and reduced stress perception phenotype of *Sms1*^{MUT}, which might correlate with the observed reduction in nociception in these animals; 3) CORT levels in *Sms1*^{MUT} rise comparable to *Sms1*^{WT}, but drop faster, converging basal levels after 15min already. In that case one could also postulate a better coping with restraint stress in *Sms1*^{MUT} animals.

As CORT is lipophilic, it cannot be stored inside the adrenal glands, but on demand, is rapidly synthesized from Chol upon its translocation into the mitochondria (Lin *et al.* 1995, Arakane *et al.* 1997). There were no major persistent alterations in the adrenal zona fasciculata, which could point to an altered synthesis of CORT. Furthermore, the perception of 15min restraint stress led to comparable elevation in CORT levels in *Sms1*^{WT} and *Sms1*^{MUT} animals, eliminating the first hypothesis on altered CORT synthesis and/or secretion. The similar CORT levels were also reflected on the behavioral level, where genotype dependent locomotion and anxiety-related parameter detected previously persisted between *Sms1*^{WT} and *Sms1*^{MUT} animals after perception of restraint stress.

As, with extended duration of restraint stress, two hours after the initial blood taking *Sms1*^{WT} and *Sms1*^{MUT} CORT levels of the control groups were back to base line, we could state that after a mild stressor, such as handling accompanied by blood taking, *Sms1*^{MUT} animals either do not show a rise in CORT levels or drop their CORT levels within 15min, while *Sms1*^{WT} animals show a more sensitive stress reaction, or a slower negative feedback. In both cases *Sms1*^{MUT} animals could be considered to be more stress-resistant.

A higher protein level of total brain GR and a higher expression levels of MR in the hippocampus of *Sms1*^{MUT} could be one reason for the described observations. MRs regulate the diurnal rhythm of CORT and have a high affinity for this steroid (Reul and de Kloet 1985, 1986). A higher expression could lead to a faster feedback regulation, lowering CORT levels in response to small fluctuations. GRs on the other side have a lower affinity for CORT and take over the negative feedback reaction

in response to stress, when larger amounts of CORT reach the brain and MRs are already saturated (Reul and de Kloet 1985, 1986, Arriza *et al.* 1988). Similar to the studies by Reichardt *et al.* (2000) and Ridder *et al.* (2005), this overexpression of GRs could lead to a faster drop in CORT levels after perception of a stressor. This could explain the observed differences in CORT down regulation in *Sms1*^{MUT} mice after perception of stress by handling and blood taking or by fixation in course of the SRT. However, GR overexpressing mice are also known to have lower basal serum CORT levels (Reichardt *et al.* 2000, Ridder *et al.* 2005), which was not observed in *Sms1*^{MUT} animals, showing that GR upregulation alone is not enough to explain the observed differences.

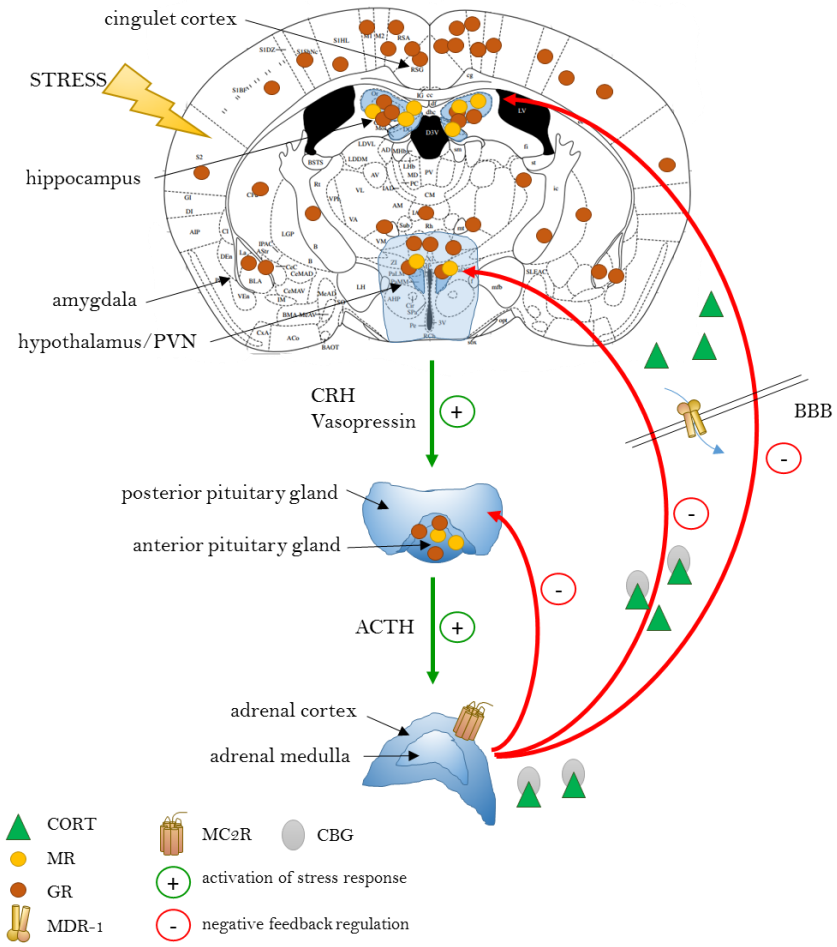

Figure 4.1: Hypothalamus-Pituitary-Adrenal axis signaling
Upon perception of an external stress the HPA-axis gets activated (green arrows). CRH triggers the release of ACTH from the pituitary, wich is distributed by the blood stream and binds to MC2R in the adrenal cortex. Upon binding CORT is released to the bloodstream, and triggers the systemic stress reaction. CORT is bound to CBG, when released to the blood and gets transported to the BBB. Here MDR-1 is a major transporter responsible for the regulation of CORT in the brain, due to efflux regulation. The negative feedback regulation mediated by CORT (red arrows) can be triggered at the level of the pituitary gland, the hypothalamus or the hippocampus. Here CORT can bind to two different kinds of receptors, MR and GR, regulating diurnal or stress-related activation of the HPA-axis.
Adenocorticotroph hormone (ACTH), blood-brain-barrier (BBB), corticosterone binding globulin (CBG), Corticosterone (CORT), corticotrophin releasing hormone (CRH), glucocorticoid receptor (GR), hypothalamus-pituitary-adranal axis (HPA-axis), melanocortin 2 receptor / adrenocorticotrophic receptor (MC2R), multidrug resistance protein 1 (MDR-1), mineralocorticoid receptor (MR), paraventricular nucleus (PVN).

It could not be definitely excluded, that CORT levels did not rise at all in *Sms1*^{MUT} after handling and the initial blood taking. A missing reaction could be due to altered signaling upstream of CORT synthesis and release. Reichardt *et al.* (2000) showed that overexpression of GR had such effects, by lowering CRH and POMC levels 2 to 3-fold, respectively, leading to reduced ACTH immunoreactivity in the pituitary gland without alteration in pituitary structure. In agreement with that study normal histological appearance of the pituitary gland was observed and reduced ACTH in the intermediate and anterior pituitary lobe, but higher pituitary *Pomc* mRNA levels were detected. This could be an indication for an altered processing of POMC in the *Sms1*^{MUT} animals. Together with reduced adrenal expression levels of *Mc2r*, these might point to restricted stress signaling in *Sms1*^{MUT} animals and the need for a stronger trigger/stressor to elicit HPA-axis signaling. Furthermore, MC2R-mediated activation of steroid synthesis and release is not just dependent on pure expression levels, but can be modulated in its sensitivity. Clark *et al.* (2003) proposes, that this could be achieved by the colocalization of MC2R with PKA in lipid rafts. PKA phosphorylates and therefore activates HSL, responsible for cholesterol synthesis and StAR, mediating Chol import to mitochondria. MC2R-mediated action of ACTH is additionally modified by internalization of the receptor (Clark *et al.* 2003). However, absent or strongly hampered MC2R signaling should be reflected in high levels of circulating ACTH with very low levels of secreted mineralo- or glucocorticoids, as it is known from MC2R knock-out animals or MC2R mutations in familial glucocorticoid deficiency (Chida *et al.* 2007, Chan *et al.* 2008), which were not found in *Sms1*^{MUT} animals. Nevertheless, altered membrane composition could affect MC2R colocalization with PKA and its internalization characteristics, contributing to altered HPA signaling parameters.

In fact, based on current results, altered sensitivity of the HPA-axis is proposed, with higher basal CORT levels, leading to increased arousal and basal activity levels and a faster down regulation of CORT in response to a stress-reaction, possibly contributing to a more stress-resistant phenotype in *Sms1*^{MUT} animals.

Overall one could say that 2h of restraint stress affected behavior only in *Sms1*^{WT} animals, elevating distance and speed of locomotion as well as number of rearings. That *Sms1*^{MUT} animals are not affected in their behavioral performance despite elevated blood CORT levels underlines again an altered stress-coping behavior between *Sms1*^{WT} and *Sms1*^{MUT} mice. Either additional stress signaling could not alter stress-related behavior anymore, due to saturation, or it outlines a more stress resistant phenotype of *Sms1*^{MUT} animals.

Measurement of MDR-1 levels in the brain showed an elevation in *Sms1*^{MUT} compared to *Sms1*^{WT}. MDR-1 or Pgp-1 belongs to the family of ATP-dependent ABC-transporters (Juranka *et al.* 1989). It is amongst others found in the BBB where it is responsible for the efflux of several substances including CORT from the brain (Wolf and Horwitz 1992, Uhr *et al.* 2002, Muller *et al.* 2003, Mittapalli *et al.* 2013), although, the transport of CORT is discussed controversially (Karssen *et al.* 2001). In case

of MDR-1-mediated CORT transport, elevated levels of MDR-1 could alter HPA-axis signaling under basal conditions, by hampering CORT transit via the BBB and the subsequent binding to the steroid receptors (Uhr *et al.* 2002, Muller *et al.* 2003). This could explain higher basal blood CORT levels and behavioral activity, which was found in *Sms1*^{MUT} animals. Despite higher MDR-1 expression, a massive rise in CORT upon perception of a stressor would be mirrored in the brain, as MDR-1-mediated efflux might not be able to compensate. In this case, the high density of steroid receptors, especially GRs, observed in the *Sms1*^{MUT} brain, would lead to a fast mediated negative feedback response, rapidly down regulating HPA-axis signaling rendering *Sms1*^{MUT} animals more stress-resistant (Reichardt *et al.* 2000, Ridder *et al.* 2005).

To clarify this topic further, one would have to set up another SRT experiment with a shorter recovery period, measuring CORT levels five or ten minutes after initial blood sampling, to check for CORT rise or rapid decrease. Additionally a dialysis set up to follow stress-induced blood and brain levels of CORT in a time-dependent manner could help to elucidate further questions, such as altered CRH/Vasopressin signaling and differences in ACTH release. Interestingly MC2R was also found to be of importance in mediation of the general lipolysis pathway in adipocytes, where shRNA targeting led amongst others to increased AA levels but in parallel to reduced desaturase expression, resulting in lower MUFAs level (Betz *et al.* 2012). These results render this receptor and other components of the HPA-axis promising candidates for further studies on lipid pathways and stress reactivity in the *Sms1* mouse line. Beyond that, the proposed higher stress-resistance of *Sms1*^{MUT} represents a crucial aspect for additional studies in the *Sms1* x *APPswe* mouse line, concerning the often discussed correlation between stress-sensitivity and AD risk (Gottfries *et al.* 1994, Nasman *et al.* 1995, Pomara *et al.* 2003, Rothman and Mattson 2010).

4.11 h*APPswe* is also expressed in lung and heart of *APPswe*^{Tg} mice

As suggested in earlier studies, h*APPswe* was found to be expressed not only in the brain, but also in heart and lung (brain>heart>lung), while a previously described expression in the spleen could not be confirmed (Kawarabayashi *et al.* 2001). Additionally, as stated before, the endogenous APP processing enzymes were expressed in different intensities in those organs (Marcinkiewicz and Seidah 2000). *In situ* expression data in P4 pups was similar to our results obtained by immunoblotting of samples from 8 week old mice for BACE1 (brain>heart=lung), but differed for ADAM10 (lung>heart>brain), where at P4 staining intensities were highest in the brain, followed by the lung and almost not detectable in the heart (Marcinkiewicz and Seidah 2000).

Enzymatic cleavage gave rise to APP degradation products such as stubs and Aβ. With regard to Aβ, levels in lung and heart were between 5 to 20-fold higher compared to the brain. Although genotype differences did not reach significance, our data suggested that amyloid production could be en-

hanced in *Sms1*^{MUT} x *APPswe*^{Tg} in comparison to *Sms1*^{WT} x *APPswe*^{Tg} animals in an organ-specific manner.

With a disruption of *Sms1*, processing of h*APPswe* seems to result in overproduction of Aβ in heart and lung. In general, an accumulation of protein cleavage products could affect systemic functions leading to early death. The investigations on expression and cleavage of h*APPswe* in lung and heart were just preliminary. Nevertheless, it would be interesting to study Aβ deposition and related organ function in those tissues with a higher number of animals and additional methods, to elucidate if the disruption of *Sms1* functions as a trigger to shift the anyway high production of Aβ in lung and heart of *Sms1*^{WT} x *APPswe*^{Tg} animals to a critical level, causing organ failure.

Vascular diseases like stroke and heart disease are also regarded as a risk factor for sporadic AD (Sparks *et al.* 1990, Soneira and Scott 1996, Knopman *et al.* 2001, Cermakova *et al.* 2015). The relevance of SM in heart disease is discussed controversially. In a multi ethnic study by Yeboah *et al.* (2010) elevated plasma SM levels could not be associated with a higher risk for coronary heart disease (CHD). Other studies, however, report high SM levels to be a risk factor for CHD and left ventricular systolic dysfunction. (Chatterjee *et al.* 2006, Chen *et al.* 2011). With respect to these studies, the mutation in *Sms1* would be rather protective than contributing to the development of heart disease. However the reduced MUFA/PUFA content observed with the *Sms1* disruption were not taken into account and moreover increased SM could point towards different dietary habits. It was also found that major changes of phospholipid and triacylglycerol content, including shifts of saturation states of these lipids, occur during postnatal heart development in the rat (Novak *et al.* 2006). An alteration of phospholipid and FA availability due to the mutation in *Sms1* might therefore affect already the development of the heart, leading to defects and failure in later life.

Sms1^{MUT} animals had higher heart weight relative to body weight and a reduced diastolic posterior wall width in males, but no functional alterations have been observed. The weight increase was not detected in animals of the *Sms1* x *APPswe* line, but all of the examined *Sms1*^{MUT} x *APPswe*^{Tg} animals showed a dilatation of the right ventricle. Importantly, this was also seen in some of the other genotypes. Therefore the relevance of these subtle changes in the *Sms1* x *APPswe* mouse line is questionable. To elucidate whether *Sms1*^{MUT} x *APPswe*^{Tg} animals suffer from Aβ-mediated heart failure contributing to the premature death phenotype would be of major interest. This question could be addressed further by studies on heart morphology, function and resilience, which could be done by immunostaining and echocardiogramms.

4.12 *Sms1* seems to be involved in regulation of the immune system and the autophagic flux

4.12.1 *Sms1*^{MUT} animals suffer from age-dependent splenomegaly

It is said that, due to its localization at the plasma membrane, SMS2 rather than SMS1 is involved in cytokine-mediated inflammatory response (Gowda *et al.* 2011). However, studies on *Sms2* and also on *Sms1* provided evidence for the importance of both enzymes in either the regulation of viral infection, such HIV-1 membrane fusion (Hayashi *et al.* 2014), or in alteration of T-cell (Dong *et al.* 2012) or macrophage function (Liu *et al.* 2009a, Li *et al.* 2012).

The spleen represents one of the most important organs of the immune system. It is responsible for the synthesis of lymphocytes and the storage of red blood cells and platelets, but also for the removal of disused blood cells (Song 1974). Relative to body weight spleen weights were slightly increased in *Sms1*^{MUT} animals, at an age of 16 weeks. Additional analysis of aged (1.7-2.3 years) *Sms1* females showed that *Sms1*^{MUT} suffered from major splenomegaly. These data go in hand with the previous description of *Sms1* knock-out animals, which at an age of up to 12 months, have a normal appearance, except of mild splenomegaly (Dong *et al.* 2012). These data suggest that disruption of *Sms1* leads to age-dependent increase in spleen weight and size.

Factors contributing to splenomegaly include viral, parasitic or bacterial infections such as endocarditis. Cirrhosis of the liver, blood cancers and blood clots as well as general inflammation are also connected to an enlargement of the spleen. In addition, LSDs such as Gaucher's disease and NPD are, besides other symptoms, characterized by splenomegaly (reviewed by: vom Dahl and Mengel (2010), Grabowski (2012), Pastores and Hughes (2015)).

One reason for LSDs and the resulting splenomegaly is a defective clearance of lipids and/or proteins by the autophagic pathway (Schulze and Sandhoff 2011). In *Sms1*^{MUT} mice autophagy, commonly monitored by LC3I/LC3II ratio and p62 levels (Jiang and Mizushima 2015), was not clearly altered and highly variable. EEA1 levels, however, were elevated and CatD levels reduced. EEA1 would point to an elevated level of early endosomes (Mu *et al.* 1995), while CatD, a lysosomal aspartyl protease, is found in the early endosomes, maturating endosomes and lysosomes, where it gets activated and degrades proteins (Benes *et al.* 2008), but is also involved in autophagy mediated cell death (Zheng *et al.* 2008). CatD translocation from the lysosome to the cytoplasm was found to be the earliest event in triggering caspase independent apoptosis, by activation of Bax, leading to outer mitochondrial membrane permeabilization and the release of AIF, which is residing in the intermembrane space of mitochondria. Release of AIF triggers early apoptotic events in T-cells (Bidere *et al.* 2003). Thus reduced CatD and reduced AIF levels in *Sms1*^{MUT} spleen could point to a reduced number of apoptotic events. Consistently, the number of TUNEL-positive cells was reduced in *Sms1*^{MUT}

with enlarged spleens. These findings could point to an inefficient removal of superfluous blood cells and other debris, after induction of endocytosis and reduced apoptosis, leading to splenomegaly.

To check for efficient removal of blood cells in spleens of *Sms1*^{WT} and *Sms1*^{MUT} animals hemosiderin and ceroid or lipofuscin pigment was labeled by PAS staining. Hemosiderin is found in macrophages and is detected in mice of all ages, while it is more prominent in females and increases with age. Normal levels reflect the removal of effete red blood cells. It can be increased in cases of chemically induced hemolytic anemia or methemoglobinemia (Travlos et al., 1996). Ceroid or lipofuscin is also found in cytoplasm of macrophages. It derives from oxidation and polymerization of fatty acids (Crichton et al., 1978). As pigment levels did not differ between both genotypes, it can be assumed that the number of splenic macrophages and therefore the removal of effete red blood cells is similar. Additionally, the oxidation and polymerization process of fatty acids seems to be unaffected by the disruption of *Sms1*.

Some unclear effects on IgG2b and TGF-β levels were found in *Sms1*^{MUT} spleen samples, which might represent a hampered secretion of IgG2b due to a lack of TGF-β signaling (Garcia *et al.* 1996). However, these results did not reach significance and should be elucidated in more detail.

4.12.2 Does the BBB provide sufficient barrier function?

The altered HPA-axis regulation and the higher expression of the BBB-residing MDR-1 in *Sms1*^{MUT} animals led me to the question if the BBB per se shows changed functionality, which could amongst others also affect the spreading of systemic inflammation to the brain. Several studies mention the regulatory task of the BBB and emphasize that the BBB can be altered in response to glucocorticoid stimuli and inflammation (Bolton *et al.* 1998, Forster *et al.* 2005, Quan and Banks 2007, McCaffrey *et al.* 2008), but is also affected in AD (Dickstein *et al.* 2006, Bowman *et al.* 2007, Viggars *et al.* 2011, Kook *et al.* 2013, Takeda *et al.* 2013, Takeda *et al.* 2014).

Misregulation of specific junction proteins could contribute to a size-selective opening of the BBB, thereby permitting infiltration of the brain (Nitta *et al.* 2003). To elucidate this topic BBB resident junction protein markers were investigated. Occludin is a crucial component of TJ (Hirase *et al.* 1997, Bolton *et al.* 1998), while Cx43 represents a marker for GJ and was recently connected to promotion of immune quiescence in the brain (Ezan *et al.* 2012, De Bock *et al.* 2014, Gaete *et al.* 2014, Boulay *et al.* 2015). Catenin-β, an AJ protein, was also found to be important for BBB development (Liebner *et al.* 2000, Liebner *et al.* 2008, Liu *et al.* 2014). Marker analysis revealed an up regulation of all of these proteins in brain samples of *Sms1*^{MUT} animals. This could be a result of disrupted TGN-mediated protein trafficking and protein secretion, which was shown by Subathra *et al.* (2011) to be constricted upon *Sms1* disruption. Thus misguidance of junction proteins to their site of destination could affect BBB functionality in means of pure permeability, but also in regulation of the immune response and development.

Additionally, to mere junctions, the BBB is made up and regulated by specific transporter proteins (Glavinas *et al.* 2004, Rautioa and Chikhale, Pardridge 2012). One of the transporters analyzed was MFSD2A. This FA-transporter is exclusively found in specialized barriers such as the BBB epithelium, where it is crucial for embryonic BBB development and adult maintenance (Ben-Zvi *et al.* 2014, Nguyen *et al.* 2014, Guemez-Gamboa *et al.* 2015). The FA transporter selectively delivers LC-lyso-PCs containing MUFAs and PUFAs into the brain and thus is responsible for the vast majority of DHA uptake (Ben-Zvi *et al.* 2014, Nguyen *et al.* 2014, Alakbarzade *et al.* 2015). Although, LC-lyso-PC were not altered in brain samples of *Sms1* x *APPswe* animals, the reduced levels of MFSD2A, found in *Sms1*^{MUT} x *APPswe*^{WT} and in *Sms1*^{MUT} x *APPswe*^{Tg} animals, could be an indicator of a misfunctional BBB. Mice bearing a homozygous mutation in MFSD2A residue (p.Ser339Leu), rendering the transporter less active, showed progressive microcephaly syndrome (Alakbarzade *et al.* 2015). Additionally, MFSD2A knock-out animals are reported to be smaller in size and leaner, with a significantly higher rate of voluntary movement (Berger *et al.* 2012). These observations are similar to those made in *Sms1*^{MUT} x *APPswe*^{Tg} animals, which showed reduced brain mass, reduced body weight gain and higher activity rates, additionally to reduced levels of MFSD2A. Thus, results could point to developmental changes in *Sms1*^{MUT} x *APPswe*^{Tg} animals due to alterations in MFSD2A function in development

MFSD2A is further known to regulate transcytosis through epithelial cells into the brain tissue, without affecting TJs (Ben-Zvi *et al.* 2014). Transcytosis allows the passage of immunoglobulins through the epithelium and is highly enhanced in MFS2A knock-out animals (Ben-Zvi *et al.* 2014). This affects the isolated character of the brain, with respect to inflammation and allows the passage of Igs into the brain.

As mentioned before, *Sms1*^{MUT} mice had enhanced IgG2b levels in the spleen. Additionally, high levels of endogenous IgGs in general and also of IgG2b in heart samples of *Sms1*^{MUT} x *APPswe*^{Tg} animals were found. Although, IgG2b differences did just partially reach significance, the elevation was more prominent in genotypes carrying the *Sms1* gene trap cassette. I wondered if the lower expression of MFSD2A in *Sms1*^{MUT} x *APPswe*^{Tg} animals would affect the passage of IgG into the brain. However, immunological staining showed that despite high IgG2b levels found in brain samples, positive staining was restricted to the blood vessels of the brain. That IgG2b did not infiltrate the brain, gives further evidence that the BBB, despite the described changes in lipid composition, junction proteins and MFSD2A levels, remains functional upon mutation of *Sms1*.

Another specific transporter contributing to BBB functionality is MDR-1 which, as mentioned before, regulates efflux from the brain (Wolf and Horwitz 1992, Uhr *et al.* 2002, Muller *et al.* 2003, Mittapalli *et al.* 2013). Interestingly, one substrate of the ATP-dependent transporter is Aβ. Changes in MDR-1-mediated efflux parameters, would therefore affect Aβ transport and its removal from the brain (Cirrito *et al.* 2005). The findings from *Sms1*^{MUT} animals could be validated, as also *Sms1*^{MUT} x

APPswe^{Tg} animals had higher MDR-1 levels compared to their *Sms1*^{WT} x *APPswe*^{Tg} controls. Knock-out animals of MDR-1 have a 50% reduced clearance rate of CNS injected I^{125} labeled Aβ40 and Aβ42. Besides this, 12 month old Tg2576/MDR-1 knock-out double mutants had higher accumulation of Aβ in the brain compared to Tg2576 mice without the additional knock-out of MDR-1 (Cirrito *et al.* 2005). A correlation of MDR-1 activity and AD is also found in AD patients with mild dementia. Reduced activity was detected in parietotemporal, frontal and posterior cingulate cortices and the hippocampus of PET examined subjects (Deo *et al.* 2014). These findings provide evidence, that BBB alterations such as higher expression of MDR-1 and specific export Aβ could prevent accumulation of Aβ oligomers and fibril formation in the brain of *Sms1*^{MUT} x *APPswe*^{Tg} mice, leading to the observed reduction in plaque formation.

In AD research, the interest for the BBB is on the rise. In Tg2576 mice a functionally compromised BBB was found already at the age of 4-10 month, prior to development of plaque pathology (Ujiie *et al.* 2003). Therefore maintenance of BBB integrity is a target for early intervention. On the other hand a recent study using ultra sound to open the BBB, resulted in reduction of plaques, improvement of spatial memory performance, a higher number of new born neurons and improved dendrite outgrowth in a model of advanced AD (Burgess *et al.* 2014), providing evidence, that a permeabilization of the BBB could also contribute to AD therapy.

Analysis of the BBB by MSOT measurement did not reveal any significant alterations in permeability with respect to ICG absorbance into the brain. However, these results are just preliminary and should be repeated. Additional experiments elucidating this topic should be conducted to analyze BBB permeability, dynamics and diffusion rates in *Sms1* animals for specific substrates. A proper positive control, meaning an animal model with known BBB dysfunction or opening of the BBB by ultra sound and staining with two differentially sized dyes would be recommendable. Thus it would be possible to better distinguish diffusion pattern of a BBB-permeable and a BBB-non-permeable dye. Furthermore, a wider range of TJ markers additionally to occludin should be investigated, including crucial TJ components such as caudin-5 and zona occludens-1, as this junction type is mainly responsible for the perpetuation of barrier function. It would also be worth it to analyze BBB alterations further in *Sms1* x *APPswe* animals, to investigate the effects on Aβ accumulation and plaque formation.

4.12.3 Neuro-inflammatory processes might be alterd in *Sms1*^{MUT} x *APPswe*^{Tg} animals

Inflammation is an important aspect in AD. The inflammatory process causes a vicious cycle, with Aβ production promoting inflammation and inflammation triggering the production of Aβ (Hjorth *et al.* 2013). AD patients show a reduction of PUFAs (Grimm *et al.* 2011a). As PUFAs (AA and EPA) also serve as precursors for lipid mediators in the inflammatory process, a reduction could lead to a lack of lipoxins and RvEs. (Serhan *et al.* 2008). Their anti-inflammatory and pro-resolving character-

istics contribute to the regulation of cytokines (reducing the levels of Il-1β, IL-6) and ROS, to a decrease of the inflammatory response and neutrophil traffic and to stimulation of Aβ-42 phagocytosis (Serhan *et al.* 2000, Serhan *et al.* 2002, Serhan 2007, Hjorth *et al.* 2013). Therefore the proposed higher release of AA and EPA for the production of lipoxins and RvE, as it was discussed above, could serve as a compensatory mechanism to reduce the inflammatory response and to prevent the outlined vicious cycle in *Sms1*^{MUT} x *APPswe*^{Tg} animals.

The inflammatory response in the brain includes the activation of microglia, which is also observed early in AD (Arends *et al.* 2000). Activated, proliferating microglia are especially found in the proximity to SPs and are thought to actively participate in the neuro-inflammatory process and Aβ-clearance (Matsuoka *et al.* 2001, Janelsins *et al.* 2005, Marlatt *et al.* 2014, Matsumura *et al.* 2015). CD68 and Iba-1 represent common markers for microglia activation and are frequently used to assess neuro-inflammation in AD models (Krabbe *et al.* 2013, Matsumura *et al.* 2015). In *Sms1* x *APPswe* animals, data on CD68 and Iba-1 were not significantly different. Nevertheless, *Sms1*^{WT} x *APPswe*^{WT} had slightly higher levels compared to the levels in *Sms1*^{MUT} x *APPswe*^{WT} and *Sms1*^{MUT} x *APPswe*^{Tg} levels dropped slightly below their respective controls with functional *Sms1*. If one would consider these data as relevant, the grade of amyloidogenic processing of APP and the number of Aβ40 positive plaques would correlate positively with activation of microglia cells. The parallel appearance of plaques and activated microglia was reported earlier (Arends *et al.* 2000, Matsuoka *et al.* 2001, Marlatt *et al.* 2014). Matsuoka *et al.* (2001) reported further that activated microglia associate with fibrillary, but also with the diffuse non-fibrillar plaques, which were observed in the *Sms1* x *APPswe* mouse line. These results could promote the assumption of a protecting effect of *Sms1* disruption on AD-related proteinopathies and neuronal inflammation.

Especially the elevated levels of EPA-containing PCs could participate in the clearance or prevention of plaques in *Sms1*^{MUT} x *APPswe*^{Tg} mice, through elevation of phagocytosis (Halvorsen *et al.* 1997, Adolph *et al.* 2012). In human M2-microglia enhanced phagocytosis of non-fibrillar Aβ-42 upon DHA and/or EPA treatment was shown (Hjorth *et al.* 2013). Co-incubation with Aβ-42 and EPA also resulted in lower production of pro-inflammatory cytokines and elevation of the neurotrophic factor BDNF (Hjorth *et al.* 2013).

Altered BDNF expression makes up another immunological characteristics of AD (Phillips *et al.* 1991, Poon *et al.* 2011). Levels of BDNF change during AD progression. While in early AD BDNF is upregulated as a kind of compensatory repair mechanism, trying to prevent neurodegeneration, in late AD BDNF levels are found to be decreased (Laske *et al.* 2006, Faria *et al.* 2014). BDNF was found elevated in *Sms1*^{WT} x *APPswe*^{Tg} animals, where EPA-containing PCaas were just slightly elevated and was decreased to *Sms1*^{WT} x *APPswe*^{WT} levels in *Sms1*^{MUT} x *APPswe*^{Tg} animals, which had the highly elevated levels of EPA-containing PCaas. These findings would fit to the results of Hjorth

et al. (2013), who reported BDNF elevation in microglia treatment only with the lowest dosage of EPA. Furthermore, *Sms1*^{WT} x *APPswe*^{Tg} were the only genotype with a higher PUFA/SFA ratio in PCs, validating the positive correlation between PUFA content and BDNF levels as AD-relevant parameters, which was stated before (Rao *et al.* 2007b, Ferreira *et al.* 2014).

Despite the difference in protein levels, not different intensities or a clustering of CD68 immunoreactivity could be seen in the brain of *Sms1*^{WT} x *APPswe*^{Tg} and *Sms1*^{MUT} x *APPswe*^{Tg}. To further investigate whether CD68 or Iba-1 positive cells accumulate in the proximity of plaques immunological co-staining with Aβ-40 and Aβ-42 should be performed and could be expanded to animals in advanced age, including *Sms1*^{HET} x *APPswe*^{Tg} mice. Furthermore it would be interesting to check for increased phagocytosis of Aβ in primary microglial cell culture derived from *Sms1* x *APPswe* animals.

4.13 Autophagy alterations in CNS, connections between LSDs and AD

The SL-influenced autophagic process and clearance of APP metabolites by the lysosomal pathway plays an important role in AD (Tamboli *et al.* 2011a, Tamboli *et al.* 2011b). Impairment of the autophagic flux, attended by hampered autophagic degradation was observed (lee, 2010, Lai and mclaurin 2012). Thus, neuronal accumulation of autophagic vacuoles (autophagosome, amphisome, autolysosome), which represent a typical pathological hallmark of LSDs, have been observed in AD brains (Nixon *et al.* 2005, Boland *et al.* 2008). On the other hand LSD also show neuronal tangles and amyloid aggregations, similar to those found in AD (Saito *et al.* 2002, Nixon *et al.* 2008, Ohmi *et al.* 2009), linking both diseases to each other.

In aSMase knock-out mice, representing a model for NPD-A, it was shown, that particularly the accumulation of SM leads to a disruption of the autophagic flux and an accumulation of autophagolysosomes due to misfunctional clearance (Gabande-Rodriguez *et al.* 2014).

Brains of *Sms1*^{MUT} x *APPswe*^{WT} and *Sms1*^{MUT} x *APPswe*^{Tg} animals both had reduced levels of p62 in comparison to *Sms1*^{WT} x *APPswe*^{WT} mice, which were underlined in *Sms1*^{MUT} x *APPswe*^{Tg} with a higher ratio of LC3II/LC3I. Elevated ratios of LC3II/LC3I are connected to an up regulation of the autophagic process as the conversion of LC3I to LC3II takes place in forming autophagosomes (Mizushima 2004, Tanida *et al.* 2004, 2008), while reduced levels of p62 reflect a fast removal of autolysosmes and a rapid degradation process (Ichimura and Komatsu 2010). Boland *et al.* (2008) proposed that neurons have a relatively high rate of autolysosomal clearance in comparison to fibroblasts. A highly efficient degradation process of autolysosomes is indicated by the reduced levels of p62 in *Sms1*^{MUT} x *APPswe*^{WT} and *Sms1*^{MUT} x *APPswe*^{Tg} and shows a negative involvement of SM levels in autophagic clearance, as it was proposed by Gabande-Rodriguez *et al.* (2014).

Lysosomes and endosomes play a dual role in APP metabolism. On the one hand they harbor BACE1 and γ-secretase, needed for the generation of Aβ and its release to the vacuolar lumen. On the other hand they content nephrilysin and cathepsins, necessary for Aβ degradation and clearance (Tamboli *et al.* 2011a, Tamboli *et al.* 2011b). SL act in two ways on this system. They enhance the induction of autophagy thereby promoting APP cleavage and they block autophagic clearance in the autolysosomes. Both actions lead to accumulation of autophagosomal and lysosomal compartments and enhanced aggregation of APP-CTFs and Aβ, promoting AD pathological characteristics (Tamboli *et al.* 2011a, Tamboli *et al.* 2011b).

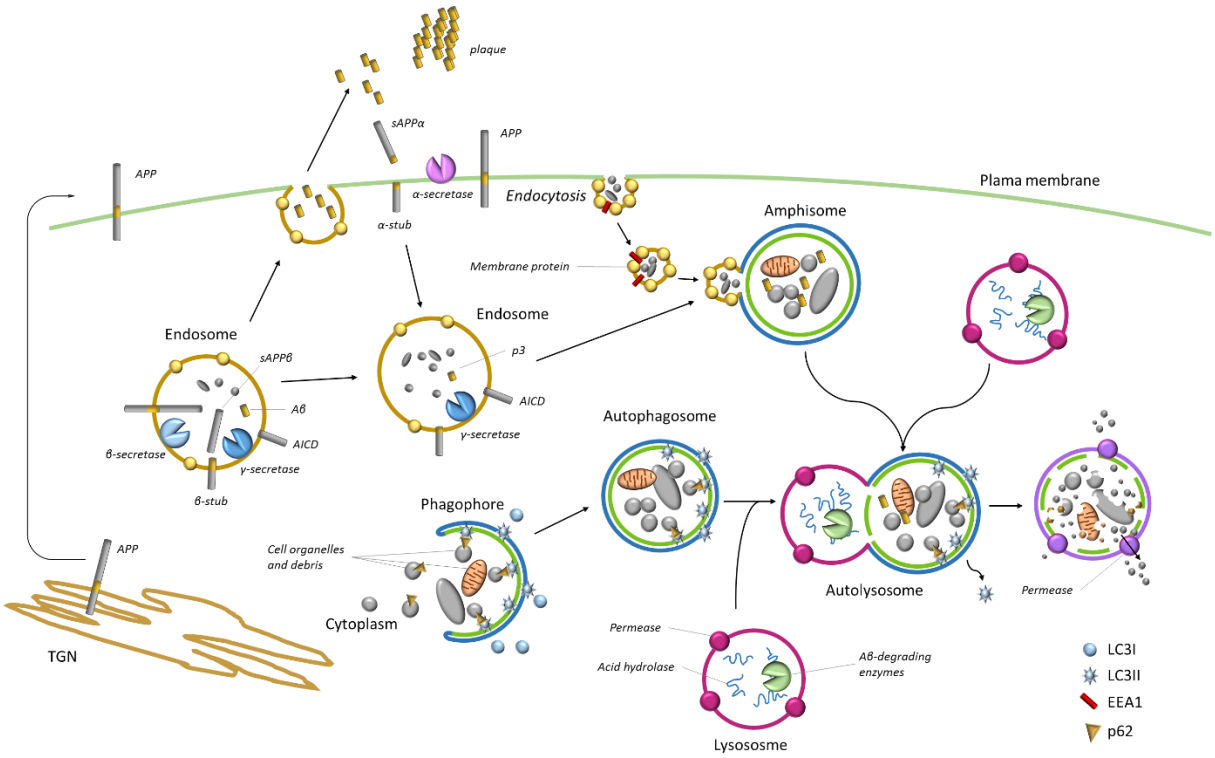

Figure 4.2: Overview on the autophagic pathway
The autophagic pathway describes a degradation process for the recycling of biomolecules. It starts with the formation of a bilaminar phagophore, which takes up cytoplasmic cell organelles, porteins or other cell debris. With the induction of phagophore formation and its closure to form the so called autophagosome, the conversion of LC3I to LC3II takes place. Furthermore, p62 serves as an adaptor protein to bind ubiquitinated proteins, labeled for degradation and to fuse them to the inner wall of the phagophore. The fusion of the autophagosome with the lysosome leads to the formation of autolysosmes with a more acidic pH. These autolysosmes can also be build out of amphisomes, fusing with lysosomes. Amphisomes arise by fusion of endodomes (characterized by EEA1 expression) with autophagosomes and therefore carry extracellular cargo and membrane associated proteins. Toghether with the delivery of acid hydrolases the acidic condiditons make the autolysosme the perfect compartment for the degradation process, where not only intravesicular components are degraded, but also anchor and adaptor proteins.
APP turn over is tightly connected to the autophagic pathway. APP is delivered from the TGN to the plasma membrane, here it can be cleaved by α-secretase and the sAPPα is released to extracellular space. By endocytosis the α-stub and full length APP can get internalized into endosomes. Here β- and γ-secretase are residing and gain higher activity due to pH changes. Within the endosomes amyloidogenic processing, but also the cleavage of the α-stub takes place, creating AICD, p3, Aβ and sAPPβ. These cleavage products can be directed to enzymatic degradation in the autolysosome or be released at the plasma membrane, leading to accumulation of Aβ in extracellular space and plaque formation.

No significant alteration of early endosome formation could be observed. B-cleavage takes place in early endosomes, from here Aβ is driven to multivesicular bodies (MVBs) and a fraction can be secreted by exosomes (Rajendran *et al.* 2006). Thus, the formation of endosomes would lead to amyloidogenic processing of APP. These results might point to a similar rate of APP processing, but also in accordance with the findings of Tamboli *et al.* (2011a) to a faster degradation of derivates in *Sms1*^{MUT} x *APPswe*^{Tg} in comparison to *Sms1*^{WT} x *APPswe*^{Tg}, which could contribute to the observed reduction in the number of SPs.

To check for differences in mTOR mediated autophagy induction and dosage effects, Rapamycin treated MEFs obtained from embryos of *Sms1* x *APPswe* breading were investigated. Results were similar to those obtained from brain lysates. With the highest dosage of Rapamycin, *Sms1*^{MUT} x *APPswe*^{Tg} MEFs showed a high LC3II/LC3I ratio and strong reduction in p62 levels, 4h after treatment. Compared to *Sms1*^{WT} x *APPswe*^{Tg} MEFs, *Sms1*^{MUT} x *APPswe*^{Tg} MEFs seem to be more sensitive to Rapamycin concerning amplitude and speed of autophagy induction, but also of autolysosomal turnover. This could be interpreted as a negative effect of SM on induction of autophagy and autolysosomal clearance.

4.14 *Sms1* is crucial for male fertility

One of the most prominent lipid fractions in sperm cell membranes is represented by PL with a high content of PUFAs, e.g. VLC-PUFA-SM. These lipids have a role in sperm capacitation, but are also found in Sertoli cells (Robinson *et al.* 1992, Lenzi *et al.* 1996, Cross 2000). The two SMSs responsible for SM generation - SMS1 and SMS2 have redundant and non-redundant functions in different organs. This was shown in knock-out animals of *Sms1* (Yano *et al.* 2011, Li *et al.* 2012, Lu *et al.* 2012), and *Sms2* (Hailemariam *et al.* 2008, Mitsutake *et al.* 2011). While there are no reports of spermatogenesis or fertility defects from *Sms2* knock-out animals, but normal reproduction was observed (Hailemariam *et al.* 2008, Liu *et al.* 2009b, Li *et al.* 2013), altered reproduction has been noted from male *Sms1* knock-out animals (Dong *et al.* 2012). Unlike this study by Dong et al., (2012), where complete infertility of male *Sms1* knock-out animals was stated, residual age dependent fertility in some male *Sms1*^{MUT} mice was observed. Controversial results might be explained by the remaining *Sms1* expression in the *Sms1*^{MUT} animals, as well as by potential differences in diet and age of the animals. A yet unknown role for SMS1 during spermatogenesis was described in *Sms1*^{MUT} animals, where disruption of *Sms1* expression leads to extended changes in the testicular lipid profile, especially in unsaturated FA containing species and sloughing of pachytene to late spermatid stages due to altered cell-cell contacts, including a dysfunctional BTB. Further, the observed accumulation of immature sperm in the epididymides of *Sms1*^{MUT}s is connected to progressive sub- to infertility, which could be in part rescued by DHA/EPA supplemented diet.

Testes SM levels of *Sms1*^{MUT} were 20% reduced as compared to *Sms1*^{WT} males, although VLC-PUFA-SMs (≥C24) were not quantified. This reduction is in agreement with previous reports (Dong *et al.* 2012, Li *et al.* 2012) and the remaining 80% are likely resulting from SMS2 activity and dietary uptake. One explanation for the different impact of SMS1 and SMS2 on male fertility is the subcellular localization and functional differences of both enzymes, as described above (Ternes *et al.* 2009, Holthuis and Menon 2014). The role of SMS1 includes the maintenance of intracellular SM homeostasis and generation of the bulk SM pool and its supply to the plasma membrane (Jeckel *et al.* 1990). The imbalance in the lipid metabolism, caused by disruption of *Sms1* in testes therefore affects intracellular, but also cell surface lipid composition, altering protein delivery, enzymatic activity and lipid based cell signaling, similar to other organs analyzed above.

4.14.1 The *Sms1* mutation altered the lipid profile of mutant testis

As stated before, although Cer and PC are the direct substrates of SMS1, they did not accumulate in *Sms1*^{MUT} testes. *Sms1*^{MUT}s maintained their levels of otherwise potentially cytotoxic Cer. As discussed above, Cer homeostasis is maintained mostly by enzymes other than SMS1. This was seen in previous studies on *Sms1*, where a complete knock-out had just marginal effects on Cer while knock-out of *Sms2* led to Cer elevation in plasma (Liu *et al.* 2009b, Mitsutake *et al.* 2011, Li *et al.* 2012). In parallel to unaltered Cer, unsaturated PCaa and PCae species were decreased. Reduction of specific PUFA (AA, EPA, DPA and DHA) containing lipids and an overall reduction in MUFA/SFA and PUFA/SFA ratios was found in the PCaa and less pronounced in the PCae profile. This alteration likely reduced the ability of Sertoli cells to support accumulation of LC-PUFA and VLC-PUFA in spermatozoa (Furland *et al.* 2007). The production of these PUFA-SMs, gaining importance during the germ cell maturation process, appears to be primarily derived from the activity of SMS1. The observed reduction in several unsaturated testicular PCaes, representing one of the major phospholipids of sperm membranes, together with a decrease in SM levels, alters membrane properties and thus affects the special composition crucial for the interaction and communication between Sertoli cells and spermatocytes necessary for the differentiation into mature sperm.

4.14.2 BTB functionality was compromised in *Sms1* mutants

Immature spermatogenic cell types ranging from pachytene to late spermatid stages were sloughed and accumulated in the epididymal lumen of *Sms1*^{MUT}s. A malfunction of the BTB as the reason for this sloughing phenotype is supported by several lines of evidence. Usually, the BTB is crossed by spermatocytes, when developing from preleptotene to leptotene stage. Meiotic prophase stage cells are held back, as long as they gain their special set of proteins and lipids, which primes them for the passage. Similar to the BBB, the BTB is made up of several distinct junction types, which build a dynamic network. In the BTB these junctions link Sertoli/Sertoli and Sertoli/germ cells, thereby regulating the passage of germ cells from the basal to the adluminal compartment (Hermo *et al.* 2010, Mital *et al.* 2011). Indications for a BTB deficiency in *Sms1*^{MUT} arose from altered junction

protein levels, mirroring those seen in the BBB. Elevated β-catenin and Cx43 were observed, representing subunits of AJ and GJ, respectively (Risley *et al.* 1992, Mital *et al.* 2011). Another GJ-protein, connexin-31 (CX31, encoded by *Gjb3*) showed elevated expression in testes microarray studies. Connexins represent a highly flexible system for intercellular contact and communication as they are continuously synthesized and degraded and are known to influence expression levels of other junctional proteins (Carette *et al.* 2010, Mital *et al.* 2011). The observed increase in testicular junction proteins may like in the brain result from disrupted TGN-mediated protein trafficking and protein secretion, which was shown to be dependent on SMS activity (Subathra *et al.* 2011). Although the subcellular localization of junctional proteins was found mostly unaltered in *Sms1*^{MUT}s, their elevated expression might reflect a disturbed Sertoli cell/germ cell interaction. The protein levels of occludin, one of the major component of TJ, had the tendency to be elevated as well in *Sms1*^{MUT}. TEM analysis of the TJ structure between Sertoli cells did not reveal any obvious morphological differences in the *Sms1*^{MUT} in comparison to *Sms1*^{WT} testes. However, the BTB is not established through TJ only, as AJ, GJ, channel proteins and transporters also play important roles in intercellular contacts and communication (Griswold 1995). After injection of ICG into tail veins of living animals followed by life imaging using MSOT we determined a significantly higher fluorescent signal from the testes lumen of *Sms1*^{MUT} animals. Different to the imaging results of the BBB, this clearly indicates BTB dysfunction and leakiness of this physiological barrier.

4.14.3 DHA/EPA diet rescued the sloughing phenotype of infertile *Sms1* mutants

Sms1^{MUT} males were found to suffer from age-dependent partial infertility, as indicated by a progressive loss in number of offspring and the decreasing ability to reproduce.

Several studies in different organisms suggested crucial role for PUFAs in male fertility already (Arscott *et al.* 1965, Zadravec *et al.* 2011, Gulliver *et al.* 2012, Yan *et al.* 2013). Additionally, epidemiological studies showed a negative impact of a SFA enriched diet ("Western diet") on the sperm quality in young men (Jensen *et al.* 2013). Evidence that the impact of PUFAs on spermatogenesis is mediated by a reduction of BTB integrity was recently described for the Δ^6-desaturase (*Fads2*) mutant mice (Stoffel *et al.* 2008, Roqueta-Rivera *et al.* 2010). *Fads2* knock-out animals shared phenotypic similarities with *Sms1*^{MUT} males, including specifically reduced DHA/EPA/ARA levels, a significant decrease in PUFA-PCaa and possible leakiness of the BTB. These common findings prompted us to supplement the diet of *Sms1*^{MUT} with n-3 PUFAs (DHA/EPA). DHA/EPA supplementation rescued the fertility status in 50% of animals tested to be infertile with normal diet. By taking into account that pregnancies last approximately three weeks and that the first litter was obtained 36 days after mating, a minimum treatment length of two weeks was calculated to be necessary to restore fertility in *Sms1*^{MUT} males. Given the fact that a full cycle of spermatogenesis takes 34 days in mice and is made up of four sub-cycles (8.6 days each), the current data support the hypothesis that DHA/EPA supplementation affects pachytene spermatocytes and spermatid stages (Hogarth and Griswold

2010). Rabionet *et al.* (2008), suggests that after passing the BTB and with the onset of *CerS3* expression, the production of SM (C16) and glycosphingolipids, which starts around prophase, switches to the production VLC-PUFAs (Rabionet *et al.* 2008). This would be in good agreement with the current findings, proposing that an external source of DHA/EPA delivers a sufficient supply for the restoration of decreased DHA and for the generation of VLC-PUFAs for pachytene spermatocytes. More recently, it was demonstrated by Rabionet *et al.* (2015) through a germ cell-specific knock-out of *CerS3* that the enzyme is involved in the formation of intercellular bridges (ICB) between syncytial spermatids. The cell-type specific knock-out of *CerS3* resulted in elevated apoptosis of spermatogenic cells (Rabionet *et al.* 2015), similarly to the phenotype of *Sms1*^{MUT} animals as ICB stability is based on ultra-long PUFA-containing SMs. Histological analysis revealed a high numbers of mature spermatozoa in epididymides of DHA/EPA-fed offspring-producing *Sms1*^{MUT} males, while only few rounded cells remained present. This suggests further that a longer treatment duration might be even more effective in restoring male fertility.

Although, the exact cause for sloughing of germ cells in *Sms1*^{MUT}s is not entirely clear, the results indicate some of the following mechanism involved. 1) A dysfunctional BTB, which is initiated in *Sms1*^{MUT}, as it was demonstrated by the existence of TJs seen in TEM and marker analysis, but also seems to be leaky, reflected by higher absorbance rates in MSOT. 2) A hampered production of LC-PUFAs, which seems to gain importance after the passage of the BTB, as it was shown by the reduction in AA, EPA, DPA and DHA containing PCaas and PCaes, and restoration of EPA/DHA levels. 3) Abnormal regulation of inter-cellular contacts and cell-cell communication after the passage of the BTB, indicated by the increase of adluminal junctional proteins.

These findings, together with the time window required to rescue fertility underline that sloughing occurred immediately after crossing the BTB, representing the time point in germ cell maturation, when PUFAs gain importance.

In summary, in absence of SMS1, the testical levels and composition of major phospholipids PCaa, PCae, SM and lyso-PC are altered. Especially the reduction in phospholipid n-3/6 PUFA content, important in the later stages of sperm development, cause male infertility. Infertility is apparently mediated by the altered formation of specified junctions between Sertoli- and maturating germ cells and likely by reduction of ICB formation, which contributes to sloughing of these stages to the epididymis. DHA/EPA supplemented diet provides both cell types with essential PUFAs, partially rescuing the observed sloughing and fertility, validating the link between SMS1-induced loss of these PUFAs and male infertility.

5. Conclusion

Sms1 could be shown to have tissue specific splice variants and that a disruption of the gene by gen-trap cassette insertion crucially affects SM levels independent on the genetic background, as a similar reduction with gene disruption was observed in the *Sms1* and the *Sms1* x *APPswe* mouse line. SMS2 was not able to compensate this loss. Additionally to SM, SMS1 substrates, such as Cer and PC species were affected. In *Sms1*^{MUT} PCaa and PCae levels correlate negatively with FA-chain length and saturation state, possibly also including action of SMS1 on Δ^9-desaturase and elongases. However, the alterations in chain length did not persist in the *Sms1* x *APPswe* mouse line, pointing to a background specific modulation. These reduced levels of MUFAs and PUFAs and particularly the reduction in SM are proposed to be the cause for reduced brain weights in *Sms1*^{MUT} x *APPswe*^{WT} and *Sms1*^{MUT} x *APPswe*^{Tg} animals, connected to myelination defects. These were found in the PNS and/or CNS of *Sms1*^{MUT} and *Sms1*^{MUT} x *APPswe*^{Tg}, leading to slightly worse performance in motor and nociception tasks in *Sms1*^{MUT}.

Sms1^{MUT} were found to suffer from age-dependent splenomegaly, possibly connected to enhanced inflammation and reduced CatD and AIF mediated apoptosis. Furthermore, *Sms1*^{MUT} males were subfertile, with an age-dependent decline in fertility. It could be shown that sloughing of germ cells occurs between the pachytene spermatocyte and round spermatid stage. This early loss of germ cells is likely to involve BTB dysfunction caused by miss-communication between Sertoli cells and germ cells and hampered ICB formation, leading to a disruption of the specific microenvironment, needed for germ cell maturation. It is proposed, that this effect is due to the lack of essential LC-PUFAs in the testes, such as DHA and EPA. DHA/EPA supplemented diet was sufficient to rescue the infertility phenotype in 50% of formerly infertile male *Sms1*^{MUT}.

Sms1^{MUT} x *APPswe*^{Tg} animals were born below Mendelian ratios and unexpectedly suffered from pre-mature death, at an age of 8 weeks, although both single mutant animal models have normal or just slightly reduced life expectancies. Furthermore, *Sms1*^{MUT} x *APPswe*^{Tg} animals had reduced weight gain during the first month. In *Sms1*^{MUT} x *APPswe*^{Tg} specific AA, and/orEPA and/or DPA containing PCaa and PCae species were accumulated, which together with enhanced lyso-PCs might be indicative of an elevated release of these PUFAs, serving as anti-inflammatory lipid mediators. Consistent with these observations, microglial activation, monitored by CD68 and Iba-1, was found to be slightly, but not significantly reduced in brain samples of *Sms1*^{MUT} x *APPswe*^{WT} and *Sms1*^{MUT} x *APPswe*^{Tg}. Thus, data on neuronal inflammation needs to be elucidated further.

Amyloidogenic processing in *Sms1*^{MUT} x *APPswe*^{Tg} was altered, leading to slightly lower Aβ levels and a reduced number of Aβ40-positive plaques, but without affecting Aβ42 plaque count. As mechanisms contributing to plaque prevention an altered autophagic process was proposed, which seemed to be enhanced in induction and in autophagic clearance.

On the behavioral level *Sms1*^{MUT} and *Sms1*^{MUT} x *APPswe*^{Tg} animals display an increased level of voluntary movement, additionally to altered HPA-axis signaling, which could be found in *Sms1*^{MUT} and was connected to higher stress-resistance. AD is negatively correlated with physical activity and chronic stress, thus, these results could be interpreted as a beneficial behavior concerning AD risk. Further behavioral testing of *Sms1*^{MUT} x *APPswe*^{Tg} animals did not reveal any genotype effect in memory performance in early life.

APP was found to be additionally expressed and cleaved in heart and lung, with slightly higher levels of Aβ generated in the *Sms1*^{MUT} x *APPswe*^{Tg} and higher IgG levels in heart samples, which could be shown to not infiltrate the brain. Thus, in summary these results could be interpreted in a way that the disruption of *Sms1* in *Sms1*^{MUT} x *APPswe*^{Tg} mice had a protective effect on AD-related aspects such as APP cleavage, autophagic clearance and plaque formation in the brain. Additionally neuro-inflammation might be reduced. Nevertheless, survival rates of these animals were strongly affected, which might be connected to APP processing in heart and lung and an enhanced accumulation of Aβ in these tissues.

6. List of Figures

7. List of Tables

8. List of abbreviations

ABBREVIATION	MEANING
aa	amino acid
AA	aracidonic acid
AAR	alternate arm return
ABCA7	ATP-Binding Cassette Sub-Family A Member 7
ACC	acetyl-CoA carboxylase
aCDase	acidic ceramidase
Acer	alkaline ceramidase
ACh	acetylcholine
ACTH	adenocorticotrophin releasing hormone
AD	Alzheimer 's disease
ADAM	A Disintegrin And Metalloproteinase
ADAM10	α-secretase
AICD	APP intracellular domain
AIF	apoptosis inducing factor
AJ	adherends junction
alkSMase	alkaline Smase
AMPK	AMP-activated protein kinase
ANOVA	analysis of variance
APH-1	anterior pharynx defective 1
ApoE	apolipoprotein E
APP	amyloid precursor protein
APP695	amyloid precursor protein variant 695
APPswe	Swedish APP
Asah	N-acylsphingosine amidohydrolase
aSMAse, ASM	acidic SMase
Asp	asparagin
α-stub	alpha-stub
ATG	start codon
ATP	adenosin-triphosphate
Aβ	amyloid beta
Aβ40	amyloid-beta 40
Aβ42	amyloid-beta 42
BACE1	beta-site APP cleavage enzyme1
BCA	bicinchoninic acid assay
BBB	blood-brain-barrier
BDNF	brain-derived neurotropic factor
BIN1	bridging integrator 1
bp	base pair
β-stub	beta-stub
BTB	blood-testes-barrier
C1P	ceramide-1-phosphate
C57Bl/6J	black 6 j mouse strain
CA1	Cornu Amonis1
CatD	catepsin D
CBG	Corticosterone binding globulin
CD2A	CD2A antigen
CD3	CD3 antigen
CD33	CD33 antigen
CD4	CD4 antigen
CD68	CD68 antigen

CDP	cytidine di-phosphate
cDNA	Copy DNA
Cer	ceramide
CERK	ceramide kinase
CERT	ceramide transfer protein
CerS	ceramide synthase
CGT	ceramide galactosyl transferase
CHAP	Chicago Health and Aging Project
CHD	coronary heart disease
CHO-cells	chinese hamster ovary cells
Chol	cholesterol
circRNA	circular RNA
Clps	colipase
CLU	clusterin
CNS	central nervous system
CoA	coenzyme A
CORT	corticosterone
$cPLA_2$	cytosolic Phospholipase A 2
CPTP	ceramide-1-phosphate transfer protein
CR1	CR1 antigen
CRH	corticotrophin releasing hormone
CRHR	corticotrophin releasing hormone receptor
CSF	cerebrospinal fluid
CTF	C-terminal fragment
CTP	cytidine tri-phosphate
Cx43	connexin 43
DAG	diacylglycerol
DEA	diethanolamine
DES	desaturase
DMEM	Dulbecco's Modified Eagle Medium
DMSO	Dimethyl sulfoxide
DNA	desoxyribonucleic acid
de novo	de novo antigen
DHA	docosahexaenoic acid
DH-Sphingosine	dihydro-sphingosine
DPA	docosapentaenoic acid
DSMIV	Diagnostic and Statistical Manual of tMental Disorders IV
DUFA	diunsaturated fatty acids
ECL	Electrochemiluminescence
EEA1	Early Endosome Antigen 1
EHC	entorhineal cortex
EPA	eicosapentaenoic acid
ER	endoplasmatic reticulum
EtOH	ethanol
FA	fatty acid
FA	formamid acid agarose
FAD	familial AD
FCS	fetal calf serum
FDR	false discovery range
FGD	familial glococorticoid deficiency
FILM-FRET	fluorescence lifetime imaging microscopy - fluorescence recovery after photobleaching
g	gram
GalCer	galactosylceramide
GCS	glucosylceramide synthase
Gdpd1	Glycerophosphodiester Phosphodiesterase Domain Containing 1

GJ	gap junction
GluCer	glucosylceramide
GluCerS	glucosylceramide synthase
GM(1,2,3)	ganglioside GM1,2,3
GMC	german mouse clinic
GMP	guanosine monophosphate
Golgi	Golgi apparatus
Gpsn2, Tecr	Trans-2,3-Enoyl-CoA Reductase
GR, Nc2r1	glucocorticoid receptor
GSL	glycosphingolipid
HDL	high density lipoprotein
HET	heterozygous
HexCer	hexosylceramides
HMGCR, HMGR	beta-hydroxy beta-methylglutaryl-CoA reductase
HOM	homozygous
HPA	hypothalamus pituitary adrenal
HSL	hormone-sensitive lipase
Hz	Hertz
ICB	intercellular bridges
ICG	iodocyanin green
Iba-1	allograft inflammatory factor 1 (AIF1)
IFN-γ	interferron gamma
IgG	immunoglobulin G
IgG2b	immunoglobulin G2b
IHC	immunohistochemistry
IL-6	interleukin-6
IQR	inter quartal range
KDHR	3-keto-dihydro-sphingosine reductase
L	liter
LC	long chain
LC3, LC3B	microtubule-associated protein 1 light chain 3 (beta)
Ldlr	low density lipoprotein receptor
LMU	Ludiwg-Maximilian-Universität
LSD	lysosomal storage disease
LTR	long terminal repeat
lyso-PC	lyso-posphatidylcholine
MAPK	microtubule associated protein kinase
MAPT	microtubule associated protein tau
MBP	myelin basic protein
MCI	mild cognitive impairment
MCR, MC2R	adrenocorticotrophic receptor
MDR-1, Pgp-1	multi-drug resistance protein
MeOH	methanol
MES	2-(N-morpholino)ethanesulfonic acid
MFSD2A	major facilitator superfamiliy domain-containing protein 2A
MOB	medulla oblongata derived protein
MOG	myelin oligodendrocyte glycoprotein
MOPS	3-(N-morpholino)propanesulfonic acid
MR, Nc3r2	mineralocorticoid receptor
mRNA	messanger RNA
MS4A4E	membrane-spanning 4-domains, subfamily A, member 4E
MS4A6A	membrane-spanning 4-domains, subfamily A, member 6A
MSOT	multispectral optoacoustic tomography
MTL	medial temporal lobe
MUFA	monounsaturated fatty acids
MUT	mutant

MVB	multivesicular bodies
µl	micro liter
n-3	omega-3
n-6	omega-6
NADPH	nicotinamide adenine dinucleotide phosphate
nCDase	neutral ceramidase
NCT	nicastrin
NFT	neurofibrillary tangle
NMD	nonsense-mediated decay
nmol	nano Mol
NPD (NPA, NPB, NPC)	Niemann Pick disease (typeA, B, C)
nSMase	neutral sphingomyelinase
OB	olfactory bulb
OD	optical density
OF	open field
p3	p3 peptide
pA	poly A
PAF	platelet activating factor
PAP2	phosphatidic acid phosphatase type2/haloperoxidase domain
PAS	Periodic acid shiff
PC	phohphatidylcholine
PCaa	diacyl-phosphatidylcholine
PCae	acyl-ethyl-phosphatidylcholine
PCR	polymerase chain reaction
PE	phosphatidylethanolamine
PEN-2	presenilin enhancer 2
PET	positron emission tomography
PFC	prefrontal cortex
pH	power of hydrogen
PHCA	phytoceramidase, alkaline
PICALM	phosphatidylinositol binding clathrin assembly protein
PKA	protein kinase A
PL	phospholipid
Pla1a	phospholipase A1 member A
PLA2	phospholipase A2
PM	plasma membrane
PNS	periferal nervous system
pA, polyA	poly adenin
POMC	pro-opiomelanocortin
Prkaa2	protein kinase, AMP-activated, alpha 2 catalytic subunit
PS	phosphatidylserine
PS1	presinilin 1
PS2	presinilin 2
PSEN-1	locus of PS1
PSEN-2	locus of PS2
pTAU	phosphorylated microtubule associated protein tau
PUFA	ployunsaturated fatty acids
PVDF	Polyvinylidene fluoride
PVN	paraventricular nucleus
RP	red pulp
RT	room temperature
RT-PCR	reverse transcription polymerase chain reaction
RNA	ribonucleic acid
ROS	reactive oxygen species
RvE	resolvins of the E-series
S-1-P	sphingosine-1-phosphate

SA	splicing adapter
SAD	sporadic AD
SAM	sterile alpha motive
s-APPα	soluble amyloid precursor peptide-a
s-APPβ	soluble amyloid precursor peptide-b
SAR	same arm return
SD	standard deviation
SDS	sodium-docecyl-sulfate
SEM	standard error of the mean
SFA	saturated fatty acids
siRNA	small interfering RNA
SJL	SJL antigen
SL	sphingolipid
SM	sphingomyelin
SMase	sphingomyelinase
Smpd	sphingomyelin phosphodiesterase
SMS	sphingomyelin synthase
SMSr	sphingomyelin synthase related protein
SP	senile plaques
SPA	spatial pattern alteration
SphK	sphingosine kinase
SPT	serine palmitoyltransferase
SPTLC2	Serine Palmitoyltransferase, Long Chain Base Subunit 2
SRT	stress reactivity test
StAR	steroidogenic acute regulatroy protein
SVM-RFE	Support Vector Mahine. Recursive Feature Extraction
TAU, MAPT	microtubule associated protein tau
TBS-T	tris-buffered saline and Tween 20
Tecr, Gspn2	trans-2,3-enoyl-CoA reductase
TEM	transmission electron microscopy
Tg	transgenic
Tg2576	h*APPswe* transgenic mouse line
TGN	trans-Golgi-network
TJ	tight junction
TM	transmembrane
TMD	transmembrane domain
TMEM23	transmembrane protein 23
TUNEL	terminal deoxynucleotidyl transferase dUTP nick end labeling
UDP	uridine-diphosphat
UV	ultra-violett
V	Volt
V1B	vasopression receptor 1b
VEH_2O	purified water
VLC	very long chain
W	Watt
WP	white pulp
WT	wild-type
ZAP-70	ZAP-70 antigen

9. References

Abbott, A., 2011. Dementia: A problem for our age. Nature 475 (7355), S2-4.

Abo El-Khair, D.M., El-Safti Fel, N., Nooh, H.Z., El-Mehi, A.E., 2014. A comparative study on the effect of high cholesterol diet on the hippocampal ca1 area of adult and aged rats. Anat Cell Biol 47 (2), 117-26.

Adolph, S., Fuhrmann, H., Schumann, J., 2012. Unsaturated fatty acids promote the phagocytosis of p. Aeruginosa and r. Equi by raw264.7 macrophages. Curr Microbiol 65 (6), 649-55.

Aguan, K., Scott, J., See, C.G., Sarkar, N.H., 1994. Characterization and chromosomal localization of the human homologue of a rat amp-activated protein kinase-encoding gene: A major regulator of lipid metabolism in mammals. Gene 149 (2), 345-50.

Alafuzoff, I., Pikkarainen, M., Arzberger, T., Thal, D.R., Al-Sarraj, S., Bell, J., Bodi, I., Budka, H., Capetillo-Zarate, E., Ferrer, I., Gelpi, E., Gentleman, S., Giaccone, G., Kavantzas, N., King, A., Korkolopoulou, P., Kovacs, G.G., Meyronet, D., Monoranu, C., Parchi, P., Patsouris, E., Roggendorf, W., Stadelmann, C., Streichenberger, N., Tagliavini, F., Kretzschmar, H., 2008. Inter-laboratory comparison of neuropathological assessments of beta-amyloid protein: A study of the brainnet europe consortium. Acta Neuropathol 115 (5), 533-46.

Alagiakrishnan, K., Gill, S.S., Fagarasanu, A., 2012. Genetics and epigenetics of alzheimer's disease. Postgrad Med J 88 (1043), 522-9.

Alakbarzade, V., Hameed, A., Quek, D.Q., Chioza, B.A., Baple, E.L., Cazenave-Gassiot, A., Nguyen, L.N., Wenk, M.R., Ahmad, A.Q., Sreekantan-Nair, A., Weedon, M.N., Rich, P., Patton, M.A., Warner, T.T., Silver, D.L., Crosby, A.H., 2015. A partially inactivating mutation in the sodium-dependent lysophosphatidylcholine transporter mfsd2a causes a non-lethal microcephaly syndrome. Nat Genet.

Alzheimer, A., Stelzmann, R.A., Schnitzlein, H.N., Murtagh, F.R., 1995. An english translation of alzheimer's 1907 paper, "uber eine eigenartige erkankung der hirnrinde". Clin Anat 8 (6), 429-31.

Andrieu-Abadie, N., Levade, T., 2002. Sphingomyelin hydrolysis during apoptosis. Biochim Biophys Acta 1585 (2-3), 126-34.

Anstey, K.J., Lipnicki, D.M., Low, L.F., 2008. Cholesterol as a risk factor for dementia and cognitive decline: A systematic review of prospective studies with meta-analysis. Am J Geriatr Psychiatry 16 (5), 343-54.

Antonakou, A., Skenderi, K.P., Chiou, A., Anastasiou, C.A., Bakoula, C., Matalas, A.L., 2013. Breast milk fat concentration and fatty acid pattern during the first six months in exclusively breastfeeding greek women. Eur J Nutr 52 (3), 963-73.

Arakane, F., King, S.R., Du, Y., Kallen, C.B., Walsh, L.P., Watari, H., Stocco, D.M., Strauss, J.F., 3rd, 1997. Phosphorylation of steroidogenic acute regulatory protein (star) modulates its steroidogenic activity. J Biol Chem 272 (51), 32656-62.

Arendash, G.W., King, D.L., 2002. Intra- and intertask relationships in a behavioral test battery given to tg2576 transgenic mice and controls. Physiol Behav 75 (5), 643-52.

Arends, Y.M., Duyckaerts, C., Rozemuller, J.M., Eikelenboom, P., Hauw, J.J., 2000. Microglia, amyloid and dementia in alzheimer disease. A correlative study. Neurobiol Aging 21 (1), 39-47.

Armstrong, R.A., 2014. A critical analysis of the 'amyloid cascade hypothesis'. Folia Neuropathol 52 (3), 211-25.

Arriza, J.L., Simerly, R.B., Swanson, L.W., Evans, R.M., 1988. The neuronal mineralocorticoid receptor as a mediator of glucocorticoid response. Neuron 1 (9), 887-900.

Arscott, G.H., Parker, J.E., Dickinson, E.M., 1965. Effect of dietary linoleic acid, vitamin e and ethoxyguin on fertility of male chickens. J Nutr 87 (1), 63-8.

Asai, M., Hattori, C., Szabo, B., Sasagawa, N., Maruyama, K., Tanuma, S., Ishiura, S., 2003. Putative function of adam9, adam10, and adam17 as app alpha-secretase. Biochem Biophys Res Commun 301 (1), 231-5.

Augustin, R., Lichtenthaler, S.F., Greeff, M., Hansen, J., Wurst, W., Trumbach, D., 2011. Bioinformatics identification of modules of transcription factor binding sites in alzheimer's disease-related genes by in silico promoter analysis and microarrays. Int J Alzheimers Dis 2011, 154325.

Aviv, T., Lin, Z., Lau, S., Rendl, L.M., Sicheri, F., Smibert, C.A., 2003. The rna-binding sam domain of smaug defines a new family of post-transcriptional regulators. Nat Struct Biol 10 (8), 614-21.

Bandaru, V.V., Troncoso, J., Wheeler, D., Pletnikova, O., Wang, J., Conant, K., Haughey, N.J., 2009. Apoe4 disrupts sterol and sphingolipid metabolism in alzheimer's but not normal brain. Neurobiol Aging 30 (4), 591-9.

Barberger-Gateau, P., Letenneur, L., Deschamps, V., Peres, K., Dartigues, J.F., Renaud, S., 2002. Fish, meat, and risk of dementia: Cohort study. BMJ 325 (7370), 932-3.

Barberger-Gateau, P., Raffaitin, C., Letenneur, L., Berr, C., Tzourio, C., Dartigues, J.F., Alperovitch, A., 2007. Dietary patterns and risk of dementia: The three-city cohort study. Neurology 69 (20), 1921-30.

Barman, A., Schurer, S., Prabhakar, R., 2011. Computational modeling of substrate specificity and catalysis of the beta-secretase (bace1) enzyme. Biochemistry 50 (20), 4337-49.

Bartzokis, G., 2004. Age-related myelin breakdown: A developmental model of cognitive decline and alzheimer's disease. Neurobiol Aging 25 (1), 5-18; author reply 49-62.

Bayer, T.A., Cappai, R., Masters, C.L., Beyreuther, K., Multhaup, G., 1999. It all sticks together--the app-related family of proteins and alzheimer's disease. Mol Psychiatry 4 (6), 524-8.

Beeler, T., Bacikova, D., Gable, K., Hopkins, L., Johnson, C., Slife, H., Dunn, T., 1998. The saccharomyces cerevisiae tsc10/ybr265w gene encoding 3-ketosphinganine reductase is identified in a screen for temperature-sensitive suppressors of the ca2+-sensitive csg2delta mutant. J Biol Chem 273 (46), 30688-94.

Ben-Zvi, A., Lacoste, B., Kur, E., Andreone, B.J., Mayshar, Y., Yan, H., Gu, C., 2014. Mfsd2a is critical for the formation and function of the blood-brain barrier. Nature 509 (7501), 507-11.

Benes, P., Vetvicka, V., Fusek, M., 2008. Cathepsin d--many functions of one aspartic protease. Crit Rev Oncol Hematol 68 (1), 12-28.

Benzing, W.C., Wujek, J.R., Ward, E.K., Shaffer, D., Ashe, K.H., Younkin, S.G., Brunden, K.R., 1999. Evidence for glial-mediated inflammation in aged app(sw) transgenic mice. Neurobiol Aging 20 (6), 581-9.

Berger, J.H., Charron, M.J., Silver, D.L., 2012. Major facilitator superfamily domain-containing protein 2a (mfsd2a) has roles in body growth, motor function, and lipid metabolism. PLoS One 7 (11), e50629.

Bergmans, B.A., De Strooper, B., 2010. Gamma-secretases: From cell biology to therapeutic strategies. Lancet Neurol 9 (2), 215-26.

Bernardo, K., Hurwitz, R., Zenk, T., Desnick, R.J., Ferlinz, K., Schuchman, E.H., Sandhoff, K., 1995. Purification, characterization, and biosynthesis of human acid ceramidase. J Biol Chem 270 (19), 11098-102.

Betz, M.J., Hatiboglu, N., Mauracher, B., Hadaschik, D., Sauter, A., Demmelmair, H., Koletzko, B., Beuschlein, F., Slawik, M., 2012. Mc2 receptor knockdown modulates differentiation and lipid composition in adipocytes. Horm Metab Res 44 (9), 670-5.

Bhattacharyya, R., Barren, C., Kovacs, D.M., 2013. Palmitoylation of amyloid precursor protein regulates amyloidogenic processing in lipid rafts. J Neurosci 33 (27), 11169-83.

Bidere, N., Lorenzo, H.K., Carmona, S., Laforge, M., Harper, F., Dumont, C., Senik, A., 2003. Cathepsin d triggers bax activation, resulting in selective apoptosis-inducing factor (aif) relocation in t lymphocytes entering the early commitment phase to apoptosis. J Biol Chem 278 (33), 31401-11.

Blaak, E., 2001. Gender differences in fat metabolism. Curr Opin Clin Nutr Metab Care 4 (6), 499-502.

Boath, A., Graf, C., Lidome, E., Ullrich, T., Nussbaumer, P., Bornancin, F., 2008. Regulation and traffic of ceramide 1-phosphate produced by ceramide kinase: Comparative analysis to glucosylceramide and sphingomyelin. J Biol Chem 283 (13), 8517-26.

Boggs, J.M., 2006. Myelin basic protein: A multifunctional protein. Cell Mol Life Sci 63 (17), 1945-61.

Boland, B., Kumar, A., Lee, S., Platt, F.M., Wegiel, J., Yu, W.H., Nixon, R.A., 2008. Autophagy induction and autophagosome clearance in neurons: Relationship to autophagic pathology in alzheimer's disease. J Neurosci 28 (27), 6926-37.

Bolton, S.J., Anthony, D.C., Perry, V.H., 1998. Loss of the tight junction proteins occludin and zonula occludens-1 from cerebral vascular endothelium during neutrophil-induced blood-brain barrier breakdown in vivo. Neuroscience 86 (4), 1245-57.

Bosco, P., Gueant-Rodriguez, R.M., Anello, G., Spada, R.S., Romano, A., Caraci, F., Ferri, R., Gueant, J.L., 2005. Allele epsilon 4 of apoe is a stronger predictor of alzheimer risk in sicily than in continental south italy. Neurosci Lett 388 (3), 168-72.

Boulay, A.C., Mazeraud, A., Cisternino, S., Saubamea, B., Mailly, P., Jourdren, L., Blugeon, C., Mignon, V., Smirnova, M., Cavallo, A., Ezan, P., Ave, P., Dingli, F., Loew, D., Vieira, P., Chretien, F., Cohen-Salmon, M., 2015. Immune quiescence of the brain is set by astroglial connexin 43. J Neurosci 35 (10), 4427-39.

Bowman, G.L., Kaye, J.A., Moore, M., Waichunas, D., Carlson, N.E., Quinn, J.F., 2007. Blood-brain barrier impairment in alzheimer disease: Stability and functional significance. Neurology 68 (21), 1809-14.

Braak, H., Braak, E., 1991. Neuropathological stageing of alzheimer-related changes. Acta Neuropathol 82 (4), 239-59.

Braak, H., Braak, E., 1995. Staging of alzheimer's disease-related neurofibrillary changes. Neurobiol Aging 16 (3), 271-8; discussion 278-84.

Brown, J.R., Daar, I.O., Krug, J.R., Maquat, L.E., 1985. Characterization of the functional gene and several processed pseudogenes in the human triosephosphate isomerase gene family. Mol Cell Biol 5 (7), 1694-706.

Buccinna, B., Piccinini, M., Prinetti, A., Scandroglio, F., Prioni, S., Valsecchi, M., Votta, B., Grifoni, S., Lupino, E., Ramondetti, C., Schuchman, E.H., Giordana, M.T., Sonnino, S., Rinaudo, M.T., 2009. Alterations of myelin-specific proteins and sphingolipids characterize the brains of acid sphingomyelinase-deficient mice, an animal model of niemann-pick disease type a. J Neurochem 109 (1), 105-15.

Burgess, A., Dubey, S., Yeung, S., Hough, O., Eterman, N., Aubert, I., Hynynen, K., 2014. Alzheimer disease in a mouse model: Mr imaging-guided focused ultrasound targeted to the hippocampus opens the blood-brain barrier and improves pathologic abnormalities and behavior. Radiology 273 (3), 736-45.

Butterfield, D.A., Reed, T., Newman, S.F., Sultana, R., 2007. Roles of amyloid beta-peptide-associated oxidative stress and brain protein modifications in the pathogenesis of alzheimer's disease and mild cognitive impairment. Free Radic Biol Med 43 (5), 658-77.

Cai, H., Wang, Y., Mccarthy, D., Wen, H., Borchelt, D.R., Price, D.L., Wong, P.C., 2001. Bace1 is the major beta-secretase for generation of abeta peptides by neurons. Nat Neurosci 4 (3), 233-4.

Capell, A., Beher, D., Prokop, S., Steiner, H., Kaether, C., Shearman, M.S., Haass, C., 2005. Gamma-secretase complex assembly within the early secretory pathway. J Biol Chem 280 (8), 6471-8.

Carette, D., Weider, K., Gilleron, J., Giese, S., Dompierre, J., Bergmann, M., Brehm, R., Denizot, J.P., Segretain, D., Pointis, G., 2010. Major involvement of connexin 43 in seminiferous epithelial junction dynamics and male fertility. Dev Biol 346 (1), 54-67.

Carman, G.M., Han, G.S., 2006. Roles of phosphatidate phosphatase enzymes in lipid metabolism. Trends Biochem Sci 31 (12), 694-9.

Carmeli, C., Donati, A., Antille, V., Viceic, D., Ghika, J., Von Gunten, A., Clarke, S., Meuli, R., Frackowiak, R.S., Knyazeva, M.G., 2013. Demyelination in mild cognitive impairment suggests progression path to alzheimer's disease. PLoS One 8 (8), e72759.

Cermakova, P., Eriksdotter, M., Lund, L.H., Winblad, B., Religa, P., Religa, D., 2015. Heart failure and alzheimer's disease. J Intern Med 277 (4), 406-25.

Chan, L.F., Clark, A.J., Metherell, L.A., 2008. Familial glucocorticoid deficiency: Advances in the molecular understanding of acth action. Horm Res 69 (2), 75-82.

Chang, P.A., Shao, H.B., Long, D.X., Sun, Q., Wu, Y.J., 2008. Isolation, characterization and molecular 3d model of human gde4, a novel membrane protein containing glycerophosphodiester phosphodiesterase domain. Mol Membr Biol 25 (6-7), 557-66.

Chao, F., Zhang, L., Luo, Y., Xiao, Q., Lv, F., He, Q., Zhou, C., Zhang, Y., Jiang, L., Jiang, R., Gu, H., Tang, Y., 2015. Running exercise reduces myelinated fiber loss in the dentate gyrus of the hippocampus in app/ps1 transgenic mice. Curr Alzheimer Res 12 (4), 377-83.

Chatterjee, S., Kolmakova, A., Miller, M., 2006. The role of the phospholipid sphingomyelin in heart disease. Curr Opin Investig Drugs 7 (3), 219-28.

Chen, X., Sun, A., Zou, Y., Ge, J., Lazar, J.M., Jiang, X.C., 2011. Impact of sphingomyelin levels on coronary heart disease and left ventricular systolic function in humans. Nutr Metab (Lond) 8 (1), 25.

Cheng, H., Zhou, Y., Holtzman, D.M., Han, X., 2010. Apolipoprotein e mediates sulfatide depletion in animal models of alzheimer's disease. Neurobiol Aging 31 (7), 1188-96.

Chida, D., Nakagawa, S., Nagai, S., Sagara, H., Katsumata, H., Imaki, T., Suzuki, H., Mitani, F., Ogishima, T., Shimizu, C., Kotaki, H., Kakuta, S., Sudo, K., Koike, T., Kubo, M., Iwakura, Y., 2007. Melanocortin 2 receptor is required for adrenal gland development, steroidogenesis, and neonatal gluconeogenesis. Proc Natl Acad Sci U S A 104 (46), 18205-10.

Choy, R.W., Cheng, Z., Schekman, R., 2012. Amyloid precursor protein (app) traffics from the cell surface via endosomes for amyloid beta (abeta) production in the trans-golgi network. Proc Natl Acad Sci U S A 109 (30), E2077-82.

Chrast, R., Saher, G., Nave, K.A., Verheijen, M.H., 2011. Lipid metabolism in myelinating glial cells: Lessons from human inherited disorders and mouse models. J Lipid Res 52 (3), 419-34.

Chung, S.Y., Moriyama, T., Uezu, E., Uezu, K., Hirata, R., Yohena, N., Masuda, Y., Kokubu, T., Yamamoto, S., 1995. Administration of phosphatidylcholine increases brain acetylcholine concentration and improves memory in mice with dementia. J Nutr 125 (6), 1484-9.

Cirrito, J.R., Deane, R., Fagan, A.M., Spinner, M.L., Parsadanian, M., Finn, M.B., Jiang, H., Prior, J.L., Sagare, A., Bales, K.R., Paul, S.M., Zlokovic, B.V., Piwnica-Worms, D., Holtzman, D.M., 2005. P-glycoprotein deficiency at the blood-brain barrier increases amyloid-beta deposition in an alzheimer disease mouse model. J Clin Invest 115 (11), 3285-90.

Clark, A.J., Baig, A.H., Noon, L., Swords, F.M., Hunyady, L., King, P.J., 2003. Expression, desensitization, and internalization of the acth receptor (mc2r). Ann N Y Acad Sci 994, 111-7.

Clarke, C.J., Snook, C.F., Tani, M., Matmati, N., Marchesini, N., Hannun, Y.A., 2006. The extended family of neutral sphingomyelinases. Biochemistry 45 (38), 11247-56.

Claus, R.A., Dorer, M.J., Bunck, A.C., Deigner, H.P., 2009. Inhibition of sphingomyelin hydrolysis: Targeting the lipid mediator ceramide as a key regulator of cellular fate. Curr Med Chem 16 (16), 1978-2000.

Coetzee, T., Li, X., Fujita, N., Marcus, J., Suzuki, K., Francke, U., Popko, B., 1996. Molecular cloning, chromosomal mapping, and characterization of the mouse udp-galactose:Ceramide galactosyltransferase gene. Genomics 35 (1), 215-22.

Cole, S.L., Vassar, R., 2007. The alzheimer's disease beta-secretase enzyme, bace1. Mol Neurodegener 2, 22.

Corcoran, C.A., He, Q., Ponnusamy, S., Ogretmen, B., Huang, Y., Sheikh, M.S., 2008. Neutral sphingomyelinase-3 is a DNA damage and nongenotoxic stress-regulated gene that is deregulated in human malignancies. Mol Cancer Res 6 (5), 795-807.

Corder, E.H., Saunders, A.M., Strittmatter, W.J., Schmechel, D.E., Gaskell, P.C., Small, G.W., Roses, A.D., Haines, J.L., Pericak-Vance, M.A., 1993. Gene dose of apolipoprotein e type 4 allele and the risk of alzheimer's disease in late onset families. Science 261 (5123), 921-3.

Cordy, J.M., Hooper, N.M., Turner, A.J., 2006. The involvement of lipid rafts in alzheimer's disease. Mol Membr Biol 23 (1), 111-22.

Coria, F., Moreno, A., Rubio, I., Garcia, M.A., Morato, E., Mayor, F., Jr., 1993. The cellular pathology associated with alzheimer beta-amyloid deposits in non-demented aged individuals. Neuropathol Appl Neurobiol 19 (3), 261-8.

Crang, A.J., Gilson, J.M., Li, W.W., Blakemore, W.F., 2004. The remyelinating potential and in vitro differentiation of mog-expressing oligodendrocyte precursors isolated from the adult rat cns. Eur J Neurosci 20 (6), 1445-60.

Cross, N.L., 2000. Sphingomyelin modulates capacitation of human sperm in vitro. Biol Reprod 63 (4), 1129-34.

Cutler, R.G., Kelly, J., Storie, K., Pedersen, W.A., Tammara, A., Hatanpaa, K., Troncoso, J.C., Mattson, M.P., 2004. Involvement of oxidative stress-induced abnormalities in ceramide and cholesterol metabolism in brain aging and alzheimer's disease. Proc Natl Acad Sci U S A 101 (7), 2070-5.

D'uscio, L.V., Das, P., Santhanam, A.V., He, T., Younkin, S.G., Katusic, Z.S., 2012. Activation of ppardelta prevents endothelial dysfunction induced by overexpression of amyloid-beta precursor protein. Cardiovasc Res 96 (3), 504-12.

Das, A.K., Uhler, M.D., Hajra, A.K., 2000. Molecular cloning and expression of mammalian peroxisomal trans-2-enoyl-coenzyme a reductase cdnas. J Biol Chem 275 (32), 24333-40.

De Bock, M., Vandenbroucke, R.E., Decrock, E., Culot, M., Cecchelli, R., Leybaert, L., 2014. A new angle on blood-cns interfaces: A role for connexins? FEBS Lett 588 (8), 1259-70.

De Strooper, B., Iwatsubo, T., Wolfe, M.S., 2012. Presenilins and gamma-secretase: Structure, function, and role in alzheimer disease. Cold Spring Harb Perspect Med 2 (1), a006304.

Degerman, E., Moos, M., Jr., Rascon, A., Vasta, V., Meacci, E., Smith, C.J., Lindgren, S., Andersson, K.E., Belfrage, P., Manganiello, V., 1994. Single-step affinity purification, partial structure and properties of human platelet cgmp inhibited camp phosphodiesterase. Biochim Biophys Acta 1205 (2), 189-98.

Delion, S., Chalon, S., Guilloteau, D., Besnard, J.C., Durand, G., 1996. Alpha-linolenic acid dietary deficiency alters age-related changes of dopaminergic and serotoninergic neurotransmission in the rat frontal cortex. J Neurochem 66 (4), 1582-91.

Dematteos, R.B., 2004. Apolipoprotein e dose-dependent modulation of beta-amyloid deposition in a transgenic mouse model of alzheimer's disease. J Mol Neurosci 23 (3), 255-62.

Dematteos, R.B., Rudel, L.L., Williams, D.L., 2001. Biochemical analysis of cell-derived apoe3 particles active in stimulating neurite outgrowth. J Lipid Res 42 (6), 976-87.

Deo, A.K., Borson, S., Link, J.M., Domino, K., Eary, J.F., Ke, B., Richards, T.L., Mankoff, D.A., Minoshima, S., O'sullivan, F., Eyal, S., Hsiao, P., Maravilla, K., Unadkat, J.D., 2014. Activity of p-glycoprotein, a beta-amyloid transporter at the blood-brain barrier, is compromised in patients with mild alzheimer disease. J Nucl Med 55 (7), 1106-11.

Dergunova, L.V., Rozhkova, A.V., Sudarkina, O.Y., Limborska, S.A., 2013. The use of alternative polyadenylation in the tissue-specific regulation of human sms1 gene expression. Mol Biol Rep.

Diaz, M., Fabelo, N., Ferrer, I., Gomez, T., Marin, R., 2014. Biophysical alterations in lipid rafts from human cerebral cortex associate with increased bace1/abetapp interaction in early stages of alzheimer's disease. J Alzheimers Dis.

Diaz, M.L., Fabelo, N., Marin, R., 2012. Genotype-induced changes in biophysical properties of frontal cortex lipid raft from app/ps1 transgenic mice. Front Physiol 3, 454.

Dickstein, D.L., Biron, K.E., Ujiie, M., Pfeifer, C.G., Jeffries, A.R., Jefferies, W.A., 2006. Abeta peptide immunization restores blood-brain barrier integrity in alzheimer disease. FASEB J 20 (3), 426-33.

Ding, T., Li, Z., Hailemariam, T., Mukherjee, S., Maxfield, F.R., Wu, M.P., Jiang, X.C., 2008. Sms overexpression and knockdown: Impact on cellular sphingomyelin and diacylglycerol metabolism, and cell apoptosis. J Lipid Res 49 (2), 376-85.

Dong, L., Watanabe, K., Itoh, M., Huan, C.R., Tong, X.P., Nakamura, T., Miki, M., Iwao, H., Nakajima, A., Sakai, T., Kawanami, T., Sawaki, T., Masaki, Y., Fukushima, T., Fujita, Y., Tanaka, M., Yano, M., Okazaki, T., Umehara, H., 2012. Cd4+ t-cell dysfunctions through the impaired lipid rafts ameliorate concanavalin a-induced hepatitis in sphingomyelin synthase 1-knockout mice. Int Immunol 24 (5), 327-37.

Duan, R.D., Bergman, T., Xu, N., Wu, J., Cheng, Y., Duan, J., Nelander, S., Palmberg, C., Nilsson, A., 2003a. Identification of human intestinal alkaline sphingomyelinase as a novel ecto-enzyme related to the nucleotide phosphodiesterase family. J Biol Chem 278 (40), 38528-36.

Duan, R.D., Cheng, Y., Hansen, G., Hertervig, E., Liu, J.J., Syk, I., Sjostrom, H., Nilsson, A., 2003b. Purification, localization, and expression of human intestinal alkaline sphingomyelinase. J Lipid Res 44 (6), 1241-50.

Duan, S., Guan, X., Lin, R., Liu, X., Yan, Y., Lin, R., Zhang, T., Chen, X., Huang, J., Sun, X., Li, Q., Fang, S., Xu, J., Yao, Z., Gu, H., 2015. Silibinin inhibits acetylcholinesterase activity and amyloid beta peptide aggregation: A dual-target drug for the treatment of alzheimer's disease. Neurobiol Aging 36 (5), 1792-807.

Edbauer, D., Winkler, E., Regula, J.T., Pesold, B., Steiner, H., Haass, C., 2003. Reconstitution of gamma-secretase activity. Nat Cell Biol 5 (5), 486-8.

Ehehalt, R., Keller, P., Haass, C., Thiele, C., Simons, K., 2003. Amyloidogenic processing of the alzheimer beta-amyloid precursor protein depends on lipid rafts. J Cell Biol 160 (1), 113-23.

El Bawab, S., Roddy, P., Qian, T., Bielawska, A., Lemasters, J.J., Hannun, Y.A., 2000. Molecular cloning and characterization of a human mitochondrial ceramidase. J Biol Chem 275 (28), 21508-13.

Engelhart, M.J., Geerlings, M.I., Ruitenberg, A., Van Swieten, J.C., Hofman, A., Witteman, J.C., Breteler, M.M., 2002. Diet and risk of dementia: Does fat matter?: The rotterdam study. Neurology 59 (12), 1915-21.

Esch, F.S., Keim, P.S., Beattie, E.C., Blacher, R.W., Culwell, A.R., Oltersdorf, T., Mcclure, D., Ward, P.J., 1990. Cleavage of amyloid beta peptide during constitutive processing of its precursor. Science 248 (4959), 1122-4.

Ezan, P., Andre, P., Cisternino, S., Saubamea, B., Boulay, A.C., Doutremer, S., Thomas, M.A., Quenech'du, N., Giaume, C., Cohen-Salmon, M., 2012. Deletion of astroglial connexins weakens the blood-brain barrier. J Cereb Blood Flow Metab 32 (8), 1457-67.

Fabelo, N., Martin, V., Marin, R., Moreno, D., Ferrer, I., Diaz, M., 2014. Altered lipid composition in cortical lipid rafts occurs at early stages of sporadic alzheimer's disease and facilitates app/bace1 interactions. Neurobiol Aging 35 (8), 1801-12.

Fabelo, N., Martin, V., Marin, R., Santpere, G., Aso, E., Ferrer, I., Diaz, M., 2012. Evidence for premature lipid raft aging in app/ps1 double-transgenic mice, a model of familial alzheimer disease. J Neuropathol Exp Neurol 71 (10), 868-81.

Fantini, J., Yahi, N., 2010. Molecular insights into amyloid regulation by membrane cholesterol and sphingolipids: Common mechanisms in neurodegenerative diseases. Expert Rev Mol Med 12, e27.

Faria, M.C., Goncalves, G.S., Rocha, N.P., Moraes, E.N., Bicalho, M.A., Gualberto Cintra, M.T., Jardim De Paula, J., Jose Ravic De Miranda, L.F., Clayton De Souza Ferreira, A., Teixeira, A.L., Gomes, K.B., Carvalho, M., Sousa, L.P., 2014. Increased plasma levels of bdnf and inflammatory markers in alzheimer's disease. J Psychiatr Res 53, 166-72.

Farooqui, A.A., Horrocks, L.A., 2006. Phospholipase a2-generated lipid mediators in the brain: The good, the bad, and the ugly. Neuroscientist 12 (3), 245-60.

Fassbender, K., Simons, M., Bergmann, C., Stroick, M., Lutjohann, D., Keller, P., Runz, H., Kuhl, S., Bertsch, T., Von Bergmann, K., Hennerici, M., Beyreuther, K., Hartmann, T., 2001. Simvastatin

strongly reduces levels of alzheimer's disease beta -amyloid peptides abeta 42 and abeta 40 in vitro and in vivo. Proc Natl Acad Sci U S A 98 (10), 5856-61.

Feijge, M.A., Ansink, K., Vanschoonbeek, K., Heemskerk, J.W., 2004. Control of platelet activation by cyclic amp turnover and cyclic nucleotide phosphodiesterase type-3. Biochem Pharmacol 67 (8), 1559-67.

Ferrari, A., Hoerndli, F., Baechi, T., Nitsch, R.M., Gotz, J., 2003. Beta-amyloid induces paired helical filament-like tau filaments in tissue culture. J Biol Chem 278 (41), 40162-8.

Ferreira, C.F., Bernardi, J.R., Bosa, V.L., Schuch, I., Goldani, M.Z., Kapczinski, F., Salum, G.A., Dalmaz, C., Manfro, G.G., Silveira, P.P., 2014. Correlation between n-3 polyunsaturated fatty acids consumption and bdnf peripheral levels in adolescents. Lipids Health Dis 13, 44.

Ferri, C.P., Prince, M., Brayne, C., Brodaty, H., Fratiglioni, L., Ganguli, M., Hall, K., Hasegawa, K., Hendrie, H., Huang, Y., Jorm, A., Mathers, C., Menezes, P.R., Rimmer, E., Scazufca, M., Alzheimer's Disease, I., 2005. Global prevalence of dementia: A delphi consensus study. Lancet 366 (9503), 2112-7.

Filippenkov, I.B., Sudarkina, O.Y., Limborska, S.A., Dergunova, L.V., 2015. Circular rna of the human sphingomyelin synthase 1 gene: Multiple splice variants, evolutionary conservatism and expression in different tissues. RNA Biol 12 (9), 1030-42.

Filley, C.M., 1997. Alzheimer's disease in women. Am J Obstet Gynecol 176 (1 Pt 1), 1-7.

Fillit, H.M., 2000. The pharmacoeconomics of alzheimer's disease. Am J Manag Care 6 (22 Suppl), S1139-44; discussion S1145-8.

Fjell, A.M., Walhovd, K.B., 2010. Structural brain changes in aging: Courses, causes and cognitive consequences. Rev Neurosci 21 (3), 187-221.

Forster, C., Silwedel, C., Golenhofen, N., Burek, M., Kietz, S., Mankertz, J., Drenckhahn, D., 2005. Occludin as direct target for glucocorticoid-induced improvement of blood-brain barrier properties in a murine in vitro system. J Physiol 565 (Pt 2), 475-86.

Forsyth, E., Ritzline, P.D., 1998. An overview of the etiology, diagnosis, and treatment of alzheimer disease. Phys Ther 78 (12), 1325-31.

Frautschy, S.A., Yang, F., Irrizarry, M., Hyman, B., Saido, T.C., Hsiao, K., Cole, G.M., 1998. Microglial response to amyloid plaques in appsw transgenic mice. Am J Pathol 152 (1), 307-17.

Fujimoto, H., Tadano-Aritomi, K., Tokumasu, A., Ito, K., Hikita, T., Suzuki, K., Ishizuka, I., 2000. Requirement of seminolipid in spermatogenesis revealed by udp-galactose: Ceramide galactosyltransferase-deficient mice. J Biol Chem 275 (30), 22623-6.

Fujino, Y., Negishi, T., Ito, S., 1968. Enzymic synthesis of sphingosylphosphorylcholine. Biochem J 109 (2), 310-1.

Fukumori, A., Okochi, M., Tagami, S., Jiang, J., Itoh, N., Nakayama, T., Yanagida, K., Ishizuka-Katsura, Y., Morihara, T., Kamino, K., Tanaka, T., Kudo, T., Tanii, H., Ikuta, A., Haass, C., Takeda, M., 2006. Presenilin-dependent gamma-secretase on plasma membrane and endosomes is functionally distinct. Biochemistry 45 (15), 4907-14.

Furland, N.E., Zanetti, S.R., Oresti, G.M., Maldonado, E.N., Aveldano, M.I., 2007. Ceramides and sphingomyelins with high proportions of very long-chain polyunsaturated fatty acids in mammalian germ cells. J Biol Chem 282 (25), 18141-50.

Futerman, A.H., Pagano, R.E., 1991. Determination of the intracellular sites and topology of glucosylceramide synthesis in rat liver. Biochem J 280 (Pt 2), 295-302.

Gabande-Rodriguez, E., Boya, P., Labrador, V., Dotti, C.G., Ledesma, M.D., 2014. High sphingomyelin levels induce lysosomal damage and autophagy dysfunction in niemann pick disease type a. Cell Death Differ 21 (6), 864-75.

Gaete, P.S., Lillo, M.A., Figueroa, X.F., 2014. Functional role of connexins and pannexins in the interaction between vascular and nervous system. J Cell Physiol 229 (10), 1336-45.

Gailus-Durner, V., Fuchs, H., Adler, T., Aguilar Pimentel, A., Becker, L., Bolle, I., Calzada-Wack, J., Dalke, C., Ehrhardt, N., Ferwagner, B., Hans, W., Holter, S.M., Holzlwimmer, G., Horsch, M., Javaheri, A., Kallnik, M., Kling, E., Lengger, C., Morth, C., Mossbrugger, I., Naton, B., Prehn, C.,

Puk, O., Rathkolb, B., Rozman, J., Schrewe, A., Thiele, F., Adamski, J., Aigner, B., Behrendt, H., Busch, D.H., Favor, J., Graw, J., Heldmaier, G., Ivandic, B., Katus, H., Klingenspor, M., Klopstock, T., Kremmer, E., Ollert, M., Quintanilla-Martinez, L., Schulz, H., Wolf, E., Wurst, W., De Angelis, M.H., 2009. Systemic first-line phenotyping. Methods Mol Biol 530, 463-509.

Gailus-Durner, V., Fuchs, H., Becker, L., Bolle, I., Brielmeier, M., Calzada-Wack, J., Elvert, R., Ehrhardt, N., Dalke, C., Franz, T.J., Grundner-Culemann, E., Hammelbacher, S., Holter, S.M., Holzlwimmer, G., Horsch, M., Javaheri, A., Kalaydjiev, S.V., Klempt, M., Kling, E., Kunder, S., Lengger, C., Lisse, T., Mijalski, T., Naton, B., Pedersen, V., Prehn, C., Przemeck, G., Racz, I., Reinhard, C., Reitmeir, P., Schneider, I., Schrewe, A., Steinkamp, R., Zybill, C., Adamski, J., Beckers, J., Behrendt, H., Favor, J., Graw, J., Heldmaier, G., Hofler, H., Ivandic, B., Katus, H., Kirchhof, P., Klingenspor, M., Klopstock, T., Lengeling, A., Muller, W., Ohl, F., Ollert, M., Quintanilla-Martinez, L., Schmidt, J., Schulz, H., Wolf, E., Wurst, W., Zimmer, A., Busch, D.H., De Angelis, M.H., 2005. Introducing the german mouse clinic: Open access platform for standardized phenotyping. Nat Methods 2 (6), 403-4.

Garcia, B., Rodriguez, R., Angulo, I., Heath, A.W., Howard, M.C., Subiza, J.L., 1996. Differential effects of transforming growth factor-beta 1 on iga vs. Igg2b production by lipopolysaccharide-stimulated lymph node b cells: A comparative study with spleen b cells. Eur J Immunol 26 (10), 2364-70.

Gault, C.R., Obeid, L.M., Hannun, Y.A., 2010. An overview of sphingolipid metabolism: From synthesis to breakdown. Adv Exp Med Biol 688, 1-23.

Geekiyanage, H., Chan, C., 2011. Microrna-137/181c regulates serine palmitoyltransferase and in turn amyloid beta, novel targets in sporadic alzheimer's disease. J Neurosci 31 (41), 14820-30.

Geeraert, L., Mannaerts, G.P., Van Veldhoven, P.P., 1997. Conversion of dihydroceramide into ceramide: Involvement of a desaturase. Biochem J 327 (Pt 1), 125-32.

Geilen, C.C., Wieder, T., Orfanos, C.E., 1997. Ceramide signalling: Regulatory role in cell proliferation, differentiation and apoptosis in human epidermis. Arch Dermatol Res 289 (10), 559-66.

Gelissen, I.C., Hochgrebe, T., Wilson, M.R., Easterbrook-Smith, S.B., Jessup, W., Dean, R.T., Brown, A.J., 1998. Apolipoprotein j (clusterin) induces cholesterol export from macrophage-foam cells: A potential anti-atherogenic function? Biochem J 331 (Pt 1), 231-7.

Gibellini, F., Smith, T.K., 2010. The kennedy pathway--de novo synthesis of phosphatidylethanolamine and phosphatidylcholine. IUBMB Life 62 (6), 414-28.

Gil, T., Ipsen, J.H., Mouritsen, O.G., Sabra, M.C., Sperotto, M.M., Zuckermann, M.J., 1998. Theoretical analysis of protein organization in lipid membranes. Biochim Biophys Acta 1376 (3), 245-66.

Ginsberg, L., Rafique, S., Xuereb, J.H., Rapoport, S.I., Gershfeld, N.L., 1995. Disease and anatomic specificity of ethanolamine plasmalogen deficiency in alzheimer's disease brain. Brain Res 698 (1-2), 223-6.

Giussani, P., Colleoni, T., Brioschi, L., Bassi, R., Hanada, K., Tettamanti, G., Riboni, L., Viani, P., 2008. Ceramide traffic in c6 glioma cells: Evidence for cert-dependent and independent transport from er to the golgi apparatus. Biochim Biophys Acta 1781 (1-2), 40-51.

Glavinas, H., Krajcsi, P., Cserepes, J., Sarkadi, B., 2004. The role of abc transporters in drug resistance, metabolism and toxicity. Curr Drug Deliv 1 (1), 27-42.

Glenner, G.G., Wong, C.W., 1984. Alzheimer's disease: Initial report of the purification and characterization of a novel cerebrovascular amyloid protein. Biochem Biophys Res Commun 120 (3), 885-90.

Godmann, M., Auger, V., Ferraroni-Aguiar, V., Di Sauro, A., Sette, C., Behr, R., Kimmins, S., 2007. Dynamic regulation of histone h3 methylation at lysine 4 in mammalian spermatogenesis. Biol Reprod 77 (5), 754-64.

Goldenberg, G., Schuri, U., Gromminger, O., Arnold, U., 1999. Basal forebrain amnesia: Does the nucleus accumbens contribute to human memory? J Neurol Neurosurg Psychiatry 67 (2), 163-8.

Gottfries, C.G., Balldin, J., Blennow, K., Brane, G., Karlsson, I., Regland, B., Wallin, A., 1994. Regulation of the hypothalamic-pituitary-adrenal axis in dementia disorders. Ann N Y Acad Sci 746, 336-43; discussion 343-4.

Govin, J., Caron, C., Lestrat, C., Rousseaux, S., Khochbin, S., 2004. The role of histones in chromatin remodelling during mammalian spermiogenesis. Eur J Biochem 271 (17), 3459-69.

Gowda, S., Yeang, C., Wadgaonkar, S., Anjum, F., Grinkina, N., Cutaia, M., Jiang, X.C., Wadgaonkar, R., 2011. Sphingomyelin synthase 2 (sms2) deficiency attenuates lps-induced lung injury. Am J Physiol Lung Cell Mol Physiol 300 (3), L430-40.

Grabowski, G.A., 2012. Gaucher disease and other storage disorders. Hematology Am Soc Hematol Educ Program 2012, 13-8.

Graf, C., Niwa, S., Muller, M., Kinzel, B., Bornancin, F., 2008. Wild-type levels of ceramide and ceramide-1-phosphate in the retina of ceramide kinase-like-deficient mice. Biochem Biophys Res Commun 373 (1), 159-63.

Greenberg, S.M., Rebeck, G.W., Vonsattel, J.P., Gomez-Isla, T., Hyman, B.T., 1995. Apolipoprotein e epsilon 4 and cerebral hemorrhage associated with amyloid angiopathy. Ann Neurol 38 (2), 254-9.

Griffin, W.S., Sheng, J.G., Roberts, G.W., Mrak, R.E., 1995. Interleukin-1 expression in different plaque types in alzheimer's disease: Significance in plaque evolution. J Neuropathol Exp Neurol 54 (2), 276-81.

Grimm, M.O., Grimm, H.S., Patzold, A.J., Zinser, E.G., Halonen, R., Duering, M., Tschape, J.A., De Strooper, B., Muller, U., Shen, J., Hartmann, T., 2005. Regulation of cholesterol and sphingomyelin metabolism by amyloid-beta and presenilin. Nat Cell Biol 7 (11), 1118-23.

Grimm, M.O., Grimm, H.S., Tomic, I., Beyreuther, K., Hartmann, T., Bergmann, C., 2008. Independent inhibition of alzheimer disease beta- and gamma-secretase cleavage by lowered cholesterol levels. J Biol Chem 283 (17), 11302-11.

Grimm, M.O., Grosgen, S., Riemenschneider, M., Tanila, H., Grimm, H.S., Hartmann, T., 2011a. From brain to food: Analysis of phosphatidylcholins, lyso-phosphatidylcholins and phosphatidylcholin-plasmalogens derivates in alzheimer's disease human post mortem brains and mice model via mass spectrometry. J Chromatogr A 1218 (42), 7713-22.

Grimm, M.O., Grosgen, S., Rothhaar, T.L., Burg, V.K., Hundsdorfer, B., Haupenthal, V.J., Friess, P., Muller, U., Fassbender, K., Riemenschneider, M., Grimm, H.S., Hartmann, T., 2011b. Intracellular app domain regulates serine-palmitoyl-coa transferase expression and is affected in alzheimer's disease. Int J Alzheimers Dis 2011, 695413.

Grimm, M.O., Kuchenbecker, J., Rothhaar, T.L., Grosgen, S., Hundsdorfer, B., Burg, V.K., Friess, P., Muller, U., Grimm, H.S., Riemenschneider, M., Hartmann, T., 2011c. Plasmalogen synthesis is regulated via alkyl-dihydroxyacetonephosphate-synthase by amyloid precursor protein processing and is affected in alzheimer's disease. J Neurochem 116 (5), 916-25.

Grimm, M.O., Rothhaar, T.L., Hartmann, T., 2012. The role of app proteolytic processing in lipid metabolism. Exp Brain Res 217 (3-4), 365-75.

Griswold, M.D., 1995. Interactions between germ cells and sertoli cells in the testis. Biol Reprod 52 (2), 211-6.

Grundke-Iqbal, I., Iqbal, K., Quinlan, M., Tung, Y.C., Zaidi, M.S., Wisniewski, H.M., 1986a. Microtubule-associated protein tau. A component of alzheimer paired helical filaments. J Biol Chem 261 (13), 6084-9.

Grundke-Iqbal, I., Iqbal, K., Tung, Y.C., Quinlan, M., Wisniewski, H.M., Binder, L.I., 1986b. Abnormal phosphorylation of the microtubule-associated protein tau (tau) in alzheimer cytoskeletal pathology. Proc Natl Acad Sci U S A 83 (13), 4913-7.

Gruning, N.M., Du, D., Keller, M.A., Luisi, B.F., Ralser, M., 2014. Inhibition of triosephosphate isomerase by phosphoenolpyruvate in the feedback-regulation of glycolysis. Open Biol 4, 130232.

Gu, M., Kerwin, J.L., Watts, J.D., Aebersold, R., 1997. Ceramide profiling of complex lipid mixtures by electrospray ionization mass spectrometry. Anal Biochem 244 (2), 347-56.

Guemez-Gamboa, A., Nguyen, L.N., Yang, H., Zaki, M.S., Kara, M., Ben-Omran, T., Akizu, N., Rosti, R.O., Rosti, B., Scott, E., Schroth, J., Copeland, B., Vaux, K.K., Cazenave-Gassiot, A., Quek, D.Q., Wong, B.H., Tan, B.C., Wenk, M.R., Gunel, M., Gabriel, S., Chi, N.C., Silver, D.L., Gleeson, J.G., 2015. Inactivating mutations in mfsd2a, required for omega-3 fatty acid transport in brain, cause a lethal microcephaly syndrome. Nat Genet.

Gulliver, C.E., Friend, M.A., King, B.J., Clayton, E.H., 2012. The role of omega-3 polyunsaturated fatty acids in reproduction of sheep and cattle. Anim Reprod Sci 131 (1-2), 9-22.

Haass, C., Hung, A.Y., Schlossmacher, M.G., Oltersdorf, T., Teplow, D.B., Selkoe, D.J., 1993a. Normal cellular processing of the beta-amyloid precursor protein results in the secretion of the amyloid beta peptide and related molecules. Ann N Y Acad Sci 695, 109-16.

Haass, C., Hung, A.Y., Schlossmacher, M.G., Teplow, D.B., Selkoe, D.J., 1993b. Beta-amyloid peptide and a 3-kda fragment are derived by distinct cellular mechanisms. J Biol Chem 268 (5), 3021-4.

Haass, C., Kaether, C., Thinakaran, G., Sisodia, S., 2012. Trafficking and proteolytic processing of app. Cold Spring Harb Perspect Med 2 (5), a006270.

Haass, C., Steiner, H., 2002. Alzheimer disease gamma-secretase: A complex story of gxgd-type presenilin proteases. Trends Cell Biol 12 (12), 556-62.

Hailemariam, T.K., Huan, C., Liu, J., Li, Z., Roman, C., Kalbfeisch, M., Bui, H.H., Peake, D.A., Kuo, M.S., Cao, G., Wadgaonkar, R., Jiang, X.C., 2008. Sphingomyelin synthase 2 deficiency attenuates nfkappab activation. Arterioscler Thromb Vasc Biol 28 (8), 1519-26.

Halvorsen, D.S., Hansen, J.B., Grimsgaard, S., Bonaa, K.H., Kierulf, P., Nordoy, A., 1997. The effect of highly purified eicosapentaenoic and docosahexaenoic acids on monocyte phagocytosis in man. Lipids 32 (9), 935-42.

Hamer, G., Roepers-Gajadien, H.L., Van Duyn-Goedhart, A., Gademan, I.S., Kal, H.B., Van Buul, P.P., De Rooij, D.G., 2003. DNA double-strand breaks and gamma-h2ax signaling in the testis. Biol Reprod 68 (2), 628-34.

Han, X., D, M.H., Mckeel, D.W., Jr., Kelley, J., Morris, J.C., 2002. Substantial sulfatide deficiency and ceramide elevation in very early alzheimer's disease: Potential role in disease pathogenesis. J Neurochem 82 (4), 809-18.

Han, X., Holtzman, D.M., Mckeel, D.W., Jr., 2001. Plasmalogen deficiency in early alzheimer's disease subjects and in animal models: Molecular characterization using electrospray ionization mass spectrometry. J Neurochem 77 (4), 1168-80.

Hanada, K., 2003. Serine palmitoyltransferase, a key enzyme of sphingolipid metabolism. Biochim Biophys Acta 1632 (1-3), 16-30.

Hanada, K., Kumagai, K., Tomishige, N., Kawano, M., 2007. Cert and intracellular trafficking of ceramide. Biochim Biophys Acta 1771 (6), 644-53.

Hannun, Y.A., 1994. The sphingomyelin cycle and the second messenger function of ceramide. J Biol Chem 269 (5), 3125-8.

Hannun, Y.A., Luberto, C., Argraves, K.M., 2001. Enzymes of sphingolipid metabolism: From modular to integrative signaling. Biochemistry 40 (16), 4893-903.

Hardie, D.G., 1992. Regulation of fatty acid and cholesterol metabolism by the amp-activated protein kinase. Biochim Biophys Acta 1123 (3), 231-8.

Hardy, J., 2003. The relationship between amyloid and tau. J Mol Neurosci 20 (2), 203-6.

Hardy, J.A., Higgins, G.A., 1992. Alzheimer's disease: The amyloid cascade hypothesis. Science 256 (5054), 184-5.

Harris, B., Pereira, I., Parkin, E., 2009. Targeting adam10 to lipid rafts in neuroblastoma sh-sy5y cells impairs amyloidogenic processing of the amyloid precursor protein. Brain Res 1296, 203-15.

Hayashi, Y., Nemoto-Sasaki, Y., Tanikawa, T., Oka, S., Tsuchiya, K., Zama, K., Mitsutake, S., Sugiura, T., Yamashita, A., 2014. Sphingomyelin synthase 2, but not sphingomyelin synthase 1, is involved in hiv-1 envelope-mediated membrane fusion. J Biol Chem.

He, X., Huang, Y., Li, B., Gong, C.X., Schuchman, E.H., 2010. Deregulation of sphingolipid metabolism in alzheimer's disease. Neurobiol Aging 31 (3), 398-408.

Hermo, L., Pelletier, R.M., Cyr, D.G., Smith, C.E., 2010. Surfing the wave, cycle, life history, and genes/proteins expressed by testicular germ cells. Part 5: Intercellular junctions and contacts between germs cells and sertoli cells and their regulatory interactions, testicular cholesterol, and genes/proteins associated with more than one germ cell generation. Microsc Res Tech 73 (4), 409-94.

Hernando, F., Schoots, O., Lolait, S.J., Burbach, J.P., 2001. Immunohistochemical localization of the vasopressin v1b receptor in the rat brain and pituitary gland: Anatomical support for its involvement in the central effects of vasopressin. Endocrinology 142 (4), 1659-68.

Herrup, K., 2015. The case for rejecting the amyloid cascade hypothesis. Nat Neurosci 18 (6), 794-9.

Herschel, J., 1972. A scaled ratio of body weight to brain weight of a comparative index for relative importance of brain size in mammals of widely varying body mass. Psychol Rep 31 (1), 84-6.

Heude, B., Ducimetiere, P., Berr, C., Study, E.V.A., 2003. Cognitive decline and fatty acid composition of erythrocyte membranes--the eva study. Am J Clin Nutr 77 (4), 803-8.

Heverin, M., Maioli, S., Pham, T., Mateos, L., Camporesi, E., Ali, Z., Winblad, B., Cedazo-Minguez, A., Bjorkhem, I., 2015. 27-hydroxycholesterol mediates negative effects of dietary cholesterol on cognition in mice. Behav Brain Res 278, 356-9.

Hicks, D.A., Nalivaeva, N.N., Turner, A.J., 2012. Lipid rafts and alzheimer's disease: Protein-lipid interactions and perturbation of signaling. Front Physiol 3, 189.

Hirase, T., Staddon, J.M., Saitou, M., Ando-Akatsuka, Y., Itoh, M., Furuse, M., Fujimoto, K., Tsukita, S., Rubin, L.L., 1997. Occludin as a possible determinant of tight junction permeability in endothelial cells. J Cell Sci 110 (Pt 14), 1603-13.

Hjorth, E., Zhu, M., Toro, V.C., Vedin, I., Palmblad, J., Cederholm, T., Freund-Levi, Y., Faxen-Irving, G., Wahlund, L.O., Basun, H., Eriksdotter, M., Schultzberg, M., 2013. Omega-3 fatty acids enhance phagocytosis of alzheimer's disease-related amyloid-beta42 by human microglia and decrease inflammatory markers. J Alzheimers Dis 35 (4), 697-713.

Hogarth, C.A., Griswold, M.D., 2010. The key role of vitamin a in spermatogenesis. J Clin Invest 120 (4), 956-62.

Holcomb, L., Gordon, M.N., Mcgowan, E., Yu, X., Benkovic, S., Jantzen, P., Wright, K., Saad, I., Mueller, R., Morgan, D., Sanders, S., Zehr, C., O'campo, K., Hardy, J., Prada, C.M., Eckman, C., Younkin, S., Hsiao, K., Duff, K., 1998. Accelerated alzheimer-type phenotype in transgenic mice carrying both mutant amyloid precursor protein and presenilin 1 transgenes. Nat Med 4 (1), 97-100.

Holcomb, L.A., Gordon, M.N., Jantzen, P., Hsiao, K., Duff, K., Morgan, D., 1999. Behavioral changes in transgenic mice expressing both amyloid precursor protein and presenilin-1 mutations: Lack of association with amyloid deposits. Behav Genet 29 (3), 177-85.

Holthuis, J.C., Menon, A.K., 2014. Lipid landscapes and pipelines in membrane homeostasis. Nature 510 (7503), 48-57.

Horinouchi, K., Erlich, S., Perl, D.P., Ferlinz, K., Bisgaier, C.L., Sandhoff, K., Desnick, R.J., Stewart, C.L., Schuchman, E.H., 1995. Acid sphingomyelinase deficient mice: A model of types a and b niemann-pick disease. Nat Genet 10 (3), 288-93.

Hosono, T., Mouri, A., Nishitsuji, K., Jung, C.G., Kontani, M., Tokuda, H., Kawashima, H., Shibata, H., Suzuki, T., Nabehsima, T., Michikawa, M., 2015a. Arachidonic or docosahexaenoic acid diet prevents memory impairment in tg2576 mice. J Alzheimers Dis 48 (1), 149-62.

Hosono, T., Nishitsuji, K., Nakamura, T., Jung, C.G., Kontani, M., Tokuda, H., Kawashima, H., Kiso, Y., Suzuki, T., Michikawa, M., 2015b. Arachidonic acid diet attenuates brain abeta deposition in tg2576 mice. Brain Res 1613, 92-9.

Houben, E., Holleran, W.M., Yaginuma, T., Mao, C., Obeid, L.M., Rogiers, V., Takagi, Y., Elias, P.M., Uchida, Y., 2006. Differentiation-associated expression of ceramidase isoforms in cultured keratinocytes and epidermis. J Lipid Res 47 (5), 1063-70.

Hsiao, J.H., Fu, Y., Hill, A.F., Halliday, G.M., Kim, W.S., 2013. Elevation in sphingomyelin synthase activity is associated with increases in amyloid-beta peptide generation. PLoS One 8 (8), e74016.

Hsiao, K., Chapman, P., Nilsen, S., Eckman, C., Harigaya, Y., Younkin, S., Yang, F., Cole, G., 1996. Correlative memory deficits, abeta elevation, and amyloid plaques in transgenic mice. Science 274 (5284), 99-102.

Huang, R.R., Hu, W., Yin, Y.Y., Wang, Y.C., Li, W.P., Li, W.Z., 2015. Chronic restraint stress promotes learning and memory impairment due to enhanced neuronal endoplasmic reticulum stress in the frontal cortex and hippocampus in male mice. Int J Mol Med 35 (2), 553-9.

Huitema, K., Van Den Dikkenberg, J., Brouwers, J.F., Holthuis, J.C., 2004. Identification of a family of animal sphingomyelin synthases. EMBO J 23 (1), 33-44.

Hur, J.Y., Welander, H., Behbahani, H., Aoki, M., Franberg, J., Winblad, B., Frykman, S., Tjernberg, L.O., 2008. Active gamma-secretase is localized to detergent-resistant membranes in human brain. FEBS J 275 (6), 1174-87.

Hussain, I., Powell, D., Howlett, D.R., Tew, D.G., Meek, T.D., Chapman, C., Gloger, I.S., Murphy, K.E., Southan, C.D., Ryan, D.M., Smith, T.S., Simmons, D.L., Walsh, F.S., Dingwall, C., Christie, G., 1999. Identification of a novel aspartic protease (asp 2) as beta-secretase. Mol Cell Neurosci 14 (6), 419-27.

Ichimura, Y., Komatsu, M., 2010. Selective degradation of p62 by autophagy. Semin Immunopathol 32 (4), 431-6.

Igal, R.A., Wang, S., Gonzalez-Baro, M., Coleman, R.A., 2001. Mitochondrial glycerol phosphate acyltransferase directs the incorporation of exogenous fatty acids into triacylglycerol. J Biol Chem 276 (45), 42205-12.

Imgrund, S., Hartmann, D., Farwanah, H., Eckhardt, M., Sandhoff, R., Degen, J., Gieselmann, V., Sandhoff, K., Willecke, K., 2009. Adult ceramide synthase 2 (cers2)-deficient mice exhibit myelin sheath defects, cerebellar degeneration, and hepatocarcinomas. J Biol Chem 284 (48), 33549-60.

Imhoff-Kunsch, B., Briggs, V., Goldenberg, T., Ramakrishnan, U., 2012. Effect of n-3 long-chain polyunsaturated fatty acid intake during pregnancy on maternal, infant, and child health outcomes: A systematic review. Paediatr Perinat Epidemiol 26 Suppl 1, 91-107.

Irizarry, M.C., Mcnamara, M., Fedorchak, K., Hsiao, K., Hyman, B.T., 1997. Appsw transgenic mice develop age-related a beta deposits and neuropil abnormalities, but no neuronal loss in ca1. J Neuropathol Exp Neurol 56 (9), 965-73.

Ishii, M., Wang, G., Racchumi, G., Dyke, J.P., Iadecola, C., 2014. Transgenic mice overexpressing amyloid precursor protein exhibit early metabolic deficits and a pathologically low leptin state associated with hypothalamic dysfunction in arcuate neuropeptide y neurons. J Neurosci 34 (27), 9096-106.

Ishikawa, K., Mihara, Y., Gondoh, K., Suzuki, E., Asano, Y., 2000. X-ray structures of a novel acid phosphatase from escherichia blattae and its complex with the transition-state analog molybdate. EMBO J 19 (11), 2412-23.

Jahn, O., Tenzer, S., Werner, H.B., 2009. Myelin proteomics: Molecular anatomy of an insulating sheath. Mol Neurobiol 40 (1), 55-72.

Janelsins, M.C., Mastrangelo, M.A., Oddo, S., Laferla, F.M., Federoff, H.J., Bowers, W.J., 2005. Early correlation of microglial activation with enhanced tumor necrosis factor-alpha and monocyte chemoattractant protein-1 expression specifically within the entorhinal cortex of triple transgenic alzheimer's disease mice. J Neuroinflammation 2, 23.

Jarrett, J.T., Berger, E.P., Lansbury, P.T., Jr., 1993. The c-terminus of the beta protein is critical in amyloidogenesis. Ann N Y Acad Sci 695, 144-8.

Jeckel, D., Karrenbauer, A., Birk, R., Schmidt, R.R., Wieland, F., 1990. Sphingomyelin is synthesized in the cis golgi. FEBS Lett 261 (1), 155-7.

Jeckel, D., Karrenbauer, A., Burger, K.N., Van Meer, G., Wieland, F., 1992. Glucosylceramide is synthesized at the cytosolic surface of various golgi subfractions. J Cell Biol 117 (2), 259-67.

Jenkins, R.W., Canals, D., Hannun, Y.A., 2009. Roles and regulation of secretory and lysosomal acid sphingomyelinase. Cell Signal 21 (6), 836-46.

Jennemann, R., Sandhoff, R., Wang, S., Kiss, E., Gretz, N., Zuliani, C., Martin-Villalba, A., Jager, R., Schorle, H., Kenzelmann, M., Bonrouhi, M., Wiegandt, H., Grone, H.J., 2005. Cell-specific deletion of glucosylceramide synthase in brain leads to severe neural defects after birth. Proc Natl Acad Sci U S A 102 (35), 12459-64.

Jensen, M.M., Skarsfeldt, T., Hoy, C.E., 1996. Correlation between level of (n - 3) polyunsaturated fatty acids in brain phospholipids and learning ability in rats. A multiple generation study. Biochim Biophys Acta 1300 (3), 203-9.

Jensen, T.K., Heitmann, B.L., Jensen, M.B., Halldorsson, T.I., Andersson, A.M., Skakkebaek, N.E., Joensen, U.N., Lauritsen, M.P., Christiansen, P., Dalgard, C., Lassen, T.H., Jorgensen, N., 2013. High dietary intake of saturated fat is associated with reduced semen quality among 701 young danish men from the general population. Am J Clin Nutr 97 (2), 411-8.

Jiang, P., Mizushima, N., 2015. Lc3- and p62-based biochemical methods for the analysis of autophagy progression in mammalian cells. Methods 75, 13-8.

Jiang, Q., Lee, C.Y., Mandrekar, S., Wilkinson, B., Cramer, P., Zelcer, N., Mann, K., Lamb, B., Willson, T.M., Collins, J.L., Richardson, J.C., Smith, J.D., Comery, T.A., Riddell, D., Holtzman, D.M., Tontonoz, P., Landreth, G.E., 2008. Apoe promotes the proteolytic degradation of abeta. Neuron 58 (5), 681-93.

Johnson, G.V., Stoothoff, W.H., 2004. Tau phosphorylation in neuronal cell function and dysfunction. J Cell Sci 117 (Pt 24), 5721-9.

Jones, L., Holmans, P.A., Hamshere, M.L., Harold, D., Moskvina, V., Ivanov, D., Pocklington, A., Abraham, R., Hollingworth, P., Sims, R., Gerrish, A., Pahwa, J.S., Jones, N., Stretton, A., Morgan, A.R., Lovestone, S., Powell, J., Proitsi, P., Lupton, M.K., Brayne, C., Rubinsztein, D.C., Gill, M., Lawlor, B., Lynch, A., Morgan, K., Brown, K.S., Passmore, P.A., Craig, D., Mcguinness, B., Todd, S., Holmes, C., Mann, D., Smith, A.D., Love, S., Kehoe, P.G., Mead, S., Fox, N., Rossor, M., Collinge, J., Maier, W., Jessen, F., Schurmann, B., Heun, R., Kolsch, H., Van Den Bussche, H., Heuser, I., Peters, O., Kornhuber, J., Wiltfang, J., Dichgans, M., Frolich, L., Hampel, H., Hull, M., Rujescu, D., Goate, A.M., Kauwe, J.S., Cruchaga, C., Nowotny, P., Morris, J.C., Mayo, K., Livingston, G., Bass, N.J., Gurling, H., Mcquillin, A., Gwilliam, R., Deloukas, P., Al-Chalabi, A., Shaw, C.E., Singleton, A.B., Guerreiro, R., Muhleisen, T.W., Nothen, M.M., Moebus, S., Jockel, K.H., Klopp, N., Wichmann, H.E., Ruther, E., Carrasquillo, M.M., Pankratz, V.S., Younkin, S.G., Hardy, J., O'donovan, M.C., Owen, M.J., Williams, J., 2010. Genetic evidence implicates the immune system and cholesterol metabolism in the aetiology of alzheimer's disease. PLoS One 5 (11), e13950.

Jorm, A.F., Jolley, D., 1998. The incidence of dementia: A meta-analysis. Neurology 51 (3), 728-33.

Juranka, P.F., Zastawny, R.L., Ling, V., 1989. P-glycoprotein: Multidrug-resistance and a superfamily of membrane-associated transport proteins. FASEB J 3 (14), 2583-92.

Kalia, M., 2003. Dysphagia and aspiration pneumonia in patients with alzheimer's disease. Metabolism 52 (10 Suppl 2), 36-8.

Kalmijn, S., Launer, L.J., Ott, A., Witteman, J.C., Hofman, A., Breteler, M.M., 1997. Dietary fat intake and the risk of incident dementia in the rotterdam study. Ann Neurol 42 (5), 776-82.

Kalmijn, S., Van Boxtel, M.P., Ocke, M., Verschuren, W.M., Kromhout, D., Launer, L.J., 2004. Dietary intake of fatty acids and fish in relation to cognitive performance at middle age. Neurology 62 (2), 275-80.

Kalvodova, L., Kahya, N., Schwille, P., Ehehalt, R., Verkade, P., Drechsel, D., Simons, K., 2005. Lipids as modulators of proteolytic activity of bace: Involvement of cholesterol, glycosphingolipids, and anionic phospholipids in vitro. J Biol Chem 280 (44), 36815-23.

Kang, J., Lemaire, H.G., Unterbeck, A., Salbaum, J.M., Masters, C.L., Grzeschik, K.H., Multhaup, G., Beyreuther, K., Muller-Hill, B., 1987. The precursor of alzheimer's disease amyloid a4 protein resembles a cell-surface receptor. Nature 325 (6106), 733-6.

Karssen, A.M., Meijer, O.C., Van Der Sandt, I.C., Lucassen, P.J., De Lange, E.C., De Boer, A.G., De Kloet, E.R., 2001. Multidrug resistance p-glycoprotein hampers the access of cortisol but not of corticosterone to mouse and human brain. Endocrinology 142 (6), 2686-94.

Katsel, P., Li, C., Haroutunian, V., 2007. Gene expression alterations in the sphingolipid metabolism pathways during progression of dementia and alzheimer's disease: A shift toward ceramide accumulation at the earliest recognizable stages of alzheimer's disease? Neurochem Res 32 (4-5), 845-56.

Kawarabayashi, T., Younkin, L.H., Saido, T.C., Shoji, M., Ashe, K.H., Younkin, S.G., 2001. Age-dependent changes in brain, csf, and plasma amyloid (beta) protein in the tg2576 transgenic mouse model of alzheimer's disease. J Neurosci 21 (2), 372-81.

Khalil, A.M., Boyar, F.Z., Driscoll, D.J., 2004. Dynamic histone modifications mark sex chromosome inactivation and reactivation during mammalian spermatogenesis. Proc Natl Acad Sci U S A 101 (47), 16583-7.

Khalil, A.M., Driscoll, D.J., 2006. Histone h3 lysine 4 dimethylation is enriched on the inactive sex chromosomes in male meiosis but absent on the inactive x in female somatic cells. Cytogenet Genome Res 112 (1-2), 11-5.

Kihara, A., 2012. Very long-chain fatty acids: Elongation, physiology and related disorders. J Biochem 152 (5), 387-95.

Kihara, A., Igarashi, Y., 2004. Fvt-1 is a mammalian 3-ketodihydrosphingosine reductase with an active site that faces the cytosolic side of the endoplasmic reticulum membrane. J Biol Chem 279 (47), 49243-50.

Kilkus, J.P., Goswami, R., Dawson, S.A., Testai, F.D., Berdyshev, E.V., Han, X., Dawson, G., 2008. Differential regulation of sphingomyelin synthesis and catabolism in oligodendrocytes and neurons. J Neurochem 106 (4), 1745-57.

Kim, C.A., Bowie, J.U., 2003. Sam domains: Uniform structure, diversity of function. Trends Biochem Sci 28 (12), 625-8.

Kim, S.I., Yi, J.S., Ko, Y.G., 2006. Amyloid beta oligomerization is induced by brain lipid rafts. J Cell Biochem 99 (3), 878-89.

King, D.L., Arendash, G.W., 2002. Behavioral characterization of the tg2576 transgenic model of alzheimer's disease through 19 months. Physiol Behav 75 (5), 627-42.

Kinoshita, A., Fukumoto, H., Shah, T., Whelan, C.M., Irizarry, M.C., Hyman, B.T., 2003. Demonstration by fret of bace interaction with the amyloid precursor protein at the cell surface and in early endosomes. J Cell Sci 116 (Pt 16), 3339-46.

Klein, J., 2000. Membrane breakdown in acute and chronic neurodegeneration: Focus on choline-containing phospholipids. J Neural Transm 107 (8-9), 1027-63.

Knopman, D., Boland, L.L., Mosley, T., Howard, G., Liao, D., Szklo, M., Mcgovern, P., Folsom, A.R., Atherosclerosis Risk in Communities Study, I., 2001. Cardiovascular risk factors and cognitive decline in middle-aged adults. Neurology 56 (1), 42-8.

Koch, J., Gartner, S., Li, C.M., Quintern, L.E., Bernardo, K., Levran, O., Schnabel, D., Desnick, R.J., Schuchman, E.H., Sandhoff, K., 1996. Molecular cloning and characterization of a full-length complementary DNA encoding human acid ceramidase. Identification of the first molecular lesion causing farber disease. J Biol Chem 271 (51), 33110-5.

Kojro, E., Gimpl, G., Lammich, S., Marz, W., Fahrenholz, F., 2001. Low cholesterol stimulates the nonamyloidogenic pathway by its effect on the alpha -secretase adam 10. Proc Natl Acad Sci U S A 98 (10), 5815-20.

Kono, M., Dreier, J.L., Ellis, J.M., Allende, M.L., Kalkofen, D.N., Sanders, K.M., Bielawski, J., Bielawska, A., Hannun, Y.A., Proia, R.L., 2006. Neutral ceramidase encoded by the asah2 gene is essential for the intestinal degradation of sphingolipids. J Biol Chem 281 (11), 7324-31.

Koo, E.H., Sisodia, S.S., Archer, D.R., Martin, L.J., Weidemann, A., Beyreuther, K., Fischer, P., Masters, C.L., Price, D.L., 1990. Precursor of amyloid protein in alzheimer disease undergoes fast anterograde axonal transport. Proc Natl Acad Sci U S A 87 (4), 1561-5.

Kook, S.Y., Seok Hong, H., Moon, M., Mook-Jung, I., 2013. Disruption of blood-brain barrier in alzheimer disease pathogenesis. Tissue Barriers 1 (2), e23993.

Kosicek, M., Malnar, M., Goate, A., Hecimovic, S., 2010. Cholesterol accumulation in niemann pick type c (npc) model cells causes a shift in app localization to lipid rafts. Biochem Biophys Res Commun 393 (3), 404-9.

Kosicek, M., Zetterberg, H., Andreasen, N., Peter-Katalinic, J., Hecimovic, S., 2012. Elevated cerebrospinal fluid sphingomyelin levels in prodromal alzheimer's disease. Neurosci Lett 516 (2), 302-5.

Krabbe, G., Halle, A., Matyash, V., Rinnenthal, J.L., Eom, G.D., Bernhardt, U., Miller, K.R., Prokop, S., Kettenmann, H., Heppner, F.L., 2013. Functional impairment of microglia coincides with beta-amyloid deposition in mice with alzheimer-like pathology. PLoS One 8 (4), e60921.

Kruger, R.A., Liu, P., Fang, Y.R., Appledorn, C.R., 1995. Photoacoustic ultrasound (paus)--reconstruction tomography. Med Phys 22 (10), 1605-9.

Krut, O., Wiegmann, K., Kashkar, H., Yazdanpanah, B., Kronke, M., 2006. Novel tumor necrosis factor-responsive mammalian neutral sphingomyelinase-3 is a c-tail-anchored protein. J Biol Chem 281 (19), 13784-93.

Kubler, K., Tho Pesch, C., Gehrke, N., Riemann, S., Dassler, J., Coch, C., Landsberg, J., Wimmenauer, V., Polcher, M., Rudlowski, C., Tuting, T., Kuhn, W., Hartmann, G., Barchet, W., 2011. Immunogenic cell death of human ovarian cancer cells induced by cytosolic poly(i:C) leads to myeloid cell maturation and activates nk cells. Eur J Immunol 41 (10), 3028-39.

Kuhn, P.H., Wang, H., Dislich, B., Colombo, A., Zeitschel, U., Ellwart, J.W., Kremmer, E., Rossner, S., Lichtenthaler, S.F., 2010. Adam10 is the physiologically relevant, constitutive alpha-secretase of the amyloid precursor protein in primary neurons. EMBO J 29 (17), 3020-32.

Kumagai, K., Kawano, M., Shinkai-Ouchi, F., Nishijima, M., Hanada, K., 2007. Interorganelle trafficking of ceramide is regulated by phosphorylation-dependent cooperativity between the ph and start domains of cert. J Biol Chem 282 (24), 17758-66.

Kumagai, K., Yasuda, S., Okemoto, K., Nishijima, M., Kobayashi, S., Hanada, K., 2005. Cert mediates intermembrane transfer of various molecular species of ceramides. J Biol Chem 280 (8), 6488-95.

Kuthe, A., Eckel, H., Stief, C.G., Uckert, S., Forssmann, W.G., Jonas, U., Magert, H.J., 1999. Molecular biological characterization of phosphodiesterase 3a from human corpus cavernosum. Chem Biol Interact 119-120, 593-8.

Lacaze-Masmonteil, T., De Keyzer, Y., Luton, J.P., Kahn, A., Bertagna, X., 1987. Characterization of proopiomelanocortin transcripts in human nonpituitary tissues. Proc Natl Acad Sci U S A 84 (20), 7261-5.

Laske, C., Stransky, E., Leyhe, T., Eschweiler, G.W., Wittorf, A., Richartz, E., Bartels, M., Buchkremer, G., Schott, K., 2006. Stage-dependent bdnf serum concentrations in alzheimer's disease. J Neural Transm 113 (9), 1217-24.

Laufer, J., Delpy, D., Elwell, C., Beard, P., 2007. Quantitative spatially resolved measurement of tissue chromophore concentrations using photoacoustic spectroscopy: Application to the measurement of blood oxygenation and haemoglobin concentration. Phys Med Biol 52 (1), 141-68.

Lauritzen, L., Hansen, H.S., Jorgensen, M.H., Michaelsen, K.F., 2001. The essentiality of long chain n-3 fatty acids in relation to development and function of the brain and retina. Prog Lipid Res 40 (1-2), 1-94.

Laviad, E.L., Albee, L., Pankova-Kholmyansky, I., Epstein, S., Park, H., Merrill, A.H., Jr., Futerman, A.H., 2008. Characterization of ceramide synthase 2: Tissue distribution, substrate specificity, and inhibition by sphingosine 1-phosphate. J Biol Chem 283 (9), 5677-84.

Lee, J.H., Jeong, S.K., Kim, B.C., Park, K.W., Dash, A., 2015. Donepezil across the spectrum of alzheimer's disease: Dose optimization and clinical relevance. Acta Neurol Scand 131 (5), 259-67.

Lee, J.K., Jin, H.K., Park, M.H., Kim, B.R., Lee, P.H., Nakauchi, H., Carter, J.E., He, X., Schuchman, E.H., Bae, J.S., 2014. Acid sphingomyelinase modulates the autophagic process by controlling lysosomal biogenesis in alzheimer's disease. J Exp Med 211 (8), 1551-70.

Lee, J.T., Xu, J., Lee, J.M., Ku, G., Han, X., Yang, D.I., Chen, S., Hsu, C.Y., 2004. Amyloid-beta peptide induces oligodendrocyte death by activating the neutral sphingomyelinase-ceramide pathway. J Cell Biol 164 (1), 123-31.

Lehner, R., Kuksis, A., 1996. Biosynthesis of triacylglycerols. Prog Lipid Res 35 (2), 169-201.

Lentz, B.R., 2003. Exposure of platelet membrane phosphatidylserine regulates blood coagulation. Prog Lipid Res 42 (5), 423-38.

Lenzi, A., Picardo, M., Gandini, L., Dondero, F., 1996. Lipids of the sperm plasma membrane: From polyunsaturated fatty acids considered as markers of sperm function to possible scavenger therapy. Hum Reprod Update 2 (3), 246-56.

Li, C.M., Park, J.H., Simonaro, C.M., He, X., Gordon, R.E., Friedman, A.H., Ehleiter, D., Paris, F., Manova, K., Hepbildikler, S., Fuks, Z., Sandhoff, K., Kolesnick, R., Schuchman, E.H., 2002. Insertional mutagenesis of the mouse acid ceramidase gene leads to early embryonic lethality in homozygotes and progressive lipid storage disease in heterozygotes. Genomics 79 (2), 218-24.

Li, X.M., Smaby, J.M., Momsen, M.M., Brockman, H.L., Brown, R.E., 2000. Sphingomyelin interfacial behavior: The impact of changing acyl chain composition. Biophys J 78 (4), 1921-31.

Li, Y., Dong, J., Ding, T., Kuo, M.S., Cao, G., Jiang, X.C., Li, Z., 2013. Sphingomyelin synthase 2 activity and liver steatosis: An effect of ceramide-mediated proliferator-activated receptor gamma2 suppression. Arterioscler Thromb Vasc Biol.

Li, Y., Liu, L., Barger, S.W., Griffin, W.S., 2003. Interleukin-1 mediates pathological effects of microglia on tau phosphorylation and on synaptophysin synthesis in cortical neurons through a p38-mapk pathway. J Neurosci 23 (5), 1605-11.

Li, Z., Fan, Y., Liu, J., Li, Y., Huan, C., Bui, H.H., Kuo, M.S., Park, T.S., Cao, G., Jiang, X.C., 2012. Impact of sphingomyelin synthase 1 deficiency on sphingolipid metabolism and atherosclerosis in mice. Arterioscler Thromb Vasc Biol 32 (7), 1577-84.

Lichtenthaler, S.F., Haass, C., 2004. Amyloid at the cutting edge: Activation of alpha-secretase prevents amyloidogenesis in an alzheimer disease mouse model. J Clin Invest 113 (10), 1384-7.

Lichtenthaler, S.F., Haass, C., Steiner, H., 2011. Regulated intramembrane proteolysis--lessons from amyloid precursor protein processing. J Neurochem 117 (5), 779-96.

Liebner, S., Corada, M., Bangsow, T., Babbage, J., Taddei, A., Czupalla, C.J., Reis, M., Felici, A., Wolburg, H., Fruttiger, M., Taketo, M.M., Von Melchner, H., Plate, K.H., Gerhardt, H., Dejana, E., 2008. Wnt/beta-catenin signaling controls development of the blood-brain barrier. J Cell Biol 183 (3), 409-17.

Liebner, S., Gerhardt, H., Wolburg, H., 2000. Differential expression of endothelial beta-catenin and plakoglobin during development and maturation of the blood-brain and blood-retina barrier in the chicken. Dev Dyn 217 (1), 86-98.

Lim, S.Y., Suzuki, H., 2000. Effect of dietary docosahexaenoic acid and phosphatidylcholine on maze behavior and fatty acid composition of plasma and brain lipids in mice. Int J Vitam Nutr Res 70 (5), 251-9.

Lin, D., Sugawara, T., Strauss, J.F., 3rd, Clark, B.J., Stocco, D.M., Saenger, P., Rogol, A., Miller, W.L., 1995. Role of steroidogenic acute regulatory protein in adrenal and gonadal steroidogenesis. Science 267 (5205), 1828-31.

Lingwood, D., Simons, K., 2010. Lipid rafts as a membrane-organizing principle. Science 327 (5961), 46-50.

Liu, J., Huan, C., Chakraborty, M., Zhang, H., Lu, D., Kuo, M.S., Cao, G., Jiang, X.C., 2009a. Macrophage sphingomyelin synthase 2 deficiency decreases atherosclerosis in mice. Circ Res 105 (3), 295-303.

Liu, J., Zhang, H., Li, Z., Hailemariam, T.K., Chakraborty, M., Jiang, K., Qiu, D., Bui, H.H., Peake, D.A., Kuo, M.S., Wadgaonkar, R., Cao, G., Jiang, X.C., 2009b. Sphingomyelin synthase 2 is one of the determinants for plasma and liver sphingomyelin levels in mice. Arterioscler Thromb Vasc Biol 29 (6), 850-6.

Liu, J.P., Tang, Y., Zhou, S., Toh, B.H., Mclean, C., Li, H., 2010. Cholesterol involvement in the pathogenesis of neurodegenerative diseases. Mol Cell Neurosci 43 (1), 33-42.

Liu, L., Wan, W., Xia, S., Kalionis, B., Li, Y., 2014. Dysfunctional wnt/beta-catenin signaling contributes to blood-brain barrier breakdown in alzheimer's disease. Neurochem Int 75, 19-25.

Livak, K.J., Schmittgen, T.D., 2001. Analysis of relative gene expression data using real-time quantitative pcr and the 2(-delta delta c(t)) method. Methods 25 (4), 402-8.

Loprinzi, P.D., 2015. Need for increased promotion of physical activity among adults at risk for alzheimer's disease: Brief report. J Phys Act Health.

Lu, M.H., Takemoto, M., Watanabe, K., Luo, H., Nishimura, M., Yano, M., Tomimoto, H., Okazaki, T., Oike, Y., Song, W.J., 2012. Deficiency of sphingomyelin synthase-1 but not sphingomyelin synthase-2 causes hearing impairments in mice. J Physiol 590 (Pt 16), 4029-44.

Luchsinger, J.A., Tang, M.X., Shea, S., Mayeux, R., 2002. Caloric intake and the risk of alzheimer disease. Arch Neurol 59 (8), 1258-63.

Luo, F., Rustay, N.R., Ebert, U., Hradil, V.P., Cole, T.B., Llano, D.A., Mudd, S.R., Zhang, Y., Fox, G.B., Day, M., 2012. Characterization of 7- and 19-month-old tg2576 mice using multimodal in vivo imaging: Limitations as a translatable model of alzheimer's disease. Neurobiol Aging 33 (5), 933-44.

Machado, A., Herrera, A.J., De Pablos, R.M., Espinosa-Oliva, A.M., Sarmiento, M., Ayala, A., Venero, J.L., Santiago, M., Villaran, R.F., Delgado-Cortes, M.J., Arguelles, S., Cano, J., 2014. Chronic stress as a risk factor for alzheimer's disease. Rev Neurosci 25 (6), 785-804.

Mahadevaiah, S.K., Turner, J.M., Baudat, F., Rogakou, E.P., De Boer, P., Blanco-Rodriguez, J., Jasin, M., Keeney, S., Bonner, W.M., Burgoyne, P.S., 2001. Recombinational DNA double-strand breaks in mice precede synapsis. Nat Genet 27 (3), 271-6.

Mahley, R.W., 1988. Apolipoprotein e: Cholesterol transport protein with expanding role in cell biology. Science 240 (4852), 622-30.

Malaplate-Armand, C., Florent-Bechard, S., Youssef, I., Koziel, V., Sponne, I., Kriem, B., Leininger-Muller, B., Olivier, J.L., Oster, T., Pillot, T., 2006. Soluble oligomers of amyloid-beta peptide induce neuronal apoptosis by activating a cpla2-dependent sphingomyelinase-ceramide pathway. Neurobiol Dis 23 (1), 178-89.

Malnar, M., Kosicek, M., Lisica, A., Posavec, M., Krolo, A., Njavro, J., Omerbasic, D., Tahirovic, S., Hecimovic, S., 2012. Cholesterol-depletion corrects app and bace1 misstrafficking in npc1-deficient cells. Biochim Biophys Acta 1822 (8), 1270-83.

Mandon, E.C., Ehses, I., Rother, J., Van Echten, G., Sandhoff, K., 1992. Subcellular localization and membrane topology of serine palmitoyltransferase, 3-dehydrosphinganine reductase, and sphinganine n-acyltransferase in mouse liver. J Biol Chem 267 (16), 11144-8.

Mao, C., Obeid, L.M., 2008. Ceramidases: Regulators of cellular responses mediated by ceramide, sphingosine, and sphingosine-1-phosphate. Biochim Biophys Acta 1781 (9), 424-34.

Mao, C., Xu, R., Szulc, Z.M., Bielawska, A., Galadari, S.H., Obeid, L.M., 2001. Cloning and characterization of a novel human alkaline ceramidase. A mammalian enzyme that hydrolyzes phytoceramide. J Biol Chem 276 (28), 26577-88.

Mao, C., Xu, R., Szulc, Z.M., Bielawski, J., Becker, K.P., Bielawska, A., Galadari, S.H., Hu, W., Obeid, L.M., 2003. Cloning and characterization of a mouse endoplasmic reticulum alkaline ceramidase: An enzyme that preferentially regulates metabolism of very long chain ceramides. J Biol Chem 278 (33), 31184-91.

Marathe, S., Miranda, S.R., Devlin, C., Johns, A., Kuriakose, G., Williams, K.J., Schuchman, E.H., Tabas, I., 2000. Creation of a mouse model for non-neurological (type b) niemann-pick disease by stable, low level expression of lysosomal sphingomyelinase in the absence of secretory sphingomyelinase: Relationship between brain intra-lysosomal enzyme activity and central nervous system function. Hum Mol Genet 9 (13), 1967-76.

Marchesini, N., Osta, W., Bielawski, J., Luberto, C., Obeid, L.M., Hannun, Y.A., 2004. Role for mammalian neutral sphingomyelinase 2 in confluence-induced growth arrest of mcf7 cells. J Biol Chem 279 (24), 25101-11.

Marcinkiewicz, M., Seidah, N.G., 2000. Coordinated expression of beta-amyloid precursor protein and the putative beta-secretase bace and alpha-secretase adam10 in mouse and human brain. J Neurochem 75 (5), 2133-43.

Marcus, J., Honigbaum, S., Shroff, S., Honke, K., Rosenbluth, J., Dupree, J.L., 2006. Sulfatide is essential for the maintenance of cns myelin and axon structure. Glia 53 (4), 372-81.

Marggraf, W.D., Kanfer, J.N., 1984. The phosphorylcholine acceptor in the phosphatidylcholine:Ceramide cholinephosphotransferase reaction. Is the enzyme a transferase or a hydrolase? Biochim Biophys Acta 793 (3), 346-53.

Marlatt, M.W., Bauer, J., Aronica, E., Van Haastert, E.S., Hoozemans, J.J., Joels, M., Lucassen, P.J., 2014. Proliferation in the alzheimer hippocampus is due to microglia, not astroglia, and occurs at sites of amyloid deposition. Neural Plast 2014, 693851.

Marquer, C., Devauges, V., Cossec, J.C., Liot, G., Lecart, S., Saudou, F., Duyckaerts, C., Leveque-Fort, S., Potier, M.C., 2011. Local cholesterol increase triggers amyloid precursor protein-bace1 clustering in lipid rafts and rapid endocytosis. FASEB J 25 (4), 1295-305.

Matsumura, A., Suzuki, S., Iwahara, N., Hisahara, S., Kawamata, J., Suzuki, H., Yamauchi, A., Takata, K., Kitamura, Y., Shimohama, S., 2015. Temporal changes of cd68 and alpha7 nicotinic acetylcholine receptor expression in microglia in alzheimer's disease-like mouse models. J Alzheimers Dis 44 (2), 409-23.

Matsuoka, Y., Picciano, M., Malester, B., Lafrancois, J., Zehr, C., Daeschner, J.M., Olschowka, J.A., Fonseca, M.I., O'banion, M.K., Tenner, A.J., Lemere, C.A., Duff, K., 2001. Inflammatory responses to amyloidosis in a transgenic mouse model of alzheimer's disease. Am J Pathol 158 (4), 1345-54.

Mccaffrey, G., Seelbach, M.J., Staatz, W.D., Nametz, N., Quigley, C., Campos, C.R., Brooks, T.A., Davis, T.P., 2008. Occludin oligomeric assembly at tight junctions of the blood-brain barrier is disrupted by peripheral inflammatory hyperalgesia. J Neurochem 106 (6), 2395-409.

Mcdermott, J.R., Gibson, A.M., 1996. Degradation of alzheimer's beta-amyloid protein by human cathepsin d. Neuroreport 7 (13), 2163-6.

Mcgahon, B.M., Martin, D.S., Horrobin, D.F., Lynch, M.A., 1999. Age-related changes in synaptic function: Analysis of the effect of dietary supplementation with omega-3 fatty acids. Neuroscience 94 (1), 305-14.

Medina, M., Avila, J., 2014. The role of extracellular tau in the spreading of neurofibrillary pathology. Front Cell Neurosci 8, 113.

Mehlhorn, G., Hollborn, M., Schliebs, R., 2000. Induction of cytokines in glial cells surrounding cortical beta-amyloid plaques in transgenic tg2576 mice with alzheimer pathology. Int J Dev Neurosci 18 (4-5), 423-31.

Mermoud, J.E., Popova, B., Peters, A.H., Jenuwein, T., Brockdorff, N., 2002. Histone h3 lysine 9 methylation occurs rapidly at the onset of random x chromosome inactivation. Curr Biol 12 (3), 247-51.

Mielke, M.M., Haughey, N.J., Ratnam Bandaru, V.V., Schech, S., Carrick, R., Carlson, M.C., Mori, S., Miller, M.I., Ceritoglu, C., Brown, T., Albert, M., Lyketsos, C.G., 2010. Plasma ceramides are altered in mild cognitive impairment and predict cognitive decline and hippocampal volume loss. Alzheimers Dement 6 (5), 378-85.

Mietelska-Porowska, A., Wasik, U., Goras, M., Filipek, A., Niewiadomska, G., 2014. Tau protein modifications and interactions: Their role in function and dysfunction. Int J Mol Sci 15 (3), 4671-713.

Mital, P., Hinton, B.T., Dufour, J.M., 2011. The blood-testis and blood-epididymis barriers are more than just their tight junctions. Biol Reprod 84 (5), 851-8.

Mitsutake, S., Igarashi, Y., 2007. Transbilayer movement of ceramide in the plasma membrane of live cells. Biochem Biophys Res Commun 359 (3), 622-7.

Mitsutake, S., Yokose, U., Kato, M., Matsuoka, I., Yoo, J.M., Kim, T.J., Yoo, H.S., Fujimoto, K., Ando, Y., Sugiura, M., Kohama, T., Igarashi, Y., 2007. The generation and behavioral analysis of ceramide kinase-null mice, indicating a function in cerebellar purkinje cells. Biochem Biophys Res Commun 363 (3), 519-24.

Mitsutake, S., Zama, K., Yokota, H., Yoshida, T., Tanaka, M., Mitsui, M., Ikawa, M., Okabe, M., Tanaka, Y., Yamashita, T., Takemoto, H., Okazaki, T., Watanabe, K., Igarashi, Y., 2011. Dynamic modification of sphingomyelin in lipid microdomains controls development of obesity, fatty liver, and type 2 diabetes. J Biol Chem 286 (32), 28544-55.

Mittapalli, R.K., Manda, V.K., Bohn, K.A., Adkins, C.E., Lockman, P.R., 2013. Quantitative fluorescence microscopy provides high resolution imaging of passive diffusion and p-gp mediated efflux at the in vivo blood-brain barrier. J Neurosci Methods 219 (1), 188-95.

Mizushima, N., 2004. Methods for monitoring autophagy. Int J Biochem Cell Biol 36 (12), 2491-502.

Mizutani, Y., Kihara, A., Chiba, H., Tojo, H., Igarashi, Y., 2008. 2-hydroxy-ceramide synthesis by ceramide synthase family: Enzymatic basis for the preference of fa chain length. J Lipid Res 49 (11), 2356-64.

Mizutani, Y., Kihara, A., Igarashi, Y., 2005. Mammalian lass6 and its related family members regulate synthesis of specific ceramides. Biochem J 390 (Pt 1), 263-71.

Mizutani, Y., Kihara, A., Igarashi, Y., 2006. Lass3 (longevity assurance homologue 3) is a mainly testis-specific (dihydro)ceramide synthase with relatively broad substrate specificity. Biochem J 398 (3), 531-8.

Moon, Y.A., Horton, J.D., 2003. Identification of two mammalian reductases involved in the two-carbon fatty acyl elongation cascade. J Biol Chem 278 (9), 7335-43.

Morales-Corraliza, J., Mazzella, M.J., Berger, J.D., Diaz, N.S., Choi, J.H., Levy, E., Matsuoka, Y., Planel, E., Mathews, P.M., 2009. In vivo turnover of tau and app metabolites in the brains of wild-type and tg2576 mice: Greater stability of sapp in the beta-amyloid depositing mice. PLoS One 4 (9), e7134.

Morell, P., Jurevics, H., 1996. Origin of cholesterol in myelin. Neurochem Res 21 (4), 463-70.

Morris, J.C., Roe, C.M., Xiong, C., Fagan, A.M., Goate, A.M., Holtzman, D.M., Mintun, M.A., 2010. Apoe predicts amyloid-beta but not tau alzheimer pathology in cognitively normal aging. Ann Neurol 67 (1), 122-31.

Morris, M.C., 2009. The role of nutrition in alzheimer's disease: Epidemiological evidence. Eur J Neurol 16 Suppl 1, 1-7.

Morris, M.C., Evans, D.A., Bienias, J.L., Tangney, C.C., Bennett, D.A., Aggarwal, N., Schneider, J., Wilson, R.S., 2003a. Dietary fats and the risk of incident alzheimer disease. Arch Neurol 60 (2), 194-200.

Morris, M.C., Evans, D.A., Bienias, J.L., Tangney, C.C., Bennett, D.A., Wilson, R.S., Aggarwal, N., Schneider, J., 2003b. Consumption of fish and n-3 fatty acids and risk of incident alzheimer disease. Arch Neurol 60 (7), 940-6.

Morris, M.C., Evans, D.A., Tangney, C.C., Bienias, J.L., Wilson, R.S., 2005. Fish consumption and cognitive decline with age in a large community study. Arch Neurol 62 (12), 1849-53.

Mountjoy, K.G., Robbins, L.S., Mortrud, M.T., Cone, R.D., 1992. The cloning of a family of genes that encode the melanocortin receptors. Science 257 (5074), 1248-51.

Mrak, R.E., 2012. Microglia in alzheimer brain: A neuropathological perspective. Int J Alzheimers Dis 2012, 165021.

Mu, F.T., Callaghan, J.M., Steele-Mortimer, O., Stenmark, H., Parton, R.G., Campbell, P.L., Mccluskey, J., Yeo, J.P., Tock, E.P., Toh, B.H., 1995. Eea1, an early endosome-associated protein. Eea1 is a conserved alpha-helical peripheral membrane protein flanked by cysteine "fingers" and contains a calmodulin-binding iq motif. J Biol Chem 270 (22), 13503-11.

Mulder, C., Wahlund, L.O., Teerlink, T., Blomberg, M., Veerhuis, R., Van Kamp, G.J., Scheltens, P., Scheffer, P.G., 2003. Decreased lysophosphatidylcholine/phosphatidylcholine ratio in cerebrospinal fluid in alzheimer's disease. J Neural Transm 110 (8), 949-55.

Mullan, M., Crawford, F., Axelman, K., Houlden, H., Lilius, L., Winblad, B., Lannfelt, L., 1992. A pathogenic mutation for probable alzheimer's disease in the app gene at the n-terminus of beta-amyloid. Nat Genet 1 (5), 345-7.

Mullen, T.D., Hannun, Y.A., Obeid, L.M., 2012. Ceramide synthases at the centre of sphingolipid metabolism and biology. Biochem J 441 (3), 789-802.

Muller, M.B., Keck, M.E., Binder, E.B., Kresse, A.E., Hagemeyer, T.P., Landgraf, R., Holsboer, F., Uhr, M., 2003. Abcb1 (mdr1)-type p-glycoproteins at the blood-brain barrier modulate the activity of the hypothalamic-pituitary-adrenocortical system: Implications for affective disorder. Neuropsychopharmacology 28 (11), 1991-9.

Musiek, E.S., Holtzman, D.M., 2015. Three dimensions of the amyloid hypothesis: Time, space and 'wingmen'. Nat Neurosci 18 (6), 800-6.

Nagai, Y., Aoki, J., Sato, T., Amano, K., Matsuda, Y., Arai, H., Inoue, K., 1999. An alternative splicing form of phosphatidylserine-specific phospholipase a1 that exhibits lysophosphatidylserine-specific lysophospholipase activity in humans. J Biol Chem 274 (16), 11053-9.

Nasman, B., Olsson, T., Viitanen, M., Carlstrom, K., 1995. A subtle disturbance in the feedback regulation of the hypothalamic-pituitary-adrenal axis in the early phase of alzheimer's disease. Psychoneuroendocrinology 20 (2), 211-20.

Nguyen, L.N., Ma, D., Shui, G., Wong, P., Cazenave-Gassiot, A., Zhang, X., Wenk, M.R., Goh, E.L., Silver, D.L., 2014. Mfsd2a is a transporter for the essential omega-3 fatty acid docosahexaenoic acid. Nature 509 (7501), 503-6.

Nishimura, R.Y., Barbieiri, P., Castro, G.S., Jordao, A.A., Jr., Perdona Gda, S., Sartorelli, D.S., 2014. Dietary polyunsaturated fatty acid intake during late pregnancy affects fatty acid composition of mature breast milk. Nutrition 30 (6), 685-9.

Nitsch, R.M., Blusztajn, J.K., Pittas, A.G., Slack, B.E., Growdon, J.H., Wurtman, R.J., 1992. Evidence for a membrane defect in alzheimer disease brain. Proc Natl Acad Sci U S A 89 (5), 1671-5.

Nitta, T., Hata, M., Gotoh, S., Seo, Y., Sasaki, H., Hashimoto, N., Furuse, M., Tsukita, S., 2003. Size-selective loosening of the blood-brain barrier in claudin-5-deficient mice. J Cell Biol 161 (3), 653-60.

Nixon, R.A., Wegiel, J., Kumar, A., Yu, W.H., Peterhoff, C., Cataldo, A., Cuervo, A.M., 2005. Extensive involvement of autophagy in alzheimer disease: An immuno-electron microscopy study. J Neuropathol Exp Neurol 64 (2), 113-22.

Nixon, R.A., Yang, D.S., Lee, J.H., 2008. Neurodegenerative lysosomal disorders: A continuum from development to late age. Autophagy 4 (5), 590-9.

Norton, W.T., Poduslo, S.E., 1973. Myelination in rat brain: Changes in myelin composition during brain maturation. J Neurochem 21 (4), 759-73.

Novak, F., Tvrzicka, E., Hamplova, B., Kolar, F., Novakova, O., 2006. Postnatal development of phospholipids and their fatty acid profile in rat heart. Mol Cell Biochem 293 (1-2), 23-33.

Nuutinen, T., Huuskonen, J., Suuronen, T., Ojala, J., Miettinen, R., Salminen, A., 2007. Amyloid-beta 1-42 induced endocytosis and clusterin/apoj protein accumulation in cultured human astrocytes. Neurochem Int 50 (3), 540-7.

Nyakas, C., Granic, I., Halmy, L.G., Banerjee, P., Luiten, P.G., 2011. The basal forebrain cholinergic system in aging and dementia. Rescuing cholinergic neurons from neurotoxic amyloid-beta42 with memantine. Behav Brain Res 221 (2), 594-603.

O'brien, R.J., Wong, P.C., 2011. Amyloid precursor protein processing and alzheimer's disease. Annu Rev Neurosci 34, 185-204.

Oddo, S., Caccamo, A., Shepherd, J.D., Murphy, M.P., Golde, T.E., Kayed, R., Metherate, R., Mattson, M.P., Akbari, Y., Laferla, F.M., 2003. Triple-transgenic model of alzheimer's disease with plaques and tangles: Intracellular abeta and synaptic dysfunction. Neuron 39 (3), 409-21.

Ohm, T.G., Muller, H., Braak, H., Bohl, J., 1995. Close-meshed prevalence rates of different stages as a tool to uncover the rate of alzheimer's disease-related neurofibrillary changes. Neuroscience 64 (1), 209-17.

Ohmi, K., Kudo, L.C., Ryazantsev, S., Zhao, H.Z., Karsten, S.L., Neufeld, E.F., 2009. Sanfilippo syndrome type b, a lysosomal storage disease, is also a tauopathy. Proc Natl Acad Sci U S A 106 (20), 8332-7.

Okino, N., He, X., Gatt, S., Sandhoff, K., Ito, M., Schuchman, E.H., 2003. The reverse activity of human acid ceramidase. J Biol Chem 278 (32), 29948-53.

Oliveira, T.G., Chan, R.B., Bravo, F.V., Miranda, A., Silva, R.R., Zhou, B., Marques, F., Pinto, V., Cerqueira, J.J., Di Paolo, G., Sousa, N., 2015. The impact of chronic stress on the rat brain lipidome. Mol Psychiatry.

Osenkowski, P., Ye, W., Wang, R., Wolfe, M.S., Selkoe, D.J., 2008. Direct and potent regulation of gamma-secretase by its lipid microenvironment. J Biol Chem 283 (33), 22529-40.

Panchal, M., Loeper, J., Cossec, J.C., Perruchini, C., Lazar, A., Pompon, D., Duyckaerts, C., 2010. Enrichment of cholesterol in microdissected alzheimer's disease senile plaques as assessed by mass spectrometry. J Lipid Res 51 (3), 598-605.

Papadimitriou, A., Priftis, K.N., 2009. Regulation of the hypothalamic-pituitary-adrenal axis. Neuroimmunomodulation 16 (5), 265-71.

Pappolla, M.A., Bryant-Thomas, T.K., Herbert, D., Pacheco, J., Fabra Garcia, M., Manjon, M., Girones, X., Henry, T.L., Matsubara, E., Zambon, D., Wolozin, B., Sano, M., Cruz-Sanchez, F.F., Thal, L.J., Petanceska, S.S., Refolo, L.M., 2003. Mild hypercholesterolemia is an early risk factor for the development of alzheimer amyloid pathology. Neurology 61 (2), 199-205.

Pardridge, W.M., 2012. Drug transport across the blood-brain barrier. J Cereb Blood Flow Metab 32 (11), 1959-72.

Pardridge, W.M., Mietus, L.J., 1979. Transport of steroid hormones through the rat blood-brain barrier. Primary role of albumin-bound hormone. J Clin Invest 64 (1), 145-54.

Parkin, E.T., Turner, A.J., Hooper, N.M., 1999. Amyloid precursor protein, although partially detergent-insoluble in mouse cerebral cortex, behaves as an atypical lipid raft protein. Biochem J 344 Pt 1, 23-30.

Parvathy, S., Hussain, I., Karran, E.H., Turner, A.J., Hooper, N.M., 1999. Cleavage of alzheimer's amyloid precursor protein by alpha-secretase occurs at the surface of neuronal cells. Biochemistry 38 (30), 9728-34.

Pastores, G.M., Hughes, D.A., 2015. Non-neuronopathic lysosomal storage disorders: Disease spectrum and treatments. Best Pract Res Clin Endocrinol Metab 29 (2), 173-182.

Pedros, I., Petrov, D., Allgaier, M., Sureda, F., Barroso, E., Beas-Zarate, C., Auladell, C., Pallas, M., Vazquez-Carrera, M., Casadesus, G., Folch, J., Camins, A., 2014. Early alterations in energy metabolism in the hippocampus of appswe/ps1de9 mouse model of alzheimer's disease. Biochim Biophys Acta 1842 (9), 1556-66.

Peters, A.H., Mermoud, J.E., O'carroll, D., Pagani, M., Schweizer, D., Brockdorff, N., Jenuwein, T., 2002. Histone h3 lysine 9 methylation is an epigenetic imprint of facultative heterochromatin. Nat Genet 30 (1), 77-80.

Pettegrew, J.W., Panchalingam, K., Hamilton, R.L., Mcclure, R.J., 2001. Brain membrane phospholipid alterations in alzheimer's disease. Neurochem Res 26 (7), 771-82.

Pettus, B.J., Bielawska, A., Subramanian, P., Wijesinghe, D.S., Maceyka, M., Leslie, C.C., Evans, J.H., Freiberg, J., Roddy, P., Hannun, Y.A., Chalfant, C.E., 2004. Ceramide 1-phosphate is a direct activator of cytosolic phospholipase a2. J Biol Chem 279 (12), 11320-6.

Phillips, H.S., Hains, J.M., Armanini, M., Laramee, G.R., Johnson, S.A., Winslow, J.W., 1991. Bdnf mrna is decreased in the hippocampus of individuals with alzheimer's disease. Neuron 7 (5), 695-702.

Pievani, M., Bocchetta, M., Boccardi, M., Cavedo, E., Bonetti, M., Thompson, P.M., Frisoni, G.B., 2013. Striatal morphology in early-onset and late-onset alzheimer's disease: A preliminary study. Neurobiol Aging 34 (7), 1728-39.

Pike, L.J., 2006. Rafts defined: A report on the keystone symposium on lipid rafts and cell function. J Lipid Res 47 (7), 1597-8.

Pomara, N., Greenberg, W.M., Branford, M.D., Doraiswamy, P.M., 2003. Therapeutic implications of hpa axis abnormalities in alzheimer's disease: Review and update. Psychopharmacol Bull 37 (2), 120-34.

Poon, W.W., Blurton-Jones, M., Tu, C.H., Feinberg, L.M., Chabrier, M.A., Harris, J.W., Jeon, N.L., Cotman, C.W., 2011. Beta-amyloid impairs axonal bdnf retrograde trafficking. Neurobiol Aging 32 (5), 821-33.

Prasad, M.R., Lovell, M.A., Yatin, M., Dhillon, H., Markesbery, W.R., 1998. Regional membrane phospholipid alterations in alzheimer's disease. Neurochem Res 23 (1), 81-8.

Puglielli, L., Ellis, B.C., Saunders, A.J., Kovacs, D.M., 2003a. Ceramide stabilizes beta-site amyloid precursor protein-cleaving enzyme 1 and promotes amyloid beta-peptide biogenesis. J Biol Chem 278 (22), 19777-83.

Puglielli, L., Tanzi, R.E., Kovacs, D.M., 2003b. Alzheimer's disease: The cholesterol connection. Nat Neurosci 6 (4), 345-51.

Qin, R., Chen, M.L., Zhu, K., Deng, J.B., Shi, Y.Y., 2010. [sphingomyelin synthase 2 deficiency decreases atherosclerosis and inhibits inflammation in mice]. Sheng Li Xue Bao 62 (4), 333-8.

Quan, N., Banks, W.A., 2007. Brain-immune communication pathways. Brain Behav Immun 21 (6), 727-35.

Raber, J., Huang, Y., Ashford, J.W., 2004. Apoe genotype accounts for the vast majority of ad risk and ad pathology. Neurobiol Aging 25 (5), 641-50.

Rabionet, M., Bayerle, A., Jennemann, R., Heid, H., Fuchser, J., Marsching, C., Porubsky, S., Bolenz, C., Guillou, F., Grone, H.J., Gorgas, K., Sandhoff, R., 2015. Male meiotic cytokinesis requires ceramide synthase 3-dependent sphingolipids with unique membrane anchors. Hum Mol Genet 24 (17), 4792-808.

Rabionet, M., Van Der Spoel, A.C., Chuang, C.C., Von Tumpling-Radosta, B., Litjens, M., Bouwmeester, D., Hellbusch, C.C., Korner, C., Wiegandt, H., Gorgas, K., Platt, F.M., Grone, H.J., Sandhoff, R., 2008. Male germ cells require polyenoic sphingolipids with complex glycosylation for completion of meiosis: A link to ceramide synthase-3. J Biol Chem 283 (19), 13357-69.

Raffin-Sanson, M.L., De Keyzer, Y., Bertagna, X., 2003. Proopiomelanocortin, a polypeptide precursor with multiple functions: From physiology to pathological conditions. Eur J Endocrinol 149 (2), 79-90.

Rajendran, L., Honsho, M., Zahn, T.R., Keller, P., Geiger, K.D., Verkade, P., Simons, K., 2006. Alzheimer's disease beta-amyloid peptides are released in association with exosomes. Proc Natl Acad Sci U S A 103 (30), 11172-7.

Rao, J.S., Ertley, R.N., Demar, J.C., Jr., Rapoport, S.I., Bazinet, R.P., Lee, H.J., 2007a. Dietary n-3 pufa deprivation alters expression of enzymes of the arachidonic and docosahexaenoic acid cascades in rat frontal cortex. Mol Psychiatry 12 (2), 151-7.

Rao, J.S., Ertley, R.N., Lee, H.J., Demar, J.C., Jr., Arnold, J.T., Rapoport, S.I., Bazinet, R.P., 2007b. N-3 polyunsaturated fatty acid deprivation in rats decreases frontal cortex bdnf via a p38 mapk-dependent mechanism. Mol Psychiatry 12 (1), 36-46.

Rautioa, J., Chikhale, P.J., 2004. Drug delivery systems for brain tumor therapy. Curr Pharm Des 10 (12), 1341-53.

Rawicz, W., Olbrich, K.C., Mcintosh, T., Needham, D., Evans, E., 2000. Effect of chain length and unsaturation on elasticity of lipid bilayers. Biophys J 79 (1), 328-39.

Razansky, D., Buehler, A., Ntziachristos, V., 2011. Volumetric real-time multispectral optoacoustic tomography of biomarkers. Nat Protoc 6 (8), 1121-9.

Razansky, D., Vinegoni, C., Ntziachristos, V., 2007. Multispectral photoacoustic imaging of fluorochromes in small animals. Opt Lett 32 (19), 2891-3.

Reichardt, H.M., Umland, T., Bauer, A., Kretz, O., Schutz, G., 2000. Mice with an increased glucocorticoid receptor gene dosage show enhanced resistance to stress and endotoxic shock. Mol Cell Biol 20 (23), 9009-17.

Reitz, C., 2013. Dyslipidemia and the risk of alzheimer's disease. Curr Atheroscler Rep 15 (3), 307.

Reul, J.M., De Kloet, E.R., 1985. Two receptor systems for corticosterone in rat brain: Microdistribution and differential occupation. Endocrinology 117 (6), 2505-11.

Reul, J.M., De Kloet, E.R., 1986. Anatomical resolution of two types of corticosterone receptor sites in rat brain with in vitro autoradiography and computerized image analysis. J Steroid Biochem 24 (1), 269-72.

Ridder, S., Chourbaji, S., Hellweg, R., Urani, A., Zacher, C., Schmid, W., Zink, M., Hortnagl, H., Flor, H., Henn, F.A., Schutz, G., Gass, P., 2005. Mice with genetically altered glucocorticoid receptor expression show altered sensitivity for stress-induced depressive reactions. J Neurosci 25 (26), 6243-50.

Riebeling, C., Allegood, J.C., Wang, E., Merrill, A.H., Jr., Futerman, A.H., 2003. Two mammalian longevity assurance gene (lag1) family members, trh1 and trh4, regulate dihydroceramide synthesis using different fatty acyl-coa donors. J Biol Chem 278 (44), 43452-9.

Rimon, G., Bazenet, C.E., Philpott, K.L., Rubin, L.L., 1997. Increased surface phosphatidylserine is an early marker of neuronal apoptosis. J Neurosci Res 48 (6), 563-70.

Risley, M.S., Tan, I.P., Roy, C., Saez, J.C., 1992. Cell-, age- and stage-dependent distribution of connexin43 gap junctions in testes. J Cell Sci 103 (Pt 1), 81-96.

Rivier, C., Vale, W., 1983. Modulation of stress-induced acth release by corticotropin-releasing factor, catecholamines and vasopressin. Nature 305 (5932), 325-7.

Roberds, S.L., Anderson, J., Basi, G., Bienkowski, M.J., Branstetter, D.G., Chen, K.S., Freedman, S.B., Frigon, N.L., Games, D., Hu, K., Johnson-Wood, K., Kappenman, K.E., Kawabe, T.T., Kola, I., Kuehn, R., Lee, M., Liu, W., Motter, R., Nichols, N.F., Power, M., Robertson, D.W., Schenk, D., Schoor, M., Shopp, G.M., Shuck, M.E., Sinha, S., Svensson, K.A., Tatsuno, G., Tintrup, H., Wijsman, J., Wright, S., Mcconlogue, L., 2001. Bace knockout mice are healthy despite lacking the primary beta-secretase activity in brain: Implications for alzheimer's disease therapeutics. Hum Mol Genet 10 (12), 1317-24.

Robinson, B.S., Johnson, D.W., Poulos, A., 1992. Novel molecular species of sphingomyelin containing 2-hydroxylated polyenoic very-long-chain fatty acids in mammalian testes and spermatozoa. J Biol Chem 267 (3), 1746-51.

Rodriguez-Martin, T., Cuchillo-Ibanez, I., Noble, W., Nyenya, F., Anderton, B.H., Hanger, D.P., 2013. Tau phosphorylation affects its axonal transport and degradation. Neurobiol Aging 34 (9), 2146-57.

Rogakou, E.P., Pilch, D.R., Orr, A.H., Ivanova, V.S., Bonner, W.M., 1998. DNA double-stranded breaks induce histone h2ax phosphorylation on serine 139. J Biol Chem 273 (10), 5858-68.

Roher, A.E., Lowenson, J.D., Clarke, S., Wolkow, C., Wang, R., Cotter, R.J., Reardon, I.M., Zurcher-Neely, H.A., Heinrikson, R.L., Ball, M.J., Et Al., 1993. Structural alterations in the peptide backbone of beta-amyloid core protein may account for its deposition and stability in alzheimer's disease. J Biol Chem 268 (5), 3072-83.

Roqueta-Rivera, M., Stroud, C.K., Haschek, W.M., Akare, S.J., Segre, M., Brush, R.S., Agbaga, M.P., Anderson, R.E., Hess, R.A., Nakamura, M.T., 2010. Docosahexaenoic acid supplementation fully restores fertility and spermatogenesis in male delta-6 desaturase-null mice. J Lipid Res 51 (2), 360-7.

Rothman, S.M., Mattson, M.P., 2010. Adverse stress, hippocampal networks, and alzheimer's disease. Neuromolecular Med 12 (1), 56-70.

Rozhkova, A.V., Dmitrieva, V.G., Zhapparova, O.N., Sudarkina, O.Y., Nadezhdina, E.S., Limborska, S.A., Dergunova, L.V., 2011. Human sphingomyelin synthase 1 gene (sms1): Organization, multiple mrna splice variants and expression in adult tissues. Gene 481 (2), 65-75.

Rozhkova, A.V., Filippenkov, I.B., Sudarkina, O.Y., Limborska, S.A., Dergunova, L.V., 2015. [alternative promoters localised in sgms1 gene introns take part in regulation of its expression in human tissues]. Mol Biol (Mosk) 49 (2), 325-33.

Rushworth, J.V., Hooper, N.M., 2010. Lipid rafts: Linking alzheimer's amyloid-beta production, aggregation, and toxicity at neuronal membranes. Int J Alzheimers Dis 2011, 603052.

Saito, Y., Suzuki, K., Nanba, E., Yamamoto, T., Ohno, K., Murayama, S., 2002. Niemann-pick type c disease: Accelerated neurofibrillary tangle formation and amyloid beta deposition associated with apolipoprotein e epsilon 4 homozygosity. Ann Neurol 52 (3), 351-5.

Salem, N., Jr., Wegher, B., Mena, P., Uauy, R., 1996. Arachidonic and docosahexaenoic acids are biosynthesized from their 18-carbon precursors in human infants. Proc Natl Acad Sci U S A 93 (1), 49-54.

Sanchez-Mejia, R.O., Newman, J.W., Toh, S., Yu, G.Q., Zhou, Y., Halabisky, B., Cisse, M., Scearce-Levie, K., Cheng, I.H., Gan, L., Palop, J.J., Bonventre, J.V., Mucke, L., 2008. Phospholipase a2 reduction ameliorates cognitive deficits in a mouse model of alzheimer's disease. Nat Neurosci 11 (11), 1311-8.

Sasahara, K., Morigaki, K., Shinya, K., 2013. Effects of membrane interaction and aggregation of amyloid beta-peptide on lipid mobility and membrane domain structure. Phys Chem Chem Phys 15 (23), 8929-39.

Sato, T., Aoki, J., Nagai, Y., Dohmae, N., Takio, K., Doi, T., Arai, H., Inoue, K., 1997. Serine phospholipid-specific phospholipase a that is secreted from activated platelets. A new member of the lipase family. J Biol Chem 272 (4), 2192-8.

Sawai, H., Domae, N., Nagan, N., Hannun, Y.A., 1999. Function of the cloned putative neutral sphingomyelinase as lyso-platelet activating factor-phospholipase c. J Biol Chem 274 (53), 38131-9.

Sawamura, N., Ko, M., Yu, W., Zou, K., Hanada, K., Suzuki, T., Gong, J.S., Yanagisawa, K., Michikawa, M., 2004. Modulation of amyloid precursor protein cleavage by cellular sphingolipids. J Biol Chem 279 (12), 11984-91.

Scahill, R.I., Schott, J.M., Stevens, J.M., Rossor, M.N., Fox, N.C., 2002. Mapping the evolution of regional atrophy in alzheimer's disease: Unbiased analysis of fluid-registered serial mri. Proc Natl Acad Sci U S A 99 (7), 4703-7.

Schaefer, E.J., Bongard, V., Beiser, A.S., Lamon-Fava, S., Robins, S.J., Au, R., Tucker, K.L., Kyle, D.J., Wilson, P.W., Wolf, P.A., 2006. Plasma phosphatidylcholine docosahexaenoic acid content and risk of dementia and alzheimer disease: The framingham heart study. Arch Neurol 63 (11), 1545-50.

Schioth, H.B., Chhajlani, V., Muceniece, R., Klusa, V., Wikberg, J.E., 1996. Major pharmacological distinction of the acth receptor from other melanocortin receptors. Life Sci 59 (10), 797-801.

Schissel, S.L., Schuchman, E.H., Williams, K.J., Tabas, I., 1996. Zn2+-stimulated sphingomyelinase is secreted by many cell types and is a product of the acid sphingomyelinase gene. J Biol Chem 271 (31), 18431-6.

Schliebs, R., Arendt, T., 2011. The cholinergic system in aging and neuronal degeneration. Behav Brain Res 221 (2), 555-63.

Schlosser Covell, G.E., Hoffman-Snyder, C.R., Wellik, K.E., Woodruff, B.K., Geda, Y.E., Caselli, R.J., Demaerschalk, B.M., Wingerchuk, D.M., 2015. Physical activity level and future risk of mild cognitive impairment or dementia: A critically appraised topic. Neurologist 19 (3), 89-91.

Schnutgen, F., De-Zolt, S., Van Sloun, P., Hollatz, M., Floss, T., Hansen, J., Altschmied, J., Seisenberger, C., Ghyselinck, N.B., Ruiz, P., Chambon, P., Wurst, W., Von Melchner, H., 2005. Genomewide production of multipurpose alleles for the functional analysis of the mouse genome. Proc Natl Acad Sci U S A 102 (20), 7221-6.

Schuchman, E.H., 2007. The pathogenesis and treatment of acid sphingomyelinase-deficient niemann-pick disease. J Inherit Metab Dis 30 (5), 654-63.

Schulze, H., Sandhoff, K., 2011. Lysosomal lipid storage diseases. Cold Spring Harb Perspect Biol 3 (6).

Separovic, D., Semaan, L., Tarca, A.L., Awad Maitah, M.Y., Hanada, K., Bielawski, J., Villani, M., Luberto, C., 2008. Suppression of sphingomyelin synthase 1 by small interference rna is associated with enhanced ceramide production and apoptosis after photodamage. Exp Cell Res 314 (8), 1860-8.

Serhan, C.N., 2007. Resolution phase of inflammation: Novel endogenous anti-inflammatory and proresolving lipid mediators and pathways. Annu Rev Immunol 25, 101-37.

Serhan, C.N., Clish, C.B., Brannon, J., Colgan, S.P., Chiang, N., Gronert, K., 2000. Novel functional sets of lipid-derived mediators with antiinflammatory actions generated from omega-3 fatty acids via cyclooxygenase 2-nonsteroidal antiinflammatory drugs and transcellular processing. J Exp Med 192 (8), 1197-204.

Serhan, C.N., Hong, S., Gronert, K., Colgan, S.P., Devchand, P.R., Mirick, G., Moussignac, R.L., 2002. Resolvins: A family of bioactive products of omega-3 fatty acid transformation circuits initiated by aspirin treatment that counter proinflammation signals. J Exp Med 196 (8), 1025-37.

Serhan, C.N., Yacoubian, S., Yang, R., 2008. Anti-inflammatory and proresolving lipid mediators. Annu Rev Pathol 3, 279-312.

Serrano-Pozo, A., Muzikansky, A., Gomez-Isla, T., Growdon, J.H., Betensky, R.A., Frosch, M.P., Hyman, B.T., 2013. Differential relationships of reactive astrocytes and microglia to fibrillar amyloid deposits in alzheimer disease. J Neuropathol Exp Neurol 72 (6), 462-71.

Shakor, A.B., Taniguchi, M., Kitatani, K., Hashimoto, M., Asano, S., Hayashi, A., Nomura, K., Bielawski, J., Bielawska, A., Watanabe, K., Kobayashi, T., Igarashi, Y., Umehara, H., Takeya, H., Okazaki, T., 2011. Sphingomyelin synthase 1-generated sphingomyelin plays an important role in transferrin trafficking and cell proliferation. J Biol Chem 286 (41), 36053-62.

Sharma, P., Sabharanjak, S., Mayor, S., 2002. Endocytosis of lipid rafts: An identity crisis. Semin Cell Dev Biol 13 (3), 205-14.

Sheng, J.G., Mrak, R.E., Griffin, W.S., 1997. Glial-neuronal interactions in alzheimer disease: Progressive association of il-1alpha+ microglia and s100beta+ astrocytes with neurofibrillary tangle stages. J Neuropathol Exp Neurol 56 (3), 285-90.

Shinto, L., Quinn, J., Montine, T., Dodge, H.H., Woodward, W., Baldauf-Wagner, S., Waichunas, D., Bumgarner, L., Bourdette, D., Silbert, L., Kaye, J., 2014. A randomized placebo-controlled pilot trial of omega-3 fatty acids and alpha lipoic acid in alzheimer's disease. J Alzheimers Dis 38 (1), 111-20.

Silva, L.C., Futerman, A.H., Prieto, M., 2009. Lipid raft composition modulates sphingomyelinase activity and ceramide-induced membrane physical alterations. Biophys J 96 (8), 3210-22.

Simanshu, D.K., Kamlekar, R.K., Wijesinghe, D.S., Zou, X., Zhai, X., Mishra, S.K., Molotkovsky, J.G., Malinina, L., Hinchcliffe, E.H., Chalfant, C.E., Brown, R.E., Patel, D.J., 2013. Non-vesicular

trafficking by a ceramide-1-phosphate transfer protein regulates eicosanoids. Nature 500 (7463), 463-7.
Simons, K., Ikonen, E., 1997. Functional rafts in cell membranes. Nature 387 (6633), 569-72.
Simons, K., Vaz, W.L., 2004. Model systems, lipid rafts, and cell membranes. Annu Rev Biophys Biomol Struct 33, 269-95.
Simons, M., Keller, P., De Strooper, B., Beyreuther, K., Dotti, C.G., Simons, K., 1998. Cholesterol depletion inhibits the generation of beta-amyloid in hippocampal neurons. Proc Natl Acad Sci U S A 95 (11), 6460-4.
Sisodia, S.S., Koo, E.H., Beyreuther, K., Unterbeck, A., Price, D.L., 1990. Evidence that beta-amyloid protein in alzheimer's disease is not derived by normal processing. Science 248 (4954), 492-5.
Slaunwhite, W.R., Jr., Sandberg, A.A., 1959. Transcortin: A corticosteroid-binding protein of plasma. J Clin Invest 38 (2), 384-91.
Slomnicki, L.P., Lesniak, W., 2008. A putative role of the amyloid precursor protein intracellular domain (aicd) in transcription. Acta Neurobiol Exp (Wars) 68 (2), 219-28.
Smith, A.D., 2002. Imaging the progression of alzheimer pathology through the brain. Proc Natl Acad Sci U S A 99 (7), 4135-7.
Smith, P.K., Krohn, R.I., Hermanson, G.T., Mallia, A.K., Gartner, F.H., Provenzano, M.D., Fujimoto, E.K., Goeke, N.M., Olson, B.J., Klenk, D.C., 1985. Measurement of protein using bicinchoninic acid. Anal Biochem 150 (1), 76-85.
Smith, S.M., Vale, W.W., 2006. The role of the hypothalamic-pituitary-adrenal axis in neuroendocrine responses to stress. Dialogues Clin Neurosci 8 (4), 383-95.
Soderberg, M., Edlund, C., Alafuzoff, I., Kristensson, K., Dallner, G., 1992. Lipid composition in different regions of the brain in alzheimer's disease/senile dementia of alzheimer's type. J Neurochem 59 (5), 1646-53.
Sola, C., Mengod, G., Probst, A., Palacios, J.M., 1993. Differential regional and cellular distribution of beta-amyloid precursor protein messenger rnas containing and lacking the kunitz protease inhibitor domain in the brain of human, rat and mouse. Neuroscience 53 (1), 267-95.
Solfrizzi, V., Capurso, C., D'introno, A., Colacicco, A.M., Santamato, A., Ranieri, M., Fiore, P., Capurso, A., Panza, F., 2008. Lifestyle-related factors in predementia and dementia syndromes. Expert Rev Neurother 8 (1), 133-58.
Soneira, C.F., Scott, T.M., 1996. Severe cardiovascular disease and alzheimer's disease: Senile plaque formation in cortical areas. Clin Anat 9 (2), 118-27.
Song, S.H., 1974. Sluggish clearance of red blood cells from microcirculation in spleen, cardiac and skeletal muscles. Yonsei Med J 15 (1), 43-9.
Soon, P.S., Gill, A.J., Benn, D.E., Clarkson, A., Robinson, B.G., Mcdonald, K.L., Sidhu, S.B., 2009. Microarray gene expression and immunohistochemistry analyses of adrenocortical tumors identify igf2 and ki-67 as useful in differentiating carcinomas from adenomas. Endocr Relat Cancer 16 (2), 573-83.
Sparks, D.L., Hunsaker, J.C., 3rd, Scheff, S.W., Kryscio, R.J., Henson, J.L., Markesbery, W.R., 1990. Cortical senile plaques in coronary artery disease, aging and alzheimer's disease. Neurobiol Aging 11 (6), 601-7.
Sparks, D.L., Scheff, S.W., Hunsaker, J.C., 3rd, Liu, H., Landers, T., Gross, D.R., 1994. Induction of alzheimer-like beta-amyloid immunoreactivity in the brains of rabbits with dietary cholesterol. Exp Neurol 126 (1), 88-94.
Spiegel, S., Merrill, A.H., Jr., 1996. Sphingolipid metabolism and cell growth regulation. FASEB J 10 (12), 1388-97.
Sribney, M., 1966. Enzymatic synthesis of ceramide. Biochim Biophys Acta 125 (3), 542-7.
Stahl, N., Jurevics, H., Morell, P., Suzuki, K., Popko, B., 1994. Isolation, characterization, and expression of cdna clones that encode rat udp-galactose: Ceramide galactosyltransferase. J Neurosci Res 38 (2), 234-42.

Stancevic, B., Kolesnick, R., 2010. Ceramide-rich platforms in transmembrane signaling. FEBS Lett 584 (9), 1728-40.

Stoffel, W., Holz, B., Jenke, B., Binczek, E., Gunter, R.H., Kiss, C., Karakesisoglou, I., Thevis, M., Weber, A.A., Arnhold, S., Addicks, K., 2008. Delta6-desaturase (fads2) deficiency unveils the role of omega3- and omega6-polyunsaturated fatty acids. EMBO J 27 (17), 2281-92.

Strittmatter, W.J., Saunders, A.M., Schmechel, D., Pericak-Vance, M., Enghild, J., Salvesen, G.S., Roses, A.D., 1993. Apolipoprotein e: High-avidity binding to beta-amyloid and increased frequency of type 4 allele in late-onset familial alzheimer disease. Proc Natl Acad Sci U S A 90 (5), 1977-81.

Subathra, M., Qureshi, A., Luberto, C., 2011. Sphingomyelin synthases regulate protein trafficking and secretion. PLoS One 6 (9), e23644.

Sudarkina, O.Y., Filippenkov, I.B., Brodsky, I.B., Limborska, S.A., Dergunova, L.V., 2015. Comparative analysis of sphingomyelin synthase 1 gene expression at the transcriptional and translational levels in human tissues. Mol Cell Biochem 406 (1-2), 91-9.

Sugar, I.P., Mizuno, N.K., Momsen, M.M., Momsen, W.E., Brockman, H.L., 2003. Regulation of lipases by lipid-lipid interactions: Implications for lipid-mediated signaling in cells. Chem Phys Lipids 122 (1-2), 53-64.

Sugimoto, M., Shimizu, Y., Yoshioka, T., Wakabayashi, M., Tanaka, Y., Higashino, K., Numata, Y., Sakai, S., Kihara, A., Igarashi, Y., Kuge, Y., 2015. Histological analyses by matrix-assisted laser desorption/ionization-imaging mass spectrometry reveal differential localization of sphingomyelin molecular species regulated by particular ceramide synthase in mouse brains. Biochim Biophys Acta 1851 (12), 1554-65.

Sugiura, M., Kono, K., Liu, H., Shimizugawa, T., Minekura, H., Spiegel, S., Kohama, T., 2002. Ceramide kinase, a novel lipid kinase. Molecular cloning and functional characterization. J Biol Chem 277 (26), 23294-300.

Sun, W., Xu, R., Hu, W., Jin, J., Crellin, H.A., Bielawski, J., Szulc, Z.M., Thiers, B.H., Obeid, L.M., Mao, C., 2008. Upregulation of the human alkaline ceramidase 1 and acid ceramidase mediates calcium-induced differentiation of epidermal keratinocytes. J Invest Dermatol 128 (2), 389-97.

Svennerholm, L., Gottfries, C.G., 1994. Membrane lipids, selectively diminished in alzheimer brains, suggest synapse loss as a primary event in early-onset form (type i) and demyelination in late-onset form (type ii). J Neurochem 62 (3), 1039-47.

Tafesse, F.G., Huitema, K., Hermansson, M., Van Der Poel, S., Van Den Dikkenberg, J., Uphoff, A., Somerharju, P., Holthuis, J.C., 2007. Both sphingomyelin synthases sms1 and sms2 are required for sphingomyelin homeostasis and growth in human hela cells. J Biol Chem 282 (24), 17537-47.

Tafesse, F.G., Ternes, P., Holthuis, J.C., 2006. The multigenic sphingomyelin synthase family. J Biol Chem 281 (40), 29421-5.

Tafesse, F.G., Vacaru, A.M., Bosma, E.F., Hermansson, M., Jain, A., Hilderink, A., Somerharju, P., Holthuis, J.C., 2014. Sphingomyelin synthase-related protein smsr is a suppressor of ceramide-induced mitochondrial apoptosis. J Cell Sci 127 (Pt 2), 445-54.

Takasugi, N., Tomita, T., Hayashi, I., Tsuruoka, M., Niimura, M., Takahashi, Y., Thinakaran, G., Iwatsubo, T., 2003. The role of presenilin cofactors in the gamma-secretase complex. Nature 422 (6930), 438-41.

Takeda, S., Sato, N., Ikimura, K., Nishino, H., Rakugi, H., Morishita, R., 2013. Increased blood-brain barrier vulnerability to systemic inflammation in an alzheimer disease mouse model. Neurobiol Aging 34 (8), 2064-70.

Takeda, S., Sato, N., Morishita, R., 2014. Systemic inflammation, blood-brain barrier vulnerability and cognitive/non-cognitive symptoms in alzheimer disease: Relevance to pathogenesis and therapy. Front Aging Neurosci 6, 171.

Takeuchi, A., Irizarry, M.C., Duff, K., Saido, T.C., Hsiao Ashe, K., Hasegawa, M., Mann, D.M., Hyman, B.T., Iwatsubo, T., 2000. Age-related amyloid beta deposition in transgenic mice overexpressing both alzheimer mutant presenilin 1 and amyloid beta precursor protein swedish mutant is not associated with global neuronal loss. Am J Pathol 157 (1), 331-9.

Tam, J.H., Seah, C., Pasternak, S.H., 2014. The amyloid precursor protein is rapidly transported from the golgi apparatus to the lysosome and where it is processed into beta-amyloid. Mol Brain 7, 54.

Tamboli, I.Y., Hampel, H., Tien, N.T., Tolksdorf, K., Breiden, B., Mathews, P.M., Saftig, P., Sandhoff, K., Walter, J., 2011a. Sphingolipid storage affects autophagic metabolism of the amyloid precursor protein and promotes abeta generation. J Neurosci 31 (5), 1837-49.

Tamboli, I.Y., Tien, N.T., Walter, J., 2011b. Sphingolipid storage impairs autophagic clearance of alzheimer-associated proteins. Autophagy 7 (6), 645-6.

Tani, M., Hannun, Y.A., 2007a. Analysis of membrane topology of neutral sphingomyelinase 2. FEBS Lett 581 (7), 1323-8.

Tani, M., Hannun, Y.A., 2007b. Neutral sphingomyelinase 2 is palmitoylated on multiple cysteine residues. Role of palmitoylation in subcellular localization. J Biol Chem 282 (13), 10047-56.

Tani, M., Iida, H., Ito, M., 2003. O-glycosylation of mucin-like domain retains the neutral ceramidase on the plasma membranes as a type ii integral membrane protein. J Biol Chem 278 (12), 10523-30.

Tani, M., Okino, N., Mori, K., Tanigawa, T., Izu, H., Ito, M., 2000. Molecular cloning of the full-length cdna encoding mouse neutral ceramidase. A novel but highly conserved gene family of neutral/alkaline ceramidases. J Biol Chem 275 (15), 11229-34.

Tanida, I., Ueno, T., Kominami, E., 2004. Lc3 conjugation system in mammalian autophagy. Int J Biochem Cell Biol 36 (12), 2503-18.

Tanida, I., Ueno, T., Kominami, E., 2008. Lc3 and autophagy. Methods Mol Biol 445, 77-88.

Taniguchi, M., Okazaki, T., 2014. The role of sphingomyelin and sphingomyelin synthases in cell death, proliferation and migration-from cell and animal models to human disorders. Biochim Biophys Acta 1841 (5), 692-703.

Tapia-Rojas, C., Aranguiz, F., Varela-Nallar, L., Inestrosa, N.C., 2015. Voluntary running attenuates memory loss, decreases neuropathological changes and induces neurogenesis in a mouse model of alzheimer's disease. Brain Pathol.

Ternes, P., Brouwers, J.F., Van Den Dikkenberg, J., Holthuis, J.C., 2009. Sphingomyelin synthase sms2 displays dual activity as ceramide phosphoethanolamine synthase. J Lipid Res 50 (11), 2270-7.

Toman, R.E., Movsesyan, V., Murthy, S.K., Milstien, S., Spiegel, S., Faden, A.I., 2002. Ceramide-induced cell death in primary neuronal cultures: Upregulation of ceramide levels during neuronal apoptosis. J Neurosci Res 68 (3), 323-30.

Tomasselli, A.G., Qahwash, I., Emmons, T.L., Lu, Y., Leone, J.W., Lull, J.M., Fok, K.F., Bannow, C.A., Smith, C.W., Bienkowski, M.J., Heinrikson, R.L., Yan, R., 2003. Employing a superior bace1 cleavage sequence to probe cellular app processing. J Neurochem 84 (5), 1006-17.

Tomidokoro, Y., Harigaya, Y., Matsubara, E., Ikeda, M., Kawarabayashi, T., Shirao, T., Ishiguro, K., Okamoto, K., Younkin, S.G., Shoji, M., 2001. Brain abeta amyloidosis in appsw mice induces accumulation of presenilin-1 and tau. J Pathol 194 (4), 500-6.

Tomiuk, S., Hofmann, K., Nix, M., Zumbansen, M., Stoffel, W., 1998. Cloned mammalian neutral sphingomyelinase: Functions in sphingolipid signaling? Proc Natl Acad Sci U S A 95 (7), 3638-43.

Turner, D.L., Silver, M.J., Baczynski, E., Holburn, R.R., Herb, S.F., Luddy, F.E., 1970. The synthesis of phosphatidylethanolamine and phosphatidylserine containing acetylenic or cyclopropane fatty acids and the activity of these phosphatides in blood coagulation. Lipids 5 (7), 650-7.

Tusher, V.G., Tibshirani, R., Chu, G., 2001. Significance analysis of microarrays applied to the ionizing radiation response. Proc Natl Acad Sci U S A 98 (9), 5116-21.

Uchida, K., Emoto, K., Daleke, D.L., Inoue, K., Umeda, M., 1998. Induction of apoptosis by phosphatidylserine. J Biochem 123 (6), 1073-8.

Uhr, M., Holsboer, F., Muller, M.B., 2002. Penetration of endogenous steroid hormones corticosterone, cortisol, aldosterone and progesterone into the brain is enhanced in mice deficient for both mdr1a and mdr1b p-glycoproteins. J Neuroendocrinol 14 (9), 753-9.

Ujiie, M., Dickstein, D.L., Carlow, D.A., Jefferies, W.A., 2003. Blood-brain barrier permeability precedes senile plaque formation in an alzheimer disease model. Microcirculation 10 (6), 463-70.

Ullman, M.D., Radin, N.S., 1974. The enzymatic formation of sphingomyelin from ceramide and lecithin in mouse liver. J Biol Chem 249 (5), 1506-12.

Vacaru, A.M., Tafesse, F.G., Ternes, P., Kondylis, V., Hermansson, M., Brouwers, J.F., Somerharju, P., Rabouille, C., Holthuis, J.C., 2009. Sphingomyelin synthase-related protein smsr controls ceramide homeostasis in the er. J Cell Biol 185 (6), 1013-27.

Vale, W., Spiess, J., Rivier, C., Rivier, J., 1981. Characterization of a 41-residue ovine hypothalamic peptide that stimulates secretion of corticotropin and beta-endorphin. Science 213 (4514), 1394-7.

Van Dam, D., De Deyn, P.P., 2006. Drug discovery in dementia: The role of rodent models. Nat Rev Drug Discov 5 (11), 956-70.

Van Der Luit, A.H., Budde, M., Zerp, S., Caan, W., Klarenbeek, J.B., Verheij, M., Van Blitterswijk, W.J., 2007. Resistance to alkyl-lysophospholipid-induced apoptosis due to downregulated sphingomyelin synthase 1 expression with consequent sphingomyelin- and cholesterol-deficiency in lipid rafts. Biochem J 401 (2), 541-9.

Van Helvoort, A., Van't Hof, W., Ritsema, T., Sandra, A., Van Meer, G., 1994. Conversion of diacylglycerol to phosphatidylcholine on the basolateral surface of epithelial (madin-darby canine kidney) cells. Evidence for the reverse action of a sphingomyelin synthase. J Biol Chem 269 (3), 1763-9.

Van Meer, G., Hoetzl, S., 2010. Sphingolipid topology and the dynamic organization and function of membrane proteins. FEBS Lett 584 (9), 1800-5.

Van Meer, G., Voelker, D.R., Feigenson, G.W., 2008. Membrane lipids: Where they are and how they behave. Nat Rev Mol Cell Biol 9 (2), 112-24.

Vance, D.E., 1989. Phosphatidylcholine metabolism CRC Press, Boca Raton, Fla.

Venkataraman, K., Riebeling, C., Bodennec, J., Riezman, H., Allegood, J.C., Sullards, M.C., Merrill, A.H., Jr., Futerman, A.H., 2002. Upstream of growth and differentiation factor 1 (uog1), a mammalian homolog of the yeast longevity assurance gene 1 (lag1), regulates n-stearoyl-sphinganine (c18-(dihydro)ceramide) synthesis in a fumonisin b1-independent manner in mammalian cells. J Biol Chem 277 (38), 35642-9.

Viggars, A.P., Wharton, S.B., Simpson, J.E., Matthews, F.E., Brayne, C., Savva, G.M., Garwood, C., Drew, D., Shaw, P.J., Ince, P.G., 2011. Alterations in the blood brain barrier in ageing cerebral cortex in relationship to alzheimer-type pathology: A study in the mrc-cfas population neuropathology cohort. Neurosci Lett 505 (1), 25-30.

Villani, M., Subathra, M., Im, Y.B., Choi, Y., Signorelli, P., Del Poeta, M., Luberto, C., 2008. Sphingomyelin synthases regulate production of diacylglycerol at the golgi. Biochem J 414 (1), 31-41.

Vita, N., Laurent, P., Lefort, S., Chalon, P., Lelias, J.M., Kaghad, M., Le Fur, G., Caput, D., Ferrara, P., 1993. Primary structure and functional expression of mouse pituitary and human brain corticotrophin releasing factor receptors. FEBS Lett 335 (1), 1-5.

Vladychenskaya, I.P., Dergunova, L.V., Dmitrieva, V.G., Limborska, S.A., 2004. Human gene mob: Structure specification and aspects of transcriptional activity. Gene 338 (2), 257-65.

Vladychenskaya, I.P., Dergunova, L.V., Limborska, S.A., 2002. In vitro and in silico analysis of the predicted human mob gene encoding a phylogenetically conserved transmembrane protein. Biomol Eng 18 (6), 263-8.

Voelker, D.R., Kennedy, E.P., 1982. Cellular and enzymic synthesis of sphingomyelin. Biochemistry 21 (11), 2753-9.
Vom Dahl, S., Mengel, E., 2010. Lysosomal storage diseases as differential diagnosis of hepatosplenomegaly. Best Pract Res Clin Gastroenterol 24 (5), 619-28.
Wahrle, S., Das, P., Nyborg, A.C., Mclendon, C., Shoji, M., Kawarabayashi, T., Younkin, L.H., Younkin, S.G., Golde, T.E., 2002. Cholesterol-dependent gamma-secretase activity in buoyant cholesterol-rich membrane microdomains. Neurobiol Dis 9 (1), 11-23.
Walker, J.J., Spiga, F., Gupta, R., Zhao, Z., Lightman, S.L., Terry, J.R., 2015. Rapid intra-adrenal feedback regulation of glucocorticoid synthesis. J R Soc Interface 12 (102), 20140875.
Walter, J., Van Echten-Deckert, G., 2013. Cross-talk of membrane lipids and alzheimer-related proteins. Mol Neurodegener 8, 34.
Weingarten, M.D., Lockwood, A.H., Hwo, S.Y., Kirschner, M.W., 1975. A protein factor essential for microtubule assembly. Proc Natl Acad Sci U S A 72 (5), 1858-62.
Weisgraber, K.H., 1994. Apolipoprotein e: Structure-function relationships. Adv Protein Chem 45, 249-302.
Westmeyer, G.G., Willem, M., Lichtenthaler, S.F., Lurman, G., Multhaup, G., Assfalg-Machleidt, I., Reiss, K., Saftig, P., Haass, C., 2004. Dimerization of beta-site beta-amyloid precursor protein-cleaving enzyme. J Biol Chem 279 (51), 53205-12.
Whitehouse, P.J., Price, D.L., Clark, A.W., Coyle, J.T., Delong, M.R., 1981. Alzheimer disease: Evidence for selective loss of cholinergic neurons in the nucleus basalis. Ann Neurol 10 (2), 122-6.
Whitehouse, P.J., Price, D.L., Struble, R.G., Clark, A.W., Coyle, J.T., Delon, M.R., 1982. Alzheimer's disease and senile dementia: Loss of neurons in the basal forebrain. Science 215 (4537), 1237-9.
Williams, P.T., 2015. Lower risk of alzheimer's disease mortality with exercise, statin, and fruit intake. J Alzheimers Dis 44 (4), 1121-9.
Williamson, R., Sutherland, C., 2011. Neuronal membranes are key to the pathogenesis of alzheimer's disease: The role of both raft and non-raft membrane domains. Curr Alzheimer Res 8 (2), 213-21.
Wolf, D.C., Horwitz, S.B., 1992. P-glycoprotein transports corticosterone and is photoaffinity-labeled by the steroid. Int J Cancer 52 (1), 141-6.
Xu, R., Jin, J., Hu, W., Sun, W., Bielawski, J., Szulc, Z., Taha, T., Obeid, L.M., Mao, C., 2006. Golgi alkaline ceramidase regulates cell proliferation and survival by controlling levels of sphingosine and s1p. FASEB J 20 (11), 1813-25.
Yacoubian, S., Serhan, C.N., 2007. New endogenous anti-inflammatory and proresolving lipid mediators: Implications for rheumatic diseases. Nat Clin Pract Rheumatol 3 (10), 570-9; quiz 1 p following 589.
Yamada, T., Kadekaru, H., Matsumoto, S., Inada, H., Tanabe, M., Moriguchi, E.H., Moriguchi, Y., Ishikawa, P., Ishikawa, A.G., Taira, K., Yamori, Y., 2002. Prevalence of dementia in the older japanese-brazilian population. Psychiatry Clin Neurosci 56 (1), 71-5.
Yamamoto, N., Saitoh, M., Moriuchi, A., Nomura, M., Okuyama, H., 1987. Effect of dietary alpha-linolenate/linoleate balance on brain lipid compositions and learning ability of rats. J Lipid Res 28 (2), 144-51.
Yamaoka, S., Miyaji, M., Kitano, T., Umehara, H., Okazaki, T., 2004. Expression cloning of a human cdna restoring sphingomyelin synthesis and cell growth in sphingomyelin synthase-defective lymphoid cells. J Biol Chem 279 (18), 18688-93.
Yamashita, T., Allende, M.L., Kalkofen, D.N., Werth, N., Sandhoff, K., Proia, R.L., 2005. Conditional loxp-flanked glucosylceramide synthase allele controlling glycosphingolipid synthesis. Genesis 43 (4), 175-80.
Yamashita, T., Wada, R., Sasaki, T., Deng, C., Bierfreund, U., Sandhoff, K., Proia, R.L., 1999. A vital role for glycosphingolipid synthesis during development and differentiation. Proc Natl Acad Sci U S A 96 (16), 9142-7.

Yan, L., Bai, X.L., Fang, Z.F., Che, L.Q., Xu, S.Y., Wu, D., 2013. Effect of different dietary omega-3/omega-6 fatty acid ratios on reproduction in male rats. Lipids Health Dis 12, 33.

Yang, Z., Jean-Baptiste, G., Khoury, C., Greenwood, M.T., 2005. The mouse sphingomyelin synthase 1 (sms1) gene is alternatively spliced to yield multiple transcripts and proteins. Gene 363, 123-32.

Yano, M., Watanabe, K., Yamamoto, T., Ikeda, K., Senokuchi, T., Lu, M., Kadomatsu, T., Tsukano, H., Ikawa, M., Okabe, M., Yamaoka, S., Okazaki, T., Umehara, H., Gotoh, T., Song, W.J., Node, K., Taguchi, R., Yamagata, K., Oike, Y., 2011. Mitochondrial dysfunction and increased reactive oxygen species impair insulin secretion in sphingomyelin synthase 1-null mice. J Biol Chem 286 (5), 3992-4002.

Yano, M., Yamamoto, T., Nishimura, N., Gotoh, T., Watanabe, K., Ikeda, K., Garan, Y., Taguchi, R., Node, K., Okazaki, T., Oike, Y., 2013. Increased oxidative stress impairs adipose tissue function in sphingomyelin synthase 1 null mice. PLoS One 8 (4), e61380.

Ye, C.Y., Lei, Y., Tang, X.C., Zhang, H.Y., 2015. Donepezil attenuates abeta-associated mitochondrial dysfunction and reduces mitochondrial abeta accumulation in vivo and in vitro. Neuropharmacology 95, 29-36.

Yeang, C., Ding, T., Chirico, W.J., Jiang, X.C., 2011. Subcellular targeting domains of sphingomyelin synthase 1 and 2. Nutr Metab (Lond) 8, 89.

Yeang, C., Varshney, S., Wang, R., Zhang, Y., Ye, D., Jiang, X.C., 2008. The domain responsible for sphingomyelin synthase (sms) activity. Biochim Biophys Acta 1781 (10), 610-7.

Yeboah, J., Mcnamara, C., Jiang, X.C., Tabas, I., Herrington, D.M., Burke, G.L., Shea, S., 2010. Association of plasma sphingomyelin levels and incident coronary heart disease events in an adult population: Multi-ethnic study of atherosclerosis. Arterioscler Thromb Vasc Biol 30 (3), 628-33.

Yet, S.F., Lee, S., Hahm, Y.T., Sul, H.S., 1993. Expression and identification of p90 as the murine mitochondrial glycerol-3-phosphate acyltransferase. Biochemistry 32 (36), 9486-91.

York, D.A., Lin, L., Thomas, S.R., Braymer, H.D., Park, M., 2006. Procolipase gene expression in the rat brain: Source of endogenous enterostatin production in the brain. Brain Res 1087 (1), 52-9.

Yu, A.S., Mccarthy, K.M., Francis, S.A., Mccormack, J.M., Lai, J., Rogers, R.A., Lynch, R.D., Schneeberger, E.E., 2005. Knockdown of occludin expression leads to diverse phenotypic alterations in epithelial cells. Am J Physiol Cell Physiol 288 (6), C1231-41.

Yuyama, K., Sun, H., Mitsutake, S., Igarashi, Y., 2012. Sphingolipid-modulated exosome secretion promotes clearance of amyloid-beta by microglia. J Biol Chem 287 (14), 10977-89.

Yuyama, K., Yanagisawa, K., 2010. Sphingomyelin accumulation provides a favorable milieu for gm1 ganglioside-induced assembly of amyloid beta-protein. Neurosci Lett 481 (3), 168-72.

Zadravec, D., Tvrdik, P., Guillou, H., Haslam, R., Kobayashi, T., Napier, J.A., Capecchi, M.R., Jacobsson, A., 2011. Elovl2 controls the level of n-6 28:5 and 30:5 fatty acids in testis, a prerequisite for male fertility and sperm maturation in mice. J Lipid Res 52 (2), 245-55.

Zhai, X., Boldyrev, I.A., Mizuno, N.K., Momsen, M.M., Molotkovsky, J.G., Brockman, H.L., Brown, R.E., 2014. Nanoscale packing differences in sphingomyelin and phosphatidylcholine revealed by bodipy fluorescence in monolayers: Physiological implications. Langmuir 30 (11), 3154-64.

Zhang, W., Colman, R.W., 2007. Thrombin regulates intracellular cyclic amp concentration in human platelets through phosphorylation/activation of phosphodiesterase 3a. Blood 110 (5), 1475-82.

Zheng, X., Chu, F., Mirkin, B.L., Sudha, T., Mousa, S.A., Rebbaa, A., 2008. Role of the proteolytic hierarchy between cathepsin l, cathepsin d and caspase-3 in regulation of cellular susceptibility to apoptosis and autophagy. Biochim Biophys Acta 1783 (12), 2294-300.

Zhou, X., Tuck, D.P., 2007. Msvm-rfe: Extensions of svm-rfe for multiclass gene selection on DNA microarray data. Bioinformatics 23 (9), 1106-14.

Zoller, I., Bussow, H., Gieselmann, V., Eckhardt, M., 2005. Oligodendrocyte-specific ceramide galactosyltransferase (cgt) expression phenotypically rescues cgt-deficient mice and

demonstrates that cgt activity does not limit brain galactosylceramide level. Glia 52 (3), 190-8.

Zumbansen, M., Stoffel, W., 2002. Neutral sphingomyelinase 1 deficiency in the mouse causes no lipid storage disease. Mol Cell Biol 22 (11), 3633-8.

Alzheimer, A. 1907. Über eine eigenartige Erkrankung der Hirnrinde. Allgmeine Zeitschrift für Psychiatrie psychisch-gerichtliche Medizin, (Berlin) 64:146-148.

Alzheimer's Disease Education and Referral Center, National Institute of Aging

Atlas and Text-book of Human Anatomy Volume III Vascular System, Lymphatic system, Nervous system and Sense Organs

http://www.servier.com/Powerpoint-image-bank

http://ensemble.org

http://lipidlibrary.aocs.org

10. Supplementary data

Table 10.1: Organ weight of *Sms1* animals.
Medians, first and third quartile and p-values calculated by a Wilcoxon rank-sum test.
[a] Number not based on the full number of animals (missing values).
(GMC report data)

	female		male		female	male	overall
	control	mutant	control	mutant			
	n=6	n=6	n=6	n=6			
	median [25%, 75%]	median [25%, 75%]	median [25%, 75%]	median [25%, 75%]	p-value	p-value	p-value
heart weight [mg]	112 [101.8 , 125.2]	106.5 [100.5 , 109.5]	150 [141 , 153]	143 [122.8 , 157.2]	0.368	0.561	0.325
tibia length [mm]	18 [17.4 , 18.8]	18.2 [17.7 , 18.5]	18.6 [18.3 , 18.8]	18.7 [18.4 , 19.5]	0.981	0.619	0.854
Liver weight [g]	1.012 [0.953 , 1.154]	1.05 [0.984 , 1.054]	1.488 [1.325 , 1.687]	1.083 [0.938 , 1.185]	0.818	0.041	0.101
Spleen weight [g]	0.071 [0.068 , 0.079]	0.073 [0.064 , 0.084]	0.08 [0.07 , 0.084]	0.078 [0.06 , 0.113]	1	0.937	0.966
Body weight [g]	20.559 [19.836 , 23.334]	20.412 [18.989 , 20.516]	30.669 [27.678 , 32.318]	24.648 [21.907 , 28.062]	0.485	0.093	0.16
Heart Weight / Tibia Length [mg/mm]	6.32 [5.95 , 6.66]	5.82 [5.62 , 5.95]	8.21 [7.58 , 8.68]	7.66 [7.26 , 7.92]	0.093	0.18	0.16
Heart Weight / Body Weight [mg/g]	5.16 [5.08 , 5.18]	5.34 [5.32 , 5.36]	5.08 [4.72 , 5.12]	5.54 [5.29 , 5.61]	0.258	0.065	0.029
Liver Weight / Tibia Length [mg/mm]	56.19 [54.29 , 63.5]	56.61 [56.04 , 56.9]	81.45 [72.92 , 89.17]	59.53 [51.74 , 62.94]	0.937	0.026	0.06
Liver Weight / Body Weight [mg/g]	49.44 [47.55 , 50.2]	51.63 [51.09 , 51.94]	49.98 [49.34 , 51.51]	47.24 [42.38 , 47.47]	0.009	0.026	1
Spleen Weight / Tibia Length [mg/mm]	4.07 [3.86 , 4.37]	4.12 [3.62 , 4.66]	4.33 [4.03 , 4.5]	4.11 [3.35 , 5.96]	0.818	1	0.932
Spleen Weight / Body Weight [mg/g]	3.38 [3.3 , 3.5]	3.77 [3.16 , 4.2]	2.54 [2.38 , 3.03]	3.29 [2.84 , 3.94]	0.699	0.093	0.128

Table 10.2: Echocardiography of *Sms1* animals.
Medians, first and third quartile and p-values calculated by a Wilcoxon rank-sum test.
[a] Number not based on the full number of animals (missing values).
(GMC report data)

	female		male		female	male	overall
	control	mutant	control	mutant			
	n=9	n=9	n=9	n=10			
	median [25%, 75%]	median [25%, 75%]	median [25%, 75%]	median [25%, 75%]	p-value	p-value	p-value
IVSs [mm]	0.79 [0.67 , 0.81]	0.8 [0.75 , 0.82]	0.84 [0.76 , 0.85]	0.82 [0.78 , 0.9]	0.287	0.889	0.447
IVSd [mm]	0.56 [0.54 , 0.6]	0.66 [0.58 , 0.68]	0.67 [0.62 , 0.68]	0.66 [0.63 , 0.69]	0.08	0.59	0.093
LVPWs [mm]	0.81 [0.72 , 0.85]	0.84 [0.82 , 0.85]	0.88 [0.84 , 0.95]	0.84 [0.77 , 0.98]	0.267	0.78	0.636
LVPWd [mm]	0.7 [0.69 , 0.73]	0.72 [0.7 , 0.77]	0.78 [0.77 , 0.82]	0.69 [0.66 , 0.71]	0.397	< 0.001	0.046
LVIDs [mm]	1.15 [0.9 , 1.43]	0.77 [0.69 , 1.08]	1 [0.84 , 1.06]	1.32 [0.82 , 1.49]	0.136	0.447	0.558
LVIDd [mm]	2.38 [2.09 , 2.78]	2.33 [2.08 , 2.57]	2.56 [2.35 , 2.71]	2.79 [2.29 , 2.87]	0.605	0.356	0.97
Weight [g]	20.8 [20.2 , 21.5]	21.3 [19.4 , 22.1]	27.4 [24.8 , 31]	26.9 [25.4 , 29.4]	0.982	0.511	0.851
Heart rate Echo [bpm]	642.86 [578.31 , 669.77]	657.53 [612.77 , 727.27]	746.11 [702.44 , 761.9]	689.01 [655.35 , 728.22]	0.622	0.056	0.466
Respiration Rate Echo [1/min]	253.52 [199.26 , 276.92]	240 [215.57 , 242.42]	295.08 [235.29 , 352.94]	281.25 [240.07 , 321.48]	0.546	0.92	0.625

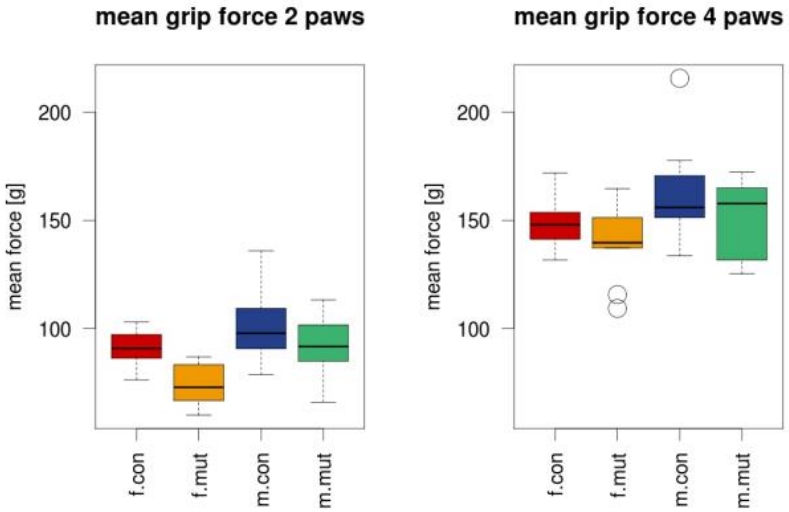

Figure 10.1: Grip Strength test results
Mean force (2 and 4 paws) boxplat, split by sex and genotype. Female (f), male (m)
(GMC report data)

Table 10.3: Grip Strength test results, 2 paws
Linear model for 2-paws grip strength (mean of 3 trials)
(GMC report data)

	Estimate	CI	p-value
(Intercept)	25.26	[-1.65 , 52.16]	0.06
genotype	5.69	[2.51 , 8.87]	<0.001
sex	3.13	[-2.28 , 8.55]	0.25
weight	3.03	[1.76 , 4.3]	<0.001

Table 10.4: Grip Strength test results, 2 and 4 paws
Group means and SD
(GMC report data)

	female		male	
	control	mutant	control	mutant
	n=10	n=10	n=10	n=10
	mean ± sd	mean ± sd	mean ± sd	mean ± sd
mean force (2 paws)	90.15 ± 8.63	73.41 ± 9.17	101.84 ± 16.71	91.35 ± 13.7
mean force (4 paws)	148.93 ± 11.64	140.5 ± 17.52	163.24 ± 22.33	151.81 ± 17.73

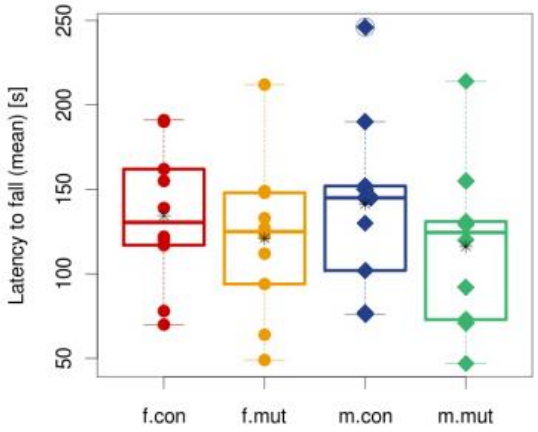

Figure 10.2: Rotarod test results
Latency to fall (mean) boxplot with stripchart split by sex and genotype.
(GMC report data)

Table 10.5: Rotarod test results
Latency to fall. Mean values and SD.
(GMC report data)

	mean (all)	std (all)	mean (1.)	std (1.)	mean (2.)	std (2.)	mean (3.)	std (3.)
f.control	134.33	63.78	94	60.6	127.3	55.05	181.7	45.28
f.mutant	120.9	66.03	76.8	37.28	130.7	55.28	155.2	77.66
m.control	141.07	67.28	114.6	74.83	137.6	63.28	171	56.5
m.mutant	116.17	56.79	85	55.45	135.6	54.88	127.9	51.51

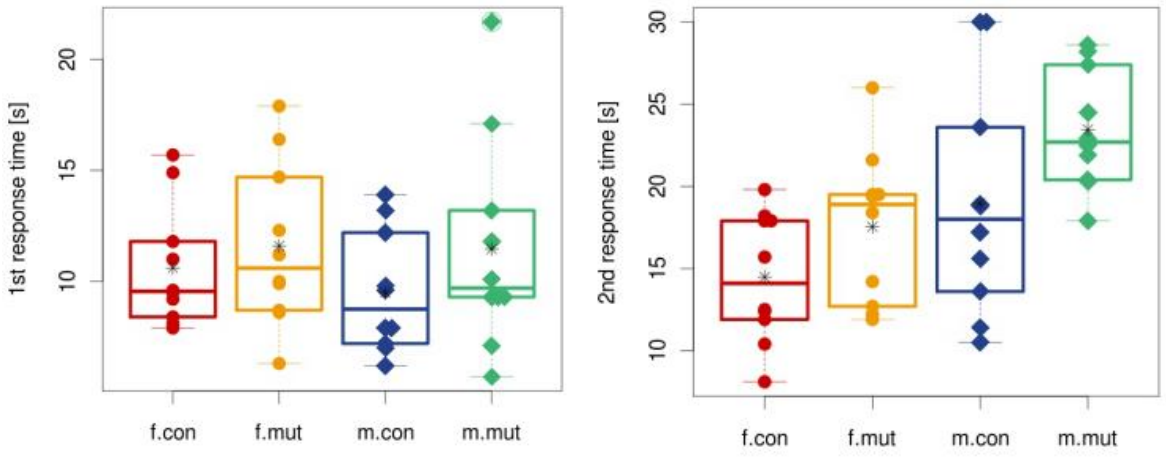

Figure 10.3: Hot plate test results.
1st and 2nd response time boxplot with stripchart, split by sex and genotype.
(GMC report data)

Table 10.6: Hot plate test results.
1st and 2nd response time, group mean and SD and ANOVA including *post hoc* calculation.
(GMC report data)

	mean ± sd	mean ± sd	mean ± sd	mean ± sd	pairwise (Tukey)	pairwise (Tukey)	ANOVA	ANOVA	ANOVA
	female	female	male	male	females	males			
	control	mutant	control	mutant	mutant-control	mutant-control	genotype	sex	sex:genotype
	N=10	N=10	N=10	N=10	adj. p-value	adj. p-value	p-value	p-value	p-value
Bodyweight	20.47 ± 1.88	20.68 ± 1.61	28.4 ± 3.37	26.6 ± 3.83	0.998	0.495	0.381	< 0.001	0.27
First response time	10.61 ± 2.76	11.6 ± 3.71	9.49 ± 2.75	11.46 ± 4.81	0.927	0.618	0.203	0.584	0.67
Second response time	14.48 ± 3.93	17.54 ± 4.65	18.96 ± 6.97	23.46 ± 3.64	0.522	0.199	0.022	0.002	0.65

Table 10.7: Flow cytometry data of *Sms1* animals.
Frequencies of Leukocyte subpopulations in peripheral blood after erythrocyte lysis [percentage of all leukocytes (CD45+ cells), or corresponding parent gate, respectively]. Means, SD and p-values calculated by a linear model.
(GMC report data)

	female		male		Linear model		
	control	mutant	control	mutant	genotype	sex	genotype:sex
	n=10	n=10	n=10	n=10			
	mean ± sd	mean ± sd	mean ± sd	mean ± sd	p-value	p-value	p-value
CD45+/T cells	28.76 ± 7.22	23.65 ± 7.31	17.03 ± 3.82	17.95 ± 4.76	0.274	< 0.001	0.119
CD45+/CD3+CD4+	16.27 ± 3.95	12.46 ± 4.3	9.29 ± 2.13	9.31 ± 2.49	0.082	< 0.001	0.078
CD45+/CD3+CD8+	11.09 ± 3.35	9.91 ± 3.48	6.85 ± 1.73	7.58 ± 2.09	0.8	0.001	0.283
CD45+/B cells	42.34 ± 8.71	47.83 ± 9.38	47.8 ± 8.67	48.38 ± 9.38	0.296	0.3	0.396
CD45+/CD5-NK+	5.21 ± 1.62	5.49 ± 1.2	4.05 ± 1.62	4.83 ± 1.64	0.285	0.068	0.613
CD45+/CD11b+Gr1+	6.5 ± 2.8	7.38 ± 2.09	10.25 ± 7.35	11.71 ± 7.84	0.516	0.03	0.871
CD45+/NK-Gr1-CD11b+	5.2 ± 2.12	4.62 ± 1.62	7.29 ± 2.47	5.66 ± 1.54	0.085	0.017	0.408
CD3+CD4+/CD25+	4.88 ± 1.66	6.28 ± 1.11	5.29 ± 1.25	5.61 ± 1.04	0.042	0.75	0.189
CD45+/CD3+gammadeltaTCR+	0.4 ± 0.13	0.4 ± 0.12	0.2 ± 0.06	0.2 ± 0.06	0.886	< 0.001	0.886
CD3+CD4+/CD62L+	45.07 ± 25.05	31.99 ± 24.6	37.76 ± 23.97	40.58 ± 21.46	0.5	0.932	0.298
CD3+CD4+/CD44+	73.01 ± 3.4	71.36 ± 4.53	73.58 ± 3.29	70.61 ± 6.32	0.117	0.95	0.649
CD3+CD8+/CD62L+	59.26 ± 29.74	50.46 ± 29.81	54.47 ± 21.88	62.49 ± 23.97	0.963	0.669	0.324
CD3+CD8+/CD44+	60.31 ± 3.16	63.37 ± 4.9	65.38 ± 5.31	65.62 ± 7.69	0.35	0.043	0.423
CD45+/CD5+NK+	0.91 ± 0.28	1.01 ± 0.28	0.61 ± 0.31	0.55 ± 0.19	0.825	< 0.001	0.397
B cells/IgD+	91.14 ± 2.08	91.8 ± 1.94	91.26 ± 1.81	90.07 ± 1.76	0.662	0.189	0.133
B cells/CD5+	4.82 ± 1.21	3.74 ± 1.25	3.04 ± 0.4	2.87 ± 0.63	0.043	< 0.001	0.136
B cells/B220+MHCclassII+	89.98 ± 2.01	90.76 ± 1.49	86.22 ± 1.79	86.87 ± 2.45	0.257	< 0.001	0.917
NK+/CD11b+	59.27 ± 5.1	65.06 ± 10.13	45.39 ± 7.8	54.65 ± 7.73	0.005	< 0.001	0.491
CD4/CD8	1.51 ± 0.22	1.32 ± 0.4	1.38 ± 0.22	1.25 ± 0.2	0.08	0.239	0.707

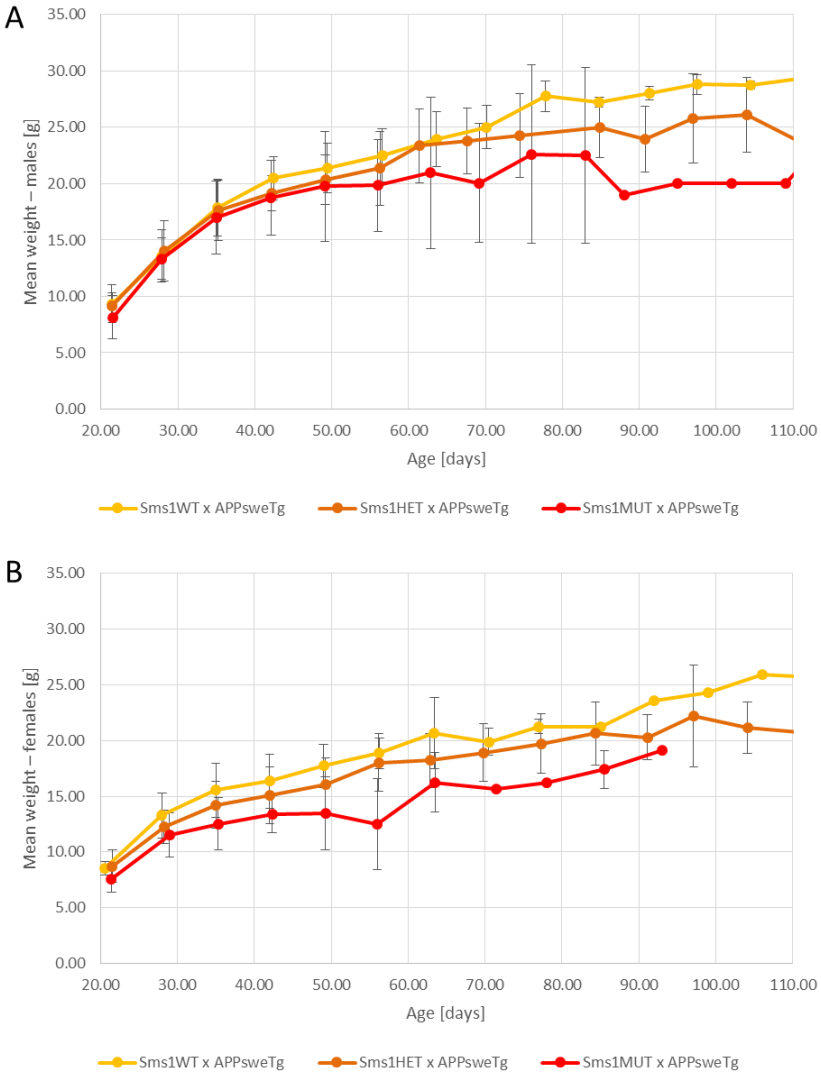

Figure 10.4: Body weigh increase with age of *Sms1* x *APPswe*Tg male and female animals.
Animals of all genotypes of the *Sms1* x *APPswe* mouse line bearing a h*APPswe* transgene where weight on a weekly basis. Mean age and mean weight per genotype and sex was calculated. Weight gain during the first 110 days is displayed. Males: $Sms1^{WT}$x $APPswe^{Tg}$ n=9-1, $Sms1^{HET}$ x $APPswe^{Tg}$ n=14-1, $Sms1^{MUT}$ x $APPswe^{Tg}$ n=12-1; Females: $Sms1^{WT}$x $APPswe^{Tg}$ n=5-2, $Sms1^{HET}$ x $APPswe^{Tg}$ n=17-4, $Sms1^{MUT}$ x $APPswe^{Tg}$ n=12-1; data is presented as mean ± SEM $p<0.01^{\#}$, $p\leq0.05$*, $p\leq0.01$**, $p\leq0.001$***.

Table 10.8: Weight difference of *Sms1*^{HET} x *APPswe*^{Tg} and *Sms1*^{MUT} x *APPswe*^{Tg} animals in comparison to *Sms1*^{WT} x *APPswe*^{Tg} animals.
Weight is given in % difference to *Sms1*^{WT} x *APPswe*^{Tg} levels and calculated corresponding to age.

% difference to *Sms1*^{WT} x *APPswe*^{Tg} weight		
mean age [days]	*Sms1*^{HET} x *APPswe*^{Tg}	*Sms1*^{MUT} x *APPswe*^{Tg}
21.33	0.24	12.61
28.22	2.32	7.37
35.11	6.12	11.78
42.17	9.15	12.66
49.21	8.22	15.09
56.21	6.60	21.86
62.98	8.75	16.59
69.84	6.24	20.49
76.80	10.99	20.86
84.57	8.45	17.60
91.06	17.38	26.21
96.78	12.62	24.67
103.78	17.52	26.81
110.71	23.37	27.40

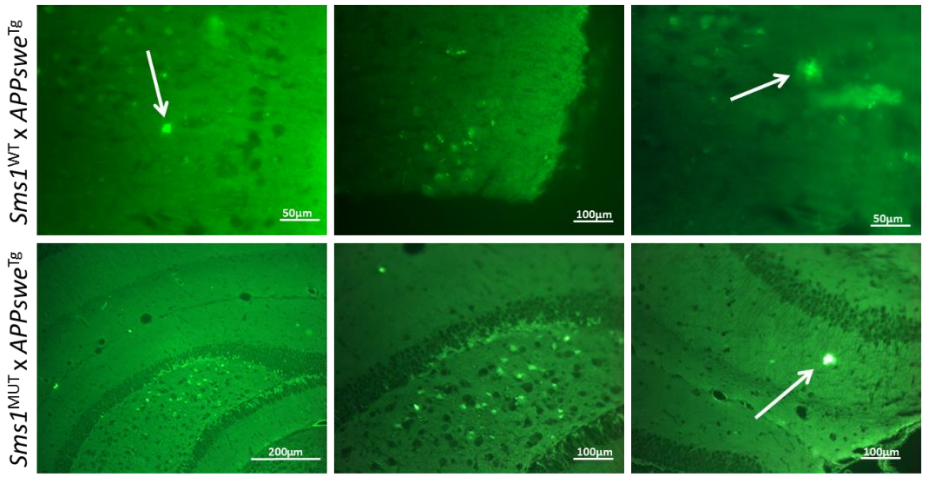

Figure 10.5: Thioflavin-S staining of brain sections from the *Sms1* x *APPswe* mouse line
Brain sections are stained with Thioflavin-S. Arrows point to Thioflavin-S positive stained plaques.

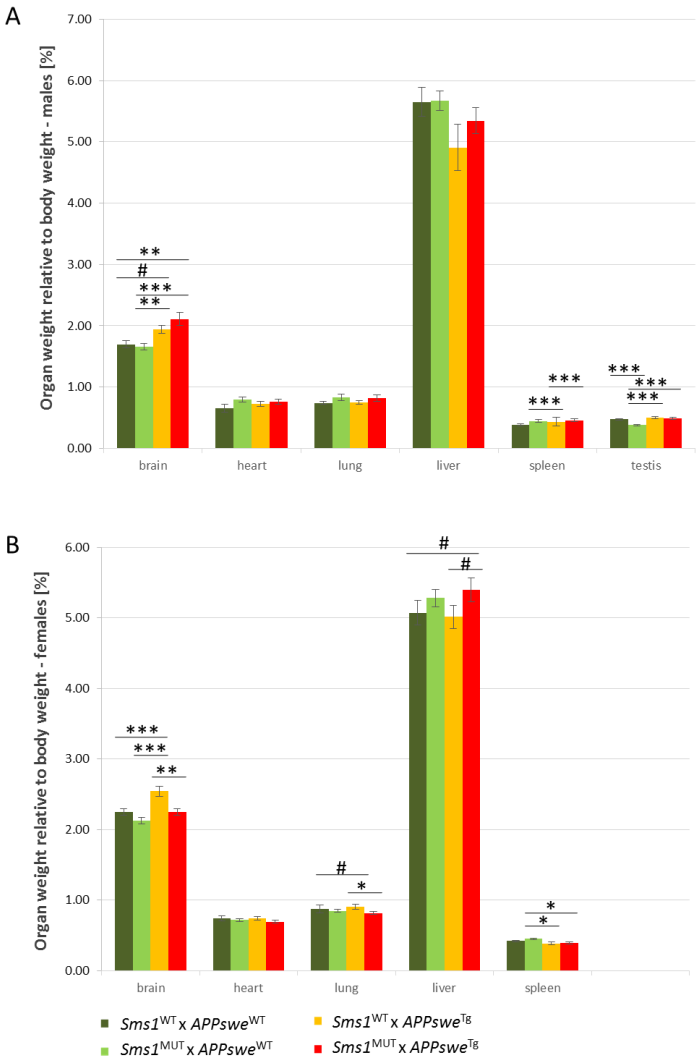

Figure 10.6: Organ weight of 8 week old male and female *Sms1* x *APPswe* mice, relative to body weight
Organ weight relative to body weight of (A) male and (B) female animals at the age of 8 weeks. Males: *Sms1*^{WT} x *APPswe*^{WT} n=8, *Sms1*^{MUT} x *APPswe*^{WT} n=12, *Sms1*^{WT} x *APPswe*^{Tg} n=16, *Sms1*^{MUT} x *APPswe*^{Tg} n=10; females: *Sms1*^{WT} x *APPswe*^{WT} n=12, *Sms1*^{MUT} x *APPswe*^{WT} n=21, *Sms1*^{WT} x *APPswe*^{Tg} n=11, *Sms1*^{MUT} x *APPswe*^{Tg} n=12. Statistical analysis was performed using one-way ANOVA and *post hoc* Tukey's test. Data is presented as percent of body weight ± SEM; $p<0.01^{\#}$, $p\leq0.05^{*}$, $p\leq0.01^{**}$, $p\leq0.001^{***}$.

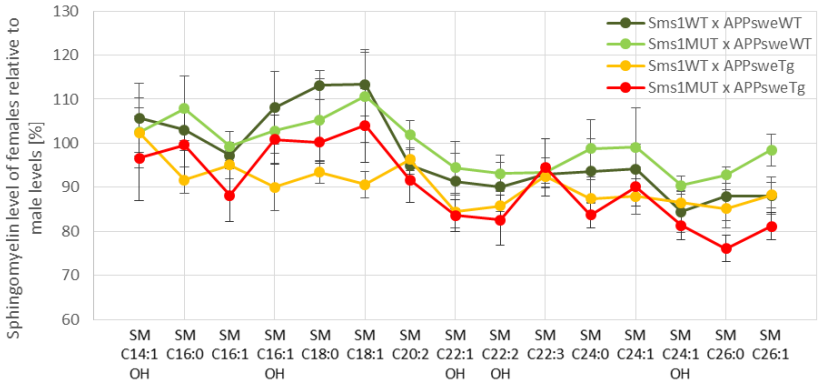

Figure 10.7: Comparison of female sphingomyelin species to male data.
Comparison of female SM species levels relative to male levels, which were set to 100%. Males: *Sms1*^{WT} x *APPswe*^{WT} n=5, *Sms1*^{MUT} x *APPswe*^{WT} n=6, *Sms1*^{WT} x *APPswe*^{Tg} n=11, *Sms1*^{MUT} x *APPswe*^{Tg} n=6; females: *Sms1*^{WT} x *APPswe*^{WT} n=6, *Sms1*^{MUT} x *APPswe*^{WT} n=11, *Sms1*^{WT} x *APPswe*^{Tg} n=13, *Sms1*^{MUT} x *APPswe*^{Tg} n=5. Age 8 weeks. Data is presented as percent difference ± SEM.

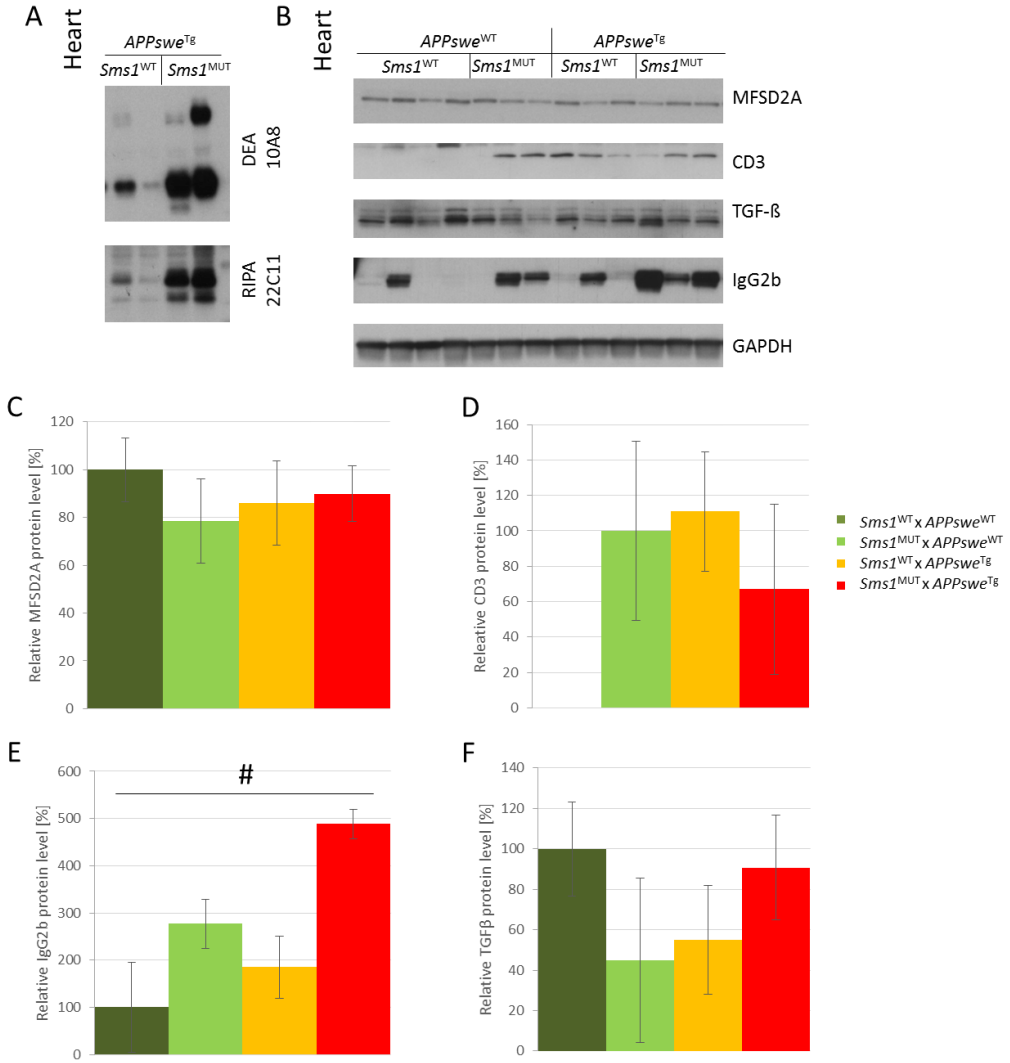

Figure 10.8: Immunological parameters of the heart.
(A) Immunoblot of heart tissue, showing high levels of endogenous mouse IgGs, detected with anti-mouse IgG secondary antibodies (B) Immunoblot of heart tissue against several inflammatory proteins. (C-F) Quantification of (C) MFSD2A, (D) CD3, (E) IgG2b and (F) TGF-β. *Sms1*^{WT} x *APPswe*^{WT} n=4, *Sms1*^{MUT} x *APPswe*^{WT} n=3, *Sms1*^{WT} x *APPswe*^{Tg} n=3, *Sms1*^{MUT} x *APPswe*^{Tg} n=3. Age 8 weeks. Statistical analysis was performed using one-way ANOVA and *post hoc* Tukey's test. Data is presented as mean ± SEM; p<0.01$^{\#}$, p≤0.05*, p≤0.01**, p≤0.001***.

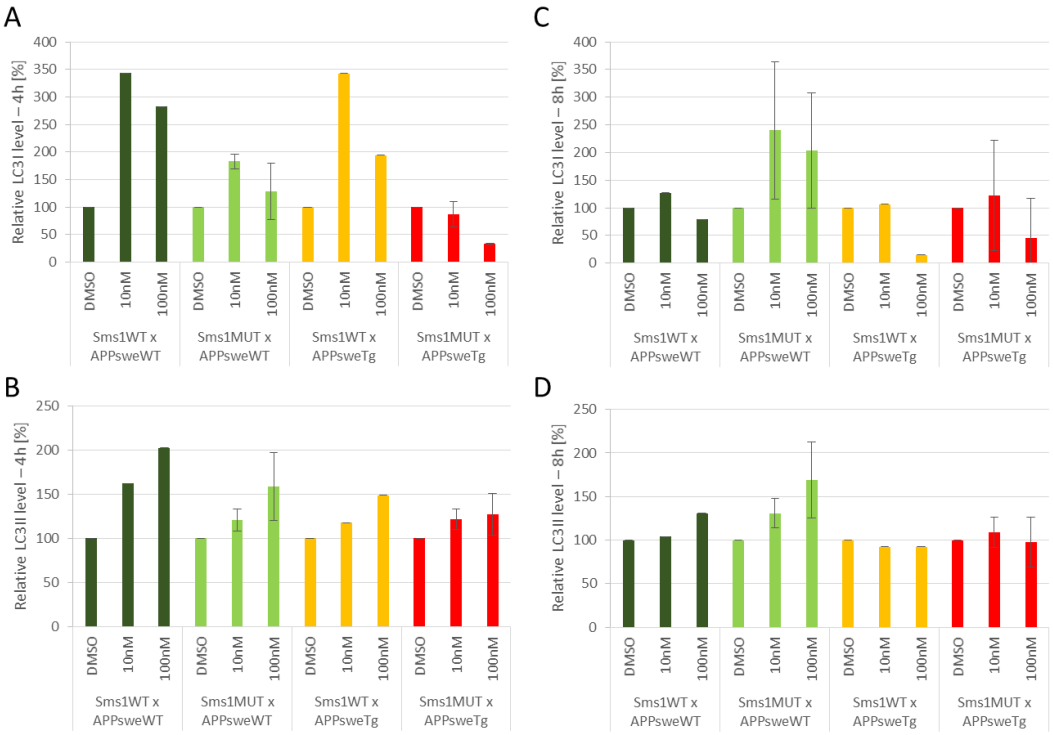

Figure 10.9: Time and dosage-dependent autophagy induction in MEFs obtained from breeding of the *Sms1* x *APPswe* mouse line
Sms1^{WT} x *APPswe*^{WT} (n=1), *Sms1*^{MUT} x *APPswe*^{WT} (n=2), *Sms1*^{WT} x *APPswe*^{Tg} (n=1) and *Sms1*^{MUT} x *APPswe*^{Tg} (n=4) MEFs obtained from E13.5 littermate embryos were treated with DMSO, 10µM or 100µM Rapamycin for 4h or 8h, respectively. (A-D) Quantification of LC3I (A,C) and LC3II (B,D) levels of immunoblots from Figure 3.43 with 4h (A,B) or 8h (C,D) incubation times relative to DMSO control, which was set to 100%. Data is presented as mean ± SEM.

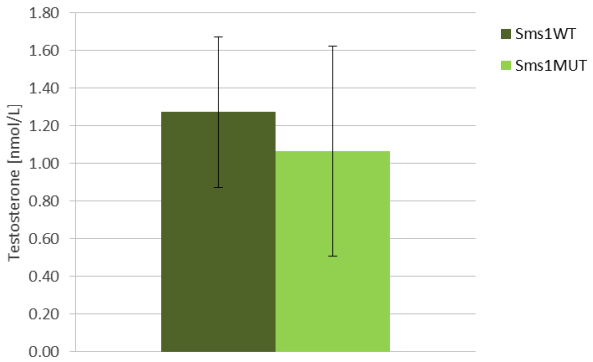

Figure 10.10: Testosterone levels of *Sms1*^{WT} and *Sms1*^{MUT} animals, measured in blood samples of 16 week old animals.
Blood testosterone levels measured in of *Sms1*^{WT} and *Sms1*^{MUT} animals at the age of 16 weeks. Statistical analysis was performed using two-tailed Student's t-test. Data is presented as mean ± SEM.

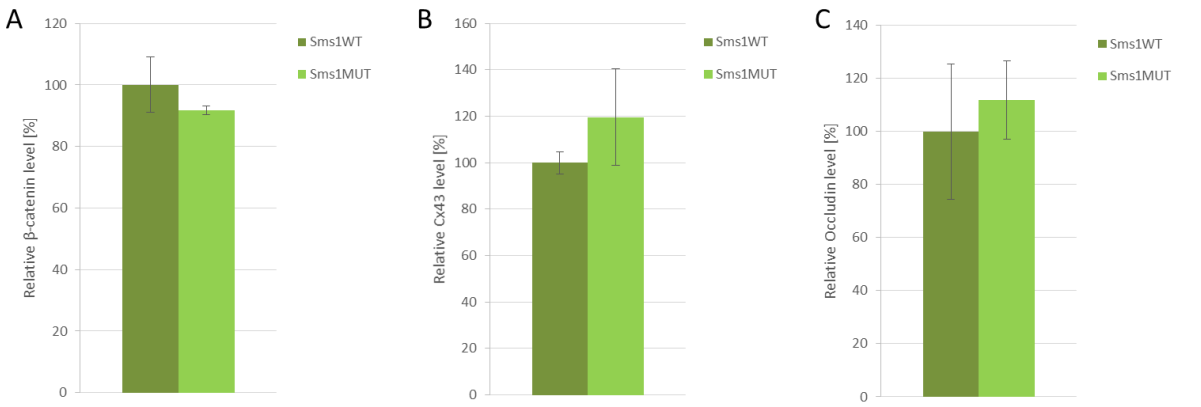

Figure 10.11: Quantification of BTB components in the epididymides of *Sms1*^{WT} and *Sms1*^{MUT} animals
(A-C) Immunoblot quantification of of junction markers. B-catenin (β-cat) was used as adherence junction marker, Connexin 43 (Cx43) as gap junction marker and occluding (Occl) as tight junction marker. Quantification of immunoblot results is based on epididymides samples shown in Figure 3.23Figure 3.23
Sms1^{WT} n=3, *Sms1*^{MUT} n=3. Statistical analysis was performed using two-tailed Student's t-test. Data is presented as mean ± SEM; *p≤0.05, **p≤0.01, ***p≤0.001.

Table 10.9: Level of SM measured in brain samples of male (A) and female (B) *Sms1*^{WT} and *Sms1*^{MUT} animals.
Statistical analysis was performed using two-tailed Student's t-test
*p≤0.05, **p≤0.01, ***p≤0.001.

A

SM species	Sms1WT (n=9)			Sms1MUT (n=9)			significance	
	Intensity	%	SEM %	Intensity	%	SEM %	ttest	significance
total SM	883293,224	100	2,1	484722,3	54,9	6,6	0,0000	***
SM C14:1 OH	361,1	100	16,5	326,7	90,5	9,1	0,6215	
SM C16:0	24945,0	100	5,6	18126,2	72,7	3,9	0,0011	**
SM C16:1	1040,0	100	6,6	871,0	83,7	3,7	0,0459	*
SM C16:1 OH	2530,2	100	3,4	1642,8	64,9	5,2	0,0000	***
SM C18:0	498513,7	100	2,6	266875,9	53,5	7,6	0,0000	***
SM C18:1	34259,9	100	4,4	22851,7	66,7	9,8	0,0068	**
SM C20:2	562,0	100	5,6	547,5	97,4	6,0	0,7583	
SM C22:1 OH	15633,0	100	2,5	8076,5	51,7	5,1	0,0000	***
SM C22:2 OH	7167,1	100	3,2	4325,7	60,4	4,7	0,0000	***
SM C22:3	4657,8	100	5,0	4558,9	97,9	8,3	0,8299	
SM C24:0	92643,1	100	2,9	49109,6	53,0	5,8	0,0000	***
SM C24:1	178317,8	100	2,0	92027,2	51,6	6,4	0,0000	***
SM C24:1 OH	4168,3	100	4,2	2820,0	67,7	4,8	0,0001	***
SM C26:0	13609,8	100	4,0	9130,7	67,1	6,0	0,0003	***
SM C26:1	4884,7	100	3,3	3431,9	70,3	5,3	0,0002	***

B

SM species	Sms1WT (n=8)			Sms1MUT (n=10)			significance	
	Intensity	%	SEM %	Intensity	%	SEM %	ttest	significance
total SM	893785,636	100	7,0	506383,0	56,7	3,4	0,0002	***
SM C14:1 OH	421,2	100	4,4	393,6	93,5	5,5	0,3681	
SM C16:0	25272,7	100	4,0	20135,4	79,7	4,2	0,0030	**
SM C16:1	1057,2	100	3,9	962,4	91,0	4,7	0,1604	
SM C16:1 OH	2572,8	100	6,0	1966,9	76,5	7,2	0,0234	*
SM C18:0	520219,2	100	8,5	263545,3	50,7	3,7	0,0004	***
SM C18:1	36768,2	100	9,0	22471,4	61,1	5,1	0,0030	**
SM C20:2	683,1	100	3,7	734,5	107,5	10,3	0,5049	
SM C22:1 OH	14232,4	100	8,1	8967,6	63,0	4,1	0,0020	**
SM C22:2 OH	7328,8	100	6,4	5837,0	79,6	6,4	0,0388	*
SM C22:3	5326,6	100	4,8	5396,4	101,3	5,8	0,8637	
SM C24:0	85632,2	100	8,7	55118,2	64,4	3,8	0,0041	**
SM C24:1	171865,8	100	9,0	103096,8	60,0	4,1	0,0024	**
SM C24:1 OH	4465,9	100	7,5	3410,2	76,4	4,1	0,0184	*
SM C26:0	13017,6	100	7,0	9863,3	75,8	4,6	0,0132	*
SM C26:1	4921,9	100	5,0	4483,9	91,1	4,5	0,2023	

Table 10.10: Level of PCaa species, measured in male *Sms1*^{WT} and *Sms1*^{MUT} brain samples.
Statistical analysis was performed using two-tailed Student's t-test.
*p≤0.05, **p≤0.01, ***p≤0.001.

PC aa species	Sms1WT (n=9)			Sms1MUT (n=9)			significance	
	Intensity	%	SEM %	Intensity	%	SEM %	ttest	significance
PC aa total	10673965,1	100,0	2,6	9682644,5	90,7	6,7	0,2155	
PC aa saturated	2174827,0	100,0	3,4	2129478,0	97,9	7,0	0,7914	
PC aa unsaturated	8499138,0	100,0	2,5	7553166,5	88,9	6,7	0,1370	
PC aa CX:1	4866174,6	100,0	1,5	4280122,8	88,0	6,0	0,0698	
PC aa CX:2	693153,8	100,0	3,3	560211,2	80,8	6,2	0,0152	*
PC aa CX:3	273326,6	100,0	4,2	250935,4	91,8	7,5	0,3568	
PC aa CX:4	1320881,2	100,0	4,3	1254124,8	94,9	8,3	0,5967	
PC aa CX:5	371894,1	100,0	4,4	340043,8	91,4	8,0	0,3607	
PC aa CX:6	973707,9	100,0	3,4	867728,7	89,1	7,8	0,2184	
PC aa C24:0	996,2	100,0	12,8	847,1	85,0	11,2	0,3916	
PC aa C26:0	1068,1	100,0	10,2	1363,6	127,7	11,4	0,0890	
PC aa C28:1	571,5	100,0	9,0	593,6	103,9	8,1	0,7538	
PC aa C30:0	43263,9	100,0	5,4	43227,7	99,9	8,1	0,9933	
PC aa C30:2	651,8	100,0	8,1	609,9	93,6	5,5	0,5227	
PC aa C32:0	1913800,0	100,0	3,4	1912953,0	100,0	7,1	0,9956	
PC aa C32:1	365221,5	100,0	3,5	279327,4	76,5	6,5	0,0057	**
PC aa C32:2	16434,0	100,0	4,4	11835,6	72,0	7,8	0,0065	**
PC aa C32:3	521,5	100,0	8,1	507,5	97,3	7,4	0,8098	
PC aa C34:1	2795900,0	100,0	0,9	2610600,0	93,4	5,8	0,2760	
PC aa C34:2	164019,3	100,0	4,9	142097,5	86,6	6,0	0,1053	
PC aa C34:3	5403,2	100,0	8,6	4612,5	85,4	2,9	0,1258	
PC aa C34:4	1316,1	100,0	5,8	1266,2	96,2	7,2	0,6891	
PC aa C36:0	188458,9	100,0	3,4	151906,4	80,6	6,7	0,0196	*
PC aa C36:1	1513844,4	100,0	2,4	1262795,2	83,4	6,6	0,0306	*
PC aa C36:2	464316,3	100,0	3,4	374348,9	80,6	6,5	0,0175	*
PC aa C36:3	144089,6	100,0	4,6	136087,5	94,4	7,6	0,5428	
PC aa C36:4	616890,0	100,0	4,1	605078,9	98,1	8,5	0,8422	
PC aa C36:5	10616,1	100,0	4,4	10491,9	98,8	8,5	0,9044	
PC aa C36:6	4195,4	100,0	4,1	4163,4	99,2	6,1	0,9189	
PC aa C38:0	22241,4	100,0	2,7	15837,1	71,2	6,0	0,0005	***
PC aa C38:1	127828,1	100,0	3,2	85783,5	67,1	6,4	0,0003	***
PC aa C38:3	112468,3	100,0	3,8	100367,0	89,2	7,7	0,2285	
PC aa C38:4	638471,5	100,0	4,6	590951,5	92,6	8,2	0,4404	
PC aa C38:5	268284,4	100,0	4,3	251831,2	93,9	8,3	0,5206	
PC aa C38:6	577558,5	100,0	3,7	533700,7	92,4	8,0	0,4010	
PC aa C40:1	35774,4	100,0	6,0	23823,2	66,6	6,3	0,0015	**
PC aa C40:2	28350,1	100,0	4,0	19029,9	67,1	6,2	0,0004	***
PC aa C40:3	10844,0	100,0	3,8	9360,8	86,3	7,2	0,1126	
PC aa C40:4	57444,4	100,0	3,5	51311,1	89,3	7,9	0,2334	
PC aa C40:5	87614,6	100,0	4,5	73542,3	83,9	7,4	0,0824	#
PC aa C40:6	385357,8	100,0	3,2	324730,4	84,3	7,6	0,0735	
PC aa C42:0	4998,6	100,0	9,3	3343,0	66,9	6,3	0,0095	**
PC aa C42:1	27034,5	100,0	9,8	17199,8	63,6	6,8	0,0077	**
PC aa C42:2	19382,3	100,0	7,8	12289,4	63,4	6,2	0,0021	**
PC aa C42:4	6759,2	100,0	4,6	5517,1	81,6	7,2	0,0465	*
PC aa C42:5	5378,9	100,0	3,8	4178,4	77,7	6,8	0,0110	*
PC aa C42:6	6596,2	100,0	3,6	5134,1	77,8	6,8	0,0109	*

PC aa	ratio	%	SEM %	ratio	%	SEM %	ttest	significance
MUFA/SFA	2,3	100,0	2,2	2,0	89,7	0,7	0,0012	**
PUFA/SFA	1,7	100,0	1,3	1,5	90,7	1,0	0,0077	**
PUFA/MUFA	0,7	100,0	2,4	0,8	101,0	0,9	0,8120	

Table 10.11: Level of PCaa species, measured in female *Sms1*^{WT} and *Sms1*^{MUT} brain samples.
* Statistical analysis was performed using two-tailed Student's t-test.
p≤0.05, **p≤0.01, ***p≤0.001.

PC aa species	Sms1WT (n=8)			Sms1MUT (n=10)			significance	
	Intensity	%	SEM %	Intensity	%	SEM %	ttest	significance
PC aa total	11147648,4	100,0	2,3	10758239,0	96,5	2,2	0,2919	
PC aa saturated	2275673,0	100,0	3,2	2316099,0	101,8	2,9	0,6851	
PC aa unsaturated	8871975,4	100,0	2,3	8442140,0	95,2	2,2	0,1430	
PC aa CX:1	4976511,9	100,0	1,6	4791147,8	96,3	2,0	0,1731	
PC aa CX:2	684527,6	100,0	3,2	640033,4	93,5	3,2	0,1716	
PC aa CX:3	281812,0	100,0	4,4	276015,2	97,9	4,0	0,7344	
PC aa CX:4	1445436,7	100,0	4,9	1388417,8	96,1	4,2	0,5506	
PC aa CX:5	411273,4	100,0	3,6	385913,7	93,8	3,1	0,2166	
PC aa CX:6	1072413,7	100,0	3,4	960612,2	89,6	3,7	0,0538	
PC aa C24:0	1173,0	100,0	4,7	1224,5	104,4	6,2	0,5801	
PC aa C26:0	1806,5	100,0	7,0	1766,3	97,8	3,1	0,7784	
PC aa C28:1	857,7	100,0	6,0	831,2	96,9	4,3	0,6845	
PC aa C30:0	45073,7	100,0	6,1	51073,6	113,3	9,0	0,2392	
PC aa C30:2	807,6	100,0	3,7	806,0	99,8	5,0	0,9759	
PC aa C32:0	2005795,8	100,0	3,5	2073383,3	103,4	3,1	0,4789	
PC aa C32:1	379158,8	100,0	4,2	321887,7	84,9	6,1	0,0598	
PC aa C32:2	17332,5	100,0	7,3	13333,3	76,9	10,5	0,0921	
PC aa C32:3	658,4	100,0	4,2	723,9	110,0	9,0	0,3360	
PC aa C34:1	2848925,0	100,0	1,2	2931923,3	102,9	2,5	0,3168	
PC aa C34:2	152340,0	100,0	4,4	161492,9	106,0	5,4	0,3994	
PC aa C34:3	4702,7	100,0	4,2	5661,4	120,4	16,0	0,2448	
PC aa C34:4	1492,6	100,0	4,0	1704,2	114,2	10,4	0,2293	
PC aa C36:0	194546,7	100,0	3,0	167791,3	86,2	3,4	0,0076	**
PC aa C36:1	1566787,5	100,0	2,5	1404437,3	89,6	2,6	0,0107	*
PC aa C36:2	469835,4	100,0	3,1	431871,3	91,9	2,8	0,0728	
PC aa C36:3	145835,4	100,0	5,0	146611,5	100,5	4,3	0,9365	
PC aa C36:4	676889,2	100,0	5,4	666849,7	98,5	4,8	0,8396	
PC aa C36:5	11991,1	100,0	4,5	12303,9	102,6	6,0	0,7328	
PC aa C36:6	6074,9	100,0	4,5	5774,7	95,1	4,6	0,4570	
PC aa C38:0	22690,5	100,0	6,1	17473,2	77,0	4,4	0,0086	**
PC aa C38:1	126681,3	100,0	6,7	94158,3	74,3	4,7	0,0078	**
PC aa C38:3	118906,5	100,0	4,0	111841,2	94,1	4,0	0,3097	
PC aa C38:4	696989,6	100,0	4,7	653773,3	93,8	3,8	0,3205	
PC aa C38:5	297861,7	100,0	4,1	284423,3	95,5	3,3	0,4085	
PC aa C38:6	629571,7	100,0	3,1	588611,7	93,5	3,8	0,2021	
PC aa C40:1	31432,8	100,0	7,6	22626,2	72,0	5,0	0,0093	**
PC aa C40:2	26919,5	100,0	6,7	20452,4	76,0	4,9	0,0122	*
PC aa C40:3	11709,0	100,0	3,3	11177,1	95,5	4,2	0,4060	
PC aa C40:4	62820,8	100,0	3,2	59728,3	95,1	4,3	0,3705	
PC aa C40:5	95613,4	100,0	3,5	84136,8	88,0	3,4	0,0253	*
PC aa C40:6	429426,7	100,0	4,1	359919,0	83,8	3,8	0,0110	*
PC aa C42:0	4586,8	100,0	9,6	3386,7	73,8	5,7	0,0378	*
PC aa C42:1	22668,9	100,0	10,2	15283,8	67,4	5,7	0,0176	*
PC aa C42:2	17292,6	100,0	10,3	12077,4	69,8	5,1	0,0244	*
PC aa C42:4	7244,6	100,0	4,3	6362,2	87,8	4,8	0,0780	
PC aa C42:5	5807,3	100,0	4,2	5049,6	87,0	3,9	0,0390	*
PC aa C42:6	7340,5	100,0	5,2	6306,8	85,9	4,3	0,0532	

PC aa	ratio	%	SEM %	ratio	%	SEM %	ttest	significance
MUFA/SFA	2,2	100,0	2,7	2,1	94,8	3,4	0,2491	
PUFA/SFA	1,7	100,0	1,6	1,6	92,0	1,3	0,0014	**
PUFA/MUFA	0,8	100,0	2,3	0,8	97,5	3,0	0,5257	

Table 10.12: Level of PCae species, measured in male *Sms1*^{WT} and *Sms1*^{MUT} brain samples.
Statistical analysis was performed using two-tailed Student's t-test.
*p≤0.05, **p≤0.01, ***p≤0.001.

PC ae species	Sms1WT (n=9)			Sms1MUT (n=9)			significance	
	Intensity	%	SEM %	Intensity	%	SEM %	ttest	significance
total PC ae	681181,887	100,0	3,9	570551,2471	83,8	6,3	0,0431	*
saturated PC ae	221361,455	100,0	3,7	191198,1867	86,4	7,1	0,1073	
unsaturated PC ae	459820,432	100,0	4,0	379353,0605	82,5	5,9	0,0267	*
PC ae CX:1	248602,92	100,0	3,9	203857,2275	82,0	6,0	0,0233	*
PC ae CX:2	74237,8383	100,0	4,4	55356,51323	74,6	4,8	0,0012	**
PC ae CX:3	37882,1754	100,0	4,5	31894,05289	84,2	6,2	0,0559	
PC ae CX:4	33331,7596	100,0	4,8	30201,75284	90,6	7,4	0,3020	
PC ae CX:5	39026,6387	100,0	4,0	33977,80423	87,1	6,7	0,1180	
PC ae CX:6	26739,0998	100,0	3,9	24065,70975	90,0	6,8	0,2194	
PC ae C30:0	1346,30688	100,0	5,2	1302,763419	96,8	5,7	0,6818	
PC ae C30:1	711,327293	100,0	6,9	703,4285667	98,9	7,1	0,9117	
PC ae C30:2	418,492822	100,0	11,9	420,382463	100,5	12,3	0,9793	
PC ae C32:1	18291,2222	100,0	4,7	17957,45427	98,2	8,0	0,8469	
PC ae C32:2	1187,1096	100,0	8,6	1035,463341	87,2	3,4	0,1844	
PC ae C34:0	47654,1852	100,0	3,8	43623,85185	91,5	7,0	0,3045	
PC ae C34:1	102329,148	100,0	3,8	88943,92593	86,9	7,0	0,1202	
PC ae C34:2	18725,7037	100,0	3,9	14612,10658	78,0	5,2	0,0041	**
PC ae C34:3	1179,44671	100,0	8,8	1053,392285	89,3	2,7	0,2624	
PC ae C36:0	17744,3704	100,0	4,7	16647,86017	93,8	5,8	0,4204	
PC ae C36:1	71652,8148	100,0	4,6	56218,85185	78,5	5,0	0,0059	**
PC ae C36:2	24177,4815	100,0	5,1	17962,88889	74,3	4,3	0,0015	**
PC ae C36:3	8559,64475	100,0	5,0	6761,931967	79,0	5,0	0,0092	**
PC ae C36:4	8432,32653	100,0	4,6	8202,977326	97,3	7,9	0,7710	
PC ae C36:5	8387,70069	100,0	5,6	8057,77173	96,1	7,1	0,6711	
PC ae C38:0	13150,0741	100,0	4,1	11476,19501	87,3	6,3	0,1113	
PC ae C38:1	23023,2593	100,0	3,8	15476,452	67,2	4,8	0,0001	***
PC ae C38:2	13004,2222	100,0	4,1	8722,353744	67,1	4,6	0,0001	***
PC ae C38:3	7575,0053	100,0	5,8	6244,328037	82,4	5,6	0,0442	
PC ae C38:4	12760,8148	100,0	4,8	11716,20862	91,8	7,8	0,3848	
PC ae C38:5	8623,15041	100,0	4,1	8058,136052	93,4	7,2	0,4394	
PC ae C38:6	14666,6296	100,0	3,8	13577,54649	92,6	6,8	0,3574	
PC ae C40:0	125417,407	100,0	4,0	106638,3333	85,0	7,7	0,1027	
PC ae C40:1	17232,6296	100,0	3,5	12914,97808	74,9	6,0	0,0023	**
PC ae C40:2	6317,69312	100,0	4,3	4363,694633	69,1	5,3	0,0003	***
PC ae C40:3	4263,11414	100,0	6,8	3610,630389	84,7	7,1	0,1393	
PC ae C40:4	5728,20862	100,0	5,7	5097,705222	89,0	7,8	0,2718	
PC ae C40:5	6879,98488	100,0	5,3	6075,856389	88,3	7,4	0,2168	
PC ae C40:6	11123,0129	100,0	3,9	9749,322752	87,7	7,0	0,1422	
PC ae C42:0	16049,1111	100,0	2,9	11509,18291	71,7	7,3	0,0023	**
PC ae C42:1	15362,5185	100,0	5,5	11642,13681	75,8	6,5	0,0120	*
PC ae C42:2	10407,1353	100,0	5,3	8239,623585	79,2	6,7	0,0270	*
PC ae C42:3	12329,9259	100,0	4,4	10992,03174	89,1	7,8	0,2422	
PC ae C42:4	2257,80196	100,0	6,5	1884,312922	83,5	7,4	0,1135	
PC ae C42:5	2249,24717	100,0	5,8	1903,297052	84,6	7,5	0,1235	
PC ae C44:3	3975,03855	100,0	3,7	3231,73847	81,3	7,6	0,0417	*
PC ae C44:4	4152,60771	100,0	5,0	3300,548748	79,5	7,4	0,0345	*
PC ae C44:5	12886,5556	100,0	3,7	9882,743007	76,7	8,5	0,0234	*
PC ae C44:6	949,457293	100,0	6,6	738,8405111	77,8	6,1	0,0251	*

Table 10.13: Level of PCae species, measured in female *Sms1*^{WT} and *Sms1*^{MUT} brain samples.
Statistical analysis was performed using two-tailed Student's t-test.
*p≤0.05, **p≤0.01, ***p≤0.001.

PC ae species	Sms1WT (n=8)			Sms1MUT (n=10)			significance	
	Intensity	%	SEM %	Intensity	%	SEM %	ttest	significance
total PC ae	725613,648	100,0	3,4	674321,68	92,9	3,7	0,1742	
saturated PC ae	245640,625	100,0	3,5	222910,1	90,7	3,3	0,0752	
unsaturated PC ae	479973,022	100,0	3,4	451411,58	94,0	4,0	0,2770	
PC ae CX:1	251309,525	100,0	2,9	239154,065	95,2	4,3	0,3706	
PC ae CX:2	73049,5053	100,0	5,6	65505,0837	89,7	4,5	0,1737	
PC ae CX:3	41373,9289	100,0	4,1	38436,7298	92,9	4,2	0,2428	
PC ae CX:4	36726,1436	100,0	2,9	36692,0708	99,9	5,0	0,9874	
PC ae CX:5	45254,692	100,0	4,3	42115,0178	93,1	5,1	0,3157	
PC ae CX:6	32259,2271	100,0	4,0	29508,6129	91,5	4,8	0,1928	
PC ae C30:0	1547,83376	100,0	3,2	1800,5979	116,3	11,9	0,2124	
PC ae C30:1	906,57795	100,0	4,2	946,603743	104,4	5,5	0,5321	
PC ae C30:2	542,724208	100,0	3,8	549,816663	101,3	5,8	0,8526	
PC ae C32:1	18901,4167	100,0	4,8	19820,4	104,9	4,9	0,4899	*
PC ae C32:2	1252,2821	100,0	3,0	1305,50391	104,2	6,5	0,5634	
PC ae C34:0	50614,9583	100,0	2,7	49934,2667	98,7	5,2	0,8233	
PC ae C34:1	105917,667	100,0	2,4	105500,6	99,6	5,8	0,9510	
PC ae C34:2	18388,6667	100,0	4,9	16547,8667	90,0	4,0	0,1321	
PC ae C34:3	1173,94728	100,0	3,6	1207,44014	102,9	5,2	0,6603	
PC ae C36:0	24431,2917	100,0	4,5	24445,4333	100,1	5,8	0,9938	
PC ae C36:1	71082,375	100,0	3,7	67474	94,9	5,5	0,4570	
PC ae C36:2	23165,2083	100,0	6,3	21670,6333	93,5	6,3	0,4783	
PC ae C36:3	8248,72144	100,0	4,8	7645,97619	92,7	5,1	0,3146	
PC ae C36:4	8942,62337	100,0	3,5	9524,27291	106,5	5,5	0,3354	
PC ae C36:5	9824,17942	100,0	4,6	9724,38401	99,0	9,1	0,9221	
PC ae C38:0	16000,9583	100,0	4,7	15407,5333	96,3	4,1	0,5601	
PC ae C38:1	22910,2917	100,0	6,0	18768	81,9	4,7	0,0325	
PC ae C38:2	12606,0833	100,0	7,4	10691,1371	84,8	4,8	0,1090	
PC ae C38:3	8231,44062	100,0	4,1	8121,1593	98,7	4,7	0,8313	
PC ae C38:4	13782,2917	100,0	3,6	14163,8333	102,8	5,9	0,6946	
PC ae C38:5	10213,9966	100,0	3,5	10113,8283	99,0	4,6	0,8666	
PC ae C38:6	18385,5417	100,0	4,0	16788,2667	91,3	4,4	0,1615	
PC ae C40:0	136080,833	100,0	3,7	117928,033	86,7	3,0	0,0149	*
PC ae C40:1	16823,5833	100,0	4,0	14494,2	86,2	4,2	0,0299	*
PC ae C40:2	6501,8497	100,0	7,0	5392,57148	82,9	4,6	0,0634	
PC ae C40:3	5120,12819	100,0	4,0	4973,76184	97,1	5,2	0,6669	
PC ae C40:4	6773,64356	100,0	3,5	6552,35402	96,7	5,3	0,6156	
PC ae C40:5	8311,10686	100,0	4,2	8132,7674	97,9	5,5	0,7608	
PC ae C40:6	12790,125	100,0	4,0	11781,2667	92,1	5,9	0,2865	
PC ae C42:0	16964,75	100,0	7,8	13394,2354	79,0	4,9	0,0407	*
PC ae C42:1	14767,6139	100,0	5,3	12150,2612	82,3	4,2	0,0202	*
PC ae C42:2	10592,691	100,0	4,6	9347,55459	88,2	3,7	0,0651	
PC ae C42:3	14000,7083	100,0	4,2	12505,385	89,3	4,0	0,0841	
PC ae C42:4	2694,30619	100,0	5,6	2463,98129	91,5	6,3	0,3232	
PC ae C42:5	2963,28415	100,0	6,7	2722,38231	91,9	6,3	0,3904	
PC ae C44:3	4598,983	100,0	6,2	3983,00731	86,6	4,8	0,1100	
PC ae C44:4	4533,27884	100,0	7,2	3987,6292	88,0	4,9	0,1880	
PC ae C44:5	13942,125	100,0	8,6	11421,6558	81,9	5,3	0,0974	
PC ae C44:6	1083,56044	100,0	7,1	939,079593	86,7	5,5	0,1611	

Table 10.14: Level of PEae measured in brain samples of male (A) and female (B) *Sms1*^{WT} and *Sms1*^{MUT} animals.
Statistical analysis was performed using two-tailed Student's t-test.
*p≤0.05, **p≤0.01, ***p≤0.001.

A

PE ae species	Sms1WT (n=9)			Sms1MUT (n=9)			significance	
	Intensity	%	SEM %	Intensity	%	SEM %	ttest	significance
PCae total	17722,4	100,0	4,3	15173,7	85,6	11,9	0,2710	
PEae 36:2	3715,2	100,0	4,7	2833,0	76,3	11,7	0,0776	
PEae 36:4	2843,6	100,0	4,0	2573,6	90,5	12,5	0,4804	
PEae 38:4	2868,5	100,0	6,0	2876,9	100,3	14,6	0,9854	
PEae 38:5	3842,0	100,0	3,8	3503,0	91,2	12,7	0,5149	
PEae 38:6	2013,3	100,0	4,7	1519,9	75,5	9,3	0,0327	*
PE ae 40:6	2439,9	100,0	5,4	1867,4	76,5	10,6	0,0661	

B

PE ae species	Sms1WT (n=8)			Sms1MUT (n=10)			significance	
	Intensity	%	SEM %	Intensity	%	SEM %	ttest	significance
PCae total	4222,8	100,0	8,7	3312,6	78,4	9,1	0,1059	
PEae 36:2	2403,7	100,0	9,7	2079,9	86,5	6,7	0,2743	
PEae 36:4	20886,2	100,0	7,4	18714,2	89,6	7,8	0,3358	
PEae 38:4	2854,5	100,0	9,0	2399,5	84,1	9,0	0,2295	
PEae 38:5	3516,2	100,0	6,6	3564,5	101,4	7,0	0,8883	
PEae 38:6	4555,8	100,0	7,1	4079,7	89,5	8,1	0,3446	
PE ae 40:6	3333,3	100,0	7,4	3278,1	98,3	8,1	0,8823	

Table 10.15: Level of lyso-PC measured in brain samples of male (A) and female (B) *Sms1*^{WT} and *Sms1*^{MUT} animals.
Statistical analysis was performed using two-tailed Student's t-test.
*p≤0.05, **p≤0.01, ***p≤0.001.

A

lyso PC a species	Sms1WT (n=9)			Sms1MUT (n=9)			significance	
	Intensity	%	SEM %	Intensity	%	SEM %	ttest	significance
total lyso PC a	54163,1	100,0	5,2	44332,6	81,9	5,6	0,0310	*
Lyso PC 6:0	44,4	100,0	6,6	51,5	116,0	4,6	0,0637	
Lyso PC 14:0	2091,1	100,0	2,5	2120,4	101,4	1,2	0,6280	
Lyso PC 16:0	22626,4	100,0	4,8	18641,8	82,4	6,3	0,0411	*
Lyso PC 16:1	646,7	100,0	6,3	704,2	108,9	7,1	0,3616	
Lyso PC 17:0	338,1	100,0	6,2	424,7	125,6	7,3	0,0167	*
Lyso PC 18:0	7908,6	100,0	4,6	6250,9	79,0	5,6	0,0111	*
Lyso PC 18:1	12486,7	100,0	6,1	9567,0	76,6	5,8	0,0132	*
Lyso PC 18:2	634,0	100,0	10,3	592,9	93,5	4,0	0,5666	
Lyso PC 20:3	439,2	100,0	6,2	352,1	80,2	6,3	0,0394	*
Lyso PC 20:4	4329,9	100,0	9,2	3144,5	72,6	6,7	0,0291	*
Lyso PC 24:0	1002,1	100,0	10,5	766,3	76,5	6,7	0,0777	
Lyso PC 26:0	546,9	100,0	11,0	573,3	104,8	10,2	0,7528	
Lyso PC 26:1	270,8	100,0	9,4	254,6	94,0	8,8	0,6486	
Lyso PC 28:0	448,2	100,0	8,9	507,8	113,3	8,8	0,3031	
Lyso PC 28:1	350,1	100,0	8,8	380,8	108,8	12,0	0,5646	

B

lyso PC a species	Sms1WT (n=8)			Sms1MUT (n=10)			significance	
	Intensity	%	SEM %	Intensity	%	SEM %	ttest	significance
total lyso PC a	62154,0	100,0	5,4	74801,6	120,3	25,6	0,4543	
Lyso PC 6:0	89,2	100,0	8,5	74,4	83,4	5,3	0,1221	
Lyso PC 14:0	2165,5	100,0	1,2	1952,1	90,1	3,3	0,0165	*
Lyso PC 16:0	25415,0	100,0	5,8	29712,9	116,9	19,7	0,4293	
Lyso PC 16:1	1183,0	100,0	8,2	1633,4	138,1	43,4	0,4097	
Lyso PC 17:0	808,2	100,0	9,6	737,0	91,2	6,1	0,4551	
Lyso PC 18:0	8947,7	100,0	5,4	8984,0	100,4	9,7	0,9714	
Lyso PC 18:1	13687,4	100,0	5,4	20734,7	151,5	56,1	0,3840	
Lyso PC 18:2	787,6	100,0	7,2	951,0	120,8	26,9	0,4726	
Lyso PC 20:3	518,1	100,0	8,6	711,5	137,3	46,2	0,4464	
Lyso PC 20:4	4864,8	100,0	9,5	5728,2	117,7	28,6	0,5678	
Lyso PC 24:0	1128,6	100,0	7,7	1027,5	91,0	5,0	0,3492	
Lyso PC 26:0	829,0	100,0	6,1	831,0	100,2	4,2	0,9750	
Lyso PC 26:1	414,6	100,0	6,9	399,8	96,4	5,3	0,6902	
Lyso PC 28:0	774,2	100,0	6,8	770,0	99,4	4,7	0,9478	
Lyso PC 28:1	541,1	100,0	5,9	554,1	102,4	5,0	0,7599	

Table 10.16: Level of SM species, measured in testes samples of *Sms1*^{WT} can *Sms1*^{MUT} animals.
Statistical analysis was performed using two-tailed Student's t-test.
*p≤0.05, **p≤0.01, ***p≤0.001.

Testes - Male	Sms1WT			Sms1MUT				
SM species	n=9			n=9				
	Intensity	Mean (%)	SEM (%)	Intensity	Mean (%)	SEM (%)	ttest to Sms1WT	
total SM	**1342032.000**	**100.00**	**1.40**	**1058783.200**	**78.90**	**2.00**	0.0000	***
SM C14:1 OH	4992.0	100.00	2.00	3799.8	78.70	2.70	0.0000	***
SM C16:0	975164.7	100.00	1.30	747365.6	79.80	1.90	0.0000	***
SM C16:1	7226.9	100.00	2.80	7036.5	94.20	4.00	0.5906	
SM C16:1 OH	6896.8	100.00	2.30	5591.1	81.60	2.50	0.0000	***
SM C18:0	83685.1	100.00	3.30	69326.0	82.30	2.80	0.0004	***
SM C18:1	3285.9	100.00	3.60	3220.2	94.40	3.70	0.7002	
SM C20:2	3182.8	100.00	2.70	2793.1	87.90	2.30	0.0016	**
SM C22:1 OH	12004.7	100.00	4.30	9305.8	78.20	2.90	0.0002	***
SM C22:2 OH	9371.2	100.00	2.40	9506.0	99.70	2.50	0.6820	
SM C22:3	11443.9	100.00	2.10	11041.3	93.60	2.10	0.2368	
SM C24:0	48828.3	100.00	3.10	37279.8	78.00	2.40	0.0000	***
SM C24:1	161722.9	100.00	2.50	138546.2	85.50	2.30	0.0002	***
SM C24:1 OH	3326.1	100.00	3.60	3258.2	96.60	3.30	0.6791	
SM C26:0	3258.0	100.00	3.40	3073.0	92.30	3.20	0.2367	
SM C26:1	7642.7	100.00	2.70	7640.8	97.70	2.80	0.9947	

Table 10.17: Level of SM species measured in brain samples of male (A) and female (B) animals of the *Sms1* x *APPswe* mouse line.
Males: *Sms1*^{WT} x *APPswe*^{WT} n=6, *Sms1*^{MUT} x *APPswe*^{WT} n=11, *Sms1*^{WT} x *APPswe*^{Tg} n=13, *Sms1*^{MUT} x *APPswe*^{Tg} n=5; females: *Sms1*^{WT} x *APPswe*^{WT} n=5, *Sms1*^{MUT} x *APPswe*^{WT} n=6, *Sms1*^{WT} x *APPswe*^{Tg} n=11, *Sms1*^{MUT} x *APPswe*^{Tg} n=6. Statistical analysis was performed using one-way ANOVA with *post hoc* Tukey's test. *p≤0.05, **p≤0.01, ***p≤0.001.

A	Sms1WT x APPsweWT		Sms1MUT x APPsweWT		One Way ANOVA		B	Sms1WT x APPsweWT		Sms1MUT x APPsweWT		One Way ANOVA	
males	%	SEM	%	SEM	p-value	sig.	females	%	SEM	%	SEM	p-value	sig.
SM C14:1 OH	100.00	6.73	85.11	4.08	0.1455	ns	SM C14:1 OH	100.00	7.43	82.55	4.44	0.4291	ns
SM C16:0	100.00	8.23	76.63	4.89	0.047	*	SM C16:0	100.00	4.61	80.29	5.43	0.047	#
SM C16:1	100.00	6.82	89.92	3.40	0.586	ns	SM C16:1	100.00	2.99	91.85	3.10	0.5157	ns
SM C16:1 OH	100.00	6.13	64.17	3.77	0.0021	*	SM C16:1 OH	100.00	7.66	61.02	2.98	0.0002	**
SM C18:0	100.00	7.20	50.86	4.70	< 0.0001	***	SM C18:0	100.00	2.94	47.31	4.26	< 0.0001	***
SM C18:1	100.00	8.71	56.17	3.29	0.0009	**	SM C18:1	100.00	6.33	54.84	5.19	< 0.0001	***
SM C20:2	100.00	5.11	100.16	4.23	> 0.9999	ns	SM C20:2	100.00	2.15	107.45	3.56	0.5447	ns
SM C22:1 OH	100.00	6.56	67.10	5.00	0.0017	*	SM C22:1 OH	100.00	6.89	69.34	4.32	0.0013	*
SM C22:2 OH	100.00	6.93	71.36	5.11	0.0099	*	SM C22:2 OH	100.00	6.24	73.78	3.26	0.003	*
SM C22:3	100.00	7.58	103.06	5.43	0.976	ns	SM C22:3	100.00	2.39	103.37	3.74	0.9438	ns
SM C24:0	100.00	7.40	69.69	5.65	0.0103	*	SM C24:0	100.00	7.88	73.48	4.84	0.016	*
SM C24:1	100.00	8.07	59.41	4.59	0.0003	**	SM C24:1	100.00	6.04	62.54	5.65	0.0004	**
SM C24:1 OH	100.00	3.93	80.97	5.35	0.0348	#	SM C24:1 OH	100.00	5.65	86.68	1.95	0.0509	#
SM C26:0	100.00	6.18	95.00	9.25	0.9577	ns	SM C26:0	100.00	6.28	100.25	2.12	> 0.9999	ns
SM C26:1	100.00	5.09	83.78	5.73	0.1901	ns	SM C26:1	100.00	4.74	93.66	3.46	0.6957	ns
SM total	100.00	7.03	57.61	4.49	< 0.0001	***	SM total	100.00	3.30	56.02	4.47	< 0.0001	***
	Sms1WT x APPsweWT		Sms1WT x APPsweTg		One Way ANOVA			Sms1WT x APPsweWT		Sms1WT x APPsweTg		One Way ANOVA	
	%	SEM	%	SEM	p-value	sig.		%	SEM	%	SEM	p-value	sig.
SM C14:1 OH	100.00	6.73	108.41	3.04	0.5059		SM C14:1 OH	100.00	7.43	105.02	8.11	0.9683	ns
SM C16:0	100.00	8.23	111.66	4.38	0.4185	ns	SM C16:0	100.00	4.61	99.34	3.18	0.9997	ns
SM C16:1	100.00	6.82	107.31	3.87	0.728	ns	SM C16:1	100.00	2.99	104.97	3.62	0.8194	ns
SM C16:1 OH	100.00	6.13	115.44	5.86	0.2202	ns	SM C16:1 OH	100.00	7.66	96.12	5.69	0.9608	ns
SM C18:0	100.00	7.20	114.10	3.52	0.1279	ns	SM C18:0	100.00	2.94	94.21	2.56	0.6757	ns
SM C18:1	100.00	8.71	113.89	6.27	0.4091	ns	SM C18:1	100.00	6.33	91.01	3.07	0.5608	ns
SM C20:2	100.00	5.11	106.80	3.55	0.6959	ns	SM C20:2	100.00	2.15	108.35	2.93	0.4245	ns
SM C22:1 OH	100.00	6.56	106.73	4.52	0.771	ns	SM C22:1 OH	100.00	6.89	98.58	4.32	0.9972	ns
SM C22:2 OH	100.00	6.93	110.86	4.64	0.465	ns	SM C22:2 OH	100.00	6.24	105.57	4.29	0.836	ns
SM C22:3	100.00	7.58	107.53	3.38	0.6729	ns	SM C22:3	100.00	2.39	106.89	2.84	0.65	ns
SM C24:0	100.00	7.40	107.51	5.03	0.7722	ns	SM C24:0	100.00	7.88	100.37	4.91	> 0.9999	ns
SM C24:1	100.00	8.07	109.49	4.66	0.5766	ns	SM C24:1	100.00	6.04	102.27	4.67	0.9919	ns
SM C24:1 OH	100.00	3.93	101.42	3.43	0.9946	ns	SM C24:1 OH	100.00	5.65	103.92	2.94	0.8453	ns
SM C26:0	100.00	6.18	104.95	5.18	0.9431	ns	SM C26:0	100.00	6.28	101.64	5.15	0.9952	ns
SM C26:1	100.00	5.09	103.79	4.55	0.9471	ns	SM C26:1	100.00	4.74	104.00	3.43	0.8925	ns
SM total	100.00	7.03	111.85	3.53	0.2272	ns	SM toal	100.00	3.30	96.75	2.66	0.9307	ns
	Sms1WT x APPsweWT		Sms1MUT x APPsweTg		One Way ANOVA			Sms1WT x APPsweWT		Sms1MUT x APPsweTg		One Way ANOVA	
	%	SEM	%	SEM	p-value	sig.		%	SEM	%	SEM	p-value	sig.
SM C14:1 OH	100.00	6.73	93.43	4.44	0.7611	ns	SM C14:1 OH	100.00	7.43	85.37	9.98	0.7045	ns
SM C16:0	100.00	8.23	82.76	4.51	0.1962	ns	SM C16:0	100.00	4.61	80.08	7.71	0.1147	ns
SM C16:1	100.00	6.82	101.27	6.12	0.9985	ns	SM C16:1	100.00	2.99	91.85	6.77	0.6533	ns
SM C16:1 OH	100.00	6.13	63.10	1.31	0.0016	*	SM C16:1 OH	100.00	7.66	58.88	5.52	0.0011	*
SM C18:0	100.00	7.20	46.95	3.05	< 0.0001	***	SM C18:0	100.00	2.94	41.57	4.79	< 0.0001	***
SM C18:1	100.00	8.71	52.75	5.16	0.0004	**	SM C18:1	100.00	6.33	48.39	8.04	< 0.0001	***
SM C20:2	100.00	5.11	121.77	4.06	0.0223	*	SM C20:2	100.00	2.15	117.49	5.54	0.0594	#
SM C22:1 OH	100.00	6.56	63.34	3.70	0.0005	**	SM C22:1 OH	100.00	6.89	57.93	4.32	0.0002	**
SM C22:2 OH	100.00	6.93	70.90	4.76	0.0087	*	SM C22:2 OH	100.00	6.24	64.99	6.88	0.0009	**
SM C22:3	100.00	7.58	122.51	2.78	0.0283	*	SM C22:3	100.00	2.39	124.45	6.81	0.01	*
SM C24:0	100.00	7.40	68.56	3.75	0.0076	*	SM C24:0	100.00	7.88	61.26	3.48	0.0025	*
SM C24:1	100.00	8.07	57.85	3.59	0.0002	**	SM C24:1	100.00	6.04	55.36	4.95	0.0004	**
SM C24:1 OH	100.00	3.93	80.45	3.98	0.0291	*	SM C24:1 OH	100.00	5.65	77.47	3.96	0.0031	*
SM C26:0	100.00	6.18	96.38	2.67	0.9831	ns	SM C26:0	100.00	6.28	83.45	3.88	0.225	ns
SM C26:1	100.00	5.09	89.99	3.02	0.5838	ns	SM C26:1	100.00	4.74	82.91	3.87	0.0843	#
SM total	100.00	7.03	55.18	1.51	< 0.0001	***	SM total	100.00	3.30	49.35	4.40	< 0.0001	***
	Sms1MUT x APPsweWT		Sms1MUT x APPsweTg		One Way ANOVA			Sms1MUT x APPsweWT		Sms1MUT x APPsweTg		One Way ANOVA	
	%	SEM	%	SEM	p-value	sig.		%	SEM	%	SEM	p-value	sig.
SM C14:1 OH	100.00	4.79	109.77	4.87	0.5702		SM C14:1 OH	100.00	5.37	103.42	10.32	0.9954	ns
SM C16:0	100.00	6.38	108.00	4.88	0.8684	ns	SM C16:0	100.00	6.76	99.74	7.69	> 0.9999	ns
SM C16:1	100.00	3.78	112.62	6.89	0.4487	ns	SM C16:1	100.00	3.38	100.00	6.77	> 0.9999	ns
SM C16:1 OH	100.00	5.87	98.33	1.29	0.9992	ns	SM C16:1 OH	100.00	4.89	96.48	5.33	0.9946	ns
SM C18:0	100.00	9.24	92.32	2.82	0.9332	ns	SM C18:0	100.00	9.01	87.88	4.21	0.7382	ns
SM C18:1	100.00	5.87	93.90	4.84	0.9832	ns	SM C18:1	100.00	9.47	88.24	7.09	0.8233	ns
SM C20:2	100.00	4.23	121.57	4.94	0.0167	*	SM C20:2	100.00	3.31	109.34	6.06	0.3416	ns
SM C22:1 OH	100.00	7.45	94.40	3.50	0.9576	ns	SM C22:1 OH	100.00	6.23	83.54	3.61	0.4736	ns
SM C22:2 OH	100.00	7.16	99.36	4.73	> 0.9999	ns	SM C22:2 OH	100.00	4.42	88.09	6.06	0.6247	ns
SM C22:3	100.00	5.27	118.87	3.31	0.0525	#	SM C22:3	100.00	3.62	120.39	8.20	0.0131	*
SM C24:0	100.00	8.11	98.39	3.69	0.9991	ns	SM C24:0	100.00	6.58	83.36	2.90	0.5169	ns
SM C24:1	100.00	7.73	97.37	3.49	0.9971	ns	SM C24:1	100.00	9.03	88.53	4.39	0.8444	ns
SM C24:1 OH	100.00	6.60	99.35	3.95	0.9998	ns	SM C24:1 OH	100.00	2.24	89.37	3.54	0.3103	ns
SM C26:0	100.00	9.74	101.45	2.71	0.9989	ns	SM C26:0	100.00	2.11	83.25	3.23	0.1368	ns
SM C26:1	100.00	6.83	107.41	3.24	0.8385	ns	SM C26:1	100.00	3.69	88.52	3.43	0.3175	ns
SM total	100.00	7.79	95.78	1.44	0.9812	ns	SM total	100.00	7.98	88.10	3.88	0.6751	ns
	Sms1WT x APPsweTg		Sms1MUT x APPsweTg		One Way ANOVA			Sms1WT x APPsweTg		Sms1MUT x APPsweTg		One Way ANOVA	
	%	SEM	%	SEM	p-value	sig.		%	SEM	%	SEM	p-value	sig.
SM C14:1 OH	100.00	2.80	86.18	3.82	0.0604	#	SM C14:1 OH	100.00	7.72	81.29	8.11	0.3572	ns
SM C16:0	100.00	3.92	74.12	3.35	0.0021	*	SM C16:0	100.00	3.20	80.61	6.22	0.0666	#
SM C16:1	100.00	3.61	94.37	5.77	0.7979	ns	SM C16:1	100.00	3.45	87.50	5.92	0.1579	ns
SM C16:1 OH	100.00	5.07	54.66	0.72	< 0.0001	***	SM C16:1 OH	100.00	5.92	61.26	3.38	0.0006	**
SM C18:0	100.00	3.08	41.15	1.26	< 0.0001	***	SM C18:0	100.00	2.72	44.13	2.11	< 0.0001	***
SM C18:1	100.00	5.51	46.31	2.39	< 0.0001	***	SM C18:1	100.00	3.38	53.16	4.27	< 0.0001	***
SM C20:2	100.00	3.32	114.02	4.63	0.0752	#	SM C20:2	100.00	2.71	108.44	6.01	0.4011	ns
SM C22:1 OH	100.00	4.23	59.35	2.20	< 0.0001	***	SM C22:1 OH	100.00	4.38	58.76	2.54	< 0.0001	***
SM C22:2 OH	100.00	4.18	63.96	3.05	< 0.0001	***	SM C22:2 OH	100.00	4.07	61.57	4.24	< 0.0001	***
SM C22:3	100.00	3.14	113.93	3.17	0.1046	ns	SM C22:3	100.00	2.66	116.43	7.93	0.0413	#
SM C24:0	100.00	4.68	63.78	2.39	0.0001	***	SM C24:0	100.00	4.89	61.03	2.13	0.0004	**
SM C24:1	100.00	4.25	52.84	1.89	< 0.0001	***	SM C24:1	100.00	4.57	54.13	2.68	< 0.0001	***
SM C24:1 OH	100.00	3.38	79.32	3.15	0.004	*	SM C24:1 OH	100.00	2.83	74.55	2.95	< 0.0001	***
SM C26:0	100.00	4.93	91.83	2.46	0.7347	ns	SM C26:0	100.00	5.07	82.11	3.19	0.0834	#
SM C26:1	100.00	4.39	86.70	2.61	0.1797	ns	SM C26:1	100.00	3.30	79.73	3.09	0.0072	*
SM total	100.00	3.16	49.34	0.74	< 0.0001	***	SM total	100.00	2.75	51.01	2.24	< 0.0001	***

Table 10.18: Level of PCaa species measured in brain samples of male (A) and female (B) animals of the *Sms1* x *APPswe* mouse line.
Males: *Sms1*^{WT} x *APPswe*^{WT} n=6, *Sms1*^{MUT} x *APPswe*^{WT} n=11, *Sms1*^{WT} x *APPswe*^{Tg} n=13, *Sms1*^{MUT} x *APPswe*^{Tg} n=5; females: *Sms1*^{WT} x *APPswe*^{WT} n=5, *Sms1*^{MUT} x *APPswe*^{WT} n=6, *Sms1*^{WT} x *APPswe*^{Tg} n=11, *Sms1*^{MUT} x *APPswe*^{Tg} n=6. Statistical analysis was performed using one-way ANOVA with *post hoc* Tukey's test. *p≤0.05, **p≤0.01, ***p≤0.001.

A	Sms1WT x APPsweWT		Sms1MUT x APPsweWT		One Way ANOVA		B	Sms1WT x APPsweWT		Sms1MUT x APPsweWT		One Way ANOVA	
males	%	SEM	%	SEM	p-value	sign.	females	%	SEM	%	SEM	p-value	sign.
PC aa C24:0	100.00	9.38	98.61	6.86	0.9991	ns	PC aa C24:0	100.00	6.22	99.88	8.20	> 0.9999	ns
PC aa C26:0	100.00	10.50	108.03	9.11	0.9573	ns	PC aa C26:0	100.00	9.18	88.90	9.08	0.9321	ns
PC aa C28:1	100.00	6.72	97.21	6.32	0.9924	ns	PC aa C28:1	100.00	6.88	87.34	6.40	0.7868	ns
PC aa C30:0	100.00	8.49	108.61	6.57	0.7051	ns	PC aa C30:0	100.00	2.58	108.62	3.66	0.8777	ns
PC aa C30:2	100.00	4.47	94.39	3.80	0.7669	ns	PC aa C30:2	100.00	5.76	90.86	4.82	0.7912	ns
PC aa C32:0	100.00	4.27	106.96	3.23	0.4738	ns	PC aa C32:0	100.00	2.48	109.13	2.39	0.0870	#
PC aa C32:1	100.00	6.22	80.69	4.22	0.0221	*	PC aa C32:1	100.00	2.38	77.08	3.01	0.0169	*
PC aa C32:2	100.00	7.88	64.46	3.22	0.0016	*	PC aa C32:2	100.00	6.02	62.64	4.51	< 0.0001	***
PC aa C32:3	100.00	5.61	99.78	5.72	> 0.9999	ns	PC aa C32:3	100.00	4.09	98.81	5.50	0.9985	ns
PC aa C34:1	100.00	2.49	101.22	1.15	0.9506	ns	PC aa C34:1	100.00	1.28	100.31	0.82	0.9977	ns
PC aa C34:2	100.00	6.61	100.81	5.56	0.9996	ns	PC aa C34:2	100.00	2.61	104.17	3.18	0.8758	ns
PC aa C34:3	100.00	6.66	100.46	5.25	> 0.9999	ns	PC aa C34:3	100.00	2.21	104.41	3.64	0.9205	ns
PC aa C34:4	100.00	6.57	104.86	4.94	0.9156	ns	PC aa C34:4	100.00	2.54	106.82	3.79	0.0374	*
PC aa C36:0	100.00	5.80	96.96	5.78	0.9752	ns	PC aa C36:0	100.00	3.21	105.60	2.51	0.6738	ns
PC aa C36:1	100.00	4.85	98.29	5.06	0.9925	ns	PC aa C36:1	100.00	2.32	104.22	1.98	0.7226	ns
PC aa C36:2	100.00	5.74	97.04	5.96	0.9745	ns	PC aa C36:2	100.00	2.61	100.59	2.24	0.9991	ns
PC aa C36:3	100.00	5.76	100.18	4.55	> 0.9999	ns	PC aa C36:3	100.00	3.14	106.29	3.53	0.6543	ns
PC aa C36:4	100.00	5.27	102.33	3.72	0.9827	ns	PC aa C36:4	100.00	3.50	104.32	3.46	0.8396	ns
PC aa C36:5	100.00	7.87	103.74	5.91	0.9616	ns	PC aa C36:5	100.00	1.66	105.38	3.76	0.7944	ns
PC aa C36:6	100.00	5.95	97.54	4.96	0.9775	ns	PC aa C36:6	100.00	2.46	103.04	2.52	0.9055	ns
PC aa C38:0	100.00	6.31	91.93	6.96	0.7883	ns	PC aa C38:0	100.00	3.80	99.02	2.49	0.9988	ns
PC aa C38:1	100.00	6.48	90.01	7.24	0.7065	ns	PC aa C38:1	100.00	6.56	97.54	2.95	0.9839	ns
PC aa C38:3	100.00	5.99	96.46	4.30	0.9595	ns	PC aa C38:3	100.00	3.08	103.60	3.27	0.8866	ns
PC aa C38:4	100.00	5.18	98.19	3.60	0.9915	ns	PC aa C38:4	100.00	2.93	102.52	2.97	0.9499	ns
PC aa C38:5	100.00	5.87	99.16	4.38	0.9993	ns	PC aa C38:5	100.00	2.24	102.22	2.93	0.9657	ns
PC aa C38:6	100.00	6.19	102.44	4.24	0.9836	ns	PC aa C38:6	100.00	2.40	109.40	3.05	0.2351	ns
PC aa C40:1	100.00	6.11	96.75	8.59	0.9869	ns	PC aa C40:1	100.00	7.48	102.85	2.71	0.9859	ns
PC aa C40:2	100.00	6.44	95.14	9.19	0.9612	ns	PC aa C40:2	100.00	5.99	100.09	2.14	> 0.9999	ns
PC aa C40:3	100.00	6.01	97.18	6.24	0.9832	ns	PC aa C40:3	100.00	8.39	109.08	3.08	0.2785	ns
PC aa C40:4	100.00	6.10	98.70	5.11	0.9951	ns	PC aa C40:4	100.00	2.81	108.81	3.58	0.3063	ns
PC aa C40:5	100.00	6.49	98.24	5.15	0.9956	ns	PC aa C40:5	100.00	3.54	105.90	3.04	0.6186	ns
PC aa C40:6	100.00	6.51	100.44	5.02	> 0.9999	ns	PC aa C40:6	100.00	4.64	107.85	3.07	0.4651	ns
PC aa C42:0	100.00	4.88	97.44	8.72	0.9914	ns	PC aa C42:0	100.00	8.43	102.13	2.62	0.9944	ns
PC aa C42:1	100.00	6.07	97.43	8.04	0.9938	ns	PC aa C42:1	100.00	9.31	101.88	3.44	0.9974	ns
PC aa C42:2	100.00	6.26	98.25	9.07	0.9977	ns	PC aa C42:2	100.00	8.45	101.84	2.57	0.9968	ns
PC aa C42:4	100.00	6.07	96.64	6.48	0.9739	ns	PC aa C42:4	100.00	2.95	105.00	2.99	0.7603	ns
PC aa C42:5	100.00	5.93	94.35	6.52	0.8865	ns	PC aa C42:5	100.00	2.47	103.51	2.29	0.8519	ns
PC aa C42:6	100.00	6.56	93.70	5.53	0.8442	ns	PC aa C42:6	100.00	4.49	105.57	2.87	0.6273	ns
Pcaa total	100.00	4.41	100.34	3.53	0.9999	ns	Pcaa total	100.00	1.76	103.13	1.96	0.7796	ns

	Sms1WT x APPsweWT		Sms1WT x APPsweTg		One Way ANOVA			Sms1WT x APPsweWT		Sms1WT x APPsweTg		One Way ANOVA	
	%	SEM	%	SEM	p-value	sig.		%	SEM	%	SEM	p-value	sig.
PC aa C24:0	100.00	9.38	98.37	5.16	0.9979	ns	**PC aa C24:0**	100.00	6.22	113.12	10.17	0.8026	ns
PC aa C26:0	100.00	10.50	104.82	8.15	0.9862	ns	**PC aa C26:0**	100.00	9.18	95.40	12.87	0.9941	ns
PC aa C28:1	100.00	6.72	105.46	4.78	0.9289	ns	**PC aa C28:1**	100.00	6.83	102.32	9.45	0.9980	ns
PC aa C30:0	100.00	8.49	111.30	3.32	0.4021	ns	**PC aa C30:0**	100.00	2.58	103.67	2.61	0.8908	ns
PC aa C30:2	100.00	4.47	104.19	2.29	0.8477	ns	**PC aa C30:2**	100.00	5.76	104.09	7.08	0.9774	ns
PC aa C32:0	100.00	4.27	100.07	2.50	> 0.9999	ns	**PC aa C32:0**	100.00	2.48	94.63	2.11	0.4571	ns
PC aa C32:1	100.00	6.22	112.63	3.15	0.1271	ns	**PC aa C32:1**	100.00	2.38	99.24	2.73	0.9985	ns
PC aa C32:2	100.00	7.88	113.77	5.19	0.2800	ns	**PC aa C32:2**	100.00	6.02	93.10	3.07	0.6946	ns
PC aa C32:3	100.00	5.61	103.32	2.52	0.9517	ns	**PC aa C32:3**	100.00	4.09	107.97	7.39	0.8654	ns
PC aa C34:1	100.00	2.49	101.50	1.22	0.8815	ns	**PC aa C34:1**	100.00	1.28	98.49	1.05	0.7884	ns
PC aa C34:2	100.00	6.61	111.67	3.51	0.3839	ns	**PC aa C34:2**	100.00	2.61	107.95	3.42	0.4647	ns
PC aa C34:3	100.00	6.66	109.90	3.38	0.6412	ns	**PC aa C34:3**	100.00	2.21	113.00	4.11	0.2416	ns
PC aa C34:4	100.00	6.57	107.03	3.62	0.7219	ns	**PC aa C34:4**	100.00	2.54	107.59	3.61	0.6070	ns
PC aa C36:0	100.00	5.80	103.68	3.89	0.9415	ns	**PC aa C36:0**	100.00	3.21	100.06	3.24	> 0.9999	ns
PC aa C36:1	100.00	4.85	103.19	3.29	0.9380	ns	**PC aa C36:1**	100.00	2.32	98.99	2.70	0.9938	ns
PC aa C36:2	100.00	5.74	108.85	3.54	0.5062	ns	**PC aa C36:2**	100.00	2.61	101.57	2.91	0.9830	ns
PC aa C36:3	100.00	5.76	105.39	3.77	0.8081	ns	**PC aa C36:3**	100.00	3.14	101.16	3.01	0.9962	ns
PC aa C36:4	100.00	5.27	104.59	3.61	0.8489	ns	**PC aa C36:4**	100.00	3.50	96.57	2.86	0.9047	ns
PC aa C36:5	100.00	7.87	107.04	3.45	0.7362	ns	**PC aa C36:5**	100.00	1.66	108.93	2.70	0.4102	ns
PC aa C36:6	100.00	5.95	108.00	2.63	0.4715	ns	**PC aa C36:6**	100.00	2.46	105.25	2.65	0.6323	ns
PC aa C38:0	100.00	6.31	106.51	4.72	0.8329	ns	**PC aa C38:0**	100.00	5.80	103.02	4.56	0.9642	ns
PC aa C38:1	100.00	6.48	104.97	5.21	0.9305	ns	**PC aa C38:1**	100.00	6.56	101.11	4.55	0.9983	ns
PC aa C38:3	100.00	5.99	105.92	4.15	0.7893	ns	**PC aa C38:3**	100.00	3.08	100.48	2.71	0.9996	ns
PC aa C38:4	100.00	5.18	105.23	3.59	0.7821	ns	**PC aa C38:4**	100.00	2.93	97.84	2.69	0.9650	ns
PC aa C38:5	100.00	5.87	107.64	3.70	0.5921	ns	**PC aa C38:5**	100.00	2.24	97.94	2.81	0.9697	ns
PC aa C38:6	100.00	6.19	103.04	3.70	0.9575	ns	**PC aa C38:6**	100.00	2.40	97.08	2.97	0.9254	ns
PC aa C40:1	100.00	6.11	100.72	4.87	0.9998	ns	**PC aa C40:1**	100.00	7.43	97.65	5.95	0.9914	ns
PC aa C40:2	100.00	6.44	105.60	5.18	0.9212	ns	**PC aa C40:2**	100.00	5.99	101.56	5.19	0.9958	ns
PC aa C40:3	100.00	6.01	105.02	4.22	0.8857	ns	**PC aa C40:3**	100.00	3.39	104.64	2.85	0.7676	ns
PC aa C40:4	100.00	6.10	105.44	4.26	0.8460	ns	**PC aa C40:4**	100.00	2.81	99.06	2.51	0.9973	ns
PC aa C40:5	100.00	6.49	107.37	4.26	0.7031	ns	**PC aa C40:5**	100.00	3.54	99.47	2.63	0.9995	ns
PC aa C40:6	100.00	6.51	104.58	4.37	0.9086	ns	**PC aa C40:6**	100.00	4.64	98.06	3.03	0.9817	ns
PC aa C42:0	100.00	4.88	95.96	4.20	0.9553	ns	**PC aa C42:0**	100.00	8.43	97.99	5.84	0.9948	ns
PC aa C42:1	100.00	6.07	96.65	5.00	0.9813	ns	**PC aa C42:1**	100.00	9.31	92.59	6.81	0.8642	ns
PC aa C42:2	100.00	6.26	100.39	4.48	> 0.9999	ns	**PC aa C42:2**	100.00	8.45	95.44	6.40	0.9522	ns
PC aa C42:4	100.00	6.07	101.64	4.26	0.9955	ns	**PC aa C42:4**	100.00	2.95	99.51	3.16	0.9996	ns
PC aa C42:5	100.00	5.93	105.00	4.15	0.8885	ns	**PC aa C42:5**	100.00	2.47	104.53	2.83	0.7116	ns
PC aa C42:6	100.00	6.56	105.45	4.25	0.8553	ns	**PC aa C42:6**	100.00	4.49	103.18	2.29	0.8931	ns
Pcaa total	100.00	4.41	103.51	2.68	0.8575	ns	**Pcaa total**	100.00	1.76	98.08	2.05	0.9320	ns

	Sms1WT x APPsweWT		Sms1MUT x APPsweTg		One Way ANOVA			Sms1WT x APPsweWT		Sms1MUT x APPsweTg		One Way ANOVA	
	%	SEM	%	SEM	p-value	sig.		%	SEM	%	SEM	p-value	sig.
PC aa C24:0	100.00	9.38	105.17	4.77	0.9565	ns	**PC aa C24:0**	100.00	6.22	96.10	10.22	0.9962	ns
PC aa C26:0	100.00	10.50	100.66	12.41	> 0.9999	ns	**PC aa C26:0**	100.00	9.18	101.43	14.35	> 0.9999	ns
PC aa C28:1	100.00	6.72	94.05	8.30	0.9343	ns	**PC aa C28:1**	100.00	6.83	92.70	10.56	0.9687	ns
PC aa C30:0	100.00	8.49	130.66	2.64	0.0041	**	**PC aa C30:0**	100.00	2.58	123.74	5.64	0.0037	**
PC aa C30:2	100.00	4.47	100.99	5.09	0.9982	ns	**PC aa C30:2**	100.00	5.76	94.93	9.16	0.9767	ns
PC aa C32:0	100.00	4.27	112.76	1.96	0.0584	#	**PC aa C32:0**	100.00	2.48	106.85	2.79	0.4235	ns
PC aa C32:1	100.00	6.22	92.84	1.76	0.6574	ns	**PC aa C32:1**	100.00	2.38	84.86	4.83	0.0597	#
PC aa C32:2	100.00	7.88	68.11	1.86	0.0046	**	**PC aa C32:2**	100.00	6.02	62.55	3.57	0.0002	***
PC aa C32:3	100.00	5.61	108.39	5.69	0.6420	ns	**PC aa C32:3**	100.00	4.09	97.93	7.53	0.9984	ns
PC aa C34:1	100.00	2.49	104.56	0.71	0.2179	ns	**PC aa C34:1**	100.00	1.28	100.71	1.37	0.9839	ns
PC aa C34:2	100.00	6.61	128.71	6.05	0.0080	**	**PC aa C34:2**	100.00	2.61	124.99	5.28	0.0036	**
PC aa C34:3	100.00	6.66	136.84	9.61	0.0033	**	**PC aa C34:3**	100.00	2.21	133.53	8.95	0.0018	**
PC aa C34:4	100.00	6.57	128.09	4.67	0.0052	**	**PC aa C34:4**	100.00	2.54	121.02	6.90	0.0412	*
PC aa C36:0	100.00	5.80	103.26	2.23	0.9696	ns	**PC aa C36:0**	100.00	3.21	95.80	3.95	0.8922	ns
PC aa C36:1	100.00	4.85	103.75	1.73	0.9298	ns	**PC aa C36:1**	100.00	2.32	95.81	3.33	0.8191	ns
PC aa C36:2	100.00	5.74	106.44	2.25	0.7984	ns	**PC aa C36:2**	100.00	2.61	98.14	3.66	0.9846	ns
PC aa C36:3	100.00	5.76	117.74	2.23	0.0670	#	**PC aa C36:3**	100.00	3.14	113.54	4.66	0.1760	ns
PC aa C36:4	100.00	5.27	115.45	2.86	0.0986	#	**PC aa C36:4**	100.00	3.50	105.04	3.84	0.8487	ns
PC aa C36:5	100.00	7.87	124.13	3.13	0.0220	*	**PC aa C36:5**	100.00	1.66	125.20	8.17	0.0056	**
PC aa C36:6	100.00	5.95	110.16	2.84	0.3650	ns	**PC aa C36:6**	100.00	2.46	106.75	4.80	0.5968	ns
PC aa C38:0	100.00	6.31	96.33	2.62	0.9737	ns	**PC aa C38:0**	100.00	5.80	86.78	3.36	0.3454	ns
PC aa C38:1	100.00	6.48	91.97	2.79	0.8220	ns	**PC aa C38:1**	100.00	6.56	82.11	3.03	0.1494	ns
PC aa C38:3	100.00	5.99	109.54	2.41	0.5501	ns	**PC aa C38:3**	100.00	3.08	103.39	4.29	0.9400	ns
PC aa C38:4	100.00	5.18	111.18	2.54	0.3006	ns	**PC aa C38:4**	100.00	2.93	101.88	4.00	0.9869	ns
PC aa C38:5	100.00	5.87	111.39	2.76	0.3549	ns	**PC aa C38:5**	100.00	2.24	103.55	4.38	0.9225	ns
PC aa C38:6	100.00	6.19	111.15	2.55	0.3734	ns	**PC aa C38:6**	100.00	2.40	105.23	3.67	0.8034	ns
PC aa C40:1	100.00	6.11	99.59	4.52	> 0.9999	ns	**PC aa C40:1**	100.00	7.43	84.41	4.39	0.4113	ns
PC aa C40:2	100.00	6.44	96.86	2.48	0.9889	ns	**PC aa C40:2**	100.00	5.99	84.01	3.44	0.2506	ns
PC aa C40:3	100.00	6.01	109.71	1.78	0.6022	ns	**PC aa C40:3**	100.00	3.39	99.81	3.85	> 0.9999	ns
PC aa C40:4	100.00	6.10	113.01	2.19	0.3264	ns	**PC aa C40:4**	100.00	2.81	101.28	4.19	0.9964	ns
PC aa C40:5	100.00	6.49	109.13	2.51	0.6361	ns	**PC aa C40:5**	100.00	3.54	100.41	4.11	0.9999	ns
PC aa C40:6	100.00	6.51	107.35	2.54	0.7767	ns	**PC aa C40:6**	100.00	4.64	100.48	3.90	0.9998	ns
PC aa C42:0	100.00	4.88	95.55	3.78	0.9576	ns	**PC aa C42:0**	100.00	8.43	83.04	4.77	0.3531	ns
PC aa C42:1	100.00	6.07	97.04	6.02	0.9907	ns	**PC aa C42:1**	100.00	9.31	81.29	4.72	0.3939	ns
PC aa C42:2	100.00	6.26	96.28	3.81	0.9790	ns	**PC aa C42:2**	100.00	8.45	84.28	3.85	0.4625	ns
PC aa C42:4	100.00	6.07	105.30	2.30	0.9081	ns	**PC aa C42:4**	100.00	2.95	90.06	3.95	0.3733	ns
PC aa C42:5	100.00	5.93	104.94	1.92	0.9202	ns	**PC aa C42:5**	100.00	2.47	93.39	3.79	0.5883	ns
PC aa C42:6	100.00	6.56	103.63	1.69	0.9643	ns	**PC aa C42:6**	100.00	4.49	95.87	3.40	0.8757	ns
Pcaa total	100.00	4.41	104.22	1.45	0.4062	ns	**Pcaa total**	100.00	1.76	103.21	2.70	0.9894	ns

	Sms1MUT x APPsweWT		Sms1MUT x APPsweTg		One Way ANOVA			Sms1MUT x APPsweWT		Sms1MUT x APPsweTg		One Way ANOVA	
	%	SEM	%	SEM	p-value	sig.		%	SEM	%	SEM	p-value	sig.
PC aa C24:0	100.00	6.96	106.65	4.84	0.9053	ns	**PC aa C24:0**	100.00	8.21	96.22	10.24	0.9951	ns
PC aa C26:0	100.00	8.43	93.17	11.48	0.9616	ns	**PC aa C26:0**	100.00	10.21	114.10	16.14	0.9722	ns
PC aa C28:1	100.00	6.50	96.75	8.54	0.9875	ns	**PC aa C28:1**	100.00	7.32	106.14	12.09	0.9820	ns
PC aa C30:0	100.00	6.05	120.30	2.43	0.0368	*	**PC aa C30:0**	100.00	3.37	113.92	5.19	0.0528	#
PC aa C30:2	100.00	4.02	107.00	5.39	0.6338	ns	**PC aa C30:2**	100.00	5.33	105.07	10.14	0.9757	ns
PC aa C32:0	100.00	3.02	105.42	1.83	0.5838	ns	**PC aa C32:0**	100.00	2.19	97.91	2.56	0.9381	ns
PC aa C32:1	100.00	5.23	115.06	2.18	0.1933	ns	**PC aa C32:1**	100.00	3.90	110.10	6.26	0.4380	ns
PC aa C32:2	100.00	5.00	105.66	2.88	0.9679	ns	**PC aa C32:2**	100.00	7.20	99.86	5.69	> 0.9999	ns
PC aa C32:3	100.00	5.73	108.63	5.71	0.5869	ns	**PC aa C32:3**	100.00	5.59	99.61	7.66	> 0.9999	ns
PC aa C34:1	100.00	1.14	103.31	0.70	0.4334	ns	**PC aa C34:1**	100.00	0.82	100.40	1.37	0.9958	ns
PC aa C34:2	100.00	5.52	127.68	6.00	0.0068	**	**PC aa C34:2**	100.00	3.06	119.98	5.07	0.0069	**
PC aa C34:3	100.00	5.23	136.22	9.57	0.0023	**	**PC aa C34:3**	100.00	3.49	127.89	8.57	0.0024	**
PC aa C34:4	100.00	4.71	122.15	4.45	0.0170	*	**PC aa C34:4**	100.00	3.55	113.29	6.46	0.1682	ns
PC aa C36:0	100.00	5.97	106.50	2.30	0.8022	ns	**PC aa C36:0**	100.00	2.37	90.72	3.74	0.2648	ns
PC aa C36:1	100.00	5.15	105.55	1.76	0.7932	ns	**PC aa C36:1**	100.00	1.90	91.94	3.19	0.2226	ns
PC aa C36:2	100.00	6.14	109.69	2.32	0.5129	ns	**PC aa C36:2**	100.00	2.22	97.56	3.64	0.9527	ns
PC aa C36:3	100.00	4.54	117.52	2.23	0.0544	#	**PC aa C36:3**	100.00	3.32	106.82	4.38	0.5933	ns
PC aa C36:4	100.00	3.64	112.81	2.79	0.1629	ns	**PC aa C36:4**	100.00	3.32	100.69	3.68	0.9992	ns
PC aa C36:5	100.00	5.70	119.65	3.02	0.0484	*	**PC aa C36:5**	100.00	3.57	118.81	7.75	0.0163	*
PC aa C36:6	100.00	5.09	112.94	2.91	0.1619	ns	**PC aa C36:6**	100.00	2.45	103.60	4.65	0.8653	ns
PC aa C38:0	100.00	7.57	104.78	2.85	0.9504	ns	**PC aa C38:0**	100.00	2.51	87.64	3.40	0.3122	ns
PC aa C38:1	100.00	8.04	102.17	3.10	0.9961	ns	**PC aa C38:1**	100.00	3.02	84.18	3.11	0.1701	ns
PC aa C38:3	100.00	4.46	113.57	2.50	0.2462	ns	**PC aa C38:3**	100.00	3.15	99.79	4.14	> 0.9999	ns
PC aa C38:4	100.00	3.66	113.22	2.59	0.1560	ns	**PC aa C38:4**	100.00	2.90	99.37	3.90	0.9992	ns
PC aa C38:5	100.00	4.42	112.34	2.79	0.2571	ns	**PC aa C38:5**	100.00	2.87	101.31	4.28	0.9934	ns
PC aa C38:6	100.00	4.14	108.50	2.49	0.5427	ns	**PC aa C38:6**	100.00	2.79	96.19	3.35	0.8510	ns
PC aa C40:1	100.00	8.88	102.93	4.68	0.9898	ns	**PC aa C40:1**	100.00	2.63	82.06	4.27	0.1814	ns
PC aa C40:2	100.00	9.66	101.80	2.60	0.9979	ns	**PC aa C40:2**	100.00	2.14	83.94	3.44	0.1630	ns
PC aa C40:3	100.00	6.42	112.90	1.83	0.3494	ns	**PC aa C40:3**	100.00	2.78	91.50	3.53	0.3061	ns
PC aa C40:4	100.00	5.18	114.51	2.22	0.2136	ns	**PC aa C40:4**	100.00	3.29	93.07	3.85	0.4938	ns
PC aa C40:5	100.00	5.24	111.08	2.56	0.4561	ns	**PC aa C40:5**	100.00	2.88	94.81	3.88	0.7106	ns
PC aa C40:6	100.00	5.00	106.88	2.53	0.7840	ns	**PC aa C40:6**	100.00	2.85	93.17	3.62	0.5692	ns
PC aa C42:0	100.00	8.95	98.06	3.88	0.9959	ns	**PC aa C42:0**	100.00	2.56	81.31	4.67	0.1700	ns
PC aa C42:1	100.00	8.25	99.60	6.18	> 0.9999	ns	**PC aa C42:1**	100.00	3.37	79.79	4.63	0.2189	ns
PC aa C42:2	100.00	9.23	98.00	3.88	0.9963	ns	**PC aa C42:2**	100.00	2.53	82.75	3.78	0.2683	ns
PC aa C42:4	100.00	6.65	108.97	2.38	0.6661	ns	**PC aa C42:4**	100.00	2.85	85.78	3.76	0.0448	*
PC aa C42:5	100.00	6.91	111.23	2.04	0.4971	ns	**PC aa C42:5**	100.00	2.21	90.22	3.66	0.1505	ns
PC aa C42:6	100.00	5.90	110.59	1.80	0.5376	ns	**PC aa C42:6**	100.00	2.72	90.81	3.22	0.2179	ns
Pcaa total	100.00	3.51	107.50	1.45	0.4037	ns	**Pcaa total**	100.00	1.90	98.15	2.62	0.9478	ns
	Sms1WT x APPsweTg		Sms1MUT x APPsweTg		One Way ANOVA			Sms1WT x APPsweTg		Sms1MUT x APPsweTg		One Way ANOVA	
	%	SEM	%	SEM	p-value	sig.		%	SEM	%	SEM	p-value	sig.
PC aa C24:0	100.00	5.25	106.91	4.85	0.8554	ns	**PC aa C24:0**	100.00	8.99	84.96	9.04	0.6919	ns
PC aa C26:0	100.00	7.77	96.03	11.84	0.9892	ns	**PC aa C26:0**	100.00	13.49	106.32	15.04	0.9200	ns
PC aa C28:1	100.00	4.53	89.18	7.87	0.5428	ns	**PC aa C28:1**	100.00	9.24	90.59	10.32	0.9019	ns
PC aa C30:0	100.00	2.99	117.39	2.37	0.0372	*	**PC aa C30:0**	100.00	2.52	119.35	5.44	0.0049	**
PC aa C30:2	100.00	2.20	96.93	4.88	0.9111	ns	**PC aa C30:2**	100.00	6.80	91.21	8.80	0.8312	ns
PC aa C32:0	100.00	2.50	112.69	1.96	0.0193	*	**PC aa C32:0**	100.00	2.23	112.92	2.95	0.0169	*
PC aa C32:1	100.00	2.80	82.43	1.56	0.0043	**	**PC aa C32:1**	100.00	2.75	85.51	4.86	0.0343	*
PC aa C32:2	100.00	4.56	59.87	1.63	< 0.0001	***	**PC aa C32:2**	100.00	3.29	67.18	3.83	0.0004	***
PC aa C32:3	100.00	2.44	104.90	5.51	0.8284	ns	**PC aa C32:3**	100.00	6.85	90.70	6.97	0.7969	ns
PC aa C34:1	100.00	1.20	103.02	0.70	0.3989	ns	**PC aa C34:1**	100.00	1.07	102.25	1.39	0.5787	ns
PC aa C34:2	100.00	3.14	115.26	5.42	0.0818	#	**PC aa C34:2**	100.00	3.17	115.78	4.89	0.0283	*
PC aa C34:3	100.00	3.08	124.52	8.75	0.0109	*	**PC aa C34:3**	100.00	3.64	118.17	7.92	0.0374	*
PC aa C34:4	100.00	3.39	119.67	4.36	0.0134	*	**PC aa C34:4**	100.00	3.36	112.48	6.42	0.1892	ns
PC aa C36:0	100.00	3.75	99.60	2.15	0.9999	ns	**PC aa C36:0**	100.00	3.24	95.75	3.95	0.8405	ns
PC aa C36:1	100.00	3.18	100.54	1.68	0.9995	ns	**PC aa C36:1**	100.00	2.72	96.79	3.36	0.8713	ns
PC aa C36:2	100.00	3.26	97.78	2.07	0.9765	ns	**PC aa C36:2**	100.00	2.86	96.63	3.61	0.8763	ns
PC aa C36:3	100.00	3.58	111.71	2.12	0.1589	ns	**PC aa C36:3**	100.00	2.98	112.24	4.61	0.1433	ns
PC aa C36:4	100.00	3.45	110.38	2.73	0.2033	ns	**PC aa C36:4**	100.00	2.96	108.76	3.97	0.4104	ns
PC aa C36:5	100.00	3.22	115.96	2.93	0.0636	#	**PC aa C36:5**	100.00	2.48	114.94	7.50	0.0535	#
PC aa C36:6	100.00	2.43	102.01	2.63	0.9741	ns	**PC aa C36:6**	100.00	2.52	101.43	4.56	0.9883	ns
PC aa C38:0	100.00	4.43	90.44	2.46	0.5095	ns	**PC aa C38:0**	100.00	4.43	84.24	3.27	0.1000	ns
PC aa C38:1	100.00	4.96	87.61	2.66	0.3591	ns	**PC aa C38:1**	100.00	4.50	81.21	3.00	0.0549	#
PC aa C38:3	100.00	3.92	103.42	2.28	0.9293	ns	**PC aa C38:3**	100.00	2.70	102.89	4.27	0.9420	ns
PC aa C38:4	100.00	3.42	105.65	2.41	0.6702	ns	**PC aa C38:4**	100.00	2.75	104.12	4.09	0.8420	ns
PC aa C38:5	100.00	3.44	103.48	2.57	0.9109	ns	**PC aa C38:5**	100.00	2.87	105.74	4.47	0.6673	ns
PC aa C38:6	100.00	3.59	107.87	2.47	0.4946	ns	**PC aa C38:6**	100.00	3.06	108.40	3.78	0.3832	ns
PC aa C40:1	100.00	4.84	98.88	4.49	0.9990	ns	**PC aa C40:1**	100.00	6.09	86.44	4.50	0.4313	ns
PC aa C40:2	100.00	4.91	91.72	2.35	0.7245	ns	**PC aa C40:2**	100.00	5.11	82.72	3.39	0.0992	#
PC aa C40:3	100.00	4.02	104.46	1.70	0.8882	ns	**PC aa C40:3**	100.00	2.72	95.38	3.68	0.7798	ns
PC aa C40:4	100.00	4.04	107.18	2.08	0.6286	ns	**PC aa C40:4**	100.00	2.54	102.24	4.22	0.9729	ns
PC aa C40:5	100.00	3.96	101.64	2.34	0.9926	ns	**PC aa C40:5**	100.00	2.65	100.95	4.13	0.9976	ns
PC aa C40:6	100.00	4.17	102.65	2.43	0.9729	ns	**PC aa C40:6**	100.00	3.09	102.48	3.98	0.9712	ns
PC aa C42:0	100.00	4.38	99.57	3.94	> 0.9999	ns	**PC aa C42:0**	100.00	5.96	84.74	4.87	0.3406	ns
PC aa C42:1	100.00	5.18	100.41	6.23	> 0.9999	ns	**PC aa C42:1**	100.00	7.36	87.79	5.10	0.6854	ns
PC aa C42:2	100.00	4.46	95.91	3.80	0.9543	ns	**PC aa C42:2**	100.00	6.71	88.31	4.04	0.6268	ns
PC aa C42:4	100.00	4.19	103.60	2.26	0.9457	ns	**PC aa C42:4**	100.00	3.17	90.51	3.97	0.2966	ns
PC aa C42:5	100.00	3.95	99.95	1.83	> 0.9999	ns	**PC aa C42:5**	100.00	2.71	89.34	3.62	0.0862	#
PC aa C42:6	100.00	4.04	98.28	1.60	0.9919	ns	**PC aa C42:6**	100.00	2.22	92.91	3.29	0.4336	ns
Pcaa total	100.00	2.59	104.22	1.40	0.7232	ns	**Pcaa total**	100.00	2.09	103.21	2.75	0.7953	ns

Table 10.19: Level of PCae species measured in brain samples of male (A) and female (B) animals of the *Sms1* x *APPswe* mouse line.
Males: *Sms1*^{WT} x *APPswe*^{WT} n=6, *Sms1*^{MUT} x *APPswe*^{WT} n=11, *Sms1*^{WT} x *APPswe*^{Tg} n=13, *Sms1*^{MUT} x *APPswe*^{Tg} n=5; females: *Sms1*^{WT} x *APPswe*^{WT} n=5, *Sms1*^{MUT} x *APPswe*^{WT} n=6, *Sms1*^{WT} x *APPswe*^{Tg} n=11, *Sms1*^{MUT} x *APPswe*^{Tg} n=6. Statistical analysis was performed using one-way ANOVA with *post hoc* Tukey's test. *p≤0.05, **p≤0.01, ***p≤0.001.

A	Sms1WT x APPsweWT		Sms1MUT x APPsweWT		One Way ANOVA		B	Sms1WT x APPsweWT		Sms1MUT x APPsweWT		One Way ANOVA	
males	%	SEM	%	SEM	p-value	sign.	females	%	SEM	%	SEM	p-value	sign.
PC ae C30:0	100.00	4.63	102.91	4.89	0.9663	ns	PC ae C30:0	100.00	4.59	103.20	2.61	0.9410	ns
PC ae C30:1	100.00	2.99	96.07	4.05	0.8663	ns	PC ae C30:1	100.00	3.26	94.16	4.32	0.9272	ns
PC ae C30:2	100.00	9.73	96.39	7.34	0.9869	ns	PC ae C30:2	100.00	6.03	100.28	9.46	> 0.9999	ns
PC ae C32:1	100.00	3.99	100.39	3.13	> 0.9999	ns	PC ae C32:1	100.00	4.88	101.70	3.28	0.9923	ns
PC ae C32:2	100.00	4.49	99.55	6.08	0.9998	ns	PC ae C32:2	100.00	3.45	99.12	3.08	0.9939	ns
PC ae C34:0	100.00	3.84	97.95	3.84	0.9932	ns	PC ae C34:0	100.00	3.55	102.98	3.28	0.9727	ns
PC ae C34:1	100.00	6.32	98.70	4.05	0.9975	ns	PC ae C34:1	100.00	3.78	102.88	2.64	0.9620	ns
PC ae C34:2	100.00	3.82	96.13	4.96	0.9566	ns	PC ae C34:2	100.00	4.46	99.60	2.41	0.9999	ns
PC ae C34:3	100.00	1.44	97.62	3.44	0.9495	ns	PC ae C34:3	100.00	3.92	95.98	3.30	0.8851	ns
PC ae C36:0	100.00	3.25	93.48	5.60	0.7331	ns	PC ae C36:0	100.00	5.12	104.08	2.37	0.8965	ns
PC ae C36:1	100.00	5.46	93.38	5.01	0.7913	ns	PC ae C36:1	100.00	6.54	102.95	3.20	0.9708	ns
PC ae C36:2	100.00	6.05	93.01	5.60	0.9922	ns	PC ae C36:2	100.00	5.52	103.37	2.38	0.9455	ns
PC ae C36:3	100.00	4.93	102.46	6.05	0.9868	ns	PC ae C36:3	100.00	4.06	103.89	2.16	0.9184	ns
PC ae C36:4	100.00	6.70	102.19	2.84	0.9893	ns	PC ae C36:4	100.00	4.10	106.99	3.39	0.7111	ns
PC ae C36:5	100.00	6.81	98.80	3.67	0.9988	ns	PC ae C36:5	100.00	4.83	108.08	3.24	0.6632	ns
PC ae C38:0	100.00	3.19	96.77	3.76	0.9664	ns	PC ae C38:0	100.00	3.13	103.97	2.26	0.8399	ns
PC ae C38:1	100.00	3.12	86.85	6.48	0.3452	ns	PC ae C38:1	100.00	6.46	95.28	2.85	0.8621	ns
PC ae C38:2	100.00	3.60	91.05	6.78	0.6863	ns	PC ae C38:2	100.00	7.13	97.28	2.82	0.9756	ns
PC ae C38:3	100.00	4.94	99.00	3.53	0.9996	ns	PC ae C38:3	100.00	4.58	107.87	3.21	0.7311	ns
PC ae C38:4	100.00	4.34	96.40	4.34	0.9708	ns	PC ae C38:4	100.00	3.83	101.61	3.05	0.9969	ns
PC ae C38:5	100.00	3.88	98.16	2.95	0.9918	ns	PC ae C38:5	100.00	3.25	102.86	2.84	0.9515	ns
PC ae C38:6	100.00	3.82	98.58	4.32	0.9964	ns	PC ae C38:6	100.00	4.01	104.69	2.45	0.8055	ns
PC ae C40:0	100.00	6.16	99.86	5.49	> 0.9999	ns	PC ae C40:0	100.00	3.82	106.78	3.31	0.6081	ns
PC ae C40:1	100.00	4.87	97.06	6.04	0.9828	ns	PC ae C40:1	100.00	3.20	103.65	2.09	0.8669	ns
PC ae C40:2	100.00	3.23	91.53	7.61	0.7104	ns	PC ae C40:2	100.00	4.91	94.59	1.69	0.6796	ns
PC ae C40:3	100.00	6.82	97.76	9.10	0.9964	ns	PC ae C40:3	100.00	3.10	101.86	3.97	0.9913	ns
PC ae C40:4	100.00	5.95	96.95	7.64	0.9875	ns	PC ae C40:4	100.00	3.76	110.26	3.22	0.5792	ns
PC ae C40:5	100.00	5.88	99.35	7.97	0.9999	ns	PC ae C40:5	100.00	4.35	110.73	3.45	0.4860	ns
PC ae C40:6	100.00	6.21	96.00	5.65	0.9535	ns	PC ae C40:6	100.00	6.79	105.85	3.00	0.8132	ns
PC ae C42:0	100.00	7.72	95.07	6.70	0.9468	ns	PC ae C42:0	100.00	7.52	108.05	3.66	0.7040	ns
PC ae C42:1	100.00	4.51	96.84	6.70	0.9718	ns	PC ae C42:1	100.00	3.82	104.64	2.06	0.8055	ns
PC ae C42:2	100.00	6.35	99.97	7.60	> 0.9999	ns	PC ae C42:2	100.00	2.88	109.97	1.65	0.1237	ns
PC ae C42:3	100.00	6.95	100.90	6.19	0.9997	ns	PC ae C42:3	100.00	2.84	110.30	3.02	0.1779	ns
PC ae C42:4	100.00	7.17	99.43	10.06	> 0.9999	ns	PC ae C42:4	100.00	4.22	114.43	4.49	0.2826	ns
PC ae C42:5	100.00	7.22	98.36	11.34	0.9992	ns	PC ae C42:5	100.00	5.93	118.82	5.20	0.1791	ns
PC ae C44:3	100.00	6.75	96.65	6.41	0.9725	ns	PC ae C44:3	100.00	4.12	111.40	2.48	0.0641	#
PC ae C44:4	100.00	6.54	100.03	7.88	> 0.9999	ns	PC ae C44:4	100.00	3.77	114.34	2.11	0.0735	#
PC ae C44:5	100.00	8.30	101.44	6.43	0.9990	ns	PC ae C44:5	100.00	7.45	115.11	4.43	0.3018	ns
PC ae C44:6	100.00	5.12	97.60	8.67	0.9930	ns	PC ae C44:6	100.00	5.44	107.99	3.47	0.6319	ns
PC ae total	100.00	5.51	97.51	4.93	0.9818		PC ae total	100.00	3.80	104.41	2.28	0.8091	ns

	Sms1WT x APPsweWT		Sms1WT x APPsweTg		One Way ANOVA			Sms1WT x APPsweWT		Sms1WT x APPsweTg		One Way ANOVA	
	%	SEM	%	SEM	p-value	sig.		%	SEM	%	SEM	p-value	sig.
PC ae C30:0	100	4.63481	107.289029	3.50516	0.5728	ns	PC ae C30:0	100	4.59053	104.25992	3.771	0.8644	ns
PC ae C30:1	100.00	2.99	103.62	2.29	0.8539	ns	PC ae C30:1	100.00	5.26	108.19	6.80	0.8133	ns
PC ae C30:2	100.00	9.75	96.95	5.29	0.9888	ns	PC ae C30:2	100.00	6.03	115.59	11.35	0.7684	ns
PC ae C32:1	100.00	5.99	106.88	3.28	0.6012	ns	PC ae C32:1	100.00	4.88	97.55	3.81	0.9761	ns
PC ae C32:2	100.00	4.49	104.26	2.04	0.8419	ns	PC ae C32:2	100.00	3.45	105.49	4.15	0.7922	ns
PC ae C34:0	100.00	5.84	104.21	4.73	0.9267	ns	PC ae C34:0	100.00	5.35	97.13	4.33	0.9736	ns
PC ae C34:1	100.00	6.32	105.23	3.89	0.8262	ns	PC ae C34:1	100.00	3.78	101.78	3.88	0.9892	ns
PC ae C34:2	100.00	5.82	106.04	3.48	0.7402	ns	PC ae C34:2	100.00	4.46	96.75	3.68	0.9331	ns
PC ae C34:3	100.00	1.44	105.91	2.23	0.4558	ns	PC ae C34:3	100.00	3.92	101.22	4.84	0.9980	ns
PC ae C36:0	100.00	3.25	101.09	3.38	0.9974	ns	PC ae C36:0	100.00	5.12	104.47	3.70	0.8549	ns
PC ae C36:1	100.00	5.46	103.16	4.07	0.9592	ns	PC ae C36:1	100.00	6.54	99.17	3.70	0.9992	ns
PC ae C36:2	100.00	6.05	104.67	3.64	0.8811	ns	PC ae C36:2	100.00	5.52	99.38	3.67	0.9996	ns
PC ae C36:3	100.00	4.93	108.04	3.80	0.6185	ns	PC ae C36:3	100.00	4.06	98.94	4.04	0.9979	ns
PC ae C36:4	100.00	6.70	108.89	4.36	0.5029	ns	PC ae C36:4	100.00	4.10	104.50	4.25	0.8936	ns
PC ae C36:5	100.00	6.81	104.99	4.62	0.9000	ns	PC ae C36:5	100.00	4.83	100.70	3.46	0.9996	ns
PC ae C38:0	100.00	5.19	102.46	3.48	0.9784	ns	PC ae C38:0	100.00	3.15	104.28	2.80	0.7941	ns
PC ae C38:1	100.00	5.12	104.98	4.12	0.8870	ns	PC ae C38:1	100.00	6.46	101.52	3.59	0.9940	ns
PC ae C38:2	100.00	5.60	106.22	4.23	0.8218	ns	PC ae C38:2	100.00	7.15	102.24	3.98	0.9853	ns
PC ae C38:3	100.00	4.94	101.37	4.69	0.9984	ns	PC ae C38:3	100.00	4.58	109.57	5.17	0.5745	ns
PC ae C38:4	100.00	4.84	108.51	5.39	0.6512	ns	PC ae C38:4	100.00	5.83	101.35	5.29	0.9980	ns
PC ae C38:5	100.00	5.88	108.51	3.94	0.4669	ns	PC ae C38:5	100.00	3.25	101.37	3.47	0.9937	ns
PC ae C38:6	100.00	5.82	107.09	3.72	0.6278	ns	PC ae C38:6	100.00	4.01	101.38	3.35	0.9928	ns
PC ae C40:0	100.00	6.16	104.02	4.48	0.9414	ns	PC ae C40:0	100.00	3.32	97.28	3.26	0.9557	ns
PC ae C40:1	100.00	4.87	102.72	4.12	0.9808	ns	PC ae C40:1	100.00	3.20	101.69	3.17	0.9828	ns
PC ae C40:2	100.00	5.23	104.52	3.57	0.9175	ns	PC ae C40:2	100.00	4.91	105.81	3.14	0.6081	ns
PC ae C40:3	100.00	6.82	101.05	5.09	0.9995	ns	PC ae C40:3	100.00	3.10	111.22	4.09	0.3003	ns
PC ae C40:4	100.00	5.95	102.83	4.92	0.9859	ns	PC ae C40:4	100.00	3.76	113.46	5.83	0.3247	ns
PC ae C40:5	100.00	5.88	100.99	4.59	0.9993	ns	PC ae C40:5	100.00	4.35	112.67	4.60	0.2701	ns
PC ae C40:6	100.00	6.21	104.38	4.23	0.9186	ns	PC ae C40:6	100.00	6.79	102.29	3.71	0.9843	ns
PC ae C42:0	100.00	7.72	105.02	4.75	0.9231	ns	PC ae C42:0	100.00	7.52	103.46	4.60	0.9634	ns
PC ae C42:1	100.00	4.51	103.23	3.62	0.9582	ns	PC ae C42:1	100.00	3.32	100.31	3.76	> 0.9999	ns
PC ae C42:2	100.00	6.35	103.71	3.86	0.9557	ns	PC ae C42:2	100.00	2.38	106.77	3.14	0.3959	ns
PC ae C42:3	100.00	6.95	103.33	5.31	0.9771	ns	PC ae C42:3	100.00	2.84	101.70	2.91	0.9845	ns
PC ae C42:4	100.00	7.17	96.74	6.01	0.9897	ns	PC ae C42:4	100.00	4.22	117.70	5.10	0.1206	ns
PC ae C42:5	100.00	7.22	95.27	5.97	0.9742	ns	PC ae C42:5	100.00	5.93	125.57	5.56	0.0313	*
PC ae C44:3	100.00	6.75	103.20	3.96	0.9668	ns	PC ae C44:3	100.00	4.12	109.14	2.41	0.1614	ns
PC ae C44:4	100.00	6.54	106.36	4.37	0.8495	ns	PC ae C44:4	100.00	5.77	107.31	3.52	0.5508	ns
PC ae C44:5	100.00	8.30	106.25	5.86	0.9068	ns	PC ae C44:5	100.00	7.45	104.21	5.39	0.9562	ns
PC ae C44:6	100.00	5.12	95.22	5.08	0.9497	ns	PC ae C44:6	100.00	5.44	113.82	4.26	0.1838	ns
PC ae total	100.00	5.51	104.44	3.62	0.8768	ns	PC ae total	100.00	3.80	100.71	3.10	0.9988	ns
	Sms1WT x APPsweWT		Sms1MUT x APPsweTg		One Way ANOVA			Sms1WT x APPsweWT		Sms1MUT x APPsweTg		One Way ANOVA	
	%	SEM	%	SEM	p-value	sig.		%	SEM	%	SEM	p-value	sig.
PC ae C30:0	100	4.63481	109.778151	1.66741	0.4241	ns	PC ae C30:0	100	4.59053	109.59977	3.09564	0.4930	ns
PC ae C30:1	100.00	2.99	101.94	3.80	0.9808	ns	PC ae C30:1	100.00	5.26	99.18	6.49	0.9999	ns
PC ae C30:2	100.00	9.75	101.45	5.73	0.9991	ns	PC ae C30:2	100.00	6.03	93.27	10.64	0.9861	ns
PC ae C32:1	100.00	5.99	106.45	2.98	0.7249	ns	PC ae C32:1	100.00	4.88	103.55	4.00	0.9615	ns
PC ae C32:2	100.00	4.49	108.00	2.56	0.5227	ns	PC ae C32:2	100.00	3.45	101.55	4.68	0.9965	ns
PC ae C34:0	100.00	5.84	99.46	3.10	0.9999	ns	PC ae C34:0	100.00	5.35	100.79	6.28	0.9997	ns
PC ae C34:1	100.00	6.32	103.06	1.85	0.9696	ns	PC ae C34:1	100.00	3.78	103.58	5.09	0.9552	ns
PC ae C34:2	100.00	5.82	98.83	2.24	0.9980	ns	PC ae C34:2	100.00	4.46	96.14	4.95	0.9386	ns
PC ae C34:3	100.00	1.44	107.70	3.16	0.3277	ns	PC ae C34:3	100.00	3.92	104.15	6.16	0.9614	ns
PC ae C36:0	100.00	3.25	96.43	2.71	0.9415	ns	PC ae C36:0	100.00	5.12	93.69	5.13	0.7957	ns
PC ae C36:1	100.00	5.46	94.85	2.50	0.8881	ns	PC ae C36:1	100.00	6.54	94.19	6.91	0.8855	ns
PC ae C36:2	100.00	6.05	99.59	2.51	> 0.9999	ns	PC ae C36:2	100.00	5.52	98.15	6.28	0.9942	ns
PC ae C36:3	100.00	4.93	102.35	3.51	0.9885	ns	PC ae C36:3	100.00	4.06	104.79	6.43	0.9116	ns
PC ae C36:4	100.00	6.70	115.61	0.84	0.1485	ns	PC ae C36:4	100.00	4.10	118.34	4.49	0.1086	ns
PC ae C36:5	100.00	6.81	113.11	4.08	0.3898	ns	PC ae C36:5	100.00	4.83	107.86	3.60	0.7832	ns
PC ae C38:0	100.00	5.19	105.59	3.11	0.8530	ns	PC ae C38:0	100.00	3.15	103.07	5.59	0.9487	ns
PC ae C38:1	100.00	5.12	87.59	3.34	0.3943	ns	PC ae C38:1	100.00	6.46	80.88	5.05	0.0610	#
PC ae C38:2	100.00	5.60	90.10	3.36	0.6152	ns	PC ae C38:2	100.00	7.15	84.47	5.74	0.2281	ns
PC ae C38:3	100.00	4.94	104.13	4.69	0.9711	ns	PC ae C38:3	100.00	4.58	98.19	7.36	0.9971	ns
PC ae C38:4	100.00	4.84	105.25	2.06	0.9172	ns	PC ae C38:4	100.00	5.83	103.58	6.72	0.9805	ns
PC ae C38:5	100.00	5.88	111.32	1.52	0.3218	ns	PC ae C38:5	100.00	3.25	109.64	4.28	0.4535	ns
PC ae C38:6	100.00	5.82	105.82	1.61	0.8139	ns	PC ae C38:6	100.00	4.01	103.85	4.16	0.9254	ns
PC ae C40:0	100.00	6.16	105.20	3.00	0.9139	ns	PC ae C40:0	100.00	3.32	99.19	4.56	0.9993	ns
PC ae C40:1	100.00	4.87	106.32	4.81	0.8595	ns	PC ae C40:1	100.00	3.20	95.65	4.29	0.8674	ns
PC ae C40:2	100.00	5.23	92.76	4.01	0.7972	ns	PC ae C40:2	100.00	4.91	84.10	3.99	0.0450	*
PC ae C40:3	100.00	6.82	105.00	5.22	0.9632	ns	PC ae C40:3	100.00	3.10	94.63	4.76	0.8977	ns
PC ae C40:4	100.00	5.95	106.79	3.93	0.8837	ns	PC ae C40:4	100.00	3.76	100.72	6.30	0.9998	ns
PC ae C40:5	100.00	5.88	106.36	3.93	0.8971	ns	PC ae C40:5	100.00	4.35	100.69	6.22	0.9998	ns
PC ae C40:6	100.00	6.21	100.97	2.45	0.9995	ns	PC ae C40:6	100.00	6.79	99.48	6.20	0.9999	ns
PC ae C42:0	100.00	7.72	101.92	3.16	0.9965	ns	PC ae C42:0	100.00	7.52	93.60	3.44	0.8882	ns
PC ae C42:1	100.00	4.51	103.49	2.79	0.9627	ns	PC ae C42:1	100.00	3.32	92.18	3.46	0.5891	ns
PC ae C42:2	100.00	6.35	106.01	2.24	0.8809	ns	PC ae C42:2	100.00	2.38	99.82	3.80	> 0.9999	ns
PC ae C42:3	100.00	6.95	111.06	3.15	0.6342	ns	PC ae C42:3	100.00	2.84	102.75	4.07	0.9654	ns
PC ae C42:4	100.00	7.17	105.40	6.10	0.9682	ns	PC ae C42:4	100.00	4.22	97.32	6.29	0.9919	ns
PC ae C42:5	100.00	7.22	103.93	6.98	0.9892	ns	PC ae C42:5	100.00	5.93	94.72	7.14	0.9605	ns
PC ae C44:3	100.00	6.75	107.78	1.64	0.7512	ns	PC ae C44:3	100.00	4.12	100.48	3.32	0.9997	ns
PC ae C44:4	100.00	6.54	110.17	2.75	0.6613	ns	PC ae C44:4	100.00	5.77	104.53	4.40	0.9067	ns
PC ae C44:5	100.00	8.30	110.67	4.53	0.7387	ns	PC ae C44:5	100.00	7.45	105.65	3.73	0.9437	ns
PC ae C44:6	100.00	5.12	103.47	5.47	0.9854	ns	PC ae C44:6	100.00	5.44	90.20	6.13	0.6321	ns
PC ae total	100.00	5.51	102.46	2.02	0.9825	ns	PC ae total	100.00	3.80	99.22	4.69	0.9991	ns

	Sms1MUT x APPsweWT		Sms1MUT x APPsweTg		One Way ANOVA			Sms1MUT x APPsweWT		Sms1MUT x APPsweTg		One Way ANOVA	
	%	SEM	%	SEM	p-value	sig.		%	SEM	%	SEM	p-value	sig.
PC ae C30:0	**100**	**4.75555**	**106.670413**	**1.77863**	**0.6677**	**ns**	**PC ae C30:0**	**100**	**2.52859**	**106.19986**	**3.28756**	**0.7116**	**ns**
PC ae C30:1	100.00	4.21	106.11	4.03	0.6275	ns	**PC ae C30:1**	100.00	4.59	105.33	6.84	0.9595	ns
PC ae C30:2	100.00	7.83	105.25	6.03	0.9606	ns	**PC ae C30:2**	100.00	9.43	93.01	9.89	0.9782	ns
PC ae C32:1	100.00	3.12	106.03	3.16	0.7341	ns	**PC ae C32:1**	100.00	3.22	101.82	4.08	0.9918	ns
PC ae C32:2	100.00	6.10	108.49	2.78	0.4363	ns	**PC ae C32:2**	100.00	3.05	102.45	4.79	0.9818	ns
PC ae C34:0	100.00	3.92	101.54	3.15	0.9968	ns	**PC ae C34:0**	100.00	3.19	97.87	6.15	0.9906	ns
PC ae C34:1	100.00	4.10	104.41	1.93	0.9083	ns	**PC ae C34:1**	100.00	2.57	100.73	5.13	0.9994	ns
PC ae C34:2	100.00	5.16	102.80	2.30	0.9736	ns	**PC ae C34:2**	100.00	2.42	96.52	4.78	0.9374	ns
PC ae C34:3	100.00	3.52	110.32	3.48	0.1076	ns	**PC ae C34:3**	100.00	3.52	110.83	6.82	0.5447	ns
PC ae C36:0	100.00	6.00	103.15	2.79	0.9608	ns	**PC ae C36:0**	100.00	2.28	90.06	4.62	0.3469	ns
PC ae C36:1	100.00	5.36	101.57	2.53	0.9963	ns	**PC ae C36:1**	100.00	3.11	91.49	6.33	0.6121	ns
PC ae C36:2	100.00	5.71	101.61	2.55	0.9954	ns	**PC ae C36:2**	100.00	2.50	94.94	5.97	0.8523	ns
PC ae C36:3	100.00	5.90	99.89	3.50	> 0.9999	ns	**PC ae C36:3**	100.00	2.08	100.86	6.49	0.9990	ns
PC ae C36:4	100.00	2.78	113.13	0.94	0.2180	ns	**PC ae C36:4**	100.00	3.17	110.61	4.97	0.3755	ns
PC ae C36:5	100.00	3.72	114.48	4.68	0.2767	ns	**PC ae C36:5**	100.00	4.85	99.83	3.60	> 0.9999	ns
PC ae C38:0	100.00	5.95	109.12	3.39	0.5560	ns	**PC ae C38:0**	100.00	2.17	99.14	5.55	0.9980	ns
PC ae C38:1	100.00	7.46	100.85	3.37	0.9996	ns	**PC ae C38:1**	100.00	2.99	84.93	4.29	0.1426	ns
PC ae C38:2	100.00	7.44	98.96	3.32	0.9993	ns	**PC ae C38:2**	100.00	2.90	86.87	4.99	0.2921	ns
PC ae C38:3	100.00	8.61	105.18	4.93	0.9395	ns	**PC ae C38:3**	100.00	2.98	91.03	6.70	0.6337	ns
PC ae C38:4	100.00	4.50	109.18	2.24	0.6714	ns	**PC ae C38:4**	100.00	3.00	101.94	6.85	0.9952	ns
PC ae C38:5	100.00	3.00	113.41	1.72	0.1719	ns	**PC ae C38:5**	100.00	2.76	106.60	4.57	0.6441	ns
PC ae C38:6	100.00	4.38	107.34	1.73	0.6623	ns	**PC ae C38:6**	100.00	2.34	99.20	4.12	0.9987	ns
PC ae C40:0	100.00	5.49	105.34	3.16	0.8955	ns	**PC ae C40:0**	100.00	3.10	92.90	4.23	0.5678	ns
PC ae C40:1	100.00	6.22	109.54	5.27	0.6267	ns	**PC ae C40:1**	100.00	2.01	92.29	3.96	0.3990	ns
PC ae C40:2	100.00	8.31	101.34	4.06	0.9984	ns	**PC ae C40:2**	100.00	1.78	88.91	3.55	0.1941	ns
PC ae C40:3	100.00	9.30	107.40	5.61	0.8859	ns	**PC ae C40:3**	100.00	3.89	92.90	4.42	0.7203	ns
PC ae C40:4	100.00	7.88	110.15	4.32	0.6867	ns	**PC ae C40:4**	100.00	2.92	91.35	5.75	0.6781	ns
PC ae C40:5	100.00	8.02	107.05	4.20	0.8509	ns	**PC ae C40:5**	100.00	3.12	90.93	5.66	0.5441	ns
PC ae C40:6	100.00	5.89	105.18	2.57	0.9048	ns	**PC ae C40:6**	100.00	2.83	93.98	5.83	0.8017	ns
PC ae C42:0	100.00	7.05	107.20	3.39	0.8556	ns	**PC ae C42:0**	100.00	3.39	86.62	2.98	0.2811	ns
PC ae C42:1	100.00	6.92	106.86	2.98	0.7728	ns	**PC ae C42:1**	100.00	1.97	88.10	3.05	0.1272	ns
PC ae C42:2	100.00	7.60	106.04	2.38	0.8640	ns	**PC ae C42:2**	100.00	1.50	90.77	3.45	0.1488	ns
PC ae C42:3	100.00	6.14	110.06	3.46	0.6610	ns	**PC ae C42:3**	100.00	2.74	93.15	3.79	0.4831	ns
PC ae C42:4	100.00	10.12	106.01	6.46	0.9518	ns	**PC ae C42:4**	100.00	3.92	85.05	5.35	0.1982	ns
PC ae C42:5	100.00	11.53	105.67	7.37	0.9662	ns	**PC ae C42:5**	100.00	4.38	79.72	5.69	0.0769	#
PC ae C44:3	100.00	6.63	111.52	1.83	0.4529	ns	**PC ae C44:3**	100.00	2.22	90.20	3.00	0.1097	ns
PC ae C44:4	100.00	7.88	110.13	3.03	0.6297	ns	**PC ae C44:4**	100.00	1.85	91.42	4.02	0.3755	ns
PC ae C44:5	100.00	6.34	109.11	4.94	0.7907	ns	**PC ae C44:5**	100.00	3.85	91.78	3.42	0.7224	ns
PC ae C44:6	100.00	8.88	106.02	5.80	0.9263	ns	**PC ae C44:6**	100.00	3.21	83.52	5.12	0.0896	#
PC ae total	100.00	5.06	105.07	2.13	0.8634	ns	**PC ae total**	100.00	2.19	95.03	4.46	0.7572	ns

	Sms1WT x APPsweTg		Sms1MUT x APPsweTg		One Way ANOVA			Sms1WT x APPsweTg		Sms1MUT x APPsweTg		One Way ANOVA	
	%	SEM	%	SEM	p-value	sig.		%	SEM	%	SEM	p-value	sig.
PC ae C30:0	**100**	**3.26703**	**102.320015**	**1.70609**	**0.9647**	**ns**	**PC ae C30:0**	**100**	**3.61692**	**105.12167**	**3.25418**	**0.7981**	**ns**
PC ae C30:1	100.00	2.21	98.37	3.74	0.9785	ns	**PC ae C30:1**	100.00	6.28	91.67	5.95	0.7985	ns
PC ae C30:2	100.00	5.45	104.64	6.00	0.9594	ns	**PC ae C30:2**	100.00	9.82	80.69	8.58	0.5700	ns
PC ae C32:1	100.00	3.06	99.60	2.97	0.9998	ns	**PC ae C32:1**	100.00	3.90	106.15	4.25	0.7807	ns
PC ae C32:2	100.00	1.95	103.59	2.65	0.8668	ns	**PC ae C32:2**	100.00	3.93	96.26	4.50	0.9243	ns
PC ae C34:0	100.00	4.54	95.45	2.96	0.8817	ns	**PC ae C34:0**	100.00	4.45	103.77	6.52	0.9561	ns
PC ae C34:1	100.00	3.70	97.94	1.81	0.9811	ns	**PC ae C34:1**	100.00	3.81	101.77	5.18	0.9906	ns
PC ae C34:2	100.00	3.28	93.20	2.08	0.5758	ns	**PC ae C34:2**	100.00	3.81	99.37	4.92	0.9996	ns
PC ae C34:3	100.00	2.10	101.69	3.21	0.9622	ns	**PC ae C34:3**	100.00	4.78	102.90	6.34	0.9786	ns
PC ae C36:0	100.00	3.35	95.39	2.58	0.8155	ns	**PC ae C36:0**	100.00	3.54	89.68	4.60	0.2908	ns
PC ae C36:1	100.00	3.95	91.95	2.29	0.5196	ns	**PC ae C36:1**	100.00	3.73	94.98	6.57	0.8895	ns
PC ae C36:2	100.00	3.48	95.14	2.39	0.8292	ns	**PC ae C36:2**	100.00	3.69	98.76	6.21	0.9973	ns
PC ae C36:3	100.00	3.52	94.74	3.32	0.7944	ns	**PC ae C36:3**	100.00	4.08	105.91	6.81	0.7907	ns
PC ae C36:4	100.00	4.01	106.17	0.89	0.6712	ns	**PC ae C36:4**	100.00	4.06	113.25	5.09	0.1952	ns
PC ae C36:5	100.00	4.40	107.74	4.40	0.6370	ns	**PC ae C36:5**	100.00	3.44	107.11	3.86	0.7582	ns
PC ae C38:0	100.00	3.39	103.06	3.20	0.9496	ns	**PC ae C38:0**	100.00	2.69	98.85	5.53	0.9949	ns
PC ae C38:1	100.00	3.93	83.44	2.79	0.0585	#	**PC ae C38:1**	100.00	3.54	79.67	4.02	0.0137	*
PC ae C38:2	100.00	3.98	84.83	2.85	0.1067	ns	**PC ae C38:2**	100.00	3.90	82.62	4.74	0.0686	#
PC ae C38:3	100.00	4.62	102.72	4.81	0.9850	ns	**PC ae C38:3**	100.00	4.72	89.61	6.59	0.4841	ns
PC ae C38:4	100.00	4.97	96.99	1.99	0.9635	ns	**PC ae C38:4**	100.00	5.21	102.19	6.87	0.9927	ns
PC ae C38:5	100.00	3.63	102.59	1.56	0.9540	ns	**PC ae C38:5**	100.00	3.43	108.17	4.63	0.4642	ns
PC ae C38:6	100.00	3.47	98.81	1.59	0.9955	ns	**PC ae C38:6**	100.00	3.31	102.43	4.26	0.9679	ns
PC ae C40:0	100.00	4.30	101.14	3.03	0.9980	ns	**PC ae C40:0**	100.00	3.36	101.97	4.65	0.9865	ns
PC ae C40:1	100.00	4.01	103.50	4.98	0.9497	ns	**PC ae C40:1**	100.00	3.12	94.07	4.04	0.6131	ns
PC ae C40:2	100.00	3.41	88.75	3.56	0.3102	ns	**PC ae C40:2**	100.00	2.97	79.48	3.17	0.0008	***
PC ae C40:3	100.00	5.04	103.91	5.42	0.9689	ns	**PC ae C40:3**	100.00	3.68	85.08	4.05	0.0842	#
PC ae C40:4	100.00	4.78	103.85	4.08	0.9563	ns	**PC ae C40:4**	100.00	5.14	88.78	5.59	0.4284	ns
PC ae C40:5	100.00	4.55	105.31	4.13	0.8951	ns	**PC ae C40:5**	100.00	4.09	89.37	5.56	0.3714	ns
PC ae C40:6	100.00	4.05	96.73	2.37	0.9514	ns	**PC ae C40:6**	100.00	3.62	97.25	6.03	0.9764	ns
PC ae C42:0	100.00	4.52	97.05	3.07	0.9763	ns	**PC ae C42:0**	100.00	4.45	90.46	3.12	0.5838	ns
PC ae C42:1	100.00	3.51	100.25	2.80	> 0.9999	ns	**PC ae C42:1**	100.00	3.75	91.90	3.18	0.4399	ns
PC ae C42:2	100.00	3.73	102.22	2.29	0.9865	ns	**PC ae C42:2**	100.00	2.94	93.49	3.55	0.4287	ns
PC ae C42:3	100.00	5.14	107.48	3.38	0.7513	ns	**PC ae C42:3**	100.00	2.86	101.04	4.11	0.9968	ns
PC ae C42:4	100.00	6.21	108.95	6.64	0.8212	ns	**PC ae C42:4**	100.00	4.33	82.69	5.20	0.0830	#
PC ae C42:5	100.00	6.26	109.10	7.61	0.8441	ns	**PC ae C42:5**	100.00	4.43	75.43	5.39	0.0123	*
PC ae C44:3	100.00	3.84	104.44	1.71	0.8952	ns	**PC ae C44:3**	100.00	2.21	92.06	3.06	0.2462	ns
PC ae C44:4	100.00	4.11	103.58	2.85	0.9547	ns	**PC ae C44:4**	100.00	3.28	97.41	4.28	0.9641	ns
PC ae C44:5	100.00	5.52	104.16	4.72	0.9571	ns	**PC ae C44:5**	100.00	5.18	101.38	3.78	0.9984	ns
PC ae C44:6	100.00	5.34	108.67	5.94	0.7610	ns	**PC ae C44:6**	100.00	3.74	79.25	4.86	0.0116	*
PC ae total	100.00	3.47	98.10	1.98	0.9843	ns	**PC ae total**	100.00	3.08	98.52	4.62	0.9912	ns

Table 10.20: Level of lyso-PC species measured in brain samples of male (A) and female (B) animals of the *Sms1* x *APPswe* mouse line.
Males: *Sms1*^{WT} x *APPswe*^{WT} n=6, *Sms1*^{MUT} x *APPswe*^{WT} n=11, *Sms1*^{WT} x *APPswe*^{Tg} n=13, *Sms1*^{MUT} x *APPswe*^{Tg} n=5; females: *Sms1*^{WT} x *APPswe*^{WT} n=5, *Sms1*^{MUT} x *APPswe*^{WT} n=6, *Sms1*^{WT} x *APPswe*^{Tg} n=11, *Sms1*^{MUT} x *APPswe*^{Tg} n=6. Statistical analysis was performed using one-way ANOVA with *post hoc* Tukey's test. *p≤0.05, **p≤0.01, ***p≤0.001.

A	Sms1WT x APPsweWT		Sms1MUT x APPsweWT		One Way ANOVA		B	Sms1WT x APPsweWT		Sms1MUT x APPsweWT		One Way ANOVA	
males	%	SEM	%	SEM	p-value	sign.	females	%	%	SEM	SEM	p-value	sign.
Lyso PC 06:0	100.00	6.15	104.48	5.87	0.9732	ns	Lyso PC 06:0	100.00	5.02	106.48	4.08	0.7923	ns
Lyso PC 14:0	100.00	8.78	105.48	10.85	0.9514	ns	Lyso PC 14:0	100.00	1.83	112.28	6.45	0.2742	ns
Lyso PC 16:0	100.00	8.80	105.28	10.17	0.9784	ns	Lyso PC 16:0	100.00	4.63	124.08	6.00	0.1399	ns
Lyso PC 16:1	100.00	11.22	104.81	11.39	0.9868	ns	Lyso PC 16:1	100.00	4.46	121.33	6.32	0.3536	ns
Lyso PC 17:0	100.00	7.93	101.78	10.44	0.9939	ns	Lyso PC 17:0	100.00	4.18	110.52	4.31	0.6968	ns
Lyso PC 18:0	100.00	7.93	102.94	10.26	0.9965	ns	Lyso PC 18:0	100.00	6.49	121.29	4.12	0.1763	ns
Lyso PC 18:1	100.00	7.69	100.97	9.06	0.9998	ns	Lyso PC 18:1	100.00	5.20	118.82	5.44	0.2663	ns
Lyso PC 18:2	100.00	7.83	101.52	8.63	0.9995	ns	Lyso PC 18:2	100.00	5.89	126.75	5.78	0.1393	ns
Lyso PC 20:3	100.00	9.65	97.85	10.18	0.9985	ns	Lyso PC 20:3	100.00	7.94	126.41	6.87	0.2048	ns
Lyso PC 20:4	100.00	8.95	98.22	11.67	0.9994	ns	Lyso PC 20:4	100.00	8.65	123.71	7.59	0.4210	ns
Lyso PC 24:0	100.00	6.00	102.84	7.38	0.9856	ns	Lyso PC 24:0	100.00	3.57	105.89	6.41	0.9491	ns
Lyso PC 26:0	100.00	8.95	104.59	8.31	0.9820	ns	Lyso PC 26:0	100.00	8.94	94.59	9.24	0.9911	ns
Lyso PC 26:1	100.00	10.20	99.53	5.58	> 0.9999	ns	Lyso PC 26:1	100.00	8.56	95.18	9.45	0.9921	ns
Lyso PC 28:0	100.00	8.42	100.16	7.45	> 0.9999	ns	Lyso PC 28:0	100.00	8.59	94.08	8.68	0.9836	ns
Lyso PC 28:1	100.00	8.96	97.71	6.78	0.9963	ns	Lyso PC 28:1	100.00	7.00	92.64	8.87	0.9728	ns
Lyso PC total	100.00	7.48	103.21	9.07	0.9921	ns	Lyso PC total	100.00	4.22	120.10	4.47	0.1248	ns
	Sms1WT x APPsweWT		Sms1WT x APPsweTg		One Way ANOVA			Sms1WT x APPsweWT		Sms1WT x APPsweTg		One Way ANOVA	
	%	SEM	%	SEM	p-value	sig.		%	SEM	%	SEM	p-value	sig.
Lyso PC 06:0	100.00	6.15	99.72	6.05	> 0.9999	ns	Lyso PC 06:0	100.00	5.02	104.94	8.68	0.8840	ns
Lyso PC 14:0	100.00	8.78	92.28	1.32	0.7800	ns	Lyso PC 14:0	100.00	1.83	103.92	1.91	0.9299	ns
Lyso PC 16:0	100.00	8.80	99.53	6.88	> 0.9999	ns	Lyso PC 16:0	100.00	4.63	114.08	6.89	0.5483	ns
Lyso PC 16:1	100.00	11.22	101.46	6.60	0.9995	ns	Lyso PC 16:1	100.00	4.46	120.02	7.38	0.3844	ns
Lyso PC 17:0	100.00	7.93	100.48	5.70	> 0.9999	ns	Lyso PC 17:0	100.00	4.18	112.81	6.52	0.5283	ns
Lyso PC 18:0	100.00	7.93	98.89	7.19	0.9991	ns	Lyso PC 18:0	100.00	6.49	115.96	7.07	0.3841	ns
Lyso PC 18:1	100.00	7.69	97.91	6.22	0.9969	ns	Lyso PC 18:1	100.00	5.20	111.94	6.41	0.6238	ns
Lyso PC 18:2	100.00	7.83	97.27	6.58	0.9961	ns	Lyso PC 18:2	100.00	5.89	123.51	7.54	0.2065	ns
Lyso PC 20:3	100.00	9.65	92.84	7.84	0.9178	ns	Lyso PC 20:3	100.00	7.94	120.90	8.66	0.3724	ns
Lyso PC 20:4	100.00	8.95	97.38	8.95	0.9975	ns	Lyso PC 20:4	100.00	8.65	120.20	9.85	0.5342	ns
Lyso PC 24:0	100.00	6.00	98.55	8.96	0.9972	ns	Lyso PC 24:0	100.00	3.57	114.70	7.41	0.5209	ns
Lyso PC 26:0	100.00	8.95	99.90	5.83	> 0.9999	ns	Lyso PC 26:0	100.00	8.94	103.04	12.95	0.9952	ns
Lyso PC 26:1	100.00	10.20	98.83	8.89	0.9990	ns	Lyso PC 26:1	100.00	8.56	106.77	11.51	0.9770	ns
Lyso PC 28:0	100.00	8.42	102.11	5.59	0.9971	ns	Lyso PC 28:0	100.00	8.59	102.58	11.93	0.9987	ns
Lyso PC 28:1	100.00	8.96	98.60	5.02	0.9988	ns	Lyso PC 28:1	100.00	7.00	106.68	11.67	0.9777	ns
Lyso PC total	100.00	7.48	98.71	6.05	0.9995	ns	Lyso PC total	100.00	4.22	113.70	5.70	0.3948	ns

	Sms1WT x APPsweWT		Sms1MUT x APPsweTg		One Way ANOVA			Sms1WT x APPsweWT		Sms1MUT x APPsweTg		One Way ANOVA	
	%	SEM	%	SEM	p-value	sig.		%	%	SEM	SEM	p-value	sig.
Lyso PC 06:0	100.00	6.15	91.01	7.50	0.8268	ns	**Lyso PC 06:0**	100.00	3.02	107.80	7.14	0.7837	ns
Lyso PC 14:0	100.00	8.78	99.15	2.83	0.9997	ns	**Lyso PC 14:0**	100.00	1.83	102.04	2.30	0.9940	ns
Lyso PC 16:0	100.00	8.80	117.71	6.53	0.5342	ns	**Lyso PC 16:0**	100.00	4.63	118.83	8.70	0.4755	ns
Lyso PC 16:1	100.00	11.22	124.48	7.03	0.3433	ns	**Lyso PC 16:1**	100.00	4.46	141.59	12.39	0.0474	*
Lyso PC 17:0	100.00	7.93	108.57	5.53	0.8867	ns	**Lyso PC 17:0**	100.00	4.18	107.27	9.26	0.9209	ns
Lyso PC 18:0	100.00	7.98	114.18	6.77	0.7216	ns	**Lyso PC 18:0**	100.00	6.49	111.49	7.71	0.7789	ns
Lyso PC 18:1	100.00	7.69	105.51	4.60	0.9628	ns	**Lyso PC 18:1**	100.00	5.20	109.58	8.82	0.8573	ns
Lyso PC 18:2	100.00	7.83	120.15	10.28	0.4850	ns	**Lyso PC 18:2**	100.00	5.89	134.94	10.33	0.0915	#
Lyso PC 20:3	100.00	9.65	100.29	5.45	> 0.9999	ns	**Lyso PC 20:3**	100.00	7.94	114.48	8.52	0.7913	ns
Lyso PC 20:4	100.00	8.98	104.71	6.10	0.9900	ns	**Lyso PC 20:4**	100.00	8.65	114.10	13.02	0.8660	ns
Lyso PC 24:0	100.00	6.00	103.95	8.41	0.9630	ns	**Lyso PC 24:0**	100.00	8.57	95.98	7.29	0.9897	ns
Lyso PC 26:0	100.00	8.93	97.95	9.42	0.9983	ns	**Lyso PC 26:0**	100.00	8.94	101.09	12.49	> 0.9999	ns
Lyso PC 26:1	100.00	10.20	99.79	5.99	> 0.9999	ns	**Lyso PC 26:1**	100.00	8.56	95.18	12.84	0.9953	ns
Lyso PC 28:0	100.00	8.42	97.80	9.69	0.9957	ns	**Lyso PC 28:0**	100.00	8.59	95.96	12.14	0.9972	ns
Lyso PC 28:1	100.00	8.96	97.79	7.45	0.9967	ns	**Lyso PC 28:1**	100.00	7.00	93.99	13.87	0.9908	ns
Lyso PC total	100.00	7.48	112.11	5.08	0.7181	ns	**Lyso PC total**	100.00	4.22	113.77	7.75	0.5643	ns

	Sms1MUT x APPsweWT		Sms1MUT x APPsweTg		One Way ANOVA			Sms1MUT x APPsweWT		Sms1MUT x APPsweTg		One Way ANOVA	
	%	SEM	%	SEM	p-value	sig.		%	%	SEM	SEM	p-value	sig.
Lyso PC 06:0	100.00	5.61	87.10	6.58	0.5433	ns	**Lyso PC 06:0**	100.00	8.83	101.29	7.28	0.9977	ns
Lyso PC 14:0	100.00	10.29	94.00	2.66	0.8860	ns	**Lyso PC 14:0**	100.00	5.75	90.88	2.09	0.4822	ns
Lyso PC 16:0	100.00	9.66	111.81	7.30	0.7629	ns	**Lyso PC 16:0**	100.00	4.83	95.77	8.83	0.9680	ns
Lyso PC 16:1	100.00	10.87	118.77	8.35	0.4897	ns	**Lyso PC 16:1**	100.00	5.21	116.70	14.46	0.4513	ns
Lyso PC 17:0	100.00	10.26	106.72	5.90	0.9293	ns	**Lyso PC 17:0**	100.00	5.90	97.05	8.99	0.9886	ns
Lyso PC 18:0	100.00	9.97	110.92	7.51	0.8181	ns	**Lyso PC 18:0**	100.00	5.40	91.92	7.08	0.8005	ns
Lyso PC 18:1	100.00	8.98	104.50	4.81	0.9754	ns	**Lyso PC 18:1**	100.00	4.58	92.22	8.18	0.8256	ns
Lyso PC 18:2	100.00	8.50	118.85	12.17	0.5109	ns	**Lyso PC 18:2**	100.00	4.52	106.46	11.00	0.9180	ns
Lyso PC 20:3	100.00	10.41	102.50	5.58	0.9975	ns	**Lyso PC 20:3**	100.00	5.48	90.57	7.72	0.8278	ns
Lyso PC 20:4	100.00	11.88	106.61	6.50	0.9710	ns	**Lyso PC 20:4**	100.00	6.14	92.24	12.01	0.9341	ns
Lyso PC 24:0	100.00	7.18	101.08	8.45	0.9990	ns	**Lyso PC 24:0**	100.00	6.05	90.64	6.60	0.8294	ns
Lyso PC 26:0	100.00	7.94	93.65	8.83	0.9416	ns	**Lyso PC 26:0**	100.00	9.76	106.88	13.34	0.9872	ns
Lyso PC 26:1	100.00	5.61	100.27	6.01	> 0.9999	ns	**Lyso PC 26:1**	100.00	9.93	100.00	12.34	> 0.9999	ns
Lyso PC 28:0	100.00	7.48	97.14	9.42	0.9941	ns	**Lyso PC 28:0**	100.00	9.23	102.00	12.39	0.9996	ns
Lyso PC 28:1	100.00	6.88	100.08	7.45	> 0.9999	ns	**Lyso PC 28:1**	100.00	9.57	101.46	14.07	0.9998	ns
Lyso PC total	100.00	8.79	108.63	5.52	0.8466	ns	**Lyso PC total**	100.00	8.72	94.78	7.35	0.9055	ns

	Sms1WT x APPsweTg		Sms1MUT x APPsweTg		One Way ANOVA			Sms1WT x APPsweTg		Sms1MUT x APPsweTg		One Way ANOVA	
	%	SEM	%	SEM	p-value	sig.		%	%	SEM	SEM	p-value	sig.
Lyso PC 06:0	100.00	6.06	91.26	6.84	0.7561	ns	**Lyso PC 06:0**	100.00	3.43	102.72	7.38	0.9785	ns
Lyso PC 14:0	100.00	1.43	107.45	3.04	0.8069	ns	**Lyso PC 14:0**	100.00	1.84	98.19	2.26	0.9928	ns
Lyso PC 16:0	100.00	6.91	118.26	7.73	0.3829	ns	**Lyso PC 16:0**	100.00	6.04	104.17	9.06	0.9741	ns
Lyso PC 16:1	100.00	6.51	122.69	8.62	0.2495	ns	**Lyso PC 16:1**	100.00	6.10	117.97	14.62	0.8752	ns
Lyso PC 17:0	100.00	5.67	108.05	5.98	0.8469	ns	**Lyso PC 17:0**	100.00	5.78	95.08	8.81	0.9443	ns
Lyso PC 18:0	100.00	7.31	116.05	7.85	0.5134	ns	**Lyso PC 18:0**	100.00	6.10	96.14	7.41	0.9738	ns
Lyso PC 18:1	100.00	6.35	107.75	4.96	0.8585	ns	**Lyso PC 18:1**	100.00	5.72	97.89	8.63	0.9959	ns
Lyso PC 18:2	100.00	6.72	128.55	12.70	0.2317	ns	**Lyso PC 18:2**	100.00	6.11	109.25	11.29	0.7964	ns
Lyso PC 20:3	100.00	7.95	108.61	5.92	0.8935	ns	**Lyso PC 20:3**	100.00	7.16	94.69	8.07	0.9647	ns
Lyso PC 20:4	100.00	9.17	107.53	6.56	0.9414	ns	**Lyso PC 20:4**	100.00	8.20	94.93	12.56	0.9804	ns
Lyso PC 24:0	100.00	4.02	105.48	8.60	0.8624	ns	**Lyso PC 24:0**	100.00	6.46	88.68	6.10	0.8675	ns
Lyso PC 26:0	100.00	5.84	98.05	9.24	0.9976	ns	**Lyso PC 26:0**	100.00	12.56	98.11	12.25	0.9996	ns
Lyso PC 26:1	100.00	8.93	100.98	6.05	0.9993	ns	**Lyso PC 26:1**	100.00	10.78	89.14	11.00	0.9142	ns
Lyso PC 28:0	100.00	5.48	95.29	9.24	0.9619	ns	**Lyso PC 28:0**	100.00	11.63	93.56	11.56	0.9821	ns
Lyso PC 28:1	100.00	5.09	99.17	7.38	0.9997	ns	**Lyso PC 28:1**	100.00	10.94	88.15	12.22	0.8894	ns
Lyso PC total	100.00	6.13	113.58	5.77	0.5139	ns	**Lyso PC total**	100.00	5.01	100.06	7.76	> 0.9999	ns

Table 10.21: Pathological examination of *Sms1* x *APPswe* animals the age of 8 weeks
Sms1^{MUT} x *APPswe*^{Tg} animals, which made a sick impression and age matched controls were transferred to the pathological institute for examination by Dr. Frauke Neff. The most prominent observations are listed.

Heart	Sms1^{WT} x APPswe^{WT}	Sms1^{MUT} x APPswe^{WT}	Sms1^{WT} x APPswe^{Tg}	Sms1^{MUT} x APPswe^{Tg}
male 1	Artefacts, NAD	NAD	Bilateral dilatation of ventricles	r.V. dilatated, focal fatt deposition in the heart interstitium
male 2	Septum and l.V. muscles strong, possible myocarddegeneration		r.V. dilatated, septum and l.V muscles strong	r.V. dilatated, septum and l.V muscles strong
male 3			NAD	r.V. dilatated, septum and l.V muscles strong
female 1	Artefacts, r.V. dilatated	Artefacts, r.V. dilatated	NAD	Bilateral dilatation of ventricles
female 2			possible hypertrophie of septum and l.V., anisocaryosis, focal fat deposition in the heart interstitium	

Lung	Sms1^{WT} x APPswe^{WT}	Sms1^{MUT} x APPswe^{WT}	Sms1^{WT} x APPswe^{Tg}	Sms1^{MUT} x APPswe^{Tg}
male 1	NAD	hyperemia	NAD	irregular hyperemia
male 2	NAD		mild oligofocal interstitial pneumonia	hyperemia
male 3			NAD	NAD
female 1	NAD	irregular hyperemia	hyperemia	NAD
female 2			NAD	

Liver	Sms1^{WT} x APPswe^{WT}	Sms1^{MUT} x APPswe^{WT}	Sms1^{WT} x APPswe^{Tg}	Sms1^{MUT} x APPswe^{Tg}
male 1	oligofocal micorgranuloma	mild to semi-strong diffuse glycogen storage, solitary microgranuloma	hyperemia, solitary microgranuloma	focal microgranuloma
male 2	semi-strong diffuse glycogen storage, oligofocal liver cell necrosis		NAD	semi-strong diffuse glycogen storage, focxal and more extended acute necrosis
male 3			mild to semi-strong diffuse glycogen storage	emi-strong to strong diffuse glycogen storage, oligofocal necrosis
female 1	semi-strong diffuse glycogen storage, focal micorgranuloma	semi-strong diffuse glycogen storage, focal micorgranuloma	mild focal histiocytic lymph infiltrations	semi-strong diffuse glycogen storage, focal micorgranuloma
female 2			strong diffuce glycogen storage	

NAD = no abnormality detected
r.V. = right ventricle
l.V. = left ventricle

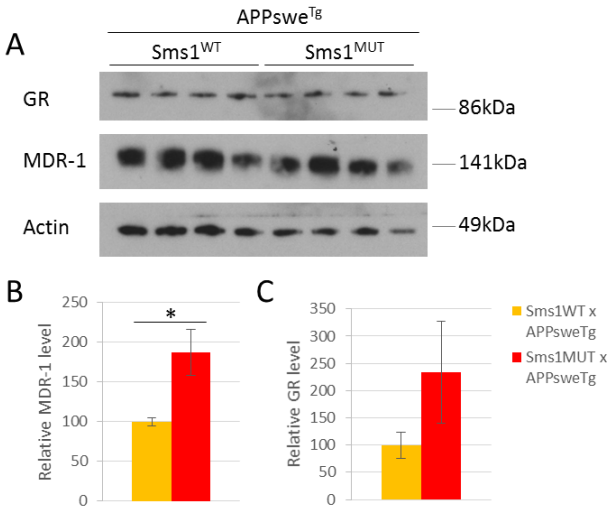

Figure 10.12: MDR-1 protein levels are elevated in *Sms1*^{MUT} x *APPswe*^{Tg} animals.
(A) Immunoblot with *Sms1*^{WT} x *APPswe*^{Tg} and *Sms1*^{MUT} x *APPswe*^{Tg} brain samples of 8 week old males for the detection of GR and MDR-1. (B) Relative quantification of MDR-1 and GR protein levels. Immunoblot data: n=4 per genotype; data is presented as mean ± SEM. Statistical analysis was performed using two-tailed Student's t-test. $p<0.01^{\#}$, $p\leq0.05^{*}$, $p\leq0.01^{**}$, $p\leq0.001^{***}$.

Table 10.22: Genes ranked highest for expression differences in brain samples from male *Sms1*^{WT} (n=3) and *Sms1*^{MUT} (n=4) animals.

ID	ILMN-ID	Frequency	Linear_ratio
1700001O22Rik	ILMN_2962336	50	1,05864814
Adam11	ILMN_1255996	50	1,13984783
Cnbp2	ILMN_2902833	50	1,46582197
Cys1	ILMN_1229578	50	0,74603352
Ddr2	ILMN_1230373	50	0,80665172
Dip2b	ILMN_2905040	50	1,31798533
Gpsn2	ILMN_2710784	50	1,19369668
LOC100047369	ILMN_1216623	50	1,10094605
Lsm14b	ILMN_2613313	50	0,83725396
Magea5	ILMN_2596441	50	1,2890377
Mus81	ILMN_2651462	50	1,2733697
Nlrp9b	ILMN_2769017	50	0,85253997
Olfr913	ILMN_2922354	50	0,82611048
Olfr982	ILMN_2698350	50	0,87030995
Pcbp2	ILMN_2843355	50	0,8402499
Prmt2	ILMN_3099751	50	1,0714766
Rnf207	ILMN_2823733	50	0,74485105
Scn3b	ILMN_1215136	50	0,83283405
Sf4	ILMN_2607953	50	0,95303142
Smpd2	ILMN_2867033	50	0,81044721
Sorcs3	ILMN_1233371	50	1,14446369
Uhrf1	ILMN_2517041	50	1,33278898
Wdr35	ILMN_1258932	50	0,82460977
Zbtb17	ILMN_1232592	50	1,24702007
Zfp191	ILMN_2421299	50	0,74117135
Rbm10	ILMN_1242598	49	1,29176447
Frzb	ILMN_2601155	48	0,77239321
Map6d1	ILMN_2761405	48	0,81663062
OTTMUSG00000010747	ILMN_3134537	48	0,83434613
Pramel1	ILMN_1253686	48	0,66741266
Runx2	ILMN_2599072	48	1,1412583
Tuba3b	ILMN_2417813	48	1,27043644
Wnt3a	ILMN_1220516	48	0,79834814
Cxcl12	ILMN_2746295	47	1,17778526
Sh3glb1	ILMN_2732362	47	0,82674582
Ccdc49	ILMN_2600813	46	1,21827142
Olfr102	ILMN_2460041	46	0,72134552
1110004E09Rik	ILMN_1257567	45	1,27444384
Gstm2	ILMN_1251449	45	1,13365337
Sin3b	ILMN_2749818	45	1,21064957
Art1	ILMN_3161382	44	1,28485528
Fbxl12	ILMN_1224697	44	1,14149549
Hectd3	ILMN_2687372	44	1,17126333
Lta	ILMN_1229804	44	1,14888931
Olfr1342	ILMN_1245835	44	0,88610651
Tmem18	ILMN_1245565	44	1,21379159
Pear1	ILMN_2609711	43	0,80597919
Bcl2l2	ILMN_2601572	42	0,79385382
Csnk1d	ILMN_2746075	42	0,77059594
Dmbx1	ILMN_3140871	42	0,8567242
Nr5a2	ILMN_2751680	42	1,34958299
Prpf40b	ILMN_1249348	42	0,78567176
Sfrs2	ILMN_2636335	42	1,06025369
Trdn	ILMN_2521511	42	0,79991148
V1re9	ILMN_1233229	42	0,86469085
Vmn2r1	ILMN_1259367	42	0,88504927
Crk	ILMN_2652663	41	0,75771953
Gria3	ILMN_2638066	41	0,83788834
Igf2bp3	ILMN_1226175	41	0,75774478
Jmy	ILMN_2437714	41	0,77286825
LOC100042777	ILMN_1217879	41	1,1398758
Olfr694	ILMN_1231923	41	0,7985543
Vsig2	ILMN_1245518	41	1,19327724
Lor	ILMN_1241825	40	1,07952333
Pla1a	ILMN_2722024	40	0,80010713
Rhbdl1	ILMN_2710802	40	1,04090486
Tdrd1	ILMN_2718442	40	0,85867129
Ypel4	ILMN_2966558	40	0,86021814
1700034I23Rik	ILMN_2862353	39	0,86256754
Csda	ILMN_2705078	39	0,83086252
Glipr2	ILMN_3130350	39	0,76066113
Mnat1	ILMN_2758631	39	0,8433011
Prl2c4	ILMN_2996648	39	0,67118262
Ranbp3l	ILMN_2734815	39	0,81186495
Slc25a31	ILMN_1228264	39	0,88424788
Swap70	ILMN_2752989	39	0,78746226
Zfp709	ILMN_1228695	39	1,19059226
4930519G04Rik	ILMN_2658753	38	1,19892494
Cbfa2t2	ILMN_2752204	38	0,7894398
Olfr273	ILMN_1255796	38	0,86551874

ID	ILMN-ID	Frequency	Linear_ratio
Slc25a26	ILMN_1256867	38	1,14781308
Thap4	ILMN_2773540	38	1,31420198
4833426J09Rik	ILMN_3057482	37	1,19986137
Arfgap1	ILMN_2700126	37	0,82591426
Asah3	ILMN_2848871	37	1,23600503
Cidec	ILMN_1222679	37	0,80150871
Crebl2	ILMN_2632162	37	0,92135785
Cyp2d26	ILMN_2704777	37	1,21916332
Ecsit	ILMN_2824167	37	1,1313109
Fuca1	ILMN_2696806	37	0,77957332
Rps12	ILMN_2956159	37	0,9376574
Rpsa	ILMN_2727876	37	1,08508268
Syne1	ILMN_3017615	37	1,17275418
Tfip11	ILMN_2961179	37	1,1034285
Vav2	ILMN_2436992	37	0,7758169
2610510B01Rik	ILMN_1217562	36	0,83509508
Cdc45l	ILMN_2919433	36	1,300341
Ino80e	ILMN_1244842	36	1,28034491
Lemd2	ILMN_1233040	36	0,91774669
Maz	ILMN_2709839	36	1,19630148
Nradd	ILMN_2690396	36	1,35155669
Olfr1065	ILMN_2744014	36	0,8473353
2310061C15Rik	ILMN_2703204	35	1,32945864
Allc	ILMN_2992073	35	1,33486544
Bmp8b	ILMN_1229350	35	1,2441441
Dtna	ILMN_2724339	35	0,85313148
Lrpprc	ILMN_2683718	35	0,74790993
Lysmd1	ILMN_1238939	35	1,07396681
Traf3ip2	ILMN_1232123	35	0,83618987
Tspyl1	ILMN_2801001	35	0,77197644
4430402I18Rik	ILMN_2719487	34	1,31825331
Cth	ILMN_2662719	34	0,90527662
EG436332	ILMN_2827515	34	0,85833362
Itgax	ILMN_2727172	34	1,33157741
LOC100047634	ILMN_1215644	34	1,19978491
Tmprss11f	ILMN_2759828	34	1,18106694
Alg12	ILMN_2869182	33	1,14343407
Atic	ILMN_2606567	33	0,89779735
Il15	ILMN_2610234	33	0,73493434
Lass4	ILMN_2880467	33	0,82490884
Fyn	ILMN_2912082	32	0,85161992
Mcm6	ILMN_1217331	32	1,65003169
Sgcb	ILMN_1255256	32	0,91812417
A430089I19Rik	ILMN_2979672	31	0,82320957
Ckap2l	ILMN_1231885	31	1,11971189
D4Ertd22e	ILMN_3129206	31	1,14573072
Gabrb3	ILMN_3044905	31	1,25035021
Ndor1	ILMN_3146204	31	1,20050826
Olfr1167	ILMN_2912805	31	1,32961447
Olfr922	ILMN_1246083	31	0,77629671
Igfl3	ILMN_1242115	30	0,83015462
Krit1	ILMN_2701155	30	0,77294745
LOC100046355	ILMN_2536080	30	1,19011773
Tle3	ILMN_2984872	30	0,7905691
Arr3	ILMN_2726271	29	0,75224703
Hfm1	ILMN_2605533	29	0,85819086
Khsrp	ILMN_3003567	29	1,19574987
Klk1b9	ILMN_2723594	29	1,29641749
LOC619597	ILMN_3087413	29	0,90447593
Lrrc48	ILMN_3071876	29	1,2392513
Smc3	ILMN_1223531	29	1,20604501
Tmem16b	ILMN_2802590	29	0,88378869
Dhx9	ILMN_2762418	28	1,24453293
Kbtbd7	ILMN_3077630	28	0,81816806
Lman2l	ILMN_1220769	28	1,13105665
Olfr877	ILMN_1243598	28	1,44600683
Tpi1	ILMN_1231447	28	0,90669448
Dusp22	ILMN_2767996	27	0,72681136
Fbln1	ILMN_2602770	27	1,18540217
LOC100048461	ILMN_1239843	27	1,31228544
Rell2	ILMN_2671794	27	0,90045091
1200011O22Rik	ILMN_2679477	26	1,12313457
Brca2	ILMN_3109564	26	1,214688
Frat1	ILMN_1251022	26	1,2175478
Rspry1	ILMN_1238609	26	0,83558875
Sgip1	ILMN_2678327	26	0,75214847
1110018J18Rik	ILMN_2647669	25	0,89256295
4930579E17Rik	ILMN_2654720	25	0,82600606
Adra2b	ILMN_2688190	25	1,25432725
Arl4d	ILMN_2593709	25	1,32807314

ID	ILMN-ID	Frequency	Linear_ratio
Fbln2	ILMN_3132949	25	0,89711195
Timp4	ILMN_2665133	25	0,85645027
Gper	ILMN_2747135	24	1,26133048
Pdzd8	ILMN_2982143	24	0,81077599
Prima1	ILMN_1234415	24	1,12318328
Sdc3	ILMN_2715042	24	0,88923985
Adap1	ILMN_1224713	23	1,09592551
Ccdc85a	ILMN_2723052	23	0,80394986
Fancb	ILMN_2689773	23	1,29033977
Pax7	ILMN_2709591	23	0,80325777
Prkaa2	ILMN_2803138	23	0,84322819
Clec4b1	ILMN_2603898	22	1,30518471
EG629734	ILMN_3162417	22	0,78380464
Igsf11	ILMN_1237582	22	0,86853071
Lypd3	ILMN_1248916	22	1,17555142
Matk	ILMN_2743902	22	1,11173665
Nrf1	ILMN_1251184	22	1,2528432
Rgr	ILMN_2957721	22	1,11566666
Rnf125	ILMN_2594109	22	1,18295402
Wdr17	ILMN_2434160	22	0,8837581
AW548124	ILMN_3104118	21	0,78997834
Clps	ILMN_2722659	21	0,80373009
Htra1	ILMN_2966104	21	1,10864375
Map4k5	ILMN_1239275	21	0,72753852
Ndufa7	ILMN_2629044	21	0,88925404
Timm17b	ILMN_2824012	21	0,80228787
2810417H13Rik	ILMN_1223045	20	0,72517647
Chrna7	ILMN_3001588	20	0,8185977
Gga3	ILMN_1242273	20	1,13363178
Klf10	ILMN_2648189	20	1,22563167
Lincr	ILMN_1229573	20	1,2577447
Ly6g6c	ILMN_1251725	20	1,26923515
Mettl9	ILMN_2713471	20	0,88738987
Pde3a	ILMN_2629556	20	0,80756396
Spire1	ILMN_2741746	20	0,69645963
A230074B11Rik	ILMN_3092518	19	1,23806952
Klk1b27	ILMN_1252131	19	1,27084791
Pomgnt1	ILMN_2722353	19	1,07996328
Ppt2	ILMN_2616827	19	1,14678972
S100a7a	ILMN_1230080	19	1,2801286
Six5	ILMN_2995454	19	0,82102492
Eif4h	ILMN_1243395	18	0,93879347
Klk15	ILMN_2726478	18	1,11380488
Mtcp1	ILMN_3162682	18	0,83832042
Rnase11	ILMN_1253337	18	1,19999992
Xpo7	ILMN_1251572	18	1,10915342
Zfp106	ILMN_2482427	18	0,83932552
9130019O22Rik	ILMN_2637604	17	1,22726228
Ampd1	ILMN_2971142	17	1,25710769
BC049730	ILMN_2907915	17	1,17479722
Epb4.9	ILMN_2615749	17	1,16538362
Gats	ILMN_3036708	17	1,12188648
Ifna11	ILMN_2769241	17	1,26298723
Kcne2	ILMN_2794237	17	0,85456569
Pabpc2	ILMN_2635205	17	1,21967948
Spink12	ILMN_2660373	17	1,23412473
2210009G21Rik	ILMN_3072319	16	0,79892235
2310047D13Rik	ILMN_2543108	16	0,86695783
Arhgef1	ILMN_2920753	16	0,79969438
Asnsd1	ILMN_1229430	16	0,86907193
Cstad	ILMN_2666764	16	1,2323487
D230010M03Rik	ILMN_1226081	16	1,28099049
Gabrb2	ILMN_1247588	16	0,82612302
Gdpd1	ILMN_2683528	16	1,10329504
Gm1008	ILMN_3021415	16	0,76877282
Gpam	ILMN_2655954	16	0,75784859
Mip	ILMN_1254280	16	1,2313741
Ogfod2	ILMN_2732896	16	1,23691346
Pag1	ILMN_2711339	16	0,70845424
Rhbdf2	ILMN_1221129	16	0,79566774
Sh3rf1	ILMN_2711279	16	1,22434323
Tmem215	ILMN_1231792	16	1,17265465
Txndc3	ILMN_2474917	16	1,13695487

Table 10.23: GO categories - biological process, obtained by analysis of expression differences in brain samples of *Sms1*^{MUT} (n=4) and *Sms1*^{WT} (n=3).
All GO categories with a p-value < 0.1 are listed. False discovery range (FDR).

Name	Total Entities	Overlap	Percent Overlap	Overlapping Entities	p-value	FDR
signal transduction	3586	44	1	RHBDL1,OR13C3,OR10S1,Vmn2r1,Vmn1r69,Olfr102,Olfr913,Olfr1167,Olfr1065,Olfr877,Olfr694,Olfr1342,Olfr922,IL15,LTA,CXCL12,ADRB1,CRK,PRKAA2,GPER,PDE3A,RPSA,CHRNA7,ADRA2B,NR5A2,DDR2,WNT3A,FRZB,TLE3,VAV2,PRMT2,ARR3,SMC3,GABRB2,SH3GLB1,GRIA3,PAG1,RGR,CSNK1D,Clec4b1,GABRB3,Nradd,IGSF11,CREBL2	2.03E-06	0.00150829
metabolic process	2421	30	1	RHBDL1,C9orf21,AADACL4,Klk1b27,Rnf125,FYN,GPAM,PDE3A,SMPD2,CTH,TPI1,FUCA1,DHX9,PRMT2,DUSP22,SH3RF1,HFM1,ART1,ACER1,CSNK1D,PPT2,GSTM2,DIP2B,PDP2,RHBDF2,Cyp2d26,MAP4K5,Harbi1,ALLC,Neurl3	9.86E-05	0.0366299
multicellular organismal development	1146	17	1	Bmp8b,FYN,PAX7,WNT3A,TPI1,UHRF1,FRZB,ZBTB17,TLE3,DUSP22,TDRD1,DMBX1,TXNDC3,SIX5,PKDCC,DOPEY2,LSM14B	0.00051795	0.08321397
innervation	6	2	33	GABRB2,GABRB3	0.00051939	0.08321397
induction of apoptosis	240	7	2	LTA,CIDEC,PRMT2,KLF10,SH3RF1,SH3GLB1,JMY	0.00061125	0.08321397
RNA splicing	323	8	2	Khsrp,SRSF2,PCBP2,DHX9,PRPF40B,TFIP11,RBM10,SUGP1	0.00073881	0.08321397
DNA-dependent DNA replication initiation	32	3	9	MCM6,CDC45,LRWD1	0.00090383	0.08321397
DNA repair	337	8	2	UHRF1,BRCA2,FANCB,MUS81,MNAT1,SMC3,CSNK1D,JMY	0.00097089	0.08321397
cell proliferation	429	9	2	LTA,UHRF1,BRCA2,ARHGEF1,MTCP1,MATK,MNAT1,KLF10,DUSP22	0.00112944	0.08321397
inner ear receptor cell development	9	2	22	GABRB2,GABRB3	0.00123197	0.08321397
positive regulation of calcium ion transport via voltage-gated calcium channel activity	9	2	22	CXCL12,ADRB1	0.00123197	0.08321397
spinal cord association neuron differentiation	10	2	20	PAX7,WNT3A	0.00153394	0.09497645
organ regeneration	87	4	4	CXCL12,NRF1,ATIC,CSDA	0.00183435	0.10042253
activated T cell proliferation	12	2	16	FYN,ITGAX	0.00223224	0.10042253
cochlea development	12	2	16	GABRB2,GABRB3	0.00223224	0.10042253
positive regulation of chondrocyte differentiation	13	2	15	RUNX2,PKDCC	0.0026278	0.10042253
adrenergic receptor signaling pathway	14	2	14	ADRB1,ADRA2B	0.00305381	0.10042253
ovulation cycle	14	2	14	TIMP4,CHRNA7	0.00305381	0.10042253
Wnt receptor signaling pathway	168	5	2	WNT3A,FRZB,TLE3,FRAT1,CSNK1D	0.00338969	0.10042253
gene expression	415	8	1	SRSF2,RPSA,NR5A2,PCBP2,DHX9,MNAT1,EIF4H,SUGP1	0.00353696	0.10042253
oocyte maturation	16	2	12	PDE3A,BRCA2	0.00399566	0.10042253
nuclear mRNA splicing, via spliceosome	175	5	2	SRSF2,PCBP2,DHX9,TFIP11,SUGP1	0.00403151	0.10042253
positive regulation of receptor-mediated endocytosis	17	2	11	SGIP1,SYNE1	0.00451078	0.10042253
positive regulation of cell proliferation	438	8	1	IL15,LTA,CXCL12,RUNX2,CHRNA7,DDR2,WNT3A,MATK	0.00487521	0.10042253
dorsal-ventral neural tube patterning	18	2	11	PAX7,WNT3A	0.00505486	0.10042253
regulation of transcription from RNA polymerase II promoter	351	7	1	CRK,NRF1,UHRF1,FRZB,MNAT1,ECSIT,JMY	0.0052076	0.10042253
ceramide biosynthetic process	19	2	10	SMPD2,LASS4	0.00562757	0.10042253
transport	1812	20	1	NDUFA7,Khsrp,CHRNA7,KCNE2,LRPPRC,GABRB2,ARFGAP1,GRIA3,MIP,SLC25A31,ANO2,SLC25A26,SCN3B,GABRB3,PKDCC,GGA3,XPO7,DOPEY2,TIMM17B,SPIRE1	0.00576812	0.10042253
lymph node development	21	2	9	IL15,LTA	0.00685739	0.10840512
protein N-linked glycosylation	21	2	9	Alg12,POMGNT1	0.00685739	0.10840512
purine ribonucleoside monophosphate biosynthetic process	21	2	9	ATIC,AMPD1	0.00685739	0.10840512
lipid biosynthetic process	128	4	3	PRKAA2,TPI1,TECR,LASS4	0.00728675	0.11279282
cellular response to heat	22	2	9	DHX9,ZNF14	0.00751382	0.11393405
gamma-aminobutyric acid signaling pathway	25	2	8	GABRB2,GABRB3	0.00964498	0.11442972
response to food	25	2	8	CLPS,CHRNA7	0.00964498	0.11442972
positive regulation of protein binding	26	2	7	WNT3A,KRIT1	0.0104082	0.11442972
response to DNA damage stimulus	309	6	1	UHRF1,BRCA2,FANCB,MUS81,SMC3,JMY	0.0106967	0.11442972
spermatogenesis	423	7	1	Bmp8b,BCL2L2,BRCA2,TLE3,CSDA,TDRD1,TXNDC3	0.0136616	0.1271539
regulation of axonogenesis	30	2	6	WNT3A,ARHGEF1	0.0137163	0.1271539
regulation of lipid metabolic process	30	2	6	PRKAA2,ACER1	0.0137163	0.1271539
mRNA transport	84	3	3	Khsrp,LRPPRC,XPO7	0.013862	0.1271539
mRNA processing	331	6	1	Khsrp,SRSF2,PRPF40B,TFIP11,RBM10,SUGP1	0.0145896	0.13074652
G1 phase of mitotic cell cycle	31	2	6	MNAT1,LRWD1	0.0146056	0.13074652
transforming growth factor beta receptor signaling pathway	88	3	3	Bmp8b,KLF10,DUSP22	0.0156926	0.13177551
brain development	245	5	2	CXCL12,BRCA2,FRZB,SYNE1,DMBX1	0.0158568	0.13177551
fatty acid biosynthetic process	89	3	3	PRKAA2,TPI1,TECR	0.0161705	0.13177551
chloride transport	91	3	3	GABRB2,ANO2,GABRB3	0.0171506	0.13177551
lens development in camera-type eye	34	2	5	MIP,SIX5	0.0174173	0.13177551
DNA strand elongation involved in DNA replication	35	2	5	MCM6,CDC45	0.0184016	0.13404303
positive regulation of cell-substrate adhesion	35	2	5	FBLN2,RELL2	0.0184016	0.13404303
cellular calcium ion homeostasis	94	3	3	CXCL12,TRDN,CHRNA7	0.0186818	0.13476289
triglyceride biosynthetic process	36	2	5	GPAM,TECR	0.0194088	0.13842909
mammary gland development	38	2	5	WNT3A,BRCA2	0.021491	0.13842909
positive regulation of canonical Wnt receptor signaling pathway	38	2	5	WNT3A,CSNK1D	0.021491	0.13842909
regulation of ARF GTPase activity	39	2	5	ADAP1,ARFGAP1	0.0225654	0.13842909
response to cold	39	2	5	ADRB1,CSDA	0.0225654	0.13842909
organ morphogenesis	180	4	2	PAX7,ITGAX,WNT3A,TLE3	0.0228205	0.13842909
regulation of cell proliferation	180	4	2	NR5A2,BRCA2,KLF10,DUSP22	0.0228205	0.13842909
chromosome organization	40	2	5	BRCA2,SMC3	0.0236615	0.13842909
neuroprotection	40	2	5	GABRB2,GABRB3	0.0236615	0.13842909
lipid metabolic process	372	6	1	GDPD1,PDE3A,CLPS,PLA1A,ACER1,TECR	0.0242895	0.13853047
blood coagulation	477	7	1	CRK,FYN,PDE3A,ADRA2B,ITGAX,IFNA1,VAV2	0.0245052	0.13853047
ossification	107	3	2	Bmp8b,RUNX2,PKDCC	0.0261672	0.13853047
cell-cell signaling	281	5	1	IL15,LTA,ADRA2B,WNT3A,KLF10	0.0267439	0.13853047
glutathione metabolic process	43	2	4	CTH,GSTM2	0.0270777	0.13853047
mesoderm development	43	2	4	WNT3A,MATK	0.0270777	0.13853047
purine base metabolic process	43	2	4	ATIC,AMPD1	0.0270777	0.13853047
response to activity	43	2	4	PRKAA2,GPAM	0.0270777	0.13853047
extracellular matrix organization	109	3	2	WNT3A,FBLN1,TFIP11	0.0274414	0.13853047
activation of JUN kinase activity	44	2	4	CRK,MAP4K5	0.028258	0.13853047
germ cell development	45	2	4	CXCL12,TDRD1	0.0294587	0.13853047
angiogenesis	200	4	2	IL15,ADRA2B,KRIT1,VAV2	0.0318952	0.14675627
defense response to virus	47	2	4	GPAM,ITGAX	0.03192	0.14675627
humoral immune response	47	2	4	LTA,TRAF3IP2	0.03192	0.14675627
adult locomotory behavior	48	2	4	CXCL12,DMBX1	0.03318	0.14675627
S phase of mitotic cell cycle	120	3	2	MCM6,CDC45,MNAT1	0.0350303	0.14675627
cellular amino acid biosynthetic process	50	2	4	ASNSD1,CTH	0.0357574	0.14842317
blood circulation	51	2	3	CXCL12,KCNE2	0.0370743	0.15218898
memory	51	2	3	ADRB1,CHRNA7	0.0370743	0.15218898
palate development	52	2	3	WNT3A,PKDCC	0.0384096	0.15680403
intracellular protein kinase cascade	125	3	2	FYN,SMPD2,MAP4K5	0.0388015	0.15753833
myelination	53	2	3	FYN,ZNF24	0.0397631	0.15803033
mitotic cell cycle	316	5	1	MCM6,CDC45,MNAT1,SMC3,CSNK1D	0.0410496	0.15803033
steroid hormone mediated signaling pathway	55	2	3	GPER,NR5A2	0.0425235	0.15852769
ion transmembrane transport	540	7	1	CHRNA7,KCNE2,GABRB2,GRIA3,ANO2,SCN3B,GABRB3	0.0432997	0.15852769
proteolysis	657	8	1	RHBDL1,TMPRSS11F,Klk1b9,Klk1b27,Klk15,HTRA1,RHBDF2,ADAM11	0.0434538	0.15852769
nerve growth factor receptor signaling pathway	224	4	1	CRK,SMPD2,ARHGEF1,VAV2	0.0452192	0.15852769
sphingolipid metabolic process	57	2	3	ACER1,LASS4	0.0453534	0.15852769
sensory perception of pain	58	2	3	ADRB1,SCN3B	0.0467938	0.15852769
Rho protein signal transduction	59	2	3	ADRB1,ARHGEF1	0.0482509	0.15852769
BMP signaling pathway	60	2	3	WNT3A,ECSIT	0.0497243	0.15852769
positive regulation of neuron differentiation	60	2	3	CXCL12,ADRA2B	0.0497243	0.15852769

Table 10.24: GO categories – cellular compartment, obtained by analysis of expression differences in brain samples of *Sms1*^{MUT} (n=4) and *Sms1*^{WT} (n=3).
All GO categories with a p-value < 0.1 are listed. False discovery range (FDR).

Name	Total Entities	Overlap	Percent Overlap	Overlapping Entities	p-value	FDR
cytoplasm	5836	70	1	NDOR1,MAP6D1,LRRC48,GDPD1,NLRP9,Khsrp,S100a7a,Dtna,IL15,ADRB1,CRK,RUNX2,PRKAA2,RPSA,NRF1,CIDEC,BCL2L2,TRDN,CTH,CHRNA7,NR5A2,FUCA1,BRCA2,FRZB,ARHGEF1,CDC45,SWAP70,PCBP2,MATK,EPB49,DHX9,VAV2,MNAT1,SGCB,PRMT2,FRAT1,LRPPRC,DUSP22,EIF4H,ARR3,ECSIT,CSDA,SH3RF1,SMC3,ADAP1,IGF2BP3,SGIP1,LOR,ARFGAP1,TDRD1,SH3GLB1,SYNE1,TXNDC3,SIX5,CSNK1D,TECR,ARL4D,GSTM2,JMY,TFIP11,FBXL12,XPO7,MAP4K5,CYS1,Harbi1,TUBA3C,ZFP106,HECTD3,LRWD1,SPIRE1	4.67E-05	0.007939
nucleus	6226	68	1	NDOR1,C21orf59,Khsrp,Sin3b,IL15,ADRB1,CRK,RUNX2,PRKAA2,SRSF2,RPSA,PAX7,NRF1,CIDEC,CTH,NR5A2,TPI1,UHRF1,BRCA2,KIAA0101,MCM6,CDC45,SWAP70,FANCB,PCBP2,ZBTB17,MATK,EPB49,TLE3,TMEM18,DHX9,MUS81,MNAT1,PRMT2,KLF10,LRPPRC,DUSP22,ECSIT,CSDA,SMC3,ADAP1,IGF2BP3,LOR,PRPF40B,CBFA2T2,ZNF24,SYNE1,LEMD2,DMBX1,SIX5,CSNK1D,ARL4D,SLC25A26,JMY,TSPYL1,TFIP11,LASS4,DIP2B,RBM10,XPO7,Harbi1,ZFP106,YPEL4,LRWD1,ZNF14,Nradd,SUGP1,CREBL2	0.0011352	0.096492
asymmetric synapse	13	2	15	CHRNA7,GRIA3	0.00449208	0.14992045
membrane fraction	724	13	1	RHBDL1,VSIG2,IL15,ADRB1,FYN,RPSA,SMPD2,CHRNA7,GABRB2,GRIA3,MIP,ZFP106,Nradd	0.00473551	0.14992045
nucleoplasm	901	15	1	PRKAA2,SRSF2,NR5A2,BRCA2,MCM6,CDC45,FANCB,PCBP2,DHX9,MNAT1,LRPPRC,SMC3,LOR,CSNK1D,SUGP1	0.0049666	0.14992045
basement membrane	89	4	4	RPSA,FBLN1,SMC3,RELL2	0.00529131	0.14992045
chloride channel complex	60	3	5	GABRB2,ANO2,GABRB3	0.0116495	0.19352687
membrane	6818	68	0	NDUFA7,RHBDL1,VSIG2,GDPD1,AADACL4,TMPRSS11F,Vmn2r1,Alg12,LTA,ADRB1,CRK,FYN,GPAM,GPER,PDE3A,RPSA,BCL2L2,TRDN,SMPD2,CHRNA7,LY6G6C,ADRA2B,ITGAX,DDR2,PEAR1,FRZB,ARHGEF1,SWAP70,EPB49,PRIMA1,TMEM18,KRIT1,SGCB,LYPD3,PRMT2,SDC3,KCNE2,LRPPRC,GABRB2,ART1,SH3GLB1,GRIA3,MIP,SLC25A31,SYNE1,LEMD2,PAG1,POMGNT1,ACER1,ANO2,RGR,TECR,ARL4D,SLC25A26,SCN3B,GABRB3,LASS4,SORCS3,FAM57A,GGA3,RHBDF2,Cyp2d26,LMAN2L,RELL2,TIMM17B,GLIPR2,ADAM11,IGSF11	0.0118335	0.19352687
nuclear outer membrane	25	2	8	LRPPRC,SYNE1	0.0162472	0.19352687
postsynaptic membrane	190	5	2	CHRNA7,GABRB2,GRIA3,SYNE1,GABRB3	0.0170759	0.19352687
sarcoplasmic reticulum membrane	28	2	7	TRDN,ART1	0.0201607	0.1952093
nuclear membrane	132	4	3	TMEM18,SYNE1,LEMD2,LASS4	0.0202408	0.1952093
clathrin adaptor complex	30	2	6	SGIP1,GGA3	0.0229658	0.1952093
gap junction	30	2	6	CSDA,MIP	0.0229658	0.1952093
nuclear inner membrane	30	2	6	LRPPRC,LEMD2	0.0229658	0.1952093
microsome	383	7	1	ADRB1,FYN,TRDN,SH3GLB1,MIP,POMGNT1,Cyp2d26	0.0316079	0.21836212
dendritic spine	93	3	3	CHRNA7,GRIA3,SYNE1	0.0366807	0.21836212
sarcoplasmic reticulum	43	2	4	TRDN,ART1	0.0446359	0.21836212
dendritic shaft	47	2	4	CHRNA7,GRIA3	0.0523688	0.21836212
lamellipodium	108	3	2	SWAP70,SH3RF1,Nradd	0.0530759	0.21836212
cytosol	2285	25	1	NDOR1,C21orf59,Khsrp,Rps12,CRK,FYN,PRKAA2,PDE3A,RPSA,CIDEC,BCL2L2,TPI1,ARHGEF1,ATIC,PCBP2,VAV2,PRMT2,EIF4H,GABRB2,IGF2BP3,ARFGAP1,AMPD1,SH3GLB1,CSNK1D,ZFP106	0.0542822	0.21836212
terminal button	49	2	4	GRIA3,GABRB3	0.0564012	0.21836212
ribonucleoprotein complex	350	6	1	RPSA,PCBP2,DHX9,CSDA,TDRD1,LSM14B	0.0578559	0.21836212
synapse	350	6	1	CHRNA7,PRIMA1,ARR3,GABRB2,GRIA3,GABRB3	0.0578559	0.21836212
plasma membrane	4022	40	0	OR13C3,OR10S1,Vmn2r1,CXCL12,ADRB1,CRK,FYN,GPER,RPSA,TRDN,SMPD2,CHRNA7,LY6G6C,ADRA2B,ITGAX,WNT3A,PEAR1,ARHGEF1,SWAP70,PRIMA1,VAV2,SGCB,LYPD3,KCNE2,GABRB2,ART1,ADAP1,SGIP1,GRIA3,MIP,PAG1,ANO2,ARL4D,SCN3B,GABRB3,FAM57A,RELL2,ADAM11,ZNF14,IGSF11	0.0608485	0.21836212
Golgi membrane	452	7	1	GPER,ARFGAP1,SH3GLB1,POMGNT1,LMAN2L,DOPEY2,GLIPR2	0.06564	0.21836212
integral to plasma membrane	1250	15	1	RHBDL1,VSIG2,TMPRSS11F,IL15,ADRB1,GPER,SMPD2,ADRA2B,DDR2,SGCB,GABRB2,ART1,MIP,RGR,GABRB3	0.0665492	0.21836212
Golgi apparatus	1046	13	1	MAP6D1,IL15,GPER,SH3RF1,ARFGAP1,SH3GLB1,SYNE1,POMGNT1,PKDCC,GGA3,LMAN2L,GLIPR2,SPIRE1	0.0679763	0.21836212
microtubule basal body	55	2	3	CYS1,TUBA3C	0.0691107	0.21836212
mitochondrial outer membrane	123	3	2	GPAM,SH3GLB1,Cstad	0.072398	0.21836212
sarcomere	58	2	3	TIMP4,SYNE1	0.0757845	0.21836212
perinuclear region of cytoplasm	480	7	1	NDOR1,LRPPRC,EIF4H,SH3RF1,SYNE1,HECTD3,SPIRE1	0.0840617	0.22683316
transcription factor complex	302	5	1	RUNX2,PAX7,NRF1,ECSIT,DMBX1	0.0893443	0.2373208
extracellular matrix	217	4	1	RPSA,HTRA1,FBLN1,RELL2	0.0913334	0.23887197
nucleolus	1213	14	1	RUNX2,BRCA2,MCM6,MATK,DHX9,MUS81,SYNE1,ARL4D,SLC25A26,TSPYL1,RBM10,ZFP106,YPEL4,SUGP1	0.0950432	0.2393499

Acknowledgments

Ich möchte mich herzlich bedanken bei…

… **Prof. Dr. Wolfgang Wurst** und **Dr. Daniela Vogt-Weisenhorn**, für die Möglichkeit meine Doktorarbeit am IDG zu verfassen. Außerdem möchte ich mich bedanken für die Hilfsbereitschaft und das Interesse an meiner Arbeit, sowie für die fachlichen Diskussionen.

… **PD Dr. Thomas Floss**, für die Betreuung meiner Arbeit, sowie für seine Hilfe und seinen Rat bei wissenschaftlichen Fragen und die angenehme, offene Arbeitsatmosphäre.

… **Prof. Dr. Tobias Hartmann** und **Dr. Marcus Grimm**, für das große Interesse an meiner Arbeit, die vielen hilfreichen und fachlich kompetenten Gespräche, sowie die Durchführung der Lipid-Messungen.

… **Dr. Michael Willem** und **Heike Hampel**, für die Unterstützung und Anleitung bei der Durchführung und Auswertung der APP-Western, sowie die freundliche und herzliche Atmosphäre in Ihrem Labor vor Ort.

… **Dr. Annemarie Zimprich**, für die Durchführung der SRT Tests, **Dr. Dietrich Trümbach** für seine Hilfe bei der Analyse der Microarray Daten und **Dr. Steven Ford** für die MSOT Messungen.

… **Prof. Dr. Luksch**, für die Übernahme des Vorsitzes in der Prüfungskommission.

… **Prof. Dr. Aphrodite Kapurniotu**, für die Übernahme der Funktion als Zweitprüfer.

… **Irina**, für Deine immer gute Laune und ruhige Art die den Stress im Labor halb so wild erscheinen ließ und für die Pflege der Mäuse!

… **Annerose**, für Deinen Zuspruch und Deine Hilfe in fachlichen wie in privaten Notlagen und Deinen kompetenten Rat.

… dem besten Büro aller Zeiten: **Clara**, **Luise**, **Bene**, **Basti** und **Flo** – zusammen mit **Helga**, **Constantin**, **Svenja** und **Anja** ohne Euch wäre die Zeit nicht dieselbe gewesen!!!

… **Michi**, für Deine Freundschaft und die Unterstützung, sowie die anregenden Diskussionen.

… **Artem**, for your patients and support and for the attitude that every obstacle one has to face represents just another opportunity, to prove oneself. спасибо большое!

… **meiner Familie**, für Eure ständige Unterstützung und Euer offenes Ohr. Außerdem möchte ich Euch danken, dass Ihr immer da seid, wenn ich Euch brauche!!